frontiers | Research Topics

Host-microbe interaction in SARS-CoV-2 infection: Mechanism and intervention

Edited by
Tengchuan Jin, Ron Geller and Penghua Wang

Published in
Frontiers in Immunology

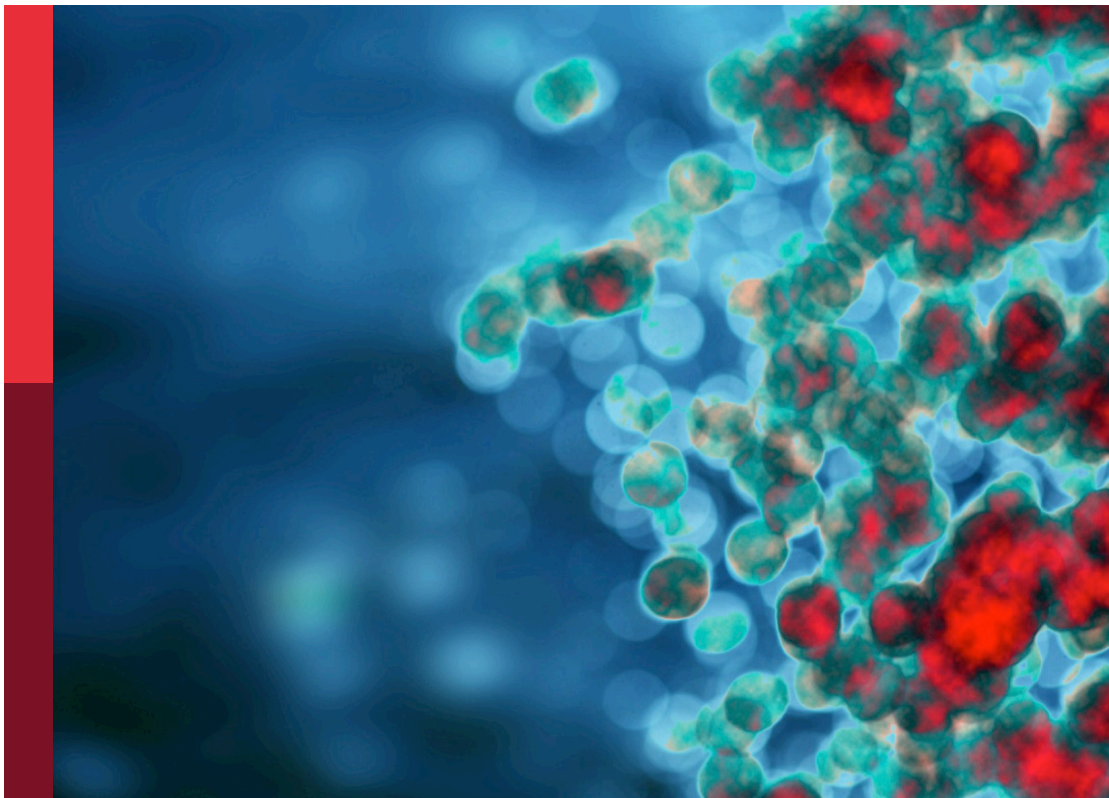

ISSN 1664-8714
ISBN 978-2-8325-2326-1
DOI 10.3389/978-2-8325-2326-1

About Frontiers

Frontiers is more than just an open access publisher of scholarly articles: it is a pioneering approach to the world of academia, radically improving the way scholarly research is managed. The grand vision of Frontiers is a world where all people have an equal opportunity to seek, share and generate knowledge. Frontiers provides immediate and permanent online open access to all its publications, but this alone is not enough to realize our grand goals.

Frontiers journal series

The Frontiers journal series is a multi-tier and interdisciplinary set of open-access, online journals, promising a paradigm shift from the current review, selection and dissemination processes in academic publishing. All Frontiers journals are driven by researchers for researchers; therefore, they constitute a service to the scholarly community. At the same time, the *Frontiers journal series* operates on a revolutionary invention, the tiered publishing system, initially addressing specific communities of scholars, and gradually climbing up to broader public understanding, thus serving the interests of the lay society, too.

Dedication to quality

Each Frontiers article is a landmark of the highest quality, thanks to genuinely collaborative interactions between authors and review editors, who include some of the world's best academicians. Research must be certified by peers before entering a stream of knowledge that may eventually reach the public - and shape society; therefore, Frontiers only applies the most rigorous and unbiased reviews. Frontiers revolutionizes research publishing by freely delivering the most outstanding research, evaluated with no bias from both the academic and social point of view. By applying the most advanced information technologies, Frontiers is catapulting scholarly publishing into a new generation.

What are Frontiers Research Topics?

Frontiers Research Topics are very popular trademarks of the *Frontiers journals series*: they are collections of at least ten articles, all centered on a particular subject. With their unique mix of varied contributions from Original Research to Review Articles, Frontiers Research Topics unify the most influential researchers, the latest key findings and historical advances in a hot research area.

Find out more on how to host your own Frontiers Research Topic or contribute to one as an author by contacting the Frontiers editorial office: frontiersin.org/about/contact

Host-microbe interaction in SARS-CoV-2 infection: Mechanism and intervention

Topic editors

Tengchuan Jin — University of Science and Technology of China, China

Ron Geller — University of Valencia, Spain

Penghua Wang — University of Connecticut Health Center, United States

Citation

Jin, T., Geller, R., Wang, P., eds. (2023). *Host-microbe interaction in SARS-CoV-2 infection: Mechanism and intervention*. Lausanne: Frontiers Media SA.

doi: 10.3389/978-2-8325-2326-1

The authors declare that the research was conducted in the absence of any commercial or financial relationships that could be construed as a potential conflict of interest

Table of contents

frontiers | Frontiers in Immunology

TYPE Editorial
PUBLISHED 18 April 2023
DOI 10.3389/fimmu.2023.1198868

OPEN ACCESS

EDITED AND REVIEWED BY
Shailendra Saxena,
King George's Medical University, India

*CORRESPONDENCE
Tengchuan Jin
jint@ustc.edu.cn

SPECIALTY SECTION
This article was submitted to Viral Immunology, a section of the journal Frontiers in Immunology

RECEIVED 02 April 2023
ACCEPTED 12 April 2023
PUBLISHED 18 April 2023

CITATION
Kombe Kombe AJ and Jin T (2023) Editorial: Host-microbe interaction in SARS-CoV-2 infection: mechanism and intervention. *Front. Immunol.* 14:1198868. doi: 10.3389/fimmu.2023.1198868

Editorial: Host-microbe interaction in SARS-CoV-2 infection: mechanism and intervention

Arnaud John Kombe Kombe[1,2,3] and Tengchuan Jin[1,2,4]*

[1]Department of Obstetrics and Gynecology, The First Affiliated Hospital of University of Science and Technology of China (USTC), Division of Life Sciences and Medicine, University of Science and Technology of China, Hefei, Anhui, China, [2]Laboratory of Structural Immunology, Chinese Academy of Sciences (C.A.S.) Key Laboratory of Innate Immunity and Chronic Disease, Division of Life Sciences and Medicine, University of Science and Technology of China, Hefei, Anhui, China, [3]Healthy Processed Foods Research Unit, United State Department of Agriculture, Agriculture Research Service (USDA-ARS), Western Regional Research Center, Albany, CA, United States, [4]CAS Center for Excellence in Molecular Cell Science, Chinese Academy of Science, Shanghai, China

KEYWORDS

COVID-19, SARS-CoV-2, immune response, virus-host interaction, intervention, pathophysiology, sepsis

Editorial on the Research Topic
Host-microbe interaction in SARS-CoV-2 infection: mechanism and intervention

Since December 2019, the world has experienced a nightmare due to the new Severe Acute Respiratory Syndrome Coronavirus 2 (SARS-CoV-2) causing the deadliest coronavirus disease known as COVID-19. This severe disease is characterized by metabolic acidosis, acute respiratory distress syndrome (ARDS), septic shock, and multiple organ dysfunction. Lacking specific treatment to contain the rapid infection spread and mitigate the disease burden, we have accumulated knowledge to understand the virus biology, its interactions with host cells, undelaying mechanisms of infection, the pathophysiology, and the immune response to the virus. However, because of the complexity of these aspects, especially the molecular interactions between SARS-CoV-2 and the host immune system, which are crucial for the successful therapeutic design, our knowledge is still limited, rendering the pandemic management challenging, talk less of the evolutionary nature of SARS-CoV-2.

This Research Topic aimed to gather novel findings and up-to-date conclusive studies from multidisciplinary expertise regarding the uncovered aspects of SARS-CoV-2–host cell interaction, which we believe, might bring light to developing effective prophylaxis and therapeutic interventions. This collection of 13 insightful studies can be put along a continuum to illustrate the immunological and molecular mechanisms underlying the COVID-19 severity, the progression of COVID-19 from the early stage board that features the later severity of the infection establishing the diverse immunological markers, and, therefore, the alternative means proposed to control the disease.

One of the major concerns (if not the first) in COVID-19 fighting strategies is the continuous emergence of new SARS-CoV-2 variants, especially the variants of concern

(VOCs) with their ability to escape the immune response. Omicron, for instance, the last known heavily mutated SARS-CoV-2 VOC, plays a crucial role in COVID-19 severity as it can escape natural and vaccine-induced immune response, and because of its high transmissibility. In their studies, Shah and Woo and Wang et al. demonstrated through and confirmed once again, at the molecular and clinical levels, the mechanism underlying the immune escape by Omicron variants, precisely the most evolved Omicron sub-strains BA.1, BA1.1, and BA.2. As previously reviewed (1) and among the over 30 mutations carried by Omicron variants, Shah and Woo demonstrated that mutations T478K, Q493K, Q498R, and E484A significantly contribute to the approved therapeutic antibody (etesevimab, bamlanivimab, and CT-p59) escape and fast transmissibility of Omicron by dampening antibody neutralizing effects and substantial enhancement of ACE2 binding affinity of RBD. More worrying, these studies showed that, as for REGEN-COV (casirivimab + imdevimab) inefficacy against Omicron (2), Omicron mutations significantly reduce neutralizing efficacy of bivalent antibody cocktails, including regdanvimab (etesevimab + CT-p59), and AZ combo (COV2-2196 + COV2-2130) targeting different SARS-CoV-2 epitopes, idea which was first thought as a better alternative to mitigate transmission and prevent the emergence of new variants (1).

Similarly, the contributive study of Tang et al. in this issue supports the before-mentioned concluding studies. In a vesicular stomatitis virus (VSV)-based pseudovirus infection system, Tang et al. showed that the infectivity of the Delta variant (B.1.617.2) critically increased, compared to that of previously evolved variants, including the D6114G variant, with the ability to resist neutralizing/inhibiting effects of RBD- and NTD-targeting antibodies and vaccinated sera, explaining its high transmissibility and severity. Therefore, even though BRII-196 + BRII-198 could retain protective effects (Wang et al.), more potent combinations of neutralizing antibodies from more than two groups (1) should be designed, or other alternatives need to be developed for more effective therapy against Omicron and Delta variants (talk less of other VOCs), potential upcoming emerging variants, and in case of infection with multiple SARS-CoV-2 variants. Saying the latter, protease inhibitors, which still can hamper entry and protect against SARS-CoV-2 infection regardless of mutational rate in spike protein [Tang et al. (3)], might be regarded as an ideal alternative.

Besides new variants, secondary bacterial coinfections can worsen primary SARS-CoV-2 infection, leading to severity. It was previously demonstrated that patients infected with respiratory tract bacteria are susceptible to SARS-CoV-2, worsening COVID-19 severity to fatality (4). The study by Smith et al. further demonstrated from the COVID-19 mice model that primary SARS-CoV-2 infection also increases susceptibility and aggravation to other respiratory infections, including pneumonia. Specifically, while the SARS-CoV-2 viral load remains steady (and low to a less extent) during the infection course, the bacterial load was progressively enhanced and accompanied by a progressive increase of neutrophils, pulmonary bacterial-associated burden, and bacteremia, which feature susceptibility to and severity of secondary bacterial infections during SARS-CoV-2. A low level of pulmonary macrophage required to clear bacteria-infected cells, which could be caused by INF response-inducing SARS-CoV-2, might be an underlying mechanism describing the pathophysiology of the coinfection. This study constitutes a point of alarm as, despite COVID-19 vaccines that reduce the severity of SARS-CoV-2 infection and thus the associated fatalities on the one hand and the observed reduced transmission of many pathogens on the other hand, asymptomatic or mild COVID-19 patients are on risk for bacterial pneumonia complication. Therefore, while encouraging COVID-19 vaccination, pneumonia diagnostic should be established in COVID-19 patients (and *vis-versa*), and adequate antibiotic treatment should be started in confirmed bacteria-co-infected patients.

The previous collection of studies highlighted new molecular and immunological aspects of the implication of SARS-CoV-2 VOCs and the pathogenic pool in the severity of COVID-19. Furthermore, several other studies have been carried out to assess the fate (mild, moderate, or severe) of a COVID-19 infection (prognostic) from the early stage (3-5 days post-symptom onset) (5, 6). Knowing the initial immune response in the early phase of SARS-CoV-2 infection and its effects on the development of respiratory failure is essential for quickly taking action to prevent fatalities. Xu et al. demonstrated that a transient high IFN-I response alongside a delayed adaptive immunity at the early stage of the infection is a hallmark of severe COVID-19. Specifically, they found that the early stage of COVID-19 severity is characterized by a strong INF response, which then drops rapidly throughout the infection in severe COVID-19 patients. In contrast, in mild COVID-19, the early INF response was low and stood steady.

Moreover, analyses starting from the early stage of severe COVID-19 showed that myeloid cells, neutrophils, and monocytes produce immune markers mediating interferon-stimulating gene transcription (IFI27, IFI35, ISG15, TXN., S100A4, S100A6, and FRP1) and pro-inflammatory cytokines, were highly detected. In contrast, the T cell titers (NK cells, T cells, mDCs, and pDCs cells) were lower than that in asymptomatic. Previous studies have reported detrimental effects of the IFN response, including its inflammatory role by recruiting more immune cells to the lungs to disrupt lung epithelial repair and the pulmonary epithelial barrier (7, 8) and suppressing pathway-related T cell functions (9) during severe COVID-19. Hence, this study by Xu et al. confirms that high IFN response (stimulated by high viral load (Nagaoka et al.) inhibits the maturation of naïve $CD8^+$ T cells triggered during the early stage of the infection. More interestingly, the early strong IFN response impairing induction of $CD8^+$ T-cells can lead to earlier fatality in patients with an already depleted titer of naïve $CD8^+$ T cells (including elderly and immunosuppressed patients).

Aligning with before mentioned Xu et al.'s findings, Nagaoka et al. found that patients who later developed severe COVID-19 (characterized by hypoxemic respiratory failure) had high titer of INF-I response, specifically INF-α (but not IFN-β) and an increased level of pro-inflammatory cytokines (IL-6, and CXCL10) in the early stage of the infection. Moreover, transcriptomic study on lung samples from succumbed COVID-19 patients revealed higher levels of pulmonary IFN inducing genes than that of mild COVID-19 recovered patients (10) and which correlated with both cytokine storm and organ failure (sepsis) caused by necrosis, apoptosis, and pyroptosis, (Zhu et al. and reviewed by Moga et al.). Therefore,

COVID-19 patients producing INF-α, IL-6, and CXCL10 at the early stage of the infection should be considered at high risk of respiratory failure and require urgent hospitalization to prevent fatalities.

While detecting IFN response at the early stage of COVID-19 infection is highly suggested to determine the potential severity of a beginning COVID-19 infection, Lai et al. revealed novel determining parameters/markers, which might also explain the severity of the infection, and, therefore, need to be monitored as well. Lai et al. confirmed that serum levels of autoantibodies against ACE2 are significantly higher in severe COVID-19 patients than in controls, and correlate with severity, suggesting that SARS-CoV-2 manage to induce anti-ACE2 antibodies leading to ACE2-specific autoimmune reaction-associated disease, possibly increasing sepsis and worsening the pathophysiology of the infection. Specifically, the amino acid residues P463, F464, E465, R466, D467, and E471 SARS-CoV-2 RBD are the primary residues recognized by the anti-ACE2-cross reactive RBD-specific antibodies. Notably, these residues are less or not reported as a variable in VOCs, suggesting that they are selective residues for the benefit of SARS-CoV-2, hence worsening pathological conditions. Besides, numerous currently available COVID-19 vaccines are developed from SARS-CoV-2 spike protein. Therefore, further studies must elucidate whether anti-ACE2-cross reactive RBD-specific antibodies are induced after SARS-CoV-2 vaccination and their potential pathological effects.

The continuous emergence of SARS-CoV-2 variants and their high ability to escape natural and vaccine-induced immunity, the reportedly life-threatening effects of respiratory bacterial coinfections, the resistance of COVID-19 to the currently repositioned treatment, and the lack of specific anti-COVID-19 treatment require more researches for safe and cost-effective alternatives to preventing COVID-19 disease.

The study by Smith et al. supports the fact that multi-pathogen coinfection with SARS-CoV-2 is a main infection pattern of increased pathological disorder. However, Cai et al. would like to draw attention to the contribution of coinfection with parasitic worms (non-pulmonary infections) in anti-COVID-19 strategies, from the hypothesis stating, "*Co-evolved microbes and other pathogens, including helminths, could help to establish appropriate immunomodulatory function and thus protect the host against a large spectrum of immune-related disorders*" (11). Hence, there is more evidence of a positive and attractive immunomodulatory response elicited by parasites, which may restore multi-system sepsis caused by other pathogens, including SARS-CoV-2. For instance, Cai et al. highlighted that chronic parasite infection induces an immunosuppressive and regulatory T-helper response that balances and lowers the inflammatory Th1/Th17 response triggered by SARS-CoV-2 infection in critically ill COVID-19 patients, restricting the severity of COVID-19 disease. Coinfection with helminths induces an anti-inflammatory Th-2 response characterized by the production of anti-inflammatory cytokines (IL-4, IL-5, and IL-13)-producing Th-2 cells. These anti-inflammatory cytokines could restore inflammatory-associated damage and thus sepsis caused by pro-inflammatory cytokines induced by activation of Th-1/Th-17 response. More precisely, these immunomodulatory responses are induced after the administration of helminth-derived products and attenuate the severity of sepsis, restoring covid-19-associated organ damages.

While Cai et al. could propose controlled helminth infection or using helminth products to control SARS-CoV-2 severity and reduce mortality, Santos et al. demonstrated an anti-SARS-CoV-2 protective activity of a carefully selected cocktail of cannabidiol and terpene, which may serve as natural extract therapeutic. In fact, the cannabinoid can boost immune response through activation of cannabinoid receptor 2 (CN2R) (12–14) and exhibit anti-inflammatory effect (15) in COVID-19 patients, while terpenes are known to enhance phytocannabinoid action; therefore, their combination was expected to synergistically protect against SARS-CoV-2, which is demonstrated in the study by Santos et al.

IgG Fc fragment plays important roles in viral clearance by activating the classical complement pathway and mediating infected cell clearance through binding to Fc gamma receptors (FcγRs), which activate antibody-dependent cellular cytotoxicity (ADCC) and antibody-dependent cellular phagocytosis (ADCP). In addition, since ACE2 is a known high-binding affinity receptor of a spike, designing ACE2-derived-Fc antibodies would be beneficial to boost effective COVID-19 immunity. In this regard, Wine and colleagues have engineered three ACE2-Fc (flACE2-Fc, EflACE2-Fc, and trACE2-Fc) by modifying ACE2 to enhance the existing binding affinity (neutralization) of ACE2 to SARS-CoV-2 S protein. The proposed high binder spike-specific ACE2-Fc demonstrated distinct but promising enhanced neutralization effects against SARS-CoV-2 and increased Fc-associated effector functions against virus-infected cells. In addition, despite the exciting results by Bahnan et al. demonstrating that non-neutralizing antibodies could be used as they can confer protection against SARS-CoV-2 through Fc-mediating phagocytosis, high-binding affinity-associated neutralizing antibodies (such as engineered ACE2-Fcs) constitute a safer way against SARS-CoV-2 infection, because neutralizing antibodies are multi-effective, whereas reported antibody-dependent enhancement (ADE) disorders are related to non-neutralizing antibodies (16).

Overall, this Research Topic compiled studies that brought novelties in aspects of SARS-CoV-2–host interactions and advanced our knowledge of the immunological mechanisms underlying COVID-19 severity. Moreover, these studies present alternative solutions for effective prophylactic and therapeutic interventions, which are essential for our preparedness to control the current pandemic state and for future emergence and re-emergence of more pathogenic SARS-CoV-2 variants or similar viruses.

Author contributions

TJ provided funding, conceptualized the idea of the topic, and edited the manuscript. JK conceived the topic and drafted and edited the manuscript. All authors contributed to the article and approved the submitted version.

Funding

This study is supported by the Strategic Priority Research Program of the Chinese Academy of Sciences (Grant No. XDB29030104), the National Natural Science Fund (Grant Nos.: 31870731), the Fundamental Research Funds for the Central Universities, and USTC new medicine joint fund training program (WK9110000136).

Acknowledgments

Special thanks to the Strategic Priorities Research Program of the Chinese Academy of Sciences, the National Natural Science Fund, the Fundamental Research Funds for the Central Universities, and the USTC new medicine joint fund training program for the funding.

Conflict of interest

The authors declare that the research was conducted in the absence of any commercial or financial relationships that could be construed as a potential conflict of interest.

Publisher's note

All claims expressed in this article are solely those of the authors and do not necessarily represent those of their affiliated organizations, or those of the publisher, the editors and the reviewers. Any product that may be evaluated in this article, or claim that may be made by its manufacturer, is not guaranteed or endorsed by the publisher.

References

1. Kombe Kombe AJ, Zahid A, Mohammed A, Shi R, Jin T. Potent molecular feature-based neutralizing monoclonal antibodies as promising therapeutics against SARS-CoV-2 infection. *Front Mol Biosci* (2021) 8:670815. doi: 10.3389/fmolb.2021.670815

2. VanBlargan LA, Errico JM, Halfmann PJ, Zost SJ, Crowe JEJr., Purcell LA, et al. An infectious SARS-CoV-2 B.1.1.529 omicron virus escapes neutralization by therapeutic monoclonal antibodies. *Nat Med* (2022) 28(3):490–5. doi: 10.1038/s41591-021-01678-y

3. Mengist HM, Fan X, Jin T. Designing of improved drugs for COVID-19: crystal structure of SARS-CoV-2 main protease m(pro). *Signal Transduct Target Ther* (2020) 5 (1):67. doi: 10.1038/s41392-020-0178-y

4. Shafran N, Shafran I, Ben-Zvi H, Sofer S, Sheena L, Krause I, et al. Secondary bacterial infection in COVID-19 patients is a stronger predictor for death compared to influenza patients. *Sci Rep* (2021) 11(1):12703. doi: 10.1038/s41598-021-92220-0

5. Schulte-Schrepping J, Reusch N, Paclik D, Bassler K, Schlickeiser S, Zhang B, et al. Severe COVID-19 is marked by a dysregulated myeloid cell compartment. *Cell* (2020) 182(6):1419–40 e23. doi: 10.1016/j.cell.2020.08.001

6. Hadjadj J, Yatim N, Barnabei L, Corneau A, Boussier J, Smith N, et al. Impaired type I interferon activity and inflammatory responses in severe COVID-19 patients. *Science* (2020) 369(6504):718–24. doi: 10.1126/science.abc6027

7. Major J, Crotta S, Llorian M, McCabe TM, Gad HH, Priestnall SL, et al. Type I and III interferons disrupt lung epithelial repair during recovery from viral infection. *Science* (2020) 369(6504):712–7. doi: 10.1126/science.abc2061

8. Broggi A, Ghosh S, Sposito B, Spreafico R, Balzarini F, Lo Cascio A, et al. Type III interferons disrupt the lung epithelial barrier upon viral recognition. *Science* (2020) 369 (6504):706–12. doi: 10.1126/science.abc3545

9. Cresse SM, Urrechaga EM, Cioci AC, Banerjee MN, Cahill A, Lieberman HM. Pexy of intraperitoneal LVAD driveline to relieve small bowel obstruction. *J Card Surg* (2020) 35(2):492–4. doi: 10.1111/jocs.14398

10. Nienhold R, Ciani Y, Koelzer VH, Tzankov A, Haslbauer JD, Menter T, et al. Two distinct immunopathological profiles in autopsy lungs of COVID-19. *Nat Commun* (2020) 11(1):5086. doi: 10.1038/s41467-020-18854-2

11. Rook GA, Adams V, Hunt J, Palmer R, Martinelli R, Brunet LR. Mycobacteria and other environmental organisms as immunomodulators for immunoregulatory disorders. *Springer Semin Immunopathol* (2004) 25(3-4):237–55. doi: 10.1007/s00281-003-0148-9

12. Zou S, Kumar U. Cannabinoid receptors and the endocannabinoid system: signaling and function in the central nervous system. *Int J Mol Sci* (2018) 19(3):833. doi: 10.3390/ijms19030833

13. Gui H, Sun Y, Luo ZM, Su DF, Dai SM, Liu X. Cannabinoid receptor 2 protects against acute experimental sepsis in mice. *Mediators Inflammation* (2013) 2013:741303. doi: 10.1155/2013/741303

14. Tahamtan A, Samieipoor Y, Nayeri FS, Rahbarimanesh AA, Izadi A, Rashidi-Nezhad A, et al. Effects of cannabinoid receptor type 2 in respiratory syncytial virus infection in human subjects and mice. *Virulence* (2018) 9(1):217–30. doi: 10.1080/21505594.2017.1389369

15. Anil SM, Shalev N, Vinayaka AC, Nadarajan S, Namdar D, Belausov E, et al. Cannabis compounds exhibit anti-inflammatory activity *in vitro* in COVID-19-related inflammation in lung epithelial cells and pro-inflammatory activity in macrophages. *Sci Rep* (2021) 11(1):1462. doi: 10.1038/s41598-021-81049-2

16. Ajmeriya S, Kumar A, Karmakar S, Rana S, Singh H. Neutralizing antibodies and antibody-dependent enhancement in COVID-19: a perspective. *J Indian Inst Sci* (2022) 102(2):671–87. doi: 10.1007/s41745-021-00268-8

frontiers in Immunology

ORIGINAL RESEARCH
published: 14 January 2022
doi: 10.3389/fimmu.2021.808932

Spike-Dependent Opsonization Indicates Both Dose-Dependent Inhibition of Phagocytosis and That Non-Neutralizing Antibodies Can Confer Protection to SARS-CoV-2

Wael Bahnan[1], Sebastian Wrighton[1], Martin Sundwall[1], Anna Bläckberg[1,2], Olivia Larsson[3], Urban Höglund[3], Hamed Khakzad[4,5], Magdalena Godzwon[6], Maria Walle[6], Elisabeth Elder[7], Anna Söderlund Strand[8], Lotta Happonen[1], Oscar André[1], Johannes Kumra Ahnlide[1], Thomas Hellmark[9], Vidar Wendel-Hansen[10], Robert PA. Wallin[11], Johan Malmstöm[1], Lars Malmström[1,12], Mats Ohlin[6,13], Magnus Rasmussen[1,2] and Pontus Nordenfelt[1]**

[1] Department of Clinical Sciences Lund, Infection Medicine, Faculty of Medicine, Lund University, Lund, Sweden, [2] Infectious Disease Clinic, Skåne University Hospital, Lund, Sweden, [3] Adlego Biomedical AB, Uppsala, Sweden, [4] Equipe Signalisation Calcique et Infections Microbiennes, Ecole Normale Supérieure Paris-Saclay, Gif-sur-Yvette, France, [5] Institut National de la Santé et de la Recherche Médicale (INSERM) U1282, Gif-sur-Yvette, France, [6] Department of Immunotechnology, Lund University, Lund, Sweden, [7] Public Health Agency of Sweden, Solna, Sweden, [8] Department of Laboratory Medicine, Clinical Microbiology, Skane University Hospital Lund, Lund University, Lund, Sweden, [9] Department of Clinical Sciences Lund, Nephrology, Skane University Hospital Lund, Lund University, Lund, Sweden, [10] Tanea Medical Ab, Uppsala, Sweden, [11] SciEd Solutions, Stockholm, Sweden, [12] Institute for Computational Science, Zurich, Switzerland, [13] SciLifeLab Drug Discovery and Development, Lund University, Lund, Sweden

Spike-specific antibodies are central to effective COVID19 immunity. Research efforts have focused on antibodies that neutralize the ACE2-Spike interaction but not on non-neutralizing antibodies. Antibody-dependent phagocytosis is an immune mechanism enhanced by opsonization, where typically, more bound antibodies trigger a stronger phagocyte response. Here, we show that Spike-specific antibodies, dependent on concentration, can either enhance or reduce Spike-bead phagocytosis by monocytes independently of the antibody neutralization potential. Surprisingly, we find that both convalescent patient plasma and patient-derived monoclonal antibodies lead to maximum opsonization already at low levels of bound antibodies and is reduced as antibody binding to Spike protein increases. Moreover, we show that this Spike-dependent modulation of opsonization correlate with the outcome in an experimental SARS-CoV-2 infection model. These results suggest that the levels of anti-Spike antibodies could influence monocyte-mediated immune functions and propose that non-neutralizing antibodies could confer protection to SARS-CoV-2 infection by mediating phagocytosis.

Keywords: antibodies, SARS – CoV – 2, antibody function, antibody binding, spike (S) protein, phagocytosis, *in vivo* model

OPEN ACCESS

Edited by:
Penghua Wang, University of Connecticut Health Center, United States

Reviewed by:
Zhanbo Zhu, Heilongjiang Bayi Agricultural University, China
Jianfeng Dai, Soochow University, China

****Correspondence:***
Pontus Nordenfelt
pontus.nordenfelt@med.lu.se
Wael Bahnan
wael.bahnan@med.lu.se

Specialty section:
This article was submitted to Viral Immunology, a section of the journal Frontiers in Immunology

Received: *04 November 2021*
Accepted: *21 December 2021*
Published: *14 January 2022*

Citation:
Bahnan W, Wrighton S, Sundwall M, Bläckberg A, Larsson O, Höglund U, Khakzad H, Godzwon M, Walle M, Elder E, Strand AS, Happonen L, André O, Ahnlide JK, Hellmark T, Wendel-Hansen V, Wallin RPA, Malmstöm J, Malmström L, Ohlin M, Rasmussen M and Nordenfelt P (2022) Spike-Dependent Opsonization Indicates Both Dose-Dependent Inhibition of Phagocytosis and That Non-Neutralizing Antibodies Can Confer Protection to SARS-CoV-2. Front. Immunol. 12:808932. doi: 10.3389/fimmu.2021.808932

INTRODUCTION

COVID19, caused by the SARS-CoV-2 virus, has since the end of 2019 resulted in millions of deaths and serious societal health effects. Treatment of patients with convalescent plasma or monoclonal antibodies was attempted early on during the pandemic, inspired by previous partial successes with Respiratory Syncytial Virus (1) and Ebola (2). Two monoclonal antibody cocktails targeting the SARS-CoV-2 Spike protein (casirivimab and imdevimab) (3) and (bamlanivimab and etesevimab) (4, 5) were given emergency use authorization by the FDA after positive phase III clinical trial data. Trials showed that antibody cocktails reduced symptoms, hospitalization, and mortality associated with COVID19 for early-stage infections. However, studies regarding their use for treating severe COVID19 showed no clinical benefit (6).

The therapeutic antibodies described previously neutralize the interaction between the Spike protein and the ACE2 receptor, thereby hindering viral entry into host cells. Considerable efforts have been made to generate neutralizing anti-Spike antibodies (7–10). Neutralizing antibodies, however, constitute only a fraction of the antibody repertoire generated by B cells against the Spike protein during COVID19 infection (11). The opsonic capability has not been a focal point in the characterization of neutralizing antibodies. Non-neutralizing antibodies, comprising the majority of the humoral immune response to a pathogen, have other immunological functions such as complement-dependent immune activation and viral phagocytosis [reviewed by Forthal (12)]. Phagocytosis plays a substantial role in the anti-viral immune response (13). Through virion or cellular phagocytosis, phagocytic cells help reduce the viral load by eliminating infection sources. In this context, we were interested in whether or not Spike antibodies might mediate phagocytosis as has been previously seen with influenza (13–15).

However, in other viral infections (such as Dengue, SARS-CoV-2, Respiratory Syncytial Virus, and others), insufficient levels of neutralizing antibodies allow non-neutralizing antibodies to mediate the entry of virions into host immune cells (16). This infection of immune cells *via* FcγR leads to Antibody-Dependent-Enhancement (ADE), exacerbating the infection and worsening patient outcomes (17). So far, studies on COVID19 vaccines and monoclonal antibodies utilized in COVID19 therapy have seen no evidence of ADE (16–21). This clinical absence of ADE remains true even when some studies report that patient sera with high titers of neutralizing antibodies could induce Spike-bead phagocytosis or FcγR-activation (ADCP) (22–24).

Our work shows evidence that convalescent patient plasma and monoclonal anti-Spike antibodies induce phagocytosis but with diminishing returns when the antibody concentrations become high. We also demonstrate that the activation and inhibition of phagocytosis are independent of neutralization potential. Finally, we present data from an experimental animal infection model showing that non-neutralizing antibodies can protect animals from SARS-CoV-2 infection. The results in this study shed light on the importance of non-neutralizing antibodies in mediating phagocytosis and how their presence translates into protection after experimental infection.

RESULTS

Convalescent Patient Plasma Reduces Spike-Monocyte Interaction

Blood plasma was obtained from 20 COVID19 convalescent patients (**Supplementary Table 1**). We used biotinylated Spike protein conjugated to streptavidin fluorescent microspheres (1 μm beads) as a model for Spike-monocyte interactions. The beads were used as bait for THP-1 monocytes. To opsonize the beads, we incubated them with the patient plasma at different dilution levels. We chose the 0.01-1% concentrations to mimic IgG levels in the mucosal niche or tissues, which would be the first place of encounter with the SARS-CoV-2 virus. The highest level of association between plasma-opsonized Spike-beads and cells was at the intermediate plasma dilution (0.1%), while the higher and lower concentrations of plasma (1 and 0.01%, respectively) showed reduced association (**Figure 1A**). In fact, the only consistent effect we saw across our patient plasma samples was a reduction in Spike-particle association with THP-1 cells at the highest plasma concentration. This phenomenon was seen in 18 out of 20 patient samples. Two patient samples (patients 8 and 18) showed no or low opsonic ability. The reduction in Spike-THP-1 cell association under high plasma concentrations was independent of patient sex, age, or disease severity (**Supplementary Table 1**).

As our results were unexpected, we checked whether the reduction in particle-to-cell association seen at higher plasma concentrations (1%) was due to a loss of Spike or antibody binding. For that purpose, we methanol-fixed the phagocytosis samples (cells and beads) from the experiment shown previously (**Figure 1A**). The samples were then stained with a fluorescently conjugated (FITC) secondary antibody (Fab anti-human Fab), which would react with the plasma anti-Spike antibodies which had bound to Spike on the beads. Unsurprisingly, increased plasma concentrations led to increased binding of Spike-specific antibodies to the Spike-beads (**Figure 1B**). In contrast, patients 8 and 18 showed no or very low binding of antibodies to Spike-beads, correlating with overall reduced opsonization (**Figure 1A**). Our results show that when assayed at higher concentrations, patient plasma is not permissive to THP-1 cell-Spike interactions, despite having antibodies that readily bind Spike protein.

Generation of Spike-Reactive Human Monoclonal Antibodies

Considering our previous data showing that high concentrations of COVID19 convalescent plasma reduced Spike-THP-1 cell interactions compared to low concentrations, we decided to identify the role monoclonal antibodies play in Spike-THP-1 cell interactions. We isolated Spike-reactive B cells from convalescent COVID19 patients and performed single-cell

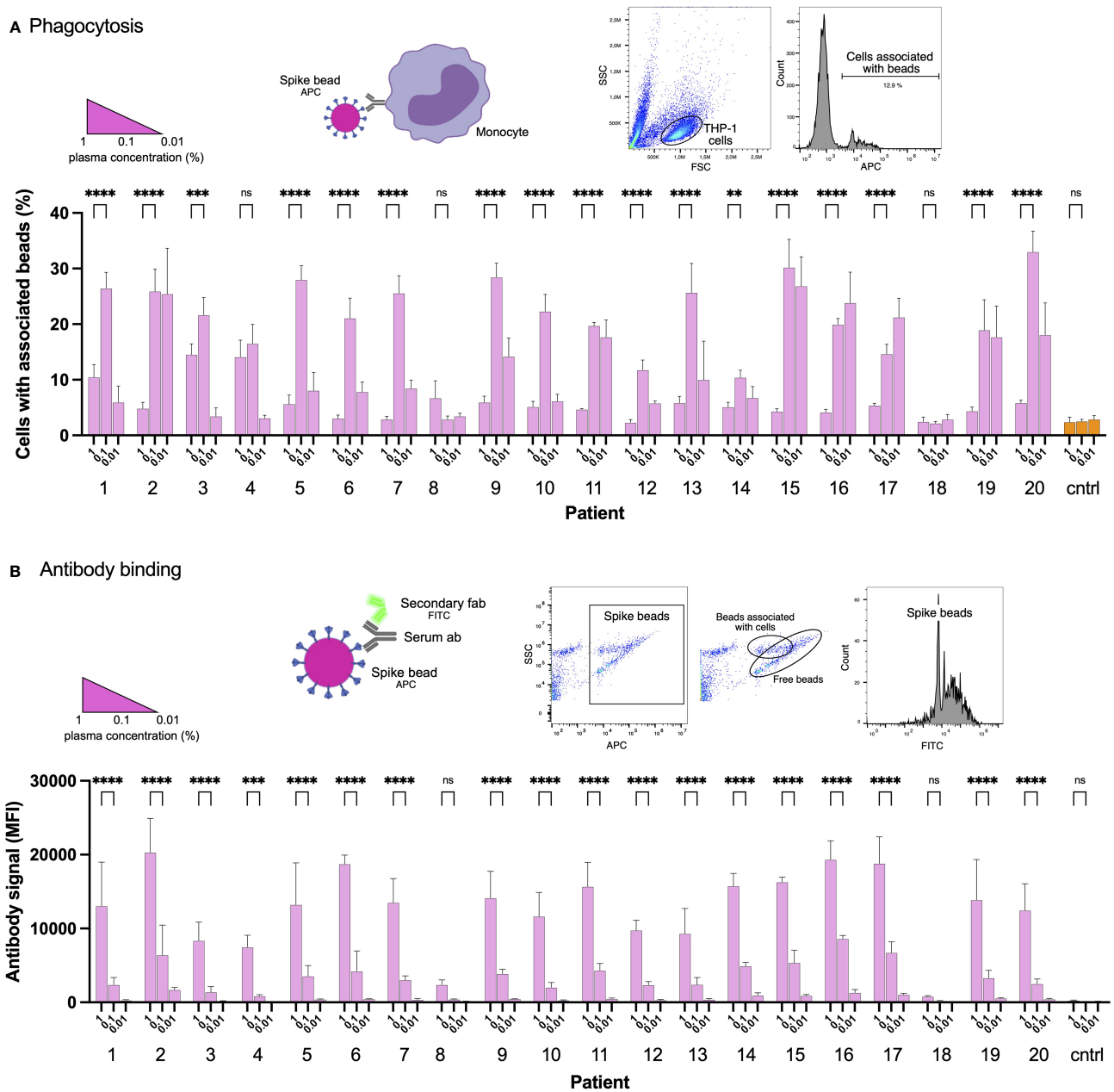

FIGURE 1 | Convalescent patient plasma reduces Spike-monocyte interaction. **(A)** Biotinylated Spike protein was conjugated to fluorescent (APC) streptavidin microspheres and was opsonized with three convalescent patient plasma concentrations (1%, 0.1%, and 0.01%). The beads were then mixed with THP-1 cells at a ratio of 2:1, and the association was measured using flow cytometry. Cells that had signal in the APC channel were considered positive. The gating strategy is shown in the top right. **(B)** The same samples of THP-1 cells and beads from **(A)** were fixed with methanol and stained with a fluorescent (FITC) Fab anti-human Fab secondary antibody. The samples were analyzed for human antibody (opsonin) binding to the Spike-beads using flow cytometry. The gating strategy is shown in the top right. The data presented are from three independent experiments. Error bars represent the SD. Statistical significance was assessed using two-way ANOVA with Dunnett's multiple comparison correction. ** denotes for $p \leq 0.01$, *** for $p \leq 0.001$ and **** for $p \leq 0.0001$. ns, not significant. Created with BioRender.com.

sequencing (**Figure 2A**). We chose 96 antibodies for production that were equidistantly spaced on the genetic clustering tree (**Supplementary Figure 1A**). The antibodies were expressed in HEK293 cells. ELISA-based screening of the antibody-containing supernatants allowed us to identify ten Spike-reactive antibodies (**Figure 2B**, **Supplementary Figures 1B, C**), which belonged to different IgG germlines (**Supplementary Figure 1D**). The Spike-reactive antibodies were then assayed for reactivity against Spike-beads using flow cytometry, where we observed that nine antibodies were reactive to the Spike-beads (**Figure 2C**). Ab11, 57, 59, 66, 77, 81, 94, and 95 showed clear reactivity (>40% positive beads) when assayed with Spike-beads

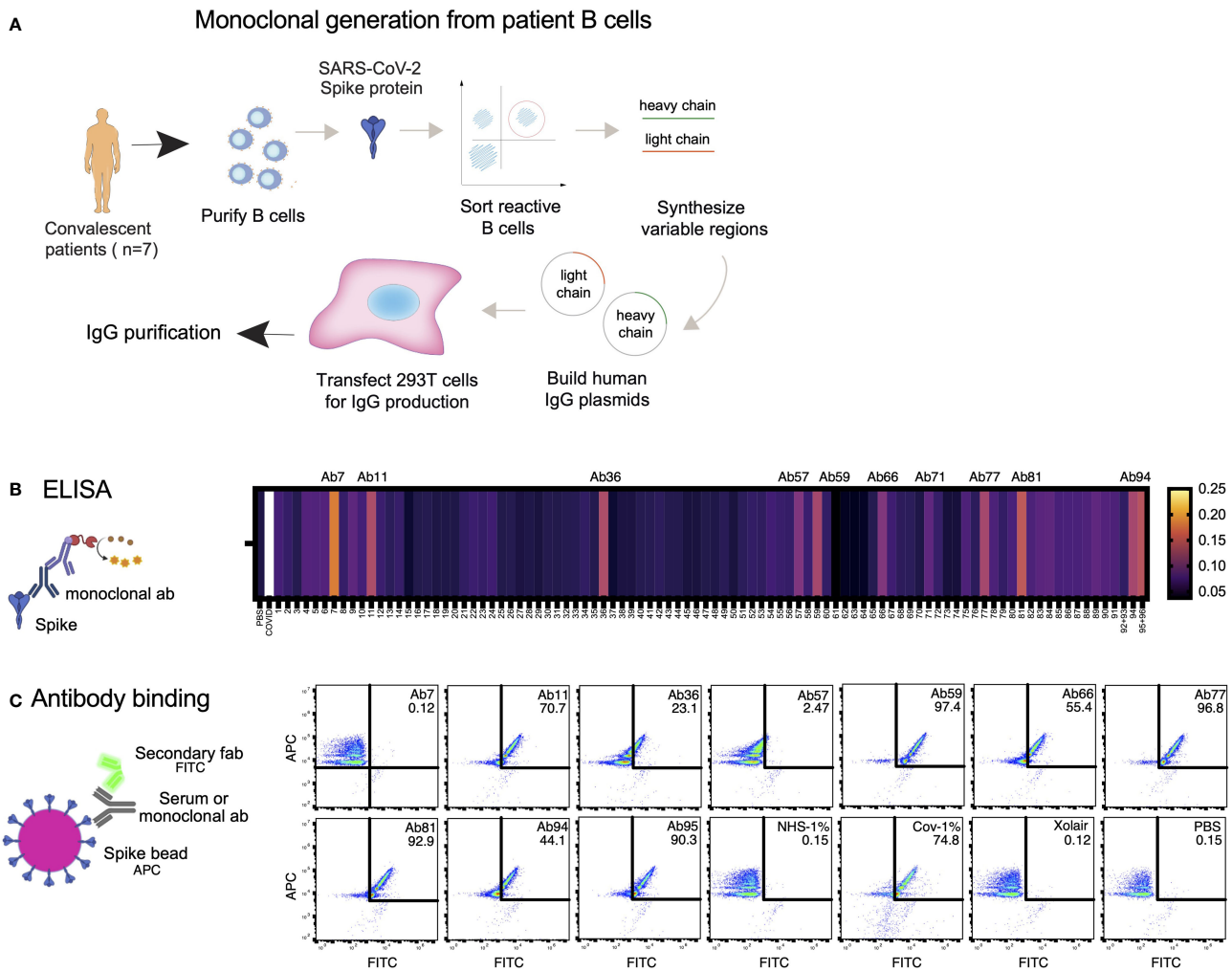

FIGURE 2 | Generation of Spike-reactive human monoclonal antibodies. **(A)** Human monoclonal antibodies were generated from convalescent donor B cells through single-cell sequencing technology. 96 antibodies derived from Spike-reactive human B cells were produced in HEK293F cells. **(B)** Cell culture supernatants containing the antibodies were assayed by ELISA for reactivity against immobilized Spike protein. Serum from a COVID19 patient was used as a positive control (external patient, not from the 20-patient cohort used in **Figure 1**). The data represent three replicate ELISAs where reproducibly reactive antibodies are indicated with their names above the heatmap. **(C)** Antibodies which were Spike-reactive in **(B)** were assayed for reactivity to Spike immobilized on beads. Fluorescent (APC) Streptavidin beads coated with biotinylated Spike protein were incubated with HEK293F-produced antibodies at a concentration of 1 μg/ml. The beads were then stained with a fluorescent (FITC) secondary anti-Fab antibody. The beads were analyzed by flow cytometry. Antibodies that shifted the beads into the FITC-positive gate were deemed reactive. Created with BioRender.com.

at a concentration of 1 μg/ml. Ab59 demonstrated strongest binding, as could be seen through the relative increase in bead staining. Xolair (used at 10 μg/ml) and normal (pre-COVID19) plasma served as negative controls, whereas COVID19 plasma from a convalescent patient was our positive control.

Epitope Mapping and Structural Mass Spectrometry Identify Antibody Binding Sites

To identify antibody binding sites, we first used ELISA to study Spike domain interactions with RBD, RBD with L452R and T478K mutations (delta), and NTD from Spike (**Figure 3A**). We could detect binding to seven antibodies, with high integrated signal (0.2-30 nM titration curves) for Ab59, Ab66, Ab81, and Ab94. Ab66 showed stronger interaction with delta RBD, and Ab 81 showed a lower signal. Ab94 only bound the NTD of Spike. We also performed relative antibody epitope mapping using the single-chain antibody fragments (scFv) isolated from an extensive combinatorial library. scFv mapping revealed that the Ab59 epitope overlaps with those of two scFv (A03_D02 and E01_C09, **Figure 3B**) that interfere in the binding of Spike to ACE2.

Next, we used TX-MS (25) to determine the binding interface between the SARS-CoV-2 specific antibodies and the RBD domain of the Spike protein. In short, we cross-linked the ten antibodies separately to the RBD domain, followed by mass

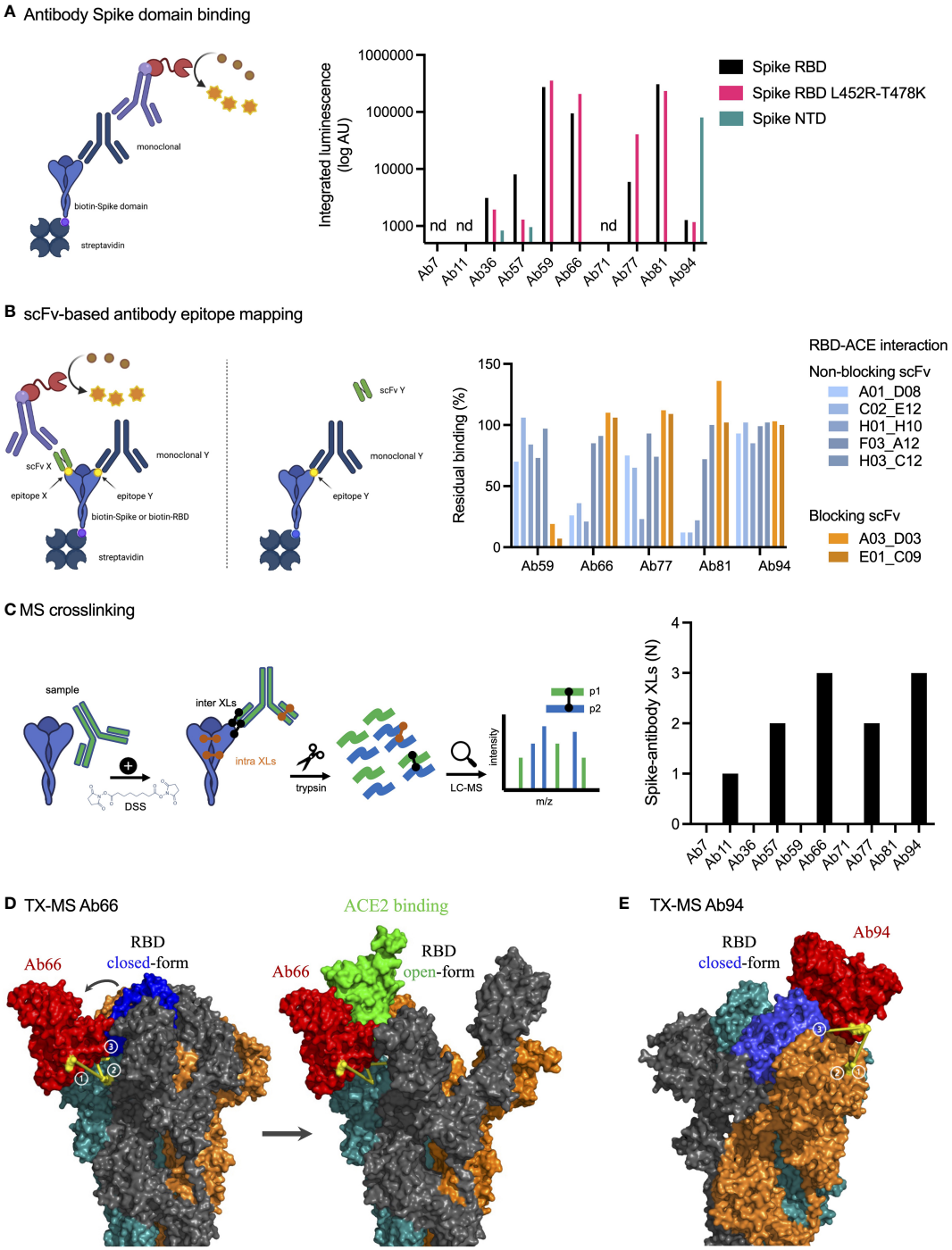

FIGURE 3 | Epitope mapping and structural mass spectrometry identify antibody binding sites. **(A)** Antibody binding to Spike domains was analyzed using ELISA as shown with HRP signal as readout. Antibodies were titrated at 0.2-30 nM, and the integrated signal was calculated. The relative binding to each Spike domain is shown. nd, not determined. **(B)** Epitope mapping was performed using scFvs targeting RBD epitopes as shown. Antibody blocking of scFv binding was measured using anti-FLAG HRP signal. Representative of two independent experiments. **(C)** Spike protein was mixed with anti-spike antibodies and the complex was cross-linked with DSS, allowing for inter and intra cross-links. After trypsinization, mass spectrometric analysis was performed. The table to the right displays the number of inter-protein cross-links detected between Spike and its corresponding antibody. **(D, E)** The binding sites for Ab66 and Ab94 were determined by TX-MS using the cross-links from c, and the data was modelled using Rosetta. Models for Ab66 **(D)** binding the Spike protein in both its open and closed conformations as well Ab94 **(E)** are shown. The cross links between Spike and antibodies are shown in yellow. Created with BioRender.com.

spectrometry analysis and structural modeling (26). This resulted in the identification of 11 confident inter-protein XLs between the RBD domain and five of the antibodies (Ab11, Ab57, Ab66, Ab77, and Ab94) in addition to 30 intra RBD XLs (**Figure 3C**, **Supplementary Figure 2**). The results show that the five antibodies can bind to the Spike protein, but they do not appear to compete with the binding site of human ACE2 directly. The interaction between Ab66 and Spike protein show binding to the open-state but not the closed-state (**Figure 3D**). Further, the structural model indicates no competition between Ab66 and human ACE2, which is in accordance with previously published work, as only the open-state is responsible for binding human ACE2 (27). In contrast, Ab94 appears to preferably bind the closed state (**Figure 3E**). The top and frontal views (with a 180°C rotation) shows the interaction cross-linked sites (**Supplementary Figure 3**). It is important to note that Ab94, after repeated modelling efforts seems to only bind to the closed conformation of Spike. The binding however, does not seem to lock the Spike protein into a closed conformation. Consistent with our other data, even though Ab94 might be able to bind to the RBD, it is non-neutralizing. The combined data from our epitope analysis approaches indicate that Ab11, 57, 59, 66, 77, 81 bind Spike RBD, that Ab94 could interact with both RBD and NTD, and that Ab59 could be a neutralizing antibody, whereas the others are likely non-neutralizing.

Neutralization Assays Identify One Monoclonal Which Blocks the ACE2-Spike Protein Interaction

Typically, the most important biological function attributed to antibodies in the context of a viral infection is neutralization. We assayed our Spike-reactive antibodies for Spike-neutralization using three different approaches: Spike RBD-ACE2 protein binding (**Figure 4A**), Spike particle-ACE2 cell interaction (**Figure 4B**), and SARS-CoV-2 pseudovirus infection neutralization (**Figure 4C**). The SPR-based Spike RBD-ACE2 binding data showed that Ab36 and Ab94 did not appear to interfere with RBD-ACE2 binding and that Ab57 reduced binding slightly. Ab59 completely blocked RBD-ACE binding, whereas Ab66, Ab77, and Ab81 seemed to bind well without interfering with the interaction. Next, we utilized ACE2-expressing HEK293 cells as a surrogate for lung epithelial cells. We measured the ability of Spike-beads to bind HEK293-ACE2+ cells after being opsonized with antibody supernatants. We assayed all 96 of our antibody-containing supernatants for Spike-particle neutralization. Only Ab59 showed a robust and reproducible reduction in Spike-particle binding to HEK293-$ACE2^+$ cells compared to COVID19 patient plasma (**Figure 4B**). As expected, pre-COVID19 plasma showed no inhibition of Spike-ACE2 interactions. Representative images of our experiments which were used for analysis, are shown in **Supplementary Figure 4**. We utilized a pseudovirus binding assay to verify the ability of our antibodies to neutralize SARS-CoV-2. Consistent with our previous experiments with RBD and Spike-beads (**Figures 4A, B**), we saw that Ab59 was the best (EC_{50}: 19 ng/ml) among our antibodies in neutralizing SARS-CoV-2 pseudovirus infection (**Figure 4C**). Taken together, our results indicate that of our 96 antibodies, only Ab59 is a potent neutralizer of the Spike-ACE2 interaction.

High Levels of Human Monoclonal Antibodies Reduce Spike-Monocyte Interaction

Antibodies are the primary mediators of FcγR-dependent cellular interactions. Given our previous data that high concentrations of convalescent patient plasma can reduce Spike-bead association with THP-1 monocytes (**Figure 1**), we tested whether this reduction was antibody-driven. We chose antibody concentrations that were in a similar range (100 - 0.01 μg/ml) than what is expected at the plasma concentrations used (1% - 0.1%) (**Figure 1**) and included a higher plasma concentration for comparison (10%). Interestingly, as with patient blood plasma, serially diluted Spike-specific monoclonal antibodies showed the same inhibition trend of bead-to-cell association at the higher concentrations (**Figure 5A**). This association was confirmed to reflect the internalization of particles (i.e., phagocytosis) by using a pH-dependent fluorescent dye (**Supplementary Figure 5**). Also, as with plasma, this inhibition was correlated with increased antibody binding to Spike (**Figure 5B**). It is important to note here that among the antibodies, Ab94 seemed to have almost half the binding efficiency of Ab59, an attribute that will be central for other experiments. The neutralizing antibody, Ab59, showed the same trend as the other non-neutralizing antibodies. We have thus identified that Spike-specific monoclonal antibodies isolated from COVID19 patients modulate the Spike-THP-1 cell interactions in a dose-dependent manner. This phenomenon is independent of the Spike-ACE2 neutralization capability of the monoclonal antibodies.

Non-Neutralizing Antibodies Can Protect Against SARS-CoV-2 Infection

We have shown that among our antibodies, Ab59 is neutralizing while the other monoclonals are not. We have also demonstrated that our Spike-bead reactive antibodies are efficient at mediating Spike-mediated phagocytosis but reach a threshold after which there is a reduction in interaction efficacy. To test the antibodies' function in a physiologically relevant context, we assessed different doses of neutralizing and non-neutralizing antibodies in an experimental animal infection model (**Figure 6A**). We infected humanized ACE2 mice intranasally with 10^5 PFU (SARS-CoV-2; Wuhan strain from Swedish isolate). As a treatment model, we administered our monoclonal antibodies intraperitoneally a day after infection. Based on previous experience, we used the pseudovirus neutralization data (**Figure 4C**) to calculate a protective dose in a prophylactic model (100 μg for Ab59). To test the effects of high dose administration, Ab59 was given at five times the calculated protective dose. For Ab94, we chose the same dose that would be considered protective for Ab59 (100 μg), as well as a higher dose (250 μg), which would be equivalent to the protective Ab59 dose based on the lower affinity of Ab94 (~2.5 times lower, **Figures 2C** and **5B**). Interestingly, the best-protected animal

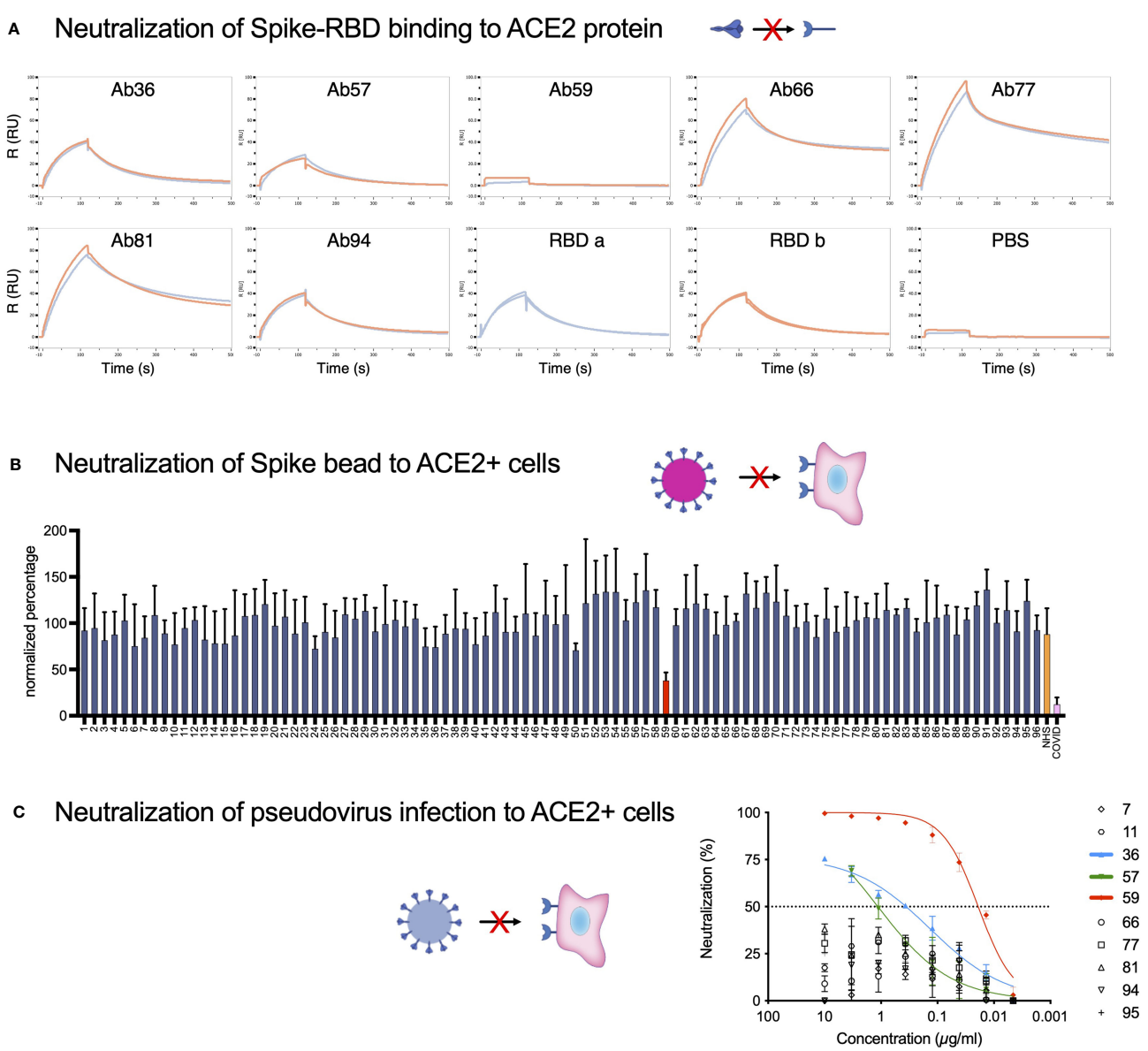

FIGURE 4 | Neutralization assays identify one monoclonal as blocking the ACE2-Spike protein interaction. **(A)** SPR analysis of the binding of monoclonal antibodies to the RBD domain of the Spike protein. PBS served as a negative control, and the intact RBD was our positive control for ACE2 binding. **(B)** The 96 antibodies which we produced were assayed for neutralization potential in a Spike-bead-based neutralization assay. Spike-beads [such as the ones used in **(B)**] were opsonized with the antibodies in 96 well plates. The beads were then centrifuged, reconstituted in fresh media, and added to HEK293-ACE2 cells at a ratio of 20 beads per cell and imaged with automated microscopy. The data is from 4 pooled experiments and is presented as bead association normalized percentage. Error bars indicate the SEM for the replicate experiments. **(C)** The 10 Spike-ELISA reactive antibodies were assayed for pseudovirus neutralization. A firefly luciferase encoding pseudotype lentivirus was used to infect HEK239-ACE2 cells. Antibody serial dilutions were used to block the viral entry into the HEK293-ACE2 cells. Nonlinear regression lines were fitted for the three antibodies that showed a higher than 50% reduction of infectivity. Those antibodies were highlighted in green (Ab57), blue (Ab36), and red (Ab59). Created with BioRender.com.

group (lower weight loss) was the one where the animals were treated with the equivalent to a protective dose of our non-neutralizing yet opsonic Ab94 (**Figure 6B**). Unexpectedly, the animals treated with a low dose of Ab59 fared better than the ones with the high dose, which had the worst outcome (more pronounced weight loss) among the treated groups. The low dose of Ab94 offered negligible improvement compared to untreated animals (**Figure 6B**). The bronchoalveolar lavage (BAL) fluids from the infected mice were harvested and the viral load in the samples were assessed. The cycle threshold (Ct) values in the BAL fluids reflected what the weight loss data showed. The animals which were untreated, or treated with the excessive dose of Ab59 (500 μg) as well as the uncorrected dose for Ab94 (100 μg) faired the worst. Those animals

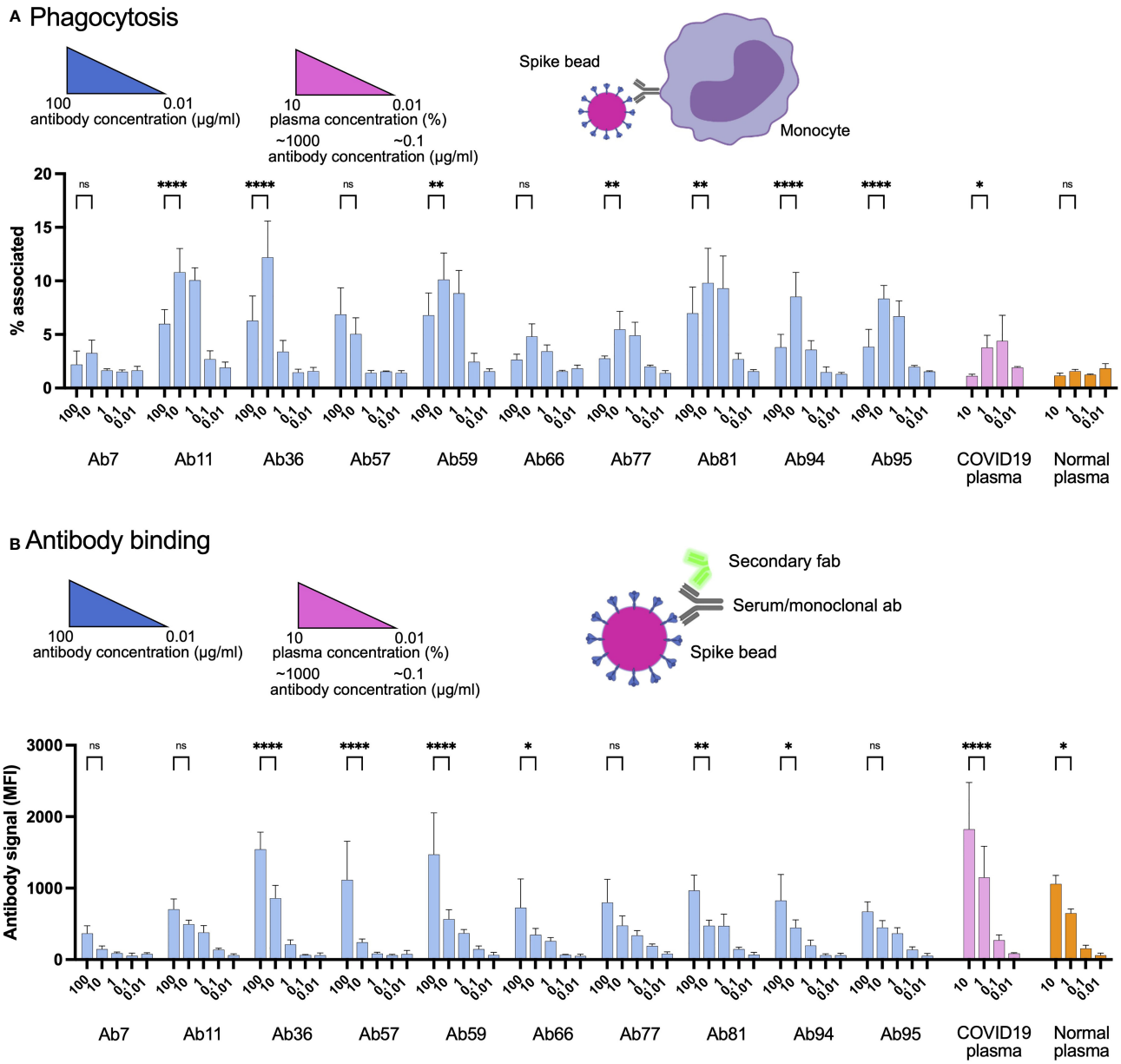

FIGURE 5 | High levels of human monoclonal antibodies reduce Spike-monocyte interaction. **(A)** Spike-reactive monoclonal antibodies at concentrations of 100, 10, 1, 0.1, and 0.01 μg/ml were used to opsonize Spike-beads. Plasma was used at serial dilutions of 10%. The beads were then incubated with THP-1 cells at a ratio of 2 beads/cell. The cells were then analyzed by flow cytometry for association with the fluorescent Spike-beads. The data show the % of bead-associated cells and is pooled from three independent experiments. Error bars represent the SD. **(B)** The cells used in **(A)** were fixed with methanol and restained with a fluorescent (FITC) Fab anti-human secondary antibody. The samples were assessed for human antibody (opsonin) binding to the Spike-beads using flow cytometry. The data are from three independent experiments. Error bars represent the SD. * denotes $p \leq 0.05$, ** for $p \leq 0.01$, and **** for $p \leq 0.0001$. ns, not significant. Created with BioRender.com.

showed the lowest Ct values for SARS-CoV-2 in the BAL fluids, corresponding to the highest titers (**Figure 6C**). Contrastingly, the animals treated with the appropriate doses of Ab94 or Ab59 faired better and showed higher Ct values, corresponding to lower viral loads. The animal data indicate that too high doses of neutralizing antibodies are not beneficial in a treatment model and that non-neutralizing antibodies can offer protection to SARS-CoV-2 infection.

DISCUSSION

In this report, we present data on antibody modulation of Spike-monocyte interactions. A previously published report showed Spike-bead phagocytosis after opsonization with 50% heat-inactivated serum and a 16 hours incubation of beads with THP-1 cells (22). We believe that the data from our experiments are more representative of the first few events after

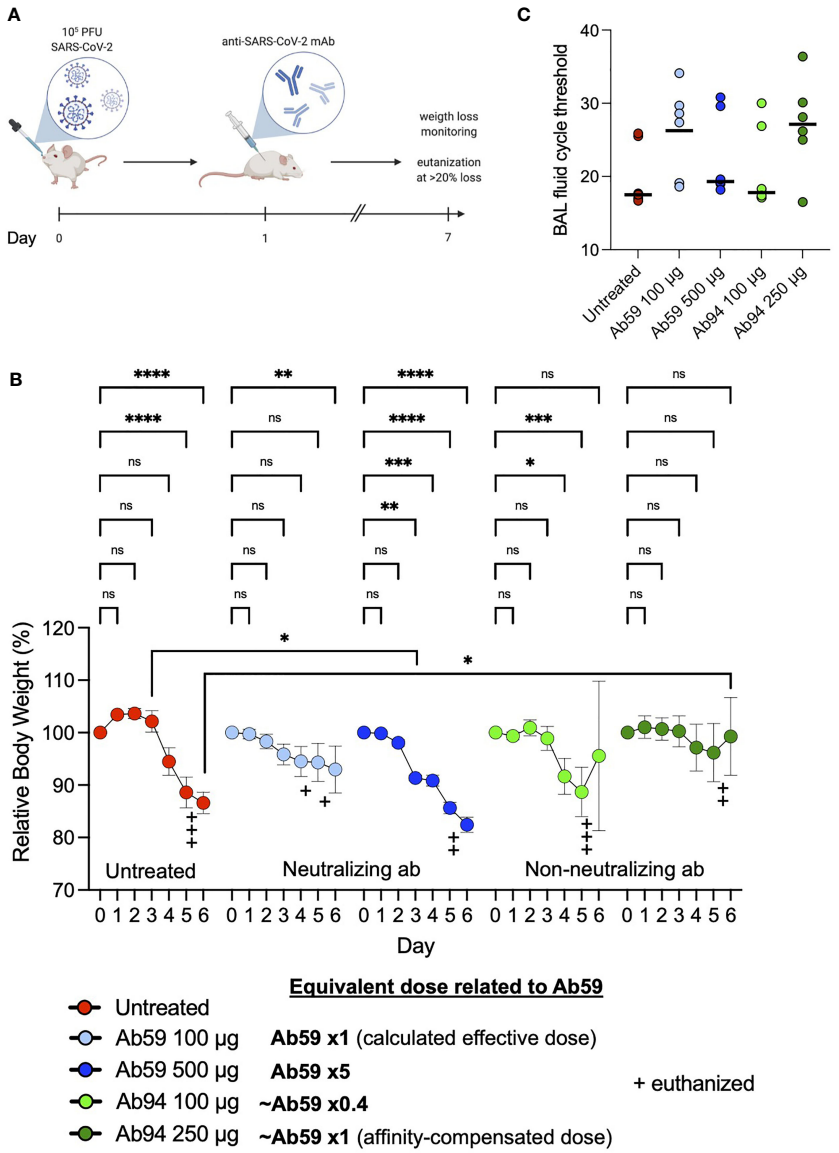

FIGURE 6 | Non-neutralizing antibodies can protect against SARS-CoV-2 infection. **(A)** Humanized ACE2 mice were infected intranasally with SARS-CoV-2 (Wuhan strain). One day after infection, the animals (N=7 per group) were treated intraperitoneally with antibodies. Relative body weights were recorded and tabulated. **(B)** Body weights relative to each individual mouse over the time course of viral infection and treatment. **(C)** Quantitative PCR analysis was performed on the BAL fluids obtained from the infected mice at the experiment termination. The cycle threshold (Ct) values were detected and graphed. Error bars represent the SD. Statistical significance was assessed using two-way ANOVA with Dunnett's multiple comparison correction both within each treatment group and across the groups for each day. * denotes $p \leq 0.05$, ** for $p \leq 0.01$, *** for $p \leq 0.001$ and **** for $p \leq 0.0001$. ns, not significant. Created with BioRender.com.

Spike-monocyte contact. Phagocytosis of small particles such as virions is a process that takes minutes, not hours (28). That is why we use shorter incubation times (30 min) and perform dose-response analysis across varying plasma concentrations. The dose-response analysis we performed exposed an antibody-mediated modulation of the Spike-monocyte interactions. It is important to elaborate on the concentrations we utilized, be it for plasma or monoclonal antibodies. For plasma, as tissues have a lower concentration of plasma proteins than whole blood, we used 1% as the highest concentration. As for the monoclonal antibody concentrations, we used 100 µg/ml as the highest concentration because it is roughly 1% of the antibody concentration present in plasma (10 mg/ml). Even though most of the experiments in this study are performed *in vitro*, we believe the effects we observe on phagocytosis efficiency could also be relevant *in vivo*, as the modulation effects occur already at relatively low antibody concentrations and would thus cover many physiological niches and scenarios.

The closest known phenomenon to the Spike-dependent phagocytosis modulation that we describe is the "Hook" or "prozone" effect. The prozone effect is a drop in antibody protection efficacy seen at very high concentrations. The prozone effect has been recognized in experiments with pneumococci, *Cryptococcus neoformans*, varicella and malaria (29–32). The mechanism is not known, but it has not been attributed to a reduction in phagocytosis per se (30) but rather to the creation of a proteinaceous coat on the organism surface, shielding them from immune recognition. Upon closer examination, we did notice a mild phagocytic differential when high antibody concentration was used in the published experiments (30). It is possible that other pathogens have evolved similar ability, and potentially through different mechanisms. That an increased binding of antibodies to a prey results in reduced or blocked phagocytosis is in contrast to the typically expected saturation at high opsonization levels, as what we and others have observed with the same type of experiment (same beads and cells) at even higher antibody concentrations (33). It cannot be explained by specific monoclonal interactions, as it is seen across diverse monoclonals as well as in convalescent polyclonal samples. It is important to note that we do not observe a Hook effect in any experiments (binding, neutralization etc.), except for phagocytosis. Also, in our experiments, the observed block in phagocytosis is only related to Spike protein and Spike-specific antibodies.

A combination of known mechanisms could potentially explain how SARS-CoV-2 could avoid phagocytosis using Spike protein. Bivalent trans-binding of antibodies is known to promote virion phagocytosis (34), where antigens are cross-linked depending on their density at the surface. Spike protein density on SARS-CoV-2 varies (35), and is increased with the D614G mutation (36). An increase in Spike antibody levels would lead to a competition of epitope binding, ultimately favoring the switch from bivalent trans-binding to monovalent binding, potentially leading to a reduction in phagocytosis. A synergistic mechanism could further aid SARS-CoV-2. Antigen height (especially below ~10 nm) is important for efficient phagocytosis (37), and most likely, a consistent antigen height is beneficial as well. Besides altering its density, SARS-CoV-2 also appears to be able to dramatically change the Spike protein conformation, where some proteins stand up vertically from the surface, and others are tilted down horizontally (35). At high anti-Spike levels, this would present an approaching phagocyte with a monovalently opsonized, irregular surface with variable antigen height (~15-25 nm), making the interaction difficult. In contrast, at low anti-Spike levels, the antibodies would be able to clasp Spike proteins in a bivalent, upright manner, presenting the phagocyte with a coherently opsonized surface at an effectively low antigen height. Careful mechanistic studies are needed to test this hypothesis.

How does the concentration-dependent phagocytosis modulation translate into an infection model? We utilized our anti-Spike antibodies as a therapeutic regimen in our animal infection. This creates a scenario where the mouse is already fighting the infection before therapy gets administered. The requirements, therefore, on therapeutic antibodies are higher than on prophylactic ones. When comparing the 100-μg dose of Ab59 and Ab94 (equivalent to 2.5 times lower binding affinity), we noticed that Ab59 showed better protection than the latter antibody. This could be attributed to either the neutralizing activity of Ab59, which Ab94 lacks, or the lower effective dose, given the lower Spike binding affinity of Ab94. Consistent with our data on phagocytosis (**Figure 5**), animals treated with the high dose of Ab59 (500 μg) fared worse than the animals that got the 100-μg dose. Interestingly, the animals that got the affinity-corrected dose for Ab94 (250 μg, equivalent to 100 μg of Ab59 in terms of binding affinity) fared the best in our cohort. The animal infection data on Ab94 protecting the mice is, most importantly, congruent with the phagocytosis data, indicating a role in infection management for non-neutralizing antibodies. In our double-blinded animal experiments, the weight loss kinetics seen is similar to other results (38), where they also analyzed viral load and lung pathology. We used the clinical standard assay for viral load assessment. Our cycle threshold values also showed that BAL viral load followed weight loss results in those animals which had better outcomes. This correlation shows that weight loss can be used to monitor the animal response to SARS-CoV-2 infection. In future studies, it remains to be established how infections would proceed in animals treated with an excessive dose of non-neutralizing antibodies. Our animal experiments show that monoclonal antibodies could be viable therapeutics even if they lack neutralizing potential.

It is widely accepted that a strong positive correlation exists between COVID19 disease severity and antibody titers (39–42). High antibody titers are generally associated with severe disease and hospitalization. The high titers are thought to be a consequence of the severe infection. Our results pose a new question: could the high anti-Spike titers seen in hospitalized patients instead (at least partially) contribute to the immune dysregulation and worsening patient outcomes? These questions are relevant in the light of the FDA's recommendation not to use monoclonal antibodies in hospitalized COVID19 patients (and who are seropositive) due to possible worsening of symptoms (3, 5). At the same time, it is important to note that convalescent plasma treatment for COVID19 was shown to be neither beneficial nor detrimental (43).

The dose variation data from Ab59-treated mice reflect the concentration-dependent modulation of Spike-bead phagocytosis. These results may explain the clinical findings seen in antibody therapy trials in the sense that having a low or excessive dosage of antibodies offers no clinical benefit (44). Recently, it has been alluded to that the differential effects seen across antibody treatment dosage in the Eli Lilly LY-CoV555 trial (44) were due to prozone-like effects (45). The authors of the clinical trial seem to disagree with the conclusions of the correspondence [please see the response from the authors in the same reference (45)]. Our results show a similar dose-dependent outcome differential as seen in the Ly-CoV555 clinical study, and suggest that a prozone-like effect could be relevant during monoclonal antibody treatment of SARS-CoV-2. Potentially, the mechanism could then be related to an antibody:

Spike-driven reduction in phagocytosis, but remains to be explained.

Coronaviruses are mutation prone (as has been the case with SARS-CoV-2), and our data indicate that non-neutralizing antibodies confer immune function *via* phagocytosis. This opsonic capability could potentially explain why anti-Spike antibodies generated even by older-generation vaccines or natural immunity can still offer protection against mutated variants (such as Beta and Delta) (46, 47). Phagocytosis, however, is not the only immune function mediated by antibodies in viral infections. Virion, as well as cellular phagocytosis and antibody-mediated killing, serve crucial roles in infection control. All those functions are independent of neutralization and can still be performed by antibodies against domains outside the RBD of Spike.

Overall, the results presented in this study highlight a concentration-dependent modulation of phagocytosis by anti-Spike antibodies. This modulation phenomenon might help explain the unclear clinical benefit seen with monoclonal antibody treatment for COVID19. This modulation is seen in patient material and translates well to animal infection experiments. The biophysical mechanism underlying the antibody-mediated phagocytic modulation is an exciting topic to pursue, as are the bridging immune steps between phagocytosis and animal protection.

MATERIALS AND METHODS

Cell Culture, Transfection, and Protein Production

THP-1 cells were maintained in RPMI medium supplemented with 10mM L-Glutamine and 10% fetal bovine serum (FBS). The cells were split kept at a density between $5x10^5$ and 10^6 cells/ml. The cells were split when they reached a density of 10^6 cells/ml, down to $5x10^5$ cells/ml. HEK293 cells (Sigma Aldrich 12022001-1VL) were maintained in DMEM supplemented with L-glutamine and 10% FBS. The cells were kept at 90% confluence and were not allowed to grow past passage 20. The plasmids for the 96 antibodies were aliquoted into 96 well plates. The cells to be transfected were grown in 24-well plates, with 500 µl of tissue culture medium. The plasmids were transfected into adherent HEK293 cells using the PEI method (48). The day after transfection the cell culture supernatant media was replaced with serum-free OptiMEM medium for 2 extra days. The supernatants containing the antibodies were distributed also in 96 well plates and stored for maximum one week for experimental use. HEK293 cells constitutively expressing the ACE2 receptor were acquired from BEI resources (NR-52511). They were maintained in DMEM supplemented with L- glutamine and 10% FBS for a maximum of 12 passages before being discarded. Expi293F suspension cells were purchased from Gibco (ThermoFisher) and routinely cultured in 125 ml Erlenmeyer flasks (Nalgene) in 30 ml Expi293 medium (Gibco) in an Eppendorf s41i shaker incubator at 37°C, 8% CO_2, 120 rpm. Cells were passaged and split to a density of 0.5 x 10^6 cells/ml every 3 to 4 days. The day before transfection, the cells were seeded at a density of 2 x 10^6 cells/ml. The next day, cells were seeded at 7.5 x 10^7 cells in 25.5 ml Expi293 medium. The transient transfection was carried out using 100 µl of Expifectamine (Gibco) according to the manufacturer's instructions. For Spike protein production, we used 40 µg of the Spike CS/PP plasmid (generously donated by Dr. Florian Krammer's lab). For antibody production, 20 µg of plasmids for the heavy and light chain was used, respectively. For all plasmids, 16 hours after transfection, 150 µl of enhancer 1 and 1.5 ml of enhancer 2 (Expifectamine transfection kit, Gibco) were added and cells cultured for an additional 3 days. The cells were then pelleted at 400 x g, 5 min, RT and the supernatant transferred to new tubes. Magne Protein G beads (Promega) were used to purify the antibodies according to the manufacturer's instructions.

Antibody Phage Selections

SARS-CoV-2 Spike RBD-specific scFv were selected by phage display technology from a human synthetic scFv library (49), similar in design and construction to previously reported (50). Briefly, selection of specific binders was performed through a process similar to the one described in the past (50) using biotinylated proteins SARS-CoV-2 S1 protein, His, Avitag™ (ACRO Biosystems, # S1N-C82E8) and SARS-CoV-2 Spike RBD, His, Avitag™ (ACRO Biosystems, # SPD-C82E9) immobilized on paramagnetic beads (Dynabeads M-280 streptavidin; Invitrogen Dynal AS, Oslo, Norway) as target antigen. Phagemid DNA from the third and fourth rounds of phage selection was isolated (Plasmid Miniprep kit, Qiagen) and the genes encoding scFv fragments were ligated into an in-house constructed screening vector providing the secreted scFv with a triple-FLAG tag and a hexahistidine (His_6) tag at the C-terminus. The constructs were subsequently transformed into TOP10 *E. coli* and individual, soluble scFv were produced as described elsewhere (50). Binding of individual selected scFv was initially assessed by ELISA against biotinylated antigen. Seven scFvs specific for RBD isolated this way were used to map relative epitope location of human IgG. The scFvs bind four epitopes on RBD, and two of them (A03-D03 and E01-C09) also interfere with the RBD-ACE2 interaction (data not shown).

COVID19 Patient Samples and B Cell Isolation

For the spike-THP-1 association experiments, 20 patients who had mild, moderate or severe COVID19 were asked to donate blood 6 weeks after infection diagnosis. Patients were classified into mild, moderate and severe COVID19 based on supportive respiratory treatment. Patients with mild COVID19 did not require oxygen treatment. Patients with moderate COVID-19 required supplementary oxygen support wheras patients with severe covid19 required non-invasive ventilation or high-flow nasal cannula oxygen therapy. All participants gave written informed consent to participate in the study which was approved by the Swedish ethical review authority (2020/01747). Blood was drawn in citrated tubes and plasma was

stored in the -80°C. For B cell isolation and antibody discovery, patients convalescing after severe COVID19 infection donated blood 6 weeks after discharge from the hospital. Thirtyml of blood were drawn into citrated tubes and the B cells were directly isolated using Rosettesep B (according to the manufacturer's instructions) and frozen at -150°C. B cells were harvested from 7 donors and were kept frozen until the sorting day when 10^7 cells were thawed, pooled and prepared for baiting which was performed in PBS +2% FBS. Spike protein (S1+S2 ECD-His Recombinant Protein) was purchased from SinoBiologicals (cat: 40589-V08B1) and was reconstituted to 1 mg/ml in PBS. Spike protein was conjugated to Alexafluor 647 microscale labeling kit (Invitrogen). The fluorescently labelled spike protein was incubated with the pooled B cells at a concentration of 0.5 µg/ml for 30 mins on ice. The cells were then washed with PBS, blocked in 2% BSA and stained with antibodies against CD19-PE (BD-555413), CD3-BV510 (BD-564713), IgG-BV421 (BD-562581) and a live/Dead Sytox stain. The cells were stained for 30 mins on ice and were later washed and prepared for sorting. Bulk cell sorting was performed using a FACSAriaFusion sorter, where the gates were set using unstained and FMO-1 controls. 7000 spike-reactive cells were sorted into RPMI + 10% FBS and were transported immediately to the RNA-sequencing facility while on ice.

10X Genomics Sequencing and Data Analysis

We performed 10X Genomics single-cell sequencing on the 7000 Spike-reactive cells (Center for Translational Genomics facility, Lund University). Cellranger suite cellranger mkfastq was used for demultiplexing and cellranger vdj for generating V(D)J sequences and annotation. Once received, we collated the V(D)J regions from our antibodies of interest using the V-Loupe software (10X Genomics software platform). 96 antibodies were chosen based on their phylogenetic distribution and the light and heavy chain variable regions were cloned into an IgG1 expression vector (Twist Biosciences). The 192 antibody plasmids (light and heavy chain constructs) were transformed into chemically competent Mix'n'go *E. coli* (Zymo research, T3002) and minipreps were prepared from the resultant colonies. Multiple sequence alignment using the ClustalW algorithm was performed on the light chain sequences and the heavy chain sequences. Single-linkage clustering was performed using the sum of the Hamming distances between the aligned light chain and the heavy chain as the similarity metric

Antibody Reactivity Screening

For ELISA, 10 µg/ml of Spike protein diluted in PBS was immobilized onto ELISA wells overnight at 4°C. The wells were washed with PBST and 100 µl of antibody supernatants were added to each well. A negative control (normal human pooled serum) and positive control (COVID patient serum) were used at 10% dilutions (in PBS). After one hour of incubation at 37°C, the wells were washed and HRP-conjugated protein G (Biorad 1706425) was added and kept for one hour at 37°C. The wells were finally washed and developed with 100 µl developing reagent (20 ml Substrate buffer NaCitrate pH 4.5 + 1 ml ABTS Peroxide substrate + 0.4 ml H2O2). OD_{450} was recorded and plotted.

For bead-based screening, fluorescent (APC) streptavidin microsphere beads (1 µm, Bangs Laboratories, Cat: CFR004) were used as Spike carriers. Spike protein was conjugated to biotin using the EZ-Link™ Micro Sulfo-NHS-LC-Biotinylation Kit (Thermofischer; Cat: 21935). The biotinylated Spike protein was attached to the streptavidin microbeads according to the bead manufacturer's instructions. For antibody reactivity testing, the Spike-beads were blocked with 5% BSA (in PBS) for 30 mins at 37°C. 150k beads were then centrifuged and incubated with 1 μ g/ml of antibody for one hour at 37°C in 96-well plates. The beads were washed with PBS and a secondary Alexa Fluor 488 conjugated Fab -Fab antibody (Jackson laboratories) was used to develop fluorescent signal. After a 30 min incubation with the secondary antibodies, the beads were further washed and fluorescence was detected using a Beckman Coulter Cytoflex flow cytometer.

Spike-THP-1 Association Assays

Spike-beads were opsonized with patient plasma or monoclonal antibodies at the specified concentrations for 30 minutes at 37°C in a 100 µl volume in 96 well plates. The beads were then centrifuged and reconstituted in 50 µl Sodium medium (5.6 mM glucose, 127 mM NaCl, 10.8 mM KCl, 2.4 mM KH_2PO_4, 1.6 mM $MgSO_4$, 10 mM HEPES, 1.8 mM $CaCl_2$; pH adjusted to 7.3 with NaOH). THP-1 cells were washed twice with PBS and reconstituted in Sodium medium. Spike beads and THP-1 cells were mixed at a ratio of 2 beads per THP-1 cell, in a final volume of 100 µl of Sodium medium. The suspension was mixed and cooled on ice for 5 minutes before incubating at 37°C in a shaking incubator for 30 minutes. The suspension was later cooled and analyzed *via* flow cytometry. Gating was first set on the cell population and the percentage of cells associated with beads (now fluorescent in the APC channel) was determined (**Figure 1A**). After cell-spike reactivity analysis was done, the cells were centrifuged and fixed with methanol (for 10 minutes at room temperature). The cells were then washed and resuspended in PBS, awaiting further flow cytometry analysis. Gates were then changed to include all the beads in the APC-fluorescent channel (**Figure 1B**, top right). For internalization analysis, Spike-beads were conjugated with pHrodo (FITC), an acid-sensitive dye that fluoresces in acidic environments. The beads were opsonized with different concentrations of antibodies and then interacted with THP-1 cells. Cells determined to be fluorescent in the APC and FITC channels by flow cytometry have had internalized as well as associated beads.

Pseudotyped Virus Neutralization Assays

Pseudotyped lentiviruses displaying the SARS-CoV-2 pandemic founder variant (Wu-Hu-1) packaging a firefly luciferase reporter gene were generated by the co-transfection of HEK293T cells using Lipofectamine 3000 (Invitrogen) per the manufacturer's protocols. Media was changed 12-16 hours after transfection, and pseudotyped viruses were harvested at 48- and 72-hours post-transfection, clarified by centrifugation, and

stored at -80°C until use. Pseudotyped viruses sufficient to generate ~50,000 relative light units (RLUs) were incubated with serial dilutions of antibodies for 60 min at 37°C in a 96-well plate, and then ~15,000 HEK293T-hACE2 cells were added to each well. For these experiments, the HEK293-ACE2 cell culture was supplemented with penicillin/streptomycin antibiotics to avoid contamination. Plates were incubated at 37°C for 48 hours, and luminescence was then measured using Bright-Glo (Promega) per the manufacturer's protocol, on a GM-2000 luminometer (Promega).

Bead-Based Neutralization Assay

HEK293-ACE2 cells were seeded at density of 35,000 cells per well in a Poly-D-Lysine coated flat bottom 96 well plate. The outer skirt wells were kept cell free and were filled with medium. The day of the experiment, Spike-beads were distributed to fresh 96 well plates, adding 700,000 beads/well. The beads were opsonized with 100 µl of antibody supernatants at 37°C for one hour. The beads were then resuspended by pipetting up and down and the bead/antibody mix was used to replace the medium on the HEK293-ACE2 cells. The cells were incubated with beads for one hour at 37°C. The cells then were washed three times with PBS and fixed with 4% paraformaldehyde at room temperature for 15 minutes. The cells were finally washed and prepared for imaging. Four images from the center of the field of each well in the 96-well plate were acquired using 10X magnification. The number of beads per field was automatically determined using the Nikon Jobs software. For each experiment, the average number of beads/quadrant per all 96 wells was calculated and used as a 100% reference. We chose to normalize our data internally this was because our hypothesis was that the majority of our antibodies would not be neutralizing. Data from four experiments were pooled and presented.

Animal Experiments

Forty-two nine-week old female K18 hACE2 (B6.Cg-Tg(K18-ACE2)2Prlmn/J) mice were inoculated intranasally with 10^5 PFU of SARS-CoV-2 (Wuhan strain, isolate SARS-CoV-2/01/human/2020/SWE, sourced from the Swedish Health Authorities). These mice are transgenic and carry the human ACE2 gene, making them permissive to SARS-CoV-2 infection (Jackson laboratories). One day after infection, the mice were split into 6 groups of 7 mice and antibodies were administered in one single dose intraperitoneally. We opted for a therapeutic model because we wanted to test the therapeutic potential of our antibodies under the most robust conditions. The body weights of the mice were recorded daily and the animals were euthanized if they lost more than 20% of their body weights or showed a severe deterioration in health status. The infection proceeded for 7 days before the animals were euthanized. Blood, tissue and bronchoalveolar lavage were harvested and stored accordingly. All the animal experiments were performed under the approval of the regional animal experimental ethics committee in Stockholm (16765–2020).

BAL Fluid qPCR Analysis

The bronchoalveolar lavage samples from mice were extracted using the MagNA pure 96 automated platform (Roche Life Science) followed by real-time RT-PCR-analysis of the SARS-CoV-2 envelope gene according to Corman et al, with some modifications (51). The thermal cycling was 48° for 10 min, then 95° for 10 min followed by 45 cycles of 95° for 15 s and 55° for 45 s. The PCR-analysis was performed using the Path-ID Multiplex one-step kit (Thermo-Fisher Scientific) and the 7500 Fast Real-time PCR system (Applied Biosystems).

Determination of IgG-Antigen Interaction Kinetics

Analysis of RBD-IgG reaction kinetics was performed on a MASS-16 biosensor instrument (Bruker, Hamburg, Germany). Anti-Human IgG (Fc) (Cytiva, Uppsala, Sweden) was diluted to 25 µg/ml in 10 mM sodium acetate buffer pH 5 and immobilized on a High Capacity Amine Sensor chip (Bruker) (time of interaction: 7 min; flow rate: 10 µl/min). S-protein-specific IgG was diluted in running buffer (Dulbecco's PBS (HyClone, South Logan, UT, USA) containing 0.01% Tween 20) and allowed to bind during a 90 s long injection (flow rate: 10 µl/min). Its capture level was set to be below 140 RU. The antigen (SARS-CoV-2 RBD (SinoBiological, Beijing, China; product number 40592-V08H) at 0.7-180 nM or Spike protein at 0.4-90 nM in running buffer) was subsequently injected (time of interaction: 2 min; flow rate: 30 µl/min). Dissociation was subsequently allowed to proceed for 5-15 min. The sensor chip was regenerated by treatment with 3 M magnesium chloride solution (Cytiva). All interactions were performed at 25°C. Apparent reaction rate kinetics was determined using a Langmuir 1:1 model using the Sierra Analyser software version 3.4.3 (Bruker).

Competition ELISA to Define Relative Epitope Location

High binding polystyrene 96-well plates (Corning Inc., Corning, NY, USA) were coated with 2 µg/ml streptavidin (Thermo Fisher Scientific, Waltham, MA, USA) diluted in Dulbecco's PBS (HyClone, South Logan, UT, USA) over night at +4°C. On the following day the plate was washed and subsequently incubated for 30 min with 30µl 30 nM biotinylated SARS-CoV-2 RBD (SinoBiological; product number:40592-V27H-B) diluted in Dulbecco's PBS containing 0.05% Tween 20 and 0.5% fish gelatine (Sigma Aldrich, St. Louis, MO, USA) (assay buffer). After washing the immobilized antigen was preincubated for 40 minutes at room temperature with 30 µl assay buffer or assay buffer containing 4.8 pmol IgG. Subsequently, 10 µl of assay buffer or assay buffer containing 4.8 pmol scFv was added to each well. After 1 hour incubation at room temperature the wells were washed and bound scFv was detected by incubation for 40 minutes at room temperature with peroxidase labelled monoclonal anti-FLAG® M2 antibody (Sigma Aldrich (30 µl diluted 1/4000 in assay buffer) and development using 1-Step™ Ultra TMB-ELISA Substrate Solution (Thermo Fisher Scientific).

Surface Plasmon Resonance Studies to Assess IgG-Specificity

The ability of IgG to interfere with the binding of SARS-CoV-2 RBD to its receptor, Angiotensin-Converting Enzyme 2 (ACE2) was examined by surface plasmon resonance-based detection in real time using a MASS-16 instrument (Bruker, Hamburg, Germany). The spots on a High Capacity Amine Sensor chip (Bruker) were immobilized with streptavidin (ThermoFisher Scientific, Waltham, MA, USA) (50 μg/ml diluted in 10 mM sodium acetate buffer pH 5.0; flow rate: 10 μl/min; time of immobilization: 6 min) to a level of approximately 1000 RU. Subsequently 50 nM biotinylated ACE2 (SinoBiological, Beijing, Shina; product number: 10108-H08H-B) was immobilized onto the chip's A spots (flow rate: 10 μl/s; time of binding: 2 min) while B spots were used as reference spots without ACE-2. 40 and 26 nM Receptor Binding Domain (RBD) was pre-incubated with 200 nM IgG diluted in Dulbecco's PBS (HyClone, South Logan, UT, USA) containing 0.01% Tween 20. The mixtures were injected over the sensor chip for 2 min, followed by a 6 min dissociation phase (flow rate: 30 μl/min). The sensor chip was regenerated by treatment with 1 M magnesium chloride solution (Sigma Aldrich, St Louis, MO, USA).

Binding of IgG to different mutated versions of SARS-CoV-2 was examined by a surface plasmon resonance assay. A High Capacity Amine Sensor chip (Bruker) was immobilized with F $(ab')_2$ Goat Anti-Human IgG, Fcγ fragment specific (Jackson, Ely, UK) at 50 μg/ml in 10 mM sodium acetate buffer pH 5 (time of interaction: 7 min; flow rate: 10 μl/min). Antibodies were diluted in Dulbecco's PBS (HyClone, South Logan, UT, USA) containing 0.01% Tween 20 and injected over the surface for 2 minutes at 10 μL/min. The antigens, produced in HEK293 cells, were obtained from SinoBiological (Beijing, China; product numbers: SARS-CoV-2 Spike RBD: 40592-V08H; SARS-CoV-2 Spike RBD-N501Y: 40592-V08H82; SARS-CoV-2 Spike RBD-E484K: 40592-V08H84; SARS-CoV-2 Spike RBD-K417N, E484K, N501Y: 40592-V08H85; SARS-CoV-2 Spike S1 HV69-70 deletion, Y144 deletion, N501Y, A570D, D614G, P681H: 40591-V08H12). All proteins were diluted to 50 nM in Dulbecco's PBS containing 0.01% Tween 20 and injected over the surface (time of interaction: 2 minutes; flow rate: 30 μl/min) followed by a dissociation phase of 6 minutes. After each cycle the surface was regenerated with 10 mM glycin pH 2.2 containing 30 mM HCl.

Crosslinking of Antibodies to Spike Protein

For the cross-linking of the antibodies to the Spike protein, 2 uG of each antibody was separately cross-linked to 2 uG of the Spike protein (Sino Biological Inc. 40589-V08H4 LC14SE2504, Recombinant SARS CoV-2 (1029-nCoV) Spike), as previously described (52). Briefly, the proteins were allowed to bind to each other in 50 uL of 1xPBS, pH 7.4 at 37°C, 500 rpm, 15 min. Heavy/light disuccinimidylsuberate (DSS; DSS-H12/D12, Creative Molecules Inc.) resuspended in dimethylformamide (DMF) was added to final concentrations 250 and 500 μM and incubated for a further of 60 min at 37°C, 800 rpm. The cross-linking reaction was quenched with a final concentration of 50 mM ammonium bicarbonate at 37°C, 800 rpm, 15 min.

Sample Preparation for MS

The cross-linked antibody-spike samples were denatured with 8 M urea - 100 mM ammonium bicarbonate, and the cysteine bonds reduced with a final concentration of 5 mM TCEP (37°C for 2h, 800 rpm) and subsequently alkylated with a final concentration of 10 mM iodoacetamide (22°C for 30 min, in the dark). The proteins were first digested with 1 μg of sequencing grade lysyl endopeptidase (Wako Chemicals) at 37°C, 800 rpm, 2h, diluted with 100 mM ammonium bicarbonate to a final urea concentration of 1.5 M, after which 1 μg sequencing grade trypsin (Promega) was added for further protein digestion (37°C, 800 rpm, 18 h). The samples were acidified to a final pH of 3.0 with 10% formic acid, and the peptides purified with C18 reverse phase spin columns according to the manufacturer's instructions (Macrospin columns, Harvard Apparatus). The peptides were dried in a speedvac and reconstituted in 2% acetonitrile, 0.2% formic acid prior to mass spectrometric analyses.

Liquid Chromatography Tandem Mass Spectrometry (LC-MS/MS)

All peptide analyses were performed on Q Exactive HF-X mass spectrometer (Thermo Scientific) connected to an EASY-nLC 1200 ultra-high-performance liquid chromatography system (Thermo Scientific), essentially as described with some minor modifications (PMID: 33411763). The peptides were loaded onto an Acclaim PepMap 100 (75μm x 2 cm) C18 (3 μm, 100 Å) pre-column and separated on an EASY-Spray column (Thermo Scientific; ID 75μm x 50 cm, column temperature 45°C) operated at a constant pressure of 800 bar. A linear gradient from 4 to 45% of 80% acetonitrile in aqueous 0.1% formic acid was run for 65 min at a flow rate of 350 nl min-1. One full MS scan (resolution 60000 @ 200 m/z; mass range 390–1 210m/z) was followed by MS/MS scans (resolution 15000 @ 200 m/z) of the 15 most abundant ion signals. The precursor ions were isolated with 2 m/z isolation width and fragmented using HCD at a normalized collision energy of 30. Charge state screening was enabled, and precursors with an unknown charge state and a charge state of 1 were rejected. The dynamic exclusion window was set to 10 s. The automatic gain control was set to 3e6 and 1e5 for MS and MS/MS with ion accumulation times of 110 ms and 60 ms, respectively. The intensity threshold for precursor ion selection was set to 1.7e4.

Computational Modeling

The variable domains (V_H-V_L) of antibodies were *de-novo* modeled and the sidechains were relaxed using Rosetta antibody (53) and relax protocols (54), respectively, from Rosetta software suite (26). For each epitope-paratope mapping, 2000 docking models were generated using Rosetta docking protocol (55) between the closed conformation of Spike protein (PDB id: 6VXX) and variable domain of target antibody. For ab66 specifically, the open conformation of Spike protein (PDB id: 7CAK) was also evaluated. The docking models for each pairwise conformation was filtered out through TX-MS protocol (25) using constraints derived from cross linking mass spectrometry experiments.

DATA AVAILABILITY STATEMENT

The raw data supporting the conclusions of this article will be made available by the authors, without undue reservation.

ETHICS STATEMENT

All participants gave written informed consent to participate in the study which was approved by the Swedish ethical review authority (2020/01747). The patients/participants provided their written informed consent to participate in this study. All the animal experiments were performed under the approval of the regional animal experimental ethics committee in Stockholm (16765–2020).

AUTHOR CONTRIBUTIONS

Conceptualization: WB, VW-H, RW, JM, LM, MO, MR, and PN. Experimentation and data analysis: WB, SW, MS, AB, UH, OL, HK, MG, MW, EE, ASS, LH, OA, JK, and TH. Writing original draft: WB and PN. All authors contributed to reading and editing the final manuscript.

FUNDING

WB, LM, JM, and PN are funded by the Knut and Alice Wallenberg Foundation. TH and equipment were funded by IngaBritt och Arne Lundbergs Forskningsstiftelse. WB, MO, JM, MR, and PN were funded by grants from the SciLifeLab National COVID-19 Research Program, financed by the Knut and Alice Wallenberg Foundation. WB was funded by the Royal Physiographic Society. HK was funded by Swiss National Science Foundation (grant no. P2ZHP3_191289).

ACKNOWLEDGMENTS

We thank Åsa Petersson for help with flow sorting and Berit Olofsson for technical assistance. We thank Benjamin Murrell and Daniel Sheward at the Karolinska Institutet for help with the pseudovirus neutralization assay. We thank Ali Mirazimi at the Public Health Agency of Sweden and Karolinska Institutet, for providing virus for the animal infection experiments performed. We thank the Department of Clinical Microbiology, Laboratory Medicine, Skåne University Hospital Lund for the qPCR analysis of BAL viral loads. We thank the Lund University Bioimaging Centre (LBIC) for use of fluorescence microscopes.

SUPPLEMENTARY MATERIAL

The Supplementary Material for this article can be found online at: https://www.frontiersin.org/articles/10.3389/fimmu.2021.808932/full#supplementary-material

REFERENCES

1. The IMpact-RSV SG. Palivizumab, a Humanized Respiratory Syncytial Virus Monoclonal Antibody, Reduces Hospitalization From Respiratory Syncytial Virus Infection in High-Risk Infants. *Pediatrics* (1998) 102:531–7. doi: 10.1542/peds.102.3.531
2. Mulangu S, Dodd LE, Davey RT, Tshiani Mbaya O, Proschan M, Mukadi D, et al. A Randomized, Controlled Trial of Ebola Virus Disease Therapeutics. *N Engl J Med* (2019) 381:2293–303. doi: 10.1056/NEJMoa1910993
3. FDA. *Fact Sheet For Health Care Providers Emergency Use Authorization (EUA) OF Regen-Covtm (Casirivimab With Imdevimab)* (2021). Available at: https://www.fda.gov/media/145611/download (Accessed May 25, 2021).
4. Gottlieb RL, Nirula A, Chen P, Boscia J, Heller B, Morris J, et al. Effect of Bamlanivimab as Monotherapy or in Combination With Etesevimab on Viral Load in Patients With Mild to Moderate COVID-19: A Randomized Clinical Trial. *JAMA* (2021) 325:632–44. doi: 10.1001/jama.2021.0202
5. FDA. *Emergency Use Authorization (EUA) OF Bamlanivimab And Etesevimab Authorized Use* (2021). Available at: https://www.fda.gov/media/145802/download#:~:text=The%20U.S.%20Food%20and%20Drug,patients%20(12%20years%20of%20age (Accessed May 25, 2021).
6. Taylor PC, Adams AC, Hufford MM, de la Torre I, Winthrop K, Gottlieb RL. Neutralizing Monoclonal Antibodies for Treatment of COVID-19. *Nat Rev Immunol* (2021) 21:382–93. doi: 10.1038/s41577-021-00542-x
7. Wu Y, Wang F, Shen C, Peng W, Li D, Zhao C, et al. A Noncompeting Pair of Human Neutralizing Antibodies Block COVID-19 Virus Binding to its Receptor ACE2. *Science* (2020) 368:1274–8. doi: 10.1126/science.abc2241
8. Cao Y, Su B, Guo X, Sun W, Deng Y, Bao L, et al. Potent Neutralizing Antibodies Against SARS-CoV-2 Identified by High-Throughput Single-Cell Sequencing of Convalescent Patients' B Cells. *Cell* (2020) 182:73–84.e16. doi: 10.1016/j.cell.2020.05.025
9. Ju B, Zhang Q, Ge J, Wang R, Sun J, Ge X, et al. Human Neutralizing Antibodies Elicited by SARS-CoV-2 Infection. *Nature* (2020) 584:115–9. doi: 10.1038/s41586-020-2380-z
10. Wang S, Peng Y, Wang R, Jiao S, Wang M, Huang W, et al. Characterization of Neutralizing Antibody With Prophylactic and Therapeutic Efficacy Against SARS-CoV-2 in Rhesus Monkeys. *Nat Commun* (2020) 11:5752. doi: 10.1038/s41467-020-19568-1
11. Yamayoshi S, Yasuhara A, Ito M, Akasaka O, Nakamura M, Nakachi I, et al. Antibody Titers Against SARS-CoV-2 Decline, But do Not Disappear for Several Months. *EClinicalMedicine* (2021) 32:100734. doi: 10.1016/j.eclinm.2021.100734
12. Forthal DN. Functions of Antibodies. *Microbiol Spectr* (2014) 2:1–17. doi: 10.1128/microbiolspec.AID-0019-2014
13. Huber VC, Lynch JM, Bucher DJ, Le J, Metzger DW. Fc Receptor-Mediated Phagocytosis Makes a Significant Contribution to Clearance of Influenza Virus Infections. *J Immunol* (2001) 166:7381–8. doi: 10.4049/jimmunol.166.12.7381
14. Fujisawa H. Neutrophils Play an Essential Role in Cooperation With Antibody in Both Protection Against and Recovery From Pulmonary Infection With Influenza Virus in Mice. *J Virol* (2008) 82:2772–83. doi: 10.1128/JVI.01210-07
15. Keeler SP, Fox JM. Requirement of Fc-Fc Gamma Receptor Interaction for Antibody-Based Protection Against Emerging Virus Infections. *Viruses* (2021) 13(6). doi: 10.3390/v13061037
16. Khandia R, Munjal A, Dhama K, Karthik K, Tiwari R, Malik YS, et al. Modulation of Dengue/Zika Virus Pathogenicity by Antibody-Dependent Enhancement and Strategies to Protect Against Enhancement in Zika Virus Infection. *Front Immunol* (2018) 9:597. doi: 10.3389/fimmu.2018.00597
17. Karthik K, Senthilkumar TMA, Udhayavel S, Raj GD. Role of Antibody-Dependent Enhancement (ADE) in the Virulence of SARS-CoV-2 and its Mitigation Strategies for the Development of Vaccines and Immunotherapies

to Counter COVID-19. *Hum Vaccin Immunother* (2020) 16:3055–60. doi: 10.1080/21645515.2020.1796425
18. Logunov DY, Dolzhikova IV, Shcheblyakov DV, Tukhvatulin AI, Zubkova OV, Dzharullaeva AS, et al. Safety and Efficacy of an Rad26 and Rad5 Vector-Based Heterologous Prime-Boost COVID-19 Vaccine: An Interim Analysis of a Randomised Controlled Phase 3 Trial in Russia. *Lancet* (2021) 397:671–81. doi: 10.1016/S0140-6736(21)00234-8
19. Baden LR, El Sahly HM, Essink B, Kotloff K, Frey S, Novak R, et al. Efficacy and Safety of the mRNA-1273 SARS-CoV-2 Vaccine. *N Engl J Med* (2021) 384:403–16. doi: 10.1056/NEJMoa2035389
20. Voysey M, Clemens SAC, Madhi SA, Weckx LY, Folegatti PM, Aley PK, et al. Safety and Efficacy of the ChAdOx1 Ncov-19 Vaccine (AZD1222) Against SARS-CoV-2: An Interim Analysis of Four Randomised Controlled Trials in Brazil, South Africa, and the UK. *Lancet* (2021) 397:99–111. doi: 10.1016/S0140-6736(20)32661-1
21. Polack FP, Thomas SJ, Kitchin N, Absalon J, Gurtman A, Lockhart S, et al. Safety and Efficacy of the BNT162b2 mRNA Covid-19 Vaccine. *N Engl J Med* (2020) 383:2603–15. doi: 10.1056/NEJMoa2034577
22. Pierce CA, Preston-Hurlburt P, Dai Y, Aschner CB, Cheshenko N, Galen B, et al. Immune Responses to SARS-CoV-2 Infection in Hospitalized Pediatric and Adult Patients. *Sci Transl Med* (2020) 12(564). doi: 10.1126/scitranslmed.abd5487
23. Alter G, Yu J, Liu J, Chandrashekar A, Borducchi EN, Tostanoski LH, et al. Immunogenicity of Ad26.COV2.S Vaccine Against SARS-CoV-2 Variants in Humans. *Nature* (2021) 596:268–72. doi: 10.1038/s41586-021-03681-2
24. Díez JM, Romero C, Cruz M, Vandeberg P, Merritt WK, Pradenas E, et al. Anti-SARS-CoV-2 Hyperimmune Immunoglobulin Provides Potent and Robust Neutralization Capacity and Antibody-Dependent Cellular Cytotoxicity and Phagocytosis Induction Through N and S Proteins. *BioRxiv* (2021). doi: 10.1101/2021.06.11.447942
25. Hauri S, Khakzad H, Happonen L, Teleman J, Malmström J, Malmström L. Rapid Determination of Quaternary Protein Structures in Complex Biological Samples. *Nat Commun* (2019) 10:192. doi: 10.1038/s41467-018-07986-1
26. Leman JK, Weitzner BD, Lewis SM, Adolf-Bryfogle J, Alam N, Alford RF, et al. Macromolecular Modeling and Design in Rosetta: Recent Methods and Frameworks. *Nat Methods* (2020) 17:665–80. doi: 10.1038/s41592-020-0848-2
27. Benton DJ, Wrobel AG, Xu P, Roustan C, Martin SR, Rosenthal PB, et al. Receptor Binding and Priming of the Spike Protein of SARS-CoV-2 for Membrane Fusion. *Nature* (2020) 588:327–30. doi: 10.1038/s41586-020-2772-0
28. Nordenfelt P, Tapper H. Phagosome Dynamics During Phagocytosis by Neutrophils. *J Leukoc Biol* (2011) 90:271–84. doi: 10.1189/jlb.0810457
29. Felton L. The Units of Protective Antibody in Antipneumococcus Serum and Antibody Solution. *J Infect Dis* (1928) 43.
30. Taborda CP, Casadevall A. Immunoglobulin M Efficacy Against Cryptococcus Neoformans: Mechanism, Dose Dependence, and Prozone-Like Effects in Passive Protection Experiments. *J Immunol* (2001) 166:2100–7. doi: 10.4049/jimmunol.166.3.2100
31. Taborda CP, Rivera J, Zaragoza O, Casadevall A. More is Not Necessarily Better: Prozone-Like Effects in Passive Immunization With IgG. *J Immunol* (2003) 170:3621–30. doi: 10.4049/jimmunol.170.7.3621
32. Asano Y, Albrecht P, Stagno S, Takahashi M. Potentiation of Neutralization of Varicella-Zoster Virus to Antibody to Immunoglobulin. *J Infect Dis* (1982) 146:524–9. doi: 10.1093/infdis/146.4.524
33. de Neergaard T, Sundwall M, Wrighton S, Nordenfelt P. High-Sensitivity Assessment of Phagocytosis by Persistent Association-Based Normalization. *J Immunol* (2021) 206:214–24. doi: 10.4049/jimmunol.2000032
34. Klein JS, Bjorkman PJ. Few and Far Between: How HIV may be Evading Antibody Avidity. *PloS Pathog* (2010) 6:e1000908. doi: 10.1371/journal.ppat.1000908
35. Ke Z, Oton J, Qu K, Cortese M, Zila V, McKeane L, et al. Structures and Distributions of SARS-CoV-2 Spike Proteins on Intact Virions. *Nature* (2020) 588:498–502. doi: 10.1038/s41586-020-2665-2
36. Zhang L, Jackson CB, Mou H, Ojha A, Peng H, Quinlan BD, et al. SARS-CoV-2 Spike-Protein D614G Mutation Increases Virion Spike Density and Infectivity. *Nat Commun* (2020) 11:6013. doi: 10.1038/s41467-020-19808-4
37. Bakalar MH, Joffe AM, Schmid EM, Son S, Podolski M, Fletcher DA. Size-Dependent Segregation Controls Macrophage Phagocytosis of Antibody-Opsonized Targets. *Cell* (2018) 174:131–42.e13. doi: 10.1016/j.cell.2018.05.059
38. Winkler ES, Bailey AL, Kafai NM, Nair S, McCune BT, Yu J, et al. SARS-CoV-2 Infection of Human ACE2-Transgenic Mice Causes Severe Lung Inflammation and Impaired Function. *Nat Immunol* (2020) 21:1327–35. doi: 10.1038/s41590-020-0778-2
39. Klein SL, Pekosz A, Park H-S, Ursin RL, Shapiro JR, Benner SE, et al. Sex, Age, and Hospitalization Drive Antibody Responses in a COVID-19 Convalescent Plasma Donor Population. *J Clin Invest* (2020) 130:6141–50. doi: 10.1172/JCI142004
40. Garcia-Beltran WF, Lam EC, Astudillo MG, Yang D, Miller TE, Feldman J, et al. COVID-19-Neutralizing Antibodies Predict Disease Severity and Survival. *Cell* (2021) 184:476–488.e11. doi: 10.1016/j.cell.2020.12.015
41. Long Q-X, Liu B-Z, Deng H-J, Wu G-C, Deng K, Chen Y-K, et al. Antibody Responses to SARS-CoV-2 in Patients With COVID-19. *Nat Med* (2020) 26:845–8. doi: 10.1038/s41591-020-0897-1
42. Bläckberg A, Fernström N, Sarbrant E, Rasmussen M, Sunnerhagen T. Antibody Kinetics and Clinical Course of COVID-19 a Prospective Observational Study. *PloS One* (2021) 16:e0248918. doi: 10.1371/journal.pone.0248918
43. RECOVERY Collaborative Group. Convalescent Plasma in Patients Admitted to Hospital With COVID-19 (RECOVERY): A Randomised Controlled, Open-Label, Platform Trial. *Lancet* (2021) 397:2049–59. doi: 10.1016/S0140-6736(21)00897-7
44. Chen P, Nirula A, Heller B, Gottlieb RL, Boscia J, Morris J, et al. SARS-CoV-2 Neutralizing Antibody LY-CoV555 in Outpatients With Covid-19. *N Engl J Med* (2021) 384:229–37. doi: 10.1056/NEJMoa2029849
45. Casadevall A, Joyner MJ, Pirofski L-A. Neutralizing Antibody LY-CoV555 for Outpatient Covid-19. *N Engl J Med* (2021) 384:189. doi: 10.1056/NEJMc2033787
46. Lopez Bernal J, Andrews N, Gower C, Gallagher E, Simmons R, Thelwall S, et al. Effectiveness of Covid-19 Vaccines Against the B.1.617.2 (Delta) Variant. *N Engl J Med* (2021) 385:585–94. doi: 10.1056/NEJMoa2108891
47. Charmet T, Schaeffer L, Grant R, Galmiche S, Chény O, Von Platen C, et al. Impact of Original, B.1.1.7 and B.1.351/P.1 SARS-CoV-2 Lineages on Vaccine Effectiveness of Two Doses of COVID-19 mRNA Vaccines: Results From a Nationwide Case-Control Study in France. *Lancet Reg Health Eur* (2021) 8:100171. doi: 10.1016/j.lanepe.2021.100171
48. Longo PA, Kavran JM, Kim M-S, Leahy DJ. Transient Mammalian Cell Transfection With Polyethylenimine (PEI). *Meth Enzymol* (2013) 529:227–40. doi: 10.1016/B978-0-12-418687-3.00018-5
49. Preger C, Wigren E, Ossipova E, Marks C, Lengqvist J, Hofström C, et al. Generation and Validation of Recombinant Antibodies to Study Human aminoacyl-tRNA Synthetases. *J Biol Chem* (2020) 295:13981–93. doi: 10.1074/jbc.RA120.012893
50. Säll A, Walle M, Wingren C, Müller S, Nyman T, Vala A, et al. Generation and Analyses of Human Synthetic Antibody Libraries and Their Application for Protein Microarrays. *Protein Eng Des Sel* (2016) 29:427–37. doi: 10.1093/protein/gzw042
51. Corman VM, Landt O, Kaiser M, Molenkamp R, Meijer A, Chu DK, et al. Detection of 2019 Novel Coronavirus (2019-Ncov) by Real-Time RT-PCR. *Euro Surveill* (2020) 25(3). doi: 10.2807/1560-7917.ES.2020.25.3.2000045
52. Bahnan W, Happonen L, Khakzad H, Kumra Ahnlide V, de Neergaard T, Wrighton S, et al. Protection Induced by a Human Monoclonal Antibody Recognizing Two Different Epitopes in a Conserved Region of Streptococcal M Proteins. *BioRxiv* (2021). doi: 10.1101/2021.03.01.433494
53. Marze NA, Lyskov S, Gray JJ. Improved Prediction of Antibody VL-VH Orientation. *Protein Eng Des Sel* (2016) 29:409–18. doi: 10.1093/protein/gzw013
54. Conway P, Tyka MD, DiMaio F, Konerding DE, Baker D. Relaxation of Backbone Bond Geometry Improves Protein Energy Landscape Modeling. *Protein Sci* (2014) 23:47–55. doi: 10.1002/pro.2389
55. Marze NA, Roy Burman SS, Sheffler W, Gray JJ. Efficient Flexible Backbone Protein-Protein Docking for Challenging Targets. *Bioinformatics* (2018) 34:3461–9. doi: 10.1093/bioinformatics/bty355

Conflict of Interest: Authors UH and OL were employed by company Adlego Biomedical AB. Author VW-H was employed by company Tanea Medical AB. Author RW was employed by company SciEd Solutions.

The remaining authors declare that the research was conducted in the absence of any commercial or financial relationships that could be construed as a potential conflict of interest.

this article, or claim that may be made by its manufacturer, is not guaranteed or endorsed by the publisher.

frontiers in Immunology

ORIGINAL RESEARCH
published: 14 January 2022
doi: 10.3389/fimmu.2021.816745

The Transient IFN Response and the Delay of Adaptive Immunity Feature the Severity of COVID-19

Gang Xu[1†], Furong Qi[1†], Haiyan Wang[1], Yu Liu[1], Xin Wang[1], Rongrong Zou[2], Jing Yuan[2], Xuejiao Liao[1], Yang Liu[1], Shuye Zhang[3] and Zheng Zhang[1,4,5*]*

[1] Institute for Hepatology, National Clinical Research Center for Infectious Disease, Shenzhen Third People's Hospital, The Second Affiliated Hospital, School of Medicine, Southern University of Science and Technology, Shenzhen, China, [2] Department for Infectious Diseases, Shenzhen Third People's Hospital, Shenzhen, China, [3] Shanghai Public Health Clinical Center, Fudan University, Shanghai, China, [4] Shenzhen Research Center for Communicable Disease Diagnosis and Treatment of Chinese Academy of Medical Science, Shenzhen, China, [5] Guangdong Key Laboratory for Anti-Infection Drug Quality Evaluation, Shenzhen, China

OPEN ACCESS

Edited by:
Tengchuan Jin,
University of Science and Technology of China, China

Reviewed by:
Lei Zhang,
Peking University, China
Ciputra Hartana,
MIT and Harvard, United States

***Correspondence:**
Zheng Zhang
zhangzheng1975@aliyun.com
Shuye Zhang
zhangshuye@shphc.org.cn

[†]These authors have contributed equally to this work

Specialty section:
This article was submitted to Viral Immunology, a section of the journal Frontiers in Immunology

Received: 17 November 2021
Accepted: 21 December 2021
Published: 14 January 2022

Citation:
Xu G, Qi F, Wang H, Liu Y, Wang X, Zou R, Yuan J, Liao X, Liu Y, Zhang S and Zhang Z (2022) The Transient IFN Response and the Delay of Adaptive Immunity Feature the Severity of COVID-19. Front. Immunol. 12:816745. doi: 10.3389/fimmu.2021.816745

COVID-19 patients show heterogeneous and dynamic immune features which determine the clinical outcome. Here, we built a single-cell RNA sequencing (scRNA-seq) dataset for dissecting these complicated immune responses through a longitudinal survey of COVID-19 patients with various categories of outcomes. The data reveals a highly fluctuating peripheral immune landscape in severe COVID-19, whereas the one in asymptomatic/mild COVID-19 is relatively steady. Then, the perturbed immune landscape in peripheral blood returned to normal state in those recovered from severe COVID-19. Importantly, the imbalance of the excessively strong innate immune response and delayed adaptive immunity in the early stage of viral infection accelerates the progression of the disease, indicated by a transient strong IFN response and weak T/B-cell specific response. The proportion of abnormal monocytes appeared early and rose further throughout the severe disease. Our data indicate that a dynamic immune landscape is associated with the progression and recovery of severe COVID-19, and have provided multiple immune biomarkers for early warning of severe COVID-19.

Keywords: COVID-19, ScRNA-seq, early immune feature, IFN response, delayed adaptive immunity

INTRODUCTION

SARS-CoV-2 infection causes COVID-19 with different severity. Most patients develop only mild symptoms, while a minor fraction develop severe diseases, especially for the elderly with pre-existing conditions (1). Immunological perturbations are associated with COVID-19 severity, including increased immature myeloid suppressor cells (2, 3), T cell depletion (4), and cytokine storm (5, 6). Thus, the successful or impaired immune responses were acknowledged playing crucial roles. Previous studies suggest that IFN response (7), T cell response (8), and potential antibody-dependent enhancement (ADE) (9) are potential factors, causing subsequent deterioration of coronavirus induced diseases. However, the reported roles of these immune elements in the pathogenesis of severe COVID-19 are often inconsistent, e.g., both heightened or impaired IFN responses in severe COVID-19 were reported (10, 11). There are also inconsistent reports of anti-

viral $CD4^+$ T-cell (12, 13), $CD8^+$ T-cell responses (14), and humoral immune responses (12, 15) in patients with different COVID-19 severity. One important cause of those discrepancies is likely due to the heterogenous nature of COVID-19 and its dynamic clinical course (16). Indeed, a COVID-19 patient may show largely different immune responses at different stages of the disease (17). Thus, mechanistic understanding of the COVID-19 pathogenesis will require a thorough understanding of the entire dynamic processes.

There were several datasets investigating non-synchronized COVID-19 samples collected primarily at peak level severity or convalescence (18–20). However, the dataset from samples taken longitudinally at an earlier stage of infection (prior to the development of serious diseases) is still absent. One mystery with COVID-19 is that patients can quickly deteriorate without any warning. Understanding such triggering events and identifying potential prediction factors may lead to more effective measures to prevent disease deterioration. However, the stressed medical system during the COVID-19 pandemic usually looks after the sickest patients first, so information/data collected prior to disease deterioration are scarce. To this end, by benefiting from strict contact tracing, quarantine measures and designated hospitalization in Shenzhen, China, we were able to study a valuable cohort of COVID-19 patients by closely following their clinical courses.

Here, we presented such a scRNA-seq dataset of peripheral immune cells in SARS-CoV-2 infected patients, containing longitudinal samples of COVID-19 patients with asymptomatic, mild, and severe diseases. This critical resource provides a great opportunity to decipher the pivotal immunological events preceding the development or resolving of the SARS-CoV-2 induced diseases. Evidence pointed to a highly dynamic circulating immune landscape, namely, remodeling of myeloid and lymphoid compartments matching with the development and recovery of severe COVID-19. In addition, our data highlighted the early immunological events that precede the stage for subsequent development of severe COVID-19. Understanding these mechanisms is the holy grail for the COVID-19 study.

RESULTS

Clinical Characteristics in a Closely Monitored Cohort of Patients With COVID-19 With Varying Severity

To identify the characteristics of the early immune response that led to the variable severity of COVID-19, we performed single cell RNA-seq of 49 PBMC samples from five asymptomatically infected, five mildly, and eight severely ill COVID-19 patients, plus 6 healthy controls (**Figure 1A** and **Table S1**). In particular, among 8 severe COVID-19 cases, conditions of 7 deteriorated after hospitalization, while another one (S7) deteriorated the same day of admission. Two severe COVID-19 cases (S7 and S8) succumbed while 6 recovered. Asymptomatic and mild COVID-19 cases had shorter duration of hospitalization and were discharged within one month (**Figure 1B**). We closely monitored clinical parameters and collected PBMCs at different stages of clinical course, as indicated in **Figure 1B**. For patients with severe COVID-19, PBMCs were collected before, during, and after disease deterioration. The first sampling (Severe Acute, SA) was around 1 week post the symptom onset, the second sampling (Severe Progression, SP) was around 17 days post the symptom onset, and the last sampling (Severe Recovery, SR) was around one month after the discharge. We collected PBMCs from mildly ill patients at times matching with those in severe COVID-19, as the MA (Mild Acute), MP (Mild Progression) and MR (Mild Recovery) groups. For asymptomatic COVID-19 cases, we collected their PBMCs shortly after their admission and one week afterwards, as the AA (Asymptomatic Acute) and AP (Asymptomatic Progression) group (**Figure 1B** and **Table S1**). Accordingly, the eight groups of COVID-19 patients exhibited varying disease severity using the WHO ordinal scale (WOS): Asymptomatic patients scored 0–2; mildly ill COVID-19 patients scored 0–4; while the severely ill patients scored 3–5 in SA, then 5–7 in SP and returned to 0 in SR (**Figure 1B**, right panel). The dynamic clinical courses are also reflected by monitoring individual parameters, such as CRP levels, which are close to normal range in asymptomatic, mildly ill and recovered patients, but increased and fluctuated in severely ill patients (**Figure 1C**).

Correlation analysis revealed the associations between disease severity and clinical parameters, assessing WOS scores and all clinical data from this cohort. We identified previously known factors, such as IL6, LDH, the neutrophils percentages, $CD4^+$/$CD8^+$ ratio, CRP (positively correlated with WOS) and $CD8^+$ T cell percentages, T cell count, lymphocyte count and percentages, $CD4^+$ T cell count (negatively correlated with WOS). Besides, we also identified previously unidentified correlations including true bound bilirubin (BC-TR), direct bilirubin (DB), immature granulocytes count and percentage (IG# and IG%), urea (positively correlated with WOS), and cholinesterase (CHE), albumin (ALB), Prealbumin (PA), basophils count (BASO#) and heart-type creatine kinase (CK-MB) (negatively correlated with WOS) (**Figures 1D, E**).

Examining disease severity associated clinical parameters among the eight studied groups, SP clearly stood out, manifested by the highest levels of neutrophils percentages (NEUT%), globulin (GLO), mean corpuscular hemoglobin (MCH), platelet-larger cell ratio (P-LCR), glutamic oxaloacetic transaminase (AST), total bilirubin (TB), mean platelet volume (MPV), direct bilirubin (DB), and BC-TR and lowest levels of estimated glomerular filtration rate (eGFR), BASO counts, the ratio of Albumin/globulin (A/G), red blood cell count (RBC), hemoglobin (HGB), lymphocyte percentages (LYMPH%), standard deviation of red blood cell distribution width (RDW-SD), and ALB, compared with other groups (**Figure 1F** and **Table S2**), whereas those differences are more heterogenous in SA patients, making it difficult to predict disease progression based on clinical parameters. This is also consistent with suddenly worsening COVID-19 in critically ill patients.

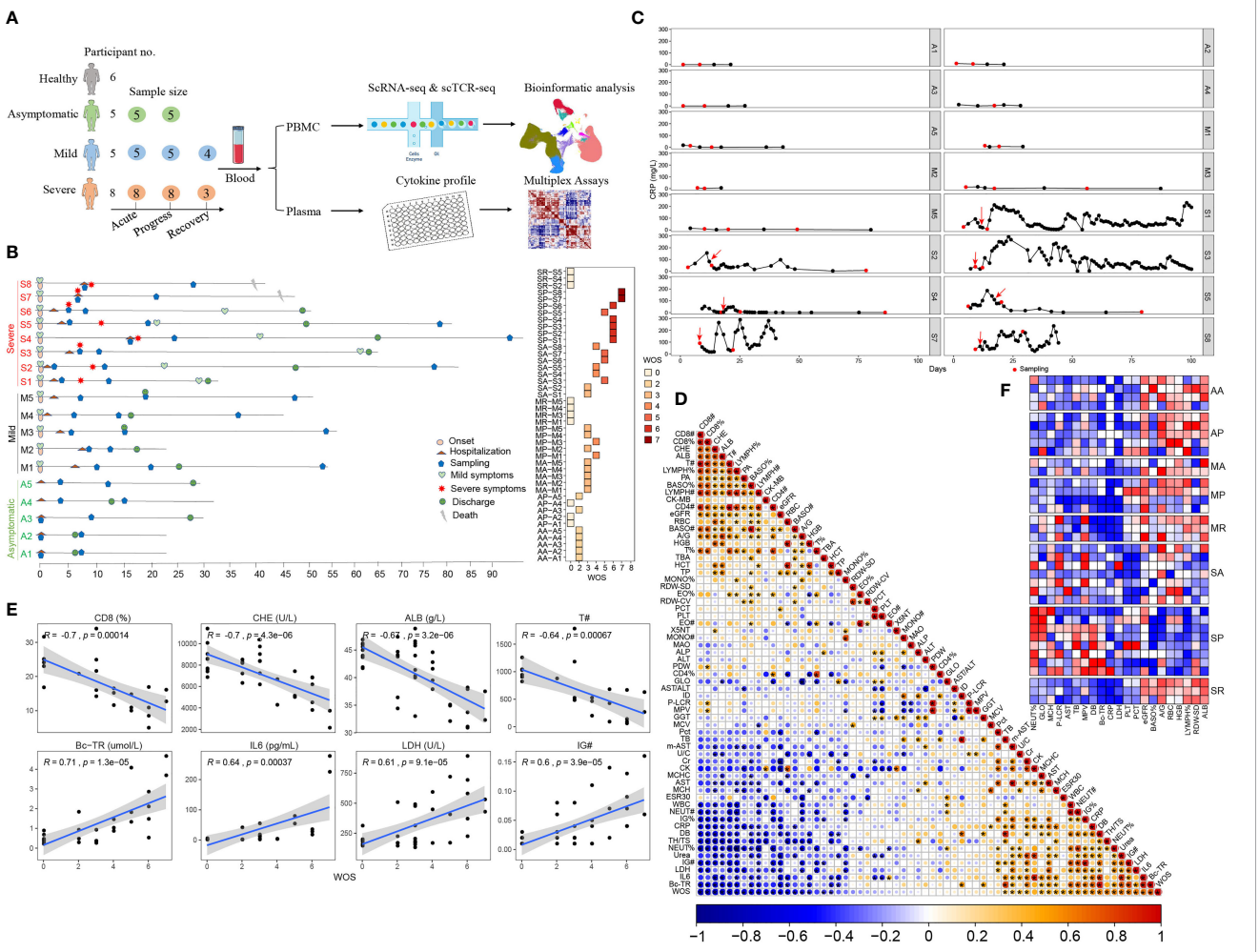

FIGURE 1 | Research scheme and clinical characteristics of the studied COVID-19 patients. **(A)** Graphical overview of the study. Blood from 5 asymptomatic, 5 mildly and 8 severely ill COVID-19 patients and 6 healthy controls were collected for scRNA-seq and cytokine profiling analysis. **(B)** Timeline of each studied COVID-19 patient enrolled in this study. Critical points indicated are hospitalization, sampling, severity turning point, discharge and death date as days after symptom onset (left). The assessment COVID-19 severity is described in the *Materials and Methods*. The right panel shows the disease severity at each sampling date according to the WHO ordinal scale (WOS). In total, 43 samples from COVID-19 patients were collected and comprised of 8 groups, namely, AA, AP, MA, MP, MR, SA, SP, and SR. **(C)** Representative dynamic monitoring of CRP levels from selected COVID-19 patients, namely, 5 asymptomatic, 4 mildly and 7 severely ill patients. The red arrow indicates when the disease becomes serious, and the red dot indicates when PBMC was sampled. **(D)** Correlation matrix of the 63 clinical parameters from the 18 studied COVID-19 patients. The bottom bar corresponds to the absolute value of the Spearman Rank correlation coefficient (*P-value < 0.05). The abbreviated terms are described in the *Materials and Methods*. **(E)** The top 4 positively and 4 negatively WOS-correlated clinical parameters, (# represents cell count). **(F)** The heatmap shows the available relative levels of WOS-correlated clinical parameters near each individual sampling, according to the 8 studied COVID-19 groups.

Characterizing the Perturbed Peripheral Immune Cell Landscape in Different Subset of COVID-19 Patients

Next, we sought to interrogate immune factors related to different COVID-19 severity by scRNA-seq. A high-quality scRNA-seq dataset composed of 498,151 cells was created and visualized by Uniform Manifold Approximation and Projection (UMAP) projection (**Figure 2A**). The clustering analysis revealed 25 clusters and 10 major cell types annotated by marker genes, namely, T cell (*CD3D*), NK cell (*KLRF1*), B cell (*CD79A*), monocyte (*CD14*, *FCGR3A*), myeloid DCs (mDCs) (*CD1C*), plasmacytoid DCs (pDCs) (*IL3RA*), and plasma cells (PCs) (*IGKC*), megakaryocyte (*MYL9*), cycling cells (*MKI67*), and erythrocytes (*HBB*) (**Figures 2A** and **S1A**). Erythrocytes, megakaryocyte, and doublets were removed in subsequent analysis. Little batch effects were observed (**Figures S1B, C**). The integrated dataset reveals a particularly dynamic immune landscape in patients with severe COVID-19 (changing from SA, to SP, to SR), whereas those in asymptomatic and mild COVID-19 are relatively stable and comparable with controls (**Figures 2B** and **S1D, E**). Consistent with previous reports, proportions of circulating NK cells, T cells, mDCs, and pDCs are significantly decreased in the SP

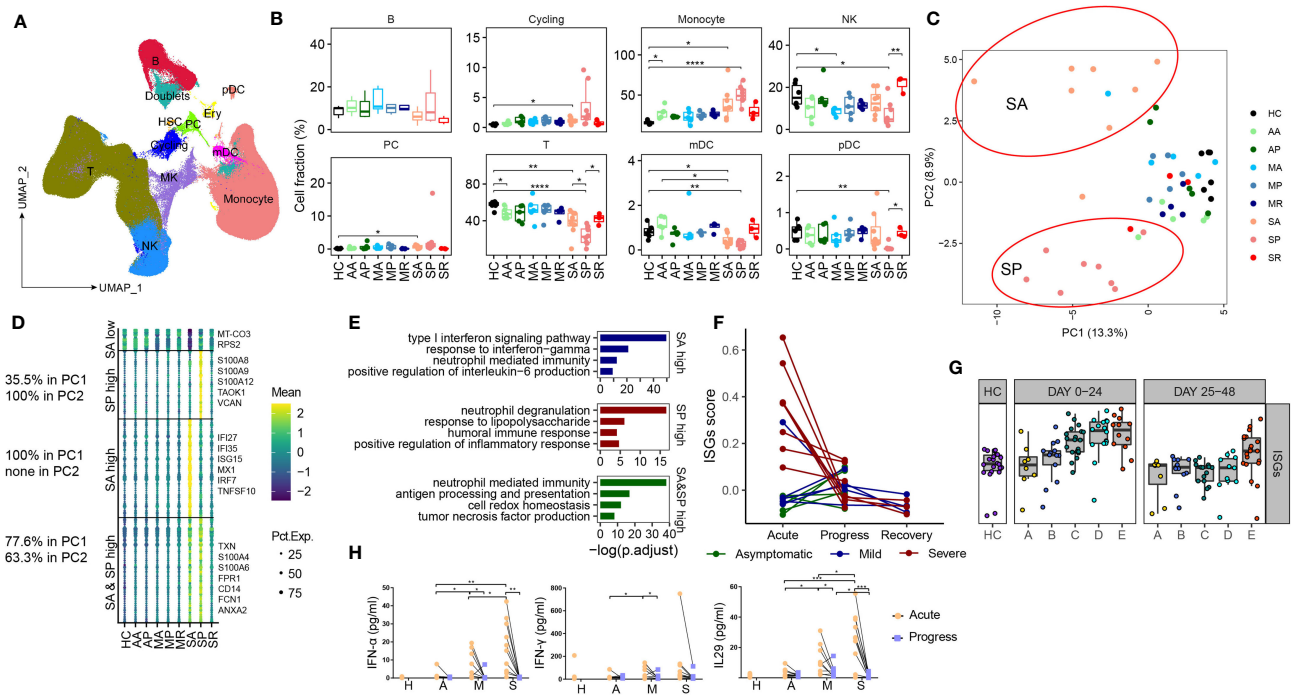

FIGURE 2 | Characterizing peripheral immune perturbations in COVID-19 patients with different clinical course. **(A)** UMAP representation of the ten cell types from the integrated PBMC scRNA-seq dataset (49 samples, 498,151 cells). **(B)** Proportions of various peripheral immune cell types from COVID-19 patients and controls (two-sided Student's t-test, *P <0.05, **P <0.01, ****P <0.0001). **(C)** Principal-component analysis of averaged transcriptome derived from each individual scRNA-seq data. **(D)** Heatmaps show the SA and SP-specific differentially expressed genes, comprising 4 groups, as higher levels in both SA and SP, higher levels in SA only, higher in SP only, or lower in SA only. Representative genes are indicated at the right side. The percentage of corresponding genes belonging to PC1 and PC2 is indicated at the left side. **(E)** Enrichment of GO biological process (BP) terms for DEGs expressed at higher levels in SA (up), in SP (middle) and in both SA and SP (bottom). **(F)** The scatter plot shows the dynamic changes of the IFN response score of each patient at different time points. **(G)** The scatter plot shows the expression of ISGs in the RNA-seq data of PBMC of 5 groups of COVID-19 patients with different severity levels and healthy controls at 2 time points. **(H)** The plasma levels of IFNα-2a, IFN-γ and IL-29 from the first two samplings of each studied COVID-19 groups and controls, (two-sided Student's t-test, *P < 0.05, **P < 0.01, ***P < 0.001,****P < 0.0001).

group, while monocyte percentage is significantly expanded. However, in SA and SP group, in whom the severe COVID-19 has yet developed or has recovered, such differences with other COVID-19 groups and controls are subtler (**Figures 2B** and **S1D, E**). Indeed, proportions of NK and pDCs are not significantly reduced in SA, while proportions of NK cells, T cells, mDCs, and pDCs are normalized in SR compared with SP (**Figures 2B** and **S1D**). Another study used RNA-seq to analyze the longitudinal immune response characteristics of a larger cohort of 207 COVID-19 patients, namely, 5 groups of multiple time points, with group A as the asymptomatical patients; group B as the mildly diseased group; group C as the patients admitted to hospital but required no oxygen supplementation; group D as the hospitalized patients need supplemental oxygen and group E as the patients who required assisted ventilation (21). The analysis of this RNA-seq dataset through MarkerBasedDecomposition function in Bisque (22) corroborates the early changes of peripheral immune cells in severe patients (**Figure S1F**). Together, these data indicated that the broad perturbation of blood immune cell compartments closely correlated with development of severe COVID-19 and mainly occurred in SP.

To search for transcriptomic differences between different subsets of COVID-19 patients, we consolidated individual scRNA-seq data as conventional RNA-seq data and performed PCA analysis, and found that PC1 distinguished SA and SP from other groups, and PC2 distinguished SA from SP (**Figure 2C**). The top 100 genes in PC1 and PC2 are listed in **Table S2**. Mapping these genes to UMAP showed that they were mainly derived from myeloid cells (**Figures S1G, H**). The data shows that SA is transcriptomically unique, suggesting that transcriptomic markers from myeloid cells may provide an early warning for developing severe COVID-19. Genes highly expressed in both SA and SP groups, namely, *TXN*, *S100A4*, *S100A6*, *FRP1*, etc., are enriched for neutrophil mediated immunity and antigen processing and presentation pathway; while those highly expressed in SP are *S100A8*, *S100A9*, *S10A12*, etc., are involved in neutrophil mediated immunity and response to LPS pathway (**Figures 2D, E**). Notably, those highly expressed in SA include *IFI27*, *IFI35*, *ISG15*, etc., as interferon-stimulating genes (ISGs) (**Figures 2D–F**), indicating a response to high levels of interferon produced *in vivo*. The high expression of ISG in peripheral immune cells of severely ill patients can also be

confirmed in the RNA-seq data set (**Figures 2G** and **S1I**). To confirm this, we measured plasma type I, II and III interferon levels from anothor cohort of patients including the different subsets. Indeed, the plasma levels of type I and III IFNs were significantly higher in acute disease stage (AA, MA, SA) versus those with progressive disease (AP, MP, SP), and were also higher in those from SA compared to the AA and MA groups (**Figure 2H**). We confirmed *in vitro* that the lung epithelial cell infected with SARS-CoV-2 induces strong IFN production (**Figure S1J**). Similar reports have been published that SARS-CoV-2 infection stimulates IFN production, which is positively correlated with viral load (23). Together, these data revealed that unique peripheral immune transcriptional signatures emerged both before and during the development of severe COVID-19.

Remodeling of Myeloid Cell Compartments and Transcriptomes Correlate With the Development of Severe COVID-19

Next, we characterized myeloid cell compartment and identified 5 subsets according to the expression of canonical markers: classical monocyte (*CD14*), intermediate monocyte (*CD14*, *FCGR3A*), nonclassical monocytes (*FCGR3A*), DC1 (*CLEA9A*) and DC2 (*CD1C*, *CLEC10A*) (**Figures 3A** and **S2A**). Notably, myeloid compartment underwent dynamic changes before, during and after progression of severe COVID-19. Proportions of DC1 and DC2 significantly decreased in SA than those in controls, reduced further in SP, but normalized in SR, whereas comparable frequencies of DCs were observed between asymptomatic, mild COVID-19 patients and controls. The proportion of $CD14^+CD16^+$ intermediate monocytes increased during acute SARS-CoV-2 infection, and normalized in those recovered. We also noticed increased proportions of $CD14^+$ classical monocytes and decreased proportions of $CD16^+$ nonclassical monocytes in SP, consistent with early reports by us and others (2, 3, 24), while proportions of classical and nonclassical monocytes were comparable among other studied groups (**Figures 3B** and **S2B–D**). We found association between high ratios of $CD14^+/CD16^+$ monocytes and acute infections, as in AA, MA and SA, while those ratios normalized in recovered patients (AP, MP, MR, and SR), but persistently high $CD14^+/CD16^+$ monocyte ratios were associated with development of severe COVID-19 in SP (**Figure 3C**). Bisque analysis of RNA-seq data of 207 COVID-19 patients also found that severe patients had higher $CD14^+/CD16^+$ monocyte ratios in the periphery at the early stage (**Figure 3D**). Thus, our data revealed that the proportion of $CD14^+$ monocytes begins to expand in the early stage of severe patients, and the $CD14^+/CD16^+$ monocyte ratios can serve as an appropriate early prognostic marker for severe COVID-19.

We further characterized the transcriptomic changes of $CD14^+$ monocyte from different subsets of COVID-19 patients. Compared with those in controls, the expression levels of genes involved in the innate immune defense were found diminished in $CD14^+$ monocytes from COVID-19 patients. The downregulated genes include ones mediating immune signaling, e.g., *RIPK2*, *RLRP3*, and *NFKBID*, etc., and genes encoding cytokine and chemokines, suggesting impaired immune functions of monocytes from COVID-19 patients (**Figure 3E**). The highest expression levels of ISGs is the most prominent feature of $CD14^+$ monocytes from SA (**Figure 3E**). Moreover, $CD14^+$ monocytes from SA and SP have similar immunosuppressive signature, including downregulation of MHC II genes (*HLA-DRB5*, *HLA-DRB1*, *HLA-DR1*, etc.) and upregulation of alarmin genes (*S100A12*, *S100A9*, *S100A8*, *S100A6*) were observed in both SA and SP, compared with other groups (**Figure 3E**). This is consistent with previous studies that $CD14^+$ monocytes from severe COVID-19 patients exhibited signature of immature monocytes, namely, downregulation of MHC II genes and upregulation of alarmin genes (2, 3, 24).

We re-clustered $CD14^+$ monocytes into HLA^{high} and HLA^{low} groups, UMAP projection of MHC-II and alarmin signature scores confirmed that HLA^{high} and HLA^{low} $CD14^+$ monocytes have a higher MHC-II and alarmin scores respectively (**Figures 3F**). We tightly monitored the MHC-II and alarmin scores at different stages of these 18 patients and found that the SA group showed a higher alarmin score and a lower MHC-II score, which worsened in SP (**Figure 3G**). The differences of "Monocyte composite scores" between different groups are even more apparent (**Figure 3H**). RNA-seq analysis of peripheral immune cells also showed that alarmin expression increased in and MHC-II expression decreased in the early stage of sever COVID-19 patients (**Figures 3I** and **S2E**). Therefore, our data suggest that during acute SARS-CoV-2 infection, the emergence of HLA^{low} population and IFN-response transcriptional signatures in monocytes, likely signify the subsequent progression of severe COVID-19.

Two Groups of $CD8^+$ T Cells With Different Phenotypes and TCR Expansion Associate With Different COVID-19 Severity

To understand the T cell response, we broadly categorized T cells into innate-like T cells (MAIT, NKT, and γδ T) and $CD4^+$ and $CD8^+$ T cells (**Figure S3A**). A high $CD4^+/CD8^+$ ratio was previously reported in severe COVID-19 (24). We found that the $CD4^+/CD8^+$ ratio started to increase in SA, reached highest levels in SP and normalized in SR (**Figures S3B–D**). Depletion of innate-like T cells is another feature previously reported in severe COVID-19 (25). We found that proportions of innate-like T cells tended to decrease in SA, reached lowest levels in SP and normalized in SR (**Figures S3C, E**). The $CD4^+/CD8^+$ ratio and proportions of innate-like T cells were comparable between non-severe COVID-19 patients and healthy controls.

Next, we identified 5 clusters of peripheral $CD8^+$ T cells, as the CD8-CCR7 (Naïve), CD8-TCF7 (central memory), CD8-GATA3, CD8-GZMK (effector memory), and CD8-GZMB (terminal differentiated effector memory) subsets based on well-studied markers (**Figures 4A** and **S4A**). The expression pattern of transcription factors (**Figure S4B**) demonstrates that CD8-GZMB strongly expresses the transcription factor *TBX21*, *PRDM1*, and *ID2*, while transcription factors *EOMES* and *BCL6* are more expressed in CD8-GZMK cells, suggesting the accuracy

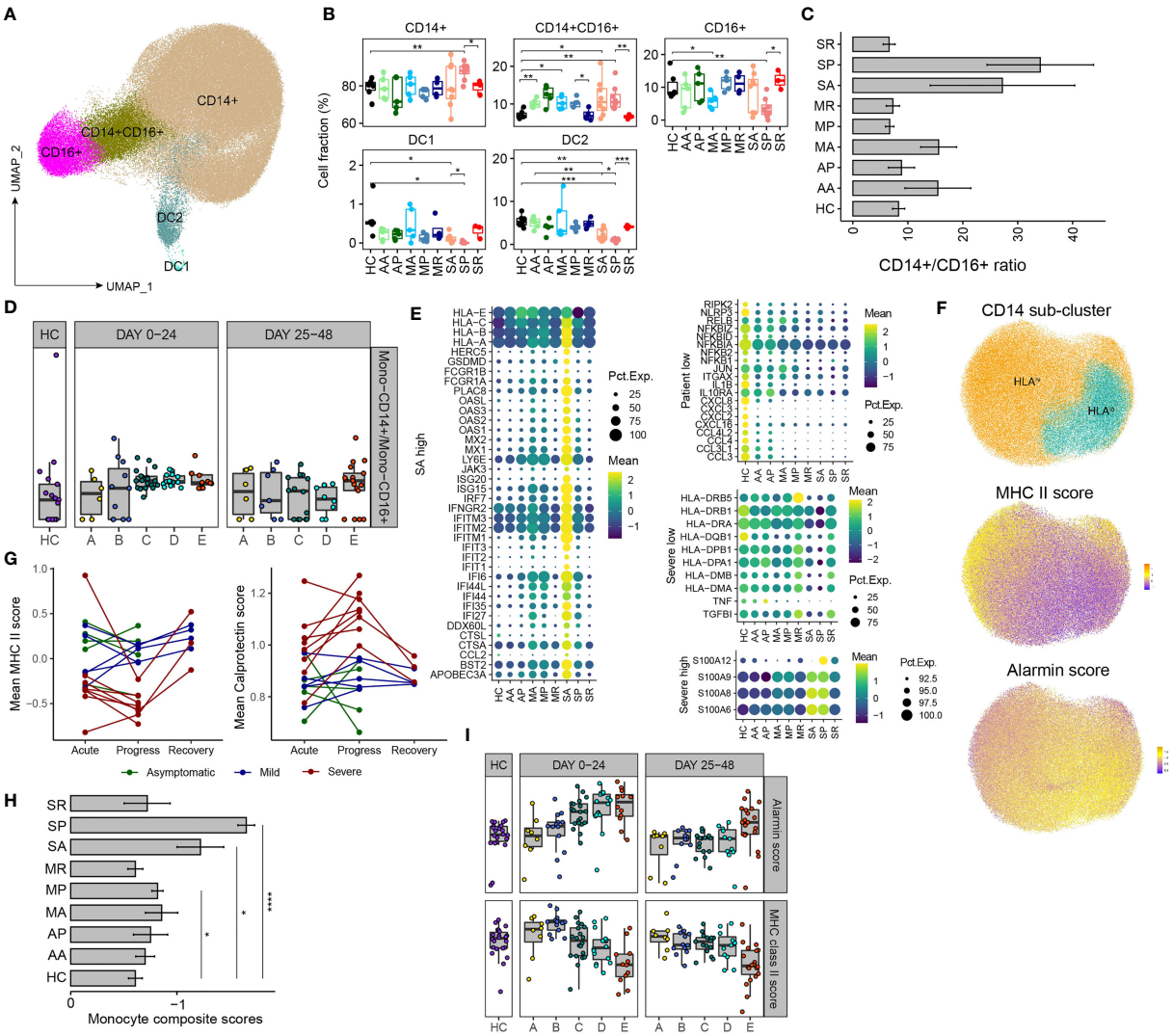

FIGURE 3 | Remodeling of myeloid cell compartment and transcriptional signatures associated with development of severe COVID-19. **(A)** UMAP plot of the major myeloid cell types within PBMCs. **(B)** Proportions of various peripheral myeloid cell types from COVID-19 patients and controls (two-sided Student's t-test, *P <0.05, **P < 0.01, ***P < 0.001). **(C)** The bar plot of the ratio of $CD14^+/CD16^+$ monocytes. **(D)** The scatter plot shows the ratio of $CD14^+/CD16^+$ monocytes of the 5 groups of COVID-19 patients and healthy controls based on the Marker Based Decomposition analysis of the RNA-seq data in the 2 time zones. **(E)** The heatmaps show the selected differentially expressed genes in $CD14^+$ monocyte from comparisons between COVID-19 patients and controls. "SA high" highlights the genes of higher levels in SA; "Patient low" as the genes of lower levels in COVID-19 patients; "Severer low" and "Severe high" as genes of lower or higher levels in both SA and SP. **(F)** UMAP plot of the $CD14^+$ monocytes, divided into HLA^{high} and HLA^{low} groups (up). MHC II score (middle) and alarmin score (down) are projected to the UMAP. **(G)** The dynamic changes of the average MHC II score (left) and alarmin score (right) of each patient at different time points. **(H)** The bar plot shows "Monocyte composite scores" across different groups, (two-sided Student's t-test, *P < 0.05, ****P < 0.0001). **(I)** The dynamic changes of the average MHC II score (bottom) and alarmin score (up) of the 5 groups of COVID-19 patients and healthy controls in the 2 time zones.

of $CD8^+$ T cell clustering. The diminished number of Naïve $CD8^+$ T cells in severe (SA, SP, and SR) COVID-19 patients (likely related to their old age), is clearly reflected by the UMAP projections (**Figure S4C**). We also found that average percentage of the peculiar CD8-GATA3 subset in SA was the highest among all studied groups (**Figure 4B** and **Figures S4D, E**). GATA3 has been reported highly expressed in peripheral $CD8^+$ T cell from patients with systemic sclerosis, and functionally related to IL13 induction. Thus, CD8-GATA3-IL13 expression have been proposed to play roles in amplifying inflammation and regarded as a highly relevant biomarker for inflammatory diseases (26). Consistently, CD8-GATA3 in the SA group produced the highest levels of IL13 (**Figures S4F**). Within the memory and effector $CD8^+$ T cell compartment, we observed a discordance of CD8-GZMK and CD8-GZMB subset in SA (with a dominance of CD8-GZMB over CD8-GZMK) compared with other COVID-19 groups (**Figure 4C**). This was also robustly confirmed in RNA-seq data set (**Figure S4G**).

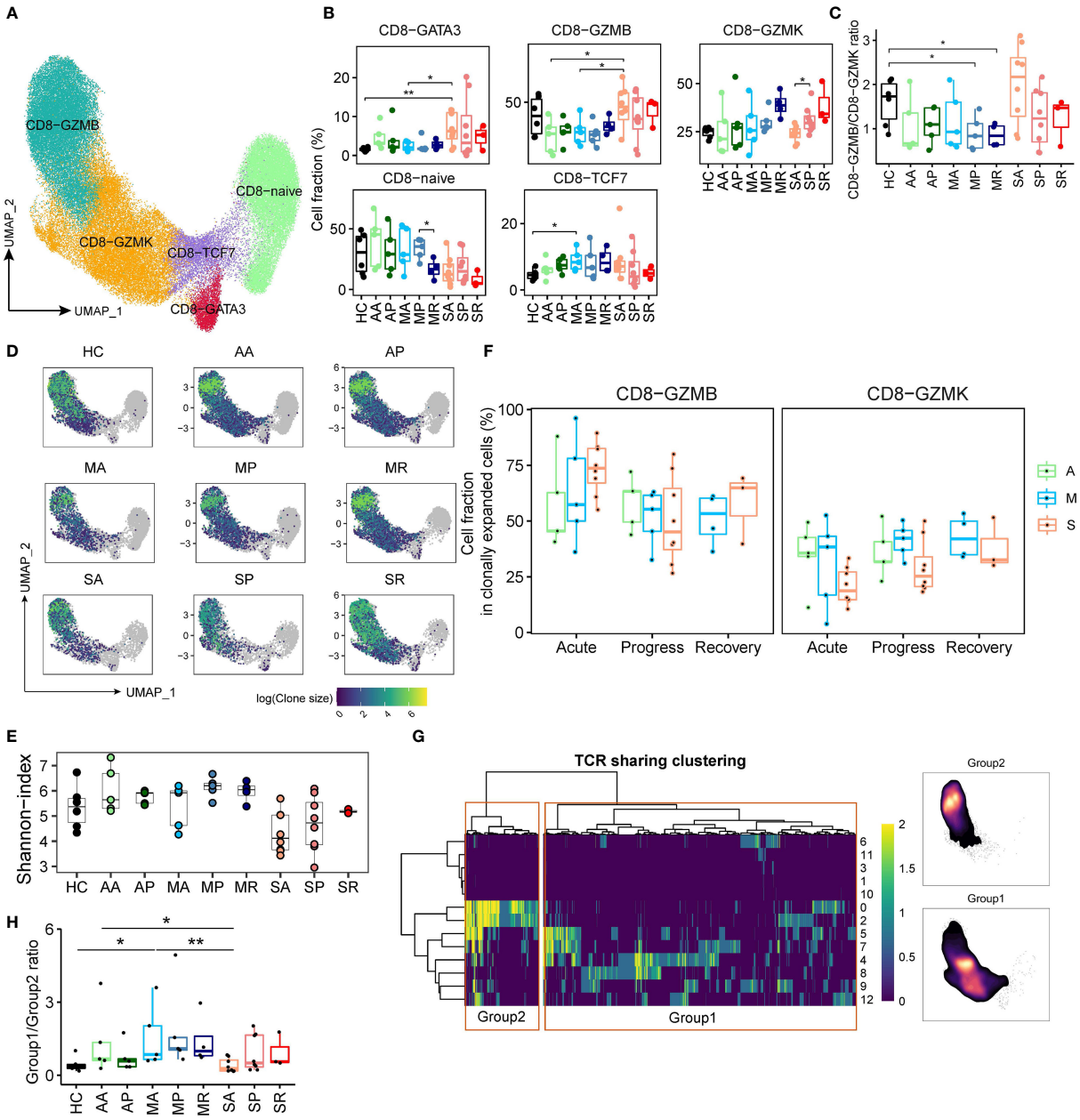

FIGURE 4 | CD8$^+$ T cell compartments respond differently in patients with severe COVID-19 versus those with non-severe diseases. **(A)** UMAP plot of the peripheral CD8$^+$ T cell subsets. **(B)** Proportions of peripheral CD8$^+$ T cell subsets from COVID-19 patients and controls (two-sided Student's t-test, *P < 0.05, **P < 0.01). **(C)** The plot indicates the ratio of CD8-GZMB/CD8-GZMK from each studied group. **(D)** UMAP projection of clonally expanded CD8$^+$ T cells from each studied group. **(E)** Shannon-index of total CD8$^+$ T cell from each studied group. **(F)** The proportions of GZMB-CD8 and GZMK-CD8 subsets within the clonally expanded CD8$^+$ T cell compartments. A, Asymptomatic; M, Mild; S, Severe. **(G)** TCR clustering analysis. Hierarchical clustering of TCRs (columns) based on TCR sharing patterns across CD8$^+$ T subsets (rows). The two distinct groups identified are indicated in left box (group 2) and right box (group 1) (left). UMAP projection of cell density from TCR-group 1 and group 2 CD8$^+$ T cells (Right). **(H)** The ratio of CD8$^+$ T cells containing TCRs from group1 over cells containing TCRs from group 2 among each studied group (*P < 0.05, **P < 0.01).

Next, we studied cycling CD8$^+$ T cells and traced clonal status using the single-cell TCR (sc-TCR) data. Consistent with viral infection triggering immune response, the frequencies of cycling immune cells, and cycling CD4$^+$ and CD8$^+$ T cells were increased among COVID-19 patients compared to controls (**Figures 2B** and **S4H**). Then, we utilized UMAP projection to overview the TCR status, and confirmed that clonally expanded populations were mainly composed of CD8-GZMB and CD8-GZMK subsets (**Figures 4D** and **S4I, J**). Using the Shannon-index to reflect diversity, we found that patients with severe COVID-19

compared to those of other groups had lower levels of TCR diversity (**Figure 4E**). Moreover, within the clonally expanded $CD8^+$ T cell compartment, a similar discordance of CD8-GZMK and CD8-GZMB subset was observed in COVID-19 patients. We found that increased proportion of clonally expanded CD8-GZMK seems to closely correlate with successful control of the SARS-CoV-2 infections, as early increase of CD8-GZMK in asymptomatic (AA/34.6% and AP/35.9%) and mildly ill (MA/31.0%, MP/41.3%, and MR/42.9%) cases, versus delayed increase of CD8-GZMK in severely ill patients (SA/20.8%, SP/29.4%, and SR/38.1%) (**Figures 4F** and **S4J**), indicating clonally expanded CD8-GZMK may play a role in viral clearance. Moreover, the percentage of CD8-GZMK cells sharing TCRs between sequential samples were higher in AA-AP and MA-MP transition than that in SA-SP (**Figure S4K**), also supporting that the clonally expanded the anti-viral CD8-GZMK population was established earlier in asymptomatic and mild cases than in severe cases.

Furthermore, integrating the scTCR-seq and scRNA-seq datasets using hierarchical clustering revealed one set of TCRs (group 1) with the cytotoxic phenotype and another set of TCRs (group 2) within the memory phenotype (**Figure 4G**). The proportions of group 1 and group 2 $CD8^+$ T cells were varied among COVID-19 groups (**Figure S4L**), with higher percentage of group 1 cells in patients with severe COVID-19. The ratio of group 1/group 2 from SA is significantly lower than that from the AA and MA (**Figure 4H**), suggesting that the dominance of group 1 $CD8^+$ T cells at the early stage of infection was associated with worse outcomes. Thus, our data suggest that the CD8-GZMK subset, as the group 2 $CD8^+$ T cell equivalent, likely contains the majority of virus-responding T cells, and helps determine COVID-19 outcomes.

Peripheral $CD4^+$ T Cell Compartments and the Development of Severe or Non-Severe COVID-19

We identified eight subpopulations of $CD4^+$ T cells, namely, CD4-Naïve (*SELL*), Tfh-like (CD4-ICOS), Th1-like (CD4-GZMK), Th2-like (CD4-*GATA3*), Th17-like (CD4-*CCR6*), Treg-SELL and Treg-CTLA4 (*FOXP3*), cytotoxic phenotype (CD4-*GZMB*) (**Figures 5A** and **S5A**). Density UMAP plots revealed the increase of non-Naive cells as one obvious perturbation of peripheral $CD4^+$ T compartments by the COVID-19 (**Figure S5B**). Notably, the percentage of Treg-CTLA4 cells increased significantly in most COVID-19 groups over controls, but the proportions of other $CD4^+$ T cell subsets did not change significantly (**Figure 5B**). Among COVID-19 patients, we observed the trend of increased Treg-CTLA4 and CD4-GZMB, and decreased CD4-Naïve and CD4-GZMK in severe over non-severe groups (**Figures 5B** and **S5C, D**). The signature of T follicular helper (Tfh) (*IL21* in the CD4-ICOS cluster) and the signature of Th17 (*IL22* in the CD4-CCR6 cluster) tend to increase in SP patients, reflecting a dysregulated immune firing, while the polarization of the response of other T helper cells was not obvious (**Figure S5E**). Except for CD4-GZMB, the remaining $CD4^+$ T cell subsets manifested lower levels of clonal expansion (**Figures 5C** and **S5C, D**). The severe COVID-19 patients had the lowest diversity of $CD4^+$ T cell clonotypes among all studied groups (**Figure 5D**). Within the clonally expanded $CD4^+$ T cell compartment, we observed overall decreased CD4-GZMB and increased Th1-, Th2-, Th17-, and cycling $CD4^+$ T cell proportions from COVID-19 patients versus controls (**Figures S5F, G**). Notably, excluding CD4-GMZB, the Th1-like CD4-GZMK subset dominated in the expanded $CD4^+$ T cell compartment in non-severe COVID-19 cases, but only represented a minor subset in severe cases (**Figures 5E** and **S5D**), indicating a discordant $CD4^+$ T cell responses likely underlying the development of severe COVID-19. Moreover, percentage of TCR-sharing Th1-like (CD4-GZMK) cells between sequential samples were higher in AA-AP and MA-MP transition than that in SA-SP (**Figure S5H**), also supporting that clonally expanded CD4-GZMK cells were established earlier in non-severe cases, and likely played an important role in viral clearance.

Next, we integrated the scTCR-seq and scRNA-seq datasets of $CD4^+$ T cells by hierarchical clustering and revealed one set of TCRs (group 1) showing the mix phenotype including the Th1-, Th2-, and Th17 subset and a group 2 within the cytotoxic phenotype (**Figure 5F**). Except that group 1 $CD4^+$ T cells were enriched in SR, there was very little $CD4^+$ T cell clonal expansion in the remaining 8 groups (**Figure S5I**). The ratio of group 1 and group 2 was also very small in 9 groups, making it hard to tell any differences (**Figure 5G**).

Characterization of B Cell Subsets in COVID-19 Patients

B cells were subclustered into three subsets by canonical markers, NAMELY, naïve B cells (*TCL1A*), memory B cells (MBC) (*CD27*) and Antibody secreting cells (ASC) (*MZB1*) (**Figures 6A** and **S6A**). Density UMAP plots clearly show that the proportion of ASCs from COVID-19 patients increases from the acute to the progressive infection stage, then subsides during the recovery stage (**Figure S6B**). We also found significantly decreased percentages of MBC in SA and SP compared to controls (**Figures 6B** and **S6C, D**). Since the proportion of ASC in patient S2 is abnormally high due to the presence of one massively expanded clone (**Figures S6E, F**), we excluded data from S2 in the following analysis.

Next, we analyzed scBCR-seq data. Notably, ASC in COVID-19 patients were more clonally expanded, consistent with the increased frequency of this population in the response to infection, whereas other B cells were non-expanded (**Figures 6C, D**). Compared to controls, asymptomatic and mildly ill patients, severely sick COVID-19 patients showed lower BCR diversity (**Figure 6E**). We examined proportions of each immunoglobulin (Ig) heavy chain isotypes within the different B cell subsets (**Figure 6F**). Indeed, naive B cells contained only IgD/IgM, while memory B cells and ASCs contained class-switched isotypes, namely, IgA and IgG. IgM presents a major fraction in naïve and memory B cells from all studied groups, while the IgG1 and IgA1 accounts for the majority of Ig isotypes in ASC. Consistent with reports showing IgG1 as the major responding Ig isotype during SARS-CoV-2 infection, the proportion of IgG1 isotype in ASC is increased among COVID-19 patients (**Figure 6F**).

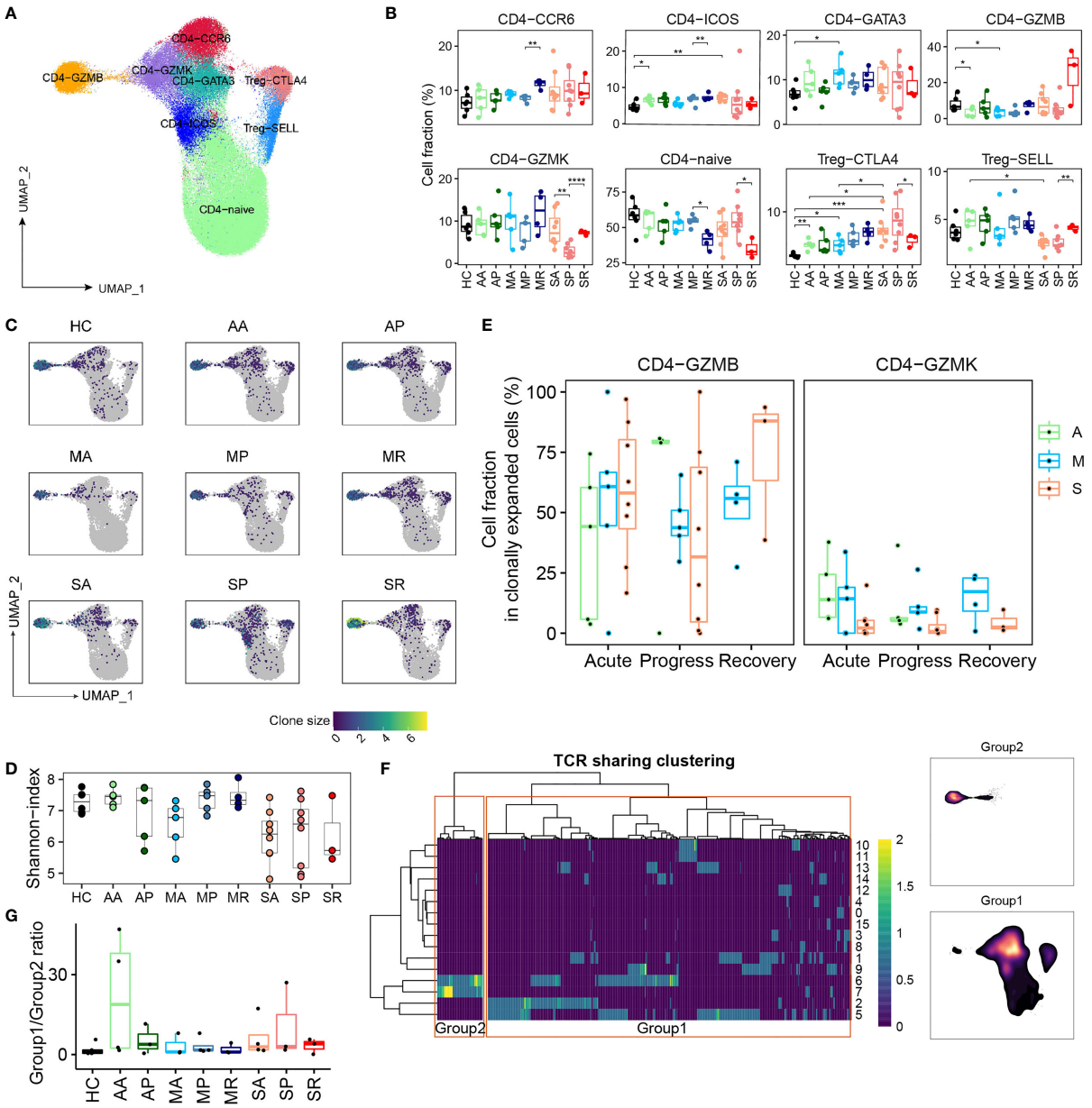

FIGURE 5 | The peripheral CD4$^+$ T cell compartment and its association with COVID-19 severity. **(A)** UMAP plot of the peripheral CD4$^+$ T cell subsets. **(B)** Proportions of peripheral CD4$^+$ T cell subsets from each studied group (two-sided Student's t-test, *P <0.05, **P <0.01, ***p <0.001, ****P <0.0001). **(C)** UMAP plot of clonally expanded CD4$^+$ T cells from each studied group. **(D)** The Shannon-index of total CD4$^+$ T cells from each studied group. **(E)** The proportions of GZMB-CD4 and GZMK-CD4 subsets within the clonally expanded CD4$^+$ T cell compartments. A, Asymptomatic; M, Mild; S, Severe. **(F)** TCR clustering analysis. Hierarchical clustering of TCRs (columns) based on TCR sharing patterns across CD4$^+$ T subsets (rows). The two distinct groups identified are indicated in left box (group 2) and right box (group 1) (left). UMAP projection of cell density from TCR-group 1 and group 2 CD4$^+$ T cells (right). **(G)** The ratio of CD4$^+$ T cells containing TCRs from group 1 over cells containing TCRs from group 2 among each studied group.

We observed significantly enriched IgM-IgA1, IgM-IgG1, and IgM-IgG2 events in most patients, especially in asymptomatic and mildly ill patients (**Figure 6G**). Previous studies have shown that SARS-CoV-2 targeting antibodies exhibit limited somatic hypermutation (SHM) (27). Since ASC is the antibody-producing population and more clonally expanded, we evaluated their SHM levels among each Ig isotypes. Indeed, SHM levels were higher in class-switched isotypes (both IgAs and IgGs) than non-class-switched IgM isotype (**Figure 6H**). However, we observed lower levels of SHM (even germline without SHM) in ASCs from COVID-19 patients, especially in the IgG1 isotype. Interestingly, the timing of germline IgG1 ASCs

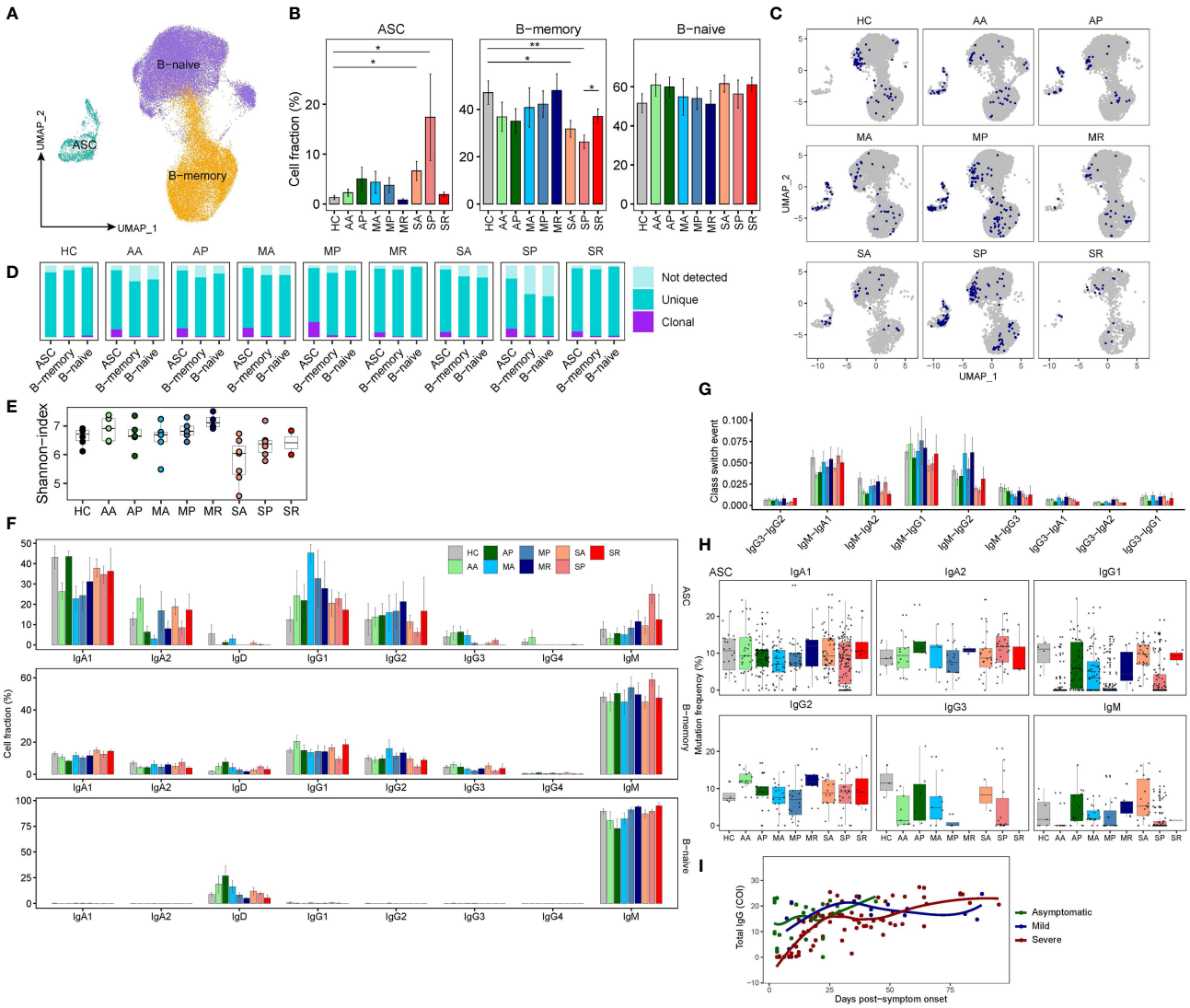

FIGURE 6 | The peripheral B cell heterogeneity and its association with COVID-19 severity. **(A)** UMAP plot peripheral B cell subsets. **(B)** Proportions of peripheral B cell subsets from each studied group (two-sided Student's t-test, *P <0.05, **P <0.01). **(C)** UMAP plot of clonally expanded B cells from each studied group. **(D)** Bar plots show the levels of clonal expansion within each B cell subsets from each studied group. **(E)** The Shannon-index of total B cells from each studied group. **(F)** Bar plots showing the proportions of cells with corresponding Ig isotypes within three B cell subsets from each studied group. **(G)** Bar plots show the class-switched ratio between different Ig isotypes across nine groups. **(H)** Bar plots show the frequency of somatic mutations of ASC with different Ig isotypes across nine groups. **(I)** The scatter plot shows the dynamics of RBD antibodies in the plasma of those 18 patients.

emergence differed in asymptomatic, mildly ill patients and severely sick patients. Those unusual ASCs, likely the virus responding ones, emerged earlier in AA and MA, and emerged later in SP. Similar trends were also present in IgG3 and IgM isotype (**Figure 6H**). We suspect that our data reveal a delayed antibody response in patients destined to become severely ill. Indeed, we found higher levels of serum SARS-CoV-2-Spike-RBD (Receptor binding domain on Spike protein)-specific antibodies in the blood of AA and MA compared to SA patients (**Figure 6I**), and made similar observations on a larger cohort of 506 COVID-19 patients (28). Thus, although many reports showed higher levels SARS-CoV-2 antibodies in patients with severe COVID-19 than those in mild COVID-19 (29), the humoral immune defense may actually be initiated earlier in patients with mild disease.

DISCUSSION

For severe COVID-19, the entire clinical course is dynamic and includes asymptomatic, symptomatic, ARDS and recovery phases (1). Thus, patients with severe COVID-19 would manifest very different symptoms, and very likely distinct immune responses at those different stages of the infection or

diseases. Understanding the pathogenic mechanisms in the deterioration and recovery of severe COVID-19 will require a complete monitoring the entire dynamic immune responses.

Many efforts have been attempted to dissect the heterogeneous immune responses in patients with different clinical manifestations, namely, multiple studies using high-throughput single-cell approaches (30–33). However, most of these previous reported datasets which investigated cross-sectional samples collected at peak level severity or convalescence. As a result, there is a lack of datasets for longitudinal samples collected from an earlier stage of infection. So far, little is known about the early immunological events that could affect the development of severe versus asymptomatic/mild diseases. In addition, previous immune investigations comparing samples collected at unsynchronized clinical phases could lead to inconsistent conclusions (18, 19). In contrast, we provide a valuable scRNA-seq analysis of peripheral immune cells in patients infected with SARS-CoV-2, covering longitudinal specimens of COVID-19 patients with asymptomatic, mild, and severe diseases collected shortly after the symptom onset. Indeed, our data reveal a highly dynamic immune landscape particularly in severe COVID-19, matching with the different stages (Acute, Progression, and Recovery) of clinical courses, whereas the composition of immune cellular compartment in patients with asymptomatic/mild COVID-19 is rather stable. Particularly, the data that we describe here provide a useful resource for precisely deciphering the early immunological events preceding the worsen or resolution of SARS-CoV-2 induced disease.

IFN response is the first line of host innate immune defense against viral infection. We and others have previously reported that IFN response is impaired in patients with severe COVID-19 based on cross-sectional samples (10, 24). But here, we were surprised to find that severe patients had a transient strong IFN response before the disease deterioration, but then dropped rapidly. While the mild patients have a weak but stable interferon response throughout the disease. High concentrations of IFN in plasma of SA patients are most likely stimulated by viral infections. SARS-CoV-2 infection can induce strong IFN production and is positively correlated with viral load (23). In the absence of animal models that can mimic severe COVID-19, it is difficult to determine whether IFNs serve a protective or a detrimental function in COVID-19. There are some studies reporting the pathological role of IFN during severe coronavirus infections (7, 34, 35). Hospitalized COVID-19 patients with high levels of pulmonary ISGs died significantly earlier than those with low levels of ISGs in a transcriptomic study of the lung samples (35). Another study found that IFN played inflammatory roles by recruiting more immune cells to the lungs (34). It has been reported that IFN disrupt lung epithelial repair and the pulmonary epithelial barrier upon viral recognition (36, 37). In addition, IFN can disrupt the urea cycle, reducing arginine levels and thus dampening the T cell functions (38). Arginine in plasma in patients with severe COVID-19 is indeed lower than in mild cases (39). Based on these data, we propose that a strong early transient IFN response may aggravate the progression of COVID-19, by impairing T-cell responses.

Regarding protective anti-viral adaptive immune components, $CD8^+$ T cells are a unique immune cell population that could precisely and efficiently clear virus-infected host cells. Although SARS-CoV-2 reacting T cells responses were detected in COVID-19 patients (14, 40–42), and their roles in determining disease severity are postulated, so far, their roles have not been definitively defined. Here, our data revealed that the $CD8^+$ T cell likely played a crucial role in controlling SARS-CoV-2 infection, especially in the early stages of infection. We found the lack of early induction of $CD8^+$ T cell responses as a prominent feature of severe COVID-19. In agreement with other recent reports (13, 43), this impaired induction of $CD8^+$ T cell responses in severe COVID-19 was likely a result of decreased numbers of naive $CD8^+$ T cells. This could also explain why old age is an important risk factor for development of severe COVID-19. Old adults are known to have a lower number of naive $CD8^+$ T cells, and therefore they are less likely to be effective responders to handle new viral pathogens.

In addition, our data demonstrated the importance of humoral immune defense in SARS-CoV-2 infection. Interestingly, sequencing the BCR repertoire showed that the early recruitment of B cells with low SHMs signatures was associated with seroconversion of SARS-CoV-2 IgG (44). It was later reported that antibodies against the SARS-CoV-2 spike protein receptor binding domain (RBD) are primarily mediated by the near-germline IgG1 antibodies with low levels of SHMs (27). Thus, the appearance of low SHM IgG1 sequences in ASCs observed in this study, likely indicates the antibody response to SARS-CoV-2 RBD. Importantly, both the low SHM IgG1 signature and RBD antibodies occurred later in patients with severe COVID-19, suggesting delayed engagement of effective humoral immunity as another predictor for onset of severe disease. This is consistent with recent studies showing delayed neutralizing antibodies correlate with fatal COVID-19 (45, 46).

In conclusion, we provided convincing evidence that the early immunological events, namely, abnormal strong interferon response, delayed $CD8^+$ T-cell engagement, and humoral immune responses, may determine the subsequent progression of severe COVID-19. Additionally, we provide a number of early prognostic markers for the onset of severe COVID-19, such as $CD14^+/CD16^+$ monocytes ratio, $CD4^+/CD8^+$T cell ratio, $GZMK^+/GZMB^+$ T cell ratio, etc., although these parameters require further validation in the larger cohorts.

MATERIALS AND METHODS

Patients

Ethics statement: This study was conducted according to the ethical principles of the Declaration of Helsinki. Ethical approval was obtained from the Research Ethics Committee of Shenzhen Third People's Hospital (2020-242).

All participants provided written informed consent for sample collection and subsequent analyses. Eighteen COVID-19 patients were enrolled at the Shenzhen Third People's Hospital for scRNA-seq study. Samples from metadata and patients were collected similarly as

previously described: The severity of COVID-19 was categorized to be mild, moderate, severe and critical according to the "Diagnosis and Treatment Protocol of COVID-19 (the 7th Tentative Version)" by the National Health Commission of China (http://www.nhc.gov.cn/yzygj/s7653p/202003/46c9294a7dfe4cef80dc7f5912eb1989.shtml). In this study, we grouped patients with mild and moderate COVID-19 as the mild group, and included those with severe and critical diseases as the severe group. Asymptomatic patients have no clinical symptoms such as cough or fever within 1–2 weeks from a positive nucleic acid test to negative. Six healthy subjects were enrolled as the control group.

Blood Samples Process

Approximately 5–10 ml of fresh blood is separated into plasma after centrifugation, which will be used for cytokine detection later. The remaining cells underwent Ficoll–Hypaque density gradient centrifugation to obtain PBMC, which can be used for single cell sequencing.

Cytokines Measurement by MSD

Plasma from 10 severe patients, 9 mild patients, and 11 asymptomatic patients was used for cytokine measurement. Twelve healthy subjects were enrolled as the control group. IFNγ, IFN-α2a, and IL-29/IFN-λ1 were detected according to the instruction (MESO SCALE DISCOVERY, K15067L-1). In brief, 25 ul samples or standards were incubated in antibody coupled plate at room temperature for 1h, detection antibodies were added for 1 h after washing by PBST. Finally, MSD GOLDTM Read Buffer B was added to read the results.

Detection of Plasma Antibodies

The plasma of 18 patients in the acute phase in this study were collected, and chemiluminescence kit (Beijing Wantai Biotech) in the Caris200 automatic chemiluminescence instrument was used to detect the level of IgG antibody against SARS-CoV-2-Spike-RBD. The relative fluorescence of sample to control (COI) was used to estimate the result. The results ≥1 COI are reactive (positive), and the results <1 COI are nonreactive (negative).

ScRNA-Seq Library Construction

ScRNA-seq libraries were prepared according to previous protocols. In brief, the recovered PBMC were counted in 0.4% trypan blued, centrifuged and re-suspended at the concentration of 2×10^6/ml. The cell suspension was loaded onto a Chromium single cell controller (10× Genomics) to generate single-cell gel beads in the emulsion (GEMs) according to the manufacturer's protocol. Reverse transcription takes place inside each GEM, after which cDNAs are pooled together for amplification and library construction. The resulting library products consist of Illumina adapters and sample indices, allowing pooling and sequencing of multiple libraries on the next-generation short read sequencer.

Single Cell Filtering, Clustering, Dimension Reduction, and Visualization

We aligned the sequenced reads against GRCh38 human reference genome by Cell Ranger (version 3.1.0, 10× genomics). The raw count matrix (UMI counts per gene per cell) was processed by Seurat (v3.2.2) (47). Cells with less than 200 and more than 6,000 expressed genes, less than 1,000 UMI and higher than 15% mitochondrial genome transcript were removed. Genes expressed in less than 3 cells were removed.

Data integration, cell clustering and dimension reduction were performed by Seurat (v3.2.2). First, the gene expression matrix were normalized using the "NormalizeData" function with default settings. The sources of cell–cell variation driven by batch were regressed out using the number of detected UMI and mitochondrial gene expression, which were implemented using the "ScaleData" function. The top 2,000 highly variable genes (HVGs) were used for the following analysis using "FindVariableFeatures" function. Next, we integrated different samples by "IntegrateData" function, which eliminates technical or batch effect by canonical correlation analysis (CCA). Using those HVGs, we calculate a PCA matrix with the top 50 components by "RunPCA" function. The cells were then clustered by "FindClusters" function after building nearest neighbor graph using "FindNeighbors" function. The parameter resolution was set to 0.4 to identify cell types in all cell populations. The cluster-specific marker genes were identified by "FindMarkers" function using MAST algorithm (v1.15.0). The clustered cells were then projected into a two-dimension space for visualization by a non-linear dimensional reduction method "RunUMAP" in Seurat package.

Integrated Analysis of Peripheral Myeloid, $CD4^+$ T, $CD8^+$ T, Innate T and B Cells

We re-clustered the peripheral myeloid, $CD4^+$ T, $CD8^+$ T, innate T, and B cells using the top 20 dimensions of PCA with the parameter resolution of 0.6, 1.3, 1.3, 0.8, and 1.3 respectively. The myeloid compartment, namely, mDCs and monocytes was re-clustered using cells annotated with monocyte and mDCs in **Figure 2**. The $CD4^+$ T and $CD8^+$ T cells were re-clustered using cells annotated with $CD4^+$ and $CD8^+$ T cells in **Figure S2**. The B cell subsets were re-clustered using B cells annotated in **Figure 2**. The re-clustered cells were annotated by canonical markers.

Differentially Expressed Gene and Gene Enrichment Analysis

The "FindMarkers" function in Seurat with MAST algorithm (v1.15.0) (48) was used to analyze DEGs. For each pairwise comparison, the "FindMarkers" function was run with the parameters of test.use = 'MAST'. Genes were defined as significantly upregulated if the average natural logarithm fold change (logFC) was >0.25 and adjusted P-value was <0.01. The genes with logFC <−0.25 and adjusted P <0.01 were considered significantly downregulated. We performed GO term enrichment analysis for the significantly upregulated and downregulated genes using clusterProfiler (v3.17.3) (49) package in R (v4.0.2). GO term of Biological Process (BP) was displayed.

Principal Component Analysis of All Samples

The principal component analysis of all samples in **Figure 1** was calculated using the average expression level of the top 4,000

HVGs across all cells in each sample utilizing "prcomp" method in R (v4.0.2).

Calculation of Immune Signature Scores

Immune signature scores in scRNA-seq data were calculated using the AddModuleScore function in the Seurat package. IFN response scores were calculated using *ADAR, APOBEC3, BST2, CD74, MB21D1, DDIT4, DDX58, DDX60, EIF2AK2, GBP1, GBP2, HPSE, IFI44L, IFI6, IFIH1, IFIT1, IRF1, IRF7, ISG15, ISG20, MAP3K14, MOV10, MS4A4A, MX1, MX2, NAMPT, NT5C3, OAS1, OAS2, OAS3, OASL, P2RY6, PHF15, PML, RSAD2, RTP4, SLC15A3, SLC25A28, SSBP3, TREX1, TRIM5, TRIM25, SUN2, ZC3HAV1, IFITM1, IFITM2*, and *IFITM3*. The MHC class II score was calculated using *HLA-DMA, HLA-DMB, HLA-DPA1, HLA-DPB1, HLA-DQA1, HLA-DQB1, HLA-DRA, HLA-DRB1*, and *HLA-DRB5*. The alarmin score was calculated using *S100A1, S100A2, S100A3, S100A4, S100A5, S100A6, S100A7, S100A7A, S100A7L2, S100A7P1, S100A7P2, S100A8, S100A9, S100A10, S100A11, S100A12, S100A13, S100A14, S100A15A, S100A16, S100B, S100G, S100P*, and *S100Z*. "Monocyte composite scores" were calculated according to the MHC-II score minus alarmin score. The cytotoxicity score was calculated using *PRF1, IFNG, GNLY, NKG7, GZMB, GZMA, GZMH, KLRK1, KLRB1, KLRD1, CTSW*, and *CST7*.

The ISGs score, MHC II score and alarmin score in a sample with bulk RNA-seq data were calculated as the geometric mean of the normalized log2-transformed expression of the genes above separately.

Estimation of Cell Composition in Bulk RNA-Seq Data

We used MarkerBasedDecomposition function in Bisque, a semi-supervised model that extracts trends in cellular composition from normalized bulk expression samples, to deduce cell type abundance using only cell-specific marker genes: CD79A, CD19, MS4A1 marked B cells. CD79A and IGKC marked PCs. CD3D, CD4 and GZMB marked CD4-GZMB. CD3D, CD4 and GZMK marked CD4-GZMK. CD3D, CD4 and FOXP3 marked CD4-Treg. CD3D, CD8A and GZMB marked CD8-GZMB. CD3D, CD8A and GZMK marked CD8-GZMK. FCN1 and CD14 marked mono-CD14+. FCN1 and FCGR3A marked mono-CD16+.

Single-Cell TCR and BCR Analysis

The amino acid and nucleotide sequence of TCR/BCR chains were assembled and annotated by cellranger vdj function in CellRanger (version 3.1.0). For TCR, only cells with paired TCRα and TCRβ chains were included in clonotype analysis. Cells sharing the same TCRα- and TCRβ-CDR3 amino acid sequences were assigned to the same TCR clonotype. For the BCR, only cells with at least one productive heavy chain (IGH) and one productive light chain (IGK or IGL) were kept for further analysis. Cells sharing the same V/J gene and the same IGH- and IGK/IGL-CDR3 amino acid was defined as a clonotype. The TCR clonotypes and the BCR clonotypes were integrated into transcriptome object using barcode information. Shannon index (TCR/BCR diversity) of each sample was calculated using "diversity" function in vegan package (v2.5.6) (https://github.com/vegandevs/vegan) in R. For each BCR, we calculated their similarity to the germline genes using the V gene on heavy chain utilizing IgBlast (v1.15.0) (50). The SHM was deduced using the difference between 1 and the above calculated similarity.

TCR sharing clustering analysis. Referring to the methods from a recent report (19), we constructed a TCR matrix of $CD4^+$ and $CD8^+$ T cells with cell cluster as rows and unique TCRs as columns with the number of cells with a given TCR in a certain cluster as values. Only the TCRs present in at least two clusters were kept for further analysis. The TCR matric were transformed *via* log1p transformation (formula = ln (value + 1)) and values were clipped at 2 (any value greater than 2 was set to 2). Both TCRs and cell clusters were subject to hierarchal clustering with the method set to "ward" using "pheatmap" function in R.

RT-qPCR

All studies involving SARS-CoV-2 infection were conducted in the biosafety level-3 (BLS-3) laboratory of Shenzhen Third People's Hospital. Lung epithelial cells Calu3 were infected with SARS-CoV-2 at 1 MOI for 24 and 48 h. Total RNA was extracted with TRIzolTM Reagent in accordance with the manufacturer's instructions and reverse-transcribed into cDNA with a High-Capacity cDNA Reverse Transcription Kit (Takara, RR036A). The expression levels of indicated RNA were determined by RT-qPCR analysis using Power SYBR Green PCR Master Mix (Vazyme, Q311-02). Primers used in RT-qPCR reactions are listed in **Table S4**.

Statistics

The Student's t-test (t-test in R, two-sided, unadjusted for multiple comparisons) was used for pairwise comparisons of the cell proportions between different groups. The Pearson correlation coefficient between clinical index and WOS was evaluated utilizing the corr.test function in R (v4.0.2). The silhouette coefficient was calculated using the following formula:

$$\frac{b_i - a_i}{\max\{a_i, b_i\}}$$

Where, a_i indicates the mean of euclidean distance from cell i to all other cells that belong to the cell type. b_i indicates the mean of euclidean distance from cell i to all other cells that is nearest to the cell type of i.

DATA AVAILABILITY STATEMENT

The raw data reported in this paper have been deposited in the Genome Sequence Archive in National Genomics Data Center, Beijing Institute of Genomics, Chinese Academy of Sciences under accession number(s) HRA000628 that are publicly accessible at http://bigd.big.ac.cn/gsa-human.

AUTHOR CONTRIBUTIONS

This study was conceived and designed by SZ and ZZ. GX conducted the major experiments. Bioinformatics analysis was

performed by FQ and YaL. HW, YuL, XW, RZ, JY, and XL contributed some experimental data. The manuscript was written by ZZ, GX, SZ, and FQ. All authors contributed to the article and approved the submitted version.

FUNDING

This study was supported by the National Science Fund for Distinguished Young Scholars (82025022), the Central Charity Fund of Chinese Academy of Medical Science (2020-PT310-009), the Shenzhen Bay Funding (2020B1111340075), the China National Natural Science Youth Foundation (82101857), the Guangdong Provincial Department of Science and Technology (2019A1515011072) and the Shenzhen Science and Technology Innovation Committee (KQTD20200909113758004). The funders had no role in study design, data collection, data analysis, data interpretation, or writing of the report.

ACKNOWLEDGMENTS

We thank professor Stanley Perlman (University of Iowa) for help with discussion and writing. We acknowledge the work and contribution of all the health providers from Shenzhen Third People's Hospital. We also thank patients for their active participation.

SUPPLEMENTARY MATERIAL

The Supplementary Material for this article can be found online at: https://www.frontiersin.org/articles/10.3389/fimmu.2021.816745/full#supplementary-material

REFERENCES

1. Guan WJ, Ni ZY, Hu Y, Liang WH, Ou CQ, He JX, et al. Clinical Characteristics of Coronavirus Disease 2019 in China. *N Engl J Med* (2020) 382:1708–20. doi: 10.1056/NEJMoa2002032
2. Schulte-Schrepping J, Reusch N, Paclik D, Bassler K, Schlickeiser S, Zhang B, et al. Severe COVID-19 Is Marked by a Dysregulated Myeloid Cell Compartment. *Cell* (2020) 182:1419–40.e1423. doi: 10.1016/j.cell.2020.08.001
3. Silvin A, Chapuis N, Dunsmore G, Goubet AG, Dubuisson A, Derosa L, et al. Elevated Calprotectin and Abnormal Myeloid Cell Subsets Discriminate Severe From Mild COVID-19. *Cell* (2020) 182:1401–18.e1418. doi: 10.1016/j.cell.2020.08.002
4. Kuri-Cervantes L, Pampena MB, Meng W, Rosenfeld AM, Ittner CAG, Weisman AR, et al. Comprehensive Mapping of Immune Perturbations Associated With Severe COVID-19. *Sci Immunol* (2020) 5(49):eabd7114. doi: 10.1126/sciimmunol.abd7114
5. Leisman DE, Ronner L, Pinotti R, Taylor MD, Sinha P, Calfee CS, et al. Cytokine Elevation in Severe and Critical COVID-19: A Rapid Systematic Review, Meta-Analysis, and Comparison With Other Inflammatory Syndromes. *Lancet Respir Med* (2020) 8:1233–44. doi: 10.1016/S2213-2600(20)30404-5
6. Remy KE, Mazer M, Striker DA, Ellebedy AH, Walton AH, Unsinger J, et al. Severe Immunosuppression and Not a Cytokine Storm Characterizes COVID-19 Infections. *JCI Insight* (2020) 5(17):e140329. doi: 10.1172/jci.insight.140329
7. Channappanavar R, Fehr AR, Vijay R, Mack M, Zhao J, Meyerholz DK, et al. Dysregulated Type I Interferon and Inflammatory Monocyte-Macrophage Responses Cause Lethal Pneumonia in SARS-CoV-Infected Mice. *Cell Host Microbe* (2016) 19:181–93. doi: 10.1016/j.chom.2016.01.007
8. Zhao J, Zhao J, Perlman S. T Cell Responses are Required for Protection From Clinical Disease and for Virus Clearance in Severe Acute Respiratory Syndrome Coronavirus-Infected Mice. *J Virol* (2010) 84:9318–25. doi: 10.1128/JVI.01049-10
9. Liu L, Wei Q, Lin Q, Fang J, Wang H, Kwok H, et al. Anti-Spike IgG Causes Severe Acute Lung Injury by Skewing Macrophage Responses During Acute SARS-CoV Infection. *JCI Insight* (2019) 4(4):e123158. doi: 10.1172/jci.insight.123158
10. Hadjadj J, Yatim N, Barnabei L, Corneau A, Boussier J, Smith N, et al. Impaired Type I Interferon Activity and Inflammatory Responses in Severe COVID-19 Patients. *Science* (2020) 369:718–24. doi: 10.1126/science.abc6027
11. Lucas C, Wong P, Klein J, Castro TBR, Silva J, Sundaram M, et al. Longitudinal Analyses Reveal Immunological Misfiring in Severe COVID-19. *Nature* (2020) 584:463–9. doi: 10.1038/s41586-020-2588-y
12. Kaneko N, Kuo HH, Boucau J, Farmer JR, Allard-Chamard H, Mahajan VS, et al. Loss of Bcl-6-Expressing T Follicular Helper Cells and Germinal Centers in COVID-19. *Cell* (2020) 183:143–157 e113. doi: 10.1016/j.cell.2020.08.025
13. Rydyznski Moderbacher C, Ramirez SI, Dan JM, Grifoni A, Hastie KM, Weiskopf D, et al. Antigen-Specific Adaptive Immunity to SARS-CoV-2 in Acute COVID-19 and Associations With Age and Disease Severity. *Cell* (2020) 183:996–1012.e1019. doi: 10.1016/j.cell.2020.09.038
14. Sekine T, Perez-Potti A, Rivera-Ballesteros O, Stralin K, Gorin JB, Olsson A, et al. Robust T Cell Immunity in Convalescent Individuals With Asymptomatic or Mild COVID-19. *Cell* (2020) 183:158–168 e114. doi: 10.1016/j.cell.2020.08.017
15. Wu F, Liu M, Wang A, Lu L, Wang Q, Gu C, et al. Evaluating the Association of Clinical Characteristics With Neutralizing Antibody Levels in Patients Who Have Recovered From Mild COVID-19 in Shanghai, China. *JAMA Intern Med* (2020) 180:1356–62. doi: 10.1001/jamainternmed.2020.4616
16. Zhou F, Yu T, Du R, Fan G, Liu Y, Liu Z, et al. Clinical Course and Risk Factors for Mortality of Adult Inpatients With COVID-19 in Wuhan, China: A Retrospective Cohort Study. *Lancet* (2020) 395:1054–62. doi: 10.1016/S0140-6736(20)30566-3
17. Bernardes JP, Mishra N, Tran F, Bahmer T, Best L, Blase JI, et al. Longitudinal Multi-Omics Analyses Identify Responses of Megakaryocytes, Erythroid Cells, and Plasmablasts as Hallmarks of Severe COVID-19. *Immunity* (2020) 53:1296–314.e1299. doi: 10.1016/j.immuni.2020.11.017
18. Mathew D, Giles JR, Baxter AE, Oldridge DA, Greenplate AR, Wu JE, et al. Deep Immune Profiling of COVID-19 Patients Reveals Distinct Immunotypes With Therapeutic Implications. *Science* (2020) 369(6508):eabc8511.
19. Su Y, Chen D, Yuan D, Lausted C, Choi J, Dai CL, et al. Multi-Omics Resolves a Sharp Disease-State Shift Between Mild and Moderate COVID-19. *Cell* (2020) 183:1479–95.e1420. doi: 10.1016/j.cell.2020.10.037
20. Combes AJ, Courau T, Kuhn NF, Hu KH, Ray A, Chen WS, et al. Global Absence and Targeting of Protective Immune States in Severe COVID-19. *Nature* (2021) 591(7848):124–30. doi: 10.1038/s41586-021-03234-7
21. Bergamaschi L, Mescia F, Turner L, Hanson AL, Kotagiri P, Dunmore BJ, et al. Longitudinal Analysis Reveals That Delayed Bystander CD8+ T Cell Activation and Early Immune Pathology Distinguish Severe COVID-19 From Mild Disease. *Immunity* (2021) 54:1257–75.e1258. doi: 10.1016/j.immuni.2021.05.010
22. Jew B, Alvarez M, Rahmani E, Miao Z, Ko A, Garske KM, et al. Accurate Estimation of Cell Composition in Bulk Expression Through Robust Integration of Single-Cell Information. *Nat Commun* (2020) 11:1971. doi: 10.1038/s41467-020-15816-6
23. Lieberman N, Peddu V, Xie H, Shrestha L, Huang ML, Mears MC, et al. In Vivo Antiviral Host Transcriptional Response to SARS-CoV-2 by Viral Load, Sex, and Age. *PloS Biol* (2020) 18:e3000849. doi: 10.1371/journal.pbio.3000849
24. Xu G, Qi F, Li H, Yang Q, Wang H, Wang X, et al. The Differential Immune Responses to COVID-19 in Peripheral and Lung Revealed by Single-Cell RNA Sequencing. *Cell Discovery* (2020) 6:73. doi: 10.1038/s41421-020-00225-2
25. Jouan Y, Guillon A, Gonzalez L, Perez Y, Boisseau C, Ehrmann S, et al. Phenotypical and Functional Alteration of Unconventional T Cells in Severe

COVID-19 Patients. *J Exp Med* (2020) 217(12):e20200872. doi: 10.1084/jem.20200872
26. Medsger TAJr., Ivanco DE, Kardava L, Morel PA, Lucas MR, Fuschiotti P. GATA-3 Up-Regulation in CD8+ T Cells as a Biomarker of Immune Dysfunction in Systemic Sclerosis, Resulting in Excessive Interleukin-13 Production. *Arthritis Rheum* (2011) 63:1738–47. doi: 10.1002/art.30489
27. Kreer C, Zehner M, Weber T, Ercanoglu MS, Gieselmann L, Rohde C, et al. Longitudinal Isolation of Potent Near-Germline SARS-CoV-2-Neutralizing Antibodies From COVID-19 Patients. *Cell* (2020) 182:1663–73. doi: 10.1016/j.cell.2020.08.046
28. Yu S, An J, Liao X, Wang H, Ma F, Li D, et al. Distinct Kinetics of Immunoglobulin Isotypes Reveal Early Diagnosis and Disease Severity of COVID-19: A 6-Month Follow-Up. *Clin Trans Med* (2021) 11:e342. doi: 10.1002/ctm2.342
29. Liu A, Li Y, Wan Z, Wang W, Lei X, Lv Y. Seropositive Prevalence of Antibodies Against SARS-CoV-2 in Wuhan, China. *JAMA Netw Open* (2020) 3:e2025717. doi: 10.1001/jamanetworkopen.2020.25717
30. Liao M, Liu Y, Yuan J, Wen Y, Xu G, Zhao J, et al. Single-Cell Landscape of Bronchoalveolar Immune Cells in Patients With COVID-19. *Nat Med* (2020) 26:842–4. doi: 10.1038/s41591-020-0901-9
31. Wen W, Su W, Tang H, Le W, Zhang X, Zheng Y, et al. Immune Cell Profiling of COVID-19 Patients in the Recovery Stage by Single-Cell Sequencing. *Cell Discovery* (2020) 6:31. doi: 10.1038/s41421-020-0168-9
32. Wilk AJ, Rustagi A, Zhao NQ, Roque J, Martinez-Colon GJ, Mckechnie JL, et al. A Single-Cell Atlas of the Peripheral Immune Response in Patients With Severe COVID-19. *Nat Med* (2020) 26:1070–6. doi: 10.1038/s41591-020-0944-y
33. Zhang JY, Wang XM, Xing X, Xu Z, Zhang C, Song JW, et al. Single-Cell Landscape of Immunological Responses in Patients With COVID-19. *Nat Immunol* (2020) 21:1107–18. doi: 10.1038/s41590-020-0762-x
34. Israelow B, Song E, Mao T, Lu P, Meir A, Liu F, et al. Mouse Model of SARS-CoV-2 Reveals Inflammatory Role of Type I Interferon Signaling. *J Exp Med* (2020) 217(12):e20201241. doi: 10.1084/jem.20201241
35. Nienhold R, Ciani Y, Koelzer VH, Tzankov A, Haslbauer JD, Menter T, et al. Two Distinct Immunopathological Profiles in Autopsy Lungs of COVID-19. *Nat Commun* (2020) 11:5086. doi: 10.1038/s41467-020-18854-2
36. Broggi A, Ghosh S, Sposito B, Spreafico R, Balzarini F, Lo Cascio A, et al. Type III Interferons Disrupt the Lung Epithelial Barrier Upon Viral Recognition. *Science* (2020) 369:706–12. doi: 10.1126/science.abc3545
37. Major J, Crotta S, Llorian M, Mccabe TM, Gad HH, Priestnall SL, et al. Type I and III Interferons Disrupt Lung Epithelial Repair During Recovery From Viral Infection. *Science* (2020) 369:712–7. doi: 10.1126/science.abc2061
38. Lercher A, Bhattacharya A, Popa AM, Caldera M, Schlapansky MF, Baazim H, et al. Type I Interferon Signaling Disrupts the Hepatic Urea Cycle and Alters Systemic Metabolism to Suppress T Cell Function. *Immunity* (2019) 51:1074–87.e1079. doi: 10.1016/j.immuni.2019.10.014
39. Shen B, Yi X, Sun Y, Bi X, Du J, Zhang C, et al. Proteomic and Metabolomic Characterization of COVID-19 Patient Sera. *Cell* (2020) 182:59–72 e15. doi: 10.1016/j.cell.2020.05.032
40. Ni L, Ye F, Cheng ML, Feng Y, Deng YQ, Zhao H, et al. Detection of SARS-CoV-2-Specific Humoral and Cellular Immunity in COVID-19 Convalescent Individuals. *Immunity* (2020) 52:971–7.e973. doi: 10.1016/j.immuni.2020.04.023
41. Weiskopf D, Schmitz KS, Raadsen MP, Grifoni A, Okba NMA, Endeman H, et al. Phenotype and Kinetics of SARS-CoV-2-Specific T Cells in COVID-19 Patients With Acute Respiratory Distress Syndrome. *Sci Immunol* (2020) 5 (48):eabd2071. doi: 10.1126/sciimmunol.abd2071
42. Rha MS, Jeong HW, Ko JH, Choi SJ, Seo IH, Lee JS, et al. PD-1-Expressing SARS-CoV-2-Specific CD8(+) T Cells Are Not Exhausted, But Functional in Patients With COVID-19. *Immunity* (2021) 54:44–52.e43. doi: 10.1016/j.immuni.2020.12.002
43. Ni L, Cheng ML, Feng Y, Zhao H, Liu J, Ye F, et al. Impaired Cellular Immunity to SARS-CoV-2 in Severe COVID-19 Patients. *Front Immunol* (2021) 12:603563. doi: 10.3389/fimmu.2021.603563
44. Nielsen SCA, Yang F, Jackson KJL, Hoh RA, Roltgen K, Jean GH, et al. Human B Cell Clonal Expansion and Convergent Antibody Responses to SARS-CoV-2. *Cell Host Microbe* (2020) 28:516–25.e515. doi: 10.1016/j.chom.2020.09.002
45. Dispinseri S, Secchi M, Pirillo MF, Tolazzi M, Borghi M, Brigatti C, et al. Neutralizing Antibody Responses to SARS-CoV-2 in Symptomatic COVID-19 is Persistent and Critical for Survival. *Nat Commun* (2021) 12:2670. doi: 10.1038/s41467-021-22958-8
46. Lucas C, Klein J, Sundaram ME, Liu F, Wong P, Silva J, et al. Delayed Production of Neutralizing Antibodies Correlates With Fatal COVID-19. *Nat Med* (2021) 27(7):1178–86. doi: 10.1038/s41591-021-01355-0
47. Stuart T, Butler A, Hoffman P, Hafemeister C, Papalexi E, Mauck WM3rd, et al. Comprehensive Integration of Single-Cell Data. *Cell* (2019) 177:1888–902.e1821. doi: 10.1016/j.cell.2019.05.031
48. Finak G, Mcdavid A, Yajima M, Deng J, Gersuk V, Shalek AK, et al. MAST: A Flexible Statistical Framework for Assessing Transcriptional Changes and Characterizing Heterogeneity in Single-Cell RNA Sequencing Data. *Genome Biol* (2015) 16:278. doi: 10.1186/s13059-015-0844-5
49. Yu G, Wang LG, Han Y, He QY. Clusterprofiler: An R Package for Comparing Biological Themes Among Gene Clusters. *OMICS* (2012) 16:284–7. doi: 10.1089/omi.2011.0118
50. Ye J, Ma N, Madden TL, Ostell JM. IgBLAST: An Immunoglobulin Variable Domain Sequence Analysis Tool. *Nucleic Acids Res* (2013) 41:W34–40. doi: 10.1093/nar/gkt382

Conflict of Interest: The authors declare that the research was conducted in the absence of any commercial or financial relationships that could be construed as a potential conflict of interest.

Publisher's Note: All claims expressed in this article are solely those of the authors and do not necessarily represent those of their affiliated organizations, or those of the publisher, the editors and the reviewers. Any product that may be evaluated in this article, or claim that may be made by its manufacturer, is not guaranteed or endorsed by the publisher.

frontiers in Immunology

ORIGINAL RESEARCH
published: 24 January 2022
doi: 10.3389/fimmu.2021.830527

Omicron: A Heavily Mutated SARS-CoV-2 Variant Exhibits Stronger Binding to ACE2 and Potently Escapes Approved COVID-19 Therapeutic Antibodies

Masaud Shah[1] *and Hyun Goo Woo*[1,2]*

[1] Department of Physiology, Ajou University School of Medicine, Suwon, South Korea, [2] Department of Biomedical Science, Graduate School, Ajou University, Suwon, South Korea

The new SARS-CoV-2 variant of concern "Omicron" was recently spotted in South Africa and spread quickly around the world due to its enhanced transmissibility. The variant became conspicuous as it harbors more than 30 mutations in the Spike protein with 15 mutations in the receptor-binding domain (RBD) alone, potentially dampening the potency of therapeutic antibodies and enhancing the ACE2 binding. More worrying, Omicron infections have been reported in vaccinees in South Africa and Hong Kong, and that post-vaccination sera poorly neutralize the new variant. Here, we investigated the binding strength of Omicron with ACE2 and monoclonal antibodies that are either approved by the FDA for COVID-19 therapy or undergoing phase III clinical trials. Computational mutagenesis and free energy perturbation could confirm that Omicron RBD binds ACE2 ~2.5 times stronger than prototype SARS-CoV-2. Notably, three substitutions, i.e., T478K, Q493K, and Q498R, significantly contribute to the binding energies and almost doubled the electrostatic potential (ELE) of the RBD^{Omic}–ACE2 complex. Omicron also harbors E484A substitution instead of the E484K that helped neutralization escape of Beta, Gamma, and Mu variants. Together, T478K, Q493K, Q498R, and E484A substitutions contribute to a significant drop in the ELE between RBD^{Omic}–mAbs, particularly in etesevimab, bamlanivimab, and CT-p59. AZD1061 showed a slight drop in ELE and sotrovimab that binds a conserved epitope on the RBD; therefore, it could be used as a cocktail therapy in Omicron-driven COVID-19. In conclusion, we suggest that the Spike mutations prudently devised by the virus facilitate the receptor binding, weakening the mAbs binding to escape the immune response.

Keywords: SARS-CoV-2, Omicron, ACE2, antibodies, immune escape, therapeutic

OPEN ACCESS

Edited by:
Tengchuan Jin, University of Science and Technology of China, China

Reviewed by:
Matias Gutiérrez-González, Ragon Institute of MGH, MIT and Harvard, United States
Chengliang Wang, UCONN Health, United States

***Correspondence:**
Hyun Goo Woo
hg@ajou.ac.kr

Specialty section:
This article was submitted to Viral Immunology, a section of the journal Frontiers in Immunology

Received: *07 December 2021*
Accepted: *31 December 2021*
Published: *24 January 2022*

Citation:
Shah M and Woo HG (2022) Omicron: A Heavily Mutated SARS-CoV-2 Variant Exhibits Stronger Binding to ACE2 and Potently Escapes Approved COVID-19 Therapeutic Antibodies. Front. Immunol. 12:830527. doi: 10.3389/fimmu.2021.830527

INTRODUCTION

Since its emergence, severe acute respiratory syndrome coronavirus 2 (SARS-CoV-2) has been found to continuously evolve and raise new variants of concerns (VOCs) to avoid host hostilities, i.e., evade the host immune response, increase transmission, and aggress the pathogenesis of coronavirus disease 2019 (COVID-19). This host adaptation by the virus has been demonstrated by

the rise of VOCs, including Alpha, Beta, Gamma, and Delta variants that weaken the neutralizing efficacy of antibodies (1–4). Most recently, a new strain of the SARS-CoV-2 named Omicron by the World Health Organization has emerged in South Africa (November 24, 2021) and spread worldwide within a short period. Researchers around the globe are racing to determine whether Omicron poses a threat to the immunity induced by the COVID-19 vaccine (5).

Omicron harbors many novel mutations in structural and non-structural proteins, leading to serious concerns over vaccine failure, immune escape (5), and increased transmissibility. More than 32 mutations were found in the Spike protein alone, where 15 of these mutations reside in the receptor-binding domain (RBD), which are vital to both receptor and viral neutralizing antibodies. The non-structural proteins encoded by the ORF1ab contain mutations in the nsp3 (K38R, V1069I, Δ1265, L1266I, A1892T), nsp4 (T492I), nsp5 (P132H), nsp6 (Δ105-107, A189V), nsp12 (P323L), and nsp14 (I42V). Nsp3 (Plpro) and nsp5 (3Clpro, main protease) are proteases that cleave the polypeptide encoded by ORF1a and ORF1ab. 3Clpro and nsp12 [RNA-dependent RNA-polymerase (RdRp)] are primary targets for drugs that block the polypeptide cleaving and viral protein synthesis (6). Using structural models and as confirmed by the preliminary data in a preprint study (7), we found that mutations in nsp5 and nsp12 are not close to the active site and may not hinder the effect of antiviral drugs; nonetheless, these proteins play a vital role in innate immune response (interferon induction), requiring further experimental investigation (6). Omicron also had mutations in the other structural proteins, including Envelope (E) (T9I), Membrane (M) (D3G, Q19E, and A63T), and Nucleocapsid (N) (P13L, Δ31-33, R203K, G204R), further enhancing their infectivity. Since N protein is highly immunogenic (8, 9), these mutations could help escape the host immune response.

In addition, Omicron had multiple mutations in the Spike protein, which are associated with increased infectivity and antibody evasion. Out of 32 mutations, half of them hold the potential to dampen the potency of therapeutic antibodies and enhance the ACE2 binding. Omicron has also been shown to infect triple-vaccinated individuals who have received BNT162b2 jabs (10). Here, we conducted molecular modeling and mutational analyses to delineate how the new variant enhances its transmissibility and escapes against the FDA-approved Spike-neutralizing COVID-19 therapeutic antibodies. Our results may provide new insights into therapeutic management against the infection caused by Omicron.

RESULTS

Mutations in the Omicron RBD Strengthen the Spike–ACE2 Interaction

Omicron is unique among the previously reported SARS-CoV-2 VOCs, showing multiple mutations in Spike and other genes. According to the unrooted phylogenic analysis using the global ~4,000 full-genome SARS-CoV-2 sequences from the Global Initiative on Sharing All Influenza Data (GISAID), Omicron stands distant from other VOCs (**Figure 1A**). A full-length trimeric 3D model was constructed by substituting the respective amino acids of previously reported reference (Wuhan strain, PDB ID: 7VNE) structure into Omicron. There are three deletion sites in the N-terminus domains (NTD) and at least 15 substitutions in the RBD region. Omicron Spike also harbors mutations that were reported in the previous VOCs such as K417, T478, E484, and N501 (**Figure 1B**). Of these, at least 11 mutations are involved in ACE2 binding (**Table 1**), substantially affecting their binding affinity (**Figure 1C**). In addition, Omicron Spike, compared with the prototype SARS-CoV-2, has three deletions, i.e., Δ69-70, Δ143-145, and Δ211, and one highly charged insertion, i.e., ins214EPE at 214 positions.

We monitored the relative binding strength of RBD–ACE2 complexes of both prototype and Omicron strains using a protein design strategy and calculating binding affinity and stability changes in terms of relative change in energies. We observed that the individually substituted residues had a slight effect on the local stability of the RBD–ACE2 complexes (**Figure 2A**). However, by performing endpoint molecular mechanics generalized born surface area (MMGBSA) binding free energy calculation, we could demonstrate a substantial increase in the binding affinity by T478K, Q493K, and Q498R, leading to an overall increase in the binding affinity of the RBD^{Omic} with ACE2 (ΔG^{WT} = −64.65 kcal/mol < ΔG^{Omic} = −83.79 kcal/mol; **Supplementary Figure 1A**). We also investigated the change in electrostatic potential of the RBD^{Omic} relative to that of RBD^{WT} because the five residues in the RBM region of RBD are mutated from the polar to the positively charged residues (i.e., N440K, T478K, Q493K, Q498R, and Y505H). Surprisingly, we could observe that the electrostatic energy of ACE2–RBD^{Omic} was double as that of ACE2–RBD^{WT}, which in turn doubled the polar solvation free energies of the ACE2–RBD^{Omic} (**Supplementary Figure 1A**). Per residues, energy distribution suggests that mutations in RBD^{Omic} directly participate in the binding, enhancing the binding strength of amino acids in the same network (**Supplementary Figure 1B**). To validate our finding, we performed molecular dynamics simulations (MDS) using GROMACS (11) and calculated their binding free energies using the widely acceptable and more authentic molecular mechanics Poisson–Boltzmann surface area (MMPBSA) approach (12). As expected, we observed that RBD^{Omic}, compared with RBD^{WT}, had over 2.5 (BFE = −2,642.5 kJ/mol) times stronger binding affinity toward ACE2 (BFE = −951.9 kJ/mol). In addition, the electrostatic potential of RBD^{Omic} was increased by ~1.5 times due to the polar-to-positive amino acids substitution (**Figure 2B**). In addition, energy perturbation per amino acid could confirm that the four amino acids, i.e., N440K, T478K, Q493K, and Q498R, directly contribute to the change of the total energy and the electrostatic potential, whereas K417N and E484A compensate the energy change (**Figure 2C**). Among 15 substituted amino acids, K417N and Y505H exhibited a slight reduction in binding energy due to the breakage of salt bridges between K417 of the RBD and D30 of ACE2; nonetheless, this breakage was compensated by the salt bridge between E35 of ACE2 and Q493K substitution in RBD^{Omic} (**Figure 2C**, right panel). Although the simulation time was short (20 ns), the root

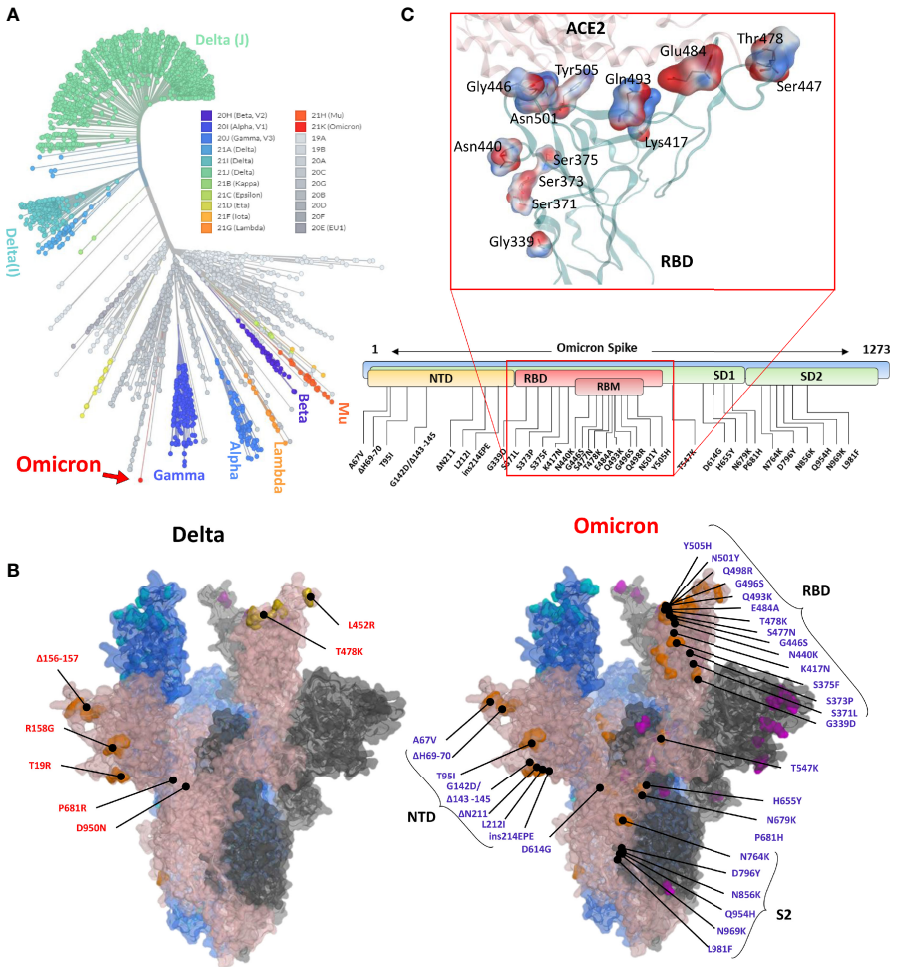

FIGURE 1 | **(A)** Phylogeny of the Omicron and annotation of the mutation in Spike protein. The unrooted phylogenetic tree was constructed from the Nextstrain servers. Wuhan-Hu-1/2019 strains were taken as a reference sequence. **(B)** The full-length Delta and Omicron Spikes were built to annotate the relative (not exact) positions of the mutations on the surface map of Spike. **(C)** The amino acids mutated in the RBD of Omicron are shown concerning the ACE2 interface. Residues are colored according to the electrostatic map of the WT strain. The respective Omicron mutations are depicted in the panel below the RBD surface map.

TABLE 1 | RBD binding interface residues of ACE2 and therapeutic antibodies.

ACE2	CT-p59	Sotrovimab	Etesevimab	Bamlanivimab	AZD1061	AZD8895	Casirivimab	Imdevimab
Lys417	Arg403	Asn334	Arg403	Tyr449	Arg346	**Lys417**	**Lys417**	Arg346
Gly446	Tyr449	Leu335	**Lys417**	Gly482	Lys444	Ala475	Tyr453	Asn440
Glu484	Asn450	Glu340	Asp420	**Glu484**	Tyr449	Gly476	Ser477	Lys444
Asn487	Tyr453	Asn343	Tyr421	Gly485	Asn450	Ser477	**Glu484**	Tyr449
Gln493	**Glu484**	Thr345	Leu455	Phe486	**Glu484**	Thr478	Phe486	**Gln498**
Gly496	Phe486	Arg346	Asn460	**Gln493**		**Asn487**	Tyr489	
Gln498	**Gln493**	Lys356	Tyr473	Ser494		Tyr489	Leu492	
Thr500	Ser494		Ala475	Tyr495		**Gln493**		
Gly502	Tyr505		**Asn487**					
Tyr505			**Gln493**					

Bold residues are shared by ACE2 and mAbs on the RBD interface.

mean square deviation (RMSD) of the RBD proteins was not much different (**Figure 2D**). However, the number of hydrogen bonds between RBD^{WT}–ACE2 showed a transient shift from high (N = ~7.5) to low (N = ~5) to high (N = ~7.5). This effect was not observed in RBD^{Omic}–ACE2, and the hydrogen bond number remained consistent (N = ~7.5) (**Figure 2E**). Taken together, we suggest that Omicron binds ACE2 with greater affinity, partly explaining its increased transmissibility.

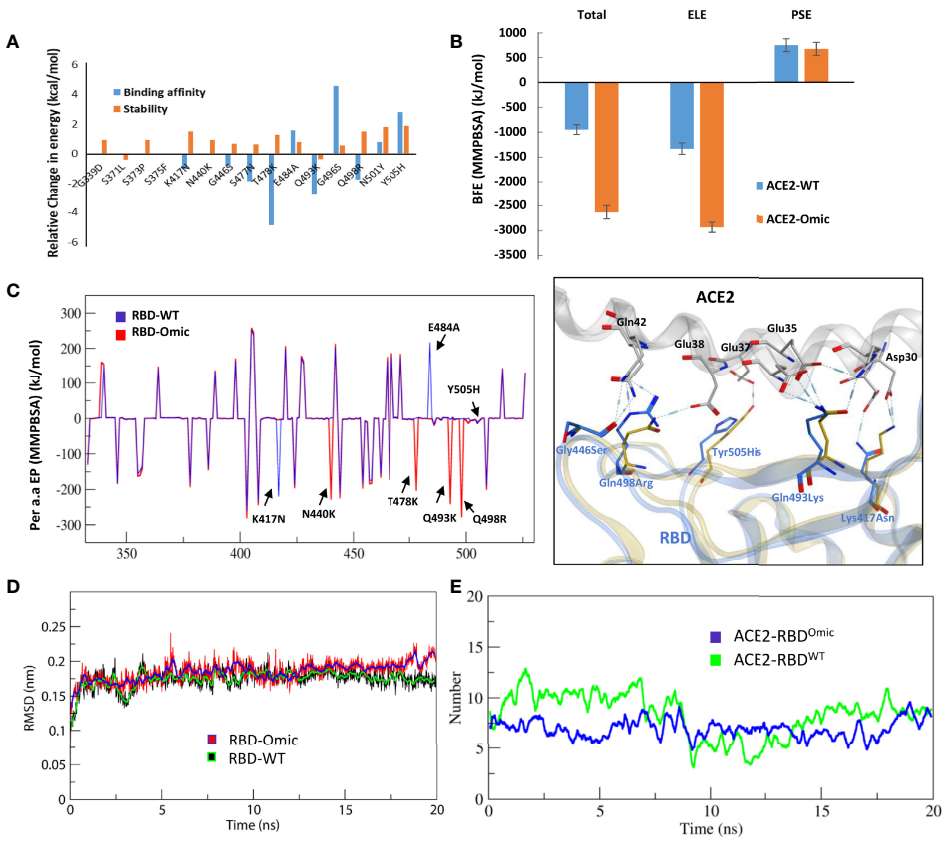

FIGURE 2 | Relative effect of mutations in Omicron RBD on the ACE2 binding. **(A)** Effect of 15 individual mutations on the binding and stability of RBD^{Omic}–ACE2 was monitored relative to that of RBD^{WT}–ACE2. **(B)** The binding free energies (measured through MMPBSA) as consequences of all 15 mutations at once were monitored for both RBD^{Omic}–ACE2 and RBD^{WT}–ACE2. **(C)** Per-residue energy contribution was monitored, and the hotspots of RBD were labeled. The change in the hydrogen bond network of the selected hotspots is shown at the right. **(D, E)** Root mean square deviation and hydrogen bonds at the RBD–ACE2 interface as a function of time are displayed for both RBD^{Omic}–ACE2 and RBD^{WT}–ACE2 complexes.

Mutations in the RBD^{Omic} Deteriorate the Binding of Therapeutic Antibodies and Garble Their Epitopes on RBD

To evaluate whether the mutations that strengthen the RBD^{Omic}–ACE2 interaction affect the RBD-targeting COVID-19 therapeutic antibodies, we constructed structural models of eight monoclonal antibodies (mAbs) bound to RBD^{Omic}. The antibodies like CT-p59, developed by Celltrion from the peripheral blood mononuclear cells (PBMCs) derived from a convalescent plasma of COVID-19 patients, and sotrovimab are used as solo COVID-19 therapeutics undergoing phase III clinical trials (13, 14). The other six mAbs were approved for COVID-19 therapies on an emergency basis (15), which are used as cocktail therapy to tackle the immune escape by the newly acquired mutants (**Figures 3A–D**).

Since mAbs in their respective cocktail therapy regimen do not share overlapping epitopes on the RBD, except etesevimab and bamlanivimab (sponsored by AbCellera) where the light chain variable domains show a slight clash (**Figure 3B** and **Table 1**) and are capable of neutralizing the virus independently, we investigated the change in their interface and binding strength of the mAbs with RBD^{Omic} individually. Remarkably, we found a substantial drop in the total binding energies of bamlanivimab and CT-p59 when bound to RBD^{Omic} (**Figure 3E**). The total binding energy is the sum of the four energies (listed in **Table 2**). We could see that vdW (Van der Waals potentials) and SA (solvation free energy) energies did not affect the binding strength; however, electrostatic potentials (ELE) had a significant shift in the calculated energies. The magnitude of the change in ELE energies was similar to that of RBD^{Omic}–ACE2; however, the effect was opposite, i.e., in RBD^{Omic}–ACE2 ELE energies favor the binding, whereas RBD^{Omic}–mAbs ELE opposed the binding strength (**Supplementary Figure 1C**). All the mAbs showed a significant drop in ELE energies, but AZD1061 (AstraZeneca) showed a slight drop (RBD-AZD1061 = −204.24 kcal/mol > RBD^{Omic}-AZD1061 = −112.35 kcal/mol). To validate the relative change of total binding energies and the shift of the electrostatic potential of RBD^{Omic}–mAbs, we analyzed the MDS of the two complexes (i.e., RBD^{Omic}–etesevimab and RBD^{Omic}–CT-p59) and calculated their BFE using MMPBSA. Interestingly, we found that the change of the electrostatic potential of both complexes

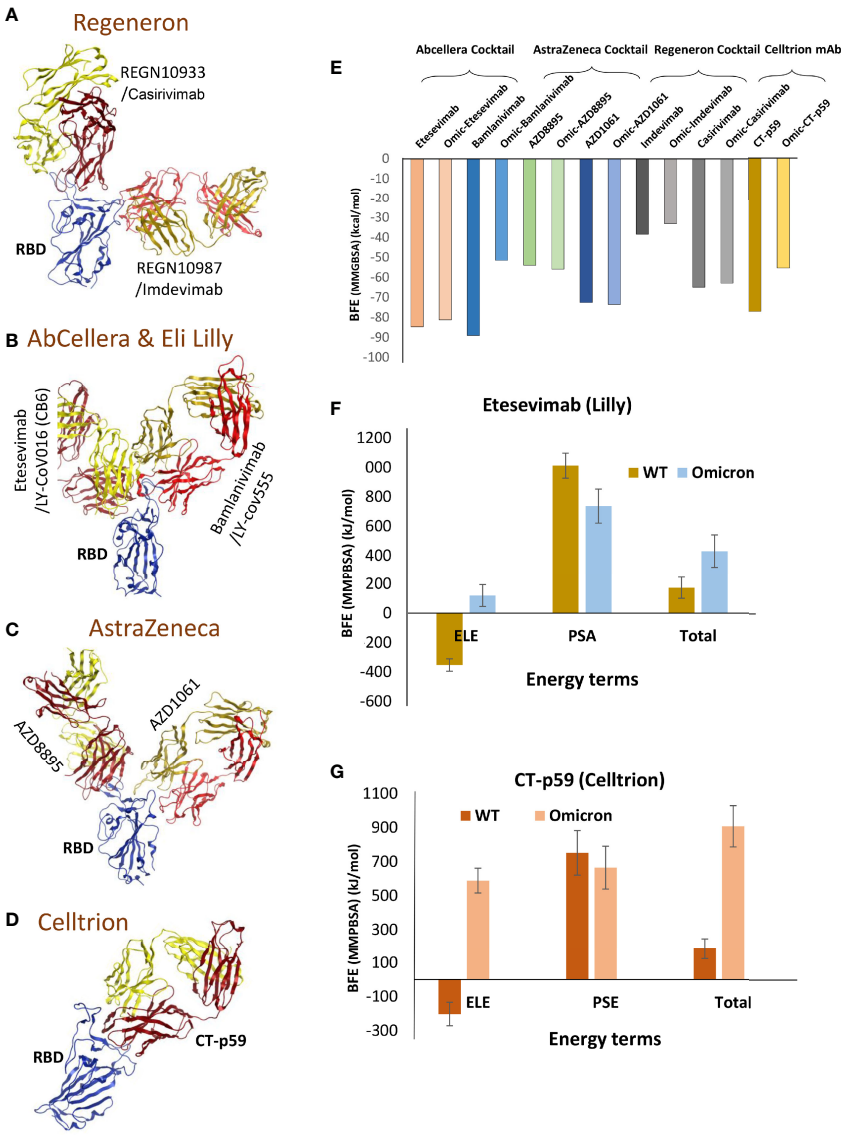

FIGURE 3 | Mutations in the Omicron RBD distort the epitopes of therapeutic mAbs. **(A–D)** Crude epitopes of seven selected mAbs are shown on the RBD. Antibodies used as cocktails are labeled with their sponsors. All variable light chains are colored yellow or orange and variable heavy chains are colored red. **(E)** Changes in the binding affinity of the RBD^{Omic}–mAbs relative to RBD^{WT}–mAbs are shown. The binding energies were calculated through endpoint MMGBSA. **(F)** The binding free energies (measured through MMPBSA) as consequences of all 15 mutations at once were monitored for RBD^{Omic}–etesevimab and RBD^{WT}–etesevimab. **(G)** The binding free energies (measured through MMPBSA) as consequences of all 15 mutations at once were monitored for RBD^{Omic}–CT-p59 and RBD^{WT}–CT-p59.

exhibited a similar trend for both MMGBSA and MMPBSA approaches. The MMPBSA values were calculated as the statistical outcome of 100 frames extracted from the 20-ns MDS trajectory (**Figures 3F, G**). The total binding energies for RBD^{Omic}–mAbs complexes were substantially higher compared with the RBD^{WT}–mAbs, suggesting that Omicron can escape both etesevimab and CT-p59 (regdanvimab) (**Figures 3F, G**).

Next, to evaluate which mutations are mainly involved in weakening the RBD^{Omic}–mAbs interactions, we calculated per amino acid energy perturbation for CT-p59 and bamlanivimab when bound to RBD^{WT} and RBD^{Omic}. We observed that two hotspots, i.e., R96 in CDRL3 and R50 in CDRH2 of bamlanivimab, established highly stable salt bridges with the E484 of RBD^{WT}, losing their binding entirely upon E484A mutation in RBD^{Omic} (**Figure 4A**). In addition, E102 and R104 in CDRH3 showed a 50% reduction in binding energies. Similarly, the hotspots in CDRL1 and CDRH3 lost their bindings due to the mutations of E484A, Q493K, and Y505H in RBD^{Omic}. By contrast, N501Y slightly strengthens the binding, establishing a hydrogen bond with D57 in CDRH2 (**Figure 4B**). Next, we extended our search and used two more SARS-CoV-2 neutralizing antibodies, C102 and C105, isolated from the

TABLE 2 | The binding energies of RBD^{Omic} and RBD^{WT} with seven therapeutic mAbs are listed.

Sponsor	mAbs	VDW	ELE	GB	SA	Total
AbCellera and Eli Lilly	Etesevimab	−131.41	−179.48	243.28	−17.15	−84.76
	Omic-Ete	−147.42	65.04	19.31	−18.16	−81.24
	Bamlanivimab	−95.81	−13.97	33.7	−13.01	−89.1
	Omic-Bam	−108.74	602.59	−532.27	−13.12	−51.54
AstraZeneca	AZD8895	−84.37	−30.35	71.27	−10.46	−53.92
	Omic-Az95	−96.77	76.73	−24.25	−11.62	−55.91
	AZD1061	−94.96	−204.24	238.04	−11.49	−72.64
	Omic-Az61	−98.83	−112.35	149.92	−12.29	−73.55
Regeneron	Imdevimab	−76.1	−27.36	74.73	−9.67	−38.4
	Omic-Imd	−81.32	−5.84	64.23	−10.15	−33.08
	Casirivimab	−103.52	−174.81	228.04	−14.66	−64.94
	Omic-Cas	−113.25	−55.14	119.9	−14.42	−62.91
Celltrion	CT-p59	−105.66	−7.38	49.61	−13.75	−77.18
	Omic-CT-p59	−114.85	352.19	−278.48	−14.27	−55.4

mAbs, monoclonal antibodies; VDW, Van der Waals potentials; ELE, electrostatic potentials; GB, polar solvation potentials (generalized born model); SA, non-polar contribution to the solvation free energy calculated by an empirical model.

convalescent plasma of a single donor for their RBD^{Omic} affinity (16). Both mAbs bind to an overlapping epitope on the RBM and predominantly utilize the heavy chain variable domain (VH) CDRs as main paratopes (**Supplementary Figure 2A**). Like other RBD-binding mAbs, both C102 and C105 exhibited a drastic reduction in binding affinity driven by a significant change in the electrostatic potential (**Supplementary Figures 2B, C**). To investigate how sotrovimab retains its neutralization efficacy, we constructed the RBD^{Omic}–sotrovimab model and found that sotrovimab binds to a highly conserved epitope on the RBD and, among 15 mutations in the RBD^{Omic}, faces only G339D mutation. The retained Omicron neutralization in pseudovirus assay (17) may indicate that the salt bridges between the CDRH3 and RBD may override the clash between RBD^{Omic} D339 and Y100 in CDRH3 that could potently destabilize the RBD^{Omic}–sotrovimab interaction (**Supplementary Figure 2D**). These results suggest that mutations in the Omicron Spike are precisely designed by the virus, facilitating receptor binding but hindering antibody binding simultaneously and that antibodies recognizing conserved epitope on the Spike of SARS-CoV-2 variants could be used as pan-variant therapeutics. Overall, the escape of Omicron from a large pool of antibodies, especially those approved by the FDA after undergoing extensive clinical trials and safety measures, raises serious concerns about the efficacy of therapeutic mAbs in Omicron-infected patients.

DISCUSSION

To this end, it is well known that SARS-CoV-2 is rapidly evolving and makes at least two mutations per month in its genome (18, 19). The virus is capable of adapting to the host environment by increasing transmissibility and evading immune response, as exemplified by the continuous rise of VOCs (20, 21). Although tremendous efforts have been made in vaccine development and COVID-19 therapeutics, including mAbs and COVID-19 pills by Merck, the emergence of VOCs has raised concerns over the efficacy of neutralizing antibodies (21, 22). Even though these variants had a limited number of mutations, they successfully escaped the immune response, at least partly if not entirely. Omicron harbors four or five times more mutations in the Spike protein than other SARS-CoV-2 VOCs and raise more serious concerns (see **Figure 1B**).

We used the previously available structural data of Spike RBD-binding antibodies, Spike itself, and Spike–ACE2 complexes and constructed the mutant Omicron Spike. Omicron Spike contains some of the mutations reported in the previous VOCs. In particular, D614 enhances the receptor binding by increasing its "up" conformation and the overall density of Spike protein at the surface of the virus (23, 24). In addition, five of the amino acids within the RBD region are mutated from polar to positively charged residues (K, R, or H) that paradoxically enhance the receptor binding and weaken the Spike neutralizing interactions (**Figures 2C** and **4**). The RBD mutation has been mapped to predict the neutralization escape from REGN-COV2 (a cocktail of REGN10933 and REGN10987) and LY-CoV016. Such mutations have already been found in patients with persistently infected COVID-19 since late 2020 or early 2021 (25). Single E406W mutation can lead to the viral escape from both antibodies in REGN-COV2, whereas F486K has been reported to escape REGN10933. N440K and K444Q can escape against REGN10987, while K417N, N460T, and A475V can successfully escape against LY-CoV016 antibody (AbCellera), currently approved by the FDA for COVID-19 therapy (25). Unfortunately, Omicron has mutations or amino acids adjacent to those predicted to escape the neutralization of antibodies.

Among the investigated antibodies here, we suggest that AZD1061 may be able to retain Omicron neutralization (**Figure 3E**). During our study, two research groups investigated the neutralization escape of Omicron from the same set of antibodies. They reported consistent results for the mAbs sponsored by Regeneron and AbCellera. Nonetheless, they demonstrated that the Omicron pseudovirus neutralization findings differed in AZD1061 (cilgavimab) and AZD8895 (tixagevimab). In support of our results, Planas et al. have shown that AZD1061 (cilgavimab) and the cocktail (AZD1061 +AZD8895), but not AZD8895 alone, could retain the Omicron pseudovirus neutralization (17).

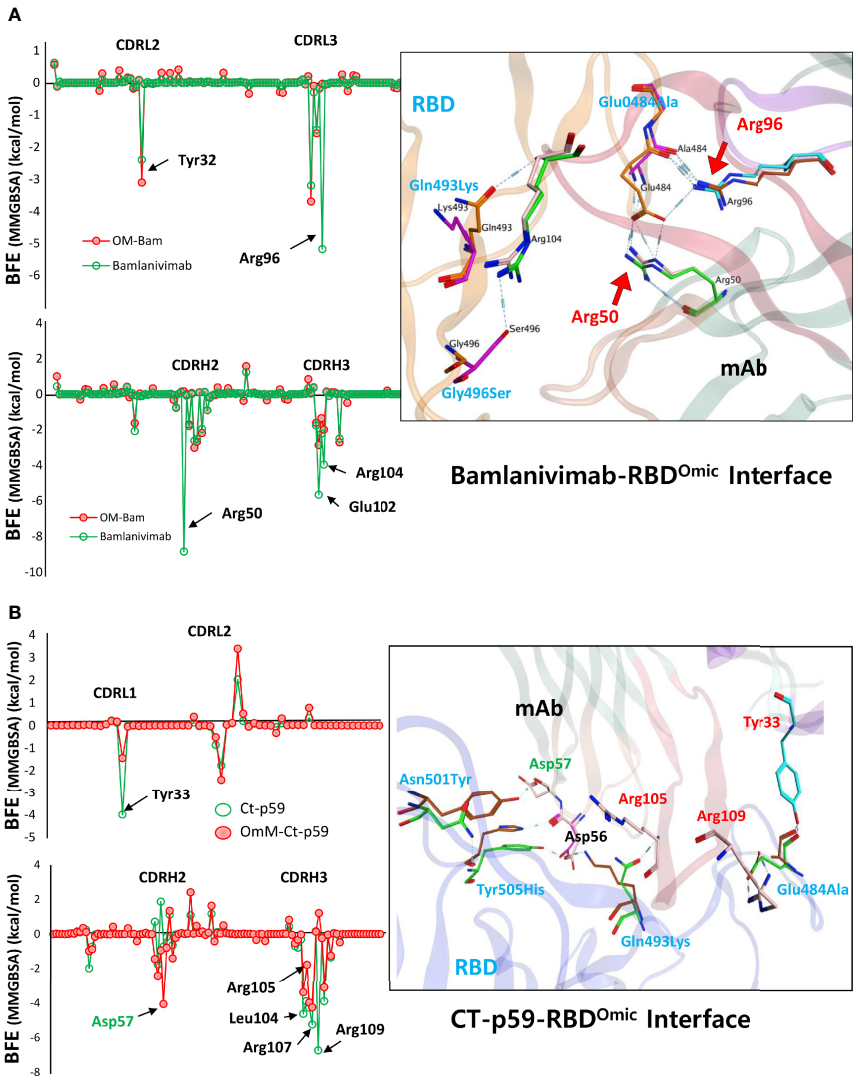

FIGURE 4 | Per-residue changes in the binding affinity of RBD–mAbs were monitored and the hotspots on CDRs of **(A)** bamlanivimab and **(B)** CT-p59 are labeled. The change in the hydrogen bond network of the selected hotspots is shown at the right.

On the other hand, Cao et al. have demonstrated that AZD8895, but not AZD1061, binds Omicron with lower affinity and slightly neutralizes the Omicron pseudovirus at a very higher concentration (26). However, they did not examine the effect of the AZD1061+AZD8895 cocktail on the Omicron. The above studies suggested that sotrovimab (VIR-7831/GSK4182136/S309) holds the promising neutralization efficacy against the Omicron pseudovirus. Thus, we constructed an RBD^{Omic}–sotrovimab model to investigate how sotrovimab retains its neutralization efficacy. Sotrovimab could bind to the highly conserved epitope on the RBD, and among the 15 mutations in the RBD^{Omic}, it faces only G339D mutation.

Although the pathological manifestations are thus far reported to be mild, the threat of Omicron is global, and it is also quite clear that the new variant is more transmissible than Delta. Vaccination has been reported to significantly drop the COVID-19 infection of emerging VOCs, including Delta (27). However, the sera from convalescent subjects infected with different variants of SARS-CoV-2 including Alpha, Beta, Gamma, and Delta and vaccines were found to be ineffective against Omicron. Nonetheless, immunity boosted by the third dose of vaccines or vaccinees infected by the Delta strain has shown effect against Omicron (28). Another study has also reported some preliminary data about the ineffectiveness of vaccines against Omicron. The sera from individuals with the 5-month post-vaccination with Pfizer (29) or AstraZeneca vaccine have failed to inhibit Omicron (30, 31). Similarly, the sera from 6- to 12-month post-infection individuals could not neutralize the new variant. Nevertheless, 5- to 31-fold lower neutralization of Omicron compared with Delta has been

reported by boosters and the previously infected vaccines (17). Thus, Omicron can escape against the therapeutic and vaccine-elicited antibodies. Our study and the preliminary data from other studies consistently suggest that a cocktail of Evusheld (AstraZeneca mAbs) and sotrovimab (GSK, S203 mAb) could effectively neutralize the Omicron.

METHODS

Model Construction and Optimization

For the full-length trimeric Spike, a previously reported PDB ID: 7VNE was used to rebuild the Omicron Spike protein using a Swiss-Model server (32). Other structures used in this study are listed as follows: RBD–ACE2 (PDB ID: 6MOJ), RBD–etesevimab (PDB ID: 7C01), RBD–bamlanivimab (PDB ID: 7KMG), RBD–CT-p59 (PDB ID: 7CM4), RBD–AZD1061 (PDB ID: 7I7E), RBD–AZD8895 (PDB ID: 7I7E), RBD–casirivimab (PDB ID: 6XDG), RBD–imdevimab (PDB ID: 6XDG), and RBD–sotrovimab (PDB ID: 7R6X). For constructing the mutant RBD, free BIOVIA Discovery Studio Visualizer was used (http://www.accelrys.com). All complexes were solvated with TIP3P water cubic box of dimension boundaries extended to 10 Å from protein atoms and neutralized with counter ions, Na^+/Cl^-, wherever needed. The neutralized systems were energy minimized in GROMACS 2019.6 (33) using CHARMM37 force field (34) and steep descent algorithm. For endpoint binding free energy calculations, the HawkDock server was utilized (35).

Molecular Dynamics Simulation

To calculate the binding free energies of RBD^{Omic} with ACE2 and antibodies, we utilized the GROMACS package for the generation of trajectories and the MMPBSA tool for the free energy perturbation. Each system was solvated in a dodecahedron box filled with TIP3P water model and neutralized by adding counter ions (Na^+/Cl^-). The neutralized systems were energy minimized as stated above. Next, a two-step equilibration was set up under constant temperature (NVT) and constant pressure (NPT) of 0.2 ns, and the systems were equilibrated. The temperature and pressure were coupled with v-rescale (modified Berendsen thermostat) and Berendsen, respectively (36). The long-range electrostatic interactions were computed by utilizing the particle mesh Ewald algorithm (37). Each system was simulated for 20 ns with all constrains removed. For the calculation of RMSD and hbonds, MD trajectories were converted by removing the jumps and translational and rotational motions using –pbc nojump and –fit rot+trans flags under the trjconv tool in GROMACS. For MMPBSA, every 20th frame was extracted from a 20-ns trajectory in a separate trajectory.

Binding Free Energy Calculation

The MMPBSA (12) approach is best suited for calculating binding free energies of the ligands bound to the same target. Here, RBD is the main target, whereas mAbs and ACE2 are considered as ligands. GROMACS is equipped with g_mmpbsa tool which was used for the calculation of binding free energies. The topology of each system was generated through the older version of GROMACS (v 5.0) as the MMPBSA package has not been updated by the developer till now. The binding energies were calculated according to the equations described in our previous study (38).

Computational Tools Used in This Project

For protein structure visualization, VMD (39), PyMOL (https://pymol.org), and Chimaera Chimera (40) packages were used. For electrostatic surfaces, isolation of the proteins, APBS and APBSrun plugins in PyMOL and VMD were utilized. The interfaces of RBD^{WT} and RBD^{Omic} with mAbs and ACE2 were analyzed by the online server PDBePISA (v1.52) (41), and the binding contribution of individual amino acids was determined. For endpoint binding free energy calculations, the HawkDock server was utilized (35). The hotspot results were validated through the DrugScorePPI web server (42). The unrooted phylogenetic tree was constructed from the Nextstrain (43) servers using ~4,000 full-length SARS-CoV-2 sequences from the GISAID (44) database with reference to Wuhan-Hu-1/2019 as a reference sequence.

DATA AVAILABILITY STATEMENT

The raw data supporting the conclusions of this article will be made available by the authors, without undue reservation.

AUTHOR CONTRIBUTIONS

MS and HW contributed toward conceptualization of the project and designed the methodology. MS and HW wrote the original manuscript draft. HW supervised the study and provided funding acquisition. All authors contributed to the article and approved the submitted version.

FUNDING

This research was supported by grants from the National Research Foundation of Korea (NRF) funded by the Ministry of Science and ICT (MSIT) (NRF-2017M3C9A6047620, NRF-2019R1A5A2026045, and NRF-2017M3A9B6061509) and grant from the Korea Health Industry Development Institute (KHIDI) funded by the Ministry of Health & Welfare, Republic of Korea (HI21C1003). In addition, this study was also supported by KREONET (Korea Research Environment Open NETwork), which is managed and operated by KISTI (Korea Institute of Science and Technology Information).

ACKNOWLEDGMENTS

A preliminary version of this manuscript has been released as a pre-print at BioRxiv by Shah et al. (45).

SUPPLEMENTARY MATERIAL

The Supplementary Material for this article can be found online at: https://www.frontiersin.org/articles/10.3389/fimmu.2021.830527/full#supplementary-material

REFERENCES

1. Garcia-Beltran WF, Lam EC, St Denis K, Nitido AD, Garcia ZH, Hauser BM, et al. Multiple SARS-CoV-2 Variants Escape Neutralization by Vaccine-Induced Humoral Immunity. *Cell* (2021) 184(9):2523. doi: 10.1016/j.cell.2021.04.006
2. Mlcochova P, Kemp SA, Dhar MS, Papa G, Meng B, Ferreira I, et al. SARS-CoV-2 B.1.617.2 Delta Variant Replication and Immune Evasion. *Nature* (2021) 599(7883):114–9. doi: 10.1038/s41586-021-03944-y
3. Yi C, Sun X, Lin Y, Gu C, Ding L, Lu X, et al. Comprehensive Mapping of Binding Hot Spots of SARS-CoV-2 RBD-Specific Neutralizing Antibodies for Tracking Immune Escape Variants. *Genome Med* (2021) 13(1):164. doi: 10.1186/s13073-021-00985-w
4. Planas D, Veyer D, Baidaliuk A, Staropoli I, Guivel-Benhassine F, Rajah MM, et al. Reduced Sensitivity of SARS-CoV-2 Variant Delta to Antibody Neutralization. *Nature* (2021) 596(7871):276–80. doi: 10.1038/s41586-021-03777-9
5. Callaway E. Heavily Mutated Omicron Variant Puts Scientists on Alert. *Nature* (2021). doi: 10.1038/d41586-021-03552-w
6. Shah M, Woo HG. Molecular Perspectives of SARS-CoV-2: Pathology, Immune Evasion, and Therapeutic Interventions. *Mol Cells* (2021) 44 (6):408–21. doi: 10.14348/molcells.2021.0026
7. Meng B, Ferreira IATM, Abdullahi A, Saito A, Kimura I, Yamasoba D, et al. SARS-CoV-2 Omicron Spike Mediated Immune Escape, Infectivity and Cell-Cell Fusion. *bioRxiv [Preprint]* (2021). doi: 10.1101/2021.12.17.473248
8. Mu J, Fang Y, Yang Q, Shu T, Wang A, Huang M, et al. SARS-CoV-2 N Protein Antagonizes Type I Interferon Signaling by Suppressing Phosphorylation and Nuclear Translocation of STAT1 and STAT2. *Cell Discov* (2020) 6:65. doi: 10.1038/s41421-020-00208-3
9. Dobano C, Santano R, Jimenez A, Vidal M, Chi J, Rodrigo Melero N, et al. Immunogenicity and Crossreactivity of Antibodies to the Nucleocapsid Protein of SARS-CoV-2: Utility and Limitations in Seroprevalence and Immunity Studies. *Transl Res* (2021) 232:60–74. doi: 10.1016/j.trsl.2021.02.006
10. Helmsdal G, Hansen OK, Møller LF, Christiansen DH, Petersen MS, Kristiansen MF. Omicron Outbreak at a Private Gathering in the Faroe Islands, Infecting 21 of 33 Triple-Vaccinated Healthcare Workers. *medRxiv* (2021). doi: 10.1101/2021.12.22.21268021
11. Pronk S, Pall S, Schulz R, Larsson P, Bjelkmar P, Apostolov R, et al. GROMACS 4.5: A High-Throughput and Highly Parallel Open Source Molecular Simulation Toolkit. *Bioinformatics* (2013) 29(7):845–54. doi: 10.1093/bioinformatics/btt055
12. Kumari R, Kumar R. Open Source Drug Discovery C, Lynn A. G_Mmpbsa–a GROMACS Tool for High-Throughput MM-PBSA Calculations. *J Chem Inf Model* (2014) 54(7):1951–62. doi: 10.1021/ci500020m
13. Kim JY, Jang YR, Hong JH, Jung JG, Park JH, Streinu-Cercel A, et al. Safety, Virologic Efficacy, and Pharmacokinetics of CT-P59, a Neutralizing Monoclonal Antibody Against SARS-CoV-2 Spike Receptor-Binding Protein: Two Randomized, Placebo-Controlled, Phase I Studies in Healthy Individuals and Patients With Mild SARS-CoV-2 Infection. *Clin Ther* (2021) 43(10):1706–27. doi: 10.1016/j.clinthera.2021.08.009
14. Gupta A, Gonzalez-Rojas Y, Juarez E, Crespo Casal M, Moya J, Falci DR, et al. Early Treatment for Covid-19 With SARS-CoV-2 Neutralizing Antibody Sotrovimab. *N Engl J Med* (2021) 385(21):1941–50. doi: 10.1056/NEJMoa2107934
15. Taylor PC, Adams AC, Hufford MM, de la Torre I, Winthrop K, Gottlieb RL. Neutralizing Monoclonal Antibodies for Treatment of COVID-19. *Nat Rev Immunol* (2021) 21(6):382–93. doi: 10.1038/s41577-021-00542-x
16. Chen EC, Gilchuk P, Zost SJ, Suryadevara N, Winkler ES, Cabel CR, et al. Convergent Antibody Responses to the SARS-CoV-2 Spike Protein in Convalescent and Vaccinated Individuals. *Cell Rep* (2021) 36(8):109604. doi: 10.1016/j.celrep.2021.109604
17. Planas D, Saunders N, Maes P, Guivel-Benhassine F, Planchais C, Buchrieser J, et al. Considerable Escape of SARS-CoV-2 Variant Omicron to Antibody Neutralization. *bioRxiv [Preprint]* (2021). doi: 10.1101/2021.12.14.472630
18. Duchene S, Featherstone L, Haritopoulou-Sinanidou M, Rambaut A, Lemey P, Baele G. Temporal Signal and the Phylodynamic Threshold of SARS-CoV-2. *Virus Evol* (2020) 6(2):veaa061. doi: 10.1093/ve/veaa061
19. Worobey M, Pekar J, Larsen BB, Nelson MI, Hill V, Joy JB, et al. The Emergence of SARS-CoV-2 in Europe and North America. *Science* (2020) 370 (6516):564–70. doi: 10.1126/science.abc8169
20. Harvey WT, Carabelli AM, Jackson B, Gupta RK, Thomson EC, Harrison EM, et al. SARS-CoV-2 Variants, Spike Mutations and Immune Escape. *Nat Rev Microbiol* (2021) 19(7):409–24. doi: 10.1038/s41579-021-00573-0
21. Krause PR, Fleming TR, Longini IM, Peto R, Briand S, Heymann DL, et al. SARS-CoV-2 Variants and Vaccines. *N Engl J Med* (2021) 385(2):179–86. doi: 10.1056/NEJMsr2105280
22. Kemp SA, Collier DA, Datir RP, et al. SARS-CoV-2 Evolution During Treatment of Chronic Infection. *Nature* (2021) 592:277–82. doi: 10.1038/s41586-021-03291-y
23. Mansbach RA, Chakraborty S, Nguyen K, Montefiori D, Korber B, Gnanakaran S. The SARS-CoV-2 Spike Variant D614G Favors an Open Conformational State. *Sci Adv* (2020) 7(16):eabf3671. doi: 10.1126/sciadv.abf3671
24. Zhang L, Jackson CB, Mou H, Ojha A, Rangarajan ES, Izard T, et al. SARS-CoV-2 Spike-Protein D614G Mutation Increases Virion Spike Density and Infectivity. *Nat Commun* (2020) 11(1):6013. doi: 10.1038/s41467-020-19808-4
25. Starr TN, Greaney AJ, Addetia A, Hannon WW, Choudhary MC, Dingens AS, et al. Prospective Mapping of Viral Mutations That Escape Antibodies Used to Treat COVID-19. *Science* (2021) 371(6531):850–4. doi: 10.1126/science.abf9302
26. Cao Y, Wang J, Jian F, Xiao T, Song W, Yisimayi A, et al. Omicron Escapes the Majority of Existing SARS-CoV-2 Neutralizing Antibodies. *bioRxiv [Preprint]* (2021). doi: 10.1101/2021.12.07.470392
27. Tartof SY, Slezak JM, Fischer H, Hong V, Ackerson BK, Ranasinghe ON, et al. Effectiveness of mRNA BNT162b2 COVID-19 Vaccine Up to 6 Months in a Large Integrated Health System in the USA: A Retrospective Cohort Study. *Lancet* (2021) 398(10309):1407–16. doi: 10.1016/S0140-6736(21)02183-8
28. Dejnirattisai W, Huo J, Zhou D, Zahradník J, Supasa P, Liu C, et al. Omicron-B.1.1.529 Leads to Widespread Escape From Neutralizing Antibody Responses. *bioRxiv [Preprint]* (2021). doi: 10.1101/2021.12.03.471045
29. Cele S, Jackson L, Khoury DS, Khan K, Moyo-Gwete T, Tegally H, et al. SARS-CoV-2 Omicron has Extensive But Incomplete Escape of Pfizer BNT162b2 Elicited Neutralization and Requires ACE2 for Infection. *medRxiv [Preprint]* (2021). doi: 10.1101/2021.12.08.21267417
30. Wilhelm A, Widera M, Grikscheit K, Toptan T, Schenk B, Pallas C, et al. Reduced Neutralization of SARS-CoV-2 Omicron Variant by Vaccine Sera and Monoclonal Antibodies. *medRxiv [Preprint]* (2021). doi: 10.1101/2021.12.07.21267432
31. Rössler A, Riepler L, Bante D, Laer DV, Kimpel J. SARS-CoV-2 B.1.1.529 Variant (Omicron) Evades Neutralization by Sera From Vaccinated and Convalescent Individuals. *medRxiv [Preprint]* (2021). doi: 10.1101/2021.12.08.21267491
32. Waterhouse A, Bertoni M, Bienert S, Studer G, Tauriello G, Gumienny R, et al. SWISS-MODEL: Homology Modelling of Protein Structures and Complexes. *Nucleic Acids Res* (2018) 46(W1):W296–303. doi: 10.1093/nar/gky427
33. Abraham MJ, Murtola T, Schulz R, Páll S, Smith JC, Hess B, et al. GROMACS: High Performance Molecular Simulations Through Multi-Level Parallelism From Laptops to Supercomputers. *SoftwareX* (2015) 1–2:19–25. doi: 10.1016/j.softx.2015.06.001
34. Huang J, Rauscher S, Nawrocki G, Ran T, Feig M, de Groot BL, et al. CHARMM36m: An Improved Force Field for Folded and Intrinsically Disordered Proteins. *Nat Methods* (2017) 14(1):71–3. doi: 10.1038/nmeth.4067
35. Feng T, Chen F, Kang Y, Sun H, Liu H, Li D, et al. HawkRank: A New Scoring Function for Protein-Protein Docking Based on Weighted Energy Terms. *J Cheminform* (2017) 9(1):66. doi: 10.1186/s13321-017-0254-7
36. Bussi G, Donadio D, Parrinello M. Canonical Sampling Through Velocity Rescaling. *J Chem Phys* (2007) 126(1):014101. doi: 10.1063/1.2408420
37. Wang H, Dommert F, Holm C. Optimizing Working Parameters of the Smooth Particle Mesh Ewald Algorithm in Terms of Accuracy and Efficiency. *J Chem Phys* (2010) 133(3):034117. doi: 10.1063/1.3446812
38. Shah M, Ahmad B, Choi S, Woo HG. Mutations in the SARS-CoV-2 Spike RBD are Responsible for Stronger ACE2 Binding and Poor Anti-SARS-CoV Mabs Cross-Neutralization. *Comput Struct Biotechnol J* (2020) 18:3402–14. doi: 10.1016/j.csbj.2020.11.002

39. Humphrey W, Dalke A, Schulten K. VMD: Visual Molecular Dynamics. *J Mol Graphics* (1996) 14(1):33–8. doi: 10.1016/0263-7855(96)00018-5
40. Pettersen EF, Goddard TD, Huang CC, Couch GS, Greenblatt DM, Meng EC, et al. UCSF Chimera–a Visualization System for Exploratory Research and Analysis. *J Comput Chem* (2004) 25(13):1605–12. doi: 10.1002/jcc.20084
41. Krissinel E, Henrick K. Inference of Macromolecular Assemblies From Crystalline State. *J Mol Biol* (2007) 372(3):774–97. doi: 10.1016/j.jmb.2007.05.022
42. Kruger DM, Gohlke H. DrugScorePPI Webserver: Fast and Accurate in Silico Alanine Scanning for Scoring Protein-Protein Interactions. *Nucleic Acids Res* (2010) 38(Web Server issue):W480–6. doi: 10.1093/nar/gkq471
43. Hadfield J, Megill C, Bell SM, Huddleston J, Potter B, Callender C, et al. Nextstrain: Real-Time Tracking of Pathogen Evolution. *Bioinformatics* (2018) 34(23):4121–3. doi: 10.1093/bioinformatics/bty407
44. Shu Y, McCauley J. GISAID: Global Initiative on Sharing All Influenza Data - From Vision to Reality. *Euro Surveill* (2017) 22(13):30494. doi: 10.2807/1560-7917.ES.2017.22.13.30494
45. Shah M, Woo HG. Omicron: A Heavily Mutated SARS-CoV-2 Variant Exhibits Stronger Binding to ACE2 and Potently Escape Approved COVID-19 Therapeutic Antibodies. *bioRxiv [Preprint]* (2021). doi: 2021:2021.12.04.471200

Conflict of Interest: The authors declare that the research was conducted in the absence of any commercial or financial relationships that could be construed as a potential conflict of interest.

Publisher's Note: All claims expressed in this article are solely those of the authors and do not necessarily represent those of their affiliated organizations, or those of the publisher, the editors and the reviewers. Any product that may be evaluated in this article, or claim that may be made by its manufacturer, is not guaranteed or endorsed by the publisher.

frontiers in Immunology

OPINION
published: 11 February 2022
doi: 10.3389/fimmu.2022.849465

The Fight Against Severe COVID-19: Can Parasitic Worms Contribute?

*Pengfei Cai**, *Yi Mu* and *Donald P. McManus**

Molecular Parasitology Laboratory, QIMR Berghofer Medical Research Institute, Brisbane, QLD, Australia

OPEN ACCESS

Edited by:
Tengchuan Jin,
University of Science and Technology of China, China

Reviewed by:
David Gems,
University College London, United Kingdom
Bruce Zhang,
University College London, United Kingdom,
in collaboration with reviewer DG Makedonka Mitreva, Washington University School of Medicine in St. Louis, United States

***Correspondence:**
Pengfei Cai
Pengfei.Cai@qimrberghofer.edu.au.
Donald P. McManus
Don.McManus@qimrberghofer.edu.au

Specialty section:
This article was submitted to Viral Immunology, a section of the journal Frontiers in Immunology

Received: *06 January 2022*
Accepted: *21 January 2022*
Published: *11 February 2022*

Citation:
Cai P, Mu Y and McManus DP (2022) The Fight Against Severe COVID-19: Can Parasitic Worms Contribute? Front. Immunol. 13:849465. doi: 10.3389/fimmu.2022.849465

Keywords: COVID-19, SARS-CoV-2, cytokine storm, viral sepsis, helminth, immunomodulatory therapy

INTRODUCTION

As of 31 December 2021, COVID-19, caused by infection with SARS-CoV-2, had been confirmed in more than 285 million people worldwide, with more than 5.4 million dead resulting in a case fatality ratio of 1.89%. This figure is likely to be vastly underestimated, as a proportion was not registered officially as COVID-19-related/excess deaths. The United States recorded the highest number (54,656,866) of confirmed cases. In Africa, there are 47 countries affected, with 7,065,972 cumulative cases and 155,081 deaths were recorded by 31 Dec 2021 (WHO African Region numbers at a glance). To date, the currently approved vaccines have been effective in preventing COVID-19, particularly in regards to severe symptoms (1). However, several immune escape mechanisms of SARS-CoV-2 and the rapid emergence of mutated variants (2) pose a great challenge to the efficacy of these vaccines.

Patients with severe COVID-19 tend to have a high concentration of pro-inflammatory cytokines (IL-2, IL-7, IL-10, G-CSF, TNF-α, CXCL10, MCP1, and MIP1α) (3), suggesting that a cytokine release syndrome (CRS) (4) (also loosely referred to as a cytokine storm), which is a form of life-threatening systemic inflammatory response syndrome (SIRS), can often feature in severe COVID-19 infections. Among the increased levels of inflammatory mediators in COVID-19 patients, the plasma levels of IL-6, an amplifier in the cytokine storm, are significantly elevated in non-survivors compared with survivors (5). The main cause of death of COVID-19 is due to severe acute respiratory distress syndrome (ARDS) with this high severity being dependent on the cytokine storm.

Sepsis has been defined as a life-threatening organ dysfunction caused by a dysregulated host response to infection (6). Endothelium damage, vascular permeability, microvascular dysfunction, coagulation pathway activation, and impaired tissue oxygenation occur during sepsis and can lead to multisystem organ dysfunction (MODS), organ failure and consequently a potentially lethal outcome. As many patients with severe COVID-19 show typical clinical manifestations of septic shock, with other symptoms meeting the diagnostic criteria for sepsis and septic shock according to the Sepsis-3 International Consensus (6), Li et al. hypothesized that viral sepsis is a crucial process in severe COVID-19 cases (7). Accumulating evidence further links the pathology of severe COVID-19, such as acute kidney injury, to sepsis (8).

IMMUNOMODULATORY THERAPY OF SEVERE COVID-19

In regards to potential immunomodulatory strategies for severe COVID-19, the IL-6-STAT3 signaling pathway has been considered a promising therapeutic target for the cytokine storm generated in the disease. Tocilizumab, a specific monoclonal antibody that blocks IL-6, has been recommended for use in critically ill COVID-19 patients with extensive bilateral pulmonary lesions and with elevated serum levels of IL-6. However, anti-cytokine therapy with Tocilizumab did not improve survival rates despite reducing the likelihood of progression to the composite outcome of mechanical ventilation or death (9). In addition, ulinastatin, a serine protease inhibitor with anti-inflammatory properties (including inhibition of IL-6), previously used in the treatment of acute pancreatitis and sepsis, has been suggested for severe COVID-19 treatment (10); yet its clinical performance and cost-effectiveness remain to be validated in large cohort studies.

The value of glucocorticoids in mitigating the inflammatory response due to COVID-19 has been widely scrutinized. Recent reliable evidence from large-scale randomized clinical trials (RCTs) revealed that the use of dexamethasone reduced 28-day mortality but only in patients requiring respiratory support (11), while another parallel, double-blind, placebo-controlled, randomized, Phase IIb clinical trial showed that the administration of methylprednisolone was able to reduce 28-day mortality in patients aged over 60 years (12). In addition, hydroxychloroquine, a disease-modifying antirheumatic drug (DMARD), used for the treatment of rheumatoid arthritis and lupus, has been studied for its potential as an immunomodulatory therapeutic for COVID-19 disease. Evidence from 12 RCTs indicated that hydroxychloroquine has little or no effect on the risk of death, probably has no effect on progression to mechanical ventilation, and that it is less likely that the drug is effective in protecting people from infection, although this was not excluded entirely (13). Other immunomodulatory agents that have been therapeutically tested in SARS-CoV-2 infection include the interleukin-1 receptor (IL-1R) antagonist anakinra, the Janus kinase inhibitors baricitinib and ruxolitinib, the anti-C5a antibody vilobelimab, the anti-gout agent colchicine, the antirheumatic drug leflunomide, convalescent plasma, interferon beta, interferon kappa and intravenous immunoglobulins (IVIg) (14). However, robust data from further RCTs are required to elucidate their potential for the treatment of severe COVID-19.

HELMINTH CO-INFECTION AND SEVERITY OF COVID-19

The "old friends" hypothesis argues that some co-evolved microbes and other pathogens, including helminths, could help to establish appropriate immunomodulatory function and thus protect the host against a large spectrum of immune-related disorders (15). Mammals infected with helminths typically elicit an anti-inflammatory Th2 immune response, including the activation of Th2 cells and the elevation of Th2-type cytokines such as IL-4, IL-5 and IL-13 (16). This host-helminth interaction could be beneficial in dampening inflammatory damage induced by the Th1/Th17 branches of the immune system, repairing injured tissue and restoring homeostasis (17). Chronic helminthic infection suppresses both Th1 and Th2 responses by actively inducing the expansion of $FOXP^{3+}$ regulatory T cells, IL-10 producing B cells and alternatively activated macrophages (AAMs), which together promote the release of regulatory cytokines such as TGF-β and IL-10 (18).

There is controversy regarding whether helminth coinfection leads to increased susceptibility and attenuated immunopathology of other pathogens (i.e., viruses, bacteria and protozoa) or, in some circumstance, exacerbated pathology due to higher infection burdens (19). And this also likely applies to the interaction between helminths and SARS-CoV-2 (20, 21). It has been suggested that the immunosuppressive and regulatory T-helper response stimulated by helminths may balance the inflammatory Th1/Th17 response triggered by SARS-CoV-2 infection, potentially restricting the severity of COVID-19 disease (22, 23). In contrast, a recent viewpoint article argued that COVID-19 patients co-infected with helminths may be unable to mount a quick and efficient immune response against SARS-CoV-2 in the early phase of the infection, thereby leading to increased patient morbidity and mortality (24). However, other evidence indicates that COVID-19 lethality rates are significantly lower in Sub-Saharan Africa than in the industrialized world (25). Wolday et al. (26) carried out a prospective observational cohort study to investigate whether there was a potential correlation between co-infection with intestinal parasites and the severity of COVID-19 in two sites in an endemic area of Ethiopia in Sub-Saharan Africa. The study revealed that patients co-infected with parasites had lower odds of developing severe COVID-19, with an adjusted odds ratio (aOR) of 0.23 ($p < 0.0001$) for all parasites, an aOR of 0.37 ($p < 0.0001$) for protozoa, and an aOR of 0.26 ($p < 0.0001$) for helminths. The authors thus concluded that co-infection with the enteric parasites, *Hymenolopis nana*, *Schistosoma mansoni* and *Trichuris trichiura* reduced the risk of severe COVID-19 occurrence in this cohort of African patients. When stratified by species, co-infection with *T. trichiura* showed the lowest probability of developing severe COVID-19. In addition, of 11 cohort patients who died, all were parasite-free (26). The results of this study thus suggested that parasites, particularly the chronic disease-associated parasitic helminths, induced a Th2-prone response in the host, which modulates COVID-19 severity by restricting the hyper-inflammation associated with the viral infection. Further epidemiological studies on helminth-mediated COVID-19 alleviation are, however, required to support this argument (27, 28).

HELMINTH-DERIVED PRODUCTS CAN ATTENUATE THE SEVERITY OF SEPSIS

The "old friends" hypothesis, together with the inverse global distribution of allergy/autoimmune diseases and helminth infections, and the proclivity for helminths to orchestrate immunomodulatory effects (typically induction of a Th2

immune response) on the host immune system stimulated the concept of developing helminth-based therapies. Robust evidence from animal model studies showed that helminth infection and helminth-derived products were able to prevent/alleviate a variety of autoimmune and inflammatory diseases/disorders (i.e., sepsis, type 2 diabetes, allergic asthma, rheumatoid arthritis, inflammatory bowel disease, type 1 diabetes and multiple sclerosis) (29, 30).

In regard to sepsis, epidemiological studies (over the period 2006-2015) indicated a rapid increase in hospitalization and mortality rates due to severe sepsis in high-income countries (31). This report added further support to the hypothesis that the lack of helminth infections may contribute to the aetiology of sepsis (32). To date, a number of helminth-derived molecular products have resulted in improved sepsis outcomes in animal models. Several studies have investigated the role of *Schistosoma japonicum* cystatin (rSj-Cys) in regulating the inflammatory response in the cecal ligation and puncture (CLP)-induced mouse sepsis model (33–35). Administration of rSj-Cys to mice provided significant therapeutic effects on CLP-induced sepsis characterized by increased survival rates, alleviated overall disease severity with reduced tissue injury in the kidney, lung and liver (33) and cardiomyopathy (34). These therapeutic effects were linked to the upregulation of regulatory cytokines (IL-10 and TGF-β1) and the downregulation of pro-inflammatory cytokines (IL-1β, IL-6 and TNF-α) as measured in serum. Similarly, treatment of mice with cyclophilin A (CsCyPA) from the liver fluke, *Clonorchis sinensis*, provided significant therapeutic effects on CLP-induced sepsis characterized by an improved survival rate (36). Furthermore, using a murine model of septic shock, Ramos-Benitez et al. demonstrated *in vitro* and *in vivo* that Fh15, a recombinant variant of the common liver fluke *Fasciola hepatica* fatty acid binding protein, suppressed the LPS-induced cytokine storm, working as an antagonist of Toll-like receptor 4 (TLR4) (37). In the gram-negative bacteria-induced sepsis rhesus macaque model, Fh15 effectively suppressed bacteremia, endotoxemia, and many other inflammatory markers, emphasizing its promise as a candidate for immunomodulatory therapy against sepsis (38). In addition, the excretory-secretory products of *Trichinella spiralis* adult worms were also shown to be beneficial to the outcome of CLP-induced sepsis by preventing exacerbated inflammation and severe pathology in treated mice (39). These effects were associated with reduced levels of pro-inflammatory cytokines (IL-1β, IL-6 and TNF-α), upregulated levels of IL-10 and TGF-β, and decreased expression of HMGB1, TLR2 and MyD88 in the lung tissues of the treated mice (39). Albeit informative, these observations were accrued from animal sepsis models and human clinical trials now need to be undertaken to validate the results obtained.

DISCUSSION

Rapid mutations in SARS-CoV-2 challenge the efficacy of the current COVID-19 vaccines and concerns about their long-term safety require an urgent need to search for safe and cost-effective alternatives for preventing severe COVID-19 disease. Increased efforts are required as, to date, conclusive evidence of effective immunomodulatory therapies for severe COVID-19 is scarce (14). Due to similarities in the pathological process, sepsis animal models provide the opportunity to evaluate the efficacy of novel candidates for the immunomodulatory therapy of critically ill COVID-19 patients. We argue that helminth-derived products and molecules that can potentially induce a Th2-biased immune response may provide a contributory role in preventing severe COVID-19 by restricting the cytokine storm associated with ARDS. The aforementioned helminth-derived molecules (i.e. rSj-Cys, CsCyPA and Fh15) have been shown to increase survival rates in animal models of sepsis, thereby representing potential candidates for immunomodulatory treatment against severe COVID-19. Such components should be validated for efficacy, first in the K18-hACE2 transgenic murine model of SARS-CoV-2 infection which shares many features of severe COVID-19 infection (40), and then in clinical cohorts. The time phase in sepsis progression is regarded as a key factor for successful immunomodulatory therapy. Due to immunosuppression and immune exhaustion, treatment with immunomodulators at the late stage of severe COVID-19 could be less effective or even deleterious; consequently, the helminth-derived molecular products should be administrated as a prophylactic therapy against severe COVID-19. The suppression of the antiviral response due to excessive immunotherapy may encourage viral replication and result in a delay of clearance of SARS-CoV-2 so that administration of helminth-derived immunomodulators that elicit a mild Th2-skewed immune response could be a useful strategy to prevent severe COVID-19, while maintaining the patient's ability to kill cells infected with the virus. Severe COVID-19 has greater incidence in older individuals, due in part to an increased inflammatory response in these patients (41), begging the question whether prophylactic therapy based on helminth-derived product should primarily target and would be more effective in older individuals? Another unanswered question is whether a well-controlled low level concomitant infection with a live helminth, such as hookworm (42), can achieve an equivalent or superior effect to an immunomodulator or vaccine in preventing serious outcomes of COVID-19. It would be valuable to test such helminthic-based therapies as these may represent a safe and cost-effective anti-inflammation approach to reducing COVID-19 severity.

AUTHOR CONTRIBUTIONS

Conceptualization: PC, YM, and DM. Writing – original draft: PC and YM. Writing – review and editing: PC and DM. All authors contributed to the article and approved the submitted version.

FUNDING

This work was partly supported by the National Health and Medical Research Council (NHMRC) of Australia (ID: APP1160046, APP2008433 and APP1098244). DPM is a NHMRC Leadership Fellow and Senior Scientist at QIMRB.

REFERENCES

1. Tregoning JS, Flight KE, Higham SL, Wang Z, Pierce BF. Progress of the COVID-19 Vaccine Effort: Viruses, Vaccines and Variants Versus Efficacy, Effectiveness and Escape. *Nat Rev Immunol* (2021) 21(10):626–36. doi: 10.1038/s41577-021-00592-1
2. Harvey WT, Carabelli AM, Jackson B, Gupta RK, Thomson EC, Harrison EM, et al. SARS-CoV-2 Variants, Spike Mutations and Immune Escape. *Nat Rev Microbiol* (2021) 19(7):409–24. doi: 10.1038/s41579-021-00573-0
3. Huang C, Wang Y, Li X, Ren L, Zhao J, Hu Y, et al. Clinical Features of Patients Infected With 2019 Novel Coronavirus in Wuhan, China. *Lancet* (2020) 395(10223):497–506. doi: 10.1016/S0140-6736(20)30183-5
4. Moore JB, June CH. Cytokine Release Syndrome in Severe COVID-19. *Science* (2020) 368(6490):473–4. doi: 10.1126/science.abb8925
5. Hojyo S, Uchida M, Tanaka K, Hasebe R, Tanaka Y, Murakami M, et al. How COVID-19 Induces Cytokine Storm With High Mortality. *Inflamm Regen* (2020) 40:37–7. doi: 10.1186/s41232-020-00146-3
6. Singer M, Deutschman CS, Seymour CW, Shankar-Hari M, Annane D, Bauer M, et al. The Third International Consensus Definitions for Sepsis and Septic Shock (Sepsis-3). *JAMA* (2016) 315(8):801–10. doi: 10.1001/jama.2016.0287
7. Li H, Liu L, Zhang D, Xu J, Dai H, Tang N, et al. SARS-CoV-2 and Viral Sepsis: Observations and Hypotheses. *Lancet* (2020) 395(10235):1517–20. doi: 10.1016/S0140-6736(20)30920-X
8. Alexander MP, Mangalaparthi KK, Madugundu AK, Moyer AM, Adam BA, Mengel M, et al. Acute Kidney Injury in Severe COVID-19 Has Similarities to Sepsis-Associated Kidney Injury: A Multi-Omics Study. *Mayo Clin Proc* (2021) 96(10):2561–75. doi: 10.1016/j.mayocp.2021.07.001
9. Salama C, Han J, Yau L, Reiss WG, Kramer B, Neidhart JD, et al. Tocilizumab in Patients Hospitalized With Covid-19 Pneumonia. *N Engl J Med* (2020) 384 (1):20–30. doi: 10.1056/NEJMoa2030340
10. Lin HY. The Severe COVID-19: A Sepsis Induced by Viral Infection? And Its Immunomodulatory Therapy. *Chin J Traumatol* (2020) 23(4):190–5. doi: 10.1016/j.cjtee.2020.06.002
11. Group RC, Horby P, Lim WS, Emberson JR, Mafham M, Bell JL, et al. Dexamethasone in Hospitalized Patients With Covid-19. *N Engl J Med* (2021) 384(8):693–704. doi: 10.1056/NEJMoa2021436
12. Jeronimo CMP, Farias MEL, Val FFA, Sampaio VS, Alexandre MAA, Melo GC, et al. Methylprednisolone as Adjunctive Therapy for Patients Hospitalized With Coronavirus Disease 2019 (COVID-19; Metcovid): A Randomized, Double-Blind, Phase IIb, Placebo-Controlled Trial. *Clin Infect Dis* (2021) 72(9):e373–81. doi: 10.1093/cid/ciaa1177
13. Singh B, Ryan H, Kredo T, Chaplin M, Fletcher T. Chloroquine or Hydroxychloroquine for Prevention and Treatment of COVID-19. *Cochrane Database Syst Rev* (2021) 2:CD013587. doi: 10.1002/14651858.CD013587.pub2
14. Alunno A, Najm A, Mariette X, De Marco G, Emmel J, Mason L, et al. Immunomodulatory Therapies for SARS-CoV-2 Infection: A Systematic Literature Review to Inform EULAR Points to Consider. *Ann Rheum Dis* (2021) 80(6):803–15. doi: 10.1136/annrheumdis-2020-219725
15. Rook GA, Adams V, Hunt J, Palmer R, Martinelli R, Brunet LR. Mycobacteria and Other Environmental Organisms as Immunomodulators for Immunoregulatory Disorders. *Springer Semin Immunopathol* (2004) 25(3-4):237–55. doi: 10.1007/s00281-003-0148-9
16. Harris NL, Loke P. Recent Advances in Type-2-Cell-Mediated Immunity: Insights From Helminth Infection. *Immunity* (2017) 47(6):1024–36. doi: 10.1016/j.immuni.2017.11.015
17. Allen JE, Maizels RM. Diversity and Dialogue in Immunity to Helminths. *Nat Rev Immunol* (2011) 11(6):375–88. doi: 10.1038/nri2992
18. Turner JD, Jackson JA, Faulkner H, Behnke J, Else KJ, Kamgno J, et al. Intensity of Intestinal Infection With Multiple Worm Species Is Related to Regulatory Cytokine Output and Immune Hyporesponsiveness. *J Infect Dis* (2008) 197(8):1204–12. doi: 10.1086/586717
19. McSorley HJ, Maizels RM. Helminth Infections and Host Immune Regulation. *Clin Microbiol Rev* (2012) 25(4):585–608. doi: 10.1128/CMR.05040-11
20. Ademe M, Girma F. The Influence of Helminth Immune Regulation on COVID-19 Clinical Outcomes: Is It Beneficial or Detrimental? *Infect Drug Resist* (2021) 14:4421–6. doi: 10.2147/idr.S335447
21. Głuchowska K, Dzieciątkowski T, Sędzikowska A, Zawistowska-Deniziak A, Młocicki D. The New Status of Parasitic Diseases in the COVID-19 Pandemic-Risk Factors or Protective Agents? *J Clin Med* (2021) 10 (11):2533. doi: 10.3390/jcm10112533
22. Cepon-Robins TJ, Gildner TE. Old Friends Meet a New Foe: A Potential Role for Immune-Priming Parasites in Mitigating COVID-19 Morbidity and Mortality. *Evol Med Public Health* (2020) 2020(1):234–48. doi: 10.1093/emph/eoaa037
23. Hays R, Pierce D, Giacomin P, Loukas A, Bourke P, McDermott R. Helminth Coinfection and COVID-19: An Alternate Hypothesis. *PloS Negl Trop Dis* (2020) 14(8):e0008628. doi: 10.1371/journal.pntd.0008628
24. Abdoli A. Helminths and COVID-19 Co-Infections: A Neglected Critical Challenge. *ACS Pharmacol Transl Sci* (2020) 3(5):1039–41. doi: 10.1021/acsptsci.0c00141
25. Fonte L, Acosta A, Sarmiento ME, Ginori M, Garcia G, Norazmi MN. COVID-19 Lethality in Sub-Saharan Africa and Helminth Immune Modulation. *Front Immunol* (2020) 11:574910. doi: 10.3389/fimmu.2020.574910
26. Wolday D, Gebrecherkos T, Arefaine ZG, Kiros YK, Gebreegzabher A, Tasew G, et al. Effect of Co-Infection With Intestinal Parasites on COVID-19 Severity: A Prospective Observational Cohort Study. *EClinicalMedicine* (2021) 39:101054. doi: 10.1016/j.eclinm.2021.101054
27. Bradbury RS, Piedrafita D, Greenhill A, Mahanty S. Will Helminth Co-Infection Modulate COVID-19 Severity in Endemic Regions? *Nat Rev Immunol* (2020) 20(6):342. doi: 10.1038/s41577-020-0330-5
28. Siles-Lucas M, Gonzalez-Miguel J, Geller R, Sanjuan R, Perez-Arevalo J, Martinez-Moreno A. Potential Influence of Helminth Molecules on COVID-19 Pathology. *Trends Parasitol* (2021) 37(1):11–4. doi: 10.1016/j.pt.2020.10.002
29. Smallwood TB, Giacomin PR, Loukas A, Mulvenna JP, Clark RJ, Miles JJ. Helminth Immunomodulation in Autoimmune Disease. *Front Immunol* (2017) 8:453. doi: 10.3389/fimmu.2017.00453
30. Mu Y, McManus DP, Hou N, Cai P. Schistosome Infection and Schistosome-Derived Products as Modulators for the Prevention and Alleviation of Immunological Disorders. *Front Immunol* (2021) 12:619776. doi: 10.3389/fimmu.2021.619776
31. Fleischmann C, Scherag A, Adhikari NK, Hartog CS, Tsaganos T, Schlattmann P, et al. Assessment of Global Incidence and Mortality of Hospital-Treated Sepsis. Current Estimates and Limitations. *Am J Respir Crit Care Med* (2016) 193(3):259–72. doi: 10.1164/rccm.201504-0781OC
32. Hubner MP, Layland LE, Hoerauf A. Helminths and Their Implication in Sepsis - A New Branch of Their Immunomodulatory Behaviour? *Pathog Dis* (2013) 69(2):127–41. doi: 10.1111/2049-632X.12080
33. Li H, Wang S, Zhan B, He W, Chu L, Qiu D, et al. Therapeutic Effect of Schistosoma Japonicum Cystatin on Bacterial Sepsis in Mice. *Parasit Vectors* (2017) 10(1):222. doi: 10.1186/s13071-017-2162-0
34. Gao S, Li H, Xie H, Wu S, Yuan Y, Chu L, et al. Therapeutic Efficacy of Schistosoma Japonicum Cystatin on Sepsis-Induced Cardiomyopathy in a Mouse Model. *Parasit Vectors* (2020) 13(1):260. doi: 10.1186/s13071-020-04104-3
35. Xie H, Wu L, Chen X, Gao S, Li H, Yuan Y, et al. Schistosoma Japonicum Cystatin Alleviates Sepsis Through Activating Regulatory Macrophages. *Front Cell Infect Microbiol* (2021) 11:617461. doi: 10.3389/fcimb.2021.617461
36. Jiang J, Yin H, Sun Y, Huang H, Hu X. Clonorchis Sinensis Cyclophilin A Immunization Protected Mice From CLP-Induced Sepsis. *Int Immunopharmacol* (2018) 59:347–53. doi: 10.1016/j.intimp.2018.03.039
37. Ramos-Benitez MJ, Ruiz-Jimenez C, Rosado-Franco JJ, Ramos-Pérez WD, Mendez LB, Osuna A, et al. Fh15 Blocks the Lipopolysaccharide-Induced Cytokine Storm While Modulating Peritoneal Macrophage Migration and CD38 Expression Within Spleen Macrophages in a Mouse Model of Septic Shock. *mSphere* (2018) 3(6):e00548–00518. doi: 10.1128/mSphere.00548-18
38. Rosado-Franco JJ, Armina-Rodriguez A, Marzan-Rivera N, Burgos AG, Spiliopoulos N, Dorta-Estremera SM, et al. Recombinant Fasciola Hepatica Fatty Acid Binding Protein as a Novel Anti-Inflammatory Biotherapeutic Drug in an Acute Gram-Negative Nonhuman Primate Sepsis Model. *Microbiol Spectr* (2021) 9(3):e0191021. doi: 10.1128/Spectrum.01910-21
39. Li H, Qiu D, Yang H, Yuan Y, Wu L, Chu L, et al. Therapeutic Efficacy of Excretory-Secretory Products of Trichinella Spiralis Adult Worms on Sepsis-

Induced Acute Lung Injury in a Mouse Model. *Front Cell Infect Microbiol* (2021) 11:653843. doi: 10.3389/fcimb.2021.653843

40 . Winkler ES, Bailey AL, Kafai NM, Nair S, McCune BT, Yu J, et al. SARS-CoV-2 Infection of Human ACE2-Transgenic Mice Causes Severe Lung Inflammation and Impaired Function. *Nat Immunol* (2020) 21(11):1327–35. doi: 10.1038/s41590-020-0778-2

41. Hou Y, Zhou Y, Jehi L, Luo Y, Gack MU, Chan TA, et al. Aging-Related Cell Type-Specific Pathophysiologic Immune Responses That Exacerbate Disease Severity in Aged COVID-19 Patients. *Aging Cell* (2022):e13544. doi: 10.1111/acel.13544

42. Chapman PR, Webster R, Giacomin P, Llewellyn S, Becker L, Pearson MS, et al. Vaccination of Human Participants With Attenuated Necator Americanus Hookworm Larvae and Human Challenge in Australia: A Dose-Finding Study and Randomised, Placebo-Controlled, Phase 1 Trial. *Lancet Infect Dis* (2021) 21(12):1725–36. doi: 10.1016/S1473-3099(21)00153-5

Conflict of Interest: The authors declare that the research was conducted in the absence of any commercial or financial relationships that could be construed as a potential conflict of interest.

Publisher's Note: All claims expressed in this article are solely those of the authors and do not necessarily represent those of their affiliated organizations, or those of the publisher, the editors and the reviewers. Any product that may be evaluated in this article, or claim that may be made by its manufacturer, is not guaranteed or endorsed by the publisher.

frontiers in Immunology

ORIGINAL RESEARCH
published: 14 February 2022
doi: 10.3389/fimmu.2022.844304

Circulating Type I Interferon Levels in the Early Phase of COVID-19 Are Associated With the Development of Respiratory Failure

Kentaro Nagaoka[1], Hitoshi Kawasuji[1], Yushi Murai[1], Makito Kaneda[1], Akitoshi Ueno[1], Yuki Miyajima[1], Yasutaka Fukui[1], Yoshitomo Morinaga[2] and Yoshihiro Yamamoto[1]*

[1] Department of Clinical Infectious Diseases, Toyama University Graduate School of Medicine and Pharmaceutical Sciences, Toyama, Japan, [2] Department of Microbiology, Toyama University Graduate School of Medicine and Pharmaceutical Sciences, Toyama, Japan

OPEN ACCESS

Edited by:
Penghua Wang, University of Connecticut Health Center, United States

Reviewed by:
Yibin Feng, The University of Hong Kong, Hong Kong SAR, China
Lucia Elena Alvarado-Arnez, Franz Tamayo University, Bolivia

***Correspondence:**
Kentaro Nagaoka
knagaoka@med.u-toyama.ac.jp

Specialty section:
This article was submitted to Viral Immunology, a section of the journal Frontiers in Immunology

Received: *27 December 2021*
Accepted: *26 January 2022*
Published: *14 February 2022*

Citation:
Nagaoka K, Kawasuji H, Murai Y, Kaneda M, Ueno A, Miyajima Y, Fukui Y, Morinaga Y and Yamamoto Y (2022) Circulating Type I Interferon Levels in the Early Phase of COVID-19 Are Associated With the Development of Respiratory Failure. Front. Immunol. 13:844304. doi: 10.3389/fimmu.2022.844304

Background: The role of type I interferons (IFNs) in the early phase of COVID-19 remains unclear.

Objectives: To evaluate the relationship between IFN-I levels in patients with COVID-19 and clinical presentation, SARS-CoV-2 viral load, and other major pro-inflammatory cytokines.

Methods: This prospective observational study recruited patients hospitalized with COVID-19. The levels of interferon-alpha (IFN-α), interferon-beta (IFN-β), interleukin-6 (IL-6), and C-X-C motif chemokine ligand (CXCL10) within 5 days after symptom onset were measured using an ELISA, in serum from blood collected within 5 days after the onset of symptoms. The SARS-CoV-2 viral load was determined *via* qPCR using nasal-swab specimens and serum.

Results: The study enrolled 50 patients with COVID-19. IFN-α levels were significantly higher in patients who presented with pneumonia or developed hypoxemic respiratory failure ($p < 0.001$). Furthermore, IFN-α levels were associated with viral load in nasal-swab specimens and RNAemia ($p < 0.05$). In contrast, there was no significant association between IFN-β levels and the presence of pneumonia or RNAemia, despite showing a stronger association with nasal-swab viral load ($p < 0.001$). Correlation analysis showed that the serum levels of IFN-α significantly correlated with those of IFN-β, IL-6, and CXCL10, while the levels of IFN-β did not correlate with those of IL-6 or CXCL10.

Conclusions: Serum IFN-I levels in the early phase of SARS-CoV-2 infection were higher in patients who developed hypoxemic respiratory failure. The association between IFN-α, IL-6, and CXCL10 may reflect the systemic immune response against SARS-CoV-2 invasion into pulmonary circulation, which might be an early predictor of respiratory failure due to COVID-19.

Keywords: COVID-19, type I interferon, pneumonia, hypoxemia, interleukin-6, CXCL10

INTRODUCTION

Coronavirus disease (COVID-19) is a potentially fatal respiratory infection caused by severe acute respiratory syndrome coronavirus 2 (SARS-CoV-2) (1). Since the first outbreak of COVID-19, this pandemic has negatively affected the capacity of local and regional healthcare systems worldwide, resulting in the temporal exhaustion of in-hospital medical services (2, 3). The necessity of hospitalization due to COVID-19 is largely affected by the presence of respiratory failure, which typically develops several days (at least 3 days) after the onset of the first symptoms (4, 5). Therefore, investigating the initial immune response in the early phase of SARS-CoV-2 infection is important because it may be related to the development of respiratory failure.

Using various integrated approaches (6–9), most studies have compared immune responses between groups of patients with COVID-19 with increasing disease severity. These studies yielded homogenous results; the most severe COVID-19 phenotype was associated with an aggressive inflammatory response with the release of a large amount of pro-inflammatory cytokines, an event known as "cytokine storm", and described altered cellular immunity, including marked lymphocytopenia and neutrophil-to-lymphocyte ratio (NLR) elevation (10).

Type I interferons (IFNs) have emerged as crucial contributors to the immune response against a SARS-CoV-2 infection (11–13). In humans, the IFN-I family mainly consists of IFN-α and IFN-β (14), which act as inhibitors of viral replication in infected cells and play a defensive role in uninfected cells. The expression of IFN-I is cell-type specific: IFN-α is mainly produced by hematopoietic cells, whereas IFN-β is produced by a broad range of cell types (15). Impairment of IFN-α and increased autoantibodies against IFN-α have been recognized as important contributors to the disease severity in SARS-CoV-2 infection (11–14). In contrast, a recent *in vitro* study reported that the antiviral activity of IFN-β was superior to that of IFN-α against SARS-CoV-2 (16). Nevertheless, the involvement of each IFN-I in the pathogenesis and outcomes of a SARS-CoV-2 infection, particularly the development of hypoxemic respiratory failure, remains unclear.

In this study, we examined the association between pneumonia, hypoxemic respiratory failure, and immune response in the early phase of COVID-19, focusing on circulating IFN-I levels. Moreover, we assessed the levels of other inflammatory cytokines, including IL-6 and CXCL-10, which are known to be initial immune triggers of the cytokine storm in a SARS-CoV-2 infection (17).

The primary outcome of the study was to validate the relationship between SARS-CoV-2 pneumonia, respiratory failure, IFN-α, and IFN-β, and the secondary outcome was to investigate the association between IFN-I and other cytokines.

MATERIALS AND METHODS

Study Design

This study was conducted as part of the Toyama University COVID-19 cohort study; an investigator-initiated, prospective, single-center study that was primarily designed to investigate the clinical, epidemiological, radiological, and microbiological features of COVID-19. In this study, the patients were diagnosed as COVID-19 positive based on quantitative reverse transcription PCR (RT-qPCR) results. Nasal specimens for RT-qPCR were collected and chest computed tomography (CT) were performed at admission. Serum samples were collected and stored at -80°C after each laboratory examination. The study was approved by the Ethical Review Board of the University of Toyama (R2019167), and written informed consent was obtained from all the patients.

The inclusion criteria were as follows: (1) men or women aged 18 years or older; (2) hospitalized at Toyama University Hospital, Toyama, Japan, between April 2021 and June 2021 (during the endemic period in Toyama that was caused by the SARS-CoV-2 B.1.1.7 lineage); (3) positively diagnosed as having a SARS-CoV-2 infection *via* qPCR using nasal-swab specimens; and (4) had the first blood sample collected within 5 days after the onset of symptom. Patients who did not have an initial CT evaluation or whose blood samples were unavailable for subsequent experiments, were excluded from the study.

Study Participants and Protocol

Data on the patients' demographics, comorbidities, clinical presentation, laboratory findings, therapy regimen, and prognosis were collected from their medical charts.

When a newly developed inflammatory lesion was detected by a chest CT that was performed on admission, COVID-19 pneumonia was confirmed by trained pulmonary radiologists, KN and YY. This method for diagnosis of pneumonia is consistent with previous reports (18, 19). The patients with no inflammatory lesions were confirmed negative for COVID-19 pneumonia. The chest CT was performed in the supine position during end-inspiration on a multidetector CT scanner by using a slice thickness of 1.0 mm, a high spatial resolution algorithm (SOMATOM Definition AS+; Siemens Healthineers, Forchheim, Germany), and SOMATOM go.Top (Siemens Healthineers).

Hypoxemia requiring oxygen therapy was defined as an SpO2 of ≤93% at rest/motion under room air. This is a universally accepted criterion for the initiation of oxygen therapy in patients with COVID-19 (20).

Blood Samples

At least 1.0 mL of serum was collected from each patient and divided into three tubes, one of which was used for the cytokine and RNAemia measurements described below. Only serum collected within 5 days after the onset of symptoms was used for the analysis.

In addition, control serum was obtained from healthy immunocompetent volunteers, from Toyama University Hospital. The volunteers were hospital staff who had no known underlying diseases. The blood sampling was conducted under afebrile conditions and the serum was stored and utilized for cytokine measurements. Written informed consent were also obtained from all the volunteers.

Cytokine Measurement

Serum cytokines and chemokines (IFN-α, IFN-β, IL-6, interleukin-10 (IL-10), and CXCL10) were measured using

commercially available ELISA assays, according to the manufacturers' instructions. The levels of IFN-α, IFN-β, IL-6, IL-10, and CXCL10 were measured using the VeriKine-HS Human IFN Alpha All Subtype ELISA Kit (PBL Assay Science, New Jersey, USA), the VeriKine-HS Human IFN Beta Serum ELISA Kit (PBL Assay Science), the AuthentiKine™ Human IL-6 ELISA Kit (Proteintech, Illinois, USA), the AuthentiKine™ Human IL-10 ELISA Kit (Proteintech), and the Human CXCL10/IP-10 ELISA Kit (Proteintech), respectively. Each sample was measured on first thaw. If an analyte signal was below the background signal, it was set to zero, and if the signal was detectable, but below the manufacturer's lower limit of quantification, it was set to the lower limit of detection.

RT-qPCR

RT-qPCR to detect SARS-CoV-2 was performed as previously described (21, 22). Briefly, RNA was extracted from 140 μL of blood serum or supernatant of nasal-swab specimens by using the QIAamp ViralRNA Mini Kit (QIAGEN, Hilden, Germany) or Nippongene Isospin RNA Virus (Nippongene, Tokyo, Japan), respectively according to the manufacturer's instructions. The viral loads of SARS-CoV-2 were quantified *via* RT-qPCR using a N2-gene-specific primer/probe set according to the Japan National Institute of Infectious Diseases protocol (23). The AcroMetrix COVID-19 RNA Control (Thermo Fisher Scientific, California, USA) was used as a positive control. The detection limit was approximately 0.4 copies/μL (2 copies/5 μL). RNAemia was determined when SARS-CoV-2 was detectable in the blood serum specimens.

Statistical Analysis

Background factors were expressed as medians (interquartile range) or numbers (percentage). To evaluate intergroup differences, the Wilcoxon test and Fisher's exact test were used to compare continuous and nominal variables, respectively. For all pairs of immune parameters and viral loads, Spearman's Rho correlation coefficients were estimated. The results regarding the association between immune parameters are summarized in a correlation matrix. Statistical significance was set at $p < 0.05$. The statistical program R (version 4.1.018) and GraphPad Prism version 9.0 (GraphPad Software, California, USA) were used for statistical analyses.

RESULTS

Study Participants

The clinical characteristics, laboratory findings, treatment, and outcomes of the 50 patients included in this study are summarized in **Table 1**. Age, underlying diseases (none or hypertension), body mass index, and febrile period were significantly different between patients with COVID-19 with and without pneumonia or hypoxemia. No patients with hypoxemic respiratory failure due to COVID-19 required invasive positive pressure ventilation; however, two patients required nasal high-flow oxygen therapy. All patients included in this study survived COVID-19, at least until 30 days after the onset of symptom. None of the patients included in this study had received antiviral medication at the time of blood sampling.

IFN-α and IFN-β Level Analysis

In this study, we performed preliminary experiments to assess the levels of each IFN at different time points in six patients who developed pneumonia (**Supplementary Table 1**). Accordingly, we found that IFN levels significantly decreased 5 days after the initial assessment in five patients. Among them, the levels of IFN-α and IFN-β decreased time-dependently in three patients, even though they developed respiratory failure thereafter. Based on these results, we focused on IFN levels within 5 days of symptom onset, which correspond to the early phase of SARS-CoV-2 infection.

Next, we assessed the levels of each IFN and cytokine. The results of IFN-α and IFN-β level analyses are summarized in

TABLE 1 | Clinical feature of patients in the study.

	Total (n=50)	Pneumonia		Developed hypoxemia required oxygen therapy	
		Positive (n=35)	negative (n=15)	Positive (n=17)	Negative (n=33)
Age, years	50.0 [34-57]	51 [40-66]**	33 [23-50]	58 [53-69] ††	39 [26-51]
Sex; male/female	33/17	26/9	7/8	14/3	19/14
Underlying disease					
None	26 (52)	14 (40)*	12 (80)	5 (29) †	21 (64)
Hypertension	12 (24)	12 (34) *	0 (0)	8 (47) †	4 (12)
Diabetes mellitus	5 (10)	5 (14)	0 (0)	4 (24) †	1 (3)
Respiratory disease	2 (4)	1 (3)	1 (7)	0 (0)	2 (6)
Body mass index	23.0 [21-26]	24.0 [22-26] *	21.0 [20-23]	24.7 [22-27] †	22.5 [21-25]
Febrile period (days)	4.5 [2-6]	5 [3-6] **	2 [2-4]	6 [6-7] ††	3 [2-5]
Treatment					
Remdesivir	18 (36)	18 (51)	0 (0)	17 (100)	1 (3)
Dexamethasone	19 (38)	19 (54)	0 (0)	17 (100)	2 (6)
Heparin	19 (38)	19 (54)	0 (0)	17 (100)	2 (6)
Nasal High Flow	2 (4)	2 (6)	0 (0)	2 (12)	0 (0)
30 days-mortality	0 (0)	0 (0)	0 (0)	0 (0)	0 (0)

*Continuous variables are reported as median [interquartile range (IQR) 25-75]. Categorical variables are reported as number (percentages). *; p<0.05, **; p<0.001 vs patients without pneumonia. †; p<0.05, ††; p<0.001 vs patients without developing hypoxemia.*

Figures 1A, B. The levels of IFN-α were detectable in all patients, but under the lower limit of quantification in three patients. The levels of IFN-β were undetectable in five patients and were below the lower limit of quantification in one patient. In the following analysis, we found that IFN-α levels were significantly higher in patients with pneumonia than in those without pneumonia [130 pg/ml (45-178) vs 51.5 pg/ml (33-85), $p < 0.001$]. Similarly, IFN-α levels were significantly higher in patients who developed hypoxemia than in those who did not [178 pg/ml [130-236] vs 51.5 pg/ml (23-91), $p < 0.001$]. In contrast, the levels of IFN-β were not significantly different between patients with and without pneumonia [5.6 pg/ml (2.1-7.5) vs 4.7 pg/ml (3.1-8.2), $p = 0.488$], but these were significantly higher in patients who developed hypoxemia than in those who did not [7.5 pg/ml (4.5-10) vs 4.5 pg/ml (1.8-6.3), $p = 0.008$]. The level of C-reactive protein (CRP) and NLR were not significantly different between patients with and without hypoxemia (**Figures 1C, D**).

Association Between Serum IFN-I Levels and SARS-CoV-2 Viral Load in the Blood/Nasal Swab

To examine the association between the microbiological findings and IFN-I levels, we assessed the viral load in nasal-swab specimens and serum. The levels of IFN-α and IFN-β were significantly associated with SARS-CoV-2 viral load in nasal-swab specimens ($r = 0.327$; $p = 0.327$ for IFN-α, and $r = 0.452$; $p = 0.001$ for IFN-β; **Figures 2A, B**). Notably, a stronger association was observed with IFN-β than with IFN-α. However, only IFN-α levels were significantly higher in patients with RNAemia than in those without RNAemia (**Figures 2C, D**). The presence of RNAemia was determined by a relatively low viral load [10.4 (4.9-30.0) copies/μL], and the qPCR results were below the detection limit in 35 patients (70% of the study participants). Thus, we analyzed the association between RNAemia and IFN-I levels by the presence of RNAemia.

Immunoinflammatory Biomarker Level Analysis

The levels of CXCL10 and IL-6 were significantly higher in patients with pneumonia and hypoxemia. In contrast, the levels of IL-10 were not significantly different between patients with and without pneumonia or hypoxemia (**Figure 3**). Further analysis revealed that the levels of CXCL10, IL-6, and IL-10 were not associated with the viral load in nasal-swab specimens (**Figures 4A–C**). Moreover, these cytokine levels were not associated with the presence of RNAemia, except for CXCL10 levels (**Figures 4D–F**).

In preliminary experiments, we assessed the levels of tumor necrosis factor (TNF-α), interleukin-17 (IL-17), vascular endothelial growth factor (VEGF), and angiotensin-converting

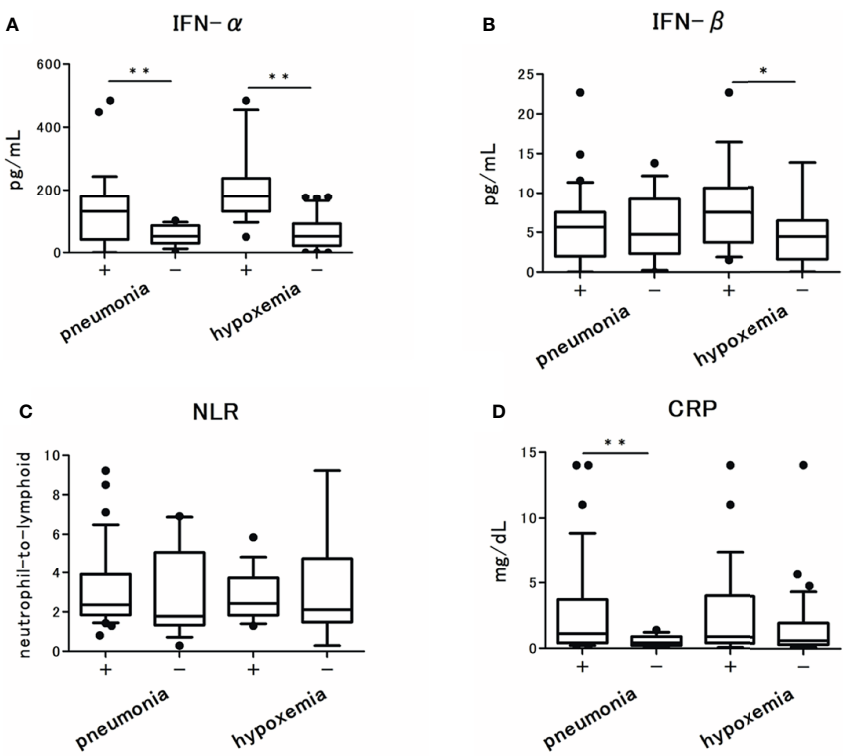

FIGURE 1 | The serum type I Interferon (IFN) levels in patients with COVID-19 and their association with pneumonia and hypoxemic respiratory failure: **(A)** IFN-α levels, **(B)** IFN-β levels. **(C)** CRP levels, and **(D)** Neutrophils-to-lymphocytes ratio in patients with COVID-19. Each level was measured at the time of admission (within 5 days after the onset of symptoms), without hypoxemic respiratory failure at the time. Data are presented as Tukey boxplots and individual values. Nonparametric Mann-Whitney test was used to compare values between groups: *$p < 0.05$. **$p < 0.001$.

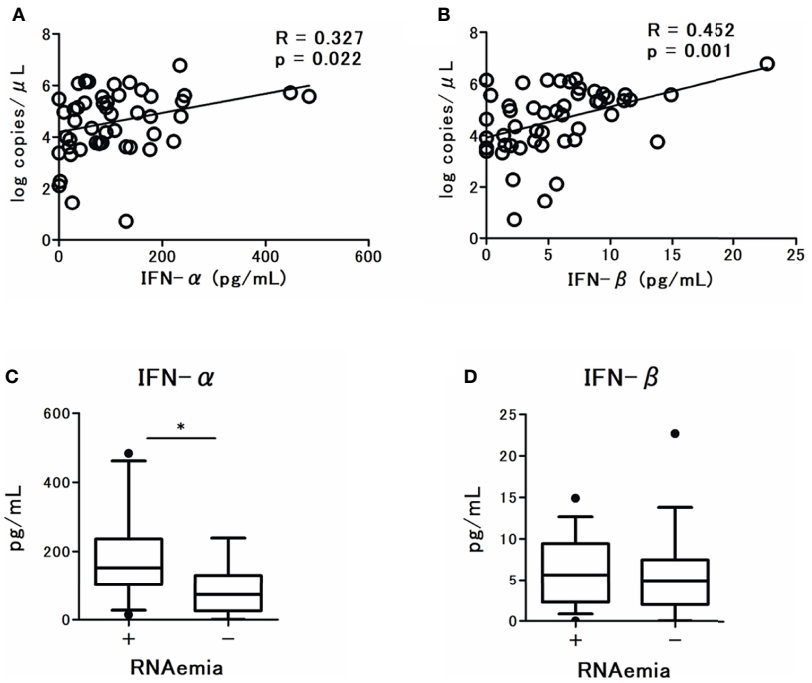

FIGURE 2 | Correlations between serum type I Interferon (IFN-I) levels and SARS-CoV-2 viral load in nasal swab specimens from patients with COVID-19: **(A)** IFN-α levels and **(B)** IFN-β levels. Spearman correlation test was used, and Spearman correlation coefficient is shown. Corresponding logarithmic trendlines are shown. Serum IFN-I levels in patients with COVID-19 and the association with RNAemia, **(C)** IFN-α levels, **(D)** IFN-β levels. Each level was measured at the time of admission (within 5 days after the onset of symptoms). Data are presented as Tukey boxplots and individual values. Nonparametric Mann-Whitney test was used to compare values between groups: *p < 0.05.

enzyme 2 (ACE-2) by using commercially available ELISA assays, according to the manufacturers' instructions (**Supplementary Table 1**): TNF-α, IL-17, and VEGF (Chondrex, Washington, USA) and ACE-2 (Abcam, Cambridge, UK). However, the analyte signals of TNF-α, IL-17, and ACE-2 were below the background signals in all patients, and those of VEGF were undetectable in 31 patients (62% of all patients). From these results, we determined that the levels of TNF-α, IL-17, VEGF, and ACE-2 were substantially low in the early phase of SARS-CoV-2 infection; therefore, we excluded these biomarkers from further analysis.

To determine the baseline levels of IFN-I and cytokines, we assessed the inflammatory biomarker levels of IFN-α, IFN-β, IL-6, CXCL10, and IL-10 in healthy volunteers (**Supplementary Table 2**). Amongst, the levels of all biomarkers in healthy volunteers were significantly lower than those in patients with SARS-CoV-2 infection, in particular with IFN-α and IFN-β.

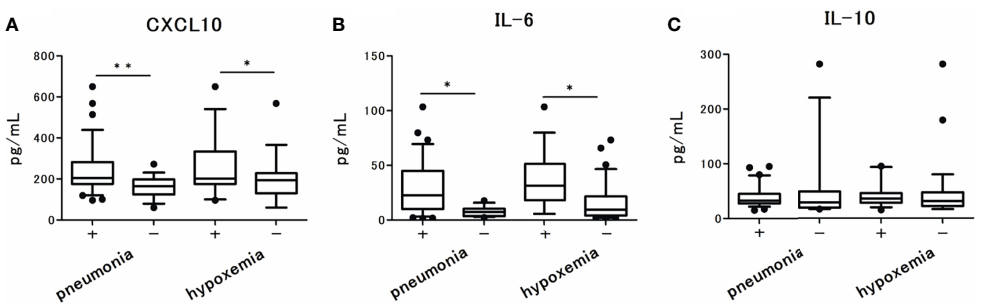

FIGURE 3 | Serum cytokine and chemokine levels in patients with COVID-19 and the associations with pneumonia and hypoxemic respiratory failure: **(A)** CXCL10 levels, **(B)** IL-6 levels, and **(C)** IL-10 levels. Each level was measured at the time of admission (within 5 days after the onset of symptoms), without hypoxemic respiratory failure. One value was excluded from the analyses of IL-6 and IL-10 as an outlier (IL-6 with 476 pg/mL, and IL-10 with 1640 pg/mL). Data are presented as Tukey boxplots and individual values. Nonparametric Mann-Whitney test was used to compare values between groups: *p < 0.05. **p < 0.001.

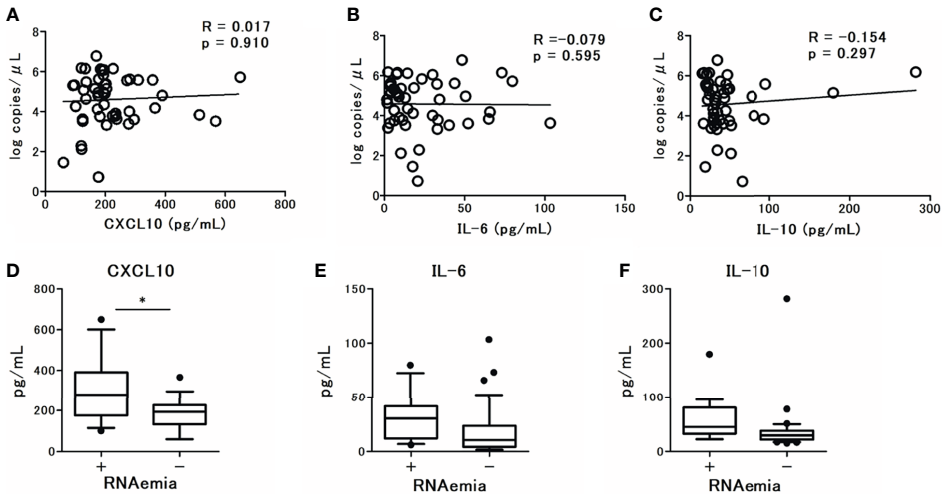

FIGURE 4 | The association observed between serum cytokine levels and SARS-CoV-2 viral load in nasal swab specimens from patients with COVID-19 at admission (within 5 days after the onset of symptoms): **(A)** CXCL10 levels, **(B)** IL-6 levels, and **(C)** IL-10 levels. Spearman correlation test was used, and Spearman correlation coefficient is shown. Corresponding logarithmic trendlines are shown. The association between serum cytokine levels in patients with COVID-19 and RNAemia: **(D)** CXCL10 levels, **(E)** IL-6 levels, and **(F)** IL-10 levels. One value was excluded from the analyses of IL-6 and IL-10 as an outlier (IL-6 with 476 pg/mL, and IL-10 with 1640 pg/mL). Data are presented as Tukey boxplots and individual values. Nonparametric Mann-Whitney test was used to compare values between groups: *p < 0.05.

Correlations Among Immunoinflammatory Biomarker Levels

Among the tested immunoinflammatory biomarkers, IFN-β (r = 0.51; p < 0.001), CXCL-10 (r = 0.45; p = 0.001), and IL-6 levels (r = 0.44; p = 0.001) were significantly associated with serum IFN-α levels (**Figure 5**). Among the tested inflammatory cytokines, IL-6 levels were strongly associated with CXCL10 (r = 0.58; p < 0.001) and CRP levels (r = 0.61; p < 0.001). However, no significant association was observed between each leukocyte level and the tested immunoinflammatory biomarker levels, except for IL-10 and neutrophil levels (r = 0.31; p = 0.028).

DISCUSSION

In this study, we demonstrated that the level of serum IFN-α in the early phase of SARS-CoV-2 infection was strongly associated with the presence of pneumonia and the development of hypoxemic respiratory failure. In addition, there was an association between IFN-α levels, the viral load in nasal-swab specimens, and the presence of RNAemia. In contrast, IFN-β levels were not associated with the presence of pneumonia or RNAemia, despite the stronger association observed with nasal-swab viral load. The serum levels of inflammatory cytokines, IL-6 and CXCL10, were significantly associated with pneumonia and hypoxemia, but not with the viral load in nasal-swab specimens. Correlation analysis showed that IFN-α significantly correlated with IFN-β, IL-6, and CXCL10 levels, while IFN-β did not correlate with IL-6 or CXCL10 levels. To our knowledge, this is the first clinical study to reveal the differential expression of IFN-α and IFN-β in the early phase of SARS-CoV-2 infection.

Previous studies suggested that an impaired IFN-I response could be a hallmark of severe COVID-19 (9, 11). However, a recent meta-analysis by Silva et al. (24), which included 15 studies examining the plasma protein levels of IFN-I (α and β), could not confirm a significant association between plasma IFN- I levels and COVID-19 disease severity. In the included studies, IFN-α was measured over 7 days after the onset of symptoms (25–32), and IFN-α levels at the early phase of SARS-CoV-2 infection (within 5 days after the onset of symptoms) were assessed only in one study (30). Galani et al. assessed the IFN-α levels in 32 patients within 5 days after onset using an ELISA kit (Abcam) and found that there was no elevation in the levels of IFN-α in the early phase of SARS-CoV-2 infection. Venet et al. evaluated serum IFN-α levels using a single molecular array in 64 critically ill patients with COVID-19 at a relatively early phase of SARS-CoV-2 infection (serum collected on admission) and compared the IFN-α levels between survivors and non-survivors (33). Although no difference was found between the cohorts, IFN-α levels were the highest in the earlier phase of SARS-CoV-2 infection and decreased time-dependently until 7 days after the initial assessment. To date, the serum levels of IFN-α during the early phase of SARS-CoV-2 infection and their association with disease progression remain unclear. Similarly, the serum levels of IFN-β during the early phase of SARS-CoV-2 infection also remain unclear because the detection of IFN-β was more difficult than that of IFN-α in the previous studies (25, 34).

In this study, we measured IFN-I and cytokine levels within 5 days after the onset of symptoms of a SARS-CoV-2 infection. Notably, our study detected relatively higher levels of IFN-α and IFN-β than those detected in previous studies. As shown by preliminary experiments (**Supplementary Table 1**), the elevation of IFN-I levels in the early phase of infection and their subsequent decrease were observed regardless of disease progression. These

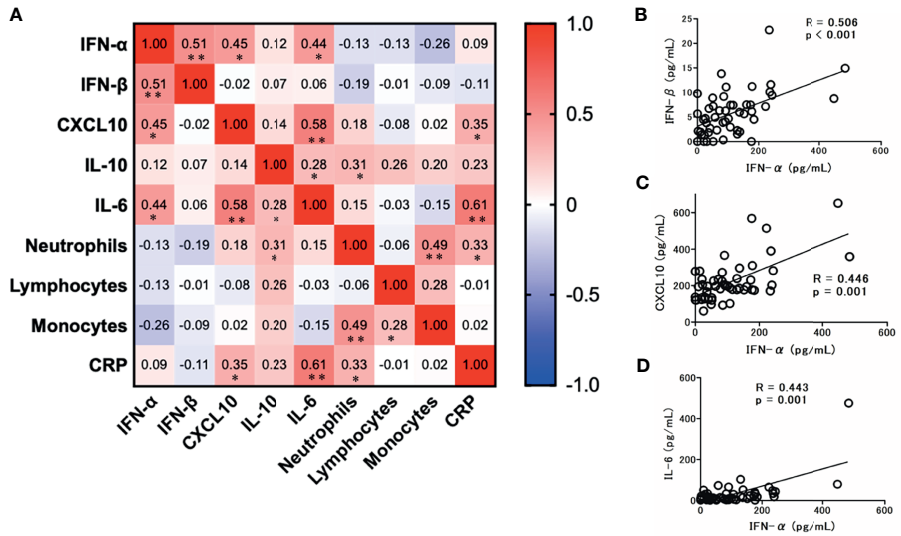

FIGURE 5 | Correlation matrix of immune parameters in patients with COVID-19 at admission (within 5 days after the onset of symptoms). **(A)** Results are presented as a correlation matrix. Spearman correlation coefficients are plotted. Cells were colored according to the strength and trend of correlations (shades of red = positive correlations; shades of blue = negative correlations). *p < 0.05. **p < 0.001. Significant correlations between serum IFN-α levels and IFN/cytokines; **(B)** IFN-β levels, **(C)** CXCL10 levels, and **(D)** IL-6 levels. Spearman correlation test was used, and Spearman correlation coefficient is shown. Corresponding logarithmic trendlines are shown.

results indicate that the temporal elevation of IFN-I levels in the early phase of infection might reflect the initial immune response against SARS-CoV-2, which might appear in a large population of patients with COVID-19. Considering the scarce evidence on IFN-I levels during the early phase of SARS-CoV-2 infection, we believe that our results could extract the crucial timing when IFN-I strongly responds to SARS-CoV-2 infection.

Furthermore, the discrepancy between IFN-α and IFN-β levels during early phase of infection is noteworthy. Our study revealed that IFN-α levels are strongly associated with the presence of pneumonia, RNAemia, and the development of hypoxemic respiratory failure. In contrast, the association between IFN-β and pneumonia or RNAemia was not significant. Serum SARS-CoV-2 RNA viral load, recently termed as RNAemia, reflects the spread of SARS-CoV-2 into circulation, which has been reported as a potential predictor of unfavorable clinical outcomes in patients with COVID-19 (35–37). RNAemia, detected by qPCR, is observed in 1.5% to 50% of patients with a mild-to-severe COVID-19. These results support our findings (RNAemia was detected in 30% of patients with COVID-19). Based on this, we speculate that the discrepancies between IFN-α and IFN-β levels during early phase of infection might be derived from the infected cell types that produce IFN-I (15). Since IFN-α is produced mainly by circulating hematopoietic cells, the elevated IFN-α levels in early phase infection might reflect a systemic immune response against the spread of SARS-CoV-2 into the blood or pulmonary circulation, rather than the local immune response in the nasopharyngeal mucosa. In contrast, the elevated IFN-β levels might reflect the latter immune response, and thus, strongly correlate with the viral load in the nasopharynx. This may explain why there was an association between the levels of IL-6 and CXCL10 with IFN-α levels, but not with those of IFN-β.

Recent evidence suggests that IL-6 and CXCL10 act as trigger signals of the cytokine storm in COVID-19 (17). A possible mechanism could involve SARS-CoV-2 invasion into the respiratory tract, which in turn stimulates lung epithelial cells to produce cytokines, including IL-6. Thereafter, the secreted IL-6 stimulates several chemokines, including CXCL10, which recruit macrophages from vessels into the interstitium. This creates a cycle involving the overproduction of IL-6 by lung-resident cells as well as by the macrophages recruited by CXCL10. In our study, the blood levels of IL-6 and CXCL10 in the early phase of SARS-CoV-2 infection were significantly associated, and this was compatible with the interactive trigger signals of the cytokine storm. Moreover, IL-6 and CXCL10 levels were significantly associated with the presence of pneumonia and the development of respiratory failure, thereby supporting the hypothesis that the elevation of these inflammatory biomarkers is possibly dominant in the pulmonary circulation. The smaller association between the biomarkers and the viral load in the nasopharynx also supports this notion. Based on these findings, we suggest that significant associations between IFN-α, IL-6, and CXCL10 levels may reflect the systemic immune response, mainly due to the spread of SARS-CoV-2 into pulmonary circulation. A diagram of the proposed mechanism regarding the observed relationship between IFN-I, CXCL10 and IL-6 is shown in **Figure 6**.

The correlation matrix of immune showed that IL-10 was associated with neutrophils, but not with IFN-I. There was no significant association between the amount of circulating leukocyte and IFN-I, IL-6 or CXCL10. These results were not consistent with a previous study which reported an inverse association between lymphocytopenia, IL-10 and IFN-α levels in 54 patients with COVID-19, which included 16 fatal cases (34). IL-10 is an

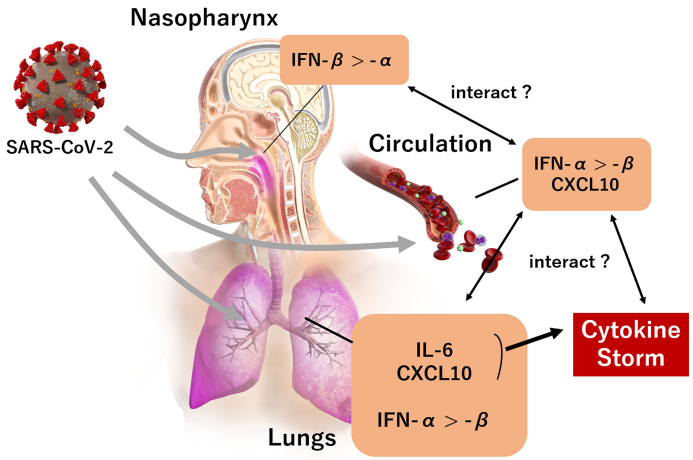

FIGURE 6 | The landscape of IFN-I and predominant cytokines (CXCL10, IL-6) during the early phase of a SARS-CoV-2 infection. A SARS-CoV-2 infection in the nasopharynx induces IFN-β expression rather than IFN-α. IFN-α, IL-6, and CXCL10 expression is induced when the infection reaches the lungs, rather than IFN-β; and the expression of IFN-α and CXCL10 is induced by the presence of SARS-CoV-2 infection in circulation. An increase of IL-6 and CXCL10 in pulmonary circulation subsequently trigger a cytokine storm.

anti-inflammatory cytokine that has pleiotropic roles and that can limit innate immune responses by inhibiting IFN-I (38). Since our study did not include data from fatal cases, the inverse effect of IL-10 on IFN-I could be underestimated. We hypothesize that, at least in the early phase of SARS-CoV-2 infection, IL-10 and circulating leukocytes are not strongly associated with IFN-I.

Aside from IFN-I, type III interferons (IFN-III) have recently received considerable attention as the predominant antiviral cytokines present at the mucosal barriers in the upper respiratory tract of SARS-CoV-2 infected patients (39, 40). Sposito et al. analyzed the pattern and level of expression of IFN-I (α and β), IFN-III (λ1, λ2, λ3) and the transcriptional programs associated with the IFN landscape in the upper or lower respiratory tract of patients with varied severity of COVID-19. They found that high levels of IFN-III, and to a lesser extent IFN-I, characterize the upper airways of patients with high viral burden but reduced disease risk or severity. In contrast, IFN-I were overrepresented in the lower airways of patients with severe COVID-19. These interferons are linked to gene pathways associated with increased apoptosis and decreased proliferation (39). Similarly, Gilbert et al. investigated the mRNA levels of IFN-I and IFN-III in nasopharyngeal swabs from 147 patients with COVID-19, and found that a SARS-CoV-2 infection induced the selective upregulation of IFN-λ1 expression in pediatric patients (≤15 years), whereas the mRNA expression levels of IFN-α, IFN-β, and IFN-λ2/3 was unaffected. Conversely, the infection triggered an upregulation of IFN-α, IFN-β, and IFN-λ2/3 in adults (15-65 years) and the elderly (≥65 years), but there was no modulation of IFN-λ1 expression (40). In these studies, it is not clear at what stage during the SARS-CoV-2 infection the blood samples were taken; therefore, circulating levels of IFN-IIIand its relationship with IFN-I in the early phase of SARS-CoV-2 infection are unclear. Concerning the local immune response, our study demonstrated that IFN-β in the early phase is possibly dominant in the nasopharyngeal mucosa rather than systemic immune response, which is similar to what is observed for IFN-III. However, the exact role and effect of the increased IFN-I levels that are observed during the early phase of SARS-CoV-2 infection are still largely unknown. Further studies are required to examine the interaction of IFN-I with proinflammatory cytokines and IFN-III in the early phase of SARS-CoV-2 infection.

To our knowledge, this is the first study to demonstrate that elevated levels of circulating IFN-I, like those of IL-6 and CXCL10, predict the further development of hypoxemic respiratory failure. Since the anti-viral treatment included in this study was initiated after blood sampling, we believe that the predictive value of IFN-I and cytokines accurately reflect the risk of hypoxemia in the early phase of SARS-CoV-2 infection. The initial elevation of serum IFN-α levels is possibly affected by SARS-CoV-2 systemic invasion, predominantly in the pulmonary circulation. Thus, the detection of IFN-α levels in the early phase of SARS-CoV-2 infection might help identify high-risk patients with respiratory failure who require urgent hospitalization. To date, elevated serum levels of CXCL-10 and IL-6 have been consistently reported in patients with COVID-19, as these are associated with an increased disease severity and risk of mortality (41, 42). We suggest that the establishment of a novel approach focusing on IFN-α and corresponding cytokines in the early phase of SARS-CoV-2 infection would contribute to the early detection of patients with COVID-19 at a high risk of respiratory failure.

The present study has several limitations. First, the single-center observational study design with a relatively small sample size may have result in selection bias. Second, we assessed IFN-I and cytokine levels in serum samples which were not stored at -80°C immediately after drawing (serum was first stored in 4°C, and then transferred to a -80°C freezer). Third, we only examined a single timepoint. Since IFN-I is rapidly and transiently induced by antiviral molecules, the association between serum IFN-I levels and the prognosis of COVID-19 should be further investigated to

confirm time-dependent changes. During this study period, patients with mild-to-moderate disease could only stay in hospital for a relatively short term (2-7 days) because of the temporal exhaustion of in-hospital medical services in the region. Thus, the longitudinal assessment of IFN-I activity was difficult in most of the patients. Moreover, IFN-I and cytokine levels in the later phase of SARS-CoV-2 infection would be largely affected by several factors including a variety of treatments and secondary bacterial infection. Future studies are necessary to investigate long-term changes in IFN-I levels, which may minimize those bias. However, this study could include various unvaccinated patients in the same endemic period, which would minimize the bias due to vaccine- or strain-dependent SARS-CoV-2 virulence. Considering the consistent correlation between IFN-I and the major cytokines, we believe that these limitations have not significantly affected the study outcomes.

In conclusion, this study demonstrated that serum IFN-I levels in the early phase of SARS-CoV-2 infection were higher in patients who developed hypoxemic respiratory failure. Analysis of the associations between IFN-I, major inflammatory cytokines, and SARS-CoV-2 viral load revealed that the early elevation of serum IFN-α levels may be affected by SARS-CoV-2 systemic invasion, which could be a predictor of disease progression, including respiratory failure. These findings would encourage further research into the specific role of IFN-I in the early phase of SARS-CoV-2 infection.

DATA AVAILABILITY STATEMENT

The original contributions presented in the study are included in the article/**Supplementary Material**. Further inquiries can be directed to the corresponding author.

ETHICS STATEMENT

The studies involving human participants were reviewed and approved by The Ethical Review Board of the University of Toyama (R2019167). The patients/participants provided their written informed consent to participate in this study.

AUTHOR CONTRIBUTIONS

KN designed and interpreted the clinical data, experimental findings, and prepared the manuscript. KN, with the assistance of YMu, MK, HK, AU, YMi, and YF collected the clinical data and blood. KN and YMo contributed to the analysis of the experimental and microbiological findings. KN, YMu, MK, HK, AU, YMi, YF, and YMo contributed to the analysis of the microbiological findings. KN and YY confirmed the radiological findings. KN and HK confirmed the accuracy of the statistical analysis. All authors contributed to discussions throughout the work. All authors contributed to the article and approved the submitted version.

FUNDING

This study was partly supported by the Research Program on Emerging and Re-emerging Infectious Diseases from AMED Grant No. JP20he0622035.

ACKNOWLEDGMENTS

We thank Yoshihiro Yoshida, Department of Microbiology, for his excellent support in qPCR for RNAemia.

SUPPLEMENTARY MATERIAL

The Supplementary Material for this article can be found online at: https://www.frontiersin.org/articles/10.3389/fimmu.2022.844304/full#supplementary-material

REFERENCES

1. Guan WJ, Ni ZY, Hu Y, Liang WH, Ou CQ, He JX, et al. Clinical Characteristics of Coronavirus Disease 2019 in China. *N Eng J Med* (2020) 382:1708–20. doi: 10.1056/NEJMoa2002032
2. Ranney ML, Griffeth V, Jha AK. Critical Supply Shortages - The Need for Ventilators and Personal Protective Equipment During the Covid-19 Pandemic. *N Engl J Med* (2020) 382:e41. doi: 10.1056/NEJMp2006141
3. Mareiniss DP. The Impending Storm: COVID-19, Pandemics and Our Overwhelmed Emergency Departments. *Am J Emerg Med* (2020) 38:1293–4. doi: 10.1016/j.ajem.2020.03.033
4. Galloway JB, Norton S, Barker RD, Brookes A, Carey I, Clarke BD, et al. A Clinical Risk Score to Identify Patients With COVID-19 at High Risk of Critical Care Admission or Death: An Observational Cohort Study. *J Infect* (2020) 81:282–8. doi: 10.1016/j.jinf.2020.05.064
5. Gentilotti E, Savoldi A, Compri M, Górska A, De Nardo P, Visentin A, et al. Assessment of COVID-19 Progression on Day 5 From Symptoms Onset. *BMC Infect Dis* (2021) 21:883. doi: 10.1186/s12879-021-06596-5
6. Laing AG, Lorenc A, Del Molino Del Barrio I, Das A, Fish M, Monin L, et al. A Dynamic COVID-19 Immune Signature Includes Associations With Poor Prognosis. *Nat Med* (2020) 26:1623–35. doi: 10.1038/s41591-020-1038-6
7. Arunachalam PS, Wimmers F, Mok CKP, Perera R, Scott M, Hagan T, et al. Systems Biological Assessment of Immunity to Mild Versus Severe COVID-19 Infection in Humans. *Science* (2020) 369:1210–20. doi: 10.1126/science.abc6261
8. Silvin A, Chapuis N, Dunsmore G, Goubet AG, Dubuisson A, Derosa L, et al. Elevated Calprotectin and Abnormal Myeloid Cell Subsets Discriminate Severe From Mild COVID-19. *Cell* (2020) 182:1401–18. doi: 10.1016/j.cell.2020.08.002
9. Schulte-Schrepping J, Reusch N, Paclik D, Bassler K, Schlickeiser S, Zhang B, et al. Severe COVID-19 Is Marked by a Dysregulated Myeloid Cell Compartment. *Cell* (2020) 182:1419–40. doi: 10.1016/j.cell.2020.08.001
10. Li X, Liu C, Mao Z, Xiao M, Wang L, Qi S, et al. Predictive Values of Neutrophil-to-Lymphocyte Ratio on Disease Severity and Mortality in COVID-19 Patients: A Systematic Review and Meta-Analysis. *Crit Care* (2020) 24:647. doi: 10.1186/s13054-020-03374-8

11. Hadjadj J, Yatim N, Barnabei L, Corneau A, Boussier J, Smith N, et al. Impaired Type I Interferon Activity and Infammatory Responses in Severe COVID-19 Patients. *Science* (2020) 369:718–24. doi: 10.1126/science.abc6027
12. Bastard P, Rosen LB, Zhang Q, Michailidis E, Hofmann HH, Zhang Y, et al. Autoantibodies Against Type I IFNs in Patients With Life-Threatening COVID-19. *Science* (2020) 370:eabd4585. doi: 10.1126/science.abd4585
13. Acharya D, Liu G, Gack MU. Dysregulation of Type I Interferon Responses in COVID-19. *Nat Rev Immunol* (2020) 20:397–8. doi: 10.1038/s41577-020-0346-x
14. Trouillet-Assant S, Viel S, Gaymard A, Pons S, Richard JC, Perret M, et al. Type I IFN Immunoprofling in COVID-19 Patients. *J Allergy Clin Immunol* (2020) 146:206–8. doi: 10.1016/j.jaci.2020.04.029
15. Crouse J, Kalinke U, Oxenius A. Regulation of Antiviral T Cell Responses by Type I Interferons. *Nat Rev Immunol* (2015) 15:231–42. doi: 10.1038/nri3806
16. Mantlo E, Bukreyeva N, Maruyama J, Paessler S, Huang C. Antiviral Activities of Type I Interferons to SARS-CoV-2 Infection. *Antiviral Res* (2020) 179:104811. doi: 10.1016/j.antiviral.2020.104811
17. Coperchini F, Chiovato L, Rotondi M. Interleukin-6, CXCL10 and Infiltrating Macrophages in COVID-19-Related Cytokine Storm: Not One for All But All for One! *Front Immunol* (2021) 12:668507. doi: 10.3389/fimmu.2021.668507
18. Prokop M, Everdingen W, Vellinga TR, Ufford HQ, Stöger L, Beenen L, et al. CORADS: A Categorical CT Assessment Scheme for Patients Suspected of Having COVID-19—Definition and Evaluation. *Radiology* (2020) 296:E97–104. doi: 10.1148/radiol.2020201473
19. Machnicki S, Patel D, Singh A, Talwar A, Mina B, Oks M, et al. The Usefulness of Chest CT Imaging in Patients With Suspected or Diagnosed COVID-19: A Review of Literature. *Chest* (2021) 160:652–70. doi: 10.1016/j.chest.2021.04.004
20. Wang YC, Lu MC, Yang SF, Bien MY, Chen YF, Li YT. Respiratory Care for the Critical Patients With 2019 Novel Coronavirus. *Respir Med* (2021) 186:106516. doi: 10.1016/j.rmed.2021.106516
21. Kawasuji H, Takegoshi Y, Kaneda M, Ueno A, Miyajima Y, Kawago K, et al. Transmissibility of COVID-19 Depends on the Viral Load Around Onset in Adult and Symptomatic Patients. *PloS One* (2020) 15:e0243597. doi: 10.1371/journal.pone.0243597
22. Kawasuji H, Morinaga Y, Tani H, Yoshida Y, Takegoshi Y, Kaneda M, et al. SARS-CoV-2 RNAemia With Higher Nasopharyngeal Viral Load Is Strongly Associated With Severity and Mortality in Patients With COVID-19. *J Med Virol* (2022) 94:147–53. doi: 10.1002/jmv.27282
23. Shirato K, Nao N, Katano H, Takayama I, Saito S, Kato F, et al. Development of Genetic Diagnostic Methods for Novel Coronavirus 2019 (Ncov-2019) in Japan. *Jpn J Infect Dis* (2020) 73:304–7. doi: 10.7883/yoken.JJID.2020.061
24. da Silva RP, Gonçalves JIB, Zanin RF, Schuch FB, de Souza APD. Circulating Type I Interferon Levels and COVID-19 Severity: A Systematic Review and Meta-Analysis. *Front Immunol* (2021) 12:657363. doi: 10.3389/fimmu.2021.657363
25. Saínchez-Cerrillo I, Landete P, Aldave B, Saínchez-Alonso S, Saínchez-Azofra A, Marcos-Jimeínez A, et al. Covid-19 Severity Associates With Pulmonary Redistribution of CD1c+ DC and Inflammatory Transitional and Nonclassical Monocytes. *J Clin Invest* (2020) 130:6290–300. doi: 10.1172/JCI140335
26. Liu Y, Zhang C, Huang F, Yang Y, Wang F, Yuan J, et al. Elevated Plasma Levels of Selective Cytokines in COVID-19 Patients Reflect Viral Load and Lung Injury. *Natl Sci Rev* (2020) 7:6. doi: 10.1093/nsr/nwaa037
27. Henry BM, Benoit S, Vikse J, Berger B, Pulvino C, Hoehn J, et al. The AntiInflammatory Cytokine Response Characterized by Elevated Interleukin-10 is a Stronger Predictor of Severe Disease and Poor Outcomes Than the Pro-Inflammatory Cytokine Response in Coronavirus Disease 2019 (COVID-19). *Clin Chem Lab Med* (2020) 59:599–607. doi: 10.1515/cclm-2020-1284
28. Lucas C, Wong P, Klein J, Castro TBR, Silva J, Sundaram M, et al. Longitudinal Analyses Reveal Immunological Misfiring in Severe Covid19. *Nature* (2020) 584:463–9. doi: 10.1038/s41586-020-2588-y
29. Chi Y, Ge Y, Wu B, Zhang W, Wu T, Wen T, et al. Serum Cytokine and Chemokine Profile in Relation to the Severity of Coronavirus Disease 2019 in China. *J Infect Dis* (2020) 222:746–54. doi: 10.1093/infdis/jiaa363
30. Thwaites RS, Uruchurtu AS, Siggins MK, Liew F, Russell CD, Moore SC. Inflammatory Profiles Across the Spectrum of Disease Reveal a Distinct Role for GM-CSF in Severe COVID-19. *Sci Immunol* (2021) 6:eabg9873. doi: 10.1126/sciimmunol.abg9873
31. Tincati C, Cannizzo ES, Giacomelli M, Badolato R, Monforte A, Marchetti G. Heightened Circulating Interferon-Inducible Chemokines, and Activated ProCytolytic Th1-Cell Phenotype Features Covid-19 Aggravation in the Second Week of Illness. *Front Immunol* (2020) 11:1–12. doi: 10.3389/fimmu.2020.580987
32. Galani IE, Rovina N, Lampropoulou V, Triantafyllia V, Manioudaki M, Pavlos E, et al. Untuned Antiviral Immunity in COVID-19 Revealed by Temporal Type IIII Interferon Patterns and Flu Comparison. *Nat Immunol* (2021) 22:32–40. doi: 10.1038/s41590-020-00840-x
33. Venet F, Cour M, Rimmelé T, Viel S, Yonis H, Coudereau R, et al. Longitudinal Assessment of IFN-I Activity and Immune Profile in Critically Ill COVID-19 Patients With Acute Respiratory Distress Syndrome. *Crit Care* (2021) 25:140. doi: 10.1186/s13054-021-03558-w
34. Contoli M, Papi A, Tomassetti L, Rizzo P, Vieceli Dalla Sega F, Fortini F, et al. Blood Interferon-α Levels and Severity, Outcomes, and Inflammatory Profiles in Hospitalized COVID-19 Patients. *Front Immunol* (2021) 12:648004. doi: 10.3389/fimmu.2021.648004
35. Miki S, Sasaki H, Horiuchi H, Miyata N, Yoshimura Y, Miyazaki K, et al. On-Admission SARS-CoV-2 RNAemia as a Single Potent Predictive Marker of Critical Condition Development and Mortality in COVID-19. *PloS One* (2021) 16:e0254640. doi: 10.1371/journal.pone.0254640
36. Ram-Mohan N, Kim D, Zudock EJ, Hashemi MM, Tjandra KC, Rogers AJ, et al. SARS-CoV-2 RNAemia Predicts Clinical Deterioration and Extrapulmonary Complications From COVID-19. *Clin Infect Dis* (2021) 74:218–26. doi: 10.1101/2020.12.19.20248561
37. van Riel D, Embregts CWE, Sips GJ, van den Akker JPC, Endeman H, van Nood E, et al. Temporal Kinetics of RNAemia and Associated Systemic Cytokines in Hospitalized COVID-19 Patients. *mSphere* (2021) 6:e0031121. doi: 10.1128/mSphere.00311-21
38. Ito S, Ansari P, Sakatsume M, Dickensheets H, Vazquez N, Donnelly RP, et al. Interleukin-10 Inhibits Expression of Both Interferon Alpha- and Interferon Gamma- Induced Genes by Suppressing Tyrosine Phosphorylation of STAT1. *Blood* (1999) 93:1456–63. doi: 10.1182/blood.V93.5.1456.404a34_1456_1463
39. Sposito B, Broggi A, Pandolfi L, Crotta S, Clementi N, Ferrarese R, et al. The Interferon Landscape Along the Respiratory Tract Impacts the Severity of COVID-19. *Cell* (2021) 184:4953–68.e16. doi: 10.1016/j.cell.2021.08.016
40. Gilbert C, Lefeuvre C, Preisser L, Pivert A, Soleti R, Blanchard S, et al. Age-Related Expression of IFN-λ1 Versus IFN-I and Beta-Defensins in the Nasopharynx of SARS-CoV-2-Infected Individuals. *Front Immunol* (2021) 12:750279. doi: 10.3389/fimmu.2021.750279
41. Lorè NI, De Lorenzo R, Rancoita PMV, Cugnata F, Agresti A, Benedetti F, et al. CXCL10 Levels at Hospital Admission Predict COVID-19 Outcome: Hierarchical Assessment of 53 Putative Inflammatory Biomarkers in an Observational Study. *Mol Med* (2021) 27:129. doi: 10.1186/s10020-021-00390-4
42. Shcherbak SG, Anisenkova AY, Mosenko SV, Glotov OS, Chernov AN, Apalko SV, et al. Basic Predictive Risk Factors for Cytokine Storms in COVID-19 Patients. *Front Immunol* (2021) 12:745515. doi: 10.3389/fimmu.2021.745515

Conflict of Interest: The authors declare that the research was conducted in the absence of any commercial or financial relationships that could be construed as a potential conflict of interest.

frontiers in Immunology

ORIGINAL RESEARCH
published: 15 February 2022
doi: 10.3389/fimmu.2022.841459

Cannabidiol and Terpene Formulation Reducing SARS-CoV-2 Infectivity Tackling a Therapeutic Strategy

Susana Santos[1,2*], *Pedro Barata*[3,4], *Adilia Charmier*[1,2], *Inês Lehmann*[1], *Suzilaine Rodrigues*[1], *Matteo M. Melosini*[1], *Patrick J. Pais*[3,4], *André P. Sousa*[3,4,5], *Catarina Teixeira*[3,4,5], *Inês Santos*[3,4,5], *Ana Catarina Rocha*[3,4], *Pilar Baylina*[3,4,5] *and Ruben Fernandes*[3,4,5]

[1] R&D&Innovation Department, EXMceuticals Portugal Lda, Lisboa, Portugal, [2] Cooperativa de Formação e Animação Cultural – Centre for Interdisciplinary Development and Research on Environment, Applied Management and Space (COFAC-DREAMS)-Universidade Lusófona, Lisboa, Portugal, [3] LABMI – Laboratório de Biotecnologia Médica e Industrial, PORTIC – Porto Research, Technology and Innovation Center, Porto, Portugal, [4] Metabesity Deopartment, i3S – Instituto de Investigação e Inovação em Saúde, Porto, Portugal, [5] Escola Superior de Saúde, Instituto Politécnico do Porto, Porto, Portugal

OPEN ACCESS

Edited by:
Tengchuan Jin, University of Science and Technology of China, China

Reviewed by:
Khalid Bougrin, Mohammed V University, Morocco
Khalid Karrouchi, Mohammed V University, Morocco

***Correspondence:**
Susana Santos
sirsantoss@gmail.com

Specialty section:
This article was submitted to Viral Immunology, a section of the journal Frontiers in Immunology

Received: *22 December 2021*
Accepted: *21 January 2022*
Published: *15 February 2022*

Citation:
Santos S, Barata P, Charmier A, Lehmann I, Rodrigues S, Melosini MM, Pais PJ, Sousa AP, Teixeira C, Santos I, Rocha AC, Baylina P and Fernandes R (2022) Cannabidiol and Terpene Formulation Reducing SARS-CoV-2 Infectivity Tackling a Therapeutic Strategy. Front. Immunol. 13:841459. doi: 10.3389/fimmu.2022.841459

In late 2019, COVID-19 emerged in Wuhan, China. Currently, it is an ongoing global health threat stressing the need for therapeutic compounds. Linking the virus life cycle and its interaction with cell receptors and internal cellular machinery is key to developing therapies based on the control of infectivity and inflammation. In this framework, we evaluate the combination of cannabidiol (CBD), as an anti-inflammatory molecule, and terpenes, by their anti-microbiological properties, in reducing SARS-CoV-2 infectivity. Our group settled six formulations combining CBD and terpenes purified from *Cannabis sativa* L, *Origanum vulgare*, and *Thymus mastichina*. The formulations were analyzed by HPLC and GC-MS and evaluated for virucide and antiviral potential by *in vitro* studies in alveolar basal epithelial, colon, kidney, and keratinocyte human cell lines.

Conclusions and Impact: We demonstrate the virucide effectiveness of CBD and terpene-based formulations. F2TC reduces the infectivity by 17%, 24%, and 99% for CaCo-2, HaCat, and A549, respectively, and F1TC by 43%, 37%, and 29% for Hek293T, HaCaT, and Caco-2, respectively. To the best of our knowledge, this is the first approach that tackles the combination of CBD with a specific group of terpenes against SARS-CoV-2 in different cell lines. The differential effectiveness of formulations according to the cell line can be relevant to understanding the pattern of virus infectivity and the host inflammation response, and lead to new therapeutic strategies.

Keywords: CBD - cannabidiol, endocannabinoid system (ECS), SARS-CoV-2, therapeutics, terpenes, formulations, essential oil (EO)

Abbreviations: ACE-2, angiotensin-converting enzyme 2; THC, tetrahydrocannabinol; ECS, endocannabinoid system; CNR2, cannabinoid receptor 2; RSV, respiratory syncytial virus; EOs, essential oils; HIV, human immunodeficiency virus; MCT, medium-chain triglyceride; CBD, cannabidiol; CPC, centrifuge partition chromatography; GC-MS, gas chromatography-mass spectrometry; HPLC, high-performance liquid chromatography; RdRp, RNA-dependent RNA polymerase; SARS-CoV, severe acute respiratory syndrome-CoV; SARS-CoV-2, severe acute respiratory syndrome-CoV-2.

1 INTRODUCTION

Since the emergence of the SARS-CoV-2 outbreak, extensive efforts have been placed regarding antiviral research for compounds with effective antiviral or virucide activity. COVID-19 is a complex disease that afflicts respiratory and gastrointestinal tract and kidney function, being one of its main features the hyperstimulation of the immune system. The spectrum of medical therapies to treat COVID-19 is growing; however, there are no 100% effective therapeutic approaches for the prevention and treatment of COVID-19.

1.1 Cannabis, Origanum, and Thymus Species as a Source of Biobased Formulations for Limiting SARS-CoV-2 Infectivity

Although vaccination and preventive medications are recognized as the most effective means of combating a virus, the treatment of COVID-19 is a real challenge prompting the need for effective drugs (1). Natural compounds from medicinal plants, such as terpenes, have gained attention as potential inhibitors of coronaviruses being the possible mechanism in the inhibition of viral replication or targeting viral proteins relevant for virus adsorption and entry (1–7). Essential oils (EOs) exhibit antiviral (4, 8–12), immunomodulatory (8, 13), and anti-inflammatory (8, 14, 15) properties, namely, regarding virus infection as *influenza* or herpes simplex viruses 1 or 2 (16, 17). EOs from *Origanum acutidens* (18), *Artemisia glabella* (19), eucalyptus and tea tree (20), *Thymus vulgaris*, *Melaleuca ericifolia*, *M. leucadendron*, and *M. armillaris* (21), among many others, have been described against those viruses. Wen et al. (22) reported EO constituents inducing a cytopathogenic effect against SARS-CoV on Vero-E6 cells. From molecular modeling studies, several terpenoids were potent inhibitors of SARS-CoV-2 replication (23). Among medicinal plants, *Origanum vulgare* has been recognized for its potential therapeutic role mainly arising from terpenes and flavonoids (24, 25) and *Thymus vulgaris* EOs have been shown to be effective against several RNA viruses including coronaviruses (21, 26). Regarding *Cannabis sativa*, it is particularly rich in terpenes, typically monoterpenes and sesquiterpenes (27–30). This plant is mostly known for containing phytocannabinoids, mainly Δ^9-tetrahydrocannabinol (THC) and cannabidiol (CBD), those widely accessed being medicinal compounds with known applications in several conditions, most of them related to inflammation processes (30–36). Phytocannabinoids are a group of terpenophenolic compounds with biological activities through interaction with the endocannabinoid system (ECS) in humans. CBD is a partial agonist for cannabinoid receptor 2 (CN2R), widely expressed in the immune system (37–39). In a mouse model for a respiratory syncytial virus (RSV) infection, CN2R activation reduced the signs of infection by modulating the immune system (10). One study demonstrates that a genetic polymorphism in CN2R, which reduces ECS-induced response (40), is associated with an increased risk of hospitalization in young children infected with RSV (n = 83), with up to 3-fold increased risk of developing severe acute respiratory tract infection. Rossi et al. (41) hypothesize that CN2R can be a therapeutic target for SARS-CoV-2 since its stimulation limits the release of pro-inflammatory cytokines, shifts the macrophage phenotype toward the anti-inflammatory M2 phenotype, and enhances the immune-modulating properties of mesenchymal stromal cells. The anti-inflammatory properties of CBD have been explored as antiviral agents for the treatment of HIV (42), *influenza* (43, 44), and most recently SARS-CoV-2 (45–48). CN2R increases as HIV infection progresses, and on infected macrophages, the exposure to CN2R to a selective agonist resulted in a dose-dependent decrease in reverse transcriptase activity/viral replication activity (17). Recently, researchers have tested CBD on 3D human models of oral, airways, and intestinal tissues and found that low THC/high CBD cultivars modulate ACE2 and TMPRSS2 levels, which might lower the virus load (49). By its turn, another study demonstrated that CBD reduced the secretion of pro-inflammatory cytokines IL-6, IL-8, CCL2, and CCL7 from the alveolar epithelial cell line A549 (50).

1.2 Why Does a Trade of *Two* Make Sense for Opposing One Single Agent? The Rationale for the Formulations

A similar study to the one proposed in this work was executed by Chatow et al. (51) who demonstrated an antiviral activity of a terpene formulation (30 terpenes) against HCoV-229E in human lung fibroblasts and the antiviral action during the viral multiplication cycle, in which the combination of the CBD with terpenes potentiated the antiviral effect. In another study, CBD exerted prolonged immunosuppression and hence might be used in chronic inflammation, and the terpenoids showed transient immunosuppression and might thus be used to relieve acute inflammation (52). Since terpenes are known to act as enhancing phytocannabinoid action (53–55), it is intended to query the action of a group of specific terpenes as virucide or antiviral agents acting in entourage effect with their selves and with the CBD as a therapeutic agent modulating inflammation. In detail, to exploit the biological action of the formulations on virus infectivity, it is a goal to understand their potential effect to act i) as a virucide agent blocking and inactivating the virus at early stages of infection, ii) as an antiviral agent blocking the virus cellular machinery, iii) as an agent against an overactive immune-inflammatory cascade at later stages of infection. This could be relevant in reversing the cytotoxic events induced by the virus and may contribute to the concept of ECS as a contributor for controlling the immune response from a virus infection.

2 MATERIALS AND METHODS

2.1 Formulation Development and Analysis

CBD and terpenes identified from *Cannabis sativa*, *Origanum vulgare subsp. virens*, and *Thymus mastichina* provided the source for 6 proprietary formulations (F1T, F2T, F3T, F1TC, F2TC, F3TC). The CBD was purified from a *Cannabis sativa* distillate (FarmCeutica Wellness, Richmond, Canada). A purified CBD sample (>99.5%) was obtained by Centrifuge

Partition Chromatography (CPC) technology using an rCPC device (RotaChrom, Purified Solutions, Budapest, Hungary). The method was internally developed through optimizing the best solvent combination and the solvent ratio (data to be published). Briefly, CPC is a liquid–liquid preparative chromatographic technique that makes use of two immiscible liquid phases, the solvent system, representing the stationary and mobile phases of a typical chromatographic apparatus. The target terpenes of EOs and CBD from the distillate were separated according to their partition coefficients. The main goal of this technology is to isolate specific compounds with a pharmaceutical purity grade (>99%) and high recovery mass yield (>95%). Relative to terpene purification, 3 groups of specific terpenes (19 in total) were purified from *Origanum vulgare subsp. virens* and *Thymus mastichina* (NBI-Natural Business Intelligence, Vila Real, Portugal) and from *Cannabis sativa* by combining a hydrodistillation clevenger with CPC (proprietary method). The formulations F1T, F2T, and F3T were prepared to contain a specific group of 7, 8, and 9 terpenes, respectively, comprising approximately 84% of terpene content and using MCT oil as carrier oil. The remaining terpenes were present at concentrations smaller than 2%. Moreover, CBD was added at a concentration of 1 µg/ml intending formulations F1TC, F2TC, and F3TC. Formulations and CBD samples were kept in dark amber glass flasks at room temperature. The EOs were obtained by the hydrodistillation clevenger, and the formulations comprising the terpenes were analyzed by gas chromatography-mass spectrometry (GC-MS, GC-MS-QP2020 NX Gas Chromatograph Mass Spectrometer, Shimadzu, Kyoto, Japan) (**Figures S1A–C** and **Supplemental Information**). The CBD isolate was analyzed by high-performance liquid chromatography (HPLC, Cannabis Analyzer™ for Potency, Shimadzu) (**Figure S1D** and **Supplemental Information**).

2.2 *In Vitro* Virucide Assays

2.2.1 Cell Culture

The Caco-2 cell line was cultured in MEM medium (VWR, Biowest, P0451-N10L, Riverside, MO, USA) supplemented with 20% of FBS (Gibco, Life Technologies, 10270, Grand Island, NY, USA) and 1% penicillin/streptomycin (Gibco, Life Technologies, 10270, USA). A549, HaCaT, and Hek293T cell lines were cultured in DMEM medium (VWR, Biowest, P0103-N10L, USA) supplemented with 10% of FBS and 1% penicillin/streptomycin. Cells were maintained at 37°C in a humidified chamber containing 5% CO_2.

2.2.2 SARS-CoV-2 Expansion

The B.1.1.7 strain of SARS-CoV-2, isolated in the laboratory, was clarified by centrifugation at 2,000 g for 15 min. The isolated virus was incubated in each cell line with 2% trypsin for 1 h, and then the cell culture was washed twice with PBS and incubated with complete cell culture medium.

2.2.3 Determination of the SARS-CoV-2 Titer

Total RNA was extracted using Lab-Aid Virus RNA Extraction Kit (Zeesan, Xiamen, China). RNA purity was measured in a microdrop 16-well microplate spectrophotometer (Thermo Scientific™ Multiskan SkyHigh Microplate Spectrophotometer, Life Technologies, Thermo Fisher Scientific, Waltham, MA, USA). Virus titer was determined by SARS-CoV-2 detection with Fosun COVID-19 RT-PCR Detection Kit (Fosun Pharma, Shanghai, China) and quantified using a calibration curve with Synthetic SARS-CoV-2 RNA SARS-CoV-2 positive control (SARS-CoV-2 Positive Control, Twist Synthetic, China).

2.2.4 Cytotoxicity Evaluation of Formulations

The MTT assay (Life Technologies, Thermo Fisher Scientific, USA) was carried out following the manufacturer's instruction. In brief, 1×10^5 cells/well were seeded and grown until 80% confluence. Each formulation and its isolated components were incubated with and without the predetermined virus titer for 24 h in cell culture. After the washing step with warm PBS, incomplete cell culture medium was added along with 0.5 mg/ml of MTT and incubated for 2 h at 37°C. The absorbance was measured using the microplate reader at 570 nm. Results were performed in triplicates and normalized to the control considered to be 100%.

2.2.5 Formulation Effect in SARS-CoV-2 Titer

Two different treatment approaches were employed: 1) treatment incubation of 24 h, followed by a rinsing step with warm PBS, and then the SARS-CoV-2 infection was executed for another 24 h; 2) incubation of SARS-CoV-2 for 24 h followed by a rinsing step with warm PBS and then the treatment incubation was employed during 24 h. Cell culture supernatant was harvested and submitted to a 3.2.3 process. The non-cytotoxic concentrations of the compounds and formulations were determined as the concentrations that did not lead to more than 50% cell death, as compared to untreated cells.

2.3 Gene Expression Under SARS-CoV-2 Infection

2.3.1 Primer and Probe Design

Four sets of primers and probes were designed based on the genome of SARS-CoV-2 (GenBank accession no. MN908947.3) using Primer Express Software (version 3.0.1 Applied Biosystems, Foster, CA, USA). The used primers and probes are identified in **Table 1**.

2.3.2 Gene Relative Quantification With the ΔCT Method Using a Reference Gene by One-Step RT-qPCR

Gene expression was estimated measuring the mRNA from cell extraction by RT-qPCR with qTOWER (3) (Analytik Jena, Germany), using One-step NZYSpeedy RT-qPCR Probe Kit, ROX (NZYTech, Lisbon, Portugal). 10 ng/µl RNA was employed, and the threshold cycle (CT) values from each biological assay were plotted with two experimental replicates following the manufacturer's procedure. Melting curve analysis was used to monitor the specificity of primers and probes. Results were normalized to the GAPDH housekeeping gene, and gene relative expression was employed by the ΔC_T expression/ΔC_T negative control ratio.

TABLE 1 | Set of primer and probe sequences for the one-step multiplex RT-qPCR.

Gene	Primer forward	Primer reverse	Probe
Spike	AAATGATCTCTGCTTTACTAATGTCTATGC	GCAGCCTGTAAAATCATCTGGTAAT	Cy5 – AAGTCAGACAAATCGCTCCAGGGCAAA – BHQ-3
RdRp (RNA-dependent RNA polymerase)	GCGGTATGTGGAAAGGTTATGG	AACGATTGTGCATCAGCTGACT	JOE – TTGTGATCAACTCCGCGAACCCATG – TAMRA
ACE2 (angiotensin converting enzyme 2)	GTGGGAGATGAAGCGAGAGATAG	TGAGTAATCATTAGAAACATGGAACAGA	JOE – CATGATGAAACATACTGTGACCCCGCA – TAMRA
TMPRSS2 (transmembrane serine protease 2)	CGGACCAAACTTCATCCTTCA	TCCAGTCGTCTTGGCACACA	Cy5 – TGTACTCATCTCAGAGGAAGTCCTGGCACC – BHQ-3
GAPDH (glyceraldehyde-3-phosphate dehydrogenase)	TCAAGATCATCAGCAATGCC	TGAGTCCTTCCACGATACC	Cy5 – CCTGCACCACCAACTGCTTAGCAC – BHQ-3

2.4 Statistical Analysis

All experiments were performed in triplicate and normalized to a negative control. Statistical analysis was performed comparing the control group results with those of the different groups with two-way analysis of variance (ANOVA) multiple-comparison and Dunnett *post hoc* tests, using GraphPad Prism 8.0.1 software (GraphPad Software, San Diego, CA, USA). Normality of data distribution was assessed using the Shapiro–Wilk test and for the homogeneity of variance with Bartlett's test. Results were considered statistically significant whenever p-value < 0.05.

3 RESULTS AND DISCUSSION

3.1 The Rationale for Data Analysis

F1T, F2T, and F3T were established using a mixture of specific terpenes purified from *Origanum virens*, *Thymus mastichina*, and *Cannabis sativa* as the genera of those plants are recognized to contain terpenes with reported antimicrobial properties (18, 21, 24–30). The concentration was based on published data and in data from our previous work (results from ecotoxicological and cytotoxic assays to be published, POCI-01-02B7-FEDER-053456-BIOBLOCKCOVID). Moreover, we intended to study the CBD-terpenes' entourage action (53–55), and so we used a lower concentration of F1T, F2T, and F3T when in combination with CBD. Despite the respiratory tract being the dominant route in SARS-CoV-2 infection, the colon, kidney, and skin comprise COVID-associated symptoms (56–66). Moreover, the colon, kidney, and skin tissues present very considerable levels of ACE2 and TMPRSS2 expression (data obtained from Human Protein Atlas available from http://www.proteinatlas.org, Uhlén M et al., Tissue-based map of the human proteome. Science (2015) PubMed: 25613900 DOI: 10.1126/science.1260419) and hence potential targets for virus infection. We performed the viral reduction assays in several cell lines and quantified ACE2 and TMPRSS2 gene expressions. Both receptors can be considered as targets for SARS-CoV-2, expecting that the coding genes are upregulated. By its turn, it is expected that RdRp and Spike gene expression is upregulated as viral infectivity progress and that gene expression diminishes because of a virucide or antiviral action. As CN2R activation could limit the release of pro-inflammatory cytokines (50) associated with COVID-19, and in this context being a potential therapeutic target for SARS-CoV-2, CBD was included in the formulations (F1TC, F2TC, F3TC) as a partial agonist of CN2R (37–39).

F1T, F2T, and F3T were established using a mixture of specific terpenes, and the concentration was based on published data and in data from our previous work (results from ecotoxicological and cytotoxic assays to be published, POCI-01-02B7-FEDER-053456-BIOBLOCKCOVID). Moreover, we intended to study the CBD-terpene entourage effect, and so we used a lower concentration of F1T, F2T, and F3T when in combination with CBD. Despite the respiratory tract being the dominant route in SARS-CoV-2 infection, the kidney and colon tissues present very considerable levels of ACE2 and TMPRSS2 expression and hence potential targets for virus infection. We performed the viral reduction assays in several cell lines and quantified ACE2 and TMPRSS2 gene expression. Both receptors can be considered as targets for SARS-CoV-2, expecting that the coding genes are upregulated. By its turn, it is expected that RdRp and Spike gene expression is upregulated as viral infectivity progress and that gene expression diminishes because of a virucide or antiviral action. As CN2R activation could limit the release of pro-inflammatory cytokines associated with COVID-19, and in this context being a therapeutic target for SARS-CoV-2, CBD was included in the formulations (F1TC, F2TC, F3TC) as a partial agonist of CN2R. **Figure 1** illustrates the adsorption and replication mechanisms as well as the potential action of CBD and terpenes and the ACE2, TMPRSS2, and CN2R expression in the lung, skin, colon, and kidney tissues. **Table 2** shows the cytotoxicity evaluation of the formulations per cell line for both pretreatment and treatment conditions, and **Table 3** shows the cytotoxicity of the components that comprises the formulations.

A two-way ANOVA analysis was performed to enquire the effect of treatment per cell line type on cytotoxicity, viral reduction, ACE2 expression, TMPRSS2 expression, RdRp expression, and Spike expression. The results of this analysis are presented in **Table 4**. A statistically significant interaction

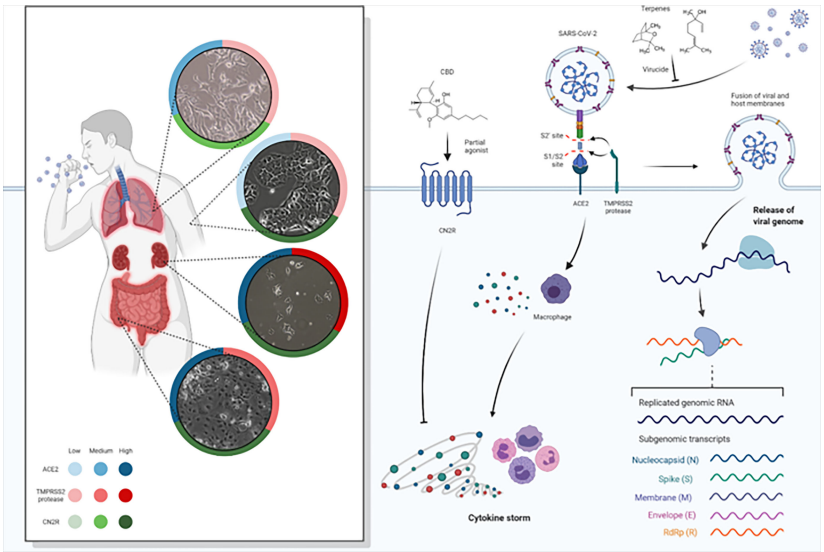

FIGURE 1 | Spike protein of SARS-CoV-2 binds to ACE2 receptors, fusing to the cell membrane and releasing the viral RNA into the host cell. SARC-CoV-2 depends on cellular serine protease, TMPRSS2, for Spike priming. Viral replication in host cells is always associated with inflammation and immune activation being that virus–host–cell interaction produces a set of immune mediators, cytokines, against the virus. It represents the ACE2, TMPRSS2, and CN2R expression levels (low, medium, high) in lung, skin, colon, and kidney tissues (data obtained from Human Protein Atlas available from http://www.proteinatlas.org, Uhlén M et al. Tissue-based map of the human proteome. Science (2015) PubMed: 25613900 DOI: 10.1126/science.1260419). CBD and terpenes (linalool and 1.8-cineole as representative of components of the formulations) are represented as virucide agents blocking and inactivating the virus at an early stage of infection, as antiviral agents blocking the virus cellular machinery and as agents against an overactive immune-inflammatory cascade. As the efficiency of Spike–ACE2 interaction determines SARS-CoV-2 transmissibility, the expression of ACE2 and TMPRSS2 could represent a major risk factor for the susceptibility to SARS-CoV-2 infection. We evaluate the hypothesis of terpenes as virucide agents that could disrupt the interaction between the Spike/TMPRSS2 proteins and the host cell ACE2 receptor. Moreover, after virus entry, terpenes could potentially have an antiviral effect by inhibiting RdRp thus preventing viral replication. Also, it was intended to better understand if a specific group of terpenes and CBD have the potential to act synergistically as therapeutic agents for SARS-CoV-2 and if the action is at early stages or later stages of infection. We assess the hypothesis that CBD may have the potential for modulating the exacerbated inflammatory process typical of COVID-19. CBD is a partial agonist CN2R that is widely expressed in the immune system and, when stimulated, promotes the inhibition of proinflammatory cytokine production, the increase of anti-inflammatory cytokines, and the induction of regulatory T cells.

between the normal treatment and the A549 cell line ($F(1, 12) = 3.773$; $p = 0.038$) and between the pretreatment and Caco-2 ($F(1, 12) = 8.181$; $p = 0.014$), A549 ($F(1, 12) = 7.406$; $p = 0.020$), and HaCaT ($F(1, 12) = 7{,}146$; $p = 0{,}020$) is denoted.

3.2 Analysis by Cell Line and per Formulation

3.2.1 Caco-2

F3T is toxic at the concentration of 50 μM. However, F3T is a promising formulation as it reduces viral titer by 35% while cell viability is 91.9%. Interestingly by adding CBD, a much higher toxicity (94.5% of cell death) is promoted; indirectly, this could be the reason why the viral reduction is 0% when using F3T *versus* F3TC. The toxicity is higher in pretreatment. Comparing F1T.100 with F1TC.10|1, in treatment and pretreatment assays it is possible to conclude those formulations as promising as the viral reduction by 29.6% and 28.6%, respectively, and as *Spike* and *RdRp* gene expressions were reduced. Comparing F2T.100 with F2TC.10|1, in treatment and pretreatment assays it was possible to conclude those formulations as promising as the viral reduction by 49.0% and 26.6%, respectively. It is an advantage to use CBD, as the concentration of terpenes, for obtaining approximately the same viral reduction, is ten times lower, and thus it is possible to conclude about an additive effect, which is also denoted when comparing F1T.100 with F1TC.10|1. An interesting fact to be explored is to understand why, comparing F1TC.10|1 pretreatment with F1TC.10|1 or F1TC.20|1 treatment, the *Spike* and *RdRp* gene expression increases. This cell line was used as COVID-19 includes gastrointestinal symptoms, and it remains uncertain if they are caused by direct infection, as aerosol droplets can be swallowed and pass the gastrointestinal tract, or whether they are a consequence of immune system activation.

3.2.2 A549

F3T is toxic at the concentration of 20 μM. Of relevance, regarding treatment assays, F3TC.10|1 reduces viral titer by 96.5% while cell viability is 22.7% and using F3TC.20|1 is less efficient in reducing viral titer. This fact is also denoted in Hek549 pointing out to a critical selection of the terpene concentration to be used when combined with CBD. By comparing F1T with F1TC and F2T with F2TC, in treatment assays, it is possible to conclude about the benefit of adding CBD as the viral titer increases, maintaining the cell viability. F2TC.20|1 is one of the most promising formulations as it reduces the viral titer by 98.7%, the best value obtained, and as expected *Spike and*

TABLE 2 | Cytotoxicity evaluation of formulations.

	Caco-2													
	Control	**[F1T.20]**	**[F1T.100]**	**[F1TC.10|1]**	**[F1TC.20|1]**	**[F2T.20]**	**[F2T.100]**	**[F2TC.10|1]**	**[F2TC.20|1]**	**[F3T.20]**	**[F3T.50]**	**[F3TC.10|1]**	**[F3TC-20|1]**	
NT	100.0 ± 5.2%	112.5 ± 12.0%	109.1 ± 4.1%	97.1 ± 4.7%	98.1 ± 2.9%	116.5 ± 6.7%	107.2 ± 14.4%	104.6 ± 1.0%	98.3 ± 4.8%	91.9 ± 12.9%	*63.1 ± 2.9%*	*5.4 ± 0.8%*	*4.7 ± 0.3%*	CV
	0.0 ± 0.0%	6.6 ± 1.1%	29.6 ± 3.3%	0.0 ± 0.0%	17.5 ± 5.0%	21.9 ± 4.7%	49.0 ± 1.9%	0.0 ± 0.0%	16.9 ± 2.2%	35.1 ± 0.0%	42.3 ± 1.7%	0.0 ± 0.0%	5.3 ± 5.1%	VR
	100.0 ± 4.0%	107.0 ± 8.0%	116.0+0.0%	115.4 ± 8.6%	116.1 ± 5.9%	107.4 ± 0.3%	111.1 ± 0.1%	0.0 ± 0.0%	112.7 ± 6.7%	0.0 ± 0.0%	0.0 ± 0.0%	130.1 ± 0.9%	0.0 ± 0.0%	Ae
	100.0 ± 1.0%	85.3 ± 9.3%	91.3 ± 0.3%	77.6 ± 7.4%	80.3 ± 7.7%	84.6 ± 5.6%	92.6 ± 5.4%	69.9 ± 0.1%	92.3 ± 11.7%	73.7 ± 2.7%	89.3 ± 4.3%	82.4 ± 2.6%	74.4 ± 1.6%	Te
	100.0 ± 5.0%	285.1 ± 2.9%	36.9 ± 0.1%	365.8 ± 12.2%	334.9 ± 6.9%	97.5 ± 1.5%	*281.0 ± 15.0%*	414.0 ± 4.0%	206.1 ± 3.9%	464.1 ± 19.1%	375.1 ± 1.9%	261.9 ± 11.1%	332.0 ± 8.0%	Re
	100.0 ± 1.2%	225.4 ± 3.6%	63.4 ± 2.6%	283.8 ± 7.2%	255.9 ± 7.9%	110.8 ± 5.2%	*222.7 ± 10.7%*	318.8 ± 9.2%	176.2 ± 1.8%	360.3 ± 5.3%	288.1 ± 0.1%	201.2 ± 3.8%	253.3 ± 3.7%	Se
PT	100 ± 4.3%	95.9 ± 10.3%	108.0 ± 4.5%	94.8 ± 7.9%	108.6 ± 8.8%	95.4 ± 2.2%	81.2 ± 0.4%	84.5 ± 8.6%	98.9 ± 4.3%	*9.9 ± 0.4%*	*9.7 ± 0.0%*	*11.5 ± 0.0%*	*11.1 ± 0.3%*	CV
	0.0 ± 0.0%	0.0 ± 0.0%	19.2 ± 5.0%	28.6 ± 3.8%	0.0 ± 0.0%	0.0 ± 0.0%	23.0 ± 3.9%	26.6 ± 1.0%	0.0 ± 0.0%	0.0 ± 0.0%	4.0 ± 3.4%	17.5 ± 2.3%	13.4 ± 3.4%	VR
	100.0 ± 0.5%	113.7 ± 4.3%	126.4 ± 1.4%	116.0 ± 5.0%	141.2 ± 0.8%	124.7 ± 4.3%	109.9 ± 4.1%	125.9 ± 3.1%	136.8 ± 3.2%	0.0 ± 0.0%	0.0 ± 0.0%	0.0 ± 0.0%	0.0 ± 0.0%	Ae
	100.0 ± 2.1%	86.50.5%	108.5 ± 1.5%	97.6 ± 4.4%	80.9 ± 0.1%	83.6 ± 9.6%	79.3 ± 1.3%	99.1 ± 2.9%	95.6 ± 0.6%	105.0 ± 1.0%	85.9 ± 11.1%	96.3 ± 2.7%	71.3 ± 1.3%	Te
	100.0 ± 0.2%	34.4 ± 1.6%	25.4 ± 0.4%	38.4 ± 0.6%	105.7 ± 4.3%	13.9 ± 0.1%	38.1 ± 0.9%	20.4 ± 0.6%	26.0 ± 1.0%	157.1 ± 0.1%	87.1 ± 0.1%	151.1 ± 0.1%	73.6 ± 3.4%	Re
	100.0 ± 2.8%	78.8 ± 3.2%	37.8 ± 0.8%	44.1 ± 5.1%	77.1 ± 7.1%	53.1 ± 5.9%	73.1 ± 5.9%	42.9 ± 8.1%	41.4 ± 4.6%	94.1 ± 6.1	60.1 ± 1.1%	150.1 ± 3.9%	110.5 ± 5.5%	Se
	A549													
	Control	[F1T.20]	[F1T.100]	[F1TC.10|1]	[F1TC.20|1]	[F2T.20]	[F2T.100]	[F2TC.10|1]	[F2TC.20|1]	[F3T.20]	[F3T.50]	[F3TC.10|1]	[F3TC-20|1]	
NT	100.0 ± 5.4%	94.0 ± 7.6%	76.1 ± 3.0%	112.1 ± 19.0%	115.8 ± 6.0%	107.9 ± 20.1%	120.6+80.5%	100.9 ± 5.1%	117.8 ± 9.7%	22.4 ± 0.2%	24.3 ± 1.1%	*22.7 ± 0.4%*	22.2 ± 0.7%	CV
	0.0 ± 0.0%	3.4 ± 0.5%	68.0 ± 4.8%	23.0 ± 0.9%	22.4 ± 0.6%	0.0 ± 0.0%	13.4 ± 4.7%	12.2 ± 0.8%	98.7 ± 5.0%	0.0 ± 0.0%	25.1 ± 0.6%	*96.5 ± 3.0%*	45.0 ± 2.2%	VR
	100.0 ± 7.0%	85.3 ± 1.7%	83.6 ± 0.6%	81.6 ± 4.4%	109.1 ± 0.1%	73.7 ± 4.3%	84.6 ± 3.4%	108.9 ± 7.1%	88.2 ± 0.8%	71.7 ± 4.7%	106.5 ± 0.5%	90.6 ± 1.4%	80.4 ± 3.6%	Ae
	100.0 ± 5.0%	101.2 ± 3.8%	83.3 ± 4.3%	73.1 ± 0.9%	100.6 ± 4.4%	69.1 ± 0.1%	82.8 ± 2.2%	106.0 ± 3.0%	80.4 ± 1.4%	72.5 ± 0.5%	132.9 ± 6.1%	86.0 ± 2.0%	70.4 ± 2.6%	Te
	100.0 ± 3.2%	63.1 ± 2.9%	79.7 ± 2.7%	60.9 ± 0.1%	45.6 ± 0.4%	48.1 ± 3.1%	27.8 ± 1.2%	73.8 ± 3.2%	70.5 ± 4.5%	30.2 ± 0.2%	28.3 ± 1.7%	61.2 ± 0.8%	31.8 ± 1.2%	Re
	100.0 ± 4.4%	59.8 ± 0.2%	76.1 ± 6.1%	66.1 ± 0.9%	44.9 ± 0.9%	51.6 ± 3.6%	33.1 ± 0.1%	75.7 ± 0.3%	73.9 ± 1.1%	24.8 ± 0.8%	39.1 ± 1.9%	60.2 ± 1.2%	43.6 ± 1.4%	Se
PT	100.0 ± 9.4%	105.0 ± 11.6%	84.6 ± 2.6%	95.7 ± 17.6%	60.7 ± 1.1%	77.4 ± 4.1%	80.2 ± 4.2%	89.8 ± 11.5%	63.7 ± 5.7%	6.0 ± 0.3%	6.6 ± 0.3%	24.0 ± 3.3%	5.4 ± 0.1%	CV
	0.0 ± 0.0%	0.0 ± 0.0%	0.0 ± 0.0%	0.0 ± 0.0%	0.0 ± 0.0%	21.9 ± 1.4%	0.0 ± 0.0%?	0.0 ± 0.0%	0.0 ± 0.0%	0.0 ± 0.0%	0.0 ± 0.0%	0.0 ± 0.0%	0.0 ± 0.0%	VR
	100.0 ± 8.0%	106.3 ± 3.7~%	112.0 ± 3.0%	103.1 ± 3.9%	114.4 ± 3.6%	105.4 ± 5.6%	104.0 ± 6.0%	97.5 ± 3.5%	98.5 ± 1.5%	105.8 ± 5.2%	74.1 ± 0.1%	104.8 ± 3.2%	95.0 ± 5.0%	Ae
	100.0 ± 11.1%	121.3 ± 5.7%	124.5 ± 7.5%	113.1 ± 5.9%	128.3 ± 0.7%	125.0 ± 8.0%	115.8 ± 3.2%	109.1 ± 5.9%	118.8 ± 8.2%	121.4 ± 4.4%	74.1 ± 3.9%	110.9 ± 2.1%	99.6 ± 6.4%	Te
	100.0 ± 2.0%	116.2 ± 6.8%	119.6 ± 1.6%	120.7 ± 1.3%	130.4 ± 0.6%	135.6 ± 9.4%	113.5 ± 3.5%	131.6 ± 6.4%	104.8 ± 2.2%	112.4 ± 1.4%	76.7 ± 1.3%	126.9 ± 8.1%	95.4 ± 1.6%	Re
	100.0 ± 2.4%	78.8 ± 3.3%	37.8 ± 0.8%	44.1 ± 5.1%	77.1 ± 7.1%	53.1 ± 5.9%	73.1 ± 5.9%	42.9 ± 8.1%	41.4 ± 4.6%	94.1 ± 6.1%	60.1 ± 1.1%	150.1 ± 3.9%	110.5 ± 5.5%	Se
	HaCaT													
	Control	[F1T.20]	[F1T.100]	[F1TC.10|1]	[F1TC.20|1]	[F2T.20]	[F2T.100]	[F2TC.10|1]	[F2TC.20|1]	[F3T.20]	[F3T.50]	[F3TC.10|1]	[F3TC-20|1]	
NT	100.0 ± 4.7%	90.4 ± 4.1%	105.8 ± 2.6%	118.1 ± 14.1%	105.3 ± 9.0%	109.4 ± 4.7%	92.5 ± 2.6%	124.6 ± 7.6%	102.8 ± 7.7%	*8.0 ± 0.1%*	*8.3 ± 0.6%*	*8.9 ± 0.2%*	*8.7 ± 0.2%*	CV
	0.0 ± 0.0%	26.1 ± 0.6%	31.9 ± 0.5%	19.7 ± 3.7%	37.7 ± 1.9%	30.0 ± 3.6%	46.1 ± 4.8%	18.6 ± 2.8%	23.5 ± 4.4%	43.8 ± 1.0%	*54.9 ± 3.0%*	30.5 ± 4.5%	54.0 ± 4.4%	VR
	100.0 ± 2.0%	136.1 ± 0.9%	134.4 ± 1.4%	168.1 ± 7.9%	143.2 ± 6.8%	139.0 ± 0.0%	160.0 ± 4.0%	124.1 ± 4.9%	0.0 ± 0.0%	151.9 ± 3.9%	120.5 ± 3.5%	0.0 ± 0.0%	0.0 ± 0.0%	Ae
	100.0 ± 1.0%	175.2 ± 7.8%	140.6 ± 7.6%	174.2 ± 0.2%	158.7 ± 5.3%	158.4 ± 2.4%	161.6 ± 1.4%	115.0 ± 5.0%	133.3 ± 2.7%	78.0 ± 8.0%	92.0 ± 2.0%	172.2 ± 5.8%	106.8 ± 3.2%	Te
	100.0 ± 7.3%	*0.4 ± 0.1%*	0.2 ± 0.2%	68.3 ± 1.7%	*0.0 ± 0.0%*	2.2 ± 1.3%	0.0 ± 0.0%	0.2 ± 0.1%	2.7 ± 0.9%	0.0 ± 0.0%	8.5 ± 6.5%	0.0 ± 0.0%	1.6 ± 0.2%	Re

(Continued)

TABLE 2 | Continued

	Caco-2													
	Control	**[F1T.20]**	**[F1T.100]**	**[F1TC.10|1]**	**[F1TC.20|1]**	**[F2T.20]**	**[F2T.100]**	**[F2TC.10|1]**	**[F2TC.20|1]**	**[F3T.20]**	**[F3T.50]**	**[F3TC.10|1]**	**[F3TC-20|1]**	
	100.0 ± 5.8%	*3.6 ± 2.4%*	129.5 ± 4.5%	52.1 ± 0.9%	*0.0 ± 0.0%*	4.2 ± 1.3%	0.0 ± 0.0%	6.5 ± 4.5%	0.9 ± 0.1%	0.0 ± 0.0%	9.1 ± 6.9%	3.0 ± 1.4%	14.0 ± 4.0%	Se
PT	100.0 ± 9.3%	109.0 ± 10.0%	130.3 ± 9.6%	145.3 ± 4.0%	103.9 ± 8.4%	124.4 ± 3.3%	137.9 ± 14.7%	141.6 ± 24.2%	136.8 ± 10.6%	*61.0 ± 10.8%*	*19.4 ± 0.3%*	*54.4 ± 5.2%*	*21.1 ± 0.9%*	CV
	0.0 ± 0.0%	0.0 ± 0.0%	0.0 ± 0.0%	0.0 ± 0.0%	0.0 ± 0.0%	0.0 ± 0.0%	0.0 ± 0.0%	0.0 ± 0.0%	0.0 ± 0.0%	0.0 ± 0.0%	0.0 ± 0.0%	0.0 ± 0.0%	0.0 ± 0.0%	VR
	100.0 ± 0.3%	87.4 ± 2.6%	94.4 ± 1.4%	108.6 ± 4.4%	100.9 ± 3.1%	102.8 ± 3.2%	90.0 ± 0.0%	106.3 ± 4.7%	0.0 ± 0.0%	109.3 ± 0.3%	104.9 ± 5.1%	0.0 ± 0.0%	0.0 ± 0.0%	Ae
	100.0 ± 8.2%	118.2 ± 0.8%	138.8 ± 4.8%	103.8 ± 5.2%	133.8 ± 6.2%	109.8 ± 2.2%	80.8 ± 2.2%	100.7 ± 4.3%	91.0 ± 2.0%	61.0 ± 1.0%	88.7 ± 2.3%	99.0 ± 0.1%	91.8 ± 2.2%	Te
	100.0 ± 1.2%	21.3 ± 0.7%	2.2 ± 1.8%	285.7 ± 4.3%	10.4 ± 0.4%	50.2 ± 0.8%	78.0 ± 4.0%	227.5 ± 4.5%	326.1 ± 0.1%	0.8 ± 0.1%	226.5 ± 8.5%	190.3 ± 3.7%	408.2 ± 1.8%	Re
	100.0 ± 2.3%	58.2 ± 1.8%	16.5 ± 0.5%	217.6 ± 10.4%	44.6 ± 0.6%	69.7 ± 1.3%	81.5 ± 4.5%	206.8 ± 5.2%	248.0 ± 12.0%	31.8 ± 0.2%	179.6 ± 4.4%	181.3 ± 3.7%	311.3 ± 7.7%	Se
							Hek293T							
	Control	[F1T.20]	[F1T.100]	[F1TC.10|1]	[F1TC.20|1]	[F2T.20]	[F2T.100]	[F2TC.10|1]	[F2TC.20|1]	[F3T.20]	[F3T.50]	[F3TC.10|1]	[F3TC-20|1]	
NT	100.0 ± 18.2%	167.7 ± 36.4%	95.1 ± 3.1%	141.9 ± 6.8%	156.2 ± 24.5%	179.5 ± 28.7%	155.8 ± 3.0%	170.5 ± 13.2%	155.6 ± 6.5%	*40.0 ± 24.7%*	*22.0 ± 0.8%*	119.4 ± 7.3%?	*37.2 ± 9.2%*	CV
	0.0 ± 0.0%	32.4 ± 3.1%	0.0 ± 0.0%	0.0 ± 0.0%	18.1 ± 7.3%	19.2 ± 2.3%	0.0 ± 0.0%	12.2 ± 1.1%	7.3 ± 1.2%	21.9 ± 1.0%	19.2 ± 0.7%	23.0 ± 2.5%	28.6 ± 0.6%	VR
	100.0 ± 9.5%	69.3 ± 1.7%	101.4 ± 2.4%	104.7 ± 2.3%	92.2 ± 3.8%	61.2 ± 2.2%	105.8 ± 4.2%	74.5 ± 1.5%	92.3 ± 0.3%	90.7 ± 3.7%	110.9 ± 3.1%	103.2 ± 0.8%	88.4 ± 0.3%	Ae
	100.0 ± 3.2%	47.7 ± 0.3%	107.2 ± 5.2%	116.9 ± 5.1%	88.9 ± 4.1%	38.2 ± 0.2%	108.4 ± 3.6%	66.6 ± 1.4%	96.1 ± 0.1%	94.9 ± 1.9%	109.9 ± 2.1%	113.3 ± 1.7%	97.6 ± 4.4%	Te
	100.0 ± 4.0%	59.3 ± 0.7%	153.3 ± 0.7%	114.2 ± 4.8%	119.5 ± 4.5%	59.1 ± 1.9%	58.1 ± 3.1%	116.9 ± 1.1%	121.8 ± 1.2%	194.2 ± 6.2%	166.1 ± 0.1%	140.9 ± 4.1%	166.2 ± 0.8%	Re
	100.0 ± 5.1%	70.1 ± 1.9%	113.5 ± 1.5%	88.9 ± 4.1%	112.8 ± 0.2%	56.9 ± 1.1%	66.3 ± 0.3%	99.2 ± 3.8%	92.9 ± 4.1%	167.3 ± 4.3%	144.0 ± 7.0%	124.3 ± 5.7%	135.3 ± 0.7%	Se
PT	100.0 ± 6.7%	94.9 ± 13.4%	103.9 ± 16.7%	131.2 ± 22.1%	108.0 ± 5.3%	132.6 ± 18.0%	110.3 ± 15.9%	117.7 ± 10.7%	97.5 ± 11.3%	*20.0 ± 0.9%*	*18.6 ± 0.0%*	118.1 ± 2.5%	*19.3 ± 0.3%*	CV
	0.0 ± 0.0%	0.0 ± 0.0%	0.0 ± 0.0%	0.0 ± 0.0%	43.1 ± 5.0%	0.0 ± 0.0%	2.7 ± 0.1%	0.0 ± 0.0%	17.5 ± 3.8%	6.0 ± 2.6%	7.9 ± 0.5%	0.0 ± 0.0%	0.0 ± 0.0%	VR
	100.0 ± 2.0%	83.1 ± 0.1%	86.5 ± 0.5%	90.2 ± 2.8%	87.6 ± 3.4%	92.2 ± 0.2%	80.3 ± 3.7%	78.0 ± 2.0	93.7 ± 2.3%	77.7 ± 3.7%	84.6 ± 3.4%	87.3 ± 1.7%	84.3 ± 3.7%	Ae
	100.0 ± 7.0%	56.2 ± 0.8%	79.7 ± 2.7%	84.6 ± 1.4%	76.1 ± 3.9%	100.8 ± 1.2%	55.9 ± 0.1%	65.6 ± 1.4%	94.7 ± 2.3%	70.8 ± 2.8%	78.6 ± 0.4%	79.4 ± 0.6%	81.8 ± 2.2%	Te
	100.0 ± 5.2%	88.9 ± 3.1%	71.7 ± 1.3%	70.7 ± 1.3%	93.6 ± 2.6%	92.6 ± 3.4%	86.2 ± 0.2%	76.5 ± 3.5%	99.2 ± 0.8%	103.1 ± 0.9%	5.1 ± 0.1%	67.7 ± 0.3%	48.9 ± 2.1%	Re
	100.0 ± 3.7%	97.5 ± 1.5%	70.5 ± 2.5%	72.7 ± 2.3%	91.2 ± 1.2%	83.5 ± 0.5%	87.1 ± 4.1%	78.0 ± 0.0%	91.7 ± 0.3%	105.9 ± 3.1%	9.4 ± 0.6%	67.4 ± 2.6%	51.2 ± 0.8%	Se

CV, cell viability; formulation effect in SARS-CoV-2 titer—VR, viral reduction; and gene relative quantification with the ΔCT method—Ae, ACE expression; Te, TMPRSS2 expression; Re, RdRp expression; Se, Spike expression; NT, normal treatment; PT, pretreatment; F1T, F2T, F3T, terpene formulations comprising a specific group of 7, 8, and 9 terpenes, respectively, in concentrations of 20, 100, or 50 μM; F1TC, F2TC, F3TC, terpene formulations added with CBD to a concentration of 1 μg/ml. In this case, the terpene concentration is 10 or 20 μM.

TABLE 3 | Formulation components evaluation regarding Caco-2, A549, HaCaT, and Hek293T cell line viability.

Components |Cell line	Caco-2	A549	HaCaT	Hek293T
T0.01%/M0.1%/D0.1%	63.9 ± 4.2%	56.5 ± 10.6%	119.1 ± 16.1%	85.7 ± 1.9%
T0.001%/M0.1%/D0.1%	115.5 ± 7.0%	137.8 ± 2.5%	108.4 ± 15.2%	88.5 ± 5.1%
T0.01%/M0.01%/D0.1%	51.7 ± 19.1%	73.1 ± 7.6%	112.9 ± 12.9%	78.8 ± 5.4%
T0.001%/M0.01%/D0.1%	100.3 ± 9.0%	130.2 ± 7.1%	105.3 ± 11.6%	68.9 ± 7.6%

T, Tween 80; M, MCT; D, DMSO.

TABLE 4 | A two-way ANOVA regarding the effect of treatment per cell line on cytotoxicity, viral reduction, and gene expression.

Treatment	Cell type	Results
Normal treatment	Caco-2	F (1, 12) = 0.424; p = 0.528
	A549	**F (1, 12) = 3.773; p = 0.038**
	HaCaT	F (1, 12) = 1.246; p = 0.306
	HEK293T	F (1, 12) = 1,988; p = 0,159
Pretreatment	Caco-2	**F (1, 12) = 8.181; p = 0.014**
	A549	**F (1, 12) = 7.406; p = 0.020**
	HaCaT	**F (1, 12) = 7,146; p = 0,020**
	HEK293T	F (1, 12) = 3,026; p = 0,108

There was a statistically significant interaction (represented in bold) between the normal treatment and the A549 cell line and between the pretreatment and Caco-2 and HaCaT.

RdRp gene expression is reduced. The additive effect of CBD is clear, as the concentration of terpenes, for obtaining approximately the same viral reduction, is ten times lower. For this cell line, the pretreatment assays have no impact in viral reduction. This cell line was used as SARS-CoV-2 propagates through aerosol droplets that can be inhaled and infect the upper airways. F2TC.20|1 could be exploited as a promising therapeutic for upper or lower airway infection.

3.2.3 HaCaT

F3T is toxic for the concentration of 20 μM. Pretreatment assays of this cell line are not adequate as viral reduction is 0%. The addition of CBD to F3T has no effect regarding viral reduction or cell viability in this cell line. A comparable effect is denoted regarding F1T.20 vs. F1TC.20|1, in that adding CBD has no (significant) additive effect in viral reduction either in *Spike* or in *RdPp* expression. F2T.20 is the most efficient formulation by reducing by 30% the viral titer and by promoting the downregulation of *Spike* and *RdPp* expression to less than 5%. The addition of CBD to F2T.20 has no additive effect. Importantly, and compared to the other cell lines, in HaCaT a higher expression of *ACE2* and *TMPRSS2* is verified. This cell line was used, as skin lesions and lesions of the vascular system in some SARS-CoV-2-positive patients have been reported. The high levels of *ACE2* and *TMPRSS2* expression could indicate that percutaneous transmission might be a potential risk route for SARS-CoV-2 infection, particularly in conditions of skin dysfunction. Also, the long-term wearing of protective clothing and having contact with disinfectants cause eczematoid dermatitis which might be a risk factor for percutaneous infection. F2T and F1T can be studied as treating skin lesions in SARS-CoV-2 patients. By its turn, F3T.50 could be used for SARS-CoV-2 control in surfaces as it reduces viral titer by 54.9%.

3.2.4 Hek293T

F3T is toxic for almost all the concentrations, except for F3TC.10|1, which is in fact a promising formulation. The addition of CBD to F1T, F2T, or F3T has no effect, regarding viral reduction or cell viability, and promotes upregulation of *Spike* and *RdRp* (F1T and F2T). F1T.20 and F2T.20 are the most promising formulations as the virus titer is 32% and 19%, respectively, and Spike and *RdRp* are downregulated. Similar to the effect in Caco-2, pretreatment and CBD addition is beneficial for this cell line as the virus titer is 43%. Comparing F1T.20 and F2T.20 with F1TC.20|1 and F2T.20|1, it is possible to conclude about a synergistic effect of CBD and terpenes, and that the terpenes from F1T have a higher effect in virus reduction compared to the terpenes from F2T. This cell line was used as COVID-19 includes kidney failure symptoms.

Table 5 intends to summarize per cell line the most promising formulations based on viral reduction and viral gene expression parameters. In **Figure 2**, it is intended to summarize the efficacy of each formulation per cell line.

4 CONCLUSIONS AND IMPACT

Up to date, a fully effective treatment for COVID-19 is still a challenge. Although the interest in CBD and EOs as therapeutic strategies grows, no scientific studies were made to evaluate the role of CBD and specific terpenes in the progression of SARS-CoV-2 infection. Our group settled an approach focused on the inhibition of both virus entry and viral replication by using biobased formulations from cannabis, thyme, and oregano. The obtained data suggest these formulations to be exploited as new therapeutics targeting COVID-19, providing evidence that CBD and terpenes could be considered for further studies as effective anti-SARS-CoV-2 agents and potentially used for treatment or as adjuvants to conventional COVID-19 therapies. Also, it demonstrates that the selection of terpenes to be used combined with CBD is relevant and points out that treatment should be targeted for afflicted tissues. The proprietary formulations F2TC and F1TC could potentially be used for treating viral infections *via* modulation of the cytokine storm. Additional studies regarding the molecular mechanism explaining both the virucide or antiviral activity and the immunomodulatory effect will be exploited by our group. It will be interesting to explore the anti-inflammatory function of CBD concerning inflammatory events that happen during severe COVID-19 disease and how it might help to prevent the progression from mild to severe disease. In this

TABLE 5 | Formulation efficacy considering viral reduction, *RdRp* expression, and *Spike* expression per cell line.

Caco-2	[F1TC 10|1.PT]	[F2TC 10|1].PT	[F2T 100]	[F1T 100]	[F2TC 20|1]	[F1TC 20|1]	[F3T 20]
Viral reduction	**28,60**	26,60	49,00	29,60	16,90	17,50	35,10
RdRp expression	✓38,4	✓20,4	↑281,0	✓36,9	↑206,1	↑334,9	↑464,0
Spike expression	✓44,10	✓42,90	↑222,70	✓63,40	↑176,20	↑255,90	↑360,0

A549	[F2TC 20|1]	[F1TC 10|1]	[F3TC 50]
Viral reduction	**98,70**	23,00	96,50
RdRp expression	✓70,5	✓60,9	✓61,0
Spike expression	✓73,9	✓66,1	✓60,0

HaCaT	[F2T 20]	[F1T 20]	[F1TC 20|1]	[F2TC 10|1]	[F3T 50]
Viral reduction	**30,00**	26,10	37,70	18,60	54,90
RdRp expression	✓2,2	✓0,4	✓0,0	✓0,2	✓8,5
Spike expression	✓4,2	✓3,6	✓0,0	✓6,5	✓9,1

Hek293T	[F1T 20]	[F2T 20]	[F1TC 20|1].PT	[F1TC 20|1]	[F2TC 10|1]	[F3TC 10|1]
Viral reduction	**32,40**	19,20	**43,10**	18,10	**12,20**	23,00
RdRp expression	✓59,3	✓59,1	✓93,6	↑119,5	↑116,9	↑140,0
Spike expression	✓70,1	✓56,9	✓91,2	↑112,8	✓99,2	↑124,0

√—downregulation, ↑—upregulation. PT—pretreatment. The bars indicate the percentage of viral reduction. For Caco-2 and A549, the combination of terpenes with CBD was the most effective treatment.

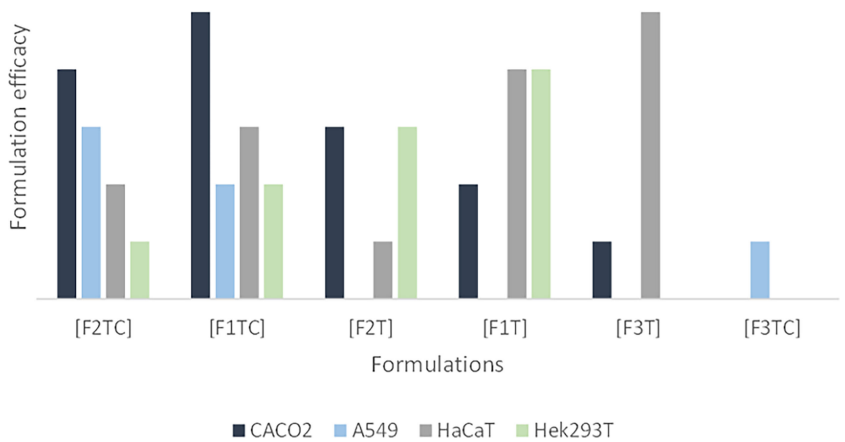

FIGURE 2 | Formulation efficacy (in terms of viral reduction) for Caco-2, A549, HaCaT, and Hek293T cell lines. In this graphic, it is possible to observe i) an additive effect of CBD and terpenes in Caco-2 and A549, ii) that adding CBD to F1T is not advantageous regarding HaCaT, iii) that adding CBD to F2T is an advantage regarding HaCaT, iv) that the terpenes of F1T are more effective than the ones from F2T for HaCaT and Hek293T, vi) that the terpenes from F1T are more effective regarding Caco-2, vii) that F3T and F3TC include terpenes that are more toxic than the ones included in F1T and F2T, being that the toxicity is higher in combination with CBD.

context, the activation of the ECS could contribute to preventing the progress and the severity of COVID-19. The current study identifies CBD and a specific group of terpenes as a promising anti-COVID-19 therapeutic strategy that warrants further *in vivo* testing and preclinical trials.

DATA AVAILABILITY STATEMENT

The original contributions presented in the study are included in the article/**Supplementary Material**. Further inquiries can be directed to the corresponding author.

AUTHOR CONTRIBUTIONS

All authors certify that they have participated sufficiently in the work to take public responsibility for the content, including participation in the concept, design, analysis, interpretation, writing, or revision of the article. All authors contributed to the article and approved the submitted version.

FUNDING

This research was partially funded by the European Commission, European Regional Development, FEDER/02/SAICT/2020/072560 SI-B7-2020-15, POCI-01-02B7-FEDER-053456, BIOBLOCKCOVID. The funding allowed to perform the collection and harvesting of the medicinal plants, extract and purify the terpenes and formulations, execute the formulations, and execute preliminary assays related to toxicity. Considering *in vitro* virucide assays and gene expression assays, the work was partially funded by FCT – Fundação para a Ciência e Tecnologia (REF UID/BIM/04293/2019) and was partially supported by grants 104 and 112 of the 1st edition of RESEARCH4COVID (FCT) and by the grant 418 from the 2nd edition of RESEARCH4COVID-19 (FCT). This work was also partially supported by FEDER-European Regional Development Fund with the grant FEDER/02/SAICT/2020/072560.

ACKNOWLEDGMENTS

We would like to acknowledge the researchers that participated in the BioBlockCOVID project, especially Prof. João Ramalho Santos for providing the A549 and HaCaT cell lines and execution of preliminary cytotoxicity assays, Prof. José Paulo Sousa, and Dr. Tiago Luz for the ecotoxicity assays, and Prof. Rui Ribeiro and Dra. Matilde Moreira Santos for the aquatic toxicity assays. We acknowledge the assistance in hydrodistillation to Prof. Ana Cristina Figueiredo, Faculdade de Ciências da Universidade de Lisboa, CESAM Lisboa.

SUPPLEMENTARY MATERIAL

The Supplementary Material for this article can be found online at: https://www.frontiersin.org/articles/10.3389/fimmu.2022.841459/full#supplementary-material

Supplementary Figure 1 | – GC-MS quantitative chromatogram of formulations F1T **(A)**, F2T **(B)** and F3T **(C)**. Peak numbering represents terpenes ranked from the higher to the lower concentration. X axis - Retention Time (min), Y axis – Intensity. The terpenes are anonymized as F1T, F2T, F3T are proprietary formulations. HPLC-UV chromatogram analysis of a CBD isolate **(D)**, X axis - Retention Time (min), Y axis - Intensity (mAU).

Supplementary Figure 2 | – Graphical representation of the cytotoxicity evaluation of formulations, formulation effect in SARS-CoV-2 titer and gene relative quantification with ΔCT method. Evaluation of the effect from formulations without (F1T=1, F2T=2, F3T=3) and with the addition of CBD (F1TC=1+, F2TC=2+, F3TC=3+). The terpenes were used in a concentration of 20 μM (L) and 100 μM (H) for F1T and F2T, 20 μM (L) and 50 μM (H) for F3T, 10 μM (L) and 20 μM (H) for F1TC and F2TC, 20 μM (H) and 10 μM (L) for F3TC. **(A)** Cytotoxicity effect; **(B)** Formulation effect on viral number copies reduction; **(C and D)** Gene expression of ACE2 and TMPRSS2 genes under the influence of the formulations; **(E and F)** Gene expression of RdRp and Spike genes under the influence of the formulations. Results are represented as mean with standard deviation and normalized to GAPDH expression. Symbols above bars represent statistical significance (* $p < 0.05$; ** $p < 0.01$; *** $p < 0.001$; **** $p < 0.0001$). **Figure 2.1 –** Treatments administrated after SARS-CoV-2 infection in Caco-2 cell line. **Figure 2.2 -** Treatments administrated before SARS-CoV-2 infection in Caco-2 cell line. **Figure 2.3 -** Treatments administrated after SARS-CoV-2 infection in A549 cell line. **Figure 2.4 –**Treatments administrated before SARS-CoV-2 infection in A549 cell line. **Figure 2.5 –** Treatments administrated after SARS-CoV-2 infection in HaCaT cell line. **Figure 2.6 -** Treatments administrated before SARS-CoV-2 infection in HaCaT cell line. **Figure 2.7 -** Treatments administrated after SARS-CoV-2 infection in Hek293T cell line. **Figure 2.8 –**Treatments administrated before SARS-CoV-2 infection in Hek293T cell line.

REFERENCES

1. Ford N, Vitoria M, Rangaraj A, Norris SL, Calmy A, Doherty M. Systematic Review of the Efficacy and Safety of Antiretroviral Drugs Against SARS, MERS or COVID-19: Initial Assessment. *J Int AIDS Soc* (2020) 23(4):e25489. doi: 10.1002/jia2.25489
2. Boukhatem MN, Setzer WN. Aromatic Herbs, Medicinal Plant-Derived Essential Oils, and Phytochemical Extracts as Potential Therapies for Coronaviruses: Future Perspectives. *Plants (Basel)* (2020) 9(6):800. doi: 10.3390/plants9060800
3. Elshabrawy HA. SARS-CoV-2: An Update on Potential Antivirals in Light of SARS-CoV Antiviral Drug Discoveries. *Vaccines (Basel)* (2020) 8(2):335. doi: 10.3390/vaccines8020335
4. Bergman ME, Davis B, Phillips MA. Medically Useful Plant Terpenoids: Biosynthesis, Occurrence, and Mechanism of Action. *Molecules* (2019) 24 (21):3961. doi: 10.3390/molecules24213961
5. Jaeger R, Cuny E. Terpenoids With Special Pharmacological Significance: A Review. *Nat Prod Commun* (2016) 11(9):1373–90. doi: 10.1177/1934578X1601100946
6. Loizzo MR, Saab AM, Tundis R, Statti GA, Menichini F, Lampronti I, et al. Phytochemical Analysis and *In Vitro* Antiviral Activities of the Essential Oils of Seven Lebanon Species. *Chem Biodivers* (2008) 5(3):461–70. doi: 10.1002/cbdv.200890045
7. Schuhmacher A, Reichling J, Schnitzler P. Virucidal Effect of Peppermint Oil on the Enveloped Viruses Herpes Simplex Virus Type 1 and Type 2 *In Vitro*. *Phytomedicine* (2003) 10(6-7):504–10. doi: 10.1078/094471103322331467
8. Asif M, Saleem M, Saadullah M, Yaseen HS, Al Zarzour R. COVID-19 and Therapy With Essential Oils Having Antiviral, Anti-Inflammatory, and Immunomodulatory Properties. *Inflammopharmacology* (2020) 28(5):1153–61. doi: 10.1007/s10787-020-00744-0. Erratum in: Inflammopharmacology. 2021 Apr;29(2):577.
9. Reichling J. Plant-Microbe Interaction and Secondary Metabolites With Antiviral, Antibacterial and Antifungal Properties. In: W Wink, editor. *Functions and Biotechnology of Plant Secondary Metabolites*. West Sussex, United Kingdom: Wiley-Blackwell (2010). p. 214–347. doi: 10.1002/9781119312994.apr0420
10. Tahamtan A, Samieipoor Y, Nayeri FS, Rahbarimanesh AA, Izadi A, Rashidi-Nezhad A, et al. Effects of Cannabinoid Receptor Type 2 in Respiratory Syncytial Virus Infection in Human Subjects and Mice. *Virulence* (2018) 9 (1):217–30. doi: 10.1080/21505594.2017.1389369
11. Sacerdote P, Martucci C, Vaccani A, Bariselli F, Panerai AE, Colombo A, et al. The Nonpsychoactive Component of Marijuana Cannabidiol Modulates Chemotaxis and IL-10 and IL-12 Production of Murine Macrophages Both

In Vivo and *In Vitro*. *J Neuroimmunol* (2005) 159(1-2):97–105. doi: 10.1016/j.jneuroim.2004.10.003
12. Nadjib BM. Effective Antiviral Activity of Essential Oils and Their Characteristic Terpenes Against Coronaviruses: An Update. *J Pharmacol Clin Toxicol* (2020) 8(1):1138.
13. Sandner G, Heckmann M, Weghuber J. Immunomodulatory Activities of Selected Essential Oils. *Biomolecules* (2020) 10(8):1139. doi: 10.3390/biom10081139
14. Juergens UR, Dethlefsen U, Steinkamp G, Gillissen A, Repges R, Vetter H. Anti-Inflammatory Activity of 1.8-Cineol (Eucalyptol) in Bronchial Asthma: A Double-Blind Placebo-Controlled Trial. *Respir Med* (2003) 97(3):250–6. doi: 10.1053/rmed.2003.1432
15. Juergens LJ, Worth H, Juergens UR. New Perspectives for Mucolytic, Anti-Inflammatory and Adjunctive Therapy With 1,8-Cineole in COPD and Asthma: Review on the New Therapeutic Approach. *Adv Ther* (2020) 37 (5):1737–53. doi: 10.1007/s12325-020-01279-0
16. Álvarez DM, Castillo E, Duarte LF, Arriagada J, Corrales N, Farías MA, et al. Current Antivirals and Novel Botanical Molecules Interfering With Herpes Simplex Virus Infection. *Front Microbiol* (2020) 11:139. doi: 10.3389/fmicb.2020.00139
17. Ramirez SH, Reichenbach NL, Fan S, Rom S, Merkel SF, Wang X, et al. Attenuation of HIV-1 Replication in Macrophages by Cannabinoid Receptor 2 Agonists. *J Leukoc Biol* (2013) 93(5):801–10. doi: 10.1189/jlb.1012523
18. Sökmen M, Serkedjieva J, Daferera D, Gulluce M, Polissiou M, Tepe B, et al. *In Vitro* Antioxidant, Antimicrobial, and Antiviral Activities of the Essential Oil and Various Extracts From Herbal Parts and Callus Cultures of Origanum Acutidens. *J Agric Food Chem* (2004) 52(11):3309–12. doi: 10.1021/jf049859g
19. Seidakhmetova RB, Beisenbaeva AA, Atazhanova GA, Suleimenov EM, Pak RN, Kulyyasov AT, et al. Chemical Composition and Biological Activity of the Essential Oil From Artemisia Glabella. *Pharma Chem J* (2002) 36:135–138.40. doi: 10.1023/A:1019630327576
20. Schnitzler P, Schön K, Reichling J. Antiviral Activity of Australian Tea Tree Oil and Eucalyptus Oil Against Herpes Simplex Virus in Cell Culture. *Pharmazie* (2001) 56(4):343–7.
21. Farag RS, Shalaby AS, El-Baroty GA, Ibrahim NA, Ali MA, Hassan EM. Chemical and Biological Evaluation of the Essential Oils of Different Melaleuca Species. *Phytother Res* (2004) 18(1):30–5. doi: 10.1002/ptr.1348
22. Wen CC, Kuo YH, Jan JT, Liang PH, Wang SY, Liu HG, et al. Specific Plant Terpenoids and Lignoids Possess Potent Antiviral Activities Against Severe Acute Respiratory Syndrome Coronavirus. *J Med Chem* (2007) 50(17):4087–95. doi: 10.1021/jm070295s
23. Diniz LRL, Perez-Castillo Y, Elshabrawy HA, Filho CDSMB, de Sousa DP. Bioactive Terpenes and Their Derivatives as Potential SARS-CoV-2 Proteases Inhibitors From Molecular Modeling Studies. *Biomolecules* (2021) 11(1):74. doi: 10.3390/biom11010074
24. Kintzios SE. The Biotechnology of Oregano (Origanum Sp. And Lippia Sp.). In: SE Kintzios, editor. *Medicinal and Aromatic Plants-Industrial Profiles, Oregano. The Genera Origanum and Lippia*, vol. 25. London: Taylor and Francis (2002). p. 237–42.
25. Pereira MMA, Morais LC, Zeneratto NJ, Reis WSM, Gómez OC, Luiz JHH, et al. Organic Management vs. Conventional Management Influence the Antimicrobial Activity of Essential Oils of Origanum Vulgare L. *Research Soc Dev* (2020) 9(11):e4239118504.
26. Catella C, Camero M, Lucente MS, Fracchiolla G, Sblano S, Tempesta M, et al. Virucidal and Antiviral Effects of Thymus Vulgaris Essential Oil on Feline Coronavirus. *Res Vet Sci* (2021) 137:44–7. doi: 10.1016/j.rvsc.2021.04.024
27. Russo EB. Taming THC: Potential Cannabis Synergy and Phytocannabinoid-Terpenoid Entourage Effects. *Br J Pharmacol* (2011) 163(7):1344–64. doi: 10.1111/j.1476-5381.2011.01238
28. Mediavilla V, Steinemann S. Essential Oil of Cannabis Sativa L. Strains. *J Int Hemp Assoc* (1997) 4:80–2.
29. Elsohly MA, Slade D. Chemical Constituents of Marijuana: The Complex Mixture of Natural Cannabinoids. *Life Sci* (2005) 78(5):539–48. doi: 10.1016/j.lfs.2005.09.011
30. Sommano SR, Chittasupho C, Ruksiriwanich W, Jantrawut P. The Cannabis Terpenes. *Molecules* (2020) 25(24):5792. doi: 10.3390/molecules25245792
31. Fasinu PS, Phillips S, ElSohly MA, Walker LA. Current Status and Prospects for Cannabidiol Preparations as New Therapeutic Agents. *Pharmacotherapy* (2016) 36(7):781–96. doi: 10.1002/phar.1780
32. Bridgeman MB, Abazia DT. Medicinal Cannabis: History, Pharmacology, And Implications for the Acute Care Setting. *P T* (2017) 42(3):180–8.
33. Burstein S. Cannabidiol (CBD) and Its Analogs: A Review of Their Effects on Inflammation. *Bioorg Med Chem* (2015) 23(7):1377–85. doi: 10.1016/j.bmc.2015.01.059
34. Amin MR, Ali DW. Pharmacology of Medical Cannabis. *Adv Exp Med Biol* (2019) 1162:151–65. doi: 10.1007/978-3-030-21737-2_8
35. De Petrocellis L, Ligresti A, Moriello AS, Allarà M, Bisogno T, Petrosino S. Effects of Cannabinoids and Cannabinoid-Enriched *Cannabis* Extracts on TRP Channels and Endocannabinoid Metabolic Enzymes. *Br J Pharmacol* (2011) 163:1479–94. doi: 10.1111/j.1476-5381.2010.01166.x
36. Robaina Cabrera CL, Keir-Rudman S, Horniman N, Clarkson N, Page C. The Anti-Inflammatory Effects of Cannabidiol and Cannabigerol Alone, and in Combination. *Pulm Pharmacol Ther* (2021) 69:102047. doi: 10.1016/j.pupt.2021.102047
37. An D, Peigneur S, Hendrickx LA, Tytgat J. Targeting Cannabinoid Receptors: Current Status and Prospects of Natural Products. *Int J Mol Sci* (2020) 21 (14):5064. doi: 10.3390/ijms21145064
38. Zou S, Kumar U. Cannabinoid Receptors and the Endocannabinoid System: Signaling and Function in the Central Nervous System. *Int J Mol Sci* (2018) 19 (3):833. doi: 10.3390/ijms19030833
39. Jordan CJ, Xi ZX. Progress in Brain Cannabinoid CB2 Receptor Research: From Genes to Behavior. *Neurosci Biobehav Rev* (2019) 98:208–20. doi: 10.1016/j.neubiorev.2018.12.026
40. Gui H, Sun Y, Luo ZM, Su DF, Dai SM, Liu X. Cannabinoid Receptor 2 Protects Against Acute Experimental Sepsis in Mice. *Mediators Inflamm* (2013) 2013:741303. doi: 10.1155/2013/741303
41. Rossi F, Tortora C, Argenziano M, Di Paola A, Punzo F. Cannabinoid Receptor Type 2: A Possible Target in SARS-CoV-2 (CoV-19) Infection? *Int J Mol Sci* (2020) 21(11):3809. doi: 10.3390/ijms21113809
42. Costiniuk CT, Saneei Z, Routy JP, Margolese S, Mandarino E, Singer J, et al. Oral Cannabinoids in People Living With HIV on Effective Antiretroviral Therapy: CTN PT028-Study Protocol for a Pilot Randomised Trial to Assess Safety, Tolerability and Effect on Immune Activation. *BMJ Open* (2019) 9(1): e024793. doi: 10.1136/bmjopen-2018-024793
43. Karmaus PW, Chen W, Crawford R, Kaplan BL, Kaminski NE. Δ9-Tetrahydrocannabinol Impairs the Inflammatory Response to Influenza Infection: Role of Antigen-Presenting Cells and the Cannabinoid Receptors 1 and 2. *Toxicol Sci* (2013) 131(2):419–33. doi: 10.1093/toxsci/kfs315
44. Buchweitz JP, Karmaus PW, Williams KJ, Harkema JR, Kaminski NE. Targeted Deletion of Cannabinoid Receptors CB1 and CB2 Produced Enhanced Inflammatory Responses to Influenza A/PR/8/34 in the Absence and Presence of Delta9-Tetrahydrocannabinol. *J Leukoc Biol* (2008) 83 (3):785–96. doi: 10.1189/jlb.0907618
45. Brown JD. Cannabidiol as Prophylaxis for SARS-CoV-2 and COVID-19? Unfounded Claims Versus Potential Risks of Medications During the Pandemic. *Res Soc Adm Pharm* (2021) 17(1):2053. doi: 10.1016/j.sapharm.2020.03.020
46. Onay A, Ertaş A, Süzerer V, Yener İ, Yilmaz MA, Ayaz-Tilkat E, et al. Cannabinoids for SARS-CoV-2 and Is There Evidence of Their Therapeutic Efficacy? *Turk J Biol* (2021) 45(4):570–87. doi: 10.3906/biy-2105-73
47. Paland N, Pechkovsky A, Aswad M, Hamza H, Popov T, Shahar E, et al. The Immunopathology of COVID-19 and the Cannabis Paradigm. *Front Immunol* (2021) 12:631233. doi: 10.3389/fimmu.2021.631233
48. El Biali M, Broers B, Besson M, Demeules J. Cannabinoids and COVID-19. *Med Cannabis Cannabinoids* (2020) 3(2):111–5. doi: 10.1159/000510799
49. Wang B, Kovalchuk A, Li D, Rodriguez-Juarez R, Ilnytskyy Y, Kovalchuk I, et al. In Search of Preventive Strategies: Novel High-CBD Cannabis Sativa Extracts Modulate ACE2 Expression in COVID-19 Gateway Tissues. *Aging (Albany NY)* (2020) 12(22):22425–44. doi: 10.18632/aging.202225
50. Anil SM, Shalev N, Vinayaka AC, Nadarajan S, Namdar D, Belausov E, et al. Cannabis Compounds Exhibit Anti-Inflammatory Activity *In Vitro* in COVID-19-Related Inflammation in Lung Epithelial Cells and Pro-Inflammatory Activity in Macrophages. *Sci Rep* (2021) 11(1):1462. doi: 10.1038/s41598-021-81049-2
51. Chatow L, Nudel A, Nesher I, Hayo Hemo D, Rozenberg P, Voropaev H, et al. *In Vitro* Evaluation of the Activity of Terpenes and Cannabidiol Against Human Coronavirus E229. *Life (Basel)* (2021) 11(4):290. doi: 10.3390/life11040290

52. Gallily R, Yekhtin Z, Hanuš LO. The Anti-Inflammatory Properties of Terpenoids From *Cannabis*. *Cannabis Cannabinoid Res* (2018) 3(1):282–90. doi: 10.1089/can.2018.0014
53. Baron EP. Medicinal Properties of Cannabinoids, Terpenes, and Flavonoids in Cannabis, and Benefits in Migraine, Headache, and Pain: An Update on Current Evidence and Cannabis Science. *Headache* (2018) 58(7):1139–86. doi: 10.1111/head.13345
54. Maayah ZH, Takahara S, Ferdaoussi M, Dyck JRB. The Molecular Mechanisms That Underpin the Biological Benefits of Full-Spectrum Cannabis Extract in the Treatment of Neuropathic Pain and Inflammation. *Biochim Biophys Acta Mol Basis Dis* (2020) 1866(7):165771. doi: 10.1016/j.bbadis.2020.165771
55. Namdar D, Voet H, Ajjampura V, Nadarajan S, Mayzlish-Gati E, Mazuz M, et al. Terpenoids and Phytocannabinoids Co-Produced in *Cannabis Sativa* Strains Show Specific Interaction for Cell Cytotoxic Activity. *Molecules* (2019) 24(17):3031. doi: 10.3390/molecules24173031
56. Bojkova D, Klann K, Koch B, Widera M, Krause D, Ciesek S, et al. Proteomics of SARS-CoV-2-Infected Host Cells Reveals Therapy Targets. *Nature* (2020) 583(7816):469–72. doi: 10.1038/s41586-020-2332-7
57. Rosa RB, Dantas WM, do Nascimento JCF, da Silva MV, de Oliveira RN, Pena LJ. *In Vitro* and *In Vivo* Models for Studying SARS-CoV-2, the Etiological Agent Responsible for COVID-19 Pandemic. *Viruses* (2021) 13(3):379. doi: 10.3390/v13030379
58. Xiao F, Tang M, Zheng X, Liu Y, Li X, Shan H. Evidence for Gastrointestinal Infection of SARS-CoV-2. *Gastroenterology* (2020) 158(6):1831–1833.e3. doi: 10.1053/j.gastro.2020.02.055
59. Lee S, Yoon GY, Myoung J, Kim SJ, Ahn DG. Robust and Persistent SARS-CoV-2 Infection in the Human Intestinal Brush Border Expressing Cells. *Emerg Microbes Infect* (2020) 9(1):2169–79. doi: 10.1080/22221751.2020.1827985
60. Kellum JA, van Till JWO, Mulligan G. Targeting Acute Kidney Injury in COVID-19. *Nephrol Dial Transplant* (2020) 35(10):1652–62. doi: 10.1093/ndt/gfaa231
61. Liakopoulos V, Roumeliotis S, Papachristou S, Papanas N. COVID-19 and the Kidney: Time to Take a Closer Look. *Int Urol Nephrol* (2021), 1–5. doi: 10.1007/s11255-021-02976-7
62. Novak N, Peng W, Naegeli MC, Galvan C, Kolm-Djamei I, Brüggen C, et al. SARS-CoV-2, COVID-19, Skin and Immunology - What Do We Know So Far? *Allergy* (2021) 76(3):698–713. doi: 10.1111/all.14498
63. Recalcati S. Cutaneous Manifestations in COVID-19: A First Perspective. *J Eur Acad Dermatol Venereol* (2020) 34(5):e212–3. doi: 10.1111/jdv.16387
64. Wollina U, Karadağ AS, Rowland-Payne C, Chiriac A, Lotti T. Cutaneous Signs in COVID-19 Patients: A Review. *Dermatol Ther* (2020) 33(5):e13549. doi: 10.1111/dth.13549
65. Matar S, Oulès B, Sohier P, Chosidow O, Beylot-Barry M, Dupin N, et al. Cutaneous Manifestations in SARS-CoV-2 Infection (COVID19): A French Experience and a Systematic Review of the Literature. *J Eur Acad Dermatol Venereol* (2020) 34(11):e686–9. doi: 10.1111/jdv.16775
66. Gisondi P, PIaserico S, Bordin C, Alaibac M, Girolomoni G, Naldi L. Cutaneous Manifestations of SARS-CoV-2 Infection: A Clinical Update. *J Eur Acad Dermatol Venereol* (2020) 34(11):2499–504. doi: 10.1111/jdv.16774

Conflict of Interest: Authors SS, AC, IL, SR and MM was employed by company EXMceuticals Portugal Lda.

The remaining authors declare that the research was conducted in the absence of any commercial or financial relationships that could be construed as a potential conflict of interest.

frontiers in Immunology

ORIGINAL RESEARCH
published: 16 March 2022
doi: 10.3389/fimmu.2022.836232

Multiple SARS-CoV-2 Variants Exhibit Variable Target Cell Infectivity and Ability to Evade Antibody Neutralization

Haijun Tang[1,2], Long Gao[1,2], Zhao Wu[1,2], Fang Meng[1,2], Xin Zhao[1,2], Yun Shao[1,2], Guocun Hou[3], Xiaohong Du[4] and F. Xiao-Feng Qin[1,2]**

[1] Institute of Systems Medicine, Chinese Academy of Medical Sciences & Peking Union Medical College, Beijing, China, [2] Suzhou Institute of Systems Medicine, Suzhou, China, [3] Department of Nephrology, Suzhou Science and Technology Town Hospital, Suzhou, China, [4] Institute of Clinical Medicine Research, Suzhou Science and Technology Town Hospital, Suzhou, China

The continuous emergence of SARS-coronavirus 2 (SARS-CoV-2) variants, especially the variants of concern (VOC), exacerbated the impact of the coronavirus disease 2019 (COVID-19) pandemic. As the key of viral entry into host cells, the spike (S) protein is the major target of therapeutic monoclonal antibodies (mAbs) and polyclonal antibodies elicited by infection or vaccination. However, the mutations of S protein in variants may change the infectivity and antigenicity of SARS-CoV-2, leading to the immune escape from those neutralizing antibodies. To characterize the mutations of S protein in newly emerging variants, the proteolytic property and binding affinity with receptor were assessed, and the vesicular stomatitis virus (VSV)-based pseudovirus system was used to assess the infectivity and immune escape. We found that some SARS-CoV-2 variants have changed significantly in viral infectivity; especially, B.1.617.2 is more likely to infect less susceptible cells than D614G, and the virus infection process can be completed in a shorter time. In addition, neutralizing mAbs and vaccinated sera partially or completely failed to inhibit host cell entry mediated by the S protein of certain SARS-CoV-2 variants. However, SARS-CoV-2 variant S protein-mediated viral infection can still be blocked by protease inhibitors and endocytosis inhibitors. This work provides a deeper understanding of the rise and evolution of SARS-CoV-2 variants and their immune evasion.

Keywords: SARS-CoV-2 variants, infectivity, CoronaVac vaccine, neutralizing antibody, BBIBP-CorV vaccine

OPEN ACCESS

Edited by:
Ron Geller,
University of Valencia, Spain

Reviewed by:
Gideon Schreiber,
Weizmann Institute of Science, Israel
Beatriz Álvarez-Rodríguez,
Instituto de Biología Integrativa de Sistemas (UV+CSIC), Spain

****Correspondence:***
Xiaohong Du
dxl4857@126.com
F. Xiao-Feng Qin
fqin1@foxmail.com

Specialty section:
This article was submitted to Viral Immunology, a section of the journal Frontiers in Immunology

Received: *15 December 2021*
Accepted: *15 February 2022*
Published: *16 March 2022*

Citation:
Tang H, Gao L, Wu Z, Meng F, Zhao X, Shao Y, Hou G, Du X and Qin FX-F (2022) Multiple SARS-CoV-2 Variants Exhibit Variable Target Cell Infectivity and Ability to Evade Antibody Neutralization. Front. Immunol. 13:836232. doi: 10.3389/fimmu.2022.836232

INTRODUCTION

The coronavirus disease 2019 (COVID-19) pandemic is threatening human health worldwide. As of November 23, 2021, SARS-coronavirus 2 (SARS-CoV-2) has infected over 256 million people and has caused more than 5 million deaths (https://covid19.who.int). SARS-CoV-2 uses its spike (S) protein to bind host receptor angiotensin-converting enzyme 2 (ACE2) and mediate virus entry into host cells (1–5). Virus entry requires the target cell protease to activate the S protein, which triggers

the cleavage between S1 and S2, activates the cleavage of the S2 site, and then mediates the fusion of the virus with the cell membrane (6–8). SARS-CoV-2 entry can be disrupted by protease inhibitors or endocytosis inhibitors (6, 8). The therapeutic applicability of these drugs for COVID-19 treatment is being evaluated within clinical trials.

The number of COVID-19 confirmed cases continues to grow rapidly, and the prospect of ending its pandemic depend on effective treatment and prevention measures. SARS-CoV-2 S protein, especially receptor-binding domain (RBD), is the main target of neutralizing monoclonal antibodies (mAbs). At present, neutralizing mAbs have shown a good therapeutic efficacy on infected individuals (9). Some antibodies have been shown to reduce viral load, relieve COVID-19 associated symptoms, and reduce hospitalization rate (10, 11). In addition, vaccines play a key role in the prevention and control of the COVID-19 epidemic in various regions of the world. At present, SARS-CoV-2 vaccines, including mRNA vaccines, adenovirus-based vaccines, protein subunit vaccines, and inactivated vaccines, all show encouragingly good clinical efficacy (12, 13). CoronaVac, an inactivated vaccine developed by Sinovac, has been demonstrated to be more than 50% effective against symptomatic infections and can reduce the risk of serious diseases (14). Similarly, another inactivated vaccine, BBIBP-CorV, developed by Sinopharm, has been confirmed to render 78.1% protection efficacy against COVID-19 symptomatic infections and reduce the hospitalization rate of patients (15).

Although the genome of SARS-CoV-2 remains relatively stable, it still has a high mutation rate during virus transmission (16–18). With the extension of the SARS-CoV-2 pandemic, a wide variety of variants have been produced in the host. In particular, SARS-CoV-2 S protein G614 has replaced the original D614 and has become the main popular SARS-CoV-2 strain (19–21). Recently, several new SARS-CoV-2 variants have appeared, which seem to be more infectious in the population. The variants make their antigenicity different from the original strain, which can reduce or even invalidate the protective efficacy of current antibodies and vaccines (18). Among the variants of concern (VOC), the B.1.351 and P.1 strains have attracted wide attention because of their extensive mutations and the ability to escape from neutralizing antibodies (22, 23). Several studies have shown that the power of neutralizing antibodies and vaccinated sera are substantially reduced in neutralization against B.1.351 and P.1 lineage variants (16, 24, 25). Moreover, due to enhanced transmission and immune evasion ability, B.1.617.2 has spread widely on a global scale, causing widespread concern (17, 26, 27). As widely employed SARS-CoV-2 vaccines in China, CoronaVac and BBIBP-CorV need to be tested for their protection ability against concerning variants.

In the work reported here, using a vesicular stomatitis virus (VSV)-based pseudovirus system, we have studied the infectivity, antigenicity, and drug inhibition characters of the major circulating SARS-CoV-2 variants. We show that some SARS-CoV-2 variants have changed significantly in viral infectivity. In addition, the antigenicity of some variants has also changed, resulting in a significant reduction in the neutralizing activity of some mAbs and vaccine sera. However, the entry of all variants into mammalian cells is effectively blocked by protease inhibitors and endocytosis inhibitors.

RESULTS

Construction of Pseudoviruses With the Major Circulating SARS-CoV-2 Variants

To study the biological characteristics of the major circulating SARS-CoV-2 variants, we generated a total of 14 pseudoviruses, including 11 main variants (D614G, B.1.1.7, B.1.351, P.1, P.2, B.1.429, B.1.525, B.1.526, B.1.617.1, B.1.617.2, and B.1.618) and 3 mutants with only RBD mutations (B.1.351 RBD, P.1 RBD, and B.1.617.1 RBD) (**Figures 1A, B** and **Figure S1**). In this study, all pseudoviruses were generated in the background of the Wuhan-1 virus strain, and D614G was used as the reference pseudovirus for the analysis of all experiments. We first analyzed the proteolytic process of the 11 main variant S proteins by Western blotting (**Figure 1C**). SARS-CoV-2 S protein mainly contains three bands, with the 180-kDa band reflecting the full-length S protein, the 90 kDa band reflecting the cleavage of S protein (S2 subunit), and the bands above 180 kDa representing trimeric S protein. The expression of full-length S protein can be detected in all variant strains, while the intensity of the S2 band was variable. The expression of S2 bands of B.1.1.7, P.1, and B.1.526 was weaker than that of D614G. But the expression of the S2 band of B.1.617.2 was stronger than that of D614G. Moreover, pseudoviruses with SARS-CoV-2 variant S protein were also analyzed for S protein incorporation and processing by Western blotting (**Figure 1C**). For all SARS-CoV-2 variants, the full-length S protein was cleaved into S2 protein to different extents. Similar to the expression of S protein in cell lysate, the intensity of S2 bands of B.1.1.7, P.1 and B.1.526 was weaker than that of D614G.

Altered Infectivity of the Major Circulating SARS-CoV-2 Variants

Next, we investigated the potential infection-related effects of pseudoviruses with variant S protein in different cells, where a difference by 2-fold in relative luminescence unit (RLU) value compared with the D614G strain was considered to be significant (**Figure 2A**). In the present study, the infectivity of the major circulating variants had no significant difference in 293T-hACE2, 293T-hACE2-TMPRSS2, Caco2-hACE2, and Vero cells, except that the infectivity of the P.1 variant was slightly reduced in 293T-hACE2 and 293T-hACE2-TMPRSS2 cells. On the other hand, in Caco2 cells, the infectivity of B.1.1.7, B.1.525, B.1.617.2, and B.1.617.1 RBD was significantly higher than that of D614G. In Huh7 cells, the infectivity of B.1.351, B.1.617.2, B.1.618, B.1.351 RBD, and P.1 RBD was higher than that of D614G. In addition, in A549 cells, the infectivity of P.2, B.1.525, B.1.617.2, B.1.351 RBD, P.1 RBD, and B.1.617.1 RBD was higher than that of D614G. Notably, in H1299 cells, the infectivity of B.1.1.7, B.1.351, P.2, B.1.525, B.1.617.1, B.1.617.2, B.1.618, B.1.351 RBD, and P.1 RBD was significantly enhanced, but the infectivity of

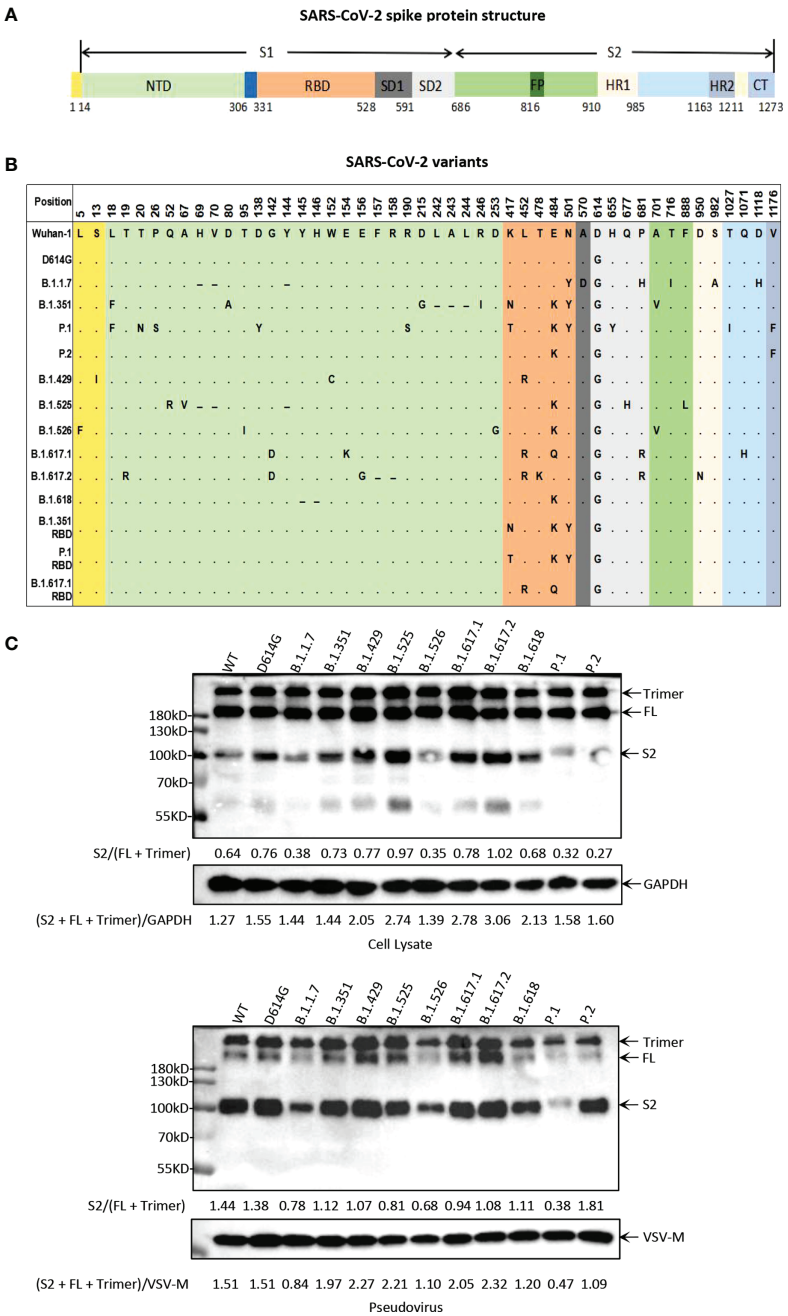

FIGURE 1 | Illustration of the major circulating SARS-CoV-2 variants. **(A)** Schematic diagram of SARS-CoV-2 spike protein structure. NTD, N-terminal domain; RBD, receptor-binding domain; SD, subdomain; FP, fusion peptide; HR1, heptad repeat 1; HR2, heptad repeat 2; CT, cytoplasmic domain. **(B)** Mutation site at the amino acid level in the viral spike protein-coding region identified in SARS-CoV-2 variants. All of the pseudoviruses in this study were generated in the background of Wuhan-1 strain. In the mutation map, a dot (·) indicates the same amino acid in that position as Wuhan-1 strain, and a dash (-) indicates a deletion. **(C)** Analysis of SARS-CoV-2 variants S protein expression and particle incorporation by Western blotting using a monoclonal antibody directed against SARS-CoV-2 S2 subunit. GAPDH (cell lysates) and VSV-M (particles) served as loading controls. The full-length S protein band is about 180 kDa, the S2 protein band is about 90 kDa, and the bands above 180 kDa represent trimeric S protein. Shown are representative blots from three experiments.

P.1, B.1.429, B.1.526, and B.1.617.1 RBD was decreased. Interestingly, mutations outside the SARS-CoV-2 RBD may also affect viral infection. In A549 cells, B.1.351 RBD was more infective than B.1.351. Similarly, in 293T-hACE2, 293T-hACE2-TMPRSS2, Huh7, and H1299 cells, the infectivity of P.1 RBD was higher than that of P.1. In addition, B.1.617.1 RBD was more infective than B.1.617.1 in Caco2 cells but decreased in H1299 cells.

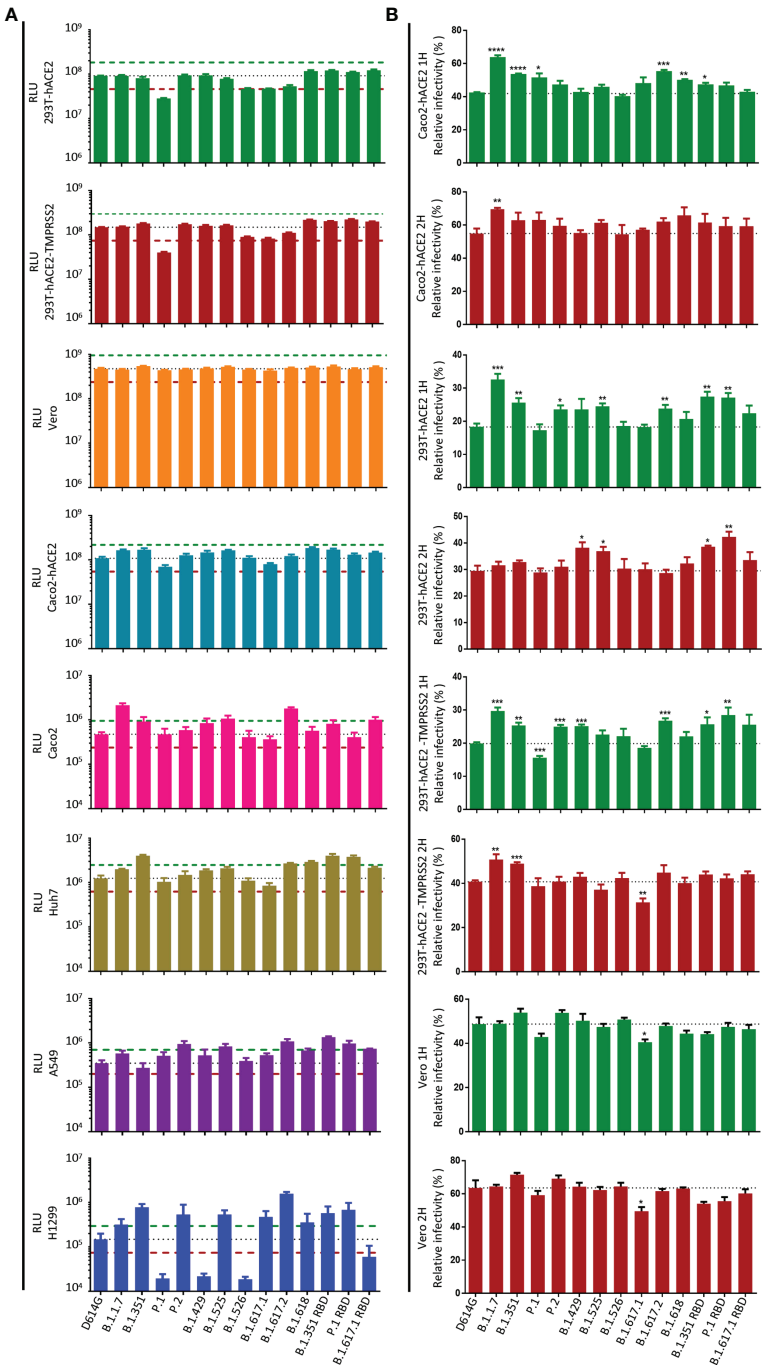

FIGURE 2 | Infectivity analysis of SARS-CoV-2 variants in mammalian cell lines. **(A)** Entry of SARS-CoV-2 variants S pseudoviruses in mammalian cells. Mammalian cells were inoculated with pseudoviruses harboring SARS-CoV-2 variants S protein. At 24 h postinoculation, luciferase activity in cell lysates was measured to detect infection efficiency. The infectivity of the D614G variant was used as a control. The dashed lines indicate the threshold value of a 2-fold difference in infectivity. **(B)** SARS-CoV-2 variants S pseudoviruses were incubated with Caco2-hACE2, 293T-hACE2, 293T-hACE2-TMPRSS2, and Vero cells, then the unbound virus was removed by washing at the specified time point (1 or 2 h), and the unwashed cells were used as the control. At 24 h, luciferase activity in cell lysates was measured to detect infection efficiency. The infection efficiency of the virus was calculated by dividing the relative luminescence unit (RLU) value at each time point by the average RLU value of the respective virus at 24 h. A p-value less than 0.05 was defined as statistically significant ($p < 0.05$ [*], $p < 0.01$ [**], $p < 0.001$ [***], $p < 0.0001$ [****]). Experiments were done in 4 replicates and repeated at least twice. One representative is shown with error bars indicating SEM.

Zhang et al. (28) showed that pseudovirus carrying the delta variant S protein infects target cells faster than D614G in the early stage, which may be the main reason for its enhanced transmissibility. To test the ability of different variants to infect target cells in the early stage, we infected target cells with pseudoviruses carrying variant S protein and removed the unbound virus by washing at the specified time point (1 or 2 h), and the unwashed cells were used as the control. At 24 h post-infection, the infection efficiency of variants was detected by measuring the luciferase activity (**Figure 2B** and **Figure S2**). We found that in the early stage of virus infection, the infection efficiency of B.1.1.7, B.1.351, and B.1.617.2 in Caco2-hACE2, 293T-hACE2, and 293T-hACE2-TMPRSS2 cells was higher than that of the reference D614G strain. Compared with D614G, the infection efficiency of P.2, B.1.429, B.1.525, B.1.618, B.1.351 RBD, and P.1 RBD may be enhanced in some cells. However, all SARS-CoV-2 variants exhibited similar infectivity in Vero cells in the early stage.

Binding of SARS-CoV-2 Variant S to Recombinant hACE2

SARS-CoV-2 RBD mediates the binding of the virus to the ACE2 receptor, which is the main determinant of the host range. Most mutations are deleterious for ACE2 binding, but some mutations are well tolerated and even enhance ACE2 binding (29). Next, we tested the binding avidity of variant S protein to ACE2 receptor. 293T cells expressing variant S protein were incubated with recombinant hACE2 and detected by flow cytometry. The mean fluorescence intensity (MFI) values of B.1.1.7 and P.1 were higher than those of D614G (**Figures 3A, B** and **Figures S3A, B**). However, the MFI values of other variants of S protein did not change significantly.

Immune Escape of SARS-CoV-2 Variants to Neutralizing Monoclonal Antibodies

To study the impact of SARS-CoV-2 variants on the antigenicity, we first measured the neutralization activity of 12 previously characterized neutralizing mAbs on pseudovirus infection in Vero cells (**Figure S4**). The neutralization profiles are shown in **Figure 4A**. Compared with the SARS-CoV-2 D614G reference strain, most of those anti-RBD mAbs showed varyingly decreased neutralizing activities to pseudovirus carrying the variant S protein. Specifically, B.1.1.7 decreased the sensitivity to mAb CB6, while P.2, B.1.429, B.1.525, and B.1.617.2 predominately decreased the sensitivity to mAb LY-CoV555. In addition, B.1.526, B.1.617.1, and B.1.618 became highly resistant to many mAbs, including LY-CoV555, CB6, AbA205, and AbB505. It is worth noting that B.1.351 and P.1 had the greatest immune escape ability on the tested neutralizing mAbs. Both of these variants reduced the sensitivity to mAbs LY-CoV555, CB6, AbA128, AbA205, AbB505, AbB606, AbE450, and AbG106. The neutralization activities of LY-CoV555, CB6, and AbA128 to B.1.351 and P.1 were below the detection limit (BDL). Previous studies have reported that SARS-CoV-2 RBD mutation could cause the decrease of neutralization activity of some mAbs (30). To verify our assay system, we also tested the same panel of mAbs against the pseudoviruses carrying just the mutations in the RBD region of B.1.351, P.1, and B.1.617.1. The results of B.1.351, P.1, and B.1.617.1 pseudoviruses were generally consistent with those of pseudoviruses with only RBD mutation. These findings indicate that the immune escape of B.1.351, P.1, and B.1.617.1 might mainly be mediated by mutations in the RBD region of SARS-CoV-2. It is worth noting that the mAbs REGN10987, S309, and VIR-7831 have a strong neutralization effect on almost all variants.

We also assessed the neutralization activity of the anti-NTD mAb 4A8 against SARS-CoV-2 variants (**Figure 4A**). B.1.1.7, B.1.351, P.1, B.1.429, B.1.525, B.1.617.1, B.1.617.2, and B.1.618 pseudoviruses showed various reductions in the sensitivity to 4A8. However, B.1.351 RBD, P.1 RBD, and B.1.617.1 RBD mutation pseudoviruses showed minimal change in neutralization activity. Therefore, the antibody targeting SARS-CoV-2 NTD can also be easily breached by certain mutations in the NTD domain of variant S protein, and the immune escape site has little to do with the RBD region.

The impaired binding affinity between the mAb and S protein is a major mechanism for SARS-CoV-2 immune escape (25). To study the correlation between variant immune escape and antibody affinity, we detected the binding affinity of mAbs to S protein expressed on 293T cells (**Figure 4B** and **Figure S5**). We found that the neutralization ability of antibodies has a strong correlation with binding affinity. In general, the weakening of the neutralization ability of mAbs is related to its decreased affinity with S protein.

Altered Reactivity of SARS-CoV-2 Variants to Inactivated Virus Vaccine Sera

We next investigated the resistance of variant pseudovirus on neutralization activity of vaccine sera obtained from 179 participants after receiving one or two doses of inactivated virus vaccine—CoronaVac or BBIBP-CorV (**Figure S6**). We first measured the neutralization titers of serum samples against the reference D614G pseudovirus and found that the majority of the vaccinated participants produced neutralizing antibodies (**Figure 5A**). The geometric mean neutralizing titers of one dose of CoronaVac, two doses of CoronaVac, one dose of BBIBP-CorV, two doses of BBIBP-CorV, and CoronaVac+BBIBP-CorV were 23, 56, 28, 69, and 92, respectively. On the other hand, undetectable neutralization activities were seen in 7 out of 65 serum samples from subjects receiving only one dose of CoronaVac, in 1 out of 24 serum samples from subjects receiving two doses of CoronaVac, and in 1 out of 29 serum samples from subjects receiving one dose of BBIBP-CorV. Consistent with the neutralization effect of serum samples on pseudoviruses, the average anti-RBD IgG levels of one dose of CoronaVac, two doses of CoronaVac, one dose of BBIBP-CorV, two doses of BBIBP-CorV, and CoronaVac+BBIBP-CorV were 3.9, 5.5, 3.5, 5.1, and 5.7 U/ml, respectively (**Figure 5B**).

Next, we selected 30 CoronaVac serum samples and 20 BBIBP-CorV serum samples to test the immune escape of SARS-CoV-2 variants. For CoronaVac serum samples, when compared with SARS-CoV-2 D614G, the neutralization activity

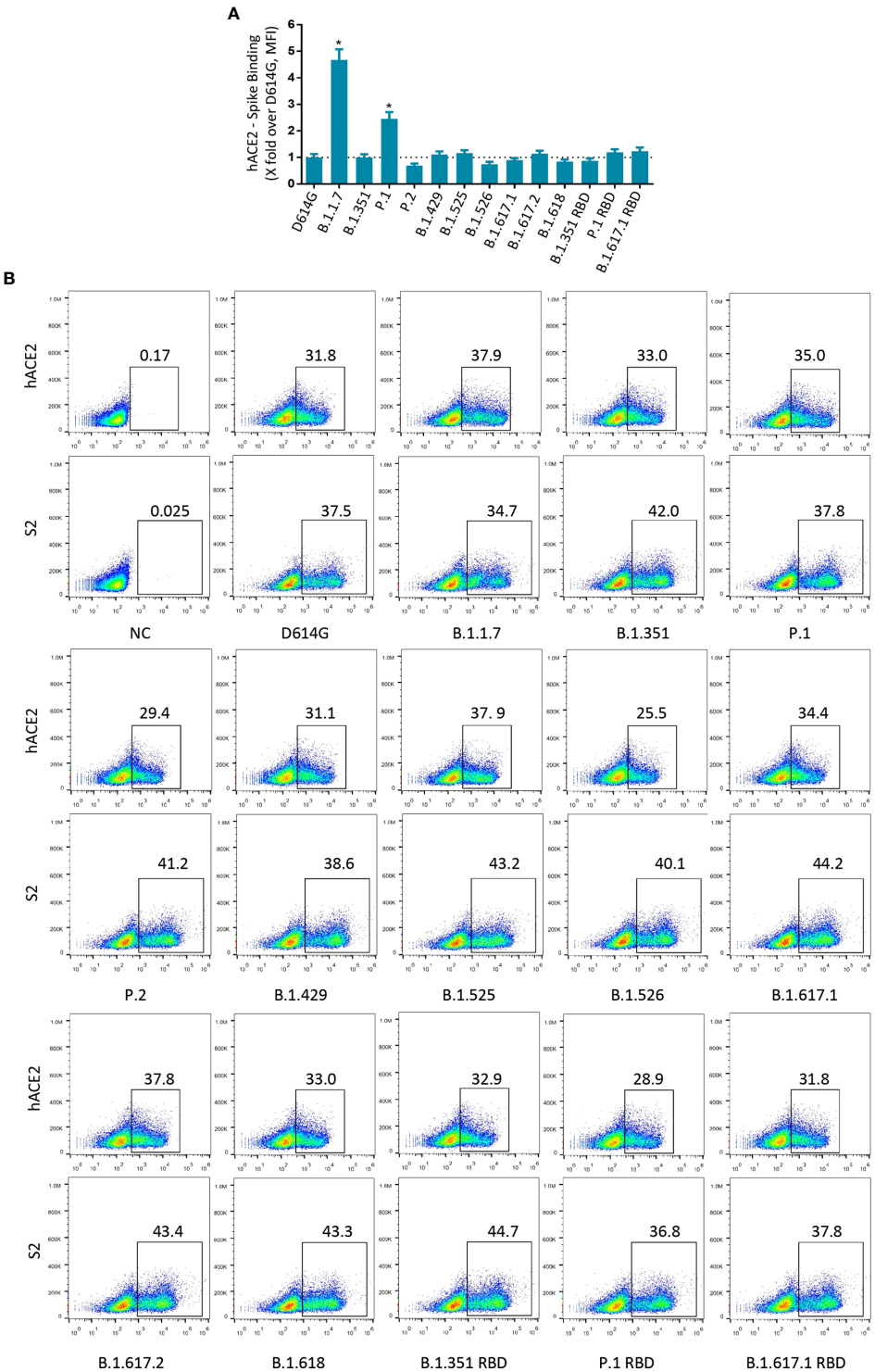

FIGURE 3 | Binding of SARS-CoV-2 variants S protein to recombinant hACE2. **(A)** The fold changes in binding activity of SARS-CoV-2 variants S protein to recombinant hACE2, measured by mean fluorescence intensity (MFI). Recombinant hACE2 protein binding percentages were calculated by the ratio between variants over D614G MFI normalized relative to that of S2 specific antibody. All MFI values were weighted by multiplying the number of positive cells in the selected gates. **(B)** 293T cells transiently expressing SARS-CoV-2 variants S proteins were incubated with recombinant hACE2 protein or anti-SARS-CoV-2 spike (S2 subunit) antibodies for 1 h. After being washed, cells were incubated with Alexa Flour 488-conjugated anti-human IgG Fc or fluorescein isothiocyanate (FITC)-conjugated anti-mouse IgG secondary antibodies. A p-value less than 0.05 was defined as statistically significant ($p < 0.05$ [*]). Experiments were done at least twice.

A

Fold changes in IC50		D614G	B.1.1.7	B.1.351	P.1	P.2	B.1.429	B.1.525	B.1.526	B.1.617.1	B.1.617.2	B.1.618	B.1.351 RBD	P.1 RBD	B.1.617.1 RBD
anti-RBD	LY-CoV555	+1	+1.4	BDL	BDL	BDL	204	BDL	BDL	BDL	BDL	BDL	BDL	BDL	BDL
	CB6	+1	-63.3	BDL	BDL	-2.3	+1.3	-1.7	-3.6	+1.2	-2.9	-2.5	BDL	BDL	-1.1
	REGN10987	+1	+2	+3.2	+2.6	+1	+1.1	+2.1	+1.2	-1.2	-1.7	+1.2	+3.1	+3.3	-1.1
	S309	+1	-2.3	+1.5	+2.6	+2	+1.5	+1.3	+1.4	+2	-1.7	+2	+1.2	+1.3	+1.1
	VIR-7831	+1	-1.3	+1.1	+2.3	+1.2	+1.3	+1.5	+1.2	+4	-2.2	+3.5	+1.2	+1.2	+1.2
	AbA128	+1	+1.4	BDL	BDL	-1.7	+1.5	-1.4	-1.3	-1.6	-1.3	-1.4	BDL	-6	-1.3
	AbA205	+1	-1.3	-52	-13.4	-2.5	-1.1	-1.5	-3.5	-2.4	-1.8	-4.1	-64.2	-25.3	-2.3
	AbB505	+1	+1	-34.8	-8.3	-2.7	-1.2	-1.6	-3.5	-3.1	+1	-3.6	-18.9	-15.4	-3.2
	AbB606	+1	+2.1	-87.2	-44.8	-2.8	+1.4	-1.9	-2.9	-1.9	+1	-2.2	-87.4	-32.2	-2.1
	AbE450	+1	+1.4	-18.1	-19.1	-2.1	+1	-1.1	-2	-2.7	+1	-3	-620.1	-20.4	-2.1
	AbG106	+1	+1.6	-9.9	-5.4	-1.4	+1.2	-1	-1.4	-1.5	-1.6	-1.5	-8.3	-6.7	-1.6
anti-NTD	4A8	+1	-26.7	BDL	-6.6	-1.1	-496.8	-618.3	-1.3	-704.7	BDL	-30.6	+1.7	+1.4	+1.3

B

Fold changes in surface binding		D614G	B.1.1.7	B.1.351	P.1	P.2	B.1.429	B.1.525	B.1.526	B.1.617.1	B.1.617.2	B.1.618	B.1.351 RBD	P.1 RBD	B.1.617.1 RBD
anti-RBD	LY-CoV555	+1	+2.3	-96.9	-594	-456.8	-4	-259.3	-563.5	-949.4	-5.1	-238.7	-1283.9	-671.3	-1146.9
	CB6	+1	+3.7	-8.6	-6.8	-1.2	+1	+1.1	-1.5	+1.4	-1.6	-1.4	-9.9	-4	-1.1
	REGN10987	+1	-1.1	+1.2	-1.7	+1	+1	+1.9	-1.3	-1.3	+1	-1.2	-1.2	+1.1	-1.1
	S309	+1	-1.2	+1	-1.7	+1	+1	+1.8	-1.3	+1.3	+1.4	+1	-1.4	+1.2	+1
	VIR-7831	+1	-1.3	-1.2	-2	-1.1	+1	+1.8	-1.4	+1	+1.2	+1	-1.6	+1	+1
	AbA128	+1	+3.2	-7.1	-1.5	-1.3	+1.2	+1	-1.8	-1.1	+1	-1.2	-6.8	-2.4	+1
	AbA205	+1	+2.7	-4.3	-1.1	-1.2	+1	+1	-1.5	-1.4	-1.5	-1.3	-4.3	-1.9	-1.2
	AbB505	+1	+4	-3	+1.1	-1.2	+1.3	+1.1	-1.1	-1.2	-1.3	-1.4	-2.8	-1.6	+1.2
	AbB606	+1	+3.4	-9.2	-3.1	-1.4	+1.1	-1.1	-1.7	-1.2	-1.5	-1.5	-11.8	-4.8	-1.2
	AbE450	+1	+3.4	-3.3	+1.8	-1.4	+1	+1.1	-1.3	-1.1	-1.5	-1.5	-3.2	-1.8	-1.1
	AbG106	+1	+3.7	-3.3	-1.7	-1.5	+1.1	+1.1	-1.3	-1.1	-1.3	-1.5	-5.4	-2	+1
anti-NTD	4A8	+1	-92	-7.1	-1.4	-1.4	-74	-68.9	-1.7	-3.8	-34.9	-152.9	-1.6	+1	-1.1

FIGURE 4 | SARS-CoV-2 variant S pseudoviruses reduce neutralization and binding of mAbs. **(A)** The fold changes in neutralizing activity (IC50) of the mAbs against SARS-CoV-2 variants pseudovirus relative to D614G. **(B)** The fold changes in binding activity [mean fluorescence intensity (MFI)] of the mAbs against SARS-CoV-2 variants pseudovirus relative to D614G. "–" represents the decrease of sensitivity to the antibody, and "+" represents the increase of sensitivity to the antibody. The values marked in red indicate that sensitivity decreased at least 3-fold for IC50 or 2-fold for MFI, while those in green indicate that sensitivity increased at least 3-fold for IC50 or 2-fold for MFI. BDL indicates neutralizing activity below the detection limit. Experiments were done once.

to most variants was somewhat decreased (**Figures 5C–E**). The average reduction of neutralization activity in serum samples of CoronaVac was 1.5-fold against B.1.1.7, 3.3-fold against B.1.351, 1.6-fold against P.1, 2.4-fold against P.2, 1.4-fold against B.1.429, 1.6-fold against B.1.525, 2.7-fold against B.1.526, 2.7-fold against B.1.617.1, 1.9-fold against B.1.617.2, and 2.7-fold against B.1.618. Consistent with the findings for anti-SARS-CoV-2 RBD mAbs, B.1.351 RBD, P.1 RBD, and B.1.617.1 RBD pseudoviruses showed similar immune escape with B.1.351, P.1, and B.1.617.1, respectively. Although the neutralization activities of vaccine sera against the variants were decreased, most of the variants still could be effectively neutralized, including the strong escaping strains B.1.351, P.1, P.2, B.1.526, B.1.617.1, and B.1.617.2. We also observed that there is significant variation in resistance to immunity escape among the vaccinated sera of participants. Some individuals showed greater reductions in neutralizing certain variants, most noticeably B.1.351, B.1.526, B1.617.1, and B.1.618, as well as B.1.351 RBD and P.1 RBD (**Figure 5C** and **Figure S6**).

For BBIBP-CorV vaccine serum samples, when compared with the neutralization activity to D614G, the sera had equal activity in neutralizing B.1.1.7, B.1.429, and B.1.525 (**Figures 5F–H**), while the neutralization efficiencies were remarkably decreased to B.1.351 (1.8-fold), P.1 (1.6-fold), P.2 (1.7-fold), B.1.526 (1.9-fold), B1.617.1 (1.5-fold), B.1.617.2 (1.7-fold), and B.1.618 (2.0-fold). Likewise, B.1.351 RBD, P.1 RBD, and B.1.617.1 RBD pseudoviruses showed a similar immune escape as B.1.351, P.1, and B.1.617.1, respectively.

Effects of Cathepsin Inhibitor and Endocytosis Inhibitors on SARS-CoV-2 Entry

SARS-CoV-2 S protein priming in cells can be activated by endosomal cysteine proteases cathepsin B and L (CatB/L) (6, 8).

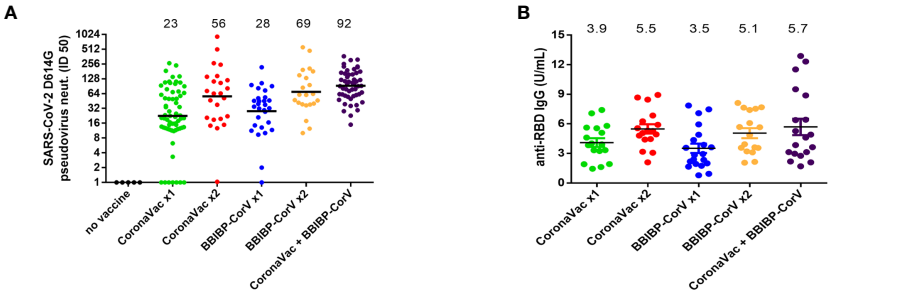

C

Fold changes in ID50		D614G	B.1.1.7	B.1.351	P.1	P.2	B.1.429	B.1.525	B.1.526	B.1.617.1	B.1.617.2	B.1.618	B.1.351 RBD	P.1 RBD	B.1.617.1 RBD
CoronaVac (1 dose)	V1	+1	-1.6	-6.1	-4.6	-10.1	-1.3	-6.3	-11.6	-7.2	-1.2	-9.3	-9	-6.3	-9.5
	V2	+1	+1.3	-4.4	-2.2	-4.5	-10.9	-6	-5.7	-6.2	-12.8	-5.3	-3.3	-3.8	-5.5
	V3	+1	-2.7	-5.8	-2.8	-2.3	-1.2	-1.6	-2.6	-1.1	-1.1	-1.7	-4.4	-16.8	-2
	V4	+1	+1	+1	-1.5	-1.3	-1.4	-1.3	-1.9	-3	-2.9	-1.4	-1.1	+1	-1.6
	V5	+1	-1.1	-1.1	-1.4	-1.3	-2	-1.1	-1.9	-1.8	-2.4	-1.6	-1.3	-1.8	-1.9
	V6	+1	-1.5	-16.3	-2.7	-3.3	-1.7	+1.3	-5.9	-4.4	-3	-3.4	-16.3	-4	-3.6
	V7	+1	-1.4	-2.8	-1.1	-5.8	-1.3	+1.7	-3	-3.7	-1.3	-5.5	-3.4	-3	-5.2
	V8	+1	-1.6	-6.6	-2.4	-6.6	+1.1	+1.3	-6.3	-5	-2.4	-5.7	-6.3	-6	-6.6
	V9	+1	-1.7	-4.3	-1.4	-2.7	-1.5	1.4	-2.5	-1.8	+1.4	-2.5	-5.2	-4.6	-1.7
	V10	+1	-1.6	-17.9	-1.4	-3.4	-1.2	-2.1	-3.5	-3.6	-1.6	-3.7	-4.6	-4	-4.3
	V11	+1	-2.1	-5.7	-2.1	-5.8	-1.8	-2.2	-4.3	-3.5	-2.1	-4.4	-6.5	-5.3	-3
	V12	+1	-1.3	-13	-1.5	-2.2	-1.1	-1.5	-2.3	-1.4	+1.6	-2.5	-2.6	-11.5	-2.1
	V13	+1	-1.2	-2.6	-2.1	-2.6	-1.8	+1	-2.3	-1.8	-1.5	-2.5	-3	-3.2	-2
	V14	+1	-1.9	-1.4	-1.4	-1.6	-1.5	-1.8	-2.1	-2.8	-1.4	-2.3	-1.5	-1.6	-1.5
	V15	+1	-2.1	-2.3	-1.8	-2.9	-2.1	-1.8	-1.6	-2.7	-1.8	-2.6	-4	-3.6	-2.8
	V16	+1	-1.8	-2.1	-1.1	-2.8	-2.4	-1.3	-1.5	-2.1	-2.8	-2.7	-3.6	-3.6	-2
	V17	+1	-1.4	-7.3	-6	-6	-1.2	-4.9	-5.9	-6.6	+1.1	-7.2	-8.5	-7.9	-7.6
	V18	+1	+1.4	-2.6	+1	-3.8	-2.2	-1.1	-3.3	-4.9	-1.7	-5.6	-4.5	-4.3	-3.3
	V19	+1	-1.6	-2.2	-1.9	-4.8	+1	-1.1	-3.4	-4.1	-1.5	-4.6	-4.5	-5.3	-3.4
	V20	+1	-1.3	-3.3	-1.2	-2.2	-1.2	-1.1	-2	-2	-1.2	-2.3	-2.8	-3	-1.9
	V21	+1	-1.9	-1.8	+1	-3.1	-1.8	-1.5	-3.2	-3.1	-1.8	-3.8	-1.8	-2.2	-2.6
	V22	+1	+1	-1.9	+1.7	-2.3	-1.2	+1.3	-2.4	1.8	+1	-2.1	-2.2	-1.9	-1.7
	V23	+1	-1.7	+1	+1	-1.1	-1.4	+1.1	-2.1	-2.3	-2.4	-1.4	+1.1	+1.1	-1.2
	V24	+1	-1.2	-3.5	+1.1	-1.5	-1.6	-1.5	-5.1	-1.3	-1.4	-2.3	-3.1	-2.5	-1.7
CoronaVac (2 dose)	V25	+1	-2.7	-13.5	-3.6	-4.6	-2.5	-4.7	-6.2	-6	-4.3	-4.2	-8.3	-7	-2.1
	V26	+1	+1.1	-1.2	+1.1	+1.4	+2.5	+1	-1.6	+1	-1.2	+1.4	+1	+1.3	+1
	V27	+1	-1.3	-3	-1.1	-1.5	-1.2	-1.1	-1.8	-1.9	-1.6	-2	-1.9	-1.9	-1.1
	V28	+1	-1.7	-1.1	+1.3	-1.3	-1.2	-1.1	-1.6	-1.3	-10.6	-1.4	-1.3	-1.1	-1.2
	V29	+1	-3.2	-2.6	-1.1	-1.7	+1	+1.1	-9.9	-1.7	-1.8	-1.9	-11.8	-1.6	-2.7
	V30	+1	-1.6	-3.4	-1.5	1.3	-1.1	+1.3	-1.3	-1.5	-2.1	-1.8	-1.5	-1.4	-1.3

D

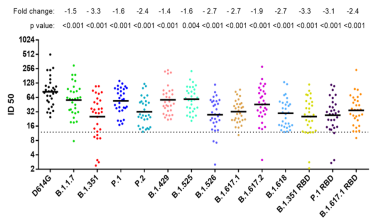

E

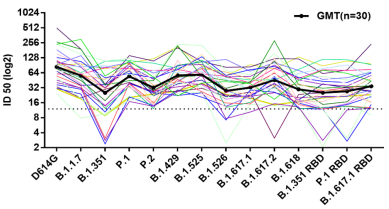

F

Fold changes in ID50		D614G	B.1.1.7	B.1.351	P.1	P.2	B.1.429	B.1.525	B.1.526	B.1.617.1	B.1.617.2	B.1.618	B.1.351 RBD	P.1 RBD	B.1.617.1 RBD
BBIBP-CorV (1 dose)	V31	+1	-1.4	-3	-3.1	-2.7	+1.3	-1.5	-3	-1.5	+1.2	-1.9	-2.9	-2.9	-2.2
	V32	+1	+1.4	-1.6	-2	+1	+1.4	+1	-1.9	+1.3	-1.2	+1.1	+1	-1.2	+1.3
	V33	+1	+1.4	+1	+1.3	+1.7	-1.3	+1.1	-1.6	-1.2	-3.2	+1.3	+1	+1.4	+1.4
	V34	+1	-1.5	-5.5	-4.1	-3	-1.2	-1.5	-1.9	-1.9	-1.9	-3.7	-3.1	-2.7	-2.2
	V35	+1	+1.3	-1.6	+1.1	-1.2	+1.1	+1.3	+1	+1.4	+1.3	-1.2	-1.1	-1.4	+1.3
	V36	+1	-1.2	-1.3	+1	-1.3	+1.3	+1.3	-1.1	+1	-1.7	-1.4	-1.5	-1.2	+1
	V37	+1	+1	-1.4	-1.5	-1.3	+1.7	+2	+1	+1.1	-3.2	-1.2	-5.6	-1.4	-1.1
BBIBP-CorV (2 dose)	V38	+1	+1.4	-2.7	-2.5	-2.6	-1.2	-1.5	-1.5	-1.7	-1.9	-2.3	-3.3	-2	-2.1
	V39	+1	+1.4	-1.2	+1	-1.1	+1	+1	-1.5	-1.5	-1.9	-1.8	-1.6	-1.6	-1.2
	V40	+1	-1.8	+1	-1.1	-2.1	-1.4	+1.4	-1.6	-2	-4.3	-3	-2.4	-2.7	-2.2
	V41	+1	+1.1	-3	-1.6	-1.3	+1.6	-2.2	-3.5	-2.1	+1	-2	-2.8	-2.5	-2
	V42	+1	+1.7	-1.4	-2.1	-1.9	+1	-1.9	-9.5	-4.9	-3.3	-4.1	-1.1	-1.3	-1.9
	V43	+1	-1.1	-1.8	-1.7	-1.9	-1.7	+1	-1.5	-1.3	+1	-2	-1.6	-1.4	+1
	V44	+1	+1	-4.3	-3.5	-5.1	-3.2	-2.8	-5.2	-5.1	-3.5	-4.4	-5.4	-5.3	-3.9
	V45	+1	+1.1	+1.1	-1.1	+1	+1.1	+1.8	-1.1	+1	-1.1	+1	-1.8	-1.7	-1.1
	V46	+1	+1.7	-3	-1.4	-3.3	-2.2	+2	-2.2	-1.3	-1.2	-3	-1.9	-2.3	-1.6
	V47	+1	+1.6	-1.5	-1.4	-1.2	+1	+1.7	-1.9	+1	+1	-1.7	-1.8	-1.9	-1.5
	V48	+1	+1.4	+1.1	-1.7	+1.1	+1.4	+2	+1.2	+1.3	-1.1	-1.4	-1.1	-1.5	+1
	V49	+1	+6.6	-3.4	-1.4	-2.4	+1	+3.7	-2.7	+1	+1	-2.9	-2.3	-2.8	-1.9
	V50	+1	+1	-2.2	-1.2	-2.3	-1.7	-1.3	-3.5	-5.5	-3.9	-4.4	-4.2	-4.2	-7.3

G

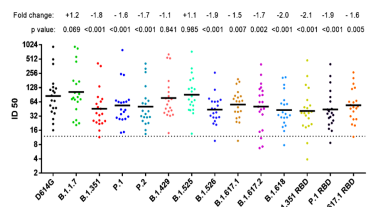

H

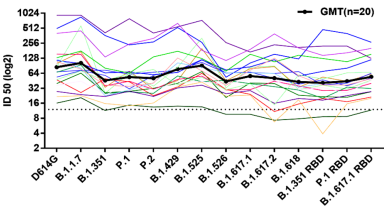

FIGURE 5 | Neutralization activity to SARS-CoV-2 variants conferred by vaccine sera (CoronaVac or BBIBP-CorV). **(A)** Neutralization ID50 values of the vaccinated sera against SARS-CoV-2 D614G reference pseudovirus. The black horizontal lines and the numbers over the lines indicate geometric mean titers. **(B)** Anti-SARS-CoV-2 RBD IgG antibody levels were measured by a quantitative ELISA against the wild-type RBD antigen. ELISAs were performed in duplicate, and average values were used. The black horizontal lines and the numbers over the lines indicate the average values of anti-SARS-CoV-2 RBD IgG. **(C, F)** SARS-CoV-2 variants reduced neutralization sensitivity to CoronaVac vaccine sera **(C)** or BBIBP-CorV vaccine sera **(F)**. Fold changes of vaccine sera neutralization activity (ID50) between variants and D614G reference strain pseudoviruses, depicted in a heat map. "–" represents the decrease of sensitivity of vaccine sera, and "+" represents the increase of sensitivity of vaccine sera. The values are marked in red, indicating that sensitivity is decreased at least 2-fold, while those in green indicate that sensitivity is increased at least 2-fold. **(D, E, G, H)** Neutralization ID50 values of the vaccinated sera [CoronaVac **(D, E)** or BBIBP-CorV **(G, H)**] against SARS-CoV-2 variant pseudoviruses. The geometric mean titer against each variant is indicated by a black horizontal line in panels **(D, G)** and a black curve in panels **(E, H)** The fold changes of ID50 between variant and D614G pseudoviruses are illustrated by the overall average at the top in **(D, G)**. The dashed line represents the initial dilution of vaccine sera. Neutralization activity is defined as the percent reduction in luciferase activity relative to the virus control wells (virus + cells).

Similarly, SARS-CoV-2 enters target cells mainly through endocytosis, and inhibiting the maturation and transport of endosomes can inhibit viral infections (6). To investigate whether the entry of SARS-CoV-2 S variants can be inhibited by cathepsin inhibitor or endocytosis inhibitor, 293T-hACE2 cells were treated with either cathepsin inhibitor E64d or endocytosis inhibitors Chloroquine, Tetrandrine, and Apilimod and then evaluated their effect on virus entry (**Figures 6A–E** and **Figures S7A–E**). All inhibitors were found to reduce the entry of variants of pseudovirus on 293T-hACE2 cells in a dose-dependent manner. The entry of B.1.1.7, B.1.429, B.1.617.1 B.1.617.2, and P.1 RBD pseudoviruses were slightly less sensitive to blockade by E64d as compared to D614G (**Figure 6E**). P.1 pseudovirus was slightly less sensitive to blockade by Apilimod as compared to D614G (**Figure 6E**). However, endocytosis inhibitors Chloroquine and Tetrandrine had similar blocking effects on all SARS-CoV-2 variants (**Figure 6E**). These results suggest that cathepsin inhibitors and endocytosis inhibitors will be active against SARS-CoV-2 variants.

DISCUSSION

As the COVID-19 pandemic persists, new SARS-CoV-2 variants will continue to emerge. Some mutations lead to changes in viral infectivity or may be able to escape neutralizing antibodies. In this study, we constructed the major circulating SARS-CoV-2 variants and identified the effects of these variants on virus infectivity, antigenicity, and sensitivity to inhibitors. The present study shows that, compared with the D614G strain, the infectivity of most variants was changed in mammalian cells. In addition, the antigenicity of some variants has also changed, resulting in a significant reduction in the neutralizing activity of a

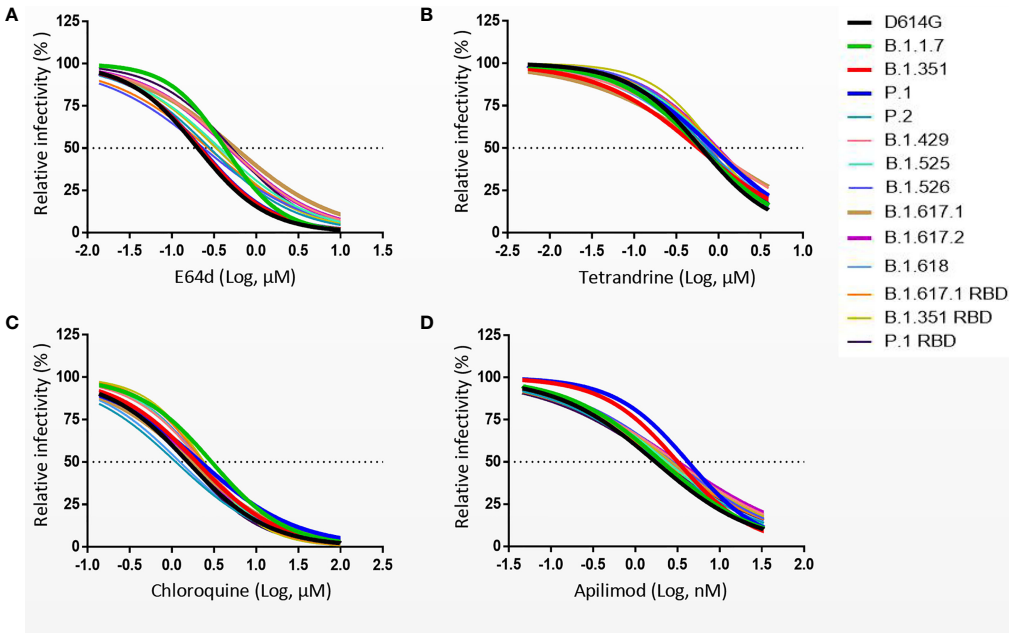

E

Fold changes in IC50	D614G	B.1.1.7	B.1.351	P.1	P.2	B.1.429	B.1.525	B.1.526	B.1.617.1	B.1.617.2	B.1.618	B.1.351 RBD	P.1 RBD	B.1.617.1 RBD
E64d	+1	-2.1	-1.1	-1.1	-1.4	-2.4	-1.8	-1.2	-2.8	-2.4	-1.7	-1.7	-2.5	-1.3
Tetrandrine	+1	+1	+1.1	-1.4	-1.2	-1.4	-1.5	-1.2	-1.2	-1.5	-1.1	-1.5	-1.1	-1.5
Chloroquine	+1	-1.9	-1.3	-1.4	+1.4	-1.5	-1.4	-1.4	-1.1	-1.2	+1.2	-1.6	+1	-1.5
Apilimod	+1	-1.2	-1.8	-2.4	-1.1	-1.8	-1.4	-1.7	-1.5	-1.8	-1.3	-1.6	-1.2	-1.3

FIGURE 6 | **(A–D)** 293T-hACE2 cells were pretreated with different concentrations of cathepsin inhibitor E64d **(A)** or endocytosis inhibitors Tetrandrine **(B)**, Chloroquine **(C)**, and Apilimod **(D)**, and then infected with SARS-CoV-2 S pseudoviruses. The luciferase activity was measured 24 h postinoculation. **(E)** The fold changes in half maximal inhibitory concentration (IC50) of inhibitors against SARS-CoV-2 variants pseudovirus relative to D614G. "-" represents the decrease of sensitivity to the inhibitor, and "+" represents the increase of sensitivity to the inhibitor. The values marked in red indicate that sensitivity decreased at least 2-fold. Experiments were done in 4 replicates and repeated at least twice. One representative is shown with error bars indicating SEM.

variety of RBD or NTD-targeting mAbs. Serum samples from individuals vaccinated with CoronaVac or BBIBP-CorV also showed the varyingly decreased neutralizing activity to many SARS-CoV-2 variants. Close monitoring of the major circulating SARS-CoV-2 variants can better control the spread of the virus, and it is also important for the development of neutralizing antibodies and vaccines.

The rapid spread of SARS-CoV-2 variants in the population raises the possibility that these viruses might exhibit altered infectivity or infection dynamics. After the SARS-CoV-2 outbreak, the D614G strain quickly replaced the original strain and became the dominant variant. Studies show that the D614G substitution leads to the enhancement of viral replication and infectivity in host cells (19, 20). Subsequently, several new SARS-CoV-2 variants were reported to spread rapidly in various countries and regions. In particular, B.1.17, B.1.351, P.1, and B.1.617.2 all showed higher infectivity than the original strain in the real world (31–34). In our study, the infectivity of the major circulating SARS-CoV-2 variants had no significant difference in 293T-hACE2, 293T-hACE2-TMPRSS2, Caco2-hACE2, and Vero cells. But the infectivity of some variants was significantly enhanced in Caco2, Huh7, A549, and H1299 cells. Recently, Zhang et al. (28) showed that the fusion activity among D614G, B.1.1.7, B.1.351, P.1, B.1.617.1, and B.1.617.2 had no significant differences when spike and ACE2 were transfected at high levels. However, B.1.617.2 can enter host cells expressing low levels of ACE2 more effectively than other variants. We also found that the infectivity of B.1.617.2 was significantly enhanced in ACE2 low-expression Caco2, Huh7, A549, and H1299 cells. This suggests that B.1.617.2 is more likely to infect less susceptible cells and then replace the previously dominant variants, leading to a global pandemic.

Priming of SARS-CoV-2 S proteins by host cell proteases is crucial for virus entry into cells (8). Insertion of a furin cleavage site with four amino acid motifs (PRRA) at the S1/S2 junction of SARS-COV-2 S protein can affect the cleavage of the viral S protein (35). The P681H, P681R, and Q677H mutation sites in the variants are located near the furin cleavage site, which may affect the cleavage of S protein (35–37). In fact, B.1.617.2 contains the P681R mutation, which results in enhanced cleavage of the S protein in cells, which may account for the enhanced infectivity of B.1.617.2 in some susceptible cells.

The main receptor for SARS-CoV-2 infection of host cells is ACE2, but several other receptors have been identified that promote SARS-CoV-2 infection (38–41). Some of these receptors affect SARS-CoV-2 infection by binding to sites outside the RBD region. Wang et al. (41) found that H1299 cells do not express the ACE2 receptor but highly express tyrosine-protein kinase receptor UFO (AXL), and it can bind to the SARS-CoV-2 NTD to mediate viral infection. In our study, most of the variants have NTD mutations, which may lead to changes in the binding ability of SARS-CoV-2 NTD to the AXL receptor, thereby affecting the ability of the virus to infect H1299 cells.

Hoffmann et al. (16) reported that pseudoviruses bearing the S protein of variants exhibit similar entry kinetics in Vero cells. In this study, we found that SARS-CoV-2 variants exhibited similar infectivity in Vero cells at an early stage. However, in Caco2-hACE2, 293T-hACE2, and 293T-hACE2-TMPRSS2 cells, B.1.1.7, B.1.351, and B.1.617.2 exhibit higher infection efficiency than D614G in shorter incubation time. These data suggest that some variants infect target cells much faster than the original strain, which may be the reason for their enhanced transmission ability.

At present, neutralizing mAbs and vaccines against SARS-CoV-2 are mainly developed against SARS-CoV-2 strains in the early stage of the pandemic (42–48). Our findings suggest that most of the circulating variants possess certain immune escape abilities to mAbs. Anti-RBD mAbs are divided into four categories according to the antibody recognition pattern and epitope structural characteristics (49). In this study, the antibody CB6 belongs to class I anti-RBD antibodies, which blocks ACE2 and bind only to "upper" RBDs. Previous studies have shown that the SARS-CoV-2 K417N/T mutation can lead to reduced neutralizing activity of CB6 (25). In our study, B.1.351, P.1, B.1.351 RBD, and P.1 RBD carrying the K417 mutation exhibited significant immune escape from CB6. LY-CoV555 is a class II anti-RBD antibody that blocks ACE2 and binds to both "upper" and "down" RBDs. LY-CoV555 has immune escape against almost all variants except D614G and B.1.17. The immune escape of some variants against LY-CoV555 may be related to the E484K/A mutation (24, 50). The mAbs REGN10987, S309, and VIR-7831 have strong neutralizing effects on almost all variants. These three antibodies belong to class III anti-RBD antibodies that bind outside the ACE2 site and recognize "up" and "down" RBDs (49), indicating that the neutralizing effect of antibodies is less affected when targeting these sites. Furthermore, 4A8 targets the SARS-CoV-2 NTD domain, and its neutralizing activity can be affected by SARS-CoV-2 Y144del, LAL242-244del, and R246I mutations (24, 25). Our studies show that its neutralizing activity is disrupted by certain mutations in the NTD domain, whereas the immune escape site is less related to the RBD region.

Similar to the neutralizing activity of antibodies, LY-CoV555 had reduced binding capacity for almost all variants except D614G and B.1.17. The binding affinity of mAbs REGN10987, S309, and VIR-7831 to variant S protein did not change significantly. The remaining anti-RBD mAbs had reduced binding ability to B.1351 or P.1. Most antibodies with reduced neutralizing activity to variant pseudoviruses also have reduced binding affinity, indicating that the antibody binding affinity is closely related to its neutralizing activity. The binding ability of these anti-RBD antibodies to the S protein is closely related to mutations in the RBD region. However, the binding ability of the 4A8 antibody to the S protein was associated with NTD mutations.

For neutralizing activity of CoronaVac and BBIBP-CorV vaccine sera, we found that most vaccine recipients were able to produce neutralizing antibodies and had the ability to neutralize the virus. Previous studies have shown that sequential booster immunizations with mRNA vaccines or subunit vaccines after two doses of inactivated vaccine are

more effective than homologous vaccines (51, 52). Indeed, mixed vaccination of CoronaVac and BBIBP-CorV vaccine resulted in higher levels of anti-RBD IgG antibodies and stronger virus neutralization than a single vaccination regimen. For neutralization activity of CoronaVac and BBIBP-CorV vaccine sera against different variants, our study is consistent with the results of recent reports using mRNA vaccine or inactivated vaccine sera (17, 18, 24, 53–55). We found that some variants, such as B.1.1.7, B.1.429, and B.1.525, have weaker immune escapes against CoronaVac or BBIBP-CorV vaccine sera. However, some variants, such as B.1.351, P.1, P.2, B.1.526, B.1.617.1, B.1.617.2, and B.1.618, have strong immune escapes against vaccine sera. Although the neutralizing activity to some SARS-CoV-2 variants was decreased, CoronaVac and BBIBP-CorV serum samples still reserved effective neutralizing abilities to all variants.

Proteolytic activation of S protein is an essential step for SARS-CoV-2 to enter target cells (6, 8, 56, 57). In this study, we confirmed that SARS-CoV-2 spread depends on cathepsin activity and further showed that the S protein-driven entry of the SARS-CoV-2 variant is effectively blocked by endosomal cysteine proteases CatB/L inhibitor. Ou et al. (6) showed that SARS-CoV-2 can enter host cells through endocytosis. The early-to-late endosomal maturation is regulated by $PI(3,5)P_2$ (58, 59). Inhibition of $PI(3,5)P_2$ synthase PIKfyve or the downstream effector TPC_2 can significantly reduce SARS-CoV-2 entry (6). Consistent with these findings, entry of all SARS-CoV-2 variants was effectively blocked by targeted endocytosis inhibitors Chloroquine, Tetrandrine, and Apilimod. Therefore, drugs targeting SARS-CoV-2 protease activity or endocytosis pathway are a commonly effective way in treating SARS-CoV-2 regardless of different mutations in the spike protein causing immune evasion.

Recently, a new SARS-CoV-2 variant, Omicron (B.1.1.529), emerged in South Africa, rapidly replacing B.1.617.2 and becoming the dominant strain. A striking feature of this variant is the large number of mutations in the S protein, most of which are located in the RBD region (60), which poses a threat to the efficacy of current COVID-19 vaccines and antibody therapies. Current studies have shown that B.1.1.529 is not only resistant to neutralization by sera from convalescent patients with COVID-19 but also significantly resistant to sera from vaccinated individuals (50, 61–63). Our published data (64) also demonstrate that pseudoviruses carrying the Omicron S protein have strong immune evasion capabilities against mAbs and vaccine sera. However, Omicron is still dependent on hACE2 for entry into target cells, and its S protein maintains a strong interaction with hACE2.

In summary, we demonstrate that the infection efficiency of pseudovirus with SARS-CoV-2 variant S protein has changed in some target cells; especially, the B.1.617.2 strain is more infectious in less susceptible cells to the original strain, and the virus infection process can be completed in a shorter time. In addition, our data suggest that SARS-CoV-2 variants may compromise the therapeutic effect of neutralizing antibodies or reduce the protective effect of vaccines. Our findings highlight the need to strengthen virus surveillance and assess the effectiveness of current antibodies and authorized vaccines against emerging SARS-CoV-2 variants. Meanwhile, increasing the proportion of people vaccinated with effective SARS-CoV-2 vaccines is the key strategy for reducing the emergence of new variants and ending the pandemic of COVID-19.

METHODS

Serum Samples

Vaccine sera were obtained from the participants who received CoronaVac and/or BBIBP-CorV vaccine at Suzhou Science and Technology Town Hospital in Suzhou City, Jiangsu Province, China, and stored at −80°C until use. Detailed vaccination information is provided in **Table S1**. The study was approved by the Institutional Review Board of Suzhou Science and Technology Town Hospital (IRB2021006). All subjects provided informed consent for the testing of their serum samples in this study.

Monoclonal Antibodies

All mAbs used in the present study were screened and provided by AtaGenix Company (Wuhan, China). Antibodies developed by other organizations, including LY-CoV555, CB6, REGN10987, S309, VIR-7831, and, 4A8, were produced based on the sequences published in Protein Data Bank (PDB). All antibodies were repackaged and stored at −80°C to avoid inconsistent results caused by repeated freeze–thaw cycles.

Cell Lines

293T (human, kidney), Caco-2 (human, colon), Huh7 (human, liver), A549 (human, lung), H1299 (human, lung), and Vero (African green monkey, kidney) cells were obtained from American Type Culture Collection (ATCC, Manassas, VA, USA). 293T-hACE2, 293T-hACE2-TMPRSS2, and Caco-2-hACE2 were produced by lentiviral mediated gene transduction. All cells were cultured in Dulbecco's modified Eagle medium (DMEM) (HyClone, Logan, UT, USA) containing 10% fetal bovine serum (FBS) (Gibco, Grand Island, NY, USA) and 100 U/ml of penicillin-streptomycin (Gibco).

Construction of SARS-CoV-2 Variant S Protein Expression Plasmids

The SARS-CoV-2 Wuhan-1 S gene (GenBank: MT_613044) was obtained from GenScript Biotech Corporation (Piscataway, NJ, USA). To effectively incorporate S protein into pseudovirus, the last 19 amino acids in the cytoplasmic tail of S protein were removed according to previously reported methods (65). To create variant S protein expression plasmids, point mutation on defined sites of the S gene was carried out using the site-directed mutagenesis kit (KOD). Subsequently, multiple PCR fragment amplification utilizing oligonucleotides containing mutation and overlapping sequence was performed for each desired mutation. Finally, overlapping fragments were assembled to produce all the mutations of each strain. The primers used to construct mutants are listed in **Table S2**.

Production of SARS-CoV-2 S Protein Pseudoviruses

Pseudoviruses with SARS-CoV-2 S protein were produced according to the methods reported in our previous study (66). Briefly, 293T cells transfected to express SARS-CoV-2 S protein under study were inoculated with G*ΔG-VSV dual reporter virus (kindly provided by UltraImmune Inc.). After 6 h of virus infection, the cells were gently washed twice with phosphate-buffered saline (PBS) to remove residual G*ΔG-VSV virus. Viral supernatant was collected at 24 or 48 h post inoculation and centrifuged at 4,000*g* for 5 min to remove cell debris.

The pseudovirus particles were quantified by RT-qPCR. Viral RNA Mini kit was used to extract virus RNA from 200 μl of pseudoviruses containing supernatant. Then, the viral RNA served as a template and reversed to cDNA. Virus particle quantification was performed by qPCR using FastStart Essential DNA Green Master (Roche, Basel, Switzerland). The copy numbers of virus particles were calculated according to VSV-P gene. Primers used to calculate pseudoviral particles are listed in **Table S3**.

Pseudovirus Infection Assay

Pseudoviral particles were normalized to the same amount using quantitative RT-PCR. Before virus infection, 2×10^4 target cells were seeded into each well of 96-well plates. Then, 100 μl of media containing pseudoviruses was inoculated into the cells. After incubation for 24 h, cells were lysed with passive lysis buffer (Promega, Madison, WI, USA) for 10 min, and then the luciferase activity was measured by the Luciferase Assay System (Promega). In order to analyze the entry of the pseudovirus into the target cells at indicated time points, the medium was removed at different time points, and the cells were washed with PBS to remove the remaining virus. Then 100 μl of fresh medium was added, and culture was continued for 24 h.

Detection of SARS-CoV-2 Variant S Protein

To detect the expression of S protein in cells, 293T cells were transfected with expression plasmids encoding SARS-CoV-2 variant S protein. After 40 h of transfection, cells were lysed by radioimmunoprecipitation assay (RIPA) Lysis Buffer (Beyotime, Shanghai, China) for 30 min on ice. To detect the cleavage of S protein on pseudoviruses, 1 ml of the SARS-CoV-2 pseudoviruses was loaded by 6% PEG8000 and shaken on the ice for 8 h. To pellet down pseudoviruses, the mixture was centrifuged at 10,000*g* for 2 h at 4°C. Next, the concentrated virus particles were resuspended in 50 μl of RIPA Lysis Buffer. The protein samples were heated at 95°C for 10 min. Then protein samples were separated in a 10% sodium dodecyl sulfate–polyacrylamide gel electrophoresis (SDS-PAGE) gel (Beyotime) and transferred onto polyvinylidene difluoride (PVDF) membranes (Millipore, Billerica, MA, USA). After protein transfer, the PVDF membranes were blocked by 5% milk for 1 h and then incubated overnight with primary antibodies. The next day, the PVDF membranes were incubated with secondary antibodies and visualized by the ChemiDoc MP system (Bio-Rad, Hercules, CA, USA). The following antibodies were used: mouse anti-SARS-CoV-2 spike (S2 subunit) mAb [1A9] (Genetex, Irvine, CA, USA; 1:2,000), mouse anti-VSV matrix protein (Kerafast, Boston, MA< USA; 1:2,500), GAPDH mAb (ProteinTech, Chicago, IL, USA; 1:2,000), and horseradish peroxidase linked anti-mouse IgG antibody (CST, Danvers, MA, USA; 1:5,000).

Enzyme-Linked Immunosorbent Assay

Anti-SARS-CoV-2 S-RBD IgG was detected using Human SARS-CoV-2 S-RBD IgG ELISA Kit (AtaGenix) according to the manufacturer's instructions. Serum samples were diluted at 1:2,000 with dilution buffer. The level of anti-RBD antibodies in the serum sample is represented by the concentration of the positive control antibody. One unit per ml (U/ml) represents the equivalent neutralization capacity of 1 ng/ml of control antibody.

Flow Cytometric Assessment of S Proteins Expression and the Binding of Monoclonal Antibodies to Cell Surface-Expressed SARS-CoV-2 S Proteins

293T cells were transfected with expression plasmids encoding SARS-CoV-2 S proteins and cultured for 36 h. Cells were digested with trypsin and washed twice with 1 ml of staining buffer (PBS containing 2% FBS). First, cells were incubated with mouse anti-SARS-CoV-2 spike (S2 subunit) antibody (Genetex, 1 μg/ml), neutralizing mAbs (AtaGenix, 0.2 μg/ml), or recombinant hACE2 protein (Sino Biological, Beijing, China; 1 μg/ml) at 4°C for 1 h. After being washed, cells were incubated with Alexa Flour 488-labeled anti-human IgG Fc (BioLegend, San Diego, CA, USA) and/or PE-labeled anti-mouse IgG (BioLegend) secondary antibodies for 1 h. After being washed, the cells were resuspended and analyzed using the Attune™ NxT Flow Cytometer (Thermo Fisher Scientific, Waltham, MA, USA).

Pseudovirus Neutralization Assays

The effects of the neutralizing antibodies and vaccinated sera on the entry inhibition of pseudoviruses were examined by detecting the reduction in luciferase gene expression (24, 30, 67). In brief, Vero or 293T-hACE2 cells were seeded in a 96-well plate at a concentration of 2×10^4 cells per well. To test the neutralization activity of the neutralizing antibodies, serial 5-fold dilution of samples were prepared at an initial concentration of 1 μg/ml and then incubated with 1,000 TCID50 pseudoviruses at 37°C for 1 h, and the mixture was added to Vero cells. To test the neutralization activity of vaccine sera, serial 3-fold dilution of samples were prepared with the starting dilution of 1:12 (all samples except V43–V50) or 1:20 (samples V43–V50) and then incubated with 1,000 TCID50 pseudoviruses at 37°C for 1 h, and the mixture was added to 293T-hACE2 cells. After incubation for 24 h, the neutralization activity was quantified by measuring the luciferase activity in cell lysates. Neutralization activity was defined as the percentage of decrease in luciferase activity compared to the virus control wells (virus + cells).

Effects of Protease and Endocytosis Inhibitors on Pseudovirus Entry

For experiments involving protease inhibitor (E64d, MCE, South Brunswick, NJ, USA) or endocytosis inhibitors (Chloroquine, MCE; Tetrandrine, Sigma, St. Louis, MO, USA; and Apilimod, MCE), 293T-hACE2 cells were pretreated with corresponding

inhibitors for 2 h before pseudovirus infection. Then, SARS-CoV-2 variants of pseudoviruses were added to the cell culture wells. The infection efficiency of viruses was quantified 24 h post-infection by measuring the luciferase activity in cell lysates.

Statistical Analysis

Half-maximal inhibitory concentration (IC50) or half-maximal inhibitory dilution (ID50) was defined as the RLU values that were reduced by 50% compared to the virus control wells (virus + cells). IC50 and ID50 were calculated by the equation of four-parameter dose inhibition response in GraphPad Prism 7. Vaccine sera, with neutralizing activity BDL, were assigned a value of 1 for geometric mean calculations and were considered as seronegative. The serum from healthy donors without vaccination was used as negative control and showed no detectable neutralization activity. The significance of neutralizing activities of serum samples against each variant pseudovirus relative to D614G was estimated using the Wilcoxon matched-pairs signed-rank test. Two-tailed p-values were reported, and $p < 0.05$ was defined as statistically significant.

DATA AVAILABILITY STATEMENT

The original contributions presented in the study are included in the article/**Supplementary Material**. Further inquiries can be directed to the corresponding authors.

ETHICS STATEMENT

The studies involving human participants were reviewed and approved by the Institutional Review Board of Suzhou Science and Technology Town Hospital (IRB2021006). The patients/participants provided their written informed consent to participate in this study. Written informed consent was obtained from the individual(s) for the publication of any potentially identifiable images or data included in this article.

AUTHOR CONTRIBUTIONS

HT performed the experiments and wrote the manuscript. HT, XD, and FQ analyzed data. LG, ZW, FM, XZ, YS, and GH contributed to revise the manuscript and approved the final manuscript. XD and FQ were responsible for research design, strategy, and supervision. All authors listed have made a substantial, direct, and intellectual contribution to the work and approved it for publication.

FUNDING

This work was supported by the National Natural Science Foundation of China (Grants 31800726 and 81773058), The Chinese Academy of Medical Sciences Initiative for Innovative Medicine (Grant CAMS-I2M, 2016-I2M-1-005), Key Research and Development Project of Zhejiang Province (No. 2021C03198), and National Grand Foreign Experts projects (G20190001633 and G20190001639).

SUPPLEMENTARY MATERIAL

The Supplementary Material for this article can be found online at: https://www.frontiersin.org/articles/10.3389/fimmu.2022.836232/full#supplementary-material

Supplementary Figure 1 | Structural diagram of mutation sites of variants S protein. The PDB number for the reference S protein structure is 7DDN. Each variant is shown from three perspectives, yellow represents the RBD region, green represents the NTD region, and turquoise represents the S2 region. Some mutation sites were not marked due to the lack of clear structural elucidation of these sites.

Supplementary Figure 2 | Infectivity analysis of SARS-CoV-2 variants in target cells in the early stage, repeated experiments of **Figures 2B**.

Supplementary Figure 3 | Binding of SARS-CoV-2 variants S protein to recombinant hACE2, repeated experiments of **Figures 3**.

Supplementary Figure 4 | Neutralization of SARS-CoV-2 variants by mAbs, related to **Figures 4**. Pseudoviruses carrying the variant S proteins were tested against a series of dilutions of each mAb. Neutralization activity was defined as the percentage of decrease in luciferase activity compared to the virus control wells (virus + cells).

Supplementary Figure 5 | Binding to cell surface expressed SARS-CoV-2 variants S proteins by neutralizing mAbs, related to **Figures 4**. SARS-CoV-2 variants S proteins were expressed on the surface of 293T cells, incubated with anti-SARS-CoV-2 spike antibody and neutralizing mAbs, followed by staining with Alexa Flour 488-conjugated anti-human IgG Fc and PE-conjugated anti-mouse IgG antibodies, and analyzed by flow cytometry. Experiments were done once. NC is 293T cells with mock transfection.

Supplementary Figure 6 | Neutralization of SARS-CoV-2 variants by vaccine sera, related to **Figures 5**. Pseudoviruses carrying the indicated variant S proteins were tested against serial dilutions of vaccine sera [CoronaVac vaccine (V1-V30) or BBIBP-CorV vaccine (V31-V50)]. Neutralization activity was defined as the percent reduction in luciferase activity relative to the virus control wells (virus + cells).

Supplementary Figure 7 | SARS-CoV-2 S pseudovirus entry into 293T-hACE cells can be blocked with endocytosis and protease inhibitors, repeated experiments of **Figures 6**.

REFERENCES

1. Benton DJ, Wrobel AG, Xu P, Roustan C, Martin SR, Rosenthal PB, et al. Receptor Binding and Priming of the Spike Protein of SARS-CoV-2 for Membrane Fusion. *Nature* (2020) 588(7837):327–30. doi: 10.1038/s41586-020-2772-0
2. Zhou P, Yang XL, Wang XG, Hu B, Zhang L, Zhang W, et al. A Pneumonia Outbreak Associated With a New Coronavirus of Probable Bat Origin. *Nature* (2020) 579(7798):270–3. doi: 10.1038/s41586-020-2012-7
3. Wan Y, Shang J, Graham R, Baric RS, Li F. Receptor Recognition by the Novel Coronavirus From Wuhan: An Analysis Based on Decade-Long Structural Studies of SARS Coronavirus. *J Virol* (2020) 94(7):e00127–20. doi: 10.1128/jvi.00127-20
4. Li W, Moore MJ, Vasilieva N, Sui J, Wong SK, Berne MA, et al. Angiotensin-Converting Enzyme 2 is a Functional Receptor for the SARS Coronavirus. *Nature* (2003) 426(6965):450–4. doi: 10.1038/nature02145
5. Shang J, Ye G, Shi K, Wan Y, Luo C, Aihara H, et al. Structural Basis of Receptor Recognition by SARS-CoV-2. *Nature* (2020) 581(7807):221–4. doi: 10.1038/s41586-020-2179-y

6. Ou X, Liu Y, Lei X, Li P, Mi D, Ren L, et al. Characterization of Spike Glycoprotein of SARS-CoV-2 on Virus Entry and its Immune Cross-Reactivity With SARS-CoV. *Nat Commun* (2020) 11(1):1620. doi: 10.1038/s41467-020-15562-9
7. Hoffmann M, Kleine-Weber H, Pöhlmann S. A Multibasic Cleavage Site in the Spike Protein of SARS-CoV-2 Is Essential for Infection of Human Lung Cells. *Mol Cell* (2020) 78(4):779–84.e5. doi: 10.1016/j.molcel.2020.04.022
8. Hoffmann M, Kleine-Weber H, Schroeder S, Krüger N, Herrler T, Erichsen S, et al. SARS-CoV-2 Cell Entry Depends on ACE2 and TMPRSS2 and Is Blocked by a Clinically Proven Protease Inhibitor. *Cell* (2020) 181(2):271–80.e8. doi: 10.1016/j.cell.2020.02.052
9. Huang Y, Sun H, Yu H, Li S, Zheng Q, Xia N. Neutralizing Antibodies Against SARS-CoV-2: Current Understanding, Challenge and Perspective. *Antib Ther* (2020) 3(4):285–99. doi: 10.1093/abt/tbaa028
10. Khan A, Zia T, Suleman M, Khan T, Ali SS, Abbasi AA, et al. Higher Infectivity of the SARS-CoV-2 New Variants is Associated With K417N/T, E484K, and N501Y Mutants: An Insight From Structural Data. *J Cell Physiol* (2021) 236(10):7045–57. doi: 10.1002/jcp.30367
11. Gottlieb RL, Nirula A, Chen P, Boscia J, Heller B, Morris J, et al. Effect of Bamlanivimab as Monotherapy or in Combination With Etesevimab on Viral Load in Patients With Mild to Moderate COVID-19: A Randomized Clinical Trial. *Jama* (2021) 325(7):632–44. doi: 10.1001/jama.2021.0202
12. Baden LR, El Sahly HM, Essink B, Kotloff K, Frey S, Novak R, et al. Efficacy and Safety of the mRNA-1273 SARS-CoV-2 Vaccine. *N Engl J Med* (2021) 384 (5):403–16. doi: 10.1056/NEJMoa2035389
13. Voysey M, Clemens SAC, Madhi SA, Weckx LY, Folegatti PM, Aley PK, et al. Safety and Efficacy of the ChAdOx1 Ncov-19 Vaccine (AZD1222) Against SARS-CoV-2: An Interim Analysis of Four Randomised Controlled Trials in Brazil, South Africa, and the UK. *Lancet* (2021) 397(10269):99–111. doi: 10.1016/s0140-6736(20)32661-1
14. Palacios R, Patiño EG, de Oliveira Piorelli R, Conde M, Batista AP, Zeng G, et al. Double-Blind, Randomized, Placebo-Controlled Phase III Clinical Trial to Evaluate the Efficacy and Safety of Treating Healthcare Professionals With the Adsorbed COVID-19 (Inactivated) Vaccine Manufactured by Sinovac - PROFISCOV: A Structured Summary of a Study Protocol for a Randomised Controlled Trial. *Trials* (2020) 21(1):853. doi: 10.1186/s13063-020-04775-4
15. Al Kaabi N, Zhang Y, Xia S, Yang Y, Al Qahtani MM, Abdulrazzaq N, et al. Effect of 2 Inactivated SARS-CoV-2 Vaccines on Symptomatic COVID-19 Infection in Adults: A Randomized Clinical Trial. *JAMA* (2021) 326(1):35–45. doi: 10.1001/jama.2021.8565
16. Hoffmann M, Arora P, Groß R, Seidel A, Hörnich BF, Hahn AS, et al. SARS-CoV-2 Variants B.1.351 and P.1 Escape From Neutralizing Antibodies. *Cell* (2021) 184(9):2384–93.e12. doi: 10.1016/j.cell.2021.03.036
17. Liu J, Liu Y, Xia H, Zou J, Weaver SC, Swanson KA, et al. BNT162b2-Elicited Neutralization of B.1.617 and Other SARS-CoV-2 Variants. *Nature* (2021) 596(7871):273–5. doi: 10.1038/s41586-021-03693-y
18. Garcia-Beltran WF, Lam EC, St Denis K, Nitido AD, Garcia ZH, Hauser BM, et al. Multiple SARS-CoV-2 Variants Escape Neutralization by Vaccine-Induced Humoral Immunity. *Cell* (2021) 184(9):2372–83.e9. doi: 10.1016/j.cell.2021.03.013
19. Plante JA, Liu Y, Liu J, Xia H, Johnson BA, Lokugamage KG, et al. Spike Mutation D614G Alters SARS-CoV-2 Fitness. *Nature* (2021) 592(7852):116–21. doi: 10.1038/s41586-020-2895-3
20. Korber B, Fischer WM, Gnanakaran S, Yoon H, Theiler J, Abfalterer W, et al. Tracking Changes in SARS-CoV-2 Spike: Evidence That D614G Increases Infectivity of the COVID-19 Virus. *Cell* (2020) 182(4):812–27.e19. doi: 10.1016/j.cell.2020.06.043
21. Hou YJ, Chiba S, Halfmann P, Ehre C, Kuroda M, Dinnon KH3rd, et al. SARS-CoV-2 D614G Variant Exhibits Efficient Replication Ex Vivo and Transmission *In Vivo*. *Science* (2020) 370(6523):1464–8. doi: 10.1126/science.abe8499
22. Baum A, Fulton BO, Wloga E, Copin R, Pascal KE, Russo V, et al. Antibody Cocktail to SARS-CoV-2 Spike Protein Prevents Rapid Mutational Escape Seen With Individual Antibodies. *Science* (2020) 369(6506):1014–8. doi: 10.1126/science.abd0831
23. Weisblum Y, Schmidt F, Zhang F, DaSilva J, Poston D, Lorenzi JC, et al. Escape From Neutralizing Antibodies by SARS-CoV-2 Spike Protein Variants. *Elife* (2020) 9:e61312. doi: 10.7554/eLife.61312
24. Wang P, Nair MS, Liu L, Iketani S, Luo Y, Guo Y, et al. Antibody Resistance of SARS-CoV-2 Variants B.1.351 and B.1.1.7. *Nature* (2021) 593(7857):130–5. doi: 10.1038/s41586-021-03398-2
25. Wang R, Zhang Q, Ge J, Ren W, Zhang R, Lan J, et al. Analysis of SARS-CoV-2 Variant Mutations Reveals Neutralization Escape Mechanisms and the Ability to Use ACE2 Receptors From Additional Species. *Immunity* (2021) 54 (7):1611–21.e5. doi: 10.1016/j.immuni.2021.06.003
26. Lopez Bernal J, Andrews N, Gower C, Gallagher E, Simmons R, Thelwall S, et al. Effectiveness of Covid-19 Vaccines Against the B.1.617.2 (Delta) Variant. *N Engl J Med* (2021) 385(7):585–94. doi: 10.1056/NEJMoa2108891
27. Mlcochova P, Kemp SA, Dhar MS, Papa G, Meng B, Ferreira I, et al. SARS-CoV-2 B.1.617.2 Delta Variant Replication and Immune Evasion. *Nature* (2021) 599(7883):114–9. doi: 10.1038/s41586-021-03944-y
28. Zhang J, Xiao T, Cai Y, Lavine CL, Peng H, Zhu H, et al. Membrane Fusion and Immune Evasion by the Spike Protein of SARS-CoV-2 Delta Variant. *Science* (2021) 374(6573):1353–60. doi: 10.1126/science.abl9463
29. Starr TN, Greaney AJ, Hilton SK, Ellis D, Crawford KHD, Dingens AS, et al. Deep Mutational Scanning of SARS-CoV-2 Receptor Binding Domain Reveals Constraints on Folding and ACE2 Binding. *Cell* (2020) 182(5):1295–10.e20. doi: 10.1016/j.cell.2020.08.012
30. Li Q, Wu J, Nie J, Zhang L, Hao H, Liu S, et al. The Impact of Mutations in SARS-CoV-2 Spike on Viral Infectivity and Antigenicity. *Cell* (2020) 182 (5):1284–94.e9. doi: 10.1016/j.cell.2020.07.012
31. Davies NG, Abbott S, Barnard RC, Jarvis CI, Kucharski AJ, Munday JD, et al. Estimated Transmissibility and Impact of SARS-CoV-2 Lineage B.1.1.7 in England. *Science* (2021) 372(6538):eabg3055. doi: 10.1126/science.abg3055
32. Tegally H, Wilkinson E, Giovanetti M, Iranzadeh A, Fonseca V, Giandhari J, et al. Detection of a SARS-CoV-2 Variant of Concern in South Africa. *Nature* (2021) 592(7854):438–43. doi: 10.1038/s41586-021-03402-9
33. Faria NR, Mellan TA, Whittaker C, Claro IM, Candido DDS, Mishra S, et al. Genomics and Epidemiology of the P.1 SARS-CoV-2 Lineage in Manaus, Brazil. *Science* (2021) 372(6544):815–21. doi: 10.1126/science.abh2644
34. Choi JY, Smith DM. SARS-CoV-2 Variants of Concern. *Yonsei Med J* (2021) 62(11):961–8. doi: 10.3349/ymj.2021.62.11.961
35. Xia S, Lan Q, Su S, Wang X, Xu W, Liu Z, et al. The Role of Furin Cleavage Site in SARS-CoV-2 Spike Protein-Mediated Membrane Fusion in the Presence or Absence of Trypsin. *Signal Transduct Target Ther* (2020) 5(1):92. doi: 10.1038/s41392-020-0184-0
36. Hossain MG, Tang YD, Akter S, Zheng C. Roles of the Polybasic Furin Cleavage Site of Spike Protein in SARS-CoV-2 Replication, Pathogenesis, and Host Immune Responses and Vaccination. *J Med Virol* (2021). doi: 10.1002/jmv.27539
37. Peacock TP, Goldhill DH, Zhou J, Baillon L, Frise R, Swann OC, et al. The Furin Cleavage Site in the SARS-CoV-2 Spike Protein is Required for Transmission in Ferrets. *Nat Microbiol* (2021) 6(7):899–909. doi: 10.1038/s41564-021-00908-w
38. Daly JL, Simonetti B, Klein K, Chen KE, Williamson MK, Antón-Plágaro C, et al. Neuropilin-1 is a Host Factor for SARS-CoV-2 Infection. *Science* (2020) 370(6518):861–5. doi: 10.1126/science.abd3072
39. Yang C, Zhang Y, Zeng X, Chen H, Chen Y, Yang D, et al. Kidney Injury Molecule-1 is a Potential Receptor for SARS-CoV-2. *J Mol Cell Biol* (2021) 13 (3):185–96. doi: 10.1093/jmcb/mjab003
40. Mori Y, Fink C, Ichimura T, Sako K, Mori M, Lee NN, et al. KIM-1/TIM-1 is a Receptor for SARS-CoV-2 in Lung and Kidney. *medRxiv* (2022). doi: 10.1101/2020.09.16.20190694
41. Wang S, Qiu Z, Hou Y, Deng X, Xu W, Zheng T, et al. AXL is a Candidate Receptor for SARS-CoV-2 That Promotes Infection of Pulmonary and Bronchial Epithelial Cells. *Cell Res* (2021) 31(2):126–40. doi: 10.1038/s41422-020-00460-y
42. Cao Y, Su B, Guo X, Sun W, Deng Y, Bao L, et al. Potent Neutralizing Antibodies Against SARS-CoV-2 Identified by High-Throughput Single-Cell Sequencing of Convalescent Patients' B Cells. *Cell* (2020) 182(1):73–84.e16. doi: 10.1016/j.cell.2020.05.025
43. Corbett KS, Flynn B, Foulds KE, Francica JR, Boyoglu-Barnum S, Werner AP, et al. Evaluation of the mRNA-1273 Vaccine Against SARS-CoV-2 in Nonhuman Primates. *N Engl J Med* (2020) 383(16):1544–55. doi: 10.1056/NEJMoa2024671

44. Hansen J, Baum A, Pascal KE, Russo V, Giordano S, Wloga E, et al. Studies in Humanized Mice and Convalescent Humans Yield a SARS-CoV-2 Antibody Cocktail. *Science* (2020) 369(6506):1010–4. doi: 10.1126/science.abd0827
45. Ju B, Zhang Q, Ge J, Wang R, Sun J, Ge X, et al. Human Neutralizing Antibodies Elicited by SARS-CoV-2 Infection. *Nature* (2020) 584(7819):115–9. doi: 10.1038/s41586-020-2380-z
46. Liu L, Wang P, Nair MS, Yu J, Rapp M, Wang Q, et al. Potent Neutralizing Antibodies Against Multiple Epitopes on SARS-CoV-2 Spike. *Nature* (2020) 584(7821):450–6. doi: 10.1038/s41586-020-2571-7
47. Vogel AB, Kanevsky I, Che Y, Swanson KA, Muik A, Vormehr M, et al. BNT162b Vaccines Protect Rhesus Macaques From SARS-CoV-2. *Nature* (2021) 592(7853):283–9. doi: 10.1038/s41586-021-03275-y
48. Wu S, Zhong GX, Zhang J, Shuai L, Zhang Z, Wen ZY, et al. A Single Dose of An Adenovirus-Vectored Vaccine Provides Protection Against SARS-CoV-2 Challenge. *Nat Commun* (2020) 11(1):4081. doi: 10.1038/s41467-020-17972-1
49. Barnes CO, Jette CA, Abernathy ME, Dam KA, Esswein SR, Gristick HB, et al. SARS-CoV-2 Neutralizing Antibody Structures Inform Therapeutic Strategies. *Nature* (2020) 588(7839):682–7. doi: 10.1038/s41586-020-2852-1
50. Liu L, Iketani S, Guo Y, Chan JF, Wang M, Liu L, et al. Striking Antibody Evasion Manifested by the Omicron Variant of SARS-CoV-2. *Nature* (2021) 602(7898):676–81. doi: 10.1038/s41586-021-04388-0
51. Ai J, Zhang H, Zhang Q, Zhang Y, Lin K, Fu Z, et al. Recombinant Protein Subunit Vaccine Booster Following Two-Dose Inactivated Vaccines Dramatically Enhanced Anti-RBD Responses and Neutralizing Titers Against SARS-CoV-2 and Variants of Concern. *Cell Res* (2022) 32(1):103–6. doi: 10.1038/s41422-021-00590-x
52. Keskin AU, Bolukcu S, Ciragil P, Topkaya AE. SARS-CoV-2 Specific Antibody Responses After Third CoronaVac or BNT162b2 Vaccine Following Two-Dose CoronaVac Vaccine Regimen. *J Med Virol* (2022) 94(1):39–41. doi: 10.1002/jmv.27350
53. Chen Y, Shen H, Huang R, Tong X, Wu C. Serum Neutralising Activity Against SARS-CoV-2 Variants Elicited by CoronaVac. *Lancet Infect Dis* (2021) 21(8):1071–2. doi: 10.1016/s1473-3099(21)00287-5
54. Wall EC, Wu M, Harvey R, Kelly G, Warchal S, Sawyer C, et al. Neutralising Antibody Activity Against SARS-CoV-2 VOCs B.1.617.2 and B.1.351 by BNT162b2 Vaccination. *Lancet* (2021) 397(10292):2331–3. doi: 10.1016/s0140-6736(21)01290-3
55. Liu Y, Liu J, Xia H, Zhang X, Fontes-Garfias CR, Swanson KA, et al. Neutralizing Activity of BNT162b2-Elicited Serum. *N Engl J Med* (2021) 384(15):1466–8. doi: 10.1056/NEJMc2102017
56. Simmons G, Gosalia DN, Rennekamp AJ, Reeves JD, Diamond SL, Bates P. Inhibitors of Cathepsin L Prevent Severe Acute Respiratory Syndrome Coronavirus Entry. *Proc Natl Acad Sci USA* (2005) 102(33):11876–81. doi: 10.1073/pnas.0505577102
57. Zhou N, Pan T, Zhang J, Li Q, Zhang X, Bai C, et al. Glycopeptide Antibiotics Potently Inhibit Cathepsin L in the Late Endosome/Lysosome and Block the Entry of Ebola Virus, Middle East Respiratory Syndrome Coronavirus (MERS-CoV), and Severe Acute Respiratory Syndrome Coronavirus (SARS-CoV). *J Biol Chem* (2016) 291(17):9218–32. doi: 10.1074/jbc.M116.716100
58. Jin X, Zhang Y, Alharbi A, Hanbashi A, Alhoshani A, Parrington J. Targeting Two-Pore Channels: Current Progress and Future Challenges. *Trends Pharmacol Sci* (2020) 41(8):582–94. doi: 10.1016/j.tips.2020.06.002
59. Sakurai Y, Kolokoltsov AA, Chen CC, Tidwell MW, Bauta WE, Klugbauer N, et al. Ebola Virus. Two-Pore Channels Control Ebola Virus Host Cell Entry and are Drug Targets for Disease Treatment. *Science* (2015) 347(6225):995–8. doi: 10.1126/science.1258758
60. Scott L, Hsiao NY, Moyo S, Singh L, Tegally H, Dor G, et al. Track Omicron's Spread With Molecular Data. *Science* (2021) 374(6574):1454–5. doi: 10.1126/science.abn4543
61. Dejnirattisai W, Huo J, Zhou D, Zahradník J, Supasa P, Liu C, et al. SARS-CoV-2 Omicron-B.1.1.529 Leads to Widespread Escape From Neutralizing Antibody Responses. *Cell* (2022) 185(3):467–84.e15. doi: 10.1016/j.cell.2021.12.046
62. Cao Y, Wang J, Jian F, Xiao T, Song W, Yisimayi A, et al. Omicron Escapes the Majority of Existing SARS-CoV-2 Neutralizing Antibodies. *Nature* (2021) 602(7898):657–63. doi: 10.1038/s41586-021-04385-3
63. Zhang X, Wu S, Wu B, Yang Q, Chen A, Li Y, et al. SARS-CoV-2 Omicron Strain Exhibits Potent Capabilities for Immune Evasion and Viral Entrance. *Signal Transduct Target Ther* (2021) 6(1):430. doi: 10.1038/s41392-021-00852-5
64. Du X, Tang H, Gao L, Wu Z, Meng F, Yan R, et al. Omicron Adopts a Different Strategy From Delta and Other Variants to Adapt to Host. *Signal Transduct Target Ther* (2022) 7(1):45. doi: 10.1038/s41392-022-00903-5
65. Whitt MA. Generation of VSV Pseudotypes Using Recombinant Δg-VSV for Studies on Virus Entry, Identification of Entry Inhibitors, and Immune Responses to Vaccines. *J Virol Methods* (2010) 169(2):365–74. doi: 10.1016/j.jviromet.2010.08.006
66. Tang H, Gao L, Wu Z, Meng F, Zhao X, Shao Y, et al. Characterization of SARS-CoV-2 Variants N501Y.V1 and N501Y.V2 Spike on Viral Infectivity. *Front Cell Infect Microbiol* (2021) 11:720357. doi: 10.3389/fcimb.2021.720357
67. Li Q, Nie J, Wu J, Zhang L, Ding R, Wang H, et al. SARS-CoV-2 501y.V2 Variants Lack Higher Infectivity But do Have Immune Escape. *Cell* (2021) 184(9):2362–71.e9. doi: 10.1016/j.cell.2021.02.042

Conflict of Interest: The authors declare that the research was conducted in the absence of any commercial or financial relationships that could be construed as a potential conflict of interest.

frontiers | Frontiers in Immunology

ORIGINAL RESEARCH
published: 04 May 2022
doi: 10.3389/fimmu.2022.868724

Antigenic Cross-Reactivity Between SARS-CoV-2 S1-RBD and Its Receptor ACE2

Yen-Chung Lai[1,2†], Yu-Wei Cheng[2,3†], Chiao-Hsuan Chao[1†], Yu-Ying Chang[2], Chi-De Chen[4], Wei-Jiun Tsai[3], Shuying Wang[5], Yee-Shin Lin[5], Chih-Peng Chang[5], Woei-Jer Chuang[6], Li-Yin Chen[2], Ying-Ren Wang[2], Sui-Yuan Chang[7], Wenya Huang[1], Jen-Ren Wang[1], Chin-Kai Tseng[8], Chun-Kuang Lin[8], Yung-Chun Chuang[1,2,9] and Trai-Ming Yeh[1*]*

[1] Department of Medical Laboratory Science and Biotechnology, College of Medicine, National Cheng Kung University, Tainan, Taiwan, [2] Leadgene Biomedical, Inc., Tainan, Taiwan, [3] The Institute of Basic Medical Sciences, College of Medicine, National Cheng Kung University, Tainan, Taiwan, [4] OmicsLab Co., Ltd., New Taipei City, Taiwan, [5] Department of Microbiology and Immunology, College of Medicine, National Cheng Kung University, Tainan, Taiwan, [6] Department of Biochemistry and Molecular Biology, College of Medicine, National Cheng Kung University, Tainan, Taiwan, [7] Department of Clinical Laboratory Sciences and Medical Biotechnology, College of Medicine, National Taiwan University, Taipei, Taiwan, [8] SIDSCO Biomedical Co., Ltd., Kaohsiung, Taiwan, [9] Department of Biomedical Sciences, Chung Shan Medical University, Taichung, Taiwan

OPEN ACCESS

Edited by:
Penghua Wang, University of Connecticut Health Center, United States

Reviewed by:
Ciro Leonardo Pierri, University of Bari Aldo Moro, Italy
Jianfeng Dai, Soochow University, China

***Correspondence:**
Yung-Chun Chuang
chasel@leadgene.com.tw
Trai-Ming Yeh
today@mail.nkcu.edu.tw

†These authors have contributed equally to this work and share first authorship

Specialty section:
This article was submitted to Viral Immunology, a section of the journal Frontiers in Immunology

Received: *03 February 2022*
Accepted: *07 April 2022*
Published: *04 May 2022*

Citation:
Lai Y-C, Cheng Y-W, Chao C-H, Chang Y-Y, Chen C-D, Tsai W-J, Wang S, Lin Y-S, Chang C-P, Chuang W-J, Chen L-Y, Wang Y-R, Chang S-Y, Huang W, Wang J-R, Tseng C-K, Lin C-K, Chuang Y-C and Yeh T-M (2022) Antigenic Cross-Reactivity Between SARS-CoV-2 S1-RBD and Its Receptor ACE2. Front. Immunol. 13:868724. doi: 10.3389/fimmu.2022.868724

Severe acute respiratory syndrome coronavirus 2 (SARS-CoV-2) is an emerging virus responsible for the ongoing COVID-19 pandemic. SARS-CoV-2 binds to the human cell receptor angiotensin-converting enzyme 2 (ACE2) through its receptor-binding domain in the S1 subunit of the spike protein (S1-RBD). The serum levels of autoantibodies against ACE2 are significantly higher in patients with COVID-19 than in controls and are associated with disease severity. However, the mechanisms through which these anti-ACE2 antibodies are induced during SARS-CoV-2 infection are unclear. In this study, we confirmed the increase in antibodies against ACE2 in patients with COVID-19 and found a positive correlation between the amounts of antibodies against ACE2 and S1-RBD. Moreover, antibody binding to ACE2 was significantly decreased in the sera of some COVID-19 patients after preadsorption of the sera with S1-RBD, which indicated that antibodies against S1-RBD can cross-react with ACE2. To confirm this possibility, two monoclonal antibodies (mAbs 127 and 150) which could bind to both S1-RBD and ACE2 were isolated from S1-RBD-immunized mice. Measurement of the binding affinities by Biacore showed these two mAbs bind to ACE2 much weaker than binding to S1-RBD. Epitope mapping using synthetic overlapping peptides and hydrogen deuterium exchange mass spectrometry (HDX-MS) revealed that the amino acid residues P463, F464, E465, R466, D467 and E471 of S1-RBD are critical for the recognition by mAbs 127 and 150. In addition, Western blotting analysis showed that these mAbs could recognize ACE2 only in native but not denatured form, indicating the ACE2 epitopes recognized by these mAbs were conformation-dependent. The protein–protein interaction between ACE2 and the higher affinity mAb 127 was analyzed by HDX-MS

and visualized by negative-stain transmission electron microscopy imaging combined with antigen-antibody docking. Together, our results suggest that ACE2-cross-reactive anti-S1-RBD antibodies can be induced during SARS-CoV-2 infection due to potential antigenic cross-reactivity between S1-RBD and its receptor ACE2.

Keywords: COVID-19, autoantibody, angiotensin converting enzyme 2, monoclonal antibody, molecular mimicry

INTRODUCTION

Severe acute respiratory syndrome coronavirus 2 (SARS-CoV-2) is a new emerging virus that is rapidly spreading in humans and thus causing the ongoing global coronavirus disease 2019 (COVID-19) pandemic (1). SARS-CoV-2 is a β-coronavirus, a subgroup that is taxonomically very close to SARS-CoV but more distantly related to MERS-CoV and common human CoVs (2). The spike (S) protein of SARS-CoV-2 is a ~180 kDa glycoprotein, which can form a trimeric structure that protrudes from the surface of the viral particle, plays a key role in the recognition of the cell surface receptor angiotensin-converting enzyme 2 (ACE2) (3) and cell membrane fusion (4). The total length of the SARS-CoV-2 S protein contains 1273 amino acids (a.a) arranged into two subunits: the S1 subunit (a.a. 14-685) contains a receptor-binding domain (S1-RBD, a.a. 319-541) that is less conserved between SARS-CoVs and other CoVs, having only a range of 20-64% identity match, whereas the S2 subunit (a.a. 686-1273) mediates viral cell membrane fusion, exhibiting higher sequence identity (~90%) (4–7). The receptor-binding motif (RBM, a.a. 437-507) is a portion of the S1-RBD that makes direct contact with ACE2, whereas S2 subunit mediates subsequent membrane fusion with the host cell membrane (8). The binding of S protein to ACE2 triggers the cleavage between S1 and S2 by host furin and TMPRRS2 proteases, which is responsible for the transition of S2 subunit to the "fusion" conformation to initiate fusion to enable viral entry into cells (9).

Since the binding of S protein to ACE2 is the first step in the process of SARS-CoV-2 infection, it is a key determinant of host cell and tissue tropism of SARS-CoV-2. Indeed, SARS-CoV-2 S1-RBD appears to exhibit improved binding efficiency to human ACE2 compared with that of the 2003 strain of SARS-CoV (3, 10). In addition to the mutation of the S1-RBD which can cause significant variation in the S1-RBD/ACE2 binding affinity (11), the distribution of ACE2 and TMPRRS2 are primary limiting cell-entry factors for the susceptibility of different tissues and cell types to SARS-CoV-2 entry and infection. A list of 28 cellular factors, referred to as SARS-CoV-2 and coronavirus-associated receptors and factors (SCARFs) are identified using single-cell transcriptomics across various human tissues, which are involved in either facilitating or restricting viral entry (9). These cellular factors are also important in determining the potential tissue tropism of SARS-CoV-2.

Analysis of SARS-CoV-2 S glycan reveals that it is heavily glycosylated, providing shielding from antibody recognition, with the exception of the S1-RBD. Intriguingly, the S1-RBD is structurally flexible which can change between an open (up) and closed (down) conformation. While S1-RBD at open conformation is required to be able to interact with ACE2, Cryo-EM study of S protein trimers reveals that on average only ~20% of S1-RBD are in the open state (12–14). Interestingly, the glycosylation of S protein is also involved in the transition between the open vs. closed state of the S1-RBD (15). Since S1-RBD at the open state increases the possibility of being recognized by host antibodies, it is likely that S protein evolved this conformational dynamic change to balance infection and immune evasion (8).

Unlike 2003 SARS, COVID-19 commonly causes tissue damage in non-respiratory organs, such as the heart, liver, kidney, and brain (16, 17). However, what leads to the wide range of clinical pathologies observed in COVID-19 patients is not yet understood. It remains unclear whether these pathological damages are caused by direct SARS-CoV-2 infection of the organs affected or indirect effects by immune responses or comorbidities. In addition to viral and cellular entry factors, many host immune responses have been proposed to contribute to the severity and multiple organs involvement of COVID-19, including dysregulated inflammatory response and autoimmunity (18–21). For example, the development of IgG, IgM, and IgA autoantibodies against ACE2 in patients with COVID-19 has been reported (22–25), and their levels in sera are associated with COVID-19 disease severity (24). However, the mechanisms through which antibodies against ACE2 are induced during SARS-CoV-2 infection are unclear.

In this study, we first confirmed the increase in antibodies against ACE2 in patients with COVID-19 and demonstrated a positive correlation between the amounts of antibodies against ACE2 and S1-RBD. In addition, the antibody binding to ACE2 was significantly decreased in the sera of some COVID-19 patients after preadsorption of the sera with S1-RBD. To confirm that antibodies against S1-RBD can indeed cross-react with ACE2, we immunized mice or rabbits using recombinant S1-RBD generated by bacteria, insect cells, or mammalian cells and found that anti-ACE2 antibodies were also increased in various sources of S1-RBD immune sera. Two monoclonal antibodies (mAbs) that could recognize both S1-RBD and ACE2 were identified. Thus, our results suggest the existence of potential antigenic cross-reactivity between S1-RBD and its receptor ACE2.

MATERIALS AND METHODS

Recombinant Proteins, Peptides, and Patient Serum

C-terminal Twin-Strep-tagged SARS-CoV-2 S1-RBD recombinant proteins (from a.a. 319 to 541 of the S1 protein, YP_009724390)

were cloned into pMT/BiP/V5-His B plasmid for S2 cell expression. The purity of SARS-CoV-2 S1-RBD from S2 cell was >90% by using SDS-PAGE analysis. The yield was around 4.6 mg/L. SARS-CoV-2 S1-RBD from *E. coli* and CHO (Cat. No. 61931/62433, Leadgene Biomedical Inc.) as well as different SARS-CoV-2 S1-RBD mutants and S1-RBD peptides were customized, purified and synthesized by Leadgene Biomedical, Inc. Tainan, Taiwan. C-terminal Fc-tagged human ACE2 recombinant protein (ACE2-hFc) was purified from CHO cells (Cat. No. 63333, Leadgene Biomedical Inc.). C-terminal His-tagged human ACE2 (10108-H08H) and other coronavirus S1 proteins (40150-V08B1, 40591-V08H, 40069-V08H, and 40600-V08H) were purchased from Sino Biological (Beijing, China). In addition, commercially available COVID-19-positive (Panel D, n=30) and COVID-19-negative patient sera (Panel E, n=60) were purchased from Access Biologicals (Vista, CA, USA). According to the manufacture, individual donor units used in the cohort have been tested and found negative by tests for antibodies to HIV 1/2, HCV and non-reactive for HBsAg. All testing was performed with kits approved by the FDA. The samples were collected under IRB approved protocols. The commercial COVID-19 positive and negative patient sera were dispensed in Biosafety Level-2 plus (BSL-2+) laboratory. All individuals participating in patient sera dispensation were fully trained according to the compliance policies of the National Cheng Kung University Hospital. Appropriate personal protective equipment was always worn when working with patient sera in the BSL-2+ room. Dispensed patient sera were inactivated at 56°C for 30 min before being used in this study (**Supplementary Table**).

Immunization and mAb Generation

For the preparation of mouse and rabbit S1-RBD-hyperimmune sera, recombinant proteins (25 μg for mice, 250 μg for rabbits) were emulsified with alum or Incomplete Freund's Adjuvant (IFA) (Sigma–Aldrich, St Louis, MO, USA). The animals were primed and challenged on days 1, 14 and 21 using alum adjuvant or on days 1, 7 and 14 using IFA. Sera were collected 7 days after the final challenge and stored at -20°C until use. For mAb generation, mice at the Leadgene Biomedical, Inc., facility were immunized with S1-RBD expressed in *E. coli* according to the hybridoma technique as previously described (26, 27). In brief, the splenocytes were fused with mouse myeloma FO cells and selected by modified selected-medium containing hypoxanthine–aminopterin–thymidine (Thermo Fisher Scientific, MA, USA), 15% fetal bovine sera (FBS) (HyClone, Logan, UT) and 2.5% HyBoost (Leadgene Biomedical Inc., Taiwan). Cloning hybridoma cells was performed by limiting dilution. Supernatants of the clones were collected and screened for antibodies against SARS-CoV-2 S1-RBD and ACE2. Hybridoma cells were injected into mouse peritoneal cavities to generate ascites, and the mAbs in ascites were harvested by protein G-Sepharose (GE Healthcare), dialyzed against phosphate-buffered saline (PBS), and stored below -20°C.

Enzyme-Linked Immunosorbent Assays

Each well of an ELISA plate (Corning Costar, Acton, MA, USA) was coated with 100 μL of antigens (1 μg/mL recombinant protein in PBS or 2 μg/mL bovine serum albumin (BSA)-conjugated peptides in carbonate coating buffer, pH 9.6) for 16 h at 4°C, washed three times with PBST (0.1% Tween 20) and blocked with 5% skim milk for 1 h at 37°C. For the detection of antibody binding to ACE2 in human sera, the ELISA plates were coated with His-tagged ACE2 instead of ACE2-hFc to prevent nonspecific binding of the secondary antibody to human Fc. In contrast, to detect antibody binding to ACE2 in immune sera from mice or rabbits, the ELISA plates were coated with ACE2-hFc to prevent nonspecific binding of anti-His antibodies in immune sera. The sera were diluted in PBST and added to the wells of the ELISA plates, and the plates were incubated for 1 h at 37°C. HRP-labeled secondary antibodies against human (C04047, Croyez, Taiwan), mouse (115-035-062, Jackson ImmunoResearch, West Grove, PA, USA), or rabbit IgG (C04010, Croyez, Taiwan) were diluted 10,000-fold in PBST and used for the detection of bound antibodies. In the competition ELISA, the Abs (1 μg/mL and 25 μg/mL for S1-RBD- and ACE2-hFc-coated plates, respectively) were preincubated with different S1-RBD polypeptides at different doses as indicated, for 1 h at 37°C. Subsequently, the Ab-peptide mixtures were incubated in S1-RBD- or ACE2-hFc (2 μg/mL)-coated plates for another 30 min, washed with PBST and incubated with HRP-labeled secondary antibodies against mouse IgG for another 1 h. For color development, 100 μL of TMB PLUS2 (Kementec Solutions A/S, Denmark) was added to the wells, the plates were incubated for 10 min at 37°C, and the reaction was stopped by the addition of 50 μL of 0.2 M sulfuric acid. The absorbance at 450 nm was determined using an ELISA reader (Multiskan, Thermo Fisher Scientific, Waltham, MA, USA).

Serum Preadsorption Assay

In the serum preadsorption assay, ELISA strip wells (Corning) were coated with BSA (10 μg/mL, 100 μL), S1-RBD (10 μg/mL, 100 μL), and ACE2-His (1 μg/mL, 100 μL). The strip wells were washed three times with PBST and blocked with 1% BSA in PBS. The sera were diluted in PBS at 1:100 dilution and then added to BSA- or S1-RBD-coated wells. After incubation at 37°C for 1 h, the diluted sera were transferred to ACE2-His-coated wells. Unbound antibodies were discarded after further incubation at 37°C for 1 h. Bound IgG against ACE2 was detected using HRP-conjugated goat anti-human IgG antibody (1:5,000, C04047, Croyez).

Western Blotting

SARS-CoV-2 NTU13-infected cell lysates provided by NTUH (28) were harvested using RIPA buffer III (Bio Basic Inc., Markham, Ontario, Canada). The cell lysates or recombinant proteins were prepared under reducing or nonreducing conditions prior to loading onto 10% or 12% SDS–PAGE gels for separation as indicated. For non-reducing condition, sample buffers containing 2% SDS and 15% glycerol were added to the samples prior to loading into SDS-PAGE; for reducing condition, sample buffers containing 2% SDS, 15% glycerol and 1% 2-ME were added to the samples, following by heat-denaturing at 95°C for 5 min prior to loading into SDS-PAGE. The separated proteins were transferred onto a PVDF membrane (Pall, Ann

Arbor, MI, USA). The membrane was blocked with 5% skim milk in TBST (0.05% Tween 20 in Tris-buffered saline, TBS), incubated with primary antibodies, namely, anti-His antibody (10411, Leadgene Biomedical Inc.), anti-SARS-CoV-2 S1 mAb (GTX635656, GeneTex Inc, Irvine, CA, USA), anti-ACE2 polyclonal antibody (anti-ACE2 pAb; ARG41099, Arigo, Taiwan) or mAbs 127 and 150 overnight at 4°C and detected with HRP-conjugated goat anti-rabbit or goat anti-mouse IgG secondary antibodies (1:10,000 dilution; Leadgene Biomedical) for another 1 h. Detection was then performed using an Enhanced Chemiluminescence Western blotting Kit (Advansta, Menlo Park, CA, USA).

Immunofluorescent Assay

Antibodies or sera were diluted in 1% BSA containing anti-microbial agent, 0.01% sodium azide. Anti-ACE2 pAb was used as a positive control. A stable clone of ACE2-overexpressing HEK293 (HEK293-ACE2) was generated by transfection with a pcDNA3.1 plasmid which was inserted tag free native sequence of full-length human ACE2 gene (NP_068576.1) within Nhe I and Xho I restriction enzyme sites. HEK293 and HEK293-ACE2 cells were fixed in 0.5% paraformaldehyde and stained with diluted antibodies or sera for 3 h. Subsequently, the cells were washed three times with PBS and then combined with fluorescence-labeled secondary antibodies against mouse, rabbit (C04025 and C04030, Croyez), or human IgG (A-11013, Thermo Fisher Scientific). An EVOS FL Auto 2 Imaging System (Thermo Fisher Scientific) was used for detection.

Biacore Surface Plasmon Resonance

All SPR measurements in this study were performed using a Biacore T200 (Cytiva/GE Healthcare Life Sciences). The recombinant proteins S1-RBD-His and ACE2-hFc were first covalently immobilized on Sensor CM5 chips (Cytiva/GE Healthcare Life Sciences) *via* amine coupling according to the manufacturer's protocol. S1-RBD-His was diluted in 10 mM sodium acetate, pH 5.0, to a final concentration of 10 μg/mL and injected into the activated flow cell to obtain an immobilization level at 884.6 and 1047.1 RU. For ACE2-hFc immobilization, a diluted concentration of 30 μg/mL in 10 mM sodium acetate, pH 4.5, was used to reach an immobilization level at 1482.1 RU. For analysis of the binding of mAb to S1-RBD-His, serial dilutions of mAb were injected into the immobilized chip, which contained 884.6 RU of S1-RBD-His, and the concentrations in these dilutions ranged from 256 nM to 8 nM. In the analysis of mAb binding to ACE2-hFc, serial dilutions of mAb with concentrations ranging from 1024 nM to 8 nM were used. All analyte injections were performed at a flow rate of 30 μL/min for 120 s and a dissociation time of 360 s (600 s was used in the assay of ACE2-hFc binding to S1-RBD-His). For regeneration, 10 mM glycine-HCl, pH 2.5 (Cytiva/GE Healthcare Life Sciences), was injected at a flow rate of 30 μL/min for 30 s. The assays were performed using the Kinetic/Affinity wizard, and all the procedures were conducted at 25°C. The binding kinetics were determined using Biacore T200 Evaluation Software version 3 (Cytiva/GE Healthcare Life Sciences).

Hydrogen Deuterium Exchange Mass Spectrometry Analysis and Peptide Identification

The footprints of mAbs 127 and 150 on S1-RBD and mAb 127 on ACE2 in the presence or absence of mAb were measured by HDX-MS analysis. The protein-antibody complex (15 pmol of antigen and 10 pmol of antibody were pre-incubated at room temperature for 1 hour) were diluted in the exchange buffer (99.9% D_2O in PBS, pH 7.4) at 1:9 ratio to initiate HD exchange at room temperature. At two time points (5 and 10 min), an aliquot (1.5 pmol of target protein) was aspired and mixed with quenching buffer (to a final concentration of 1.5 M guanidine hydrochloride, 150 mM tris (2-carboxyethyl) phosphine, and 0.8% formic acid). The mixture was immediately loaded onto homemade pepsin column for online digestion. The MS/MS spectra of pepsin-digested fragments were searched against the antigen protein database using the SEQUEST search engine. The HD exchange number of two independent HDX-MS experiments (duplicates) was then averaged and presented as differential levels of HD exchange [(exchanged D in antigen – exchanged D in antigen/antibody)/(exchanged D in antigen/antibody)]. Peptide identification was conducted using Proteome Discoverer software (version 2.2, Thermo Fisher Scientific).

Negative-Stain Transmission Electron Microscopy Analysis for mAb 127 and ACE2-hFc Image Analysis by 2D Class Averaging

Negative-stain transmission electron microscopy analysis for mAb 127 and ACE2-hFc image analysis by 2D class averaging was performed with a mixture of mAb 127 and ACE2-hFc (the total concentration of sample mixture was 10 ng/mL at 4:1 molar ratio) in PBS. The samples were stained with 1% uranyl acetate and then added to charged carbon-coated grids. The images were taken with a JEM1400 electron transmission microscope (Jeol Ltd., Tokyo, Japan) at 12,000× magnification using a 4k × 4k Gatan 895 CCD camera.

Structural Prediction and Docking of the Antigen-Binding Fragment of mAb 127 and Antigens

We used AlphaFold2 to create a predicted structure of mAb 127 Fab, and the interaction between mAb 127 Fab and S1-RBD (PDB ID: 7VN) or mAb 127 Fab and ACE2 (PDB ID: 1R42) were modeled by Maestro v10.1 (Schrödinger) docking analysis. AlphaFold2 is a neural network deep learning modeling which was used to predict the structure of proteins (29). It leverages neural networks and multiple alignments to predict structure. The sequence of mAb 127 was inputted with pair_msa option to generate a predicted structure which was further used to perform docking analysis by Maestro software. In brief, Protein Preparation Wizard was used to add hydrogens and created zero-order bonds to metals and disulfide bonds of antigens and mAb 127 Fab. Optimization H-bind assignment was used PROPKA (pH 7.0) and restrained minimization was applied

OPLS3e of force field. For protein-protein docking, we chose "antibody" mode to perform the analysis and visualized the result using PyMol version 2.4.1.

Statistical Analysis

All statistical data were analyzed using unpaired Student's t test to compare two independent groups or using one-way ANOVA to compare more than two groups. The analyses were performed using Prism software (GraphPad Software Inc., CA, USA). All data are presented as the means ± standard deviations (S.Ds.) from at least two independent experiments. *P < 0.05, **P < 0.01, ***P < 0.001, and ns indicates no significance based on 95% two-tailed confidence intervals.

RESULTS

Antibodies Against SARS-CoV-2 S1-RBD in Sera From Patients with COVID-19 Cross-React With ACE2

To confirm the presence of antibodies against ACE2 in sera from patients with COVID-19, a panel of 30 commercial serum samples collected from patients with COVID-19 and 60 serum samples from normal individuals were screened for the presence of antibodies against S1-RBD and ACE2 by ELISA. We found that the mean optical density (OD) of antibodies against ACE2 in sera from patients with COVID-19 was indeed significantly higher than that in healthy cohorts (**Figure 1A**). Moreover, a positive correlation was found between the titer of antibodies against the S1-RBD protein and that of antibodies against ACE2 in sera from patients with COVID-19 (Pearson r = 0.8132, p value < 0.0001) (**Figure 1B**). Among the 30 serum samples from patients with COVID-19, PC26 exhibited the highest antibody titer against both ACE2 and S1-RBD. To prevent the analysis from being skewed by this patient, we also analyzed the correlation after omitting the data from PC26. Even though the omission of these data decreased the Pearson r to 0.7049, the p value remained < 0.0001. To further characterize the properties of these ACE2-reactive antibodies in sera from patients with COVID-19, PC26 was used to stain HEK293-ACE2 cells. As shown in **Figure 1C**, antibodies from PC26 were able to bind to HEK293-ACE2 but not wild-type (WT) HEK293 cells, as demonstrated by immunofluorescent assay. A similar staining pattern was found using an anti-ACE2 pAb (**Figure 1C**). To confirm that antibodies against SARS-CoV-2 S1-RBD can indeed cross-react with ACE2, sera from patients with COVID-19 were preadsorbed to S1-RBD or BSA-coated ELISA plates and then tested for anti-ACE2 antibodies by ELISA. Approximately 20% of the sera from patients with COVID-19 (6 out of 30) showed significantly decreased levels of antibody binding to ACE2 after S1-RBD preadsorption **(Figure 1D)**. Notably, the sera

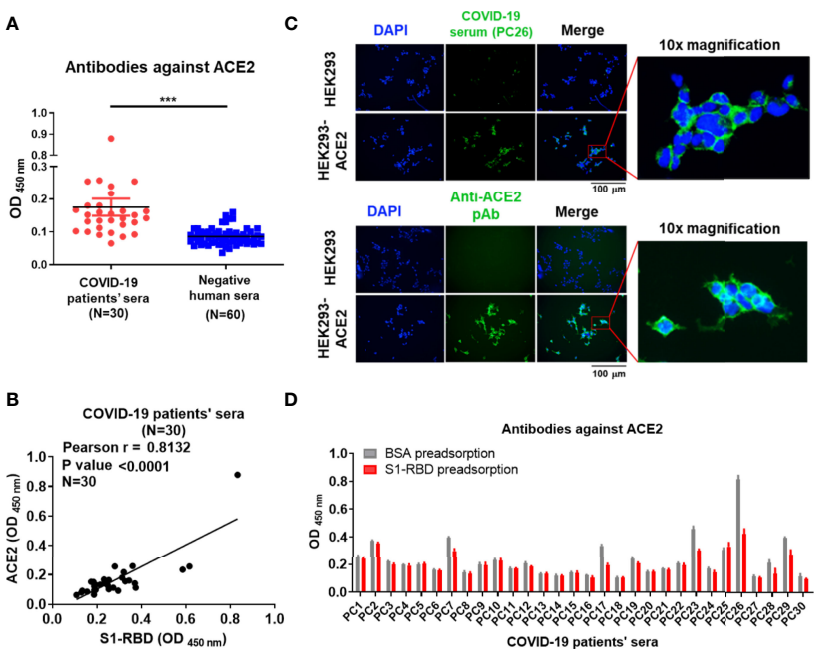

FIGURE 1 | Antibodies against S1-RBD in sera from patients with COVID-19 cross-react with ACE2. **(A)** The binding of sera (1:400 dilution) collected from 30 SARS-CoV-2-infected patients or 60 healthy humans to ACE2 was analyzed by ELISA using ACE2-His-coated plates. **(B)** Correlation of the OD of anti-S1-RBD (x-axis) and anti-ACE2 (y-axis) antibodies in the sera of patients with COVID-19 (N = 30). The binding ability was analyzed by indirect ELISA. **(C)** HEK293 and HEK293-ACE2 cells were fixed and stained with either COVID-19-positive PC26 serum (1:400 dilution) or an anti-ACE2 pAb (5 µg/mL) and then visualized using an immunofluorescent assay. Scale bar = 100 µm. The right images were derived from the original photographs at 10× magnification. The PC26 serum and anti-ACE2 pAb reacted with ACE2 expressing on the surface of HEK293 was visualized by fluorescent secondary antibody in green. All statistical data are presented as the means ± S.Ds. from at least two independent experiments. ***P < 0.001 **(D)** The sera (1:100 dilution) collected from 30 SARS-CoV-2-infected patients were preadsorbed by either BSA or S1-RBD prior to binding to ACE2-coated plates. The binding ability of preadsorbed sera to ACE2 was analyzed by indirect ELISA.

of these patients with COVID-19 usually had higher amounts of antibodies against ACE2 before adsorption than the sera of other patients with COVID-19.

SARS-CoV-2 S1-RBD Immunization Induces Antibody Binding to ACE2

To further confirm that SARS-CoV-2 S1-RBD can indeed induce ACE2 cross-reactive antibodies, mice or rabbits were immunized with recombinant SARS-CoV-2 S1-RBD produced by *E. coli*, mammalian cells (CHO cells) and insect cells (S2) emulsified with IFA or alum. Mice immunized with SARS-CoV-2 S1-RBD from *E. coli* or CHO cells produced significantly higher amounts of antibodies against ACE2 than those found in sera from control or SARS-CoV-2 nucleoprotein (NP)-immunized mice (**Figures 2A–C**). Nevertheless, the titers of antibodies against ACE2 (from >800 to >2550) were less than 1% of the titers of antibody against S1-RBD (from >64,000 to >256,000) in these S1-RBD immune sera (**Figure 2D**).

mAbs 127 and 150 Specifically Recognize SARS-CoV-2 S1-RBD but not Other Coronavirus S1 Proteins

To confirm that antibodies against S1-RBD can indeed cross-react with ACE2, about 200 hybridoma clones isolated from SARS-CoV-2 S1-RBD-immunized mice were generated. Among 21 candidates which could bind to SARS-CoV-2 S1-RBD, two mAbs, 127 (IgG2b) and 150 (IgG1) could bind to ACE2 as well. Both of these two mAbs did not show neutralizing activity against SARS-CoV-2 infection of Vero E6 cells *in vitro*. The binding affinity (KD) of mAbs 127 and 150 to S1-RBD was determined by Biacore™ SPR with S1-RBD-His-immobilized Sensor CM5 chips. The results showed that the binding affinities (KD) of mAbs 127 and 150 to S1-RBD were 2.44E-09 M and 3.87E-09 M, respectively (**Figure 3A**). Interestingly, although the amino acid identity among SARS-CoV-2 S1 protein and other coronavirus S1 protein are as high as 35~76%, both mAbs bound only to the SARS-CoV-2 S1 protein but not to the S1 proteins of SARS-CoV or other human CoVs (**Figure 3B**). In addition, the specific recognition of the authentic S1 subunit of the S protein of SARS-CoV-2 by mAbs 127 and 150 was confirmed by Western blotting analysis using cell lysates of SARS-CoV-2 (NTU-13)-infected Vero-E6 cells (**Figure 3C**). As shown in **Figure 3C**, a major band with a molecular weight (MW) of approximately 120 kDa, as predicted for the SARS-CoV-2 S1 subunit of the S protein, was recognized by the commercially available anti-SARS-CoV-2 S1 mAb and by mAbs 127 and 150. However, a higher number of nonspecific bands in cell lysates with or without virus infection were recognized by mAb 150 than by mAb 127.

Characterization of the Binding Properties of mAbs 127 and 150 to ACE2

To characterize the binding ability of mAbs 127 and 150 to ACE2, an ELISA plate or SPR Sensor CM5 chips were coated with recombinant ACE2-hFc. The mAbs 127 and 150 could recognize recombinant ACE2-hFc in a dose-dependent manner

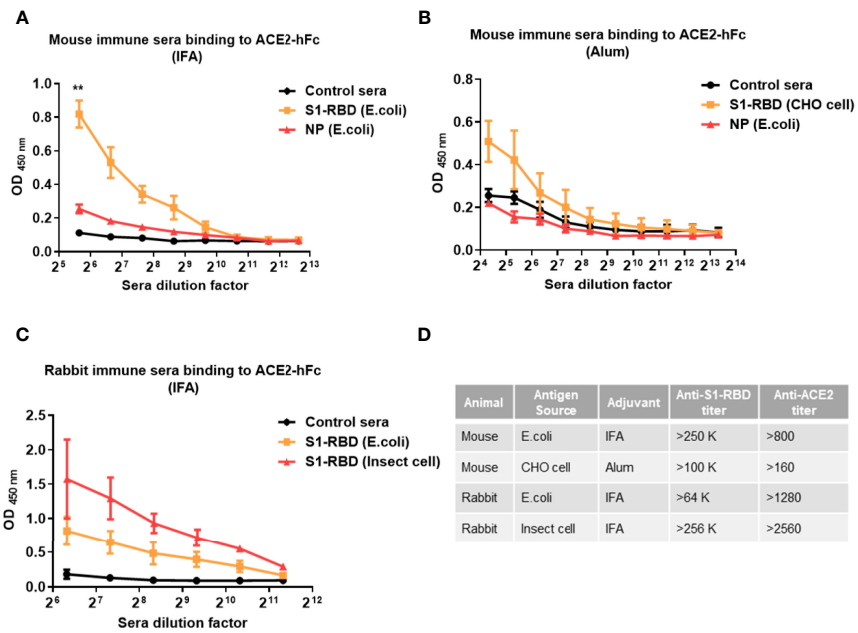

Animal	Antigen Source	Adjuvant	Anti-S1-RBD titer	Anti-ACE2 titer
Mouse	E.coli	IFA	>250 K	>800
Mouse	CHO cell	Alum	>100 K	>160
Rabbit	E.coli	IFA	>64 K	>1280
Rabbit	Insect cell	IFA	>256 K	>2560

FIGURE 2 | Immunization with SARS-CoV-2 S1-RBD elicits antibodies that cross-react with human ACE2. Mice or rabbits were immunized with recombinant S1-RBD generated from different sources, such as E. coli, mammalian cells (CHO cells) and insect cells (S2), using IFA or alum as indicated. Four mice or rabbits were included in each group for N value **(A–C)** Different dilutions of serum antibodies binding to ACE2 from S1-RBD- or NP-immunized mice or rabbits were measured by ELISA as indicated. In addition, normal mouse or rabbit sera were used as control sera. **(D)** Comparison of antibody titers against S1-RBD or ACE2-hFc in different immune sera samples measured by ELISA. The titer indicates that the highest dilution of end-point titers of sera that still showed a positive reaction. All statistical data are presented as the means ± S.Ds. from at least two independent experiments. $^{**}P < 0.01$.

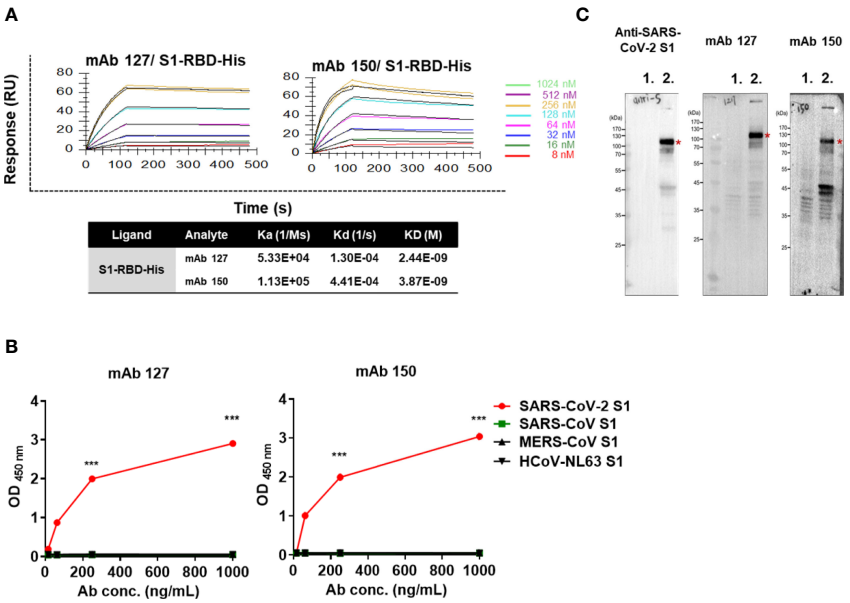

FIGURE 3 | The mAbs 127 and 150 specifically bind to SARS-CoV-2 S1-RBD. **(A)** Affinity of mAbs 127 and 150 for S1-RBD. The S1-RBD-His-bound sensors were incubated with the different concentrations of mAbs 127 or 150 (indicated by different colors) for a set time interval to allow association. The sensors were then moved to protein-free solution and allowed to dissociate over a time interval. The binding kinetics were determined using Biacore T200 Evaluation Software version 3 with 1:1 binding model fitting. **(B)** The binding ability of mAbs 127 and 150 to SARS-CoV-2 S1, SARS-CoV S1, MERS-CoV S1 or HCoV-NL63 (1 μg/mL) was analyzed by indirect ELISA. **(C)** Cell lysates of mock-infected or SARS-CoV-2 NTU13-infected Vero-E6 cells (MOI=0.1, 24 h post-infection) were separated by SDS–PAGE under reducing condition and stained with 1 μg/mL commercial anti-SARS-CoV-2 S1 mAb or mAb 127 or 150 as indicated and visualized by Western blotting. Lane 1: lysates of mock-infected Vero-E6 cells; lane 2: lysates of NTU13-infected Vero-E6 cells. The asterisks indicate the SARS-CoV-2 S1 subunit of the S protein, which has a predicted MW of approximately 120 kDa. All statistical data are presented as the means ± S.Ds. from at least two independent experiments. ***$P < 0.001$.

(**Figure 4A**). In addition, the KDs of mAbs 127 and 150 to ACE2-hFc was 1.61E-08 M and 2.77E-06 M, respectively (**Figure 4B**). Furthermore, similar to the commercially available anti-ACE2 pAbs, mAb 127 and 150 and SARS-CoV-2 S1-RBD-immunized sera could recognize HEK293-ACE2 and showed a similar pattern to that obtained with the immunofluorescence assay (**Figure 4C**). However, the Western blotting analysis revealed that these mAbs could only recognize recombinant ACE2-hFc under nonreducing conditions migrated at ~210 kDa but not reducing conditions migrated at ~140 kDa (**Figure 4D**).

Epitope Mapping of mAbs 127 and 150 on SARS-CoV-2 S1-RBD

To map the epitope region of mAbs 127 and 150 on SARS-CoV-2 S1-RBD, nineteen overlapping S1-RBD polypeptides were synthesized (**Supplementary Figure 1**). The binding ability of mAbs 127 and 150 to each of these peptides was analyzed by ELISA. Our results showed that both mAbs 127 and 150 strongly binds to peptide 13 (PFERDISTEIYQAGS, a.a. 463-477) (**Figure 5A**). This result was further supported by an analysis of the antibody footprints obtained by HDX-MS analysis. After deuterium/hydrogen exchange, the S1-RBD protein was digested into several peptides by appropriate proteolytic digestion. Among these peptides, the peptide YRLFRKSNLKPFERD (a.a. 453-467) showed the highest H-D exchange in the presence of either mAb (**Supplementary Figure 2**), and this peptide shares an overlapping sequence with peptide 13. Based on these results, we speculated that part of the epitope recognized by mAbs 127 and 150 is located near a.a. 463-466 (PFERD). The epitopes of these mAbs were further delineated by peptide competitive ELISA. The results showed that the presence of peptide 13 but not the control peptide decreased the binding of these two mAbs to S1-RBD in a dose-dependent manner (**Figure 5B**). Similar competitive inhibition of the binding of mAb 127 and 150 to ACE2 was also observed in the presence of peptide 13 but not the control peptide (**Figure 5C**). To explore the proximity of the boundaries of the epitope on S1-RBD recognized by these mAbs, we individually changed three SARS-CoV-2 S1-RBD-specific amino acids downstream of the PFERD sequence, T470, E471, and I472, to alanine for further investigation. In addition, two deletion mutants were constructed: one was based on the HDX-MS (a.a. 453-467) results, and the other was based on the mapping results for peptide 13 (a.a. 463-477). The binding ability of these two mAbs to WT S1-RBD protein was compared with that of five different His-tagged mutant S1-RBD recombinant proteins, namely, the HDX-MS-determined epitope sequence deletion (δ453-467), the peptide 13 deletion (δ463-477), a 470 site-directed mutant (T470A), a 471 site-directed mutant (E471A), and a 472 site-directed mutant (I472A), by Western blotting analysis. The results showed that the mAbs 127 and 150 were unable to bind to either deletion

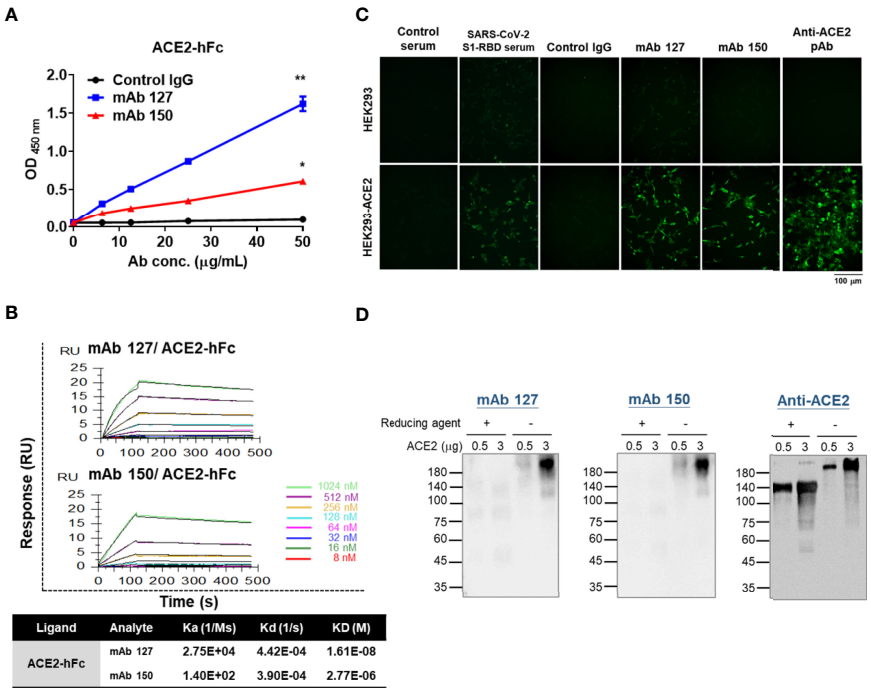

Ligand	Analyte	Ka (1/Ms)	Kd (1/s)	KD (M)
ACE2-hFc	mAb 127	2.75E+04	4.42E-04	1.61E-08
	mAb 150	1.40E+02	3.90E-04	2.77E-06

FIGURE 4 | Characterization of the binding properties of mAbs 127 and 150 to ACE2. **(A)** The dose response of mAbs 127 and 150 and control IgG binding to ACE2-hFc was analyzed by indirect ELISA. **(B)** Binding affinity of mAbs 127 and 150 to ACE2. ACE2-hFc-bound sensors were incubated with the indicated concentrations of mAb 127 or 150 for a set time interval to allow association. The sensors were moved to protein-free solution and allowed to dissociate over a time interval. The binding kinetics were determined using Biacore T200 Evaluation Software version 3 with 1:1 binding model fitting. **(C)** HEK293 and HEK293-ACE2 cells were fixed and stained with control sera, SARS-CoV-2 S1-RBD-immunized sera (1:400), control IgG, mAb 127 or 150 or anti-ACE2 pAb (5 μg/mL) and then visualized with an immunofluorescent assay. **(D)** Western blotting analysis of mAb 127 or 150 or anti-ACE2 pAb binding to 0.5 or 3 μg of ACE2 in the presence or absence of a reducing agent as indicated. All statistical data are presented as the means ± S.Ds. from at least two independent experiments. *P < 0.05, **P < 0.01.

mutant (**Figure 5D**). Additionally, compared with their binding abilities to WT S1-RBD, the binding ability of mAb 127 to the E471A mutant protein was reduced, and the binding of mAb 150 to the E471A mutant protein was abolished. In contrast, the binding ability of mAb 127 to the T470A and I472A mutant proteins was slightly decreased, even though the binding ability of mAb 150 to these two mutant proteins was slightly lower (**Figure 5D**). The binding abilities of mAbs 127 and 150 to these different SARS-CoV-2 S1-RBD mutant proteins were also confirmed by ELISA (**Supplementary Figure 3**). Because the a.a. 463-467 are conserved between SARS-CoV-2 and SARS-CoV, these results suggest that in addition to a.a. 463-467, a.a. 471 is also critical for the recognition of S1-RBD by both mAbs 127 and 150 (**Figure 5E**).

Footprints of mAb 127 on S1-RBD and ACE2

To investigate how these S1-RBD-specific mAbs cross react with ACE2, one of these two mAbs, mAb 127 was chosen to identify the protein–protein interaction between mAb and ACE2 by HDX-MS due to its higher binding affinity to ACE2 (**Supplementary Figure 4**). Among all ACE2 peptides, the peptide KGEIPKDQWMKKWWEM (a.a. 465-480), which is also located on the surface of ACE2, showed the highest H-D exchange in the presence of mAb 127. To confirm the footprints of mAb 127 on S1-RBD and ACE2, the amino acid sequence of the mAb 127 variable region was analyzed for further interaction prediction (**Supplementary Figure 5**). We used AlphaFold2 to build the 3D structure models of the Fab of mAb 127 to S1-RBD and ACE2. The binding regions between the mAb 127 Fab to S1-RBD or ACE2 were further analyzed and predicted by antibody-antigen docking (**Figures 6A, B**). As shown in **Figure 6A**, the interaction was predicted to occur between VH-CDR1, VH-CDR2, VL-CDR1, VL-CDR3, and a.a. 346, 355, 399, 450, 464, 467, 470, 471 of S1-RBD, which matched partial mapping result from S1-RBD HDX-MS (a.a. 453-467) and S1-RBD peptide 13 (a.a. 463-477). For docking on ACE2, a major chain interaction was predicted to occur on VL-CDR1, VH-CDR3, and a.a. 467-471 of ACE2. Side chain interactions were predicted on VH-CDR2, VH-CDR3, and a.a. 493 and 475 of ACE2 (**Figure 6B**). The docking interaction region was located within the same peptide region found by ACE2 HDX-MS (peptide KGEIPKDQWMKKWWEM). To visualize the interaction between ACE2 and mAb 127, freshly prepared mAb 127 and ACE2-hFc were coincubated prior to negative staining on grids. The negative-stained TEM analysis showed that mAb 127 bound

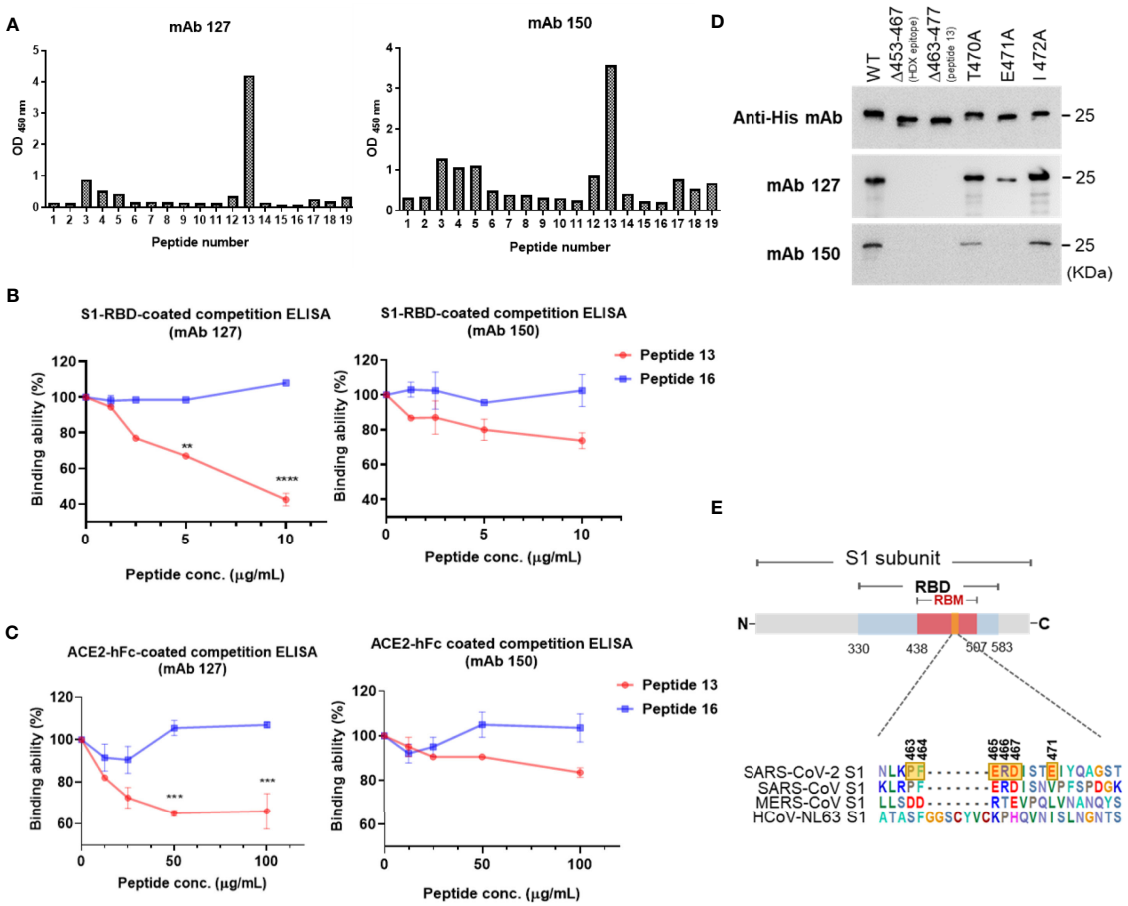

FIGURE 5 | Epitope mapping of the ACE2-cross reactive sequence on SARS-CoV-2 S1-RBD. **(A)** The binding ability of mAbs 127 and 150 (0.5 μg/mL) to 19 different SARS-CoV-2 S1-RBD polypeptides (2 μg/mL) was analyzed by indirect ELISA. Competition ELISA showing the blockage of the binding of mAbs 127 and 150 to **(B)** SARS-CoV-2 S1-RBD or **(C)** ACE2-hFc by different doses of peptide 13 and control peptide 16. The binding ability (%) represents the percentage of preincubated peptides to antibodies compared with that obtained without peptide preincubation. **(D)** One hundred nanograms of wild-type (WT) and five different mutant His-tagged S1-RBD recombinant proteins, namely, HDX-MS sequence deletion (Δ453-467), peptide 13 deletion (Δ463-477), 470 mutant (T470A), 471 mutant (E471A), and 472 mutant (I472A), were separated by SDS–PAGE and then stained with 1 μg/mL anti-His mAb, mAbs 127 and 150. The binding ability was visualized by Western blotting. **(E)** The schematic sequence of the mAb epitope compared with the S1-RBD of four strains of CoV, namely, SARS-CoV-2 (YP_009724390.1), SARS-CoV (WH20 strain AAX16192.1), MERS-CoV (AFS88936.1), and HCoV-NL63 (APF29071.1), was aligned using BioEdit software. The epitope of mAb 127 is presented with six transparent yellow blocks (463, 464, 465, 466, 467, and 471) in the SARS-CoV-2 S1 sequence. All statistical data are presented as the means ± S.Ds. from at least two independent experiments. $^{**}P < 0.01$, $^{***}P < 0.001$, $^{****}P < 0.0001$.

to ACE2-hFc with one arm (**Figure 6C**). Collectively, these data suggest that S1-RBD-specific mAb 127 can bind to not only S1-RBD but also ACE2.

DISCUSSION

In this study, we confirmed that ACE2 cross-reactive antibodies were increased in the sera of some patients with COVID-19 and found a positive association between the amount of antibody binding to ACE2 and S1-RBD in sera from patients with COVID-19. Additionally, the antibody binding to ACE2 was significantly diminished in six out of 30 serum samples from patients with COVID-19 after preadsorption with S1-RBD. Interestingly, five of these six serum samples were collected from African American. However, the possible correlation between race and the production of ACE2 cross-reactive anti-S1-RBD antibodies should be further investigated. Nevertheless, these results suggest the presence of at least two different types of anti-ACE2 antibodies in patients with COVID-19. One type of these antibodies can cross-react with S1-RBD, which is probably induced by antigenic cross-reactivity between S1-RBD and ACE2 during SARS-CoV-2 infection. The other type of anti-ACE2 antibodies that cannot be adsorbed by S1-RBD preadsorption may be induced by other mechanisms which were discussed below. To further confirm that S1-RBD can indeed induce antibody cross-reactivity with ACE2, we immunized mice or rabbits with S1-RBD recombinant proteins generated from multiple sources, such as *E. coli*, mammalian cells and insect cells, and found that antibodies that cross-reacted with ACE2

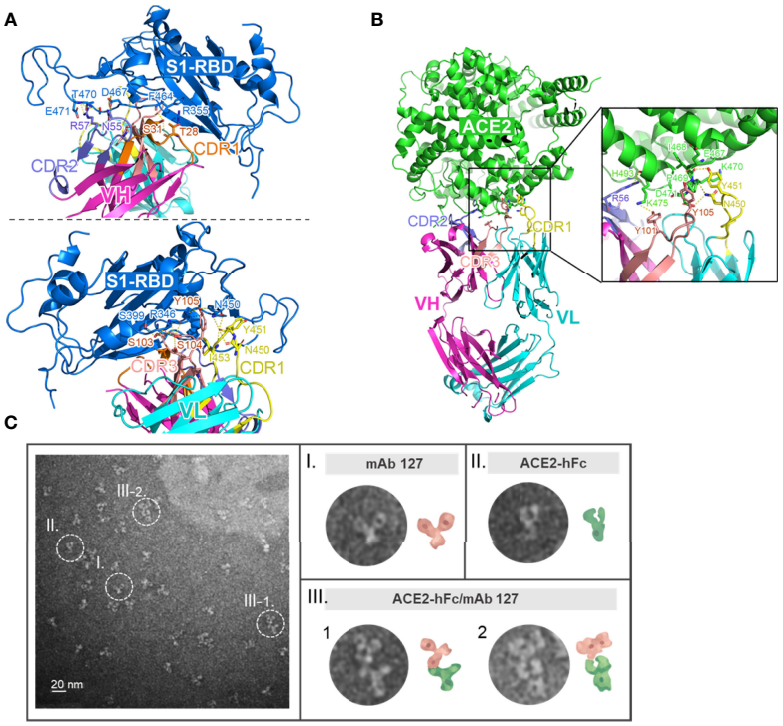

FIGURE 6 | Footprints of mAb 127 binding to S1-RBD and ACE2. **(A)** A modeled structure of mAb 127 Fab/S1-RBD complex. mAb 127 Fab is generated by AlphaFold2 and the interaction is predicted by antigen-antibody docking. The interaction of the variable region of heavy chain (VH) (upper panel) and the light chain (VL) (lower panel) of mAb 127 with S1-RBD are visualized by Pymol. VH, magenta; VL, cyan; S1-RBD, blue. **(B)** A modeled structure of mAb 127 Fab/ACE complex. VH, magenta; VL, cyan; ACE2, green. **(C)** Negative-stain electron microscopy of samples containing mAb 127 (I) and ACE2-hFc (II). Representative two-dimensional class averages of ACE2-hFc bound by mAb 127 (III-1.2).

could be detected in all these cases. In addition, two mAbs, 127 and 150, which could recognize both S1-RBD and ACE2, were isolated from SARS-CoV-2 S1-RBD-immunized mice. Even though the binding affinities of these two mAbs to ACE2 vs. S1-RBD were relatively low (10-1000 fold difference based on Biacore analysis), these results suggest a potential less-than-optimal structural mimicry between SARS-CoV-2 S1-RBD and ACE2.

Several different mechanisms have been proposed to explain the development of autoantibodies during SARS-CoV-2 infection. Dysregulation of the immune response during SARS-CoV-2 infection may lead to the breakdown of self-tolerance (30). Indeed, the activation of extrafollicular B cells, which share the B cell repertoire features previously described in autoimmune settings, has been found in critically ill patients with COVID-19 (31). Polyclonal B cell activation has also been detected in primary SARS-CoV-2 infection (32). In contrast, based on the theory of the idiotype and anti-idiotype network (33), a robust neutralizing anti-S1-RBD antibody response may induce an anti-idiotype antibody that can cross-react with the S1-RBD receptor ACE2 during SARS-CoV-2 infection (23). Alternatively, epitope spreading has also been proposed to explain the development of antibodies against ACE2 during SARS-CoV-2 infection due to the endocytosis of the complex of S protein and soluble ACE2 by macrophages (34, 35). In this study, we proposed molecular mimicry as another possible mechanism to explain the development of autoantibodies against ACE2 during SARS-CoV-2 infection. Molecular mimicry, which refers to sequence homology or structural similarity between molecules of the host and pathogens, is a common strategy used by viruses to counteract the immune response and evade immune recognition (36). Molecular mimicry has been proposed to explain the multiorgan damage observed in patients with COVID-19 (37–39). However, many of these reports are based on sequence homology between SARS-CoV-2 and host proteins and contain little clinical or experimental evidence supporting their findings. Here, we found that antibodies against S1-RBD in the sera of SARS-CoV-2-infected patients could also recognize ACE2. In addition, mAbs (127 and 150) which could recognize both S1-RBD and ACE2 were isolated from S1-RBD immunized mice. Although the binding affinities of these two mAbs to ACE2 vs. S1-RBD were low, these results suggest that the potential antigenic similarity between S1-RBD and ACE2 may induce ACE2 cross-reactive anti-S1-RBD antibodies during SARS-CoV-2 infection, which may represent one of the strategies used by SARS-CoV-2 to evade immune recognition.

In this study, a.a. 463-466 (PFERF) of S1-RBD recognized by mAbs 127 and 150 was identified using synthetic overlapping peptides and HDX-MS-based epitope mapping. The sequence of this epitope of S1-RBD on SARS-CoV-2 is distinct from other three CoVs, which shares less than 20% sequence identity. In

addition, the SARS-CoV-2-specific a.a. 471 was identified by alanine substitution and sequence comparison of the S1-RBD between SARS-CoV-2 and SARS-CoV. It indicated that the a.a. 463-467 and 471 of the S1-RBD are critical and may imply the possible correlation between autoimmunity and unique pathology of SARS-CoV-2. The recognition of the authentic S protein of SARS-CoV-2 by mAbs 127 and 150 was confirmed by Western blotting analysis using cell lysates from SARS-CoV-2 (NTU-13)-infected Vero-E6 cells (**Figure 3C**). In addition to the S1 protein, some nonspecific bands were also recognized by mAb 150, which may be due to the lower affinity of mAb 150 to S1-RBD as compared with that of mAb 127 (3.87E-09 M vs. 2.44E-09 M, respectively). To our surprise, we found VL and VH genes of mAb 127 and 150 are the same as determined by 5' RACE PCR. Since the isotypes of mAb 127 (IgG2b) and mAb 150 (IgG1) are different as defined by isotyping antibodies and isotype switching may cause the change of mAb affinity (40, 41), whether the decrease of the affinity of mAb 150 to S1-RBD is due to the isotype difference or other reasons remain unclear.

Different approaches were performed to understand the interaction between these mAbs and ACE2. Given that hFc fusion results in ACE2 dimerization (42), we found that mAbs 127 and 150 could only recognize native structure of ACE2-hFc in conditions without a reducing agent but not under reducing conditions as shown by Western blotting analysis. These results suggest the recognition of mAb 127 and 150 to ACE2 as compared to S1-RBD is more conformation-dependent. Negative-stained TEM images confirmed mAb 127 could bind to ACE2-hFc molecule with one of its arms. In addition, based on the HDX-MS analysis of the ACE2 heatmap recognized by mAb 127 and the docking model of mAb 127 on ACE2, we predicted the epitope recognized by the variable region of the light chain and heavy chain of mAb 127 on ACE2 was around a.a. 467-471. Interestingly, when we superimposed the epitopes of S1-RBD and ACE2 recognized by mAb 127 as predicted by AlphaFold2 on a S1-RBD/ACE2 complex 3D model (**Supplementary Figure 6**), we found that the regions of S1-RBD and ACE2 recognized by mAb 127 were different from the regions involved in the direct contact between S1-RBD and ACE2. This may explain why these S1-RBD specific mAbs cannot neutralize SARS-CoV-2 infection. However, more experiments such as crystal structure analysis of the mAb 127 Fab in complex with S1-RBD or ACE2 is required to fully define the precise interaction of mAb 127 and S1-RBD or ACE2.

Since the emergence of SARS-CoV-2 in late 2019, many mutations have emerged in different variants of concern (VOCs) to escape neutralization by antibodies (43, 44). Intriguingly, we found that the epitope recognized by mAbs 127 and 150 on S1-RBD is unique for SARS-CoV-2 among other CoVs, which shares only 0~50% similarity but highly conserved in all SARS-CoV-2 VOCs found thus far (43). Whether this finding indicates some evolutionary advantage for SARS-CoV-2 to preserve this structure remains unclear. Nevertheless, it indicates that antibody response induced by SARS-CoV-2 S1-RBD may play a dual role in protection and immunopathogenesis. Indeed, antibodies against SARS-CoV-2 S1-RBD which may drive significant complement activation and cellular inflammation that could have negative consequences during COVID-19 have been reported (45). In addition, higher anti-S antibody titers have been associated with worse clinical outcomes during SARS-CoV-2 infection (46). However, the pathogenic roles of ACE2-cross-reactive anti-RBD antibodies in COVID-19 infection remain to be explored.

Autoantibodies to ACE2 that can inhibit ACE2 activity have been found in patients with COVID-19 as well as patients with connective tissue diseases associated with vasculopathies (23, 47). In contrast, autoantibodies against ACE2 have been found to be correlated with elevated proinflammatory responses and increased COVID-19 severity (22). Moreover, IgM antibodies against ACE2 in sera from patients with COVID-19 may bind to ACE2-expressing tissues and activate complement to cause tissue damage (24). Therefore, in addition to the quantity of antibodies, the quality (such as the specificity, affinity, and isotype) of the anti-S antibodies may determine whether the antibodies are protective or pathogenic in patients with COVID-19 (30).

In summary, this study revealed potential antigenic cross-reactivity between SARS-CoV-2 S1-RBD and its receptor, ACE2, which could induce ACE2 cross-reactive antibodies during SARS-CoV-2 infection and in S1-RBD-immunized mice. Currently, several different types of SARS-CoV-2 vaccines have been developed, and some of them have been massively immunized in humans (48). For example, AstraZeneca (AZ) vaccine which is a SARS-CoV-2 vaccine based on a replication incompetent chimpanzee adenovirus expresses a native-like SARS-CoV-2 S glycoprotein (49). It is possible different structure and conformation of recombinant S1-RBD and native-like spike glycoprotein may contribute to the recognition of different epitopes of S1-RBD by B cells during S1-RBD immunization as reported here and AZ vaccination in humans (12–14). In addition, antibody response to SARS-CoV-2 vaccination can also be influenced by genetic background and immune status of different individuals. Therefore, whether ACE2 cross-reactive S1-RBD antibodies are induced after SARS-CoV-2 vaccination remains to be investigated (48). Nonetheless, the ACE2 cross-reactive S1-RBD mAbs found in this study provide valuable reagents to address the contribution of these ACE2 cross-reactive S1-RBD antibodies in the immunopathogenesis of COVID-19 during SARS-CoV-2 infection in the future.

DATA AVAILABILITY STATEMENT

The mAbs sequences presented in the study are deposited in figshare. (https://doi.org/10.6084/m9.figshare.19550272.v1).

ETHICS STATEMENT

The studies involving human participants were reviewed and approved by IRB approved protocol (SDP-001-FDA Licensed Plasmapheresis Center; SDP-002- U.S. Physician Network; SDP-003 Reference Laboratory Network). Samples were purchased from Access Biologicals LLC. Written informed consent for

participation was not required for this study in accordance with the national legislation and the institutional requirements. The animal study was reviewed and approved by the Institutional Animal Care and Use Committee (IACUC) under the number IACUC-10908006.

AUTHOR CONTRIBUTIONS

Y-CC, Y-WC, Y-CL, C-HC and T-MY conceived and designed the experiments. Y-CL, T-MY and Y-CC wrote and edited the paper. Y-CL, Y-YC, Y-CC, C-HC, Y-WC, Y-RW, L-YC, C-KT, C-KL, C-DC and W-JT performed the experiments and analyzed the data. SW, Y-SL, C-PC, W-JC, S-YC, WH and J-RW provided comments and suggestions during the preparation of the manuscript. All authors contributed to the article and approved the submitted version.

FUNDING

This study was supported by the board of directors of Leadgene Biomedical, Inc., the Ministry of Science and Technology of Taiwan (MOST 109-2327-B-006-005, MOST 109-2327-B-006-007, MOST 109-2320-B-006-050, MOST 110-2320-B-006-033) and the National Health Research Institute (MR-110-CO-07).

ACKNOWLEDGMENTS

We thank Lili Kuo from Wadsworth Center (New York State Department of Health, Slingerlands, New York, USA) for providing wonderful suggestions regarding the writing and proofreading of the manuscript. We thank Joseph Chen from NovoPro Bioscience Inc. for the technical support provided for the structural prediction. We appreciate the technical services provided by "the i-MANI center of the National Core Facility for Biopharmaceuticals, Ministry of Science and Technology, Taiwan" as well as the technical service provided by the Instrument Development Center of the National Cheng Kung University.

SUPPLEMENTARY MATERIAL

The Supplementary Material for this article can be found online at: https://www.frontiersin.org/articles/10.3389/fimmu.2022.868724/full#supplementary-material

REFERENCES

1. Vabret N, Britton GJ, Gruber C, Hegde S, Kim J, Kuksin M, et al. Immunology of COVID-19: Current State of the Science. *Immunity* (2020) 52(6):910–41. doi: 10.1016/j.immuni.2020.05.002
2. Cui J, Li F, Shi ZL. Origin and Evolution of Pathogenic Coronaviruses. *Nat Rev Microbiol* (2019) 17(3):181–92. doi: 10.1038/s41579-018-0118-9
3. Shang J, Ye G, Shi K, Wan Y, Luo C, Aihara H, et al. Structural Basis of Receptor Recognition by SARS-CoV-2. *Nature* (2020) 581(7807):221–4. doi: 10.1038/s41586-020-2179-y
4. Huang Y, Yang C, Xu XF, Xu W, Liu SW. Structural and Functional Properties of SARS-CoV-2 Spike Protein: Potential Antivirus Drug Development for COVID-19. *Acta Pharmacol Sin* (2020) 41(9):1141–9. doi: 10.1038/s41401-020-0485-4
5. Premkumar L, Segovia-Chumbez B, Jadi R, Martinez DR, Raut R, Markmann A, et al. The Receptor Binding Domain of the Viral Spike Protein is an Immunodominant and Highly Specific Target of Antibodies in SARS-CoV-2 Patients. *Sci Immunol* (2020) 5(48):eabc8413. doi: 10.1126/sciimmunol.abc841
6. Shah P, Canziani GA, Carter EP, Chaiken I. The Case for S2: The Potential Benefits of the S2 Subunit of the SARS-CoV-2 Spike Protein as an Immunogen in Fighting the COVID-19 Pandemic. *Front Immunol* (2021) 12:637651. doi: 10.3389/fimmu.2021.637651
7. Walls AC, Park YJ, Tortorici MA, Wall A, McGuire AT, Veesler D. Structure, Function, and Antigenicity of the SARS-CoV-2 Spike Glycoprotein. *Cell* (2020) 181(2):281–92. doi: 10.1016/j.cell.2020.02.058
8. Nugent MA. The Future of the COVID-19 Pandemic: How Good (or Bad) can the SARS-CoV2 Spike Protein Get? *Cells* (2022) 11(5):855. doi: 10.3390/cells11050855
9. Singh M, Bansal V, Feschotte C. A Single-Cell RNA Expression Map of Human Coronavirus Entry Factors. *Cell Rep* (2020) 32(12):108–75. doi: 10.1016/j.celrep.2020.108175
10. Andersen KG, Rambaut A, Lipkin WI, Holmes EC, Garry RF. The Proximal Origin of SARS-CoV-2. *Nat Med* (2020) 26(4):450–2. doi: 10.1038/s41591-020-0820-9
11. Tragni V, Preziusi F, Laera L, Onofrio A, Mercurio I, Todisco S, et al. Modeling SARS-CoV-2 Spike/ACE2 Protein-Protein Interactions for Predicting the Binding Affinity of New Spike Variants for ACE2, and Novel ACE2 Structurally Related Human Protein Targets, for COVID-19 Handling in the 3PM Context. *EPMA J* (2022) 13(1):1–27. doi: 10.1007/s13167-021-00267-w
12. Ismail AM, Elfiky AA. SARS-CoV-2 Spike Behavior *in Situ*: A Cryo-EM Images for a Better Understanding of the COVID-19 Pandemic. *Signal Transduct Target Ther* (2020) 5(1):252. doi: 10.1038/s41392-020-00365-7
13. Wrapp D, Wang N, Corbett KS, Goldsmith JA, Hsieh CL, Abiona O, et al. Cryo-EM Structure of the 2019-Ncov Spike in the Prefusion Conformation. *Science* (2020) 367(6483):1260–3. doi: 10.1126/science.abb2507
14. Turonova B, Sikora M, Schurmann C, Hagen WJH, Welsch S, Blanc FEC, et al. *In Situ* Structural Analysis of SARS-CoV-2 Spike Reveals Flexibility Mediated by Three Hinges. *Science* (2020) 370(6513):203–8. doi: 10.1126/science.abd5223
15. Sztain T, Ahn SH, Bogetti AT, Casalino L, Goldsmith JA, Seitz E, et al. A Glycan Gate Controls Opening of the SARS-CoV-2 Spike Protein. *Nat Chem* (2021) 13(10):963–8. doi: 10.1038/s41557-021-00758-3
16. Puelles VG, Lutgehetmann M, Lindenmeyer MT, Sperhake JP, Wong MN, Allweiss L, et al. Multiorgan and Renal Tropism of SARS-CoV-2. *N Engl J Med* (2020) 383(6):590–2. doi: 10.1056/NEJMc2011400
17. Gupta A, Madhavan MV, Sehgal K, Nair N, Mahajan S, Sehrawat TS, et al. Extrapulmonary Manifestations of COVID-19. *Nat Med* (2020) 26(7):1017–32. doi: 10.1038/s41591-020-0968-3
18. van Eijk LE, Binkhorst M, Bourgonje AR, Offringa AK, Mulder DJ, Bos EM, et al. COVID-19: Immunopathology, Pathophysiological Mechanisms, and Treatment Options. *J Pathol* (2021) 254(4):307–31. doi: 10.1002/path.5642
19. Wong AKH, Woodhouse I, Schneider F, Kulpa DA, Silvestri G, Maier CL. Broad Auto-Reactive IgM Responses Are Common in Critically Ill Patients, Including Those With COVID-19. *Cell Rep Med* (2021) 2(6):100321. doi: 10.1016/j.xcrm.2021.100321
20. Wang EY, Mao T, Klein J, Dai Y, Huck JD, Jaycox JR, et al. Diverse Functional Autoantibodies in Patients With COVID-19. *Nature* (2021) 595(7866):283–8. doi: 10.1038/s41586-021-03631-y
21. Chang SE, Feng A, Meng W, Apostolidis SA, Mack E, Artandi M, et al. New-Onset IgG Autoantibodies in Hospitalized Patients With COVID-19. *Nat Commun* (2021) 12(1):5417. doi: 10.1038/s41467-021-25509-3

22. Rodriguez-Perez AI, Labandeira CM, Pedrosa MA, Valenzuela R, Suarez-Quintanilla JA, Cortes-Ayaso M, et al. Autoantibodies Against ACE2 and Angiotensin Type-1 Receptors Increase Severity of COVID-19. *J Autoimmun* (2021) 122:102683. doi: 10.1016/j.jaut.2021.102683
23. Arthur JM, Forrest JC, Boehme KW, Kennedy JL, Owens S, Herzog C, et al. Development of ACE2 Autoantibodies After SARS-CoV-2 Infection. *PloS One* (2021) 16(9):e0257016. doi: 10.1371/journal.pone.0257016
24. Casciola-Rosen L, Thiemann DR, Andrade F, Trejo Zambrano MI, Hooper JE, Leonard E, et al. IgM Autoantibodies Recognizing ACE2 are Associated With Severe COVID-19. *medRxiv* (2020). doi: 10.1101/2020.10.13.20211664
25. Amiral J, Busch MH, Timmermans S, Reutelingsperger CP, van Paassen P. Development of IgG, IgM, and IgA Autoantibodies Against Angiotensin Converting Enzyme 2 in Patients With COVID-19. *J Appl Lab Med* (2022) 7(1):382–6. doi: 10.1093/jalm/jfab065
26. Jackson LR, Trudel LJ, Fox JG, Lipman NS. Monoclonal Antibody Production in Murine Ascites. I. Clinical and Pathologic Features. *Lab Anim Sci* (1999) 49 (1):70–80.
27. Nelson PN, Reynolds GM, Waldron EE, Ward E, Giannopoulos K, Murray PG. Monoclonal Antibodies. *Mol Pathol* (2000) 53(3):111–7. doi: 10.1136/mp.53.3.111
28. Huang KY, Lin MS, Kuo TC, Chen CL, Lin CC, Chou YC, et al. Humanized COVID-19 Decoy Antibody Effectively Blocks Viral Entry and Prevents SARS-CoV-2 Infection. *EMBO Mol Med* (2021) 13(1):e12828. doi: 10.15252/emmm.202012828
29. Jumper J, Evans R, Pritzel A, Green T, Figurnov M, Ronneberger O, et al. Highly Accurate Protein Structure Prediction With AlphaFold. *Nature* (2021) 596(7873):583–9. doi: 10.1038/s41586-021-03819-2
30. Frasca D, Reidy L, Romero M, Diaz A, Cray C, Kahl K, et al. The Majority of SARS-CoV-2-Specific Antibodies in COVID-19 Patients With Obesity are Autoimmune and Not Neutralizing. *Int J Obes (Lond)* (2022) 46(2):427–32. doi: 10.1038/s41366-021-01016-9
31. Woodruff MC, Ramonell RP, Nguyen DC, Cashman KS, Saini AS, Haddad NS, et al. Extrafollicular B Cell Responses Correlate With Neutralizing Antibodies and Morbidity in COVID-19. *Nat Immunol* (2020) 21(12):1506–16. doi: 10.1038/s41590-020-00814-z
32. Nielsen SCA, Yang F, Jackson KJL, Hoh RA, Röltgen K, Jean GH, et al. Human B Cell Clonal Expansion and Convergent Antibody Responses to SARS-CoV-2. *Cell Host Microbe* (2020) 28(4):516–25.e5. doi: 10.1016/j.chom.2020.09.002
33. Jerne NK. Towards a Network Theory of the Immune System. *Ann Immunol (Paris)* (1974) 125c(1-2):373–89.
34. McMillan P, Dexhiemer T, Neubig RR, Uhal BD. COVID-19-A Theory of Autoimmunity Against ACE-2 Explained. *Front Immunol* (2021) 12:582166. doi: 10.3389/fimmu.2021.582166
35. Amiral J, Vissac AM, Seghatchian J. Covid-19, Induced Activation of Hemostasis, and Immune Reactions: Can An Auto-Immune Reaction Contribute to the Delayed Severe Complications Observed in Some Patients? *Transfus Apher Sci* (2020) 59(3):102804. doi: 10.1016/j.transci.2020.102804
36. Lin YS, Yeh TM, Lin CF, Wan SW, Chuang YC, Hsu TK, et al. Molecular Mimicry Between Virus and Host and its Implications for Dengue Disease Pathogenesis. *Exp Biol Med (Maywood)* (2011) 236(5):515–23. doi: 10.1258/ebm.2011.010339
37. Angileri F, Legare S, Marino Gammazza A, Conway de Macario E, Jl Macario A, Cappello F. Molecular Mimicry May Explain Multi-Organ Damage in COVID-19. *Autoimmun Rev* (2020) 19(8):102591. doi: 10.1016/j.autrev.2020.102591
38. Kanduc D. From Anti-SARS-CoV-2 Immune Responses to COVID-19 *via* Molecular Mimicry. *Antibodies (Basel)* (2020) 9(3):33. doi: 10.3390/antib9030033
39. Angileri F, Légaré S, Marino Gammazza A, Conway de Macario E, Macario AJL, Cappello F. Is Molecular Mimicry the Culprit in the Autoimmune Haemolytic Anaemia Affecting Patients With COVID-19? *Br J Haematol* (2020) 190(2):e92–3. doi: 10.1111/bjh.16883
40. Varshney AK, Wang X, Aguilar JL, Scharff MD, Fries BC. Isotype Switching Increases Efficacy of Antibody Protection Against Staphylococcal Enterotoxin B-Induced Lethal Shock and Staphylococcus Aureus Sepsis in Mice. *mBio* (2014) 5(3):e01007–14. doi: 10.1128/mBio.01007-14
41. Torres M, Fernandez-Fuentes N, Fiser A, Casadevall A. The Immunoglobulin Heavy Chain Constant Region Affects Kinetic and Thermodynamic Parameters of Antibody Variable Region Interactions With Antigen. *J Biol Chem* (2007) 282(18):13917–27. doi: 10.1074/jbc.M700661200
42. Bernardi A, Huang Y, Harris B, Xiong Y, Nandi S, McDonald KA, et al. Development and Simulation of Fully Glycosylated Molecular Models of ACE2-Fc Fusion Proteins and Their Interaction With the SARS-CoV-2 Spike Protein Binding Domain. *PloS One* (2020) 15(8):e0237295. doi: 10.1371/journal.pone.0237295
43. VanBlargan LA, Errico JM, Halfmann PJ, Zost SJ, Crowe JEJr., Purcell LA, et al. An Infectious SARS-CoV-2 B.1.1.529 Omicron Virus Escapes Neutralization by Therapeutic Monoclonal Antibodies. *Nat Med* (2022) 28 (3):490–5. doi: 10.1038/s41591-021-01678-y
44. Harvey WT, Carabelli AM, Jackson B, Gupta RK, Thomson EC, Harrison EM, et al. SARS-CoV-2 Variants, Spike Mutations and Immune Escape. *Nat Rev Microbiol* (2021) 19(7):409–24. doi: 10.1038/s41579-021-00573-0
45. Jarlhelt I, Nielsen SK, Jahn CXH, Hansen CB, Pérez-Alós L, Rosbjerg A, et al. SARS-CoV-2 Antibodies Mediate Complement and Cellular Driven Inflammation. *Front Immunol* (2021) 12:767981. doi: 10.3389/fimmu.2021.767981
46. Jiang HW, Li Y, Zhang HN, Wang W, Yang X, Qi H, et al. SARS-CoV-2 Proteome Microarray for Global Profiling of COVID-19 Specific IgG and IgM Responses. *Nat Commun* (2020) 11(1):3581. doi: 10.1038/s41467-020-17488-8
47. Takahashi Y, Haga S, Ishizaka Y, Mimori A. Autoantibodies to Angiotensin-Converting Enzyme 2 in Patients With Connective Tissue Diseases. *Arthritis Res Ther* (2010) 12(3):R85. doi: 10.1186/ar3012
48. Krammer F. SARS-CoV-2 Vaccines in Development. *Nature* (2020) 586 (7830):516–27. doi: 10.1038/s41586-020-2798-3
49. Watanabe Y, Mendonca L, Allen ER, Howe A, Lee M, Allen JD, et al. Native-Like SARS-CoV-2 Spike Glycoprotein Expressed by ChAdOx1 Ncov-19/AZD1222 Vaccine. *ACS Cent Sci* (2021) 7(4):594–602. doi: 10.1021/acscentsci.1c00080

Conflict of Interest: Y-CL was employed by Leadgene Biomedical, Inc. Y-WC, Y-YC, L-YC, Y-RW, and Y-CC are employed by Leadgene Biomedical, Inc. C-DC is employed by OmicsLab Co., Ltd. C-KT and C-KL are employed by SIDSCO Biomedical Co., Ltd.

The remaining authors declare that the research was conducted in the absence of any commercial or financial relationships that could be construed as a potential conflict of interest.

frontiers | Frontiers in Immunology

ORIGINAL RESEARCH
published: 12 May 2022
doi: 10.3389/fimmu.2022.894534

Time-Dependent Increase in Susceptibility and Severity of Secondary Bacterial Infections During SARS-CoV-2

Amanda P. Smith[1], Evan P. Williams[2], Taylor R. Plunkett[2], Muneeswaran Selvaraj[3†], Lindey C. Lane[4], Lillian Zalduondo[2], Yi Xue[2], Peter Vogel[5], Rudragouda Channappanavar[2,3,6†], Colleen B. Jonsson[2,6] and Amber M. Smith[1,2,6*]*

[1] Department of Pediatrics, University of Tennessee Health Science Center, Memphis, TN, United States, [2] Department of Microbiology, Immunology and Biochemistry, University of Tennessee Health Science Center, Memphis, TN, United States, [3] Department of Acute and Tertiary Care, University of Tennessee Health Science Center, Memphis, TN, United States, [4] College of Pharmacy, University of Tennessee Health Science Center, Memphis, TN, United States, [5] Animal Resources Center and Veterinary Pathology Core, St. Jude Children's Research Hospital, Memphis, TN, United States, [6] Institute for the Study of Host-Pathogen Systems, University of Tennessee Health Science Center, Memphis, TN, United States

Secondary bacterial infections can exacerbate SARS-CoV-2 infection, but their prevalence and impact remain poorly understood. Here, we established that a mild to moderate infection with the SARS-CoV-2 USA-WA1/2020 strain increased the risk of pneumococcal (type 2 strain D39) coinfection in a time-dependent, but sex-independent, manner in the transgenic K18-hACE2 mouse model of COVID-19. Bacterial coinfection increased lethality when the bacteria was initiated at 5 or 7 d post-virus infection (pvi) but not at 3 d pvi. Bacterial outgrowth was accompanied by neutrophilia in the groups coinfected at 7 d pvi and reductions in B cells, T cells, IL-6, IL-15, IL-18, and LIF were present in groups coinfected at 5 d pvi. However, viral burden, lung pathology, cytokines, chemokines, and immune cell activation were largely unchanged after bacterial coinfection. Examining surviving animals more than a week after infection resolution suggested that immune cell activation remained high and was exacerbated in the lungs of coinfected animals compared with SARS-CoV-2 infection alone. These data suggest that SARS-CoV-2 increases susceptibility and pathogenicity to bacterial coinfection, and further studies are needed to understand and combat disease associated with bacterial pneumonia in COVID-19 patients.

Keywords: SARS-CoV-2, COVID-19, Streptococcus pnemoniae, pneumococcus, immune response, coinfection

OPEN ACCESS

Edited by:
Penghua Wang, University of Connecticut Health Center, United States

Reviewed by:
Zhanbo Zhu, Heilongjiang Bayi Agricultural University, China
Erez Bar-Haim, Israel Institute for Biological Research (IIBR), Israel

***Correspondence:**
Amber M. Smith
amber.smith@uthsc.edu
Colleen B. Jonsson
cjonsson@uthsc.edu

***Present address:**
Muneeswaran Selvarajc, Department of Veterinary Pathobiology, Oklahoma State University, Stillwater, OK, United States,
Rudragouda Channappanavar, Department of Veterinary Pathobiology, Oklahoma State University, Stillwater, OK, United States

Specialty section:
This article was submitted to Viral Immunology, a section of the journal Frontiers in Immunology

Received: *11 March 2022*
Accepted: *11 April 2022*
Published: *12 May 2022*

Citation:
Smith AP, Williams EP, Plunkett TR, Selvaraj M, Lane LC, Zalduondo L, Xue Y, Vogel P, Channappanavar R, Jonsson CB and Smith AM (2022) Time-Dependent Increase in Susceptibility and Severity of Secondary Bacterial Infections During SARS-CoV-2. Front. Immunol. 13:894534. doi: 10.3389/fimmu.2022.894534

INTRODUCTION

Throughout the coronavirus disease 2019 (COVID-19) pandemic caused by the severe acute respiratory syndrome coronavirus 2 (SARS-CoV-2), there have been case reports, multi-center cohort studies, systematic reviews, and meta-analyses assessing the extent and severity of coinfections with secondary pathogens including viruses, fungi, and bacteria (1–31). Although coinfection rates

varied across studies, some studies suggested that coinfecting respiratory bacteria were predictors of severe SARS-CoV-2-related disease and mortality (23–31). Bacterial pathogens that were detected included *Mycoplasma pneumoniae*, *Legionella pneumophila*, *Chlamydophila pneumoniae*, *Klebsiella pneumoniae*, *Pseudomonas aeruginosa*, *Haemophilus influenzae*, *Acinetobacter baumanii, Staphylococcus aureus*, and *Streptococcus pneumoniae* (pneumococcus). Pneumococcus, which is a major cause of community-acquired pneumonia (32–34), was detected by throat swab in 0.8% (8) to 7.2% (5) of hospitalized COVID-19 patients not requiring intensive care unit (ICU) admission or invasive respiratory support, while the frequency tended to be higher [6.5% (24) to 59.5% (4)] in patients with severe respiratory distress. Because bacterial transmission has largely been dampened by non-pharmaceutical measures (e.g., masking and physical distancing), it is important to understand whether SARS-CoV-2 infection predisposes individuals to bacterial infections and, if so, what clinical and immunological changes occur as a result of coinfection.

In general, viral-bacterial coinfections are not uncommon, where *S. aureus* and pneumococcus are widely documented as complicating pathogens during infection with other viruses, most notably influenza A virus (IAV) [Reviewed in (35–46)]. During influenza pandemics, 45-95% of the mortality has been attributed to bacterial coinfections (47–50). Fortunately, the impact of these complications has appeared to be lower during the SARS-CoV-2 pandemic, but these could increase as novel variants arise and as SARS-CoV-2 becomes endemic. IAV and SARS-CoV-2 both cause infections that range from asymptomatic to severe, but SARS-CoV-2 has a longer incubation period, longer and more varied duration of viral shedding and symptoms, and more pathological effects on tissues outside of the respiratory tract [Reviewed in (51–54)]. Although viral burden does not directly correlate to disease (55–61), both viruses can induce significant lung damage [Reviewed in (52–54)]. Some host responses also differ in timing and magnitude, including the delayed type I interferon (IFN-α,β), increased proinflammatory cytokines like TNF-α and IL-6, and reduced immune regulation that have been detected in COVID-19 patients (62–66). Further, neutrophils and macrophages, which are important for efficient bacterial clearance during viral-bacterial coinfection (67–72), are dysregulated during COVID-19 (73–75). Thus, the potential for bacterial invasion during SARS-CoV-2 infection may also differ from that observed in influenza infection with respect to timing and host-pathogen mechanisms.

While the investigation of viral and immune dynamics in the lower respiratory tract is difficult to assess in humans, they have been clarified in animal models. One study using SARS-CoV-1 suggested that bacteria can enhance pathogenicity of coronaviruses (76), and numerous studies of influenza-bacterial coinfection indicate that susceptibility and pathogenicity of bacterial coinfections are time-dependent with the greatest mortality observed when bacteria is initiated at 7 d pvi (77). The progressive increase in susceptibility to bacterial coinfection during influenza is largely due to the depletion and/or dysfunction of resident alveolar macrophages (AMΦ) during IAV infection, which is dynamic throughout the infection (55, 67) and maximal at 7 d pvi (55, 67–69). Following bacterial establishment, dysfunction of neutrophils (78–81), which may be in part facilitated by bacterial metabolic interactions (82) and type I IFNs (71, 82, 83), and additional depletion of AMΦ (55) contribute to bacterial growth and coinfection pathogenesis [Reviewed in (39–41, 45, 84, 85)]. Currently, the effect of SARS-CoV-2 infection on AMΦs remains somewhat unclear, although human, murine, and *in vitro* data indicate that AMΦs become productively infected with SARS-CoV-2, leading to altered cytokine production and responsiveness (86–89). In addition, SARS-CoV-2 seems particularly adept at delaying and avoiding innate immune responses, resulting in delayed or decreased T cell responses, accumulation of neutrophils and inflammatory monocytes, and enhanced lung pathology [Reviewed in (90–93)]. IAV also has mechanisms of immune evasion [Reviewed in (94, 95)] but induces a robust $CD8^+$ T cell response in the lungs that efficiently clears virus. During IAV-pneumococcal coinfection, $CD8^+$ T cells are depleted (96), and viral loads rebound (55, 68, 82). Mechanisms for both of these are being investigated, but direct viral-bacterial interactions (97) that allow the virus to enter new areas of the lung in addition to a bacterial-mediated increase in virus production (55, 68, 98) contribute to the increased viral loads. However, these effects are overshadowed by the robust bacterial growth and bacterial-mediated effects on host responses. Given these potential mechanisms and the reported myeloid dysfunction (73–75), delayed IFN responses (62–66), and $CD8^+$ T cell depletion (99–103) during SARS-CoV-2, a better understanding of the potential for bacterial invasion and the effects of coinfection on immune cell, viral, and pathological dynamics is needed and the focus of this study. To assess bacterial susceptibility during COVID-19 and determine whether a synergism exists between SARS-CoV-2 and pneumococcus, we infected K18-hACE2 mice with a low dose of SARS-CoV-2 to initiate a mild-moderate infection and coinfected the animals 3, 5, or 7 days later with pneumococcus. Bacteria were unable to establish at 3 d post-virus infection (pvi), but coinfections at 5 or 7 d pvi resulted in increased lethality in a sex-independent manner. Although viral dynamics and lung pathology were unchanged within the first 24 h of coinfection, select immune cells and proinflammatory cytokines were decreased in the lungs of animals coinfected at 5 d pvi but not at 7 d pvi. These findings support the increased susceptibility of SARS-CoV-2-infected individuals to bacteria and highlight numerous distinct features from other viral-bacterial coinfections.

RESULTS

Time-Dependent Increases in Lethality During SARS-CoV-2-Pneumococcal Coinfection

To examine the susceptibility and pathogenicity of pneumococcus coinfection during SARS-CoV-2 infection, K18-hACE2 mice (male and female, 10 to 13 weeks old) were infected with 250 PFU of SARS-CoV-2 or PBS followed by 10^3 CFU of pneumococcal strain D39 (coinfected) or PBS (mock coinfected) at either 3, 5, or 7 d pvi. During mock coinfection, the selected

viral dose was lethal in 35% of mice (**Figure 1A**) and caused weight loss from 5 to 11 d pvi with maximum weight loss (average 7%) at 8 d pvi (**Figure 1B**) and clinical scores peaking at 6 d pvi (**Figure 1C**). In the absence of viral infection, the selected bacterial dose was lethal in 1/6 mice (17% lethality) at 4 d post bacterial infection (pbi) (**Figure S1A**) and caused only mild, transient weight loss (~3%) (**Figure S1B**) and increased temperatures (**Figure S1C**) after 1 to 2 d pbi.

When the bacterial coinfection was initiated at 3 d pvi, lethality was not enhanced (P = 0.73) (**Figure 1A**). Interestingly, weight loss in coinfected animals was reduced at 1 d (P = 0.03) and 2 d (P = 0.04) pbi (**Figure 1B**) and the cumulative clinical score was lower at 2 d pbi (P = 0.03) (**Figure 1C**) compared with mock coinfected controls. In addition, the temperature of coinfected animals was higher at 2 d (P = 0.003) and 3 d (P = 0.01) pbi and lower at 5 d (P = 0.02) and 8 d (P = 0.045) pbi (**Figure 1D**). A coinfection initiated at 5 d pvi was slightly more lethal than the SARS-CoV-2 infection alone, where additional mortality was observed at 5 to 6 d pbi, but this was not statistically significant (P = 0.14) (**Figure 1A**).

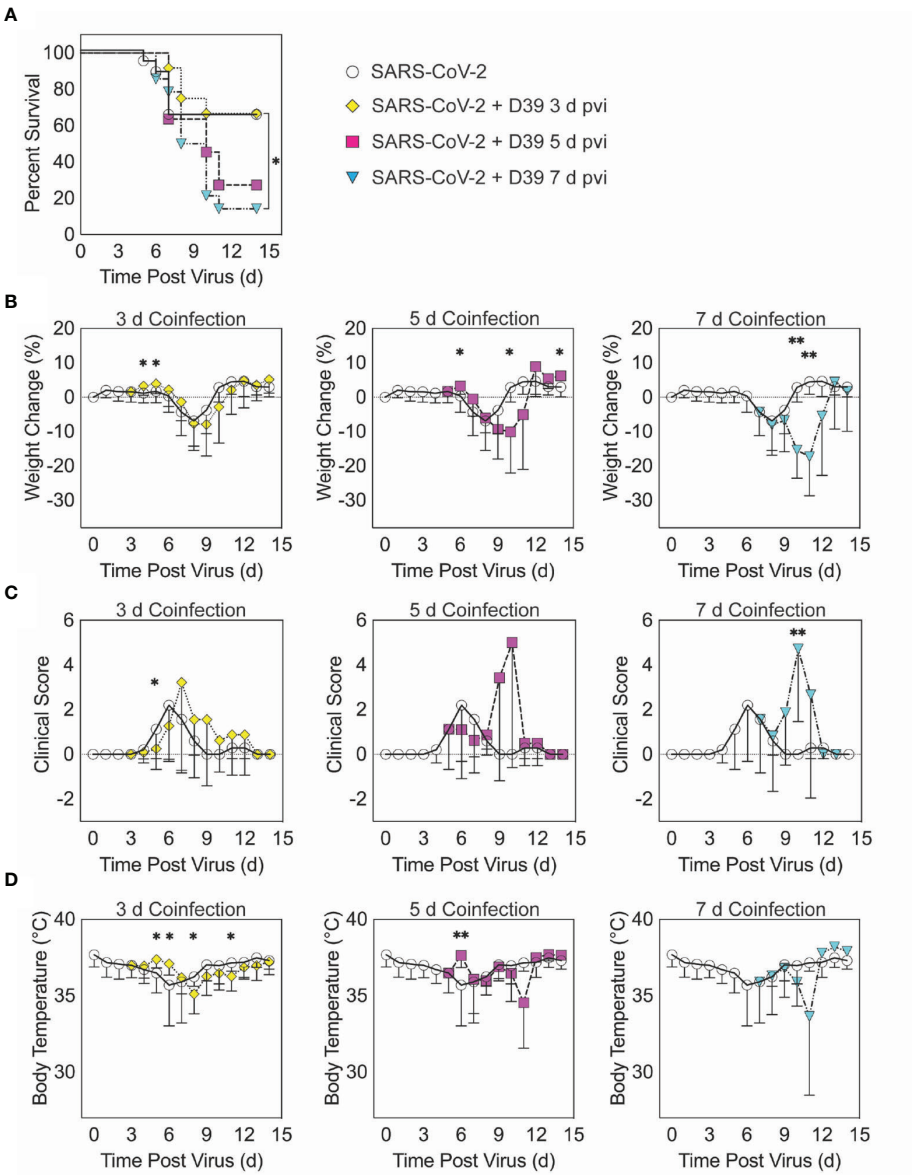

FIGURE 1 | SARS-CoV-2-pneumococcal coinfection in K18-hACE2 mice. Kaplan-Meier survival curves **(A)**, percent weight loss **(B)**, cumulative clinical score **(C)**, and temperature **(D)** of mice infected with SARS-CoV-2 (250 PFU; white circles, solid lines) followed by 10^3 CFU D39 at 3 d (yellow diamonds, dotted lines), 5 d (magenta squares, dashed lines), or 7 d (cyan triangles, dash-dotted lines) pvi. Data are shown as the mean ± standard deviation (SD) and significant differences are indicated by *,P < 0.05; **,P < 0.01 for comparisons between SARS-CoV-2 infection and SARS-CoV-2-pneumococcal coinfection.

The average weight loss was reduced ($P = 0.01$) and temperature was increased ($P = 0.001$) at 1 d pbi in the coinfected animals (**Figures 1B, D**). Coinfected animals lost more weight than animals infected with SARS-CoV-2 alone at 5 d pbi ($P = 0.03$) (**Figure 1B**), but no significant difference in their clinical scores was detected (**Figure 1C**). Comparatively, a coinfection at 7 d pvi was significantly more severe than SARS-CoV-2 infection alone ($P = 0.03$) and resulted in additional lethality at earlier times than the coinfection at 5 d pvi, with additional animals succumbing to the infection within 1, 3, or 4 d pbi (**Figure 1A**). Significantly more weight loss at 3 d ($P < 0.001$) and 4 d ($P = 0.002$) pbi (**Figure 1B**) and higher clinical scores at 3 d pbi ($P = 0.01$) (**Figure 1C**) occurred without altering temperature (**Figure 1D**).

SARS-CoV-2 Coinfection Increased Bacterial Loads but Not Viral Loads

To evaluate whether SARS-CoV-2-bacterial coinfection alters pathogen burden, we measured viral loads in the lung and bacterial loads in the lung and blood of infected animals. In mice infected with bacteria alone or with SARS-CoV-2 followed by bacteria at 3 d pvi, no bacteria were recovered from the lungs of 7/8 mice at 24 h pbi (**Figures 2A**, **S1D**). However, when the bacteria was introduced at 5 d pvi, bacterial loads in the lung remained at a level similar to the inoculum in 7/8 mice and was cleared in 1/8 mice (**Figure 2A**). Bacteria were not detected in the blood of mice infected with bacteria alone (data not shown) or SARS-CoV-2-bacteria coinfected at 3 or 5 d pvi (**Figure 2B**). However, in mice coinfected at 7 d pvi, significant bacterial

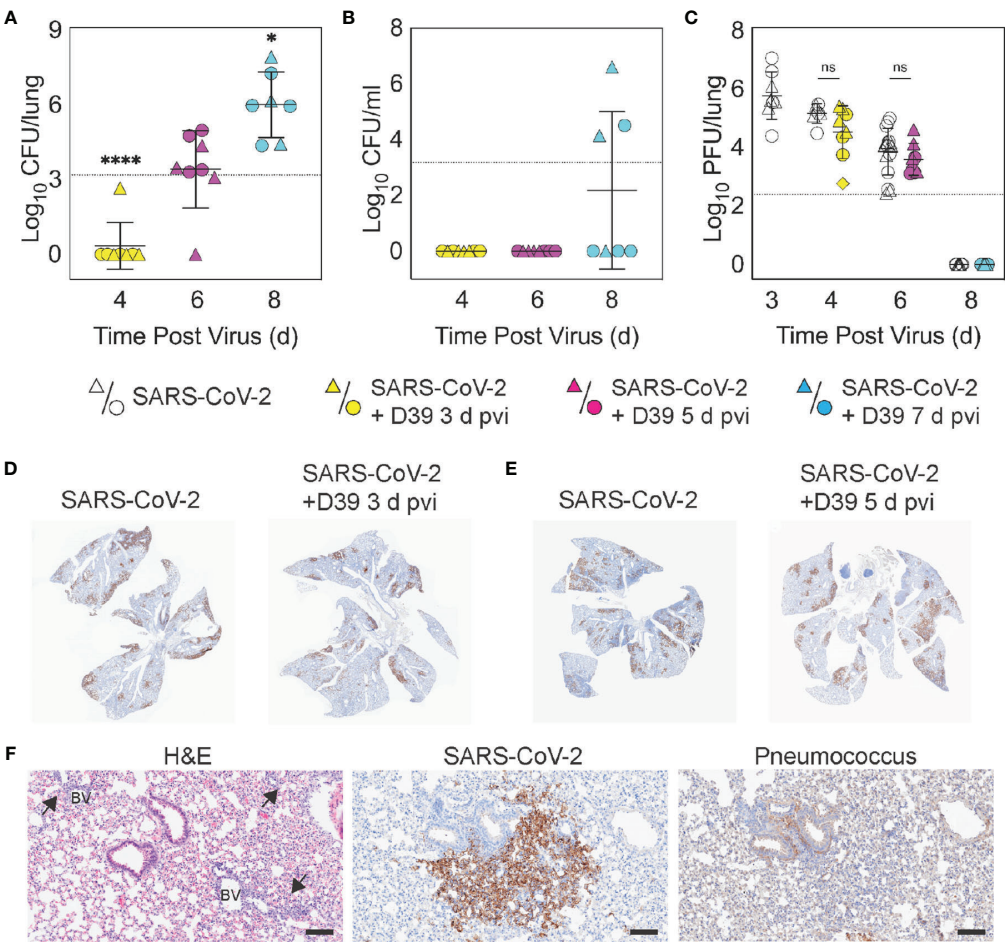

FIGURE 2 | Dynamics of pathogen loads during SARS-CoV-2 infection and pneumococcal coinfection. Lung bacterial loads (CFU/lung) **(A)**, blood bacterial loads **(B)**, and lung viral loads (PFU/lung) **(C)** in female (circles) and male (triangles) mice infected with SARS-CoV-2 (250 PFU; white) followed 10^3 CFU D39 at 3 d (yellow), 5 d (magenta), or 7 d (cyan) pvi. Each symbol represents a single mouse and the mean ± standard deviation (SD) are for combined male and female groups. Significant differences are indicated by ns, not significant; $^*P < 0.05$; $^{****}P < 0.0001$. For bacterial titers, comparison was with the inoculum (dotted line). **(D, E)** Representative immunohistochemical (IHC) staining for SARS-CoV-2 nucleocapsid protein in whole lung sections following (24 h pbi) infection with SARS-CoV-2 (250 PFU) then PBS or 10^3 CFU D39 at 3 d **(D)** or 5 d **(E)** pvi. **(F)** Representative lung sections stained with H&E, SARS-CoV-2 nucleocapsid protein, or pneumococcus from infection with SARS-CoV-2 (250 PFU) followed by 10^3 CFU D39 at 5 d pvi. Lesions with perivascular inflammatory cell infiltration are indicated by arrows; blood vessel (BV). Scale bar = 100 µm.

growth occurred in the lungs of all animals (P = 0.02; Mann-Whitney test) and the blood of some animals (3/7) with titers reaching 4.4 to 7.9 $\log_{10}$ CFU/lung (**Figure 2A**) and 4.1 to 6.6 $\log_{10}$ CFU/mL (**Figure 2B**), respectively, within 24 h pbi.

Pulmonary viral loads were unchanged by bacterial coinfection whether coinfection was initiated at 3 d (P = 0.12) or 5 d (P = 0.18) pvi (**Figure 2C**) and the amount and distribution of viral antigen in the lung tissue were also unchanged (**Figures 2D, E**). Although some areas of the lung contained colocalized virus and bacteria, both intracellular and extracellular bacterial antigen were detected in areas containing no viral antigen (**Figure 2F**). The virus had cleared by 8 d pvi in the groups that were mock coinfected or bacterial coinfected at 7 d pvi (**Figure 2C**). No significant differences were found in viral or bacterial loads between males and females.

Select Changes in Pulmonary Immune Responses After SARS-CoV-2-Pneumococcal Coinfection

To investigate whether bacterial coinfection altered immune response dynamics, several immune cells, cytokines, and chemokines were quantified in the lung 24 h after mock coinfection or bacterial coinfection in SARS-CoV-2 infected mice (**Figures 3**, **4**, **S3, S6**). In animals infected with SARS-CoV-2 only, natural killer (NK) T cells (**Figure S3D**) and total $CD19^+$ B cells (**Figure 3E**) were reduced at 4 d pvi compared with naïve (P = 0.007 and P = 0.018, respectively). The absolute numbers of other cells were unchanged at this time point (**Figures 3**, **S3**); however, increases in the proportion of activated ($CD69^+$) immune cells were evident (**Figure S4**). SARS-CoV-2 infection also resulted in many cytokines and chemokines above baseline levels (all $P < 0.05$) throughout the infection, including IFN-γ, IL-1β, IL-4, IL-28, CXCL10, GM-CSF, LIF, CCL2, CCL7, MIP-1α, MIP-1β, RANTES, IFN-α, and IFN-β. IL-5, IL-6, IL-15, IL-18, M-CSF, and TNF-α were elevated at both 4 d and 6 d pvi while CXCL5, CXCL1, G-CSF, IL-3, IL-13, and IL-17A were increased only at 6 d pvi. MIP-2α, IL-2, and IL-22 were elevated at 6 d and 10 d pvi, and increased IL-10 and IL-23 were detected only at 8 d pvi (absolute values of cytokines are in **Figure 4**, **S5**; $\log_2$ changes over naïve in **Figure S6**).

As expected, a significant influx of $CD45^+$ immune cells was evident at 6 and 8 d pvi in animals infected with SARS-CoV-2 only (both $P < 0.001$) (**Figure S3A**), including neutrophils ($Ly6G^{hi}$; both $P < 0.01$; **Figure 3A**), the F4/$80^{mid}CD11c^{mid}CD11b^+$ monocyte/macrophage subset (both $P < 0.001$; **Figure 3B**), inflammatory macrophages (F4/$80^{hi}CD11c^{hi}CD11b^+$, iMΦ; P = 0.02 and $P < 0.001$, respectively; **Figure 3C**), F4/$80^{mid}CD11c^-$ cells (both $P < 0.001$; **Figure S3B**), NK cells (both $P < 0.001$; **Figure S3C**), $CD4^+$ T cells (P = 0.02 and $P < 0.001$, respectively; **Figure 3F**), and $CD8^+$ T cells (both $P < 0.001$; **Figure 3G**). Unlike the pathogen loads, some of the immune cells were different between males and female that were mock coinfected at 5 d pvi, including neutrophils (P = 0.047), resident alveolar macrophages (F4/$80^{hi}CD11c^{hi}CD11b^-$MHC-$II^{low/-}$, AMΦ; P = 0.047), $CD4^+$ T cells (P = 0.02), NK cells (P = 0.03), and NK T cells (P = 0.02), which were higher in females than males.

In the groups coinfected with bacteria at 3 d pvi, no changes were observed in the absolute number (**Figures 3**, **S3**) or activation (**Figure S4**) of any quantified immune cell subset or the amount of cytokines and cytokines (**Figures 4**, **S5**) within 24 h pbi compared with mock coinfection. A bacterial coinfection at 5 d pvi resulted in fewer total CD45+ cells (P = 0.03; **Figure S3A**), including neutrophils (**Figure 3A**), $CD19^+$ B cells (**Figure 3E**), $CD8^+$ T cells (**Figure 3G**), and F4/$80^{mid}CD11c^-$ cells (**Figure S3B**) (all $P < 0.05$) compared with the mock coinfected groups. In addition, iMΦ (P = 0.01) and AMΦ (P = 0.047) were again higher in females than males following coinfection at 5 d pvi (**Figures 3C, D**). The extent of activation was not different between the mock coinfection and bacterial coinfection at 5 d pvi (**Figure S4**), but reduced IL-6, IL-18, LIF (all P = 0.04), and IL-15 (P = 0.02) was observed at 24 h pbi (**Figures 4A-D**).

Coinfection at 7 d pvi induced a significant increase in neutrophils at 24 h pbi ($P < 0.001$) (**Figure 3A**) without altering the number or activation of any other immune cell quantified (**Figures 3**, **S3, S4**). AMΦ were reduced in the mock coinfected group compared with naïve animals (P = 0.001) but were not different between the mock coinfection and bacterial coinfection (P = 0.29) (**Figure 3D**). Absolute cell numbers and activation did not differ between male and female mice following coinfection at 7 d pvi (**Figures 3**, **S3, S4**). Perhaps unexpectedly, none of the measured cytokines were significantly different between animals that were mock coinfected and animals that were bacterial coinfected at 7 d pvi (**Figure 4** and **Figure S5**).

Pneumococcal Coinfection Resulted in Sustained Increases in Pulmonary Immune Responses After Recovery

To investigate whether bacterial coinfection altered immune cell dynamics and activation in recovered animals, pulmonary immune cells, cytokines, and chemokines were quantified at 17 d pvi following mock coinfection or bacterial coinfection at 3, 5, or 7 d pvi. The number of iMΦ (P = 0.01) (**Figure 3C**) and $CD8^+$ T cells (P = 0.02) (**Figure 3G**), as well as the activated proportion of iMΦ (P = 0.004), $CD8^+$ T cells (P = 0.001), $CD4^+$ T cells P 0.001), and CD19+ B cells (P = 0.005) (**Figure S4**), remained increased above naïve levels in the lungs of animals that recovered from SARS-CoV-2 infection alone. These changes were accompanied by elevated IFN-γ, CXCL10, and RANTES (P = 0.01, P = 0.03, and P = 0.04, respectively) at 17 d pvi compared to naïve (**Figures 4**, **S5, S6**). However, many measured cytokines and chemokines were below naive levels at 17 d pvi in the lungs of animals infected with SARS-CoV-2 only, including eotaxin, IL-2, IL-3, IL-17A, IL-22, IL-27, IL-28, M-CSF, and MIP-2α (all $P < 0.05$) (**Figures 4**, **S5, S6**).

A sustained increase in immune cell accumulation and activation was evident in animals that recovered from SARS-CoV-2-pneumococcal coinfection. At 17 d pvi, an increased absolute number and activated proportion of F4/$80^{mid}CD11c^{mid}CD11b^+$ monocytes/macrophages (P = 0.01; **Figures 3B**, **4B**), iMΦ (P = 0.01; **Figures 3C**, **S4C**), and $CD4^+$

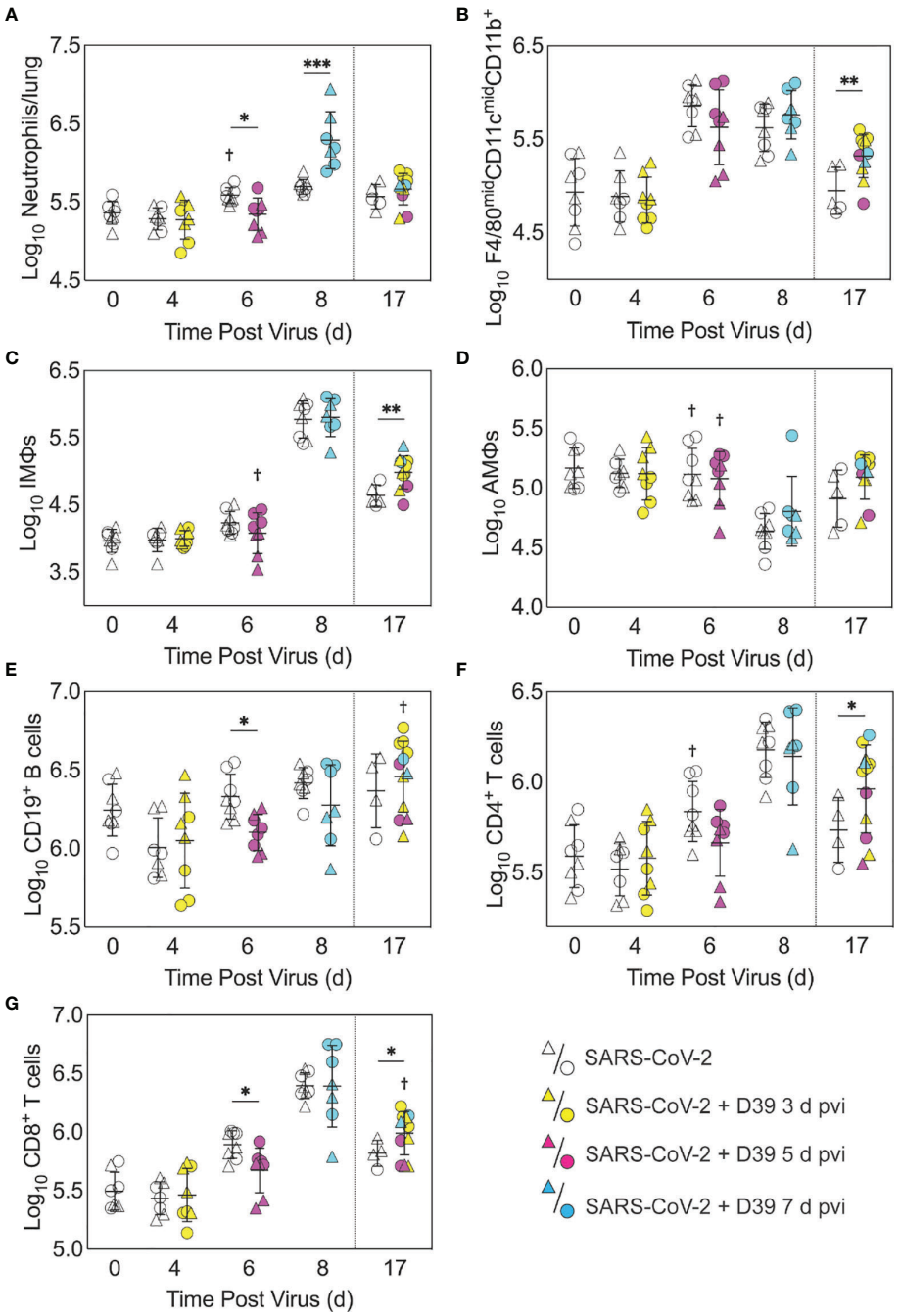

FIGURE 3 | Immune cell dynamics during SARS-CoV-2 infection and pneumococcal coinfection. Total neutrophils **(A)**, F4/80^{mid}CD11c^{mid}CD11b^{+} monocytes/macrophages **(B)**, inflammatory macrophages (iMΦ) (F4/80^{hi}CD11c^{hi}CD11b^{+}) **(C)**, alveolar macrophages (AMΦ) (F4/80^{hi}CD11c^{hi}CD11b^{-}MHC-II$^{low/-}$) **(D)**, CD19^{+} B cells **(E)**, CD4^{+} T cells **(F)**, and CD8^{+} T cells **(G)** in the lungs of female (circles) and male (triangles) mice infected with SARS-CoV-2 (250 PFU; open symbols) followed by 10^{3} CFU D39 at 3 d (yellow), 5 d (magenta), or 7 d (cyan) pvi. Each symbol represents a single mouse and the mean ± standard deviation (SD) are for combined male and female groups. Significant differences are indicated by *,$P < 0.05$; **,$P < 0.01$; ***,$P < 0.001$ for comparisons between indicated groups and by †,$P < 0.05$ for differences between males and females within a group or between coinfection times within 17 d group.

and CD8^{+} T cells ($P = 0.03$ and 0.02, respectively; **Figures 3F, G**, **S4F, G**) were present in coinfected mice compared with mock coinfected mice. Comparison between the coinfected groups indicated that more CD8^{+} T cells were present at 17 d pvi in mice that were coinfected at 3 d or 7 d pvi than those coinfected at 5 d pvi (both $P = 0.02$; **Figure 3G**). In addition, animals that recovered from a coinfection at 7 d pvi had more activated neutrophils or iMΦ than those who recovered from a coinfection

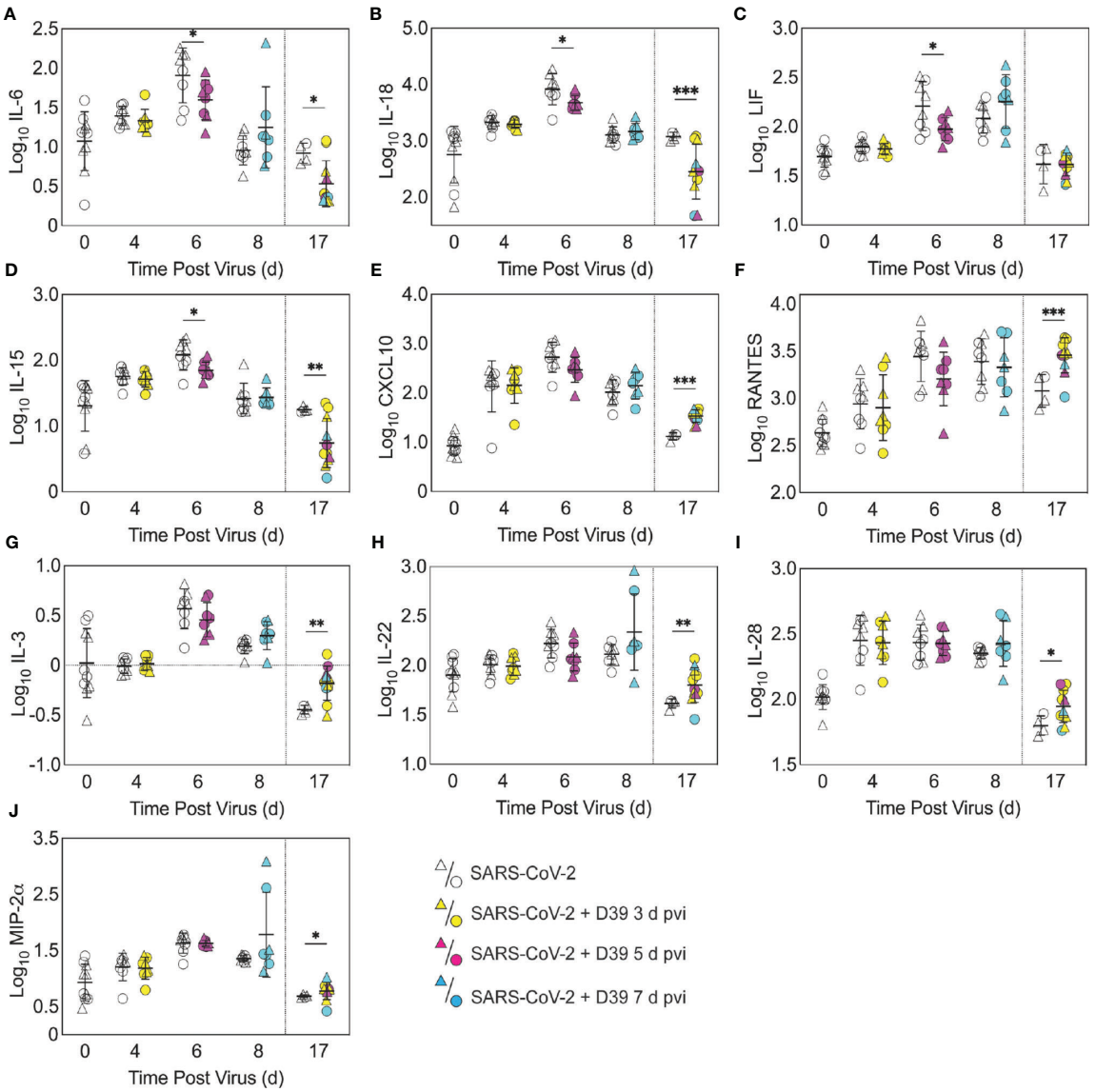

FIGURE 4 | Pulmonary cytokines and chemokines during SARS-CoV-2 infection and SARS-CoV-2-pneumococcal coinfection. Total IL-6 **(A)**, IL-18 **(B)**, LIF **(C)**, IL-15 **(D)**, CXCL10 **(E)**, RANTES **(F)**, IL-3 **(G)**, IL-22 **(H)**, IL-28 **(I)**, and MIP-2α **(J)** in the lungs of female (circles) and male (triangle) mice infected with SARS-CoV-2 (250 PFU; white) followed by infection with 10^3 CFU D39 at 3 d (yellow), 5 d (magenta), or 7 d (cyan) pvi. Each symbol represents a single mouse and the mean ± standard deviation (SD) are for combined male and female groups. Significant differences are indicated by *,$P < 0.05$; **,$P < 0.01$; ***,$P < 0.001$ for comparisons between indicated groups. Plots depicting additional cytokine and chemokine quantities (absolute $\log_{10}$ picograms) are in **Figure S5** and a heatmap representing the normalized quantity (average $\log_2$ change over naïve) is in **Figures S6**.

at 3 d pvi ($P = 0.04$) or 5 d pvi ($P = 0.03$), respectively (**Figures S4A, C**). These changes were accompanied by higher levels of CXCL-10 ($P < 0.001$), MIP-2α ($P = 0.04$), IL-3 ($P = 0.001$), IL-22 ($P < 0.008$), IL-28 ($P = 0.01$), and RANTES ($P < 0.001$) in the lungs of mice that had recovered from a bacterial coinfection compared with those recovered from SARS-CoV-2 alone (17 d pvi; **Figure 4E–J**). In addition, select cytokines and chemokines were reduced in animals that recovered from bacterial coinfection compared with those that were mock coinfected, including CXCL-1 ($P = 0.01$), IL-1α ($P = 0.04$), IL-6 ($P = 0.03$), IL-9 ($P = 0.03$), IL-10 ($P < 0.001$), IL-13 ($P < 0.001$), IL-15 ($P = 0.001$), IL-18 ($P < 0.001$), G-CSF ($P = 0.03$), and TNF-α ($P = 0.02$) (17 d pvi; **Figures 4**, **S5**). These cytokines, except for IL-1α ($P = 0.19$) and IL-18 ($P = 0.09$), were also below baseline levels (all $P < 0.05$). In addition, IL-2 ($P = 0.02$), IL-5 ($P = 0.02$), IL-17A ($P = 0.04$), and eotaxin ($P = 0.01$) were below baseline in both the bacterial coinfected and mock coinfected groups (**Figures 4**, **S5**).

Bacterial Coinfection Did Not Enhance Lung Pathology

To examine whether lung pathology was enhanced during SARS-CoV-2-pneumococcal coinfection, we assessed seven pathological features (endothelial hypertrophy/margination, peribronchiolar/perivascular lymphoid cells, interstitial inflammation/septal thickening, alveolar inflammation, alveolar edema/hemorrhage, the extent of alveolar involvement, and consolidation (**Figure 5**). There were no significant differences in any of these measurements between mock coinfected animals and those coinfected with bacteria at 3 or 5 d pvi at either 24 h pbi or 17 d pvi.

DISCUSSION

Currently, clinical data suggests variable, but moderate, frequency of bacterial coinfections in hospitalized COVID-19 patients (1–29). The wide range of reported rates is, at least in part, due to heterogeneous study designs, variability in the disease severity, age, and/or comorbidities of each cohort, the collection and detection methods used, and the panel of pathogens screened. Further, the reduced transmission of many pathogens (104–108) might have kept the rates of SARS-CoV-2-related bacterial pneumonia at an artificially low level during the COVID-19 pandemic. The results from this study suggest that we might expect more complications from bacterial pathogens going forward even in mild SARS-CoV-2 scenarios, which are becoming more common due to vaccine availability (109–111).

Here, we used the K18-hACE2 mouse model to establish that SARS-CoV-2 infection increases the risk of bacterial coinfection in a time-dependent manner with increased disease severity, pulmonary bacterial burden, bacteremia, and neutrophilia. This time dependency is similar to that of influenza-bacterial coinfections, but the lethality during the SARS-CoV-2-pneumococcal coinfection (**Figure 1**) was delayed comparatively (77) and some animals survived. In contrast, influenza-pneumococcal coinfections at similar doses consistently result in 100% lethality within 1-3 d pbi (77). Although further studies are needed to assess the potential for more severe coinfections at later time points, this may indicate a larger window for administration of antibacterial therapies in coinfected patients.

Mechanisms that contribute to increased risk and severity of bacterial coinfection during acute pulmonary diseases are complex and varied [Reviewed in (36, 39–41, 45, 84, 85, 112)]. While the mechanisms for SARS-CoV-2-bacterial coinfections remain unknown, the similar time-dependent susceptibility

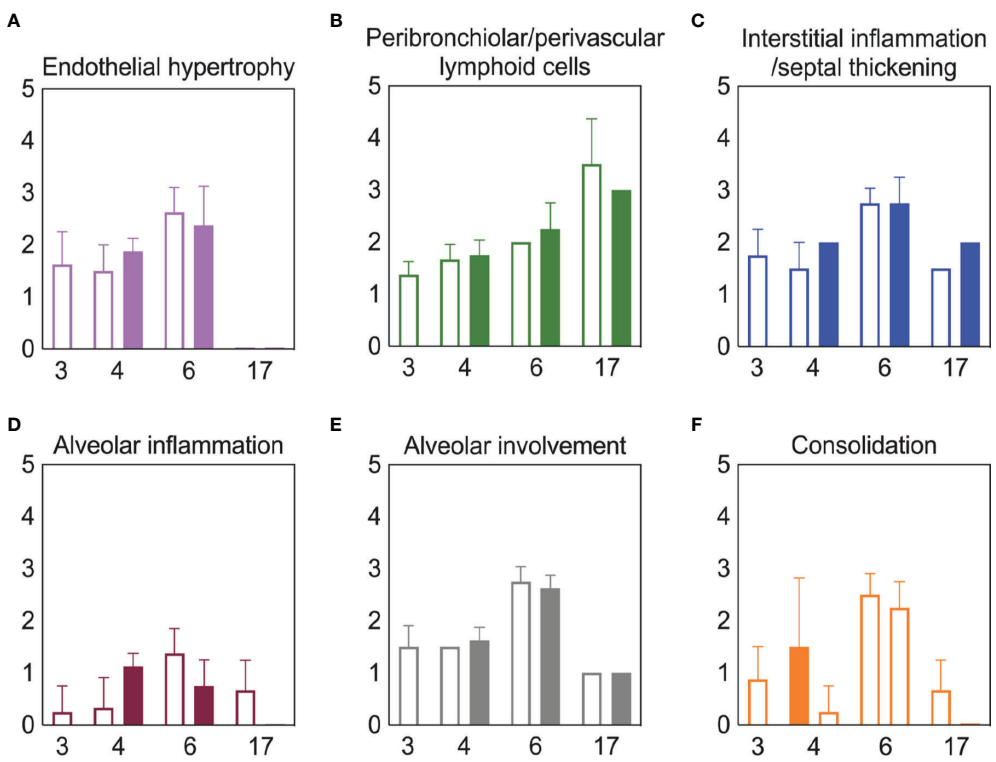

FIGURE 5 | Lung pathology during SARS-CoV-2 infection and pneumococcal coinfection. Average endothelial hypertrophy **(A)**, peribronchiolar/perivascular lymphoid cells **(B)**, interstitial inflammation/septal thickening **(C)**, alveolar inflammation **(D)**, extent of alveolar involvement **(E)**, and consolidation **(F)** in lungs of mice infected with SARS-CoV-2 (250 PFU; open bars) followed by 10^3 CFU D39 at 3 or 5 d pvi (filled bars). Plots represent the mean ± standard deviation (SD) bars for combined male and female groups.

during influenza may yield insight. We and others have shown that viral-induced changes to the number (67, 69, 70) or functionality (70, 72, 113–115) of AMΦs, which may be mediated by IFN-γ (55, 115, 116), render these cells less capable of clearing bacteria. Here, SARS-CoV-2-pneumococcal coinfection did coincide with a virally induced reduction in AMΦ (**Figure 3**), which may suggest a contribution of these cells to the acquisition of bacteria during COVID-19 particularly when paired with evidence of a dysfunctional myeloid response in patients with severe infections (75). Further studies to determine how a productive SARS-CoV-2 infection of AMΦ alters infection dynamics, their production of IFN, and their phagocytic capacity (86–89) are needed. In addition, IFN-independent mechanisms of macrophage dysfunction should also be investigated because some studies suggest that RSV coinfection severity is mediated by Gas6/Axl polarization of AMΦ to non-antibacterial (M2) type cells (117). Other mechanisms, including viral-mediated changes in bacterial receptor expression and binding (77, 118–121) and the degradation of epithelial tight junction integrity (122, 123) may also promote bacterial adherence during IAV or RSV infections, and some evidence suggests that these also occur during SARS-CoV-2 infection (124–126). However, the limited colocalization of pneumococcus with SARS-CoV-2 suggests a limited role (**Figure 2**).

Several studies have found that neutrophil dysfunction contributes to pathogenicity of IAV-pneumococcal coinfection, and this seems to be mediated by bacterial metabolism (82) and type I IFNs (71, 83, 127). However, unlike IAV-pneumococcal coinfections, type I IFNs were unchanged after SARS-CoV-2-pneumococcal coinfection (**Figure S5**) and neutrophil infiltration was only observed in coinfection at 7 d pvi (**Figure 3A**), suggesting that there may be different mechanisms underlying the enhanced pathogenicity of SARS-CoV-2 pneumococcal coinfection. This may, in part, be related to the low dose used here, where some studies have found that the SARS-CoV-related alterations to the IFN and iMΦ responses occur during more severe infections (128). It was intriguing to see here that cytokine production was largely unchanged at 24 h pbi (**Figures 4**, **S5**), which is in contrast with the robust proinflammatory cytokine/chemokine production during other viral-bacterial coinfections (39–41, 45, 84, 85). Perhaps unexpectedly, several cytokines associated with severe COVID-19 and damaging cytokine overproduction (IL-6, IL-15, and IL-18) (129, 130) were reduced following coinfection at 5 d pvi (**Figure 4**).

Although coinfections are typically thought to be hyperinflammatory with enhanced disease severity, tissue inflammation does not seem to be altered during SARS-CoV-2-pneumococcal (**Figure 5**) or influenza-pneumococcal (55) coinfections even with large neutrophil infiltrations (55, 82) (**Figure 3A**), at least within the first few days of coinfection. This may be owed to the nonlinearities between host immune responses, tissue inflammation, and disease severity (55, 56). Although the pathogenicity was increased during the coinfections at 5 d and 7 d pvi, there seemed to be little contribution from SARS-CoV-2, where the burden and distribution did not change within the first 24 h pbi (**Figure 2**) despite reduced $CD8^+$ T cells in some groups (**Figure 3G**). In IAV-pneumococcal coinfections, invading bacteria result in robustly increased viral loads (55, 68, 82, 131–133) regardless of timing (55) and viral dissemination in the lung is increased by 30-50% (55). Our prior work (55) suggests this is due to a combination of direct viral-bacterial interactions (97) that lead to viral access to new areas of the lung in addition to increased virus production rates (68) that may be mediated by alterations to the antiviral IFN response (98). The lack of detection of SARS-CoV-2 in new areas of the lung and the lack of significant colocalization of virus and bacteria (**Figure 2**) may suggest that SARS-CoV-2 cannot as readily attach to pneumococcus like other viruses (97, 134), which is positive news given that pneumococci easily invade the blood [Reviewed in (135)] and SARS-CoV-2 affects numerous other organs (51–54).

Although the long-term effects of viral-bacterial coinfections are not well studied, these data suggest they may be important where the SARS-CoV-2-bacterial coinfection resulted in lasting immunologic changes in recovered individuals. The higher macrophages and T cells (**Figure 3**) and their associated cytokines (**Figures 4**, **S5**) at 17 d pvi in animals recovered from bacterial coinfection is intriguing and suggests sustained immunopathology (55, 56, 136, 137). Many of the elevated responses are indicators of acute respiratory distress syndrome (ARDS) (138, 139) and are upregulated to promote tissue recovery and reduce pathology (140–143). This was reflected in the slightly greater interstitial inflammation 17 d pvi (**Figure 5**) in coinfected animals. However, several cytokines were lower in animals that had recovered from bacterial coinfection with some below that of a naïve animal (**Figures S5 and S6**), which may support a remodeling environment induced, in part, by hyporesponsive epithelial cells downregulating inflammatory cytokine production to minimize local immune activation [Reviewed in (144)]. In addition, the reductions in Th2 cytokines (e.g., IL-13, IL-5, and IL-9) may be an attempt to improve lung function (145–148) while limiting hyperreactivity and further damage. Nevertheless, our results suggest a lengthy recovery of the lung from both SARS-CoV-2 and SARS-CoV-2-related secondary bacterial infections.

Vaccinating against SARS-CoV-2 is likely to prove important for reducing the incidence and severity of bacterial coinfections as it has for influenza (149). The robust efficacy of the SARS-CoV-2 vaccines is encouraging (150–153), but infection is still possible with viral replication in the nasopharynx in some vaccinated individuals (154–157). This could present an opportunity for bacterial pathogens to invade and worsen the infection. With few vaccines available for coinfecting bacteria (149), the interactions within the nasopharynx between this virus and both commensal and pathogenic bacteria will be important to study.

In summary, we used the transgenic K18-hACE2 mouse model (158) to establish that a low dose SARS-CoV-2 infection increases the risk of pneumococcal coinfection in a time-dependent manner. The data importantly highlight many

differences with other viral-bacterial coinfections and the need for further studies to clarify the host-pathogen interplay that enhance susceptibility and pathogenicity during SARS-CoV-2-bacterial coinfection. This information may be crucial going forward, particularly because a sustained immune activation following coinfection suggests an increased risk of developing ARDS even in patients with mild COVID-19. In addition, as new SARS-CoV-2 variants emerge and nonpharmaceutical measures, such as wearing masks and physical distancing, become less common, we might anticipate an increase in risk of bacterial transmission and acquisition in COVID-19-infected individuals.

MATERIALS AND METHODS

Mice

Adult (10-13 week old) male and female K18-hACE2 transgenic mice (B6.Cg-Tg(K18-ACE2)2Prlmn/J) were obtained from Jackson Laboratories (Bar Harbor, ME). Mice were housed in groups of 4 in solid–bottom polysulfone individually ventilated cages (Allentown BCU) in rooms maintained on a 12:12-hour light:dark cycle at 22 ± 2°C with 30-70% humidity in the Regional Biocontainment Laboratory (animal biosafety level 3 facility) at UTHSC (Memphis, TN). Mice were acclimated for 1 day before being lightly anesthetized with 2% inhaled isoflurane (Baxter, Deerfield, IL) and implanted subcutaneously with an IPTT300 transponder (Bio Medic Data Systems, Seaford, DE) for identification and temperature monitoring, followed by an additional 3 days of acclimation before inclusion in the experiments. Envigo irradiated rodent diet (catalog no. 7912) and autoclaved water were available ad libitum during the acclimation and study periods; gel food and hydrogel were provided at the time of infection. All experimental procedures were performed under protocol 20-0132 approved by the Institutional Animal Care and Use Committee at University of Tennessee Health Science Center (UTHSC) under relevant institutional and American Veterinary Medical Association (AVMA) guidelines and were performed in a animal biosafety level 3 facility that is accredited by the American Association for Laboratory Animal Science (AALAS).

Infection Experiments

All experiments were done using 2019-nCoV/USA-WA1/2020 (BEI Resources NR-52281) (SARS-CoV-2) and type 2 pneumococcal strain D39. The viral infectious dose [plaque forming units (PFU)] was determined by plaque assay of serial dilutions on Vero E6 cells. Virus seed stocks were sequenced using next-generation sequencing with ARTIC primers on the Illumina MiSeq. Bacterial infectious dose [colony forming units (CFU)] was determined by using serial dilutions on tryptic soy agar plates supplemented with 3% sheep erythrocytes (TSA). Doses of virus and bacteria were selected that elicited mild-moderate disease independently to ensure that changes in disease severity following coinfection would be evident. Frozen stocks were diluted in sterile PBS and administered intranasally to groups of 4 mice, lightly anesthetized with 2.5% inhaled isoflurane (Baxter, Deerfield, IL) in a total volume of 50 µl (25 µl per nostril). Mice were inoculated with either PBS or SARS-CoV-2 at day 0 then with 10^3 CFU of D39 or PBS, either 3 or 5 days later. Assessment of symptom severity was performed twice daily after the onset of symptoms by assigning a score (scale 0-3) to clinical features, including weight loss (0, <15%; 1, 15-20%; 2, 21-25%; 3, >25%), temperature change (0, >34°C; 1, 34-31°C; 2, 30-26°C; 3, <26°C), body condition/appearance (0, normal; 1, roughened fur; 2, roughened fur, hunched posture, mild grimace, active; 3, roughened fur, hunched posture, grimace, inactive, conjunctivitis, head-tilt), respiratory effort (0, normal; 2, increased respiratory rate and effort; 3, weak, intermittent breathing), behavior (0, normal; 1, slow, unprovoked movement; 2, slow, provoked movement; 3, minimal response/unresponsive or spinning), and dehydration (0, normal; 1, ≤ 2 second skin tent, mildly sunken eyes; 2, 2-3 second skin tent, sunken eyes; 3, > 3 second skin tent, sunken eyes). Mice were euthanized if they lost >25% of their starting body weight or became moribund based on clinical scores (a score of 3 in any single category or a cumulative score of ≥9 in respiratory effort, dehydration, temperature reduction, behavior, body condition/appearance).

Harvest and Processing of Lungs and Blood

Mice were euthanized by 33% isoflurane inhalation. Lungs were aseptically harvested, washed in PBS, and fixed in 10% neutral buffered formalin for histology or digested with collagenase (1 mg/ml, Sigma C0130) and physical homogenization against a 40 µm cell strainer for immune cell staining. Lung digest supernatants were used to quantify cytokines and chemokines and to determine viral and bacterial titers as above; bacterial titers were also measured in peripheral blood. Following red blood cell lysis, lung cells were washed in staining buffer (PBS, 5mM EDTA, 10mM HEPES, and 0.5% bovine serum albumin), counted with trypan blue exclusion using a Cell Countess System (Invitrogen, Grand Island, NY), and prepared for flow cytometric analysis as described below.

Flow Cytometric Analysis

Flow cytometry (BD FACSAria; San Jose, CA) was performed on single cell suspensions after Fc receptor blocking (TruStainFcX, Biolegend) and viability staining (Zombie Violet Fixable Viability, Biolegend), 25 min surface staining, and fixation (BD Cytofix). The followed anti-mouse antibody panels were used for cell subset analysis: CD45 (clone 30-F11, Pe-Cy7, Biolegend), CD3e (clone 145-2C11, FITC, Biolegend), CD4 (clone RM4-5, V500, BD Biosciences), CD8α (clone 53-6.7, PerCP-Cy5.5, Biolegend), CD19 (clone 6D5, PE, Biolegend), CD335 (clone 29A1.4, APC-Fire750, Biolegend), and CD69 (clone H1.2F3, APC, Biolegend) or CD45 (clone 30-F11, Pe-Cy7, Biolegend), Ly6G (clone 1A8, PerCP-Cy5.5, Biolegend), F4/80 (clone BM8, PE, eBioscience), CD11b (clone M1/70, V500, BD Biosciences), CD11c (clone N418, APC-Fire750, Biolegend), MHC-II (clone I-A/I-E, FITC, eBioscience), and CD69 (clone H1.2F3, APC, Biolegend). The data were analyzed using FlowJo 10.7.2 (Tree

Star, Ashland, OR). Data were cleaned using the flowAI application (159) followed by gating viable cells from a forward scatter/side scatter plot, singlet inclusion, and viability dye exclusion. $CD45^+$ cells were selected for further analyses. Neutrophils ($Ly6G^{hi}$), alveolar macrophages (AMΦ) ($F4/80^{hi}CD11c^{hi}CD11b^-MHC\text{-}II^{low/-}$), inflammatory/exudate macrophages (iMΦ) ($F4/80^{hi}CD11c^{hi}CD11b^+MHC\text{-}II^{mid/hi}$), other monocyte/macrophage populations ($F4/80^{mid}CD11c^{mid}CD11b^+$ and $F4/80^{mid}CD11c^-CD11b^{+/-}$), NK cells ($CD3e^-CD19^-CD335^+$), CD4 T cells ($CD3^+CD8^-CD4^+CD335^-$), CD8 T cells ($CD3^+CD8^+CD4^-CD335^-$), NK T cells ($CD3e^+CD335^+$), B cells ($CD3e^-CD19^+$), and recently activated subsets thereof ($CD69^+$) were gated as in **Figure S2**.

Cytokine and Chemokine Quantification

Cytokines G-CSF (CSF-3), GM-CSF, IFN-γ, IL-1α, IL-1β, IL-2, IL-3, IL-4, IL-5, IL-6, IL-9, IL-10, IL-12p70, IL-13, IL-15/IL-15R, IL-17A (CTLA-8), IL-18, IL-22, IL-23, IL-27, IL-28, IL-31, LIF, MCP-3 (CCL7), M-CSF, TNF-α) and chemokines (ENA-78 (CXCL5), eotaxin (CCL11), GROα (CXCL1), IP-10 (CXCL10), MCP-1 (CCL2), MIP-1α (CCL3), MIP-1β (CCL4), MIP-2α (CXCL2), RANTES (CCL5) were measured in lung supernatant by Luminex and ELISA (IFN-α,β). Before use, cell debris and aggregates were removed by centrifugation at 4°C, 400 x *g*. ProcartaPlex magnetic bead cytokine/chemokine plates (Invitrogen) were prepared according to the manufacturer's instructions. Data were acquired using a MagPix (Luminex) with Luminex xPonent software (v4.2) and analyzed with the ProcartaPlex Analysis App (ThermoFisher Connect). ELISAs for IFNα and IFNβ (PBL Assay Science) were prepared according to the manufacturer's instructions, read at 450 nm, and analyzed using GraphPad Prism 9.2.0. Mean concentrations of duplicate samples were calculated by the construction of standard curves using a weighted 5PL and 4PL regression for the ProcartaPlex and ELISA data, respectively. Absolute quantities of each cytokine/chemokine were calculated based on the mean concentration of replicate samples normalized to the lung supernatant volume collected during tissue processing. Internal plate controls were used to adjust values obtained between plates and fold changes in cytokine and chemokine quantities were calculated for each animal, normalized to the average of naïve controls (pooled males/females).

Histology

Following euthanasia and tissue removal as above, lungs were continually fixed in 10% neutral-buffered formalin solution (NBF; ThermoFisher Scientific, Waltham, MA) before being embedded in paraffin, sectioned at 4μm, and mounted on positively charged glass slides (Superfrost Plus; Thermo Fisher Scientific, Waltham, MA). Tissue sections were stained with hematoxylin and eosin (H&E) or subjected to immunohistochemical (IHC) staining to detect SARS-CoV-2 antigen or pneumococcus. Tissue sections were deparaffinized and rehydrated before undergoing antigen retrieval in a citrate-based solution (pH 6.0) at 97°C for SARS-CoV-2 detection or a tris-based solution (pH 9.0) for pneumococcal detection (Vector Laboratories, Burlingame, CA). For IHC, a primary monoclonal antibody against SARS-CoV-2 nucleoprotein (NP) (Sino Biological, Wayne, PA) or a rabbit polyclonal antibody against pneumococcus (Novus Biologicals, Littleton, CO) was used at 1:1000 followed by a biotinylated anti-rabbit antibody (Vector Laboratories, Burlingame, CA) at 1:200, the Vectastain Elite ABC-HRP kit (Vector Laboratories, Burlingame, CA), and 3,3'-Diaminobenzidine (DAB) solution development. Stained sections were counterstained with hematoxylin, dehydrated, and examined by a pathologist blinded to the experimental group assignments. Pathology was scored on a scale from 0-5, where 0 = normal, no tissue affected; 1 = minimal: rare or inconspicuous lesions; 2 = mild: multifocal or small, focal, or widely separated, but conspicuous lesions; 3 = moderate: multifocal, prominent lesions; 4 = marked: extensive to coalescing lesions or areas of inflammation with some loss of structure; 5 = severe: diffuse lesion with effacement of normal structure. Intermediate severity grades were assigned where necessary. To quantify the extent of viral infection in the lungs, digital images of whole lung sections stained for viral antigen were first captured using the Aperio ScanScope XT Slide Scanner (Aperio Technologies, Inc., Vista, CA). The areas of both the entire lung parenchyma (alveoli and bronchioles) and the virus-positive regions were outlined manually with areas determined using ImageScope software (Aperio Technologies, Inc.). Representative images and quantitative analyses of viral spread and lung pathology during infection are shown in **Figures 2**, **5**, respectively.

Statistical Analysis

Significant differences in Kaplan-Meier survival curves were calculated using the log-rank test. Linear values of lung and blood bacterial loads, viral loads, immune cells, and cytokines/chemokines were compared using an unpaired *t* test with Welch correction except where the Mann-Whitney test was used due to unequal variances (GraphPad Prism 9.2.0 and Rv4.0.3). The confidence interval of significance was set to 95%, and $P \leq 0.05$ was considered significant.

DATA AVAILABILITY STATEMENT

The original contributions presented in the study are included in the article/**Supplementary Material**. Further inquiries can be directed to the corresponding authors. The following reagent was deposited by the Centers for Disease Control and Prevention and obtained through BEI Resources, NIAID, NIH: SARS-Related Coronavirus 2, Isolate USA-WA1/2020, NR-52281.

ETHICS STATEMENT

The animal study was reviewed and approved by Institutional Animal Care and Use Committee at the University of Tennessee Health Science Center.

AUTHOR CONTRIBUTIONS

APS, RC, CJ, and AMS conceived and designed the experiments. APS, EW, TP, MS, LL, LZ, and YX performed the experiments. YX and PV performed histological analysis. APS and AMS wrote the manuscript with input from all authors. All authors contributed to the article and approved the submitted version.

FUNDING

This work was supported by the UTHSC Institute for the Study of Host Pathogen Systems, the University of Tennessee Research Foundation, and NIH grant number AI139088.

ACKNOWLEDGMENTS

We thank the staff of the Regional Biocontainment Laboratory and Deidre Daria, Ph.D. for technical support, and Jyothi Parvathareddy and Dong Yang for the generation and characterization of viral stocks.

SUPPLEMENTARY MATERIAL

The Supplementary Material for this article can be found online at: https://www.frontiersin.org/articles/10.3389/fimmu.2022.894534/full#supplementary-material

REFERENCES

1. Toombs JM, Van den Abbeele K, Democratis J, Mandal AKJ, Missouris CG. Pneumococcal Coinfection in COVID-19 Patients. *J Med Virol* (2021) 93:177–9. doi: 10.1002/jmv.26278
2. Tsukamoto T, Nakajima N, Sakurai A, Nakajima M, Sakurai E, Sato Y, et al. Lung Pathology of Mutually Exclusive Co-Infection With SARS-CoV-2 and Streptococcus Pneumoniae. *Emerg Infect Dis* (2021) 27:919–23. doi: 10.3201/eid2703.204024
3. Adler H, Ball R, Fisher M, Mortimer K, Vardhan MS. Low Rate of Bacterial Co-Infection in Patients With COVID-19. *Lancet Microbe* (2020) 1:e62. doi: 10.1016/S2666-5247(20)30036-7
4. Zhu X, Ge Y, Wu T, Zhao K, Chen Y, Wu B, et al. Co-Infection With Respiratory Pathogens Among COVID-2019 Cases. *Virus Res* (2020) 285:198005. doi: 10.1016/j.virusres.2020.198005
5. He F, Xia X, Nie D, Yang H, Jiang Y, Huo X, et al. Respiratory Bacterial Pathogen Spectrum Among COVID-19 Infected and Non-COVID-19 Virus Infected Pneumonia Patients. *Diagn Microbiol Infect Dis* (2020) 98:115199. doi: 10.1016/j.diagmicrobio.2020.115199
6. Garcia-Vidal C, Sanjuan G, Moreno-Garcia E, Puerta-Alcalde P, Garcia-Pouton N, Chumbita M, et al. Incidence of Co-Infections and Superinfections in Hospitalized Patients With COVID-19: A Retrospective Cohort Study. *Clin Microbiol Infect* (2021) 27:83–8. doi: 10.1016/j.cmi.2020.07.041
7. Kreitmann L, Monard C, Dauwalder O, Simon M, Argaud L. Early Bacterial Co-Infection in ARDS Related to COVID-19. *Intensive Care Med* (2020) 46:1787–9. doi: 10.1007/s00134-020-06165-5
8. Bordi L, Nicastri E, Scorzolini L, Di Caro A, Capobianchi MR, Castilletti C, et al. Differential Diagnosis of Illness in Patients Under Investigation for the Novel Coronavirus (SARS-CoV-2), Italy, February 2020. *Euro Surveill* (2020) 25(8):2000170. doi: 10.2807/1560-7917.ES.2020.25.8.2000170
9. Chen N, Zhou , M, Dong X, Qu J, Gong F, Han Y, et al. Epidemiological and Clinical Characteristics of 99 Cases of 2019 Novel Coronavirus Pneumonia in Wuhan, China: A Descriptive Study. *Lancet* (2020) 395:507–13. doi: 10.1016/S0140-6736(20)30211-7
10. Kim D, Quinn J, Pinsky B, Shah NH, Brown I. Rates of Co-Infection Between SARS-CoV-2 and Other Respiratory Pathogens. *JAMA* (2020) 323:2085–6. doi: 10.1001/jama.2020.6266
11. Nowak MD, Sordillo EM, Gitman MR, Paniz Mondolfi AE. Coinfection in SARS-CoV-2 Infected Patients: Where Are Influenza Virus and Rhinovirus/Enterovirus? *J Med Virol* (2020) 92:1699–700. doi: 10.1002/jmv.25953
12. Zhou S, Yang Y, Zhang X, Li Z, Liu X, Hu C, et al. Clinical Course of 195 Critically Ill COVID-19 Patients: A Retrospective Multicenter Study. *Shock* (2020) 54:644–51. doi: 10.1097/SHK.0000000000001629
13. Hazra A, Collison M, Pisano J, Kumar M, Oehler C, Ridgway JP, et al. Coinfections With SARS-CoV-2 and Other Respiratory Pathogens. *Infect Control Hosp Epidemiol* (2020) 41:1228–9. doi: 10.1017/ice.2020.322
14. Koehler P, Cornely OA, Bottiger BW, Dusse F, Eichenauer DA, Fuchs F, et al. COVID-19 Associated Pulmonary Aspergillosis. *Mycoses* (2020) 63:528–34. doi: 10.1111/myc.13096
15. Hughes S, Troise O, Donaldson H, Mughal N, Moore LSP. Bacterial and Fungal Coinfection Among Hospitalized Patients With COVID-19: A Retrospective Cohort Study in a UK Secondary-Care Setting. *Clin Microbiol Infect* (2020) 26:1395–9. doi: 10.1016/j.cmi.2020.06.025
16. Massey BW, Jayathilake K, Meltzer HY. Respiratory Microbial Co-Infection With SARS-CoV-2. *Front Microbiol* (2020) 11:2079. doi: 10.3389/fmicb.2020.02079
17. Lai CC, Wang CY, Hsueh PR. Co-Infections Among Patients With COVID-19: The Need for Combination Therapy With Non-Anti-SARS-CoV-2 Agents? *J Microbiol Immunol Infect* (2020) 53:505–12. doi: 10.1016/j.jmii.2020.05.013
18. Langford BJ, So M, Raybardhan S, Leung V, Westwood D, MacFadden DR, et al. Bacterial Co-Infection and Secondary Infection in Patients With COVID-19: A Living Rapid Review and Meta-Analysis. *Clin Microbiol Infect* (2020) 26:1622–9. doi: 10.1016/j.cmi.2020.07.016
19. Richardson S, Hirsch JS, Narasimhan M, Crawford JM, McGinn T, Davidson KW, et al. Presenting Characteristics, Comorbidities, and Outcomes Among 5700 Patients Hospitalized With COVID-19 in the New York City Area. *JAMA* (2020) 323:2052–9. doi: 10.1001/jama.2020.6775
20. Singh V, Upadhyay P, Reddy J, Granger J. SARS-CoV-2 Respiratory Co-Infections: Incidence of Viral and Bacterial Co-Pathogens. *Int J Infect Dis* (2021) 105:617–20. doi: 10.1016/j.ijid.2021.02.087
21. Guan Z, Chen C, Li Y, Yan D, Zhang X, Jiang D, et al. Impact of Coinfection With SARS-CoV-2 and Influenza on Disease Severity: A Systematic Review and Meta-Analysis. *Front Public Health* (2021) 9:773130. doi: 10.3389/fpubh.2021.773130
22. Amin-Chowdhury Z, Aiano F, Mensah A, Sheppard C, Litt D, Fry NK, et al. Impact of the COVID-19 Pandemic on Invasive Pneumococcal Disease and Risk of Pneumococcal Coinfection With SARS-CoV-2: Prospective National Cohort Study, England. *Clin Infect Dis* (2020) 72(5):e65–75. doi: 10.1093/cid/ciaa1728
23. Shafran N, Shafran I, Ben-Zvi H, Sofer S, Sheena L, Krause I, et al. Secondary Bacterial Infection in COVID-19 Patients is a Stronger Predictor for Death Compared to Influenza Patients. *Sci Rep* (2021) 11:12703. doi: 10.1038/s41598-021-92220-0
24. Contou D, Claudinon A, Pajot O, Micaelo M, Longuet Flandre P, Dubert M, et al. Bacterial and Viral Co-Infections in Patients With Severe SARS-CoV-2 Pneumonia Admitted to a French ICU. *Ann Intensive Care* (2020) 10:119. doi: 10.1186/s13613-020-00736-x
25. Sharifipour E, Shams S, Esmkhani M, Khodadadi J, Fotouhi-Ardakani R, Koohpaei A, et al. Evaluation of Bacterial Co-Infections of the Respiratory Tract in COVID-19 Patients Admitted to ICU. *BMC Infect Dis* (2020) 20:646. doi: 10.1186/s12879-020-05374-z
26. Mirzaei R, Goodarzi P, Asadi M, Soltani A, Aljanabi HAA, Jeda AS, et al. Bacterial Co-Infections With SARS-CoV-2. *IUBMB Life* (2020) 72:2097–111. doi: 10.1002/iub.2356
27. Musuuza JS, Watson L, Parmasad V, Putman-Buehler N, Christensen L, Safdar N. Prevalence and Outcomes of Co-Infection and Superinfection With SARS-CoV-2 and Other Pathogens: A Systematic Review and Meta-Analysis. *PloS One* (2021) 16:e0251170. doi: 10.1371/journal.pone.0251170
28. Rodriguez-Nava G, Yanez-Bello MA, Trelles-Garcia DP, Chung CW, Egoryan G, Friedman HJ. A Retrospective Study of Coinfection of SARS-CoV-2 and Streptococcus Pneumoniae in 11 Hospitalized Patients With Severe COVID-19 Pneumonia at a Single Center. *Med Sci Monit* (2020) 26:e928754. doi: 10.12659/MSM.928754
29. Feldman C, Anderson R. The Role of Co-Infections and Secondary Infections in Patients With COVID-19. *Pneumonia (Nathan)* (2021) 13:5. doi: 10.1186/s41479-021-00083-w

30. Rawson TM, Moore LSP, Zhu N, Ranganathan N, Skolimowska K, Gilchrist M, et al. Bacterial and Fungal Coinfection in Individuals With Coronavirus: A Rapid Review To Support COVID-19 Antimicrobial Prescribing. *Clin Infect Dis* (2020) 71:2459–68. doi: 10.1093/cid/ciaa530
31. Bengoechea JA, Bamford CG. SARS-CoV-2, Bacterial Co-Infections, and AMR: The Deadly Trio in COVID-19? *EMBO Mol Med* (2020) 12:e12560. doi: 10.15252/emmm.202012560
32. Bartlett JG, Mundy LM. Community-Acquired Pneumonia. *N Engl J Med*. (1995) 333(24):1618–24. doi: 10.1056/NEJM199512143332408
33. Ruiz-Gonzalez A, Falguera M, Nogues A, Rubio-Caballero M. Is Streptococcus Pneumoniae the Leading Cause of Pneumonia of Unknown Etiology? A Microbiologic Study of Lung Aspirates in Consecutive Patients With Community-Acquired Pneumonia. *Am J Med* (1999) 106:385–90. doi: 10.1016/s0002-9343(99)00050-9
34. Bartlett JG, Dowell SF, Mandell LA, File Jr. TM, Musher DM, Fine MJ. Practice Guidelines for the Management of Community-Acquired Pneumonia in Adults. Infectious Diseases Society of America. *Clin Infect Dis* (2000) 31:347–82. doi: 10.1086/313954
35. Brundage JF. Interactions Between Influenza and Bacterial Respiratory Pathogens: Implications for Pandemic Preparedness. *Lancet Infect Dis* (2006) 6:303–12. doi: 10.1016/S1473-3099(06)70466-2
36. McCullers JA. The Co-Pathogenesis of Influenza Viruses With Bacteria in the Lung. *Nat Rev Microbiol* (2014) 12:252–62. doi: 10.1038/nrmicro3231
37. Morris DE, Cleary DW, Clarke SC. Secondary Bacterial Infections Associated With Influenza Pandemics. *Front Microbiol* (2017) 8:1041. doi: 10.3389/fmicb.2017.01041
38. Cawcutt K, Kalil AC. Pneumonia With Bacterial and Viral Coinfection. *Curr Opin Crit Care* (2017) 23:385–90. doi: 10.1097/MCC.0000000000000435
39. Smith AM, McCullers JA. Secondary Bacterial Infections in Influenza Virus Infection Pathogenesis. In: R Compans and M Oldstone (eds) *Influenza Pathogenesis and Control - Volume I. Current Topics in Microbiology and Immunology, vol 385*. Cham: Springer (2014). doi: 10.1007/82_2014_394
40. Short KR, Habets MN, Hermans PWM, Diavatopoulos DA. Interactions Between Streptococcus Pneumoniae and Influenza Virus: A Mutually Beneficial Relationship? *Future Microbiol* (2012) 7:609–24. doi: 10.2217/fmb.12.29
41. Metzger DW, Sun K. Immune Dysfunction and Bacterial Coinfections Following Influenza. *J Immunol* (2013) 191:2047–52. doi: 10.4049/jimmunol.1301152
42. Smith AM. Host-Pathogen Kinetics During Influenza Infection and Coinfection: Insights From Predictive Modeling. *Immunol Rev* (2018) 285:97–112. doi: 10.1111/imr.12692
43. Weinberger DM, Simonsen L, Jordan R, Steiner C, Miller M, Viboud C. Impact of the 2009 Influenza Pandemic on Pneumococcal Pneumonia Hospitalizations in the United States. *J Infect Dis* (2012) 205:458–65. doi: 10.1093/infdis/jir749
44. Robinson KM, Kolls JK, Alcorn JF. The Immunology of Influenza Virus-Associated Bacterial Pneumonia. *Curr Opin Immunol* (2015) 34:59–67. doi: 10.1016/j.coi.2015.02.002
45. Rynda-Apple A, Robinson KM, Alcorn JF. Influenza and Bacterial Superinfection: Illuminating the Immunologic Mechanisms of Disease. *Infect Immun* (2015) 83:3764–70. doi: 10.1128/IAI.00298-15
46. Bellinghausen C, Rohde GGU, Savelkoul PHM, Wouters EFM, Stassen FRM. Viral-Bacterial Interactions in the Respiratory Tract. *J Gen Virol* (2016) 97:3089–102. doi: 10.1099/jgv.0.000627
47. Chien Y-W, Klugman KP, Morens DM. Bacterial Pathogens and Death During the 1918 Influenza Pandemic. *N Engl J Med* (2009) 361:2582–3. doi: 10.1056/NEJMc0908216
48. MacIntyre CR, Chughtai AA, Barnes M, Ridda I, Seale H, Toms R, et al. The Role of Pneumonia and Secondary Bacterial Infection in Fatal and Serious Outcomes of Pandemic Influenza a(H1N1)Pdm09. *BMC Infect Dis* (2018) 18:637. doi: 10.1186/s12879-018-3548-0
49. Gill JR, Sheng Z, Ely SF, Guinee DG, Beasley MB, Suh J, et al. Pulmonary Pathologic Findings of Fatal 2009 Pandemic Influenza A/H1N1 Viral Infections. *Arch Pathol Lab Med* (2010) 134:235–43. doi: 10.1043/1543-2165-134.2.235
50. Morens, David M, Taubenberger, Jeffery K, Fauci AS. Predominant Role of Bacterial Pneumonia as a Cause of Death in Pandemic Influenza: Implications for Pandemic Influenza Preparedness. *J Infect Dis* (2008) 198:962–70. doi: 10.1086/591708
51. Petersen E, Koopmans M, Go U, Hamer DH, Petrosillo N, Castelli F, et al. Comparing SARS-CoV-2 With SARS-CoV and Influenza Pandemics. *Lancet Infect Dis* (2020) 20:e238–44. doi: 10.1016/S1473-3099(20)30484-9
52. Abdelrahman Z, Li M, Wang X. Comparative Review of SARS-CoV-2, SARS-CoV, MERS-CoV, and Influenza A Respiratory Viruses. *Front Immunol* (2020) 11:552909. doi: 10.3389/fimmu.2020.552909
53. Simmonds P, Williams S, Harvala H. Understanding the Outcomes of COVID-19 - Does the Current Model of an Acute Respiratory Infection Really Fit? *J Gen Virol* (2021) 102(3):001545. doi: 10.1099/jgv.0.001545
54. Flerlage T, Boyd DF, Meliopoulos V, Thomas PG, Schultz-Cherry S. Influenza Virus and SARS-CoV-2: Pathogenesis and Host Responses in the Respiratory Tract. *Nat Rev Microbiol* (2021) 19:425–41. doi: 10.1038/s41579-021-00542-7
55. Smith AP, Lane LC, Ramirez Zuniga I, Moquin D, Vogel P, Smith AM. Increased Virus Dissemination Leads to Enhanced Lung Injury But Not Inflammation During Influenza-Associated Secondary Bacterial Infection.
56. Myers MA, Smith AP, Lane LC, Moquin DJ, Aogo R, Woolard S, et al. Dynamically Linking Influenza Virus Infection Kinetics, Lung Injury, Inflammation, and Disease Severity. *Elife* (2021) 10:e68864. doi: 10.7554/eLife.68864
57. Granados A, Peci A, McGeer A, Gubbay JB. Influenza and Rhinovirus Viral Load and Disease Severity in Upper Respiratory Tract Infections. *J Clin Virol* (2017) 86:14–9. doi: 10.1016/j.jcv.2016.11.008
58. Oshansky CM, Gartland AJ, Wong SS, Jeevan T, Wang D, Roddam PL, et al. Mucosal Immune Responses Predict Clinical Outcomes During Influenza Infection Independently of Age and Viral Load. *Am J Respir Crit Care Med* (2014) 189:449–62. doi: 10.1164/rccm.201309-1616OC
59. Lee CK, Lee HK, Loh TP, Lai FY, Tambyah PA, Chiu L, et al. Comparison of Pandemic (H1N1) 2009 and Seasonal Influenza Viral Loads, Singapore. *Emerg Infect Dis* (2011) 17:287–91. doi: 10.3201/eid1702.100282
60. Abdulrahman A, Mallah SI, Alqahtani M. COVID-19 Viral Load Not Associated With Disease Severity: Findings From a Retrospective Cohort Study. *BMC Infect Dis* (2021) 21:688. doi: 10.1186/s12879-021-06376-1
61. Cocconcelli E, Castelli G, Onelia F, Lavezzo E, Giraudo C, Bernardinello N, et al. Disease Severity and Prognosis of SARS-CoV-2 Infection in Hospitalized Patients Is Not Associated With Viral Load in Nasopharyngeal Swab. *Front Med (Lausanne)* (2021) 8:714221. doi: 10.3389/fmed.2021.714221
62. Mudd PA, Crawford JC, Turner JS, Souquette A, Reynolds D, Bender D, et al. Distinct Inflammatory Profiles Distinguish COVID-19 From Influenza With Limited Contributions From Cytokine Storm. *Sci Adv* (2020) 6(50): eabe3024. doi: 10.1126/sciadv.abe3024
63. Paget C, Trottein F. COVID-19 and Flu: Conserved or Specific Immune Signature? *Cell Mol Immunol* (2021) 18:245–6. doi: 10.1038/s41423-020-00595-3
64. Zhu L, Yang P, Zhao Y, Zhuang Z, Wang Z, Song R, et al. Single-Cell Sequencing of Peripheral Mononuclear Cells Reveals Distinct Immune Response Landscapes of COVID-19 and Influenza Patients. *Immunity* (2020) 53:685–696 e683. doi: 10.1016/j.immuni.2020.07.009
65. Lee JS, Park S, Jeong HW, Ahn JY, Choi SJ, Lee H, et al. Immunophenotyping of COVID-19 and Influenza Highlights the Role of Type I Interferons in Development of Severe COVID-19. *Sci Immunol* (2020) 5(49):eabd1554. doi: 10.1126/sciimmunol.abd1554
66. Galani IE, Rovina N, Lampropoulou V, Triantafyllia V, Manioudaki M, Pavlos E, et al. Untuned Antiviral Immunity in COVID-19 Revealed by Temporal Type I/III Interferon Patterns and Flu Comparison. *Nat Immunol* (2021) 22:32–40. doi: 10.1038/s41590-020-00840-x
67. Ghoneim HE, Thomas PG, McCullers JA. Depletion of Alveolar Macrophages During Influenza Infection Facilitates Bacterial Superinfections. *J Immunol* (2013) 191:1250–9. doi: 10.4049/jimmunol.1300014
68. Smith AM, Adler FR, Ribeiro RM, Gutenkunst RN, McAuley JL, McCullers JA, et al. Kinetics of Coinfection With Influenza A Virus and Streptococcus Pneumoniae. *PloS Pathog* (2013) 9:e1003238. doi: 10.1371/journal.ppat.1003238
69. Smith AM, Smith AP. A Critical, Nonlinear Threshold Dictates Bacterial Invasion and Initial Kinetics During Influenza. *Sci Rep* (2016) 6(1):38703. doi: 10.1038/srep38703

70. Califano D, Furuya Y, Metzger DW. Effects of Influenza on Alveolar Macrophage Viability Are Dependent on Mouse Genetic Strain. *J Immunol* (2018) 201:134–44. doi: 10.4049/jimmunol.1701406
71. Shahangian A, Chow EK, Tian X, Kang JR, Ghaffari A, Liu SY, et al. Type I IFNs Mediate Development of Postinfluenza Bacterial Pneumonia in Mice. *J Clin Invest* (2009) 119:1910–20. doi: 10.1172/JCI35412
72. McNamee LA, Harmsen AG. Both Influenza-Induced Neutrophil Dysfunction and Neutrophil-Independent Mechanisms Contribute to Increased Susceptibility to a Secondary Streptococcus Pneumoniae Infection. *Infect Immun* (2006) 74:6707–21. doi: 10.1128/IAI.00789-06
73. Knoll R, Schultze JL, Schulte-Schrepping J. Monocytes and Macrophages in COVID-19. *Front Immunol* (2021) 12:720109. doi: 10.3389/fimmu.2021.720109
74. Reusch N, De Domenico E, Bonaguro L, Schulte-Schrepping J, Baßler K, Schultze JL, et al. Neutrophils in COVID-19. *Front Immunol* (2021) 12:652470. doi: 10.3389/fimmu.2021.652470
75. Schulte-Schrepping J, Reusch N, Paclik D, Baßler K, Schlickeiser S, Zhang B, et al. Severe COVID-19 Is Marked by a Dysregulated Myeloid Cell Compartment. *Cell* (2020) 182:1419–1440 e1423. doi: 10.1016/j.cell.2020.08.001
76. Ami Y, Nagata N, Shirato K, Watanabe R, Iwata N, Nakagaki K, et al. Co-Infection of Respiratory Bacterium With Severe Acute Respiratory Syndrome Coronavirus Induces an Exacerbated Pneumonia in Mice. *Microbiol Immunol* (2008) 52:118–27. doi: 10.1111/j.1348-0421.2008.00011.x
77. McCullers JA, Rehg JE. Lethal Synergism Between Influenza Virus and Streptococcus Pneumoniae: Characterization of a Mouse Model and the Role of Platelet-Activating Factor Receptor. *J Infect Dis* (2002) 186:341–50. doi: 10.1086/341462
78. Abramson JS, Lewis JC, Lyles DS, Heller KA, Mills EL, Bass DA, et al. Inhibition of Neutrophil Lysosome-Phagosome Fusion Associated With Influenza Virus Infection *In Vitro*. Role in Depressed Bactericidal Activity. *J Clin Invest* (1982) 69:1393–7. doi: 10.1172/JCI110580
79. Abramson JS, Wheeler JG. Virus-Induced Neutrophil Dysfunction: Role in the Pathogenesis of Bacterial Infections. *Pediatr Infect Dis J* (1994) 13:643–52. doi: 10.1097/00006454-199407000-00012
80. Colamussi ML, White MR, Crouch E, Hartshorn KL. Influenza A Virus Accelerates Neutrophil Apoptosis and Markedly Potentiates Apoptotic Effects of Bacteria. *Blood* (1999) 93:2395–403. doi: 10.1182/blood.V93.7.2395
81. Engelich G, White M, Hartshorn KL. Neutrophil Survival Is Markedly Reduced by Incubation With Influenza Virus and Streptococcus Pneumoniae: Role of Respiratory Burst. *J Leukoc Biol* (2001) 69:50–6. doi: 10.1189/jlb.69.1.50
82. Smith AP, Lane LC, van Opijnen T, Woolard S, Carter R, Iverson A, et al. Dynamic Pneumococcal Genetic Adaptations Support Bacterial Growth and Inflammation During Coinfection With Influenza. *Infect Immun* (2021) 89:e0002321. doi: 10.1128/IAI.00023-21
83. Shepardson KM, Larson K, Morton RV, Prigge JR, Schmidt EE, Huber VC, et al. Differential Type I Interferon Signaling Is a Master Regulator of Susceptibility to Postinfluenza Bacterial Superinfection. *MBio* (2016) 7(3):e00506-16. doi: 10.1128/mBio.00506-16
84. McCullers JA. Insights Into the Interaction Between Influenza Virus and Pneumococcus. *Clin Microbiol Rev* (2006) 19:571–82. doi: 10.1128/CMR.00058-05
85. Kash JC, Taubenberger JK. The Role of Viral, Host, and Secondary Bacterial Factors in Influenza Pathogenesis. *Am J Pathol* (2015) 185:1528–36. doi: 10.1016/j.ajpath.2014.08.030
86. Chu H, Chan JF, Wang Y, Yuen TT, Chai Y, Hou Y, et al. Comparative Replication and Immune Activation Profiles of SARS-CoV-2 and SARS-CoV in Human Lungs: An *Ex Vivo* Study With Implications for the Pathogenesis of COVID-19. *Clin Infect Dis* (2020) 71:1400–9. doi: 10.1093/cid/ciaa410
87. Lv J, Wang Z, Qu Y, Zhu H, Zhu Q, Tong W, et al. Distinct Uptake, Amplification, and Release of SARS-CoV-2 by M1 and M2 Alveolar Macrophages. *Cell Discov* (2021) 7:24. doi: 10.1038/s41421-021-00258-1
88. Dalskov L, Møhlenberg M, Thyrsted J, Blay-Cadanet J, Poulsen ET, Folkersen BH, et al. SARS-CoV-2 Evades Immune Detection in Alveolar Macrophages. *EMBO Rep* (2020) 21:e51252. doi: 10.15252/embr.202051252
89. Grant RA, Morales-Nebreda L, Markov NS, Swaminathan S, Querrey M, Guzman ER, et al. Circuits Between Infected Macrophages and T Cells in SARS-CoV-2 Pneumonia. *Nature* (2021) 590:635–41. doi: 10.1038/s41586-020-03148-w
90. Taefehshokr N, Taefehshokr S, Hemmat N, Heit B. Covid-19: Perspectives on Innate Immune Evasion. *Front Immunol* (2020) 11:580641. doi: 10.3389/fimmu.2020.580641
91. Beyer DK, Forero A. Mechanisms of Antiviral Immune Evasion of SARS-CoV-2. *J Mol Biol* (2021) 167265. doi: 10.1016/j.jmb.2021.167265
92. Lazarevic I, Pravica V, Miljanovic D, Cupic M. Immune Evasion of SARS-CoV-2 Emerging Variants: What Have We Learnt So Far? *Viruses* (2021) 13(7):1192. doi: 10.3390/v13071192
93. Sette A, Crotty S. Adaptive Immunity to SARS-CoV-2 and COVID-19. *Cell* (2021) 184:861–80. doi: 10.1016/j.cell.2021.01.007
94. Schmolke M, Garcia-Sastre A. Evasion of Innate and Adaptive Immune Responses by Influenza A Virus. *Cell Microbiol* (2010) 12:873–80. doi: 10.1111/j.1462-5822.2010.01475.x
95. Kikkert M. Innate Immune Evasion by Human Respiratory RNA Viruses. *J Innate Immun* (2020) 12:4–20. doi: 10.1159/000503030
96. Blevins LK, Wren JT, Holbrook BC, Hayward SL, Swords WE, Parks GD, et al. Coinfection With Streptococcus Pneumoniae Negatively Modulates the Size and Composition of the Ongoing Influenza-Specific CD8 + T Cell Response. *J Immunol* (2014) 193:5076–87. doi: 10.4049/jimmunol.1400529
97. Rowe HM, Meliopoulos VA, Iverson A, Bomme P, Schultz-Cherry S, Rosch JW. Direct Interactions With Influenza Promote Bacterial Adherence During Respiratory Infections. *Nat Microbiol* (2019) 4:1328–36. doi: 10.1038/s41564-019-0447-0
98. Warnking K, Klemm C, Löffler B, Niemann S, van Krüchten A, Peters G, et al. Super-Infection With S Taphylococcus Aureus Inhibits Influenza Virus-Induced Type I IFN Signalling Through Impaired STAT1-STAT2 Dimerization: Influenza Virus- and S. Aureus -Mediated Signalling. *Cell Microbiol* (2015) 17:303–17. doi: 10.1111/cmi.12375
99. Mathew D, Giles JR, Baxter AE, Oldridge DA, Greenplate AR, Wu JE, et al. Deep Immune Profiling of COVID-19 Patients Reveals Distinct Immunotypes With Therapeutic Implications. *Science* (2020) 369:1210. doi: 10.1126/science.abc8511
100. Song JW, Zhang C, Fan X, Meng P, Xu Z, Xia P, et al. Immunological and Inflammatory Profiles in Mild and Severe Cases of COVID-19. *Nat Commun* (2020) 11:3410. doi: 10.1038/s41467-020-17240-2
101. Kuri-Cervantes L, Pampena MB, Meng W, Rosenfeld AM, Ittner CAG, Weisman AR, et al. Comprehensive Mapping of Immune Perturbations Associated With Severe COVID-19. *Sci Immunol* (2020) 5:eabd7114. doi: 10.1126/sciimmunol.abd7114
102. Zheng HY, Zhang M, Yang CX, Zhang N, Wang XC, Yang XP, et al. Elevated Exhaustion Levels and Reduced Functional Diversity of T Cells in Peripheral Blood May Predict Severe Progression in COVID-19 Patients. *Cell Mol Immunol* (2020) 17:541–3. doi: 10.1038/s41423-020-0401-3
103. Diao B, Wang C, Tan Y, Chen X, Liu Y, Ning L, et al. Reduction and Functional Exhaustion of T Cells in Patients With Coronavirus Disease 2019 (COVID-19). *Front Immunol* (2020) 11:827. doi: 10.3389/fimmu.2020.00827
104. Brueggemann AB, Jansen van Rensburg MJ, Shaw D, McCarthy ND, Jolley KA, Maiden MCJ, et al. Changes in the Incidence of Invasive Disease Due to Streptococcus Pneumoniae, Haemophilus Influenzae, and Neisseria Meningitidis During the COVID-19 Pandemic in 26 Countries and Territories in the Invasive Respiratory Infection Surveillance Initiative: A Prospective Analysis of Surveillance Data. *Lancet Digit Health* (2021) 3:e360–70. doi: 10.1016/S2589-7500(21)00077-7
105. Huh K, Kim Y, Ji W, Kim DW, Lee E, Kim J, et al. Decrease in Hospital Admissions for Respiratory Diseases During the COVID-19 Pandemic: A Nationwide Claims Study. *Thorax* (2021) 76:939–41. doi: 10.1136/thoraxjnl-2020-216526
106. Rodgers L, Sheppard M, Smith A, Dietz S, Jayanthi P, Yuan Y, Bull L, et al. Changes in Seasonal Respiratory Illnesses in the United States During the Coronavirus Disease 2019 (COVID-19) Pandemic. *Clin Infect Dis* (2021) 73:S110–7. doi: 10.1093/cid/ciab311
107. Olsen SJ, Winn AK, Budd AP, Prill MM, Steel J, Midgley CM, et al. Changes in Influenza and Other Respiratory Virus Activity During the COVID-19

Pandemic-United States, 2020-2021. *Am J Transplant* (2021) 21:3481–6. doi: 10.1111/ajt.16049
108. Huang QS, Wood T, Jelley L, Jennings T, Jefferies S, Daniells K, et al. Impact of the COVID-19 Nonpharmaceutical Interventions on Influenza and Other Respiratory Viral Infections in New Zealand. *Nat Commun* (2021) 12:1001. doi: 10.1038/s41467-021-21157-9
109. Antonelli M, Penfold R, Merino J, Sudre C, Molteni E, Berry S, et al. Risk Factors and Disease Profile of Post-Vaccination SARS-CoV-2 Infection in UK Users of the COVID Symptom Study App: A Prospective, Community-Based, Nested, Case-Control Study. *Lancet Infect Dis* (2021) 22(1):43–55. doi: 10.1016/S1473-3099(21)00460-6
110. Tenforde MW, Self WH, Adams K, Gaglani M, Ginde AA, McNeal T, et al. Association Between mRNA Vaccination and COVID-19 Hospitalization and Disease Severity. *JAMA* (2021) 326(20):2043–54. doi: 10.1001/jama.2021.19499
111. National Center for Immunization and Respiratory Diseases (NCIRD), D. o. V. D. *The Possibility of COVID-19 After Vaccination: Breakthrough Infections* (2021). Available at: https://www.cdc.gov/coronavirus/2019-ncov/vaccines/effectiveness/why-measure-effectiveness/breakthrough-cases.html.
112. Hament JM, Kimpen JL, Fleer A, Wolfs TF. Respiratory Viral Infection Predisposing for Bacterial Disease: A Concise Review. *FEMS Immunol Med Microbiol* (1999) 26:189–95. doi: 10.1111/j.1574-695X.1999.tb01389.x
113. Karlström Å, Heston SM, Boyd KL, Tuomanen EI, McCullers JA. Toll-Like Receptor 2 Mediates Fatal Immunopathology in Mice During Treatment of Secondary Pneumococcal Pneumonia Following Influenza. *J Infect Dis* (2011) 204:1358–66. doi: 10.1093/infdis/jir522
114. LeVine AM, Koeningsknecht V, Stark JM. Decreased Pulmonary Clearance of S. Pneumoniae Following Influenza A Infection in Mice. *J Virol Methods* (2001) 94:173–86. doi: 10.1016/S0166-0934(01)00287-7
115. Verma AK, Bansal S, Bauer C, Muralidharan A, Sun K. Influenza Infection Induces Alveolar Macrophage Dysfunction and Thereby Enables Noninvasive Streptococcus Pneumoniae to Cause Deadly Pneumonia. *J Immunol* (2020) 205:1601–7. doi: 10.4049/jimmunol.2000094
116. Hang do TT, Choi EJ, Song JY, Kim SE, Kwak J, Shin YK, et al. Differential Effect of Prior Influenza Infection on Alveolar Macrophage Phagocytosis of Staphylococcus Aureus and Escherichia Coli: Involvement of Interferon-Gamma Production. *Microbiol Immunol* (2011) 55:751–9. doi: 10.1111/j.1348-0421.2011.00383.x
117. Shibata T, Makino A, Ogata R, Nakamura S, Ito T, Nagata K, et al. Respiratory Syncytial Virus Infection Exacerbates Pneumococcal Pneumonia *via* Gas6/Axl-Mediated Macrophage Polarization. *J Clin Invest* (2020) 130:3021–37. doi: 10.1172/JCI125505
118. McCullers JA, Bartmess KC. Role of Neuraminidase in Lethal Synergism Between Influenza Virus and Streptococcus Pneumoniae. *J Infect Dis* (2003) 187:1000–9. doi: 10.1086/368163
119. Plotkowski MC, Puchelle E, Beck G, Jacquot J, Hannoun C. Adherence of Type I Streptococcus Pneumoniae to Tracheal Epithelium of Mice Infected With Influenza A/PR8 Virus. *Am Rev Respir Dis* (1986) 134:1040–4. doi: 10.1164/arrd.1986.134.5.1040
120. Avadhanula V, Rodriguez CA, Devincenzo P, Wang Y, Webby RJ, Ulett GC, et al. Respiratory Viruses Augment the Adhesion of Bacterial Pathogens to Respiratory Epithelium in a Viral Species- and Cell Type-Dependent Manner. *J Virol* (2006) 80:1629–36. doi: 10.1128/JVI.80.4.1629-1636.2006
121. Stark JM, Stark MA, Colasurdo GN, LeVine AM. Decreased Bacterial Clearance From the Lungs of Mice Following Primary Respiratory Syncytial Virus Infection. *J Med Virol* (2006) 78:829–38. doi: 10.1002/jmv.20631
122. Rezaee F, DeSando SA, Ivanov AI, Chapman TJ, Knowlden SA, Beck LA, et al. Sustained Protein Kinase D Activation Mediates Respiratory Syncytial Virus-Induced Airway Barrier Disruption. *J Virol* (2013) 87:11088–95. doi: 10.1128/JVI.01573-13
123. Ruan T, Sun J, Liu W, Prinz RA, Peng D, Liu X, Xu X, et al. H1N1 Influenza Virus Cross-Activates Gli1 to Disrupt the Intercellular Junctions of Alveolar Epithelial Cells. *Cell Rep* (2020) 31:107801. doi: 10.1016/j.celrep.2020.107801
124. Shepley-McTaggart A, Sagum CA, Oliva I, Rybakovsky E, DiGuilio K, Liang J, et al. SARS-CoV-2 Envelope (E) Protein Interacts With PDZ-Domain-2 of Host Tight Junction Protein ZO1. *PloS One* (2021) 16:e0251955. doi: 10.1371/journal.pone.0251955
125. De Maio F, Lo Cascio E, Babini G, Sali M, Della Longa S, Tilocca B, et al. Improved Binding of SARS-CoV-2 Envelope Protein to Tight Junction-Associated PALS1 Could Play a Key Role in COVID-19 Pathogenesis. *Microbes Infect* (2020) 22:592–7. doi: 10.1016/j.micinf.2020.08.006
126. Teoh KT, Siu YL, Chan WL, Schlüter MA, Liu CJ, Peiris JS, et al. The SARS Coronavirus E Protein Interacts With PALS1 and Alters Tight Junction Formation and Epithelial Morphogenesis. *Mol Biol Cell* (2010) 21:3838–52. doi: 10.1091/mbc.E10-04-0338
127. Nakamura S, Davis KM, Weiser JN. Synergistic Stimulation of Type I Interferons During Influenza Virus Coinfection Promotes Streptococcus Pneumoniae Colonization in Mice. *J Clin Invest* (2011) 121:3657–65. doi: 10.1172/JCI57762
128. Channappanavar R, Fehr AR, Vijay R, Mack M, Zhao J, Meyerholz DK, et al. Dysregulated Type I Interferon and Inflammatory Monocyte-Macrophage Responses Cause Lethal Pneumonia in SARS-CoV-Infected Mice. *Cell Host Microbe* (2016) 19:181–93. doi: 10.1016/j.chom.2016.01.007
129. Zhou Z, Ren L, Zhang L, Zhong J, Xiao Y, Jia Z, et al. Heightened Innate Immune Responses in the Respiratory Tract of COVID-19 Patients. *Cell Host Microbe* (2020) 27:883–890 e882. doi: 10.1016/j.chom.2020.04.017
130. Blanco-Melo D, Nilsson-Payant BE, Liu WC, Uhl S, Hoagland D, Møller R, et al. Imbalanced Host Response to SARS-CoV-2 Drives Development of COVID-19. *Cell* (2020) 181:1036–1045 e1039. doi: 10.1016/j.cell.2020.04.026
131. Weeks-Gorospe JN, Hurtig HR, Iverson AR, Schuneman MJ, Webby RJ, McCullers JA, et al. Naturally Occurring Swine Influenza A Virus PB1-F2 Phenotypes That Contribute to Superinfection With Gram-Positive Respiratory Pathogens. *J Virol* (2012) 86:9035–43. doi: 10.1128/JVI.00369-12
132. Iverson AR, Boyd KL, McAuley JL, Plano LR, Hart ME, McCullers JA, et al. Influenza Virus Primes Mice for Pneumonia From Staphylococcus Aureus. *J Infect Dis* (2011) 203:880–8. doi: 10.1093/infdis/jiq113
133. Tashiro M, Ciborowski P, Klenk HD, Pulverer G, Rott R. Role of Staphylococcus Protease in the Development of Influenza Pneumonia. *Nature* (1987) 325:536–7. doi: 10.1038/325536a0
134. Hament JM, Aerts PC, Fleer A, van Dijk H, Harmsen T, Kimpen JL, et al. Direct Binding of Respiratory Syncytial Virus to Pneumococci: A Phenomenon That Enhances Both Pneumococcal Adherence to Human Epithelial Cells and Pneumococcal Invasiveness in a Murine Model. *Pediatr Res* (2005) 58:1198–203. doi: 10.1203/01.pdr.0000188699.55279.1b
135. Weiser JN, Ferreira DM, Paton JC. Streptococcus Pneumoniae: Transmission, Colonization and Invasion. *Nat Rev Microbiol* (2018) 16:355–67. doi: 10.1038/s41579-018-0001-8
136. Hoffmann J, Machado D, Terrier O, Pouzol S, Messaoudi M, Basualdo W, et al. Viral and Bacterial Co-Infection in Severe Pneumonia Triggers Innate Immune Responses and Specifically Enhances IP-10: A Translational Study. *Sci Rep* (2016) 6:38532. doi: 10.1038/srep38532
137. Machado D, Hoffmann J, Moroso M, Rosa-Calatrava M, Endtz H, Terrier O, et al. RSV Infection in Human Macrophages Promotes CXCL10/IP-10 Expression During Bacterial Co-Infection. *Int J Mol Sci* (2017) 18:2654. doi: 10.3390/ijms18122654
138. Taghavi S, Jackson-Weaver O, Abdullah S, Wanek A, Drury R, Packer J, et al. Interleukin-22 Mitigates Acute Respiratory Distress Syndrome (ARDS). *PloS One* (2021) 16:e0254985. doi: 10.1371/journal.pone.0254985
139. Xu F, Liu Q, Lin S, Shen N, Yin Y, Cao J, et al. IL-27 Is Elevated in Acute Lung Injury and Mediates Inflammation. *J Clin Immunol* (2013) 33:1257–68. doi: 10.1007/s10875-013-9923-0
140. Pociask DA, Scheller EV, Mandalapu S, McHugh KJ, Enelow RI, Fattman CL, et al. IL-22 is Essential for Lung Epithelial Repair Following Influenza Infection. *Am J Pathol* (2013) 182:1286–96. doi: 10.1016/j.ajpath.2012.12.007
141. Liu FD, Kenngott EE, Schröter MF, Kühl A, Jennrich S, Watzlawick R, et al. Timed Action of IL-27 Protects From Immunopathology While Preserving Defense in Influenza. *PloS Pathog* (2014) 10:e1004110. doi: 10.1371/journal.ppat.1004110
142. Ivanov S, Renneson J, Fontaine J, Barthelemy A, Paget C, Fernandez EM, et al. Interleukin-22 Reduces Lung Inflammation During Influenza A Virus Infection and Protects Against Secondary Bacterial Infection. *J Virol* (2013) 87:6911–24. doi: 10.1128/JVI.02943-12
143. Barthelemy A, Sencio V, Soulard D, Deruyter L, Faveeuw C, Le Goffic R, et al. Interleukin-22 Immunotherapy During Severe Influenza Enhances Lung

Tissue Integrity and Reduces Secondary Bacterial Systemic Invasion. *Infect Immun* (2018) 86:e00706-17. doi: 10.1128/IAI.00706-17
144. Weitnauer M, Mijosek V, Dalpke AH. Control of Local Immunity by Airway Epithelial Cells. *Mucosal Immunol* (2016) 9:287–98. doi: 10.1038/mi.2015.126
145. Atamas SP, Chapoval SP, Keegan AD. Cytokines in Chronic Respiratory Diseases. *F1000 Biol Rep* (2013) 5:3. doi: 10.3410/B5-3
146. Gieseck RL3rd, Wilson MS, Wynn TA. Type 2 Immunity in Tissue Repair and Fibrosis. *Nat Rev Immunol* (2018) 18:62–76. doi: 10.1038/nri.2017.90
147. Fulkerson PC, Fischetti CA, Hassman LM, Nikolaidis NM, Rothenberg ME. Persistent Effects Induced by IL-13 in the Lung. *Am J Respir Cell Mol Biol* (2006) 35:337–46. doi: 10.1165/rcmb.2005-0474OC
148. Marone G, Granata F, Pucino V, Pecoraro A, Heffler E, Loffredo S, et al. The Intriguing Role of Interleukin 13 in the Pathophysiology of Asthma. *Front Pharmacol* (2019) 10:1387. doi: 10.3389/fphar.2019.01387
149. Smith AM, Huber VC. The Unexpected Impact of Vaccines on Secondary Bacterial Infections Following Influenza. *Viral Immunol* (2018) 31:159–73. doi: 10.1089/vim.2017.0138
150. Haas EJ, Angulo FJ, McLaughlin JM, Anis E, Singer SR, Khan F, et al. Impact and Effectiveness of mRNA BNT162b2 Vaccine Against SARS-CoV-2 Infections and COVID-19 Cases, Hospitalisations, and Deaths Following a Nationwide Vaccination Campaign in Israel: An Observational Study Using National Surveillance Data. *Lancet* (2021) 397:1819–29. doi: 10.1016/S0140-6736(21)00947-8
151. Polack FP, Thomas SJ, Kitchin N, Absalon J, Gurtman A, Lockhart S, et al. Safety and Efficacy of the BNT162b2 mRNA Covid-19 Vaccine. *N Engl J Med* (2020) 383:2603–15. doi: 10.1056/NEJMoa2034577
152. Dagan N, Barda N, Kepten E, Miron O, Perchik S, Katz MA, et al. BNT162b2 mRNA Covid-19 Vaccine in a Nationwide Mass Vaccination Setting. *N Engl J Med* (2021) 384:1412–23. doi: 10.1056/NEJMoa2101765
153. Baden LR, El Sahly HM, Essink B, Kotloff K, Frey S, Novak R, et al. Efficacy and Safety of the mRNA-1273 SARS-CoV-2 Vaccine. *N Engl J Med* (2021) 384:403–16. doi: 10.1056/NEJMoa2035389
154. Bergwerk M, Gonen T, Lustig Y, Amit S, Lipsitch M, Cohen C, et al. Covid-19 Breakthrough Infections in Vaccinated Health Care Workers. *N Engl J Med* (2021) 385:1474–84. doi: 10.1056/NEJMoa2109072
155. Lipsitch M, Krammer F, Regev-Yochay G, Lustig Y, Balicer RD. SARS-CoV-2 Breakthrough Infections in Vaccinated Individuals: Measurement, Causes and Impact. *Nat Rev Immunol* (2022) 22:57–65. doi: 10.1038/s41577-021-00662-4
156. Brown C, Vostok J, Johnson H, Burns M, Gharpure R, Sami S, et al. Outbreak of SARS-CoV-2 Infections, Including COVID-19 Vaccine Breakthrough Infections, Associated With Large Public Gatherings - Barnstable County, Massachusetts, July 2021. *MMWR Morb Mortal Wkly Rep* (2021) 70:1059–62. doi: 10.15585/mmwr.mm7031e2
157. Hacisuleyman E, Hale C, Saito Y, Blachere NE, Bergh M, Conlon EG, et al. Vaccine Breakthrough Infections With SARS-CoV-2 Variants. *N Engl J Med* (2021) 384:2212–8. doi: 10.1056/NEJMoa2105000
158. McCray Jr PB, Pewe L, Wohlford-Lenane C, Hickey M, Manzel L, Shi L, et al. Lethal Infection of K18-Hace2 Mice Infected With Severe Acute Respiratory Syndrome Coronavirus. *J Virol* (2007) 81:813–21. doi: 10.1128/JVI.02012-06
159. Monaco G, Chen H, Poidinger M, Chen J, de Magalhães JP, Larbi A, et al. flowAI: Automatic and Interactive Anomaly Discerning Tools for Flow Cytometry Data. *Bioinformatics* (2016) 32:2473–80. doi: 10.1093/bioinformatics/btw191

Conflict of Interest: The authors declare that the research was conducted in the absence of any commercial or financial relationships that could be construed as a potential conflict of interest.

Publisher's Note: All claims expressed in this article are solely those of the authors and do not necessarily represent those of their affiliated organizations, or those of the publisher, the editors and the reviewers. Any product that may be evaluated in this article, or claim that may be made by its manufacturer, is not guaranteed or endorsed by the publisher.

frontiers | Frontiers in Immunology

REVIEW
published: 17 May 2022
doi: 10.3389/fimmu.2022.870216

Therapy Targets SARS-CoV-2 Infection-Induced Cell Death

Zhoujie Zhu[1], Jiayi Shi[1], Long Li[1,2], Jinling Wang[3]*, Yufen Zhao[1,2] and Huabin Ma[1,2]**

[1] Institute of Drug Discovery Technology, Ningbo University, Ningbo, China, [2] Qian Xuesen Collaborative Research Center of Astrochemistry and Space Life Sciences, Ningbo University, Ningbo, China, [3] School of Medicine, Xiamen University, Xiamen, China

Coronavirus Disease 2019 (COVID-19) caused by SARS-CoV-2 has become a global health issue. The clinical presentation of COVID-19 is highly variable, ranging from asymptomatic and mild disease to severe. However, the mechanisms for the high mortality induced by SARS-CoV-2 infection are still not well understood. Recent studies have indicated that the cytokine storm might play an essential role in the disease progression in patients with COVID-19, which is characterized by the uncontrolled release of cytokines and chemokines leading to acute respiratory distress syndrome (ARDS), multi-organ failure, and even death. Cell death, especially, inflammatory cell death, might be the initiation of a cytokine storm caused by SARS-CoV-2 infection. This review summarizes the forms of cell death caused by SARS-CoV-2 *in vivo* or *in vitro* and elaborates on the dedication of apoptosis, necroptosis, NETosis, pyroptosis of syncytia, and even SARS-CoV-2 E proteins forming channel induced cell death, providing insights into targets on the cell death pathway for the treatment of COVID-19.

Keywords: SARS-CoV-2, cell death, apoptosis, necroptosis, syncytia pyroptosis

OPEN ACCESS

Edited by:
Tengchuan Jin,
University of Science and Technology of China, China

Reviewed by:
Zhenlong Liu,
McGill University, Canada
Ahmed Yaqinuddin,
Alfaisal University, Saudi Arabia

***Correspondence:**
Long Li
lilong@nbu.edu.cn
Jinling Wang
wjl0920@qq.com
Huabin Ma
mahuabin@nbu.edu.cn

Specialty section:
This article was submitted to Viral Immunology, a section of the journal Frontiers in Immunology

Received: *06 February 2022*
Accepted: *19 April 2022*
Published: *17 May 2022*

Citation:
Zhu Z, Shi J, Li L, Wang J, Zhao Y and Ma H (2022) Therapy Targets SARS-CoV-2 Infection-Induced Cell Death. Front. Immunol. 13:870216. doi: 10.3389/fimmu.2022.870216

INTRODUCTION

Human coronaviruses (HCoVs) are known respiratory pathogens that could cause multiple respiratory diseases, ranging from the common cold and bronchitis to serious pneumonia (1, 2). Three of these viruses have been causing serious symptoms over the last years, including Severe Acute Respiratory Syndrome (SARS), Middle East Respiratory Syndrome Coronavirus (MERS), and now SARS Coronavirus 2 (SARS-CoV-2), especially SARS-CoV-2, which is responsible for the Coronavirus Disease 2019 (COVID-19) and has become a pandemic worldwide, causing millions of deaths and massive property losses (3–7). SARS-CoV-2 is a single-stranded RNA virus; belongs to the β-coronavirus; contains 29,903 nucleotides; encodes 16 non-structural proteins (NSP1–NSP16), 9 putative accessory factors, and 4 structural proteins, i.e., spike (S), envelope (E), membrane (M), and nucleocapsid (N); and spreads *via* respiratory droplets or close contact, which triggers mild or severe diseases (8–11) (**Figure 1A**). The main clinical symptoms of infected patients are cough, fever, and tachypnea; a CT scan usually reveals multiple patchy shadows. Severe infection can cause cytokine storms within the body, leading to multi-organ failure and even death (12–14). Cytokine storm is a life-threatening systemic inflammatory response syndrome that can be induced by pathogens, autoimmune disorders, or inflammatory cell death (15–18).

The autopsy of patients infected with SARS-CoV-2 is of great significance to truly understand the pathological changes of COVID-19 (19–27). Gupta et al. have well-reviewed that SARS-CoV-2

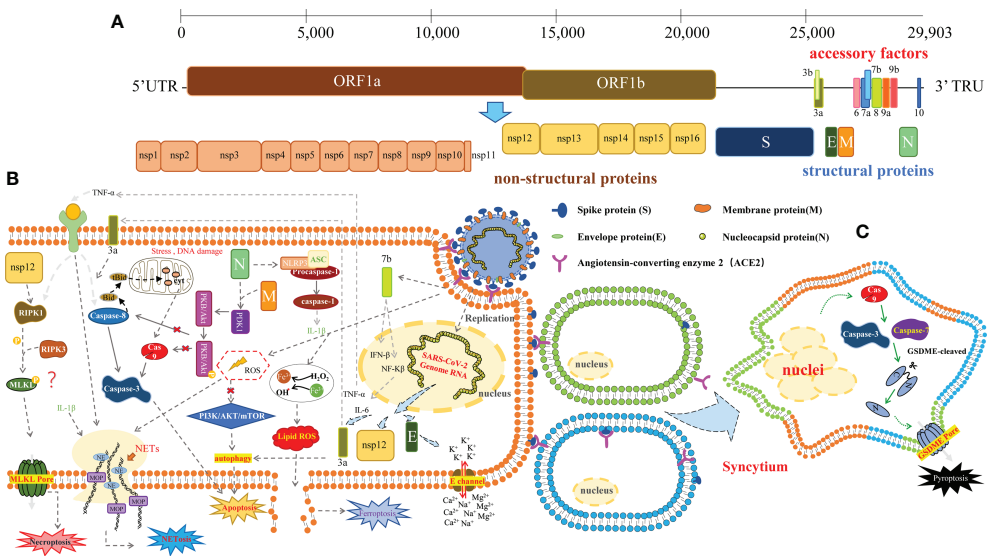

FIGURE 1 | The schematic of SARS-CoV-2-induced cell death. **(A)** The SARS-CoV-2 virus particle and genome. The genome is a single-stranded RNA genome of which the full length is 29,903 bp. It includes ORF1a and ORF1b, which encode the 16 non-structural proteins, 9 accessory factors, and 4 structural proteins: spike protein (S), envelope protein (E), mbrane protein (M), and nucleocapsid protein (N). **(B)** SARS-CoV-2 induces various cellular stress: *apoptosis*, triggered by the extrinsic pathway (death receptor pathway), or the intrinsic pathway (mitochondrial pathway), involving the caspase cleavage. SARS-CoV-2 ORF3a caused apoptosis *via* the caspase-8/Bid extrinsic pathway; ORF7b can activate TNFα-induced apoptosis. Membrane (M) protein with nucleocapsid (N) protein *via* interacting with PDK1 and inhibiting the activation of PDK1-PKB/Akt signaling to trigger caspase-dependent apoptosis. Another structural protein spike of SARS-CoV-2 also induced autophagy and apoptosis by ROS-suppressed PI3K/AKT/mTOR signaling; *necroptosis*, mediated by RIPK1/RIPK3/MLKL. MLKL can be recruited by the autophosphorylated RIPK3 and subsequently phosphorylated by RIPK3 of human MLKL. Phosphorylated MLKL will form an MLKL pore, resulting in necroptosis. Nsp12 interacted with RIPK1 and activated it; *NLRP3 inflammasome*, consisting of NLRP3, ASC, and caspase-1, activated by N protein of SARS-CoV-2 interacted directly with NLRP3; SARS-CoV-2 E proteins form cation channels to trigger cell death independent of MLKL and gasdermins; NETosis, triggered by neutrophils and formed neutrophil extracellular traps (NETs) to release of chromatin structures containing myeloperoxidase and antimicrobial proteins to neutralize intruders. MPO, myeloperoxidase; NE, Neutrophil Elastase. *Ferroptosis*, triggered by iron accumulation and overload, or reactive oxygen species (ROS). **(C)** *Pyroptosis*, mediated by the gasdermin (GSDM) protein family. The N-terminal fragments of GSDM protein could induce the formation of membrane pores. SARS-CoV-2 S induces cell–cell fusion and syncytia formation driving caspase-9/GSDME-mediated syncytia pyroptosis.

infection caused various injuries ranging from substantial respiratory to many extrapulmonary organs failure, including thrombotic complications, myocardial dysfunction and arrhythmia, acute coronary syndromes, acute kidney injury (AKI), gastrointestinal symptoms, hepatocellular injury, hyperglycemia and ketosis, neurologic illnesses, ocular symptoms, and dermatologic complications (28). Here, we mainly summarized how the different types of cell death caused by SARS-CoV-2 infection contribute to the organic failure directly, or indirectly, and discussed the therapy targets on the cell death signaling transduction molecules for treatment for COVID-19.

MULTIPLE CELL DEATH PATHWAYS WERE INDUCED IN SARS-COV-2 INFECTION

The cytopathic effect of cell death caused by the virus invading the host cells is a common result after the infection (29). Cell death in some instances can inhibit viral replication, but in more cases, it can enhance viral dissemination and affect the physiology of cells, leading to tissue and organ damage (30). The replication of coronaviruses in cells is regulated by many host factors, which can induce drastic structural and physiological changes in cells (2). During infection, SARS-CoV-2 could induce diverse cell death pathways (31, 32), such as apoptosis, necroptosis, pyroptosis, and NETosis in the host cells (**Figure 1B**).

Apoptosis is a major type of programmed cell death, morphologically characterized by cellular shrinkage, nuclear condensation, chromosomal DNA fragmentation, cytosolic membrane blebbing, and apoptotic body formation. It is triggered by the extrinsic (death receptor pathway) pathway, or the intrinsic (mitochondrial pathway) pathway, involving a group of cysteinyl aspartate proteases (caspases) cleavage (activation) (33–37).

SARS-CoV-2 infection can induce apoptosis *via* a variety of signaling pathways. It has been reported that the accessory protein ORF3a of SARS-CoV-1 caused cell death, vesicle formation, and Golgi fragmentation in VERO cells (38). To survey whether SARS-CoV-2 ORF3a can induce apoptosis, Ren and colleagues (39) overexpressed SARS-CoV-2 ORF3a in cultured HEK293T, HepG2, and VERO E6 cells; then stained the cells by annexin V-fluorescein 5-isothiocyanate (FITC)/propidium iodide (PI); and analyzed the apoptotic cells by flow

cytometry. They found that SARS-CoV-2 ORF3a caused apoptosis *via* the caspase-8/Bid extrinsic pathway, which can be restored by z-VAD-fmk, a pan-caspase inhibitor. Importantly, SARS-CoV-2 ORF3a showed weaker proapoptotic activity than SARS-CoV-1 ORF3a in cultured cells, which might lead the virus to spread more widely. Consistently, two more groups demonstrated that SARS-CoV-2 ORF3a inhibited autophagic flux by blocking the fusion of autophagosomes/amphisomes with lysosomes, causing lysosomal destruction, which allowed the virus to escape the degradation by lysosomal (40, 41). These studies facilitated strategies targeting SARS-CoV-2 ORF3a or autophagic pathway for conferring potential protection against the spread of SARS-CoV-2. In support of this concept, a study by Gassen and colleagues demonstrated that targeting autophagic pathways on the polyamine pathway, and the control of BECN1 abundance through AKT1/SKP2 signaling by exogenous administration of spermidine and spermine, the selective AKT1 inhibitor MK-2206, and the BECN1-stabilizing anthelmintic drug niclosamide inhibited SARS-CoV-2 propagation *in vitro* and *in vivo* (42). Thus, both MK-2206 and niclosamide might be promising candidates for clinical trials.

ORF7b is another accessory protein of SARS-CoV-2, which can induce the transcription of IFN-β, TNF-α, and IL-6, activating type-I IFN signaling through IRF3 phosphorylation and activating TNFα-induced apoptosis in HEK293T cells and VERO E6 cells (43).

The membrane glycoprotein M of SARS-CoV-2 could trigger caspase-dependent apoptosis with the assistance of the nucleocapsid (N) protein *via* interacting with PDK1 and inhibiting the activation of PDK1-PKB/Akt signaling. Disruption of the M–N interaction by certain rationally designed peptides, abolished M-induced apoptosis, shedding light on a new aspect of drug designs on M–N interaction to prevent SARS-CoV-2 infection, which caused apoptosis (44).

Another structural protein spike of SARS-CoV-2 also induced autophagy and apoptosis in human bronchial epithelial and microvascular endothelial cells by reactive oxygen species (ROS)-suppressed PI3K/AKT/mTOR signaling, which then led to inflammatory responses, raising important implications for developing anti-inflammatory therapies, such as ROS and autophagy inhibitors, for COVID-19 patients (45).

In addition, a clinical report showed that a total of 17 of the 18 patients who died of COVID-19 suffered from lymphocytopenia, which is the main feature of severe COVID-19 disease (46). TUNEL staining showed that spleens and hilar lymph nodes (LNs) exhibited many lymphocyte apoptosis processes, which were caused by SARS-CoV-2 promoting Fas-mediated apoptosis of T and B lymphocytes.

Further, elevated serum levels of creatinine, tubular necrosis, and renal inflammation were observed in critically ill COVID-19 patients, consistent with AKI symptoms (47–49). To identify and uncover mechanisms specifically related to a SARS-CoV-2 protein that can induce cell death in AKI after SARS-CoV-2 infection, the SARS-CoV-2 nucleocapsid (N) structural protein-expressing plasmid was delivered into the normal mouse kidneys using a well-established non-invasive ultrasound-microbubble technique, which can induce AKI and exacerbate AKI under ischemic stress conditions. The mechanism lies in SARS-CoV-2 N interacting with Smad3 and enhances TGF-β/Smad3 signaling to arrest the G1 cell cycle leading to renal tubular epithelial cell apoptosis as labeled by TUNEL-positive cells. Moreover, both deletion of Smad3 and treatment with SIS3, the inhibitor of Smad3, can restore the SARS-CoV-2 N-induced AKI, which indicated that targeting Smad3 may represent a novel therapy for COVID-19-associated AKI (50).

Although we have summarized the apoptosis caused *via* different mechanisms induced by SARS-CoV-2, the underlying mechanisms of the massive inflammatory responses triggered by SARS-CoV-2 are largely limited. In contrast to necrosis, apoptosis is a form of clear cell death because the apoptotic bodies can be cleared through the phagocytic pathway by neighboring cells, without the release of cellular contents (51). We wonder whether inflammatory cell death occurred during SARS-CoV-2 infection. Indeed, analysis of the postmortem lung sections of fatal COVID-19 patients revealed that not only apoptosis but also necroptosis occurred in the lung, and the necrotic cell debris promoted massive inflammatory cell infiltration leading to lung damage in COVID-19 patients (52).

Necroptosis is an inflammatory type of programmed cell death mediated by RIPK1/RIPK3/MLKL. The occurrence of programmed necrosis could induce a series of morphological alterations in cells: with slight changes in the ultrastructure of the nucleus (especially the expansion of the nuclear membrane and the formation of small, irregular, and circumscribed patches by chromatin condensation), with increasing lucent cytoplasm and swelling organelles, the increased permeability of the cell membrane causes the cell to grow in size, resulting in the cell rupturing and the outflow of intracellular contents and provoking the inflammatory response of the surrounding tissues (53, 54). Mixed-lineage kinase domain-like (MLKL) is the main effector protein in necroptosis, which contains an N-terminal coiled-coil domain and a C-terminal kinase-like domain. MLKL can be recruited by the autophosphorylated RIPK3 and subsequently phosphorylated by RIPK3 at the threonine 357 and serine 358 residues of human MLKL (serine at positions 345, 347, and 352 and threonine at position 349 for mouse MLKL) (55–57). Phosphorylated MLKL will oligomerize and traffic to the plasma membrane, forming an MLKL pore, resulting in necroptosis (58).

As an important mediator of inflammation and cell death, RIPK1 can mediate the activation of caspase-8 to promote apoptosis or promote necroptosis by activating RIPK3 and MLKL (59–62). Based on some evidence of RIPK1 activation found in COVID-19 (63–65), Xu et al. used the lung pathological samples of COVID-19 patients and cultured human lung organoids and ACE2 transgenic mice infected by SARS-CoV-2 to explore the role of RIPK1 in SARS-CoV-2 infection. Although autopsy detection revealed that the expression of its downstream signaling molecule RIPK3 was found to be very low, and phosphorylated RIPK3 and MLKL were also undetectable, they found that the RNA-dependent RNA polymerase of SARS-CoV-2, NSP12, directly interacted with RIPK1 to promote its

activation, resulting in the transcriptional induction of proinflammatory cytokines and host factors including ACE2 and EGFR, which promote viral entry into cells (66). As multiple RIPK1 inhibitors (Nec-1s, GSK′481/GSK′772, etc.) have been advanced beyond Phase I safety studies in human clinical trials (67, 68), the authors suggested that the RIPK1 kinase inhibitors may provide effective therapy for severe COVID-19.

During SARS-CoV-2 infection, the inhibitor of necroptosis did not completely block IL-1β secretion, suggesting that there may be other pathways involved in the inflammatory responses such as pyroptosis (52).

Pyroptosis is a lytic and inflammatory type of programmed cell death, which is characterized by the swelling of cells, forming a big balloon on the plasma membrane, destructing the cell plasma membrane, releasing the cellular contents, and causing lysis of cells (69, 70). This type of cell death is mediated by the gasdermin (GSDM) protein family (71), which is activated and cleaved by caspase protein or other proteases (72–79). The N-terminal fragments of GSDM protein could induce the formation of membrane pores, disrupting the cell membrane and causing eventual lysis (80, 81).

The participation of the inflammasome in COVID-19 has been highly speculated as to its main contribution to excessive inflammatory responses upon SARS-CoV-2 infection (82, 83). The NLRP3 inflammasome, consisting of NLRP3, ASC, and caspase-1, is activated in response to SARS-CoV-2 infection and is active in COVID-19 patients, which is associated with the clinical outcome of the disease (84). Furthermore, Pan and colleagues found that the N protein of SARS-CoV-2 interacted directly with NLRP3, promoted the recruitment of ASC, and facilitated NLRP3 inflammasome assembly, which resulted in the maturation of proinflammatory cytokines and triggered proinflammatory responses in cultured HEK293T or A549 cells. Notably, treatment with MCC950 (a specific inhibitor of NLRP3) and Ac-YVAD-cmk (an inhibitor of caspase-1) or genetic deletion of Nlrp3 inhibited N protein-induced lung injury and cytokine production (85). However, in cultured Calu-3 cells, the inhibitors of caspase-1 and NLRP3 had no effects on the production of IL-1β induced by SARS-CoV-2 infection but blocks caspase-8 using the inhibitor, or siRNA knockdown decreased the production and secretion of IL-1β (52). In this scenario, it is important to further determine specific mechanisms by which SARS-CoV-2 triggers the inflammasome activation and investigate which specific inflammasome platforms are activated during the disease for effective therapeutic strategies to target COVID-19.

NETosis, a form of regulated neutrophil death, is characterized by the formation and release of neutrophil extracellular traps (NETs), which are networks of myriad pathogen-associated molecular patterns (PAMPs), consisting of extracellular fibers composed of DNA containing histones and granule-derived enzymes (such as lactoferrin, cathepsins, neutrophil elastase (NE), and myeloperoxidase (MPO)), as well as cytoplasmic and cytoskeletal proteins. In addition to the NADPH oxidase (NOX)/ROS-, peptidylarginine deiminase 4 (PADI4)-, and NE-dependent pathways on the activation of NETosis, RIPK3/MLKL-mediated necroptosis and GSDMD-driven pyroptosis linked the excessive inflammatory response to NETosis (86–89). Emerging evidence from the clinic severe cases of COVID-19 implicated that NETosis and NET formation/release played a central role in the pathophysiology of inflammation, coagulopathy, immunothrombosis, and even organ damage during SARS-CoV-2 infection (90–94). With the growing roles of NETosis and NETs in COVID-19 reported, targeting dysregulated NETosis and NET formation/release is a new aspect of severe COVID-19 treatment. NETosis inhibitors (fostamatinib targeting SYK, etc.), or NET degraders (GSK 484 targeting PAD 4, Dornase alfa degrading cfDNA) were used in preclinical or clinical development as anti-COVID-19 drugs, which was well-summarized by other groups (93, 95–97). Here, we emphasized the Food and Drug Administration (FDA)-approved alcoholism-averting drug, disulfiram, which was identified as an inhibitor of GSDMD pore formation by covalently modifying human/mouse Cys191/Cys192 in GSDMD and preventing IL-1β release and pyroptosis (98). Although the linkage of GSDMD-mediated pyroptosis with NETosis has been reported (99, 100), Egeblad and colleagues recently found that treatment with disulfiram reduced NET formation, as well as lung inflammation and perivascular fibrosis in a golden hamster SARS-CoV-2 infection model *via* downregulated innate immune and complement/coagulation pathways (101).

SARS-COV-2 S INDUCED CELL–CELL FUSION AND SYNCYTIA DEATH

Cell fusion between eukaryotic cells is a common phenomenon, caused by various pathogens, including bacteria, parasites, and viruses, which involves a broad range of physiological and pathological processes (102). The virus-mediated cell–cell fusion will lead to the fusion of cell membrane and cytoplasmic contents between cells, forming the multinucleated giant cells, also known as syncytia. SARS-CoV-2 infection can induce cell–cell fusion and syncytia formation, which has been widely confirmed in the lungs and other tissues of infected patients (103–105), or *in vitro* cell culture systems (106–108), which was well-summarized by Schwartz and colleagues (109). Syncytia formation was mediated by cell–cell fusion occurring between the surfaces of cell membranes. Within the syncytia, cellular contents from different cells mixed and interacted, triggering various cellular responses. We aimed to discuss the fate determination of syncytia and its role in COVID-19 progress, providing insights into targeting syncytia death on COVID-19 treatment.

Recent works reported that both DNA damage response and cGAS-STING signaling pathway were activated upon cell–cell fusion, which was important for host antiviral responses (110, 111). Furthermore, Zhang and colleagues demonstrated that the multinucleate syncytia formed by SARS-CoV-2 infection could internalize multiple lines of lymphocytes to form typical cell-in-cell structures, remarkably leading to the death of internalized cells (112). Moreover, we found that syncytia formed by HeLa–spike

cell fusion with HeLa-ACE2 cells died in parallel with the increased activity of caspase-3/7/9 and the cleavage of GSDME (108). Interestingly, the deletion of caspase-9 not only blocked the cleavage of GSDME and cell death but also abolished the S2′ fragment of SARS-CoV-2-S-Flag induced by cell–cell fusion, indicating a linkage between caspase-9 and SARS-CoV-2 S protein cleavage. Thus, targeting caspase-9 might be a promising strategy to prevent syncytia cell death (**Figure 1C**). To extend the pathophysiological role of this caspase-9/GSDME-mediated syncytia pyroptosis, single-cell RNA-sequencing (scRNA-Seq) data from eight normal human lung transplant donors with a total of 42,225 cells were analyzed, showing that both ACE2 and GSDME were expressed in AT2 cells in the human lung. Finally, we proposed that this lytic pyroptosis of syncytia may contribute to the excessive inflammatory responses in severe COVID-19 patients. In line with this idea, treatment with caspase-9 selective inhibitor, z-LEHD-fmk, markedly reduced SARS-CoV-2-induced lung damage in K18-hACE2 transgenic mouse model, which was evidenced by the reduced hemorrhage and inflammatory cell infiltration, as well as the alleviated proinflammatory response in the lung (113), while the authors demonstrated that this effect was due to intrinsic apoptosis inhibition by z-LEHD-fmk. Whether apoptosis switched to pyroptosis needs further investigation.

SARS-COV-2 E PROTEINS FORM CATION CHANNELS TO TRIGGER CELL DEATH

Interestingly, consistent with the executors of pyroptosis (GSDMs) or necroptosis (p-MLKL) destroying the membrane integrity by forming either pores or channels, the envelope (E) protein, another structural protein of SARS-CoV-2, can form a cation channel to induce rapid cell death in myriad susceptible cell types and robust secretion of cytokines and chemokines in macrophages resulting in acute respiratory distress syndrome (ARDS)-like damages *in vitro* and *in vivo* (**Figure 1B**). Using a planar lipid bilayer recording system, the authors found that BE-12 (berbamine), a type of bisbenzylisoquinoline alkaloid, might be a candidate inhibitor for 2-E channels. Furthermore, to improve the antiviral activity, four more channel inhibitors (BE-30~33) were designed and synthesized based on BE-12. Finally, a new class of 2-E channel inhibitor BE-33 was identified, which exhibited not only high efficiency for antiviral activity both *in vitro* and *in vivo* but also negligible cytotoxicity, raising a promising antiviral strategy targeting 2-E channel (114). To discover SARS-CoV-2-E channel inhibitors, Wang and coworkers developed a cell-based high-throughput screening (HTS) assay and screened 4,376 compounds. Proanthocyanidins, a natural product widely used in cosmetics, were identified (115).

DISCUSSION AND PERSPECTIVES

The abovementioned different types of cell death induced by SARS-CoV-2 infection have been demonstrated in all kinds of cells including epithelial cells, macrophages, and neutrophils. It was reported that ACE2-mediated SARS-CoV-2 spike infection could induce inflammatory responses and apoptosis of human bronchial epithelial and microvascular endothelial cells *via* enhancing autophagy, which might result in organ dysfunction (45). It was also found that SARS-CoV-2 N protein-mediated AKI may be caused by tubular epithelial cell apoptosis through the TGF/Smad3 signaling-dependent G1 cell cycle arrest (50). Using gene expression profiling, Jha et al. revealed that the apoptosis signaling pathway was activated in SARS-CoV-2-infected human lung epithelial cells, which may lead to cardiovascular complications of COVID-19 (116). A recent study showed that the non-structural protein 6 (NSP6) of SARS-CoV-2 could induce NLRP3-dependent pyroptosis in lung epithelial cells *via* binding to the vacuolar ATPase proton pump component ATP6AP1, while pharmacological rectification of autophagic flux by 1α,25-dihydroxyvitamin D3, metformin, or polydatin could be a novel therapeutic strategy to reduce pyroptosis in lung epithelial cells and improve clinical outcomes of COVID-19 (117). T- and B-lymphocyte apoptosis was also observed after SARS-CoV-2 infection, which may be the cause of lymphopenia, a common symptom in severe COVID-19 patients (46, 118). Aside from apoptosis, SARS-CoV-2-induced lymphocyte loss may also be due to cell–cell fusion-mediated syncytia death, which could be a potential therapeutic target for antiviral therapy in patients with COVID-19 (112). It was found that apoptotic markers were increased in plasmacytoid dendritic cells (pDCs), a cell type that is specialized in antiviral immunity to produce abundant type I interferons (IFNs). Hence, the diminished pDCs in COVID-19 patients may be associated with increased cell apoptosis (119). Ongoing pyroptosis was also found in circulating monocytes from COVID-19 patients with increased caspase-1 activation and lytic death (120, 121). Abundant cleared caspase-3 positive macrophages have been found in the lungs of patients with COVID-19, indicating that apoptosis may mediate the death of macrophages in COVID-19 lung tissues (66). Furthermore, SARS-CoV-2 spike infection can upregulate caspase-3 and caspase-6 expression to induce apoptosis in THP-1-like macrophages, which is likely mediated by the increase of ROS and intracellular calcium release (122). The pathological investigation of a clinical study demonstrated that SARS-CoV-2 infection caused severe lung injury *via* cell pyroptosis in pneumocytes and apoptosis in endothelial cells (123). Additionally, SARS-CoV-2 infection-induced apoptosis of endothelial cells may also lead to endotheliitis in various tissues including the lung, heart, kidney, and liver (124). Moreover, SARS-CoV-2 can promote NET formation in neutrophils under a process called NETosis, a form of neutrophil death, leading to multi-organ damage during the pathogenesis of COVID-19. Indeed, increased concentration of NETs has been detected in circulating and lung-infiltrating neutrophils from COVID-19 patients. Mechanistically, SARS-CoV-2-induced release of NETs might be mediated by ACE2, serine protease, virus replication, and PAD-4 (92, 125).

SARS-CoV-2 infection can cause severe respiratory tract disease and lung injury and threaten human life, while there is still no special prevention or treatment at present. When the virus infects cells, many factors are involved in the pathogenesis of the host disease, leading to human death. In this review, we focused on the multiple types of cell death such as apoptosis, necroptosis, pyroptosis, NETosis, and other undefined death triggered by SARS-CoV-2 infection *in vivo* or *in vitro*; then we discussed the relationship between inflammatory cell death and cytokine storm, raising the possibility for targeting cell death pathway for the treatment of COVID-19 (**Figure 2**). Among these, we highlighted some potential compounds or drugs targeting the molecules of cell death pathway, such as RIPK1 (66), caspase-9 (108), Smad (50), SARS-CoV-2 Orf3a (39–41), and E protein (114). What is more, iron metabolism dysfunction has also been found in COVID-19 patients; for example, the serum ferritin levels were higher in severe COVID-19 patients than in mild cases, which may cause iron accumulation and overload, which trigger ferroptosis (126). Yang and Lai hypothesized that ferroptosis might serve as a new treatment target, and the improved ferrostatin-1 and liproxstatin-1 analogs might be potential drug candidates for COVID-19 (127). Interestingly, disulfiram, an alcoholism-averting drug approved by the FDA, was recommended to be a potential therapeutic target for SARS-CoV-2 infection in Phase 2 clinical trials by targeting SARS-CoV-2 main protease, 3CLpro (128–130). However, it has been identified that disulfiram is covalently targeted on human/mouse Cys191/Cys192 of GSDMD protein leading to blocking the GSDMD pore formation, IL-1β release, and pyroptosis (98). Furthermore, another study showed that disulfiram can inhibit the NET formation and protect rodents from SARS-CoV-2 infection (101). All these raise a common point that one drug/compound might target various proteins even on multiple signaling pathways to either synergically exert effects or trigger off-target toxicities. Therefore, we need to deeply explore the cell types of death caused by SARS-CoV-2 infection, reveal the molecular mechanism of cell death, and accurately regulate cell death by using specific pharmacological therapies to reduce the occurrence and prognosis of COVID-19.

Nevertheless, the impact of the damaged or dead cells on the injured tissues and organs is still not well understood. Furthermore, whether cytokines released by cell death participate in cytokine storms has not been well described yet. However, research on the mechanism of SARS-CoV-2 infection-induced cell death may provide additional perspectives for antiviral therapies and the development of anti-SARS-CoV-2 drugs.

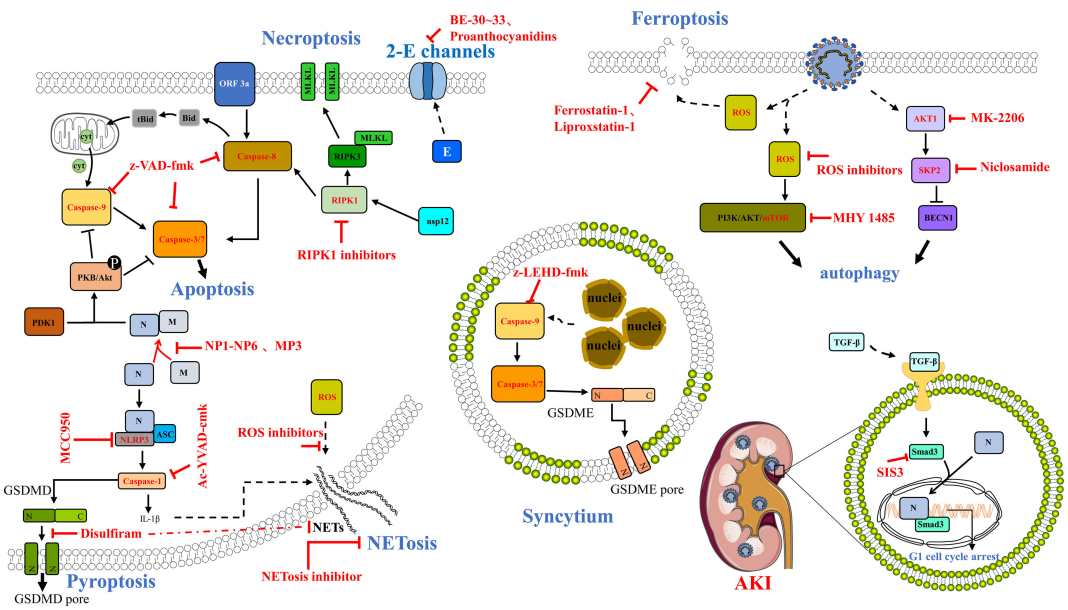

FIGURE 2 | Potential compounds or drugs that targeted different cell death pathways. The potential therapeutics of drugs or compounds to inhibit cell death, including the use of z-VAD-fmk, a pan-caspase inhibitor, to reduce the caspase activity and block the apoptosis induced by SARS-CoV-2 ORF3a, and the use of RIPK1 inhibitors (Nec-1s, GSK′481/GSK′772, etc.), as well as using peptides such as NP1-NP6 and MP3 to disrupt the M–N interaction, and abolish the activity of N on the M-triggered apoptosis. In addition, a specific inhibitor of NLRP3 called MCC950 and an inhibitor of caspase-1 named Ac-YVAD-cmk can block NLRP3 inflammasome activation induced by SARS-CoV-2 N protein. Interestingly, disulfiram was revealed as an inhibitor of GSDMD that can effectively block pyroptosis and NET formation. BE-30~33 and proanthocyanidins could inhibit 2-E channel activity as channel inhibitors. Autophagy could be regulated using various treatments, such as the ROS inhibitor MHY1485, the AKT1 inhibitor MK-2206, and the BECN1-stabilizing anthelmintic drug/SKP2 inhibitor, niclosamide. Ferroptosis inhibitors including ferrostatin-1 and liproxstatin-1 might also be potential drug candidates for COVID-19. Further, z-LEHD-fmk, the caspase-9 selective inhibitor could suppress syncytium formation. SIS3, Smad3 pharmacological inhibitor, can inhibit SARS-CoV-2 N-induced AKI. The compounds or drugs are marked in bold and red.

AUTHOR CONTRIBUTIONS

LL, JW, YZ, and HM: conceptualization. ZZ and JS: investigation and writing—original draft preparation. LL, JW, and HM: writing—review and editing. All authors have read and agreed to the published version of the manuscript.

FUNDING

This work was supported by the Natural Science Foundation of Zhejiang Province (No. LQ21H030002), the Scientific Research Grant of Ningbo University (215–432000282), and the Ningbo Top Talent Project (215–432094250).

REFERENCES

1. Lim YX, Ng YL, Tam JP, Liu DX. Human Coronaviruses: A Review of Virus-Host Interactions. *Diseases* (2016) 4(3):26. doi: 10.3390/diseases4030026
2. Fung TS, Liu DX. Human Coronavirus: Host-Pathogen Interaction. *Annu Rev Microbiol* (2019) 73:529–57. doi: 10.1146/annurev-micro-020518-115759
3. Harrison AG, Lin T, Wang P. Mechanisms of SARS-CoV-2 Transmission and Pathogenesis. *Trends Immunol* (2020) 41(12):1100–15. doi: 10.1016/j.it.2020.10.004
4. Tang D, Comish P, Kang R. The Hallmarks of Covid-19 Disease. *PLoS Pathog* (2020) 16(5):e1008536. doi: 10.1371/journal.ppat.1008536
5. Hu B, Guo H, Zhou P, Shi ZL. Characteristics of SARS-CoV-2 and Covid-19. *Nat Rev Microbiol* (2020) 19:1–14. doi: 10.1038/s41579-020-00459-7
6. Zhou P, Yang XL, Wang XG, Hu B, Zhang L, Zhang W, et al. A Pneumonia Outbreak Associated With a New Coronavirus of Probable Bat Origin. *Nature* (2020) 579(7798):270–3. doi: 10.1038/s41586-020-2012-7
7. Gorbalenya AE, Baker SC, Baric RS, de Groot RJ, Drosten C, Gulyaeva AA, et al. The Species Severe Acute Respiratory Syndrome-Related Coronavirus: Classifying 2019-Ncov and Naming it SARS-CoV-2. *Nat Microbiol* (2020) 5 (4):536–44. doi: 10.1038/s41564-020-0695-z
8. Ashour HM, Elkhatib WF, Rahman MM, Elshabrawy HA. Insights Into the Recent 2019 Novel Coronavirus (SARS-CoV-2) in Light of Past Human Coronavirus Outbreaks. *Pathogens* (2020) 9(3):186. doi: 10.3390/pathogens9030186
9. Wu F, Zhao S, Yu B, Chen YM, Wang W, Song ZG, et al. A New Coronavirus Associated With Human Respiratory Disease in China. *Nature* (2020) 579(7798):265–9. doi: 10.1038/s41586-020-2008-3
10. Kim D, Lee JY, Yang JS, Kim JW, Kim VN, Chang H. The Architecture of SARS-CoV-2 Transcriptome. *Cell* (2020) 181(4):914–21.e10. doi: 10.1016/j.cell.2020.04.011
11. Gordon DE, Jang GM, Bouhaddou M, Xu J, Obernier K, White KM, et al. A Sars-Cov-2 Protein Interaction Map Reveals Targets for Drug Repurposing. *Nature* (2020) 583(7816):459–68. doi: 10.1038/s41586-020-2286-9
12. Guan WJ, Ni ZY, Hu Y, Liang WH, Ou CQ, He JX, et al. Clinical Characteristics of Coronavirus Disease 2019 in China. *N Engl J Med* (2020) 382(18):1708–20. doi: 10.1056/NEJMoa2002032
13. Zhou F, Yu T, Du R, Fan G, Liu Y, Liu Z, et al. Clinical Course and Risk Factors for Mortality of Adult Inpatients With Covid-19 in Wuhan, China: A Retrospective Cohort Study. *Lancet* (2020) 395(10229):1054–62. doi: 10.1016/s0140-6736(20)30566-3
14. Merad M, Martin JC. Pathological Inflammation in Patients With Covid-19: A Key Role for Monocytes and Macrophages. *Nat Rev Immunol* (2020) 20 (6):355–62. doi: 10.1038/s41577-020-0331-4
15. Fajgenbaum DC, June CH. Cytokine Storm. *N Engl J Med* (2020) 383 (23):2255–73. doi: 10.1056/NEJMra2026131
16. Long Q-X, Tang X-J, Shi Q-L, Li Q, Deng H-J, Yuan J, et al. Clinical and Immunological Assessment of Asymptomatic SARS-CoV-2 Infections. *Nat Med* (2020) 26(8):1200–+. doi: 10.1038/s41591-020-0965-6
17. Wilk AJ, Rustagi A, Zhao NQ, Roque J, Martinez-Colon GJ, McKechnie JL, et al. A Single-Cell Atlas of the Peripheral Immune Response in Patients With Severe Covid-19. *Nat Med* (2020) 26(7):1070–+. doi: 10.1038/s41591-020-0944-y
18. Jose RJ, Manuel A. Covid-19 Cytokine Storm: The Interplay Between Inflammation and Coagulation. *Lancet Respir Med* (2020) 8(6):e46–7. doi: 10.1016/s2213-2600(20)30216-2
19. Bian XW, Team C-P. Autopsy of Covid-19 Patients in China. *Natl Sci Rev* (2020) 7(9):1414–8. doi: 10.1093/nsr/nwaa123
20. Liu Q, Shi Y, Cai J, Duan Y, Wang R, Zhang H, et al. Pathological Changes in the Lungs and Lymphatic Organs of 12 Covid-19 Autopsy Cases. *Natl Sci Rev* (2020) 7(12):1868–78. doi: 10.1093/nsr/nwaa247
21. Wichmann D, Sperhake J-P, Luegehetmann M, Steurer S, Edler C, Heinemann A, et al. Autopsy Findings and Venous Thromboembolism in Patients With Covid-19. *Ann Internal Med* (2020) 173(4):268–+. doi: 10.7326/m20-2003
22. Franks TJ, Chong PY, Chui P, Galvin JR, Lourens RM, Reid AH, et al. Lung Pathology of Severe Acute Respiratory Syndrome (Sars): A Study of 8 Autopsy Cases From Singapore. *Hum Pathol* (2003) 34(8):743–8. doi: 10.1016/s0046-8177(03)00367-8
23. Edler C, Schroeder AS, Aepfelbacher M, Fitzek A, Heinemann A, Heinrich F, et al. Dying With Sars-Cov-2 Infection-An Autopsy Study of the First Consecutive 80 Cases in Hamburg, Germany. *Int J Legal Med* (2020) 134 (4):1275–84. doi: 10.1007/s00414-020-02317-w
24. Hanley B, Lucas SB, Youd E, Swift B, Osborn M. Autopsy in Suspected Covid-19 Cases. *J Clin Pathol* (2020) 73(5):239–42. doi: 10.1136/jclinpath-2020-206522
25. Fox SE, Akmatbekov A, Harbert JL, Li G, Brown JQ, Heide RSV. Pulmonary and Cardiac Pathology in African American Patients With Covid-19: An Autopsy Series From New Orleans. *Lancet Respir Med* (2020) 8(7):681–6. doi: 10.1016/s2213-2600(20)30243-5
26. Bussani R, Schneider E, Zentilin L, Collesi C, Ali H, Braga L, et al. Persistence of Viral Rna, Pneumocyte Syncytia and Thrombosis are Hallmarks of Advanced Covid-19 Pathology. *EBioMedicine* (2020) 61:103104. doi: 10.1016/j.ebiom.2020.103104
27. Tian S, Hu W, Niu L, Liu H, Xu H, Xiao S-Y. Pulmonary Pathology of Early-Phase 2019 Novel Coronavirus (Covid-19) Pneumonia in Two Patients With Lung Cancer. *J Thorac Oncol* (2020) 15(5):700–4. doi: 10.1016/j.jtho.2020.02.010
28. Gupta A, Madhavan MV, Sehgal K, Nair N, Mahajan S, Sehrawat TS, et al. Extrapulmonary Manifestations of Covid-19. *Nat Med* (2020) 26(7):1017–32. doi: 10.1038/s41591-020-0968-3
29. Fung SY, Yuen KS, Ye ZW, Chan CP, Jin DY. A Tug-Of-War Between Severe Acute Respiratory Syndrome Coronavirus 2 and Host Antiviral Defence: Lessons From Other Pathogenic Viruses. *Emerg Microbes Infect* (2020) 9 (1):558–70. doi: 10.1080/22221751.2020.1736644
30. Danthi P. Viruses and the Diversity of Cell Death. *Annu Rev Virol* (2016) 3 (1):533–53. doi: 10.1146/annurev-virology-110615-042435
31. Bader SM, Cooney JP, Pellegrini M, Doerflinger M. Programmed Cell Death: The Pathways to Severe Covid-19? *Biochem J* (2022) 479(5):609–28. doi: 10.1042/bcj20210602
32. Morais da Silva M, Lira de Lucena AS, Paiva Júnior SSL, Florêncio De Carvalho VM, Santana de Oliveira PS, da Rosa MM, et al. Cell Death Mechanisms Involved in Cell Injury Caused by Sars-Cov-2. *Rev Med Virol* (2021):e2292. doi: 10.1002/rmv.2292
33. Denecker G, Vercammen D, Declercq W, Vandenabeele P. Apoptotic and Necrotic Cell Death Induced by Death Domain Receptors. *Cell Mol Life Sci* (2001) 58(3):356–70. doi: 10.1007/pl00000863
34. Jiang X, Wang X. Cytochrome C-Mediated Apoptosis. *Annu Rev Biochem* (2004) 73:87–106. doi: 10.1146/annurev.biochem.73.011303.073706
35. Green DR, Llambi F. Cell Death Signaling. *Cold Spring Harbor Perspect Biol* (2015) 7(12):a006080. doi: 10.1101/cshperspect.a006080
36. Galluzzi L, Vitale I, Aaronson SA, Abrams JM, Adam D, Agostinis P, et al. Molecular Mechanisms of Cell Death: Recommendations of the Nomenclature Committee on Cell Death 2018. *Cell Death Differ* (2018) 25 (3):486–541. doi: 10.1038/s41418-017-0012-4

37. Xu X, Lai Y, Hua ZC. Apoptosis and Apoptotic Body: Disease Message and Therapeutic Target Potentials. *Biosci Rep* (2019) 39(1):BSR20180992. doi: 10.1042/bsr20180992
38. Freundt EC, Yu L, Goldsmith CS, Welsh S, Cheng A, Yount B, et al. The Open Reading Frame 3a Protein of Severe Acute Respiratory Syndrome-Associated Coronavirus Promotes Membrane Rearrangement and Cell Death. *J Virol* (2010) 84(2):1097–109. doi: 10.1128/jvi.01662-09
39. Ren Y, Shu T, Wu D, Mu J, Wang C, Huang M, et al. The Orf3a Protein of Sars-Cov-2 Induces Apoptosis in Cells. *Cell Mol Immunol* (2020) 17(8):881–3. doi: 10.1038/s41423-020-0485-9
40. Miao G, Zhao H, Li Y, Ji M, Chen Y, Shi Y, et al. Orf3a of the Covid-19 Virus Sars-Cov-2 Blocks Hops Complex-Mediated Assembly of the Snare Complex Required for Autolysosome Formation. *Dev Cell* (2021) 56 (4):427–42.e5. doi: 10.1016/j.devcel.2020.12.010
41. Zhang Y, Sun H, Pei R, Mao B, Zhao Z, Li H, et al. The SARS-CoV-2 Protein Orf3a Inhibits Fusion of Autophagosomes With Lysosomes. *Cell Discov* (2021) 7(1):31. doi: 10.1038/s41421-021-00268-z
42. Gassen NC, Papies J, Bajaj T, Emanuel J, Dethloff F, Chua RL, et al. Sars-Cov-2-Mediated Dysregulation of Metabolism and Autophagy Uncovers Host-Targeting Antivirals. *Nat Commun* (2021) 12(1):3818. doi: 10.1038/s41467-021-24007-w
43. Yang R, Zhao Q, Rao J, Zeng F, Yuan S, Ji M, et al. SARS-CoV-2 Accessory Protein Orf7b Mediates Tumor Necrosis Factor-A-Induced Apoptosis in Cells. *Front Microbiol* (2021) 12:654709. doi: 10.3389/fmicb.2021.654709
44. Ren Y, Wang A, Fang Y, Shu T, Wu D, Wang C, et al. SARS-CoV-2 Membrane Glycoprotein M Triggers Apoptosis With the Assistance of Nucleocapsid Protein N in Cells. *Front Cell Infect Microbiol* (2021) 11:706252. doi: 10.3389/fcimb.2021.706252
45. Li F, Li J, Wang PH, Yang N, Huang J, Ou J, et al. SARS-CoV-2 Spike Promotes Inflammation and Apoptosis Through Autophagy by Ros-Suppressed Pi3k/Akt/Mtor Signaling. *Biochim Biophys Acta Mol Basis Dis* (2021) 1867(12):166260. doi: 10.1016/j.bbadis.2021.166260
46. Xiang Q, Feng Z, Diao B, Tu C, Qiao Q, Yang H, et al. SARS-CoV-2 Induces Lymphocytopenia by Promoting Inflammation and Decimates Secondary Lymphoid Organs. *Front Immunol* (2021) 12:661052. doi: 10.3389/fimmu.2021.661052
47. Diao B, Wang C, Wang R, Feng Z, Zhang J, Yang H, et al. Human Kidney Is a Target for Novel Severe Acute Respiratory Syndrome Coronavirus 2 Infection. *Nat Commun* (2021) 12(1):2506. doi: 10.1038/s41467-021-22781-1
48. Pei G, Zhang Z, Peng J, Liu L, Zhang C, Yu C, et al. Renal Involvement and Early Prognosis in Patients With Covid-19 Pneumonia. *J Am Soc Nephrol JASN* (2020) 31(6):1157–65. doi: 10.1681/asn.2020030276
49. Cheng Y, Luo R, Wang K, Zhang M, Wang Z, Dong L, et al. Kidney Disease Is Associated With in-Hospital Death of Patients With Covid-19. *Kidney Int* (2020) 97(5):829–38. doi: 10.1016/j.kint.2020.03.005
50. Wang W, Chen J, Hu D, Pan P, Liang L, Wu W, et al. SARS-CoV-2 N Protein Induces Acute Kidney Injury *Via* Smad3-Dependent G1 Cell Cycle Arrest Mechanism. *Adv Sci (Weinh)* (2021) 9(3):e2103248. doi: 10.1002/advs.202103248
51. Boada-Romero E, Martinez J, Heckmann BL, Green DR. The Clearance of Dead Cells by Efferocytosis. *Nat Rev Mol Cell Biol* (2020) 21(7):398–414. doi: 10.1038/s41580-020-0232-1
52. Li S, Zhang Y, Guan Z, Li H, Ye M, Chen X, et al. Sars-Cov-2 Triggers Inflammatory Responses and Cell Death Through Caspase-8 Activation. *Signal Transduct Tar Ther* (2020) 5(1):235. doi: 10.1038/s41392-020-00334-0
53. Xia X, Lei L, Wang S, Hu J, Zhang G. Necroptosis and Its Role in Infectious Diseases. *Apoptosis* (2020) 25(3-4):169–78. doi: 10.1007/s10495-019-01589-x
54. Gong Y, Fan Z, Luo G, Yang C, Huang Q, Fan K, et al. The Role of Necroptosis in Cancer Biology and Therapy. *Mol Cancer* (2019) 18(1):100. doi: 10.1186/s12943-019-1029-8
55. Zhang J, Yang Y, He W, Sun L. Necrosome Core Machinery: Mlkl. *Cell Mol Life Sci* (2016) 73(11-12):2153–63. doi: 10.1007/s00018-016-2190-5
56. Xu Y, Zhang J, Ma L, Zhao S, Li S, Huang T, et al. The Pathogenesis of Necroptosis-Dependent Signaling Pathway in Cerebral Ischemic Disease. *Behav Neurol* (2018) 2018:6814393. doi: 10.1155/2018/6814393
57. Moriwaki K, Chan FK. Rip3: A Molecular Switch for Necrosis and Inflammation. *Genes Dev* (2013) 27(15):1640–9. doi: 10.1101/gad.223321.113
58. Petrie EJ, Czabotar PE, Murphy JM. The Structural Basis of Necroptotic Cell Death Signaling. *Trends Biochem Sci* (2019) 44(1):53–63. doi: 10.1016/j.tibs.2018.11.002
59. Chan FK, Luz NF, Moriwaki K. Programmed Necrosis in the Cross Talk of Cell Death and Inflammation. *Annu Rev Immunol* (2015) 33:79–106. doi: 10.1146/annurev-immunol-032414-112248
60. Lin J, Kumari S, Kim C, Van TM, Wachsmuth L, Polykratis A, et al. Ripk1 Counteracts Zbp1-Mediated Necroptosis to Inhibit Inflammation. *Nature* (2016) 540(7631):124–8. doi: 10.1038/nature20558
61. Newton K, Wickliffe KE, Maltzman A, Dugger DL, Strasser A, Pham VC, et al. Ripk1 Inhibits Zbp1-Driven Necroptosis During Development. *Nature* (2016) 540(7631):129–33. doi: 10.1038/nature20559
62. Dannappel M, Vlantis K, Kumari S, Polykratis A, Kim C, Wachsmuth L, et al. Ripk1 Maintains Epithelial Homeostasis by Inhibiting Apoptosis and Necroptosis. *Nature* (2014) 513(7516):90–4. doi: 10.1038/nature13608
63. Riebeling T, Jamal K, Wilson R, Kolbrink B, von Samson-Himmelstjerna FA, Moerke C, et al. Primidone Blocks Ripk1-Driven Cell Death and Inflammation. *Cell Death Differ* (2021) 28(5):1610–26. doi: 10.1038/s41418-020-00690-y
64. Feng L, Yin YY, Liu CH, Xu KR, Li QR, Wu JR, et al. Proteome-Wide Data Analysis Reveals Tissue-Specific Network Associated With SARS-CoV-2 Infection. *J Mol Cell Biol* (2020) 12(12):946–57. doi: 10.1093/jmcb/mjaa033
65. Belyaeva A, Cammarata L, Radhakrishnan A, Squires C, Yang KD, Shivashankar GV, et al. Causal Network Models of Sars-Cov-2 Expression and Aging to Identify Candidates for Drug Repurposing. *Nat Commun* (2021) 12(1):1024. doi: 10.1038/s41467-021-21056-z
66. Xu G, Li Y, Zhang S, Peng H, Wang Y, Li D, et al. Sars-Cov-2 Promotes Ripk1 Activation to Facilitate Viral Propagation. *Cell Res* (2021) 31:1230–43. doi: 10.1038/s41422-021-00578-7
67. Mifflin L, Ofengeim D, Yuan J. Receptor-Interacting Protein Kinase 1 (Ripk1) as a Therapeutic Target. *Nat Rev Drug Discov* (2020) 19(8):553–71. doi: 10.1038/s41573-020-0071-y
68. Liu L, Lalaoui N. 25 Years of Research Put Ripk1 in the Clinic. *Semin Cell Dev Biol* (2021) 109:86–95. doi: 10.1016/j.semcdb.2020.08.007
69. Fink SL, Cookson BT. Apoptosis, Pyroptosis, and Necrosis: Mechanistic Description of Dead and Dying Eukaryotic Cells. *Infect Immun* (2005) 73 (4):1907–16. doi: 10.1128/IAI.73.4.1907-1916.2005
70. Jorgensen I, Miao EA. Pyroptotic Cell Death Defends Against Intracellular Pathogens. *Immunol Rev* (2015) 265(1):130–42. doi: 10.1111/imr.12287
71. Shi J, Gao W, Shao F. Pyroptosis: Gasdermin-Mediated Programmed Necrotic Cell Death. *Trends Biochem Sci* (2017) 42(4):245–54. doi: 10.1016/j.tibs.2016.10.004
72. Shi J, Zhao Y, Wang K, Shi X, Wang Y, Huang H, et al. Cleavage of Gsdmd by Inflammatory Caspases Determines Pyroptotic Cell Death. *Nature* (2015) 526(7575):660–5. doi: 10.1038/nature15514
73. He WT, Wan H, Hu L, Chen P, Wang X, Huang Z, et al. Gasdermin D is an Executor of Pyroptosis and Required for Interleukin-1β Secretion. *Cell Res* (2015) 25(12):1285–98. doi: 10.1038/cr.2015.139
74. Rogers C, Fernandes-Alnemri T, Mayes L, Alnemri D, Cingolani G, Alnemri ES. Cleavage of Dfna5 by Caspase-3 During Apoptosis Mediates Progression to Secondary Necrotic/Pyroptotic Cell Death. *Nat Commun* (2017) 8:14128. doi: 10.1038/ncomms14128
75. Wang Y, Gao W, Shi X, Ding J, Liu W, He H, et al. Chemotherapy Drugs Induce Pyroptosis Through Caspase-3 Cleavage of a Gasdermin. *Nature* (2017) 547(7661):99–103. doi: 10.1038/nature22393
76. Fritsch M, Gunther SD, Schwarzer R, Albert MC, Schorn F, Werthenbach JP, et al. Caspase-8 Is the Molecular Switch for Apoptosis, Necroptosis and Pyroptosis. *Nature* (2019) 575(7784):683–7. doi: 10.1038/s41586-019-1770-6
77. Sarhan J, Liu BC, Muendlein HI, Li P, Nilson R, Tang AY, et al. Caspase-8 Induces Cleavage of Gasdermin D to Elicit Pyroptosis During Yersinia Infection. *Proc Natl Acad Sci USA* (2018) 115(46):E10888–97. doi: 10.1073/pnas.1809548115
78. Zhou Z, He H, Wang K, Shi X, Wang Y, Su Y, et al. Granzyme a From Cytotoxic Lymphocytes Cleaves Gsdmb to Trigger Pyroptosis in Target Cells. *Science* (2020) 368(6494):eaaz7548. doi: 10.1126/science.aaz7548. New York, NY.

79. Kayagaki N, Stowe IB, Lee BL, O'Rourke K, Anderson K, Warming S, et al. Caspase-11 Cleaves Gasdermin D for Non-Canonical Inflammasome Signalling. *Nature* (2015) 526(7575):666–71. doi: 10.1038/nature15541
80. Ding J, Wang K, Liu W, She Y, Sun Q, Shi J, et al. Pore-Forming Activity and Structural Autoinhibition of the Gasdermin Family. *Nature* (2016) 535 (7610):111–6. doi: 10.1038/nature18590
81. Broz P, Pelegrín P, Shao F. The Gasdermins, A Protein Family Executing Cell Death and Inflammation. *Nat Rev Immunol* (2020) 20(3):143–57. doi: 10.1038/s41577-019-0228-2
82. Freeman TL, Swartz TH. Targeting the Nlrp3 Inflammasome in Severe Covid-19. *Front Immunol* (2020) 11:1518. doi: 10.3389/fimmu.2020.01518
83. van den Berg DF, Te Velde AA. Severe Covid-19: Nlrp3 Inflammasome Dysregulated. *Front Immunol* (2020) 11:1580. doi: 10.3389/fimmu.2020.01580
84. Rodrigues TS, de Sá KSG, Ishimoto AY, Becerra A, Oliveira S, Almeida L, et al. Inflammasomes Are Activated in Response to SARS-CoV-2 Infection and Are Associated With Covid-19 Severity in Patients. *J Exp Med* (2021) 218(3):e20201707. doi: 10.1084/jem.20201707
85. Pan P, Shen M, Yu Z, Ge W, Chen K, Tian M, et al. SARS-CoV-2 N Protein Promotes Nlrp3 Inflammasome Activation to Induce Hyperinflammation. *Nat Commun* (2021) 12(1):4664. doi: 10.1038/s41467-021-25015-6
86. Brinkmann V, Reichard U, Goosmann C, Fauler B, Uhlemann Y, Weiss DS, et al. Neutrophil Extracellular Traps Kill Bacteria. *Science* (2004) 303 (5663):1532–5. doi: 10.1126/science.1092385
87. Fuchs TA, Abed U, Goosmann C, Hurwitz R, Schulze I, Wahn V, et al. Novel Cell Death Program Leads to Neutrophil Extracellular Traps. *J Cell Biol* (2007) 176(2):231–41. doi: 10.1083/jcb.200606027
88. Gupta S, Kaplan MJ. The Role of Neutrophils and Netosis in Autoimmune and Renal Diseases. *Nat Rev Nephrol* (2016) 12(7):402–13. doi: 10.1038/nrneph.2016.71
89. Papayannopoulos V. Neutrophil Extracellular Traps in Immunity and Disease. *Nat Rev Immunol* (2018) 18(2):134–47. doi: 10.1038/nri.2017.105
90. Arcanjo A, Logullo J, Menezes CCB, de Souza Carvalho Giangiarulo TC, Dos Reis MC, de Castro GMM, et al. The Emerging Role of Neutrophil Extracellular Traps in Severe Acute Respiratory Syndrome Coronavirus 2 (Covid-19). *Sci Rep* (2020) 10(1):19630. doi: 10.1038/s41598-020-76781-0
91. Middleton EA, He XY, Denorme F, Campbell RA, Ng D, Salvatore SP, et al. Neutrophil Extracellular Traps Contribute to Immunothrombosis in Covid-19 Acute Respiratory Distress Syndrome. *Blood* (2020) 136(10):1169–79. doi: 10.1182/blood.2020007008
92. Veras FP, Pontelli MC, Silva CM, Toller-Kawahisa JE, de Lima M, Nascimento DC, et al. Sars-Cov-2-Triggered Neutrophil Extracellular Traps Mediate Covid-19 Pathology. *J Exp Med* (2020) 217(12):e20201129. doi: 10.1084/jem.20201129
93. Ackermann M, Anders H-J, Bilyy R, Bowlin GL, Daniel C, De Lorenzo R, et al. Patients With Covid-19: In the Dark-Nets of Neutrophils. *Cell Death Differ* (2021) 28(11):3125–39. doi: 10.1038/s41418-021-00805-z
94. Hong W, Yang J, Zou J, Bi Z, He C, Lei H, et al. Histones Released by Netosis Enhance the Infectivity of Sars-Cov-2 by Bridging the Spike Protein Subunit 2 and Sialic Acid on Host Cells. *Cell Mol Immunol* (2022) 19:577–87. doi: 10.1038/s41423-022-00845-6
95. Gillot C, Favresse J, Mullier F, Lecompte T, Dogné J-M, Douxfils J. Netosis and the Immune System in Covid-19: Mechanisms and Potential Treatments. *Front Pharmacol* (2021) 12:708302. doi: 10.3389/fphar.2021.708302
96. Zhu Y, Chen X, Liu X. Netosis and Neutrophil Extracellular Traps in Covid-19: Immunothrombosis and Beyond. *Front Immunol* (2022) 13:838011. doi: 10.3389/fimmu.2022.838011
97. Pastorek M, Dúbrava M, Celec P. On the Origin of Neutrophil Extracellular Traps in Covid-19. *Front Immunol* (2022) 13:821007. doi: 10.3389/fimmu.2022.821007
98. Hu JJ, Liu X, Xia S, Zhang Z, Zhang Y, Zhao J, et al. Fda-Approved Disulfiram Inhibits Pyroptosis by Blocking Gasdermin D Pore Formation. *Nat Immunol* (2020) 21(7):736–45. doi: 10.1038/s41590-020-0669-6
99. Kambara H, Liu F, Zhang X, Liu P, Bajrami B, Teng Y, et al. Gasdermin D Exerts Anti-Inflammatory Effects by Promoting Neutrophil Death. *Cell Rep* (2018) 22(11):2924–36. doi: 10.1016/j.celrep.2018.02.067
100. Chen KW, Monteleone M, Boucher D, Sollberger G, Ramnath D, Condon ND, et al. Noncanonical Inflammasome Signaling Elicits Gasdermin D-Dependent Neutrophil Extracellular Traps. *Sci Immunol* (2018) 3(26): eaar6676. doi: 10.1126/sciimmunol.aar6676
101. Adrover JM, Carrau L, Daßler-Plenker J, Bram Y, Chandar V, Houghton S, et al. Disulfiram Inhibits Neutrophil Extracellular Trap Formation and Protects Rodents From Acute Lung Injury and Sars-Cov-2 Infection. *JCI Insight* (2022) 7(5):e157342. doi: 10.1172/jci.insight.157342
102. Leroy H, Han M, Woottum M, Bracq L, Bouchet J, Xie M, et al. Virus-Mediated Cell-Cell Fusion. *Int J Mol Sci* (2020) 21(24):9644. doi: 10.3390/ijms21249644
103. Sanders DW, Jumper CC, Ackerman PJ, Bracha D, Donlic A, Kim H, et al. Sars-Cov-2 Requires Cholesterol for Viral Entry and Pathological Syncytia Formation. *Elife* (2021) 10:e65962. doi: 10.7554/eLife.65962
104. Asarnow D, Wang B, Lee WH, Hu Y, Huang CW, Faust B, et al. Structural Insight Into Sars-Cov-2 Neutralizing Antibodies and Modulation of Syncytia. *Cell* (2021) 184(12):3192–204.e16. doi: 10.1016/j.cell.2021.04.033
105. Stadlmann S, Hein-Kuhnt R, Singer G. Viropathic Multinuclear Syncytial Giant Cells in Bronchial Fluid From a Patient With Covid-19. *J Clin Pathol* (2020) 73(9):607–8. doi: 10.1136/jclinpath-2020-206657
106. Buchrieser J, Dufloo J, Hubert M, Monel B, Planas D, Rajah MM, et al. Syncytia Formation by Sars-Cov-2-Infected Cells. *EMBO J* (2020) 39(23): e106267. doi: 10.15252/embj.2020106267
107. Braga L, Ali H, Secco I, Chiavacci E, Neves G, Goldhill D, et al. Drugs That Inhibit Tmem16 Proteins Block Sars-Cov-2 Spike-Induced Syncytia. *Nature* (2021) 594:88–93. doi: 10.1038/s41586-021-03491-6
108. Ma H, Zhu Z, Lin H, Wang S, Zhang P, Li Y, et al. Pyroptosis of Syncytia Formed by Fusion of Sars-Cov-2 Spike and Ace2-Expressing Cells. *Cell Discov* (2021) 7(1):73. doi: 10.1038/s41421-021-00310-0
109. Rajah MM, Bernier A, Buchrieser J, Schwartz O. The Mechanism and Consequences of SARS-CoV-2 Spike-Mediated Fusion and Syncytia Formation. *J Mol Biol* (2021) 434(6):167280. doi: 10.1016/j.jmb.2021.167280
110. Zhou Z, Zhang X, Lei X, Xiao X, Jiao T, Ma R, et al. Sensing of Cytoplasmic Chromatin by Cgas Activates Innate Immune Response in Sars-Cov-2 Infection. *Signal Transduct Target Ther* (2021) 6(1):382. doi: 10.1038/s41392-021-00800-3
111. Ren H, Ma C, Peng H, Zhang B, Zhou L, Su Y, et al. Micronucleus Production, Activation of DNA Damage Response and Cgas-Sting Signaling in Syncytia Induced by Sars-Cov-2 Infection. *Biol direct* (2021) 16(1):20. doi: 10.1186/s13062-021-00305-7
112. Zhang Z, Zheng Y, Niu Z, Zhang B, Wang C, Yao X, et al. SARS-CoV-2 Spike Protein Dictates Syncytium-Mediated Lymphocyte Elimination. *Cell Death Differ* (2021) 28:2765–77. doi: 10.1038/s41418-021-00782-3
113. Chu H, Shuai H, Hou Y, Zhang X, Wen L, Huang X, et al. Targeting Highly Pathogenic Coronavirus-Induced Apoptosis Reduces Viral Pathogenesis and Disease Severity. *Sci Adv* (2021) 7(25):eabf8577. doi: 10.1126/sciadv.abf8577
114. Xia B, Shen X, He Y, Pan X, Liu FL, Wang Y, et al. SARS-CoV-2 Envelope Protein Causes Acute Respiratory Distress Syndrome (Ards)-Like Pathological Damages and Constitutes an Antiviral Target. *Cell Res* (2021) 31(8):847–60. doi: 10.1038/s41422-021-00519-4
115. Wang Y, Fang S, Wu Y, Cheng X, Zhang LK, Shen XR. Discovery of Sars-Cov-2-E Channel Inhibitors as Antiviral Candidates. *Acta Pharmacol Sin* (2021) 43:781–87. doi: 10.1038/s41401-021-00732-2
116. Jha PK, Vijay A, Halu A, Uchida S, Aikawa M. Gene Expression Profiling Reveals the Shared and Distinct Transcriptional Signatures in Human Lung Epithelial Cells Infected With Sars-Cov-2, Mers-Cov, or Sars-Cov: Potential Implications in Cardiovascular Complications of Covid-19. *Front Cardiovasc Med* (2020) 7:623012. doi: 10.3389/fcvm.2020.623012
117. Sun X, Liu Y, Huang Z, Xu W, Hu W, Yi L, et al. Sars-Cov-2 Non-Structural Protein 6 Triggers Nlrp3-Dependent Pyroptosis by Targeting Atp6ap1. *Cell Death Differ* (2022). doi: 10.1038/s41418-021-00916-7
118. Xiong Y, Liu Y, Cao L, Wang D, Guo M, Jiang A, et al. Transcriptomic Characteristics of Bronchoalveolar Lavage Fluid and Peripheral Blood Mononuclear Cells in Covid-19 Patients. *Emerg Microbes Infect* (2020) 9 (1):761–70. doi: 10.1080/22221751.2020.1747363
119. Saichi M, Ladjemi MZ, Korniotis S, Rousseau C, Ait Hamou Z, Massenet-Regad L, et al. Single-Cell Rna Sequencing of Blood Antigen-Presenting Cells

in Severe Covid-19 Reveals Multi-Process Defects in Antiviral Immunity. *Nat Cell Biol* (2021) 23(5):538–51. doi: 10.1038/s41556-021-00681-2

120. Junqueira C, Crespo A, Ranjbar S, Lewandrowski M, Ingber J, de Lacerda LB, et al. SARS-CoV-2 Infects Blood Monocytes to Activate Nlrp3 and Aim2 Inflammasomes, Pyroptosis and Cytokine Release. *Res Sq* (2021). doi: 10.21203/rs.3.rs-153628/v1
121. Ferreira AC, Soares VC, de Azevedo-Quintanilha IG, Dias S, Fintelman-Rodrigues N, Sacramento CQ, et al. Sars-Cov-2 Engages Inflammasome and Pyroptosis in Human Primary Monocytes. *Cell Death Discov* (2021) 7(1):43. doi: 10.1038/s41420-021-00428-w
122. Barhoumi T, Alghanem B, Shaibah H, Mansour FA, Alamri HS, Akiel MA, et al. Sars-Cov-2 Coronavirus Spike Protein-Induced Apoptosis, Inflammatory, and Oxidative Stress Responses in Thp-1-Like-Macrophages: Potential Role of Angiotensin-Converting Enzyme Inhibitor (Perindopril). *Front Immunol* (2021) 12:728896. doi: 10.3389/fimmu.2021.728896
123. Li S, Jiang L, Li X, Lin F, Wang Y, Li B, et al. Clinical and Pathological Investigation of Patients With Severe Covid-19. *JCI Insight* (2020) 5(12):e138070. doi: 10.1172/jci.insight.138070
124. Varga Z, Flammer AJ, Steiger P, Haberecker M, Andermatt R, Zinkernagel AS, et al. Endothelial Cell Infection and Endotheliitis in Covid-19. *Lancet* (2020) 395(10234):1417–8. doi: 10.1016/S0140-6736(20)30937-5
125. Gillot C, Favresse J, Mullier F, Lecompte T, Dogne JM, Douxfils J. Netosis and the Immune System in Covid-19: Mechanisms and Potential Treatments. *Front Pharmacol* (2021) 12:708302. doi: 10.3389/fphar.2021.708302
126. Phua J, Weng L, Ling L, Egi M, Lim CM, Divatia JV, et al. Intensive Care Management of Coronavirus Disease 2019 (Covid-19): Challenges and Recommendations. *Lancet Respir Med* (2020) 8(5):506–17. doi: 10.1016/s2213-2600(20)30161-2
127. Yang M, Lai CL. Sars-Cov-2 Infection: Can Ferroptosis be a Potential Treatment Target for Multiple Organ Involvement? *Cell Death Discov* (2020) 6:130. doi: 10.1038/s41420-020-00369-w
128. Fillmore N, Bell S, Shen C, Nguyen V, La J, Dubreuil M, et al. Disulfiram Use Is Associated With Lower Risk of Covid-19: A Retrospective Cohort Study. *PloS One* (2021) 16(10):e0259061. doi: 10.1371/journal.pone.0259061
129. Lobo-Galo N, Terrazas-López M, Martínez-Martínez A, Díaz-Sánchez ÁG. Fda-Approved Thiol-Reacting Drugs That Potentially Bind Into the Sars-Cov-2 Main Protease, Essential for Viral Replication. *J Biomol Struct Dyn* (2021) 39(9):3419–27. doi: 10.1080/07391102.2020.1764393
130. Tamburin S, Mantovani E, De Bernardis E, Zipeto D, Lugoboni F. Covid-19 and Related Symptoms in Patients Under Disulfiram for Alcohol Use Disorder. *Intern Emerg Med* (2021) 16(6):1729–31. doi: 10.1007/s11739-021-02633-y

Conflict of Interest: The authors declare that the research was conducted in the absence of any commercial or financial relationships that could be construed as a potential conflict of interest.

Publisher's Note: All claims expressed in this article are solely those of the authors and do not necessarily represent those of their affiliated organizations, or those of the publisher, the editors and the reviewers. Any product that may be evaluated in this article, or claim that may be made by its manufacturer, is not guaranteed or endorsed by the publisher.

frontiers | Frontiers in Immunology

ORIGINAL RESEARCH
published: 17 June 2022
doi: 10.3389/fimmu.2022.854952

SARS-CoV-2 Omicron Variants Reduce Antibody Neutralization and Acquire Usage of Mouse ACE2

Ruoke Wang[1,2†], Qi Zhang[1†], Rui Zhang[1†], Zhen Qin Aw[3,4,5†], Peng Chen[1†], Yi Hao Wong[3,4,5], Junxian Hong[1], Bin Ju[6,7], Xuanling Shi[1], Qiang Ding[8,9], Zheng Zhang[6,7], Justin Jang Hann Chu[3,4,5] and Linqi Zhang[1,10,11*]*

[1] Center for Global Health and Infectious Diseases, Comprehensive AIDS Research Center, Department of Basic Medical Sciences, School of Medicine, Tsinghua University, Beijing, China, [2] Tsinghua-Peking Joint Center for Life Sciences, Beijing, China, [3] Biosafety Level 3 Core Facility, Yong Loo Lin School of Medicine, National University of Singapore, Singapore, Singapore, [4] Laboratory of Molecular RNA Virology and Antiviral Strategies, Department of Microbiology and Immunology, Yong Loo Lin School of Medicine, National University of Singapore, Singapore, Singapore, [5] Infectious Disease Translation Research Programme, Yong Loo Lin School of Medicine, National University of Singapore, Singapore, Singapore, [6] Institute for Hepatology, National Clinical Research Center for Infectious Disease, Shenzhen Third People's Hospital, The Second Affiliated Hospital, School of Medicine, Southern University of Science and Technology, Shenzhen, China, [7] The Second Affiliated Hospital, School of Medicine, Southern University of Science and Technology, Shenzhen, China, [8] Center for Infectious Disease Research, School of Medicine, Tsinghua University, Beijing, China, [9] Beijing Advanced Innovation Center for Structural Biology, Tsinghua University, Beijing, China, [10] Institute of Biopharmaceutical and Health Engineering, Tsinghua Shenzhen International Graduate School, Tsinghua University, Shenzhen, China, [11] Shenzhen Bay Laboratory, Institute of Biomedical Health Technology and Engineering, Shenzhen, China

OPEN ACCESS

Edited by:
Shailendra Saxena, King George's Medical University, India

Reviewed by:
Katherine Schultheis, Inovio Pharmaceuticals, United States
Jie Hu, Chongqing Medical University, China

***Correspondence:**
Justin Jang Hann Chu
miccjh@nus.edu.sg
Linqi Zhang
zhanglinqi@tsinghua.edu.cn

[†]These authors have contributed equally to this work

Specialty section:
This article was submitted to Viral Immunology, a section of the journal Frontiers in Immunology

Received: *14 January 2022*
Accepted: *27 April 2022*
Published: *17 June 2022*

Citation:
Wang R, Zhang Q, Zhang R, Aw ZQ, Chen P, Wong YH, Hong J, Ju B, Shi X, Ding Q, Zhang Z, Chu JJH and Zhang L (2022) SARS-CoV-2 Omicron Variants Reduce Antibody Neutralization and Acquire Usage of Mouse ACE2. Front. Immunol. 13:854952. doi: 10.3389/fimmu.2022.854952

Striking number of mutations found in the spike protein of recently emerged SARS-CoV-2 Omicron subvariants BA.1, BA.2, BA.3 and BA.4/5 has raised serious concerns regarding the escape from current antibody therapies and vaccine protection. Here, we conducted comprehensive analysis on the extent of two major Omicron lineages BA.1/BA.1.1 and BA.2 to escape neutralization from the therapeutic antibodies approved by the regulatory authorities and convalescent plasma from SARS-CoV-2 patients infected during initial wave of pandemic in early 2020. We showed that Omicron BA.1/BA.1.1 were the most resistant in both magnitude and breadth against antibodies and convalescent plasma, followed by Beta, BA.2, Gamma, Delta and Alpha. While the majority of therapeutic antibodies lost binding and neutralization to Omicron variants, BRII combo (BRII-196 + BRII-198), S309, and AZ combo (COV2-2196 + COV2-2130) maintained neutralization despite of reduction due to either conserved epitope or combinational effect between the two designated antibodies. A single intraperitoneal injection of BRII combo as a prophylactic treatment protected animals from Omicron infection. Treated animals manifested normal body weight, survived infection up to 14 days, undetectable levels of infectious viruses in the lungs, and reduced lung pathology compared to the controls. Analyzing ACE2 from diverse host species showed that Omicron variants acquired ability

to use mouse ACE2 for entry. These results demonstrate major antigenic shifts and potentially broadening the host range of two major Omicron lineages BA.1/BA.1.1 and BA.2, posing serious challenges to current antibody therapies and vaccine protection as well as increasing danger of spillover into the wildlife.

Keywords: Omicron variant, antibody neutralization, ACE2 orthologues, SARS-CoV-2 infection (COVID-19), plasma neutralization

INTRODUCTION

As the severe acute respiratory syndrome coronavirus 2 (SARS-CoV-2) continues to rage around the world, we have witnessed the rapid emergence and turnover of multiple variants of concerns (VOCs) such as Alpha (B.1.1.7), Beta (B.1.351), Gamma (P.1), Delta (B.1.617.2), and Omicron (BA.1/BA.1.1 BA.2, BA.3, and BA.4/5). There is growing concern that they could become antigenically distinct from the original strain to the extent that render current therapeutic antibody and vaccine strategies ineffective. Among the previous identified Alpha, Beta, Gamma, and Delta VOCs, Beta is the most discrete in antigenic properties which leads to the substantial reduction in its sensitivity to therapeutic antibodies and plasma neutralization from convalescent and vaccinated individuals (1–5). However, Beta appears to be less transmissible and has mostly been circulating in South Africa since it was initially identified there. By contrast, Delta has spread far beyond original country of India and continues dominating in many parts of the world due to its superior transmissibility albeit relative minor changes in antigenicity (6–11).

Recently, increased attention has been paid to Omicron variants (BA.1, BA.2, BA.3 and BA.4/5), the new member of VOCs that was initially identified in November 2021 in Botswana and South Africa (WHO or CDC) (12–14). According to the recent report from the World Health Organization (WHO) (8), Omicron variants have already spread to many countries around world and is associated with steeply increased infections among unvaccinated population as well as breakthrough infections among vaccinated individuals (15–17). One alarming aspect of Omicron variants is the largest number of mutations found in the S protein among all VOCs identified so far (**Supplementary Figure 1**). It is currently unknow how Omicron accumulated such high number of mutations in such a short period, although some speculated that it may derive from immunocompromised individuals or spillback from other animal species (18, 19). A total of 32 mutations in the spike (S) protein has been found in the predominant Omicron strain. Of which, at least 15 substitutions are located in the receptor-binding domain (RBD) and 8 substitutions and insertons/deletions are in the N-terminal domain (NTD) (**Supplementary Figure 1**). As RBD and NTD are the major target of neutralizing antibodies upon infection and vaccination, these changes may result in Omicron's escape from antibody treatment and vaccine protection. Indeed, preliminary results indicate that two major lineages of Omicron (BA.1/BA.1.1 and BA.2) can escape from some of the approved therapeutic antibodies under emergency use authorization (EUA) (18, 20–27). Serum neutralizing activities from convalescent and vaccinated individuals are also severely compromised regardless of infection status or type of vaccines used (17, 18, 20–23, 25, 28–32). However, to what extent Omicron lineages BA.1/BA.1.1, and BA.2 could escape therapeutic antibodies and convalescent plasma from the early wave of SARS-CoV-2 pandemic remains unclear. The impact of highly mutated BA.1/BA.1.1 and BA.2 spike on its interaction with ACEs from human and diverse animal hosts is also unclear. Here, we show that two major lineages of Omicron BA.1/BA.1.1 and BA.2 substantially reduces neutralization of majority of therapeutic antibodies and convalescent plasma collected during the early pandemic. However, despite of reduction, BRII combo (BRII-196 + BRII-198), S309, and AZ combo (COV2-2196 + COV2-2130) maintained neutralizing activity, perhaps due to conserved epitope or combinational effect between the two designated antibodies. Furthermore, a single intraperitoneal injection of BRII combo protected animals from Omicron infection, suggesting its neutralizing activity *in vitro* could be translated into protectivity *in vivo* in this animal model. Finally, Omicron lineages BA.1/BA.1.1 and BA.2 also acquire ability to use mouse ACE2 for entry. These results clearly show major antigenic shifts and potentially expanding the host range of Omicron BA.1/BA.1.1 and BA.2, posing serious challenges to antibody and vaccine protection as well as further spread into the wildlife.

RESULTS

Substantial Reduction in Antibody Neutralization of Omicron BA.1, BA.1.1 and BA.2

To study the impact of Omicron subvariants BA.1, BA.1.1, and BA.2 on antibody neutralization, we focused on antibodies approved by the regulatory agencies such as BRII-196 (also known as amubarvimab) and BRII-198 (also known as romlusevimab) developed by Brii Biosciences, S309 (the parental antibody of sotrovimab) by GlaxoSmithKline and Vir Biotechnology, REGN10933 (also known as casirivimab) and REGN10987 (also known as imdevimab) by Regeneron, COV2-2196 (the parental antibody of AZD8895) and COV2-2130 (the parental antibody of AZD1061) by AstraZeneca, and CB6 (the parental antibody of etesevimab) by Eli Lilly. We chose to test these antibodies first against Omicron subvariants BA.1, BA.1.1, and BA.2 and compared with that against original wildtype strain

Wuhan-Hu-1 (WT, Genbank reference MN908947) as they had well been studied already against previously identified VOCs such as Alpha, Beta, Gamma and Delta (1, 2, 33–37). Pseudoviruses bearing the spike protein of Omicron variants BA.1, BA.1.1, BA.2, and WT were subjected to neutralization analysis against 8 therapeutic antibodies individually and in combination as developed clinically (**Figure 1** and **Table 1**). To improve assay representation, the neutralization was conducted in two different cell lines: HeLa cells stably expressing human ACE2 (HeLa-hACE2) and Huh7 cells previously used for SARS-CoV-2 infection and neutralization (1, 38). In HeLa-hACE2 cell line, BRII combo (BRII-196 + BRII-198), S309, and AZ combo (COV2-2196 and COV2-2130) maintained neutralizing activity below single-digit μg/mL concentration. The rest antibodies, however, demonstrated substantially reduced or lost activity against all three Omicron variants (**Figure 1A** and **Table 1**). Among the three Omicron variants, BA.1.1 had the most adverse effect on BRII combo and AZ combo, resulting in approximately 47.4- and 912.5-fold reduction in IC50, relative to the WT (**Table 1**). BA.2, on the other hand, was the most disruptive against S309 and reduced its IC50 by about 27.4-fold (**Table 1**). Interestingly, despite of marked reduction in neutralization for individual COV2-2196 and COV2-2130, AZ combo regained neutralization to Omicron with IC50 of 0.370 μg/mL to BA.1, 3.493 μg/mL to BA.1.1, and 0.026 μg/mL to BA.2, perhaps due to the synergistic effect between the two antibodies (**Figure 1A** and **Table 1**). In Huh7 cells, the estimated IC50 and fold changes relative to WT remained largely consistent with that in HeLa-hACE2 cells (**Figure 1B** and **Table 1**). BRII combo, S309, and AZ combo maintained similar trend against the Omicron strains tested, although all of them appeared to perform better in Huh7 cells than in HeLa-hACE2 cells. This was particular true for S309 where its respective IC50 to BA.1, BA.1.1 and BA.2 improved from 0.376 μg/mL, 0.629 μg/mL, and 6.438 μg/mL in HeLa-hACE2 cells to 0.069 μg/mL (5.4-fold), 0.137 μg/mL (4.6-fold), and 0.378 μg/mL (17.0-fold) in Huh7 cells. This is consistent with previous finding that neutralizing activity of S309 varied in cell lines overexpressing ACE2 (39). For BRII combo, BRII-196, and BRII-198, neutralizing activity against live authentic Omicron BA.1 virus demonstrated the similar trend with IC50 of 0.168 μg/mL, 2.370 μg/mL and 0.632 μg/mL, respectively (**Supplementary Figure 2**). Furthermore, when comparing the linear regression between experimental IC50 values of all tested

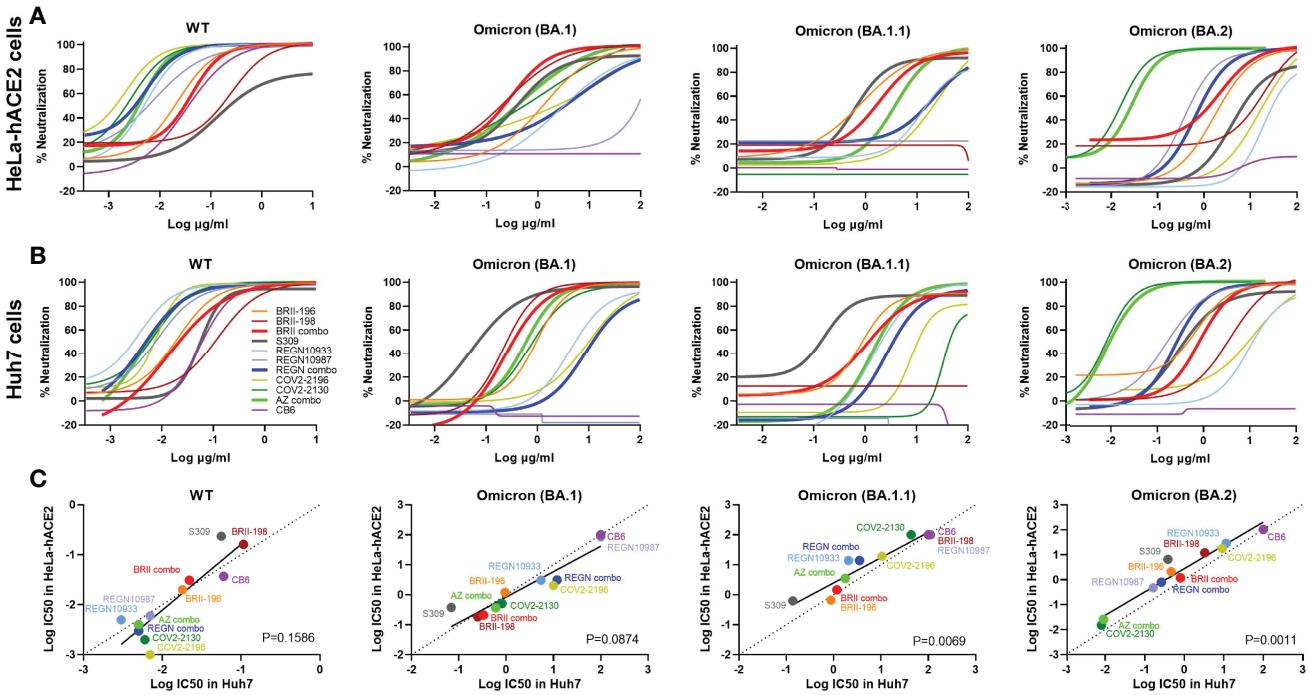

FIGURE 1 | Substantial reduction in antibody neutralization to Omicron BA.1, BA.1.1, and BA.2. Neutralizing activity of each therapeutic antibody and their designated combinations to wildtype (WT), Omicron BA.1, BA.1.1, and BA.2 pseudoviruses analyzed in **(A)** HeLa cells expressing human ACE2 (HeLa-hACE2) and **(B)** in Huh7 cells. WT and Omicron pseudoviruses were tested against serial dilutions of each antibody and relevant combinations. Neutralizing activity was defined as the percent reduction in luciferase activities compared to no antibody controls. Results were derived from two independent experiments and each included two technical replicates. **(C)** Correlation between Log IC50 for all tested mAbs and their clinical-relevant combinations in HeLa-hACE2 and Huh7 cells. The R^2 and P values of correlation were 0.7963 and 2.2e-4 for WT, 0.8768 and 2.2e-5 for BA.1, 0.9017 and 7.9e-6 for BA.1.1, and 0.9374 and 1.0e-6 for BA.2, determined by two-tailed Spearman correlation. Linear regression of experimental Log IC50 was estimated (solid line) and compared with a hypothetical regression (dotted line) for assumption of equal IC50s in both HeLa-hACE2 and Huh7 cell lines. No significant differences were detected between experimental and hypothetical regression for WT (P = 0.1586) and BA.1 (P = 0.0874), but significantly lower levels in Huh7 cells was found than in HeLa-hACE2 cells for BA.1.1 (P = 0.0069) and BA.2 (P = 0.0011).

TABLE 1 | Neutralizing and binding activities of therapeutic antibodies against WT and Omicron variants.

	Neut in Hela-hACE2 cells						Neut in Huh 7 cells						Fold Change of Spike binding		
	IC50 (μg/ml)			Fold Change			IC50 (μg/ml)			Fold Change					
	WT	BA.1	BA.1.1	BA. 2	BA .1	BA. 1. 1	BA. 2	WT	BA.1	BA.1.1	BA. 2	BA .1	BA. 1. 1	BA. 2	BA .1	BA. 1. 1	BA. 2
BRII-196	0.020	1.210	0.665	2.087	-61.5	-33.8	-106.1	0.018	0.949	0.877	0.463	-52.5	-48.5	-25.6	-2.0	-2.1	-4.3
BRII-198	0.162	0.184	>100	11.690	-1.1	<-617.6	-72.2	0.107	0.251	>100	3.303	-2.4	<-938.6	-31.0	+4.2	-198.9	-19.8
BRII-Combo	0.031	0.211	1.467	1.177	-6.8	-47.4	-38.1	0.022	0.332	1.168	0.801	-15.5	-54.3	-37.3	+1.9	-2.2	-3.9
S309	0.235	0.376	0.629	6.438	-1.6	-2.7	-27.4	0.056	0.069	0.137	0.387	-1.2	-2.4	-6.9	-1.3	-1.2	-3.4
REGN 10933	0.005	3.058	13.939	28.239	-625.9	-2852.7	-5779.1	0.003	5.463	2.055	11.507	-1959.2	-737.1	-4126.6	-5.8	-4.4	-7.3
REGN 10987	0.006	85.540	>100	0.465	-14398.4	<-16832.3	-78.3	0.007	>100	>100	0.163	<-13402.2	<-13402.2	-21.9	-70.7	-34.7	-1.4
REGN Combo	0.003	3.131	13.890	0.794	-962.9	-4271.2	-244.2	0.005	11.958	3.523	0.264	-2468.0	-727.1	-54.4	-7.0	-6.8	-1.3
COV2-2196	0.001	2.048	19.246	17.467	-1517.5	-1426.6	-12942.9	0.007	9.977	10.494	9.089	1387.9	-1459.8	-1264.3	+1.5	+1.6	-1.3
COV2-2130	0.002	0.512	>100	0.015	-233.0	<-45499.2	-6.9	0.006	0.818	43.402	0.008	-140.9	-7478.3	-1.4	-1.3	-6.0	-1.0
AZ como	0.004	0.370	3.493	0.026	-96.7	-912.5	-6.7	0.005	0.600	1.755	0.009	-113.4	-331.6	-1.7	+1.2	+1.1	+1.0
CB6	0.037	>100	>100	>100	<-2734.9	<-2734.9	<-2734.9	0.060	>100	>100	>100	<-1662.2	<-1662.2	<-1662.2	<-200	<-200	<-200

mAbs and their clinical-relevant combinations (solid line) and hypothetical regression (dotted line) for assumption of equal IC50s in both cell lines, we found no significant differences for WT (P=0.1586) and BA.1 (P=0.0874), but significantly higher activity in Huh7 than in HeLa-hACE2 cells for BA.1.1 (P=0.0069) and BA.2 (P=0.0011) (**Figure 1C**). These results indicate that substantial differences do exist between different cell lines which need to be taken into account when interpreting the antibody neutralizing activity.

Substantial Reduction in Antibody Binding to Omicron BA.1, BA.1.1, and BA.2

We next studied the binding activity of these antibodies individually or in combination to the spike protein of the three Omicron variants expressed on the surface of HEK293T (**Figure 2**). The fold-changes in normalized total fluorescence intensity (nTFI) relative to that of D614G spike were calculated and indicated in **Table 1**. Consistent with neutralization activity, BRII combo, S309, and AZ combo maintained binding to all three variants with less than five-fold reduction, although some of the antibodies, when tested singly, either markedly reduced or lost binding to at least one of the variants tested (**Figure 2**). BRII combo demonstrated somewhat increased binding to BA.1 (+1.9-fold) while decreased binding to BA.1.1 (-2.2-fold) and BA.2 (-3.9-fold), relative to WT (**Table 1**). S309 reduced binding to the spike protein of all three variants, most notably to BA.2 (-3.4-fold) (**Table 1**). By contrast, AZ combo demonstrated relatively consistent binding to BA.1 (+1.2-fold), BA.1.1 (+1.1-fold), and BA.2 (+1.0-fold), providing some mechanistic basis for its synergistic neutralizing activity, particularly against BA.2 (**Table 1** and **Figure 1**). This was perhaps owing to specific mutations in BA.2 restored the neutralizing activity of COV2-2130 (**Figure 2** and **Table 1**). These results suggest a relation between antibody binding and neutralization and reduced or lost neutralization to the three Omicron variant was largely attributed to the reduced binding to the spike protein.

BRII Combo Protects K18-hACE2 Mice From Infection With Authentic SARS-CoV-2 Omicron

We next studied the protective potential of BRII combo against infection of authentic Omicron in a K18-hACE2 mouse model of SARS-CoV-2 infection, as previously described (40) (**Figure 3A**). A total of 24 mice were used in the experiment. Of which, 12 mice were intraperitoneally administered with BRII combo at a dose of 10 + 10 mg/kg body weight (BRII-196 + BRII-198) and the other 12 remained untreated. Twenty-four hours later, all animals were intranasally challenged with 1.7×10^3 plaque-forming units (PFU) of authentic SARS-CoV-2 Omicron and monitored daily throughout the following 14 days for their body weight and survival. Six each from BRII combo treated and untreated animals were euthanized on day 3 post challenge to obtain lung and brain tissues for viral load and histopathological analysis. As shown in **Figure 3B**, BRII combo treated animals remained healthy and survived infection while one of the six untreated animals succumbed to disease on day 11 after

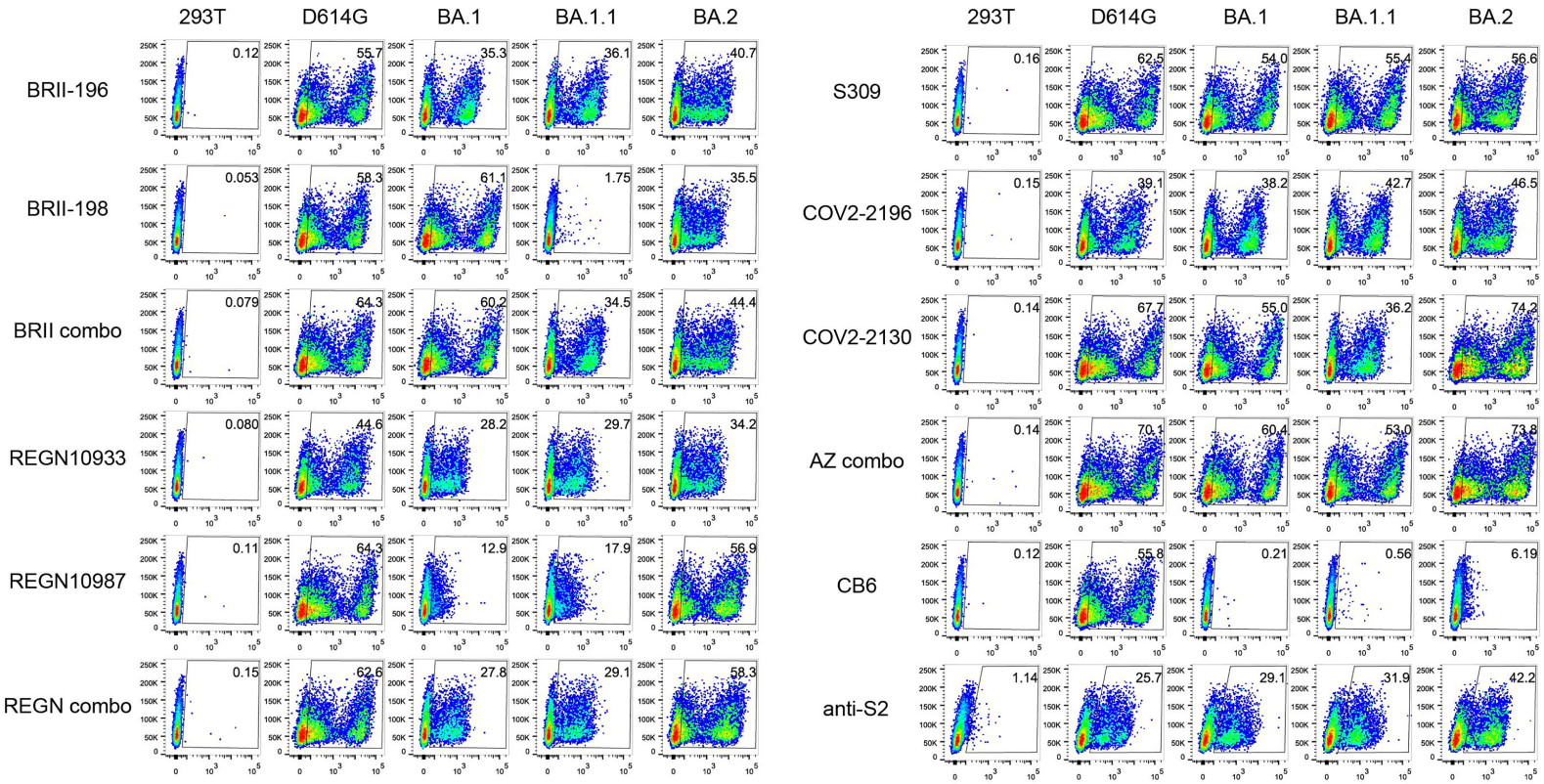

FIGURE 2 | Antibody binding to spikes of Omicron BA.1, BA.1.1, and BA.2 expressed on the cell surface. Binding of all tested mAbs, and their clinical-relevant combinations to the spike protein of WT D614G, Omicron BA.1, BA.1.1, and BA.2 expressed on the surface of HEK293T, measured by flow cytometry. Anti-S2 is a S2-specific antibody used for positive control. The numbers highlighted in the gates represent the percent of positive cells detected by indicated antibodies or combinations. The result shown was representative of two independent experiments.

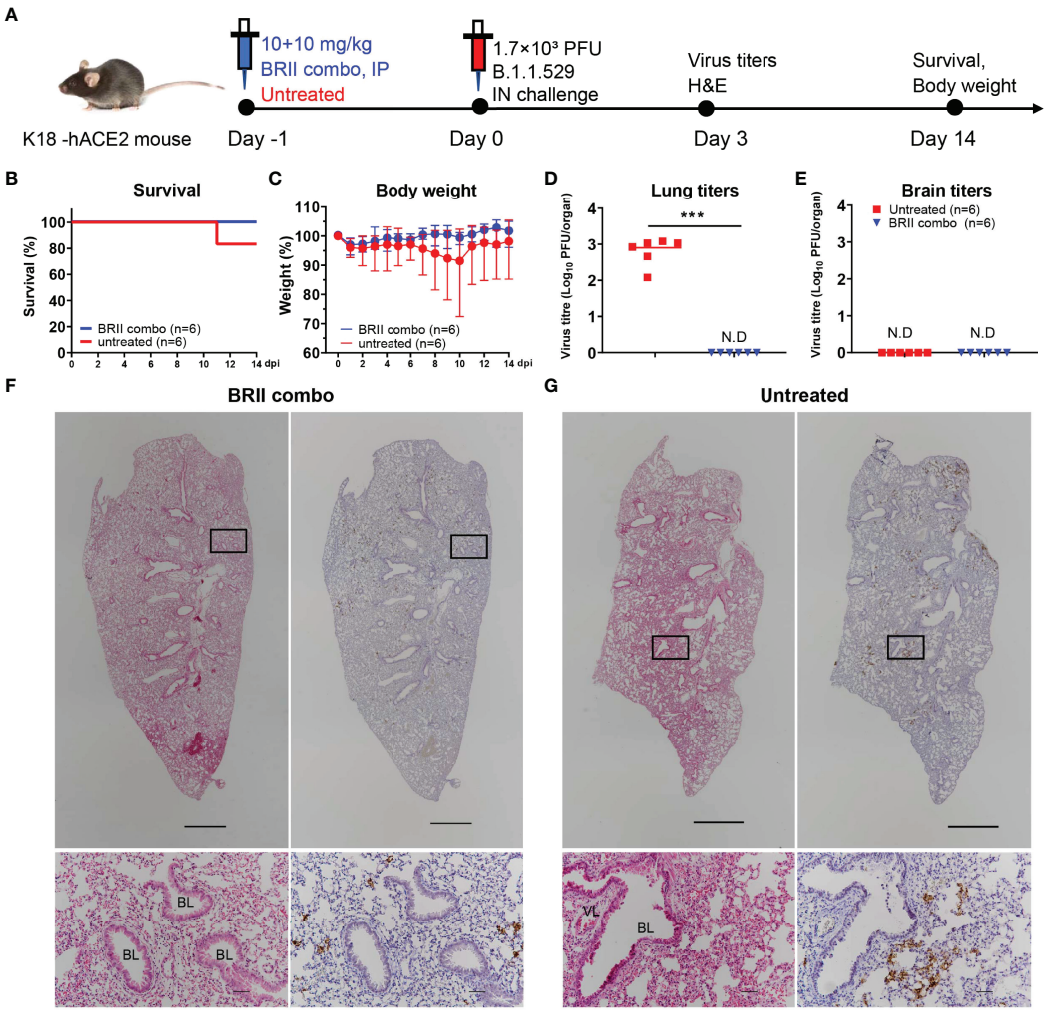

FIGURE 3 | BRII combo protects K18-hACE-2 mice from the infection of authentic SARS-CoV-2 Omicron. **(A)** Experimental schedule for BRII combo prophylaxis. Eight-week-old K18-hACE2 transgenic female mice were administered with 20 (10 + 10) mg/kg body weight of BRII combo (BRII-196 + BRII-198) intraperitoneally or remained untreated. One day later, all animals were challenged with 1.7×10^3 plaque-forming units (PFU) infectious SARS-CoV-2 Omicron *via* the intranasal route. **(B)** The survival percentage and **(C)** body-weight were recorded daily after infection until the occurrence of death or until the end of experiment. The viral load in **(D)** the lung and **(E)** the brain tissues was measured by plaque forming assays in the tissue homogenates at 3 days post inoculation. Data are presented as the means ± SEM. N.D: not detected. Mann-Whitney test was used to analyze statistical significance. ***$P < 0.001$. **(F, G)** H&E and immunohistochemistry staining of lung tissue from BRII combo-treated or untreated mice at 3 days post inoculation. The upper panels show the whole lung sections (5x; Scale bars=1000μm) while the lower panels displayed the enlarged view of the boxed regions (50x; Scale bars=50μm). Dark brown in the enlarged view are SARS-CoV-2 N protein positive cells. VL, vascular lumen; BL, bronchiolar lumen. Images were derived from one representative animal in each group.

challenge. The body weight followed the similar changes, with moderate increase in BRII combo treated animals while minor loss in untreated animals (**Figure 3C**). In BRII combo treated animals, no detectable levels of live viruses were found in the lungs on day 3 post challenge. In untreated animals, however, the live virus titer reached an average as high as 10^3 PFU/tissue (**Figure 3D**). No detectable levels of live viruses were found in the brain in either BRII combo treated nor untreated animals (**Figure 3E**). Immunohistochemistry analysis showed that the lung tissue of BRII combo-treated mice remained intact and scattered virial antigen positive cells could be detected (**Figure 3F**). The lung sections of untreated mice, however, presented moderate damage and inflammation with marked infiltration of inflammatory cells. Infected cells were readily detectable using anti-N protein specific antibody (**Figure 3G**).

Substantial Reduction in Neutralizing Activity of Convalescent Plasma to Omicron BA.1, BA.1.1 and BA.2

We next studied to what extent Omicron BA.1, BA.1.1, and BA.2 could escape from neutralization of convalescent plasma collected during the early wave of the pandemic. A total of 18

convalescent plasma samples were obtained between one or two months after wildtype strain Wuhan-Hu-1 infection. Of which, eleven patients had only mild symptoms while the remaining seven developed severe disease. The average age was 54 ranging between 29 and 81 years old. Ten were men and eight were women. For each plasma sample, eight 3-fold serial dilutions were made starting from 1:60 and neutralization activity was estimated based on half-maximal inhibitory dilution (ID50) and fold changes relative to that against D614G pseudovirus (**Figure 4** and **Supplementary Figure 3**). The data on Alpha, Beta, and Gamma have been previously reported (1) and included here for comparison only. A complete loss in neutralization activity (below the limit of detection, BDL) was found in 17 of the 18 plasma samples tested against Omicron BA.1 and BA.1.1, 8 against Beta, 6 against BA.2, 4 against Gamma, and none against Alpha and Delta (**Figure 4A**). The remaining plasma demonstrated varying degree of reduction or increase in neutralization potency against VOCs tested (**Figure 4A**, and **Supplementary Figure 3**). As a result, the greatest reduction in plasma neutralization was against Omicron BA.1 (10.3-fold), followed by BA.1.1 (9.7-fold), Beta (5.6-fold), BA.2 (2.9-fold), Gamma (2.5-fold), Delta (1.5-fold), and Alpha (1.2-fold) (**Figures 4B, C**). Furthermore, we also measured plasma binding to the spike protein of the three Omicron variants expressed on the surface of HEK293T. The fold-changes in normalized total fluorescence intensity (nTFI) relative to that of D614G spike were calculated and presented in **Figures 4D, E**. Consistent with neutralization activity, the plasma binding activity also reduced to the three variants regardless of in absolute values or fold-reduction compared to the WT (**Figures 4D, E**, and **Supplementary Figure 4**). These results clearly show that Omicron BA.1 and BA.1.1 variants were the most resistant followed by BA.2 against the convalescent plasma tested. It is possible the such reduction and loss were attributed to the striking number of mutations found in the Omicron spike including 142-144del in the NTD and G339D, S371L, S373P, S375F, K417N, E484A, Q493R, and N501Y in the RBD that had previously been shown to confer resistance against antibody and serum neutralization (1–3, 41–43), although other mutations might have made additional contribution (**Supplementary Figure 1**). Interestingly, the reduction in neutralization to BA.2 appeared to be smaller compared to BA.1 and BA.1.1, perhaps due to the relative conserved NTD region compared to BA.1 and BA.1.1 (**Supplementary Figure 1**). Finally, individual convalescent plasma samples appear to respond differently to Omicron variants and other VOCs pseudoviruses, perhaps reflecting their different compositions and proportions of neutralizing antibodies in each individual generated during natural infection.

A

Fold changes in ID50	WT	Variants						
	D614G	Alpha	Beta	Gamma	Delta	Omicron BA.1	Omicron BA.1.1	Omicron BA.2
C-plasma3	+1.0	-1.2	-3.7	-1.4	-1.2	BDL	BDL	-2.2
C-plasma4	+1.0	-1.3	-2.5	-1.2	+1.1	BDL	BDL	-3.2
C-plasma5	+1.0	-1.8	-6.7	-2.0	-2.8	BDL	BDL	+1.1
C-plasma6	+1.0	-1.3	-7.2	-2.2	+1.5	BDL	BDL	-4.7
C-plasma7	+1.0	-1.3	-7.2	-1.5	-1.0	BDL	BDL	-1.7
C-plasma8	+1.0	-1.3	BDL	-5.0	-1.9	BDL	BDL	-4.1
C-plasma9	+1.0	-1.5	BDL	BDL	-2.2	BDL	BDL	BDL
C-plasma10	+1.0	+1.3	-18.7	-8.0	-10.3	BDL	BDL	-8.4
C-plasma11	+1.0	-1.2	-6.7	-1.4	-1.6	BDL	BDL	-1.5
C-plasma12	+1.0	+1.1	BDL	-3.1	-6.2	BDL	BDL	-2.7
C-plasma13	+1.0	-1.1	-4.4	-1.0	-1.4	-22.6	-8.3	-2.3
C-plasma14	+1.0	-1.1	BDL	-3.9	-2.0	BDL	BDL	-1.7
C-plasma15	+1.0	+1.1	BDL	BDL	-3.0	BDL	BDL	BDL
C-plasma16	+1.0	+1.1	BDL	BDL	+5.4	BDL	BDL	BDL
C-plasma17	+1.0	-1.3	BDL	BDL	+1.2	BDL	BDL	BDL
C-plasma18	+1.0	-2.1	-3.7	-2.3	+2.9	BDL	BDL	BDL
C-plasma19	+1.0	-1.2	-1.1	-1.4	-1.1	BDL	BDL	BDL
C-plasma20	+1.0	-1.3	BDL	-2.8	-2.0	BDL	BDL	-2.5

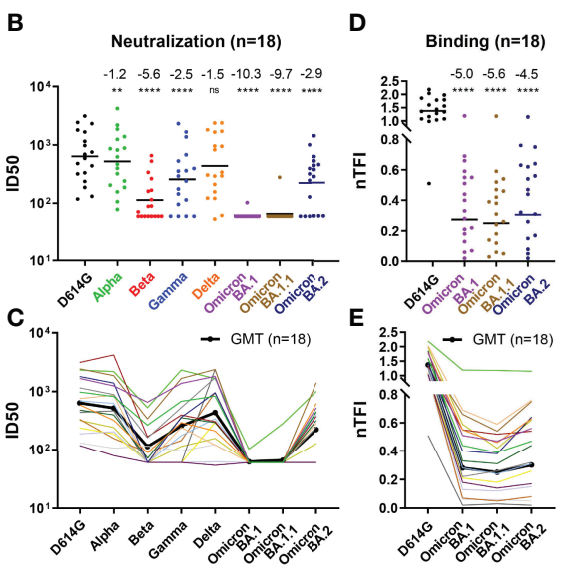

FIGURE 4 | Substantial reduction in neutralizing activity of convalescent plasma to Omicron variants. Reciprocal plasma dilutions (ID50) against SARS-CoV-2 variants are shown either by **(A)** fold changes relative to D614G pseudoviruses, or absolute values in **(B)** colored dots and **(C)** colored curves. The average fold changes in ID50 between each variant and D614G pseudoviruses are shown individually in **(A)** or as a group at the top in **(B)**. The symbol "-" indicates an increase in resistance while the symbol "+" indicates an increase in sensitivity. Those in light red indicate a minimum of 2-fold increase in resistance; dark red a minimum of 20-fold increase in resistance; blue a minimum 2-fold increase in sensitivity; and white a less than 2-fold change in either resistance or sensitivity. BDL (Below Detection Limit) indicates the highest concentration of plasma (1:60 for D614G, Alpha, Beta, and Gamma and 1:20 for Delta and Omicron) failed to confer 50% neutralization. **(B, C)** Each dot or curve represents a different plasma sample. The geometric mean titer of ID50 against each variant is indicated by a black solid line. **(D, E)** Plasma binding to spike proteins on the cell surface measured by FACS and presented as normalized total fluorescent intensity (nTFI) in **(D)** colored dots and **(E)** colored curves. The results were calculated from two independent experiments, and each included two experimental replicates. **P < 0.01; and ****P < 0.0001. ns, not significant.

Omicron Variant Acquires Usage of Mouse ACE2 for Viral Entry

To study the potential impact of Omicron variants on host range and cross-species transmission, we evaluated the ability of ACE2 from five host species to support entry of Delta and Omicron BA.1, BA.1.1, and BA.2 pseudoviruses. HeLa cell lines stably expressing ACE2 molecules from human, mink, mouse, deer, and hamster that have recently been shown susceptible to SARS-CoV-2 infection (44–47) were subjected to analysis. The entry efficiency was measured and presented as fold-changes relative to D614G (**Figure 5A**). Delta acquired substantial ability to infect HeLa cells expressing mink-ACE2 (HeLa Mink-ACE2) and mouse-ACE2 (HeLa Mouse-ACE2), and to a lesser extent deer-ACE2 (HeLa Deer-ACE2). The improved efficiency was about 82.3-fold, 131.7-fold, and 3.4-fold, respectively (**Figure 5A**). Compared to Delta, all three Omicron variants moderately improved their entry efficiency only to infection HeLa Mouse-ACE2, with improve efficiency about 12.4-fold, 8.2-fold, and 8.3-fold, respectively. To pinpoint the potential mutation(s) responsible for enhanced entry efficiency, we generated a total of 21 single-mutant pseudoviruses carrying the specific mutations found within RBD of Delta and the three Omicron variants. Comparing the entry efficiency of these mutant pseudoviruses into HeLa Mouse-ACE2 cells to WT D614G, we found 7 single substitutions (R408S, K417N, Q493R, Q493K, G496S, Q498R, and N501Y highlighted in dark red) substantially improved while 3 (S371L, S371F, and S375F in dark blue) decreased infection (**Figure 5A**). Additional mutations only moderately impacted on the entry efficiency either by improvement (L452R and T478K) or deterioration (T376A, D405N, G446S, and Y505H). This agrees well with the recent reports where either single N501Y, Q493K, or triple K417N-Q493H-N501Y mutations were found in the mouse-adapted SARS-CoV-2 strains, although the triple mutant causes more severe acute respiratory symptoms and mortality in standard laboratory mice (45, 48–50). This is also compatible with the elegant structural analysis on interaction between human ACE2 and RBD of Omicron BA.1 where Q493R substitution was proposed to enhance mouse ACE2 binding through formation of electrostatic interactions with the N31 side chain amide (51). When analysis of entry efficiency into HeLa Mink-ACE2 cells, three substitutions (L452R, T478K, and N501Y) moderately improved whereas two (S371L and S375F) severely compromised the infection (**Figure 5A**). Structurally, these critical mutations are either located on or approximate to the interface between ACE2 and RBD of Delta, Omicron BA.1, and BA.2 (**Figure 5D**). Lastly, substitutions in the inner face (S371L, S371F, S375F, and T376A) and at "mesa" region (G446S and Y505H) of RBD (4) resulted in considerable decrease in entry efficiency to all cell lines studied, suggesting their critical role in upholding overall structure and function for RBD in mediating interaction with ACE2 (**Figures 5A, D**).

To test whether therapeutic antibodies and relevant combinations could inhibit Omicron BA.1 infection of HeLa Mouse-ACE2 cells, serial dilutions of antibodies were incubated with Omicron BA.1 pseudovirus before applied onto HeLa Mouse-ACE2 cells. After 48h, the infected cells were lysed and measured for luciferase-activity. Neutralizing activity was defined as the percent reduction in luciferase activities compared to no antibody controls. As shown in **Figure 5B**, BRII combo was the most potent in inhibiting Omicron BA.1 entry into HeLa Mouse-ACE2 cells, followed by AZ combo, BRII-198, and S309. The rest of antibodies and combinations, however, demonstrated substantial weaker neutralizing activity. Interestingly, linear regression analysis on the IC50 of the tested antibodies and combinations revealed neutralizing activities were more potent in HeLa Human-ACE2 than in HeLa Mouse-ACE2 (P=0.0001), although strong correlation was found between the two systems (**Figure 5C**). This may suggest that Omicron BA.1 spike interacts with mouse ACE2 in a way that is different from that with human ACE2. Nevertheless, given the capacity of BRII combo and AZ combo in inhibiting Omicron BA.1, vaccine capable of inducing antibodies like BRII combo and AZ combo would be expected to provide protection against cross transmission of Omicron BA.1 from human to mouse. Taken together, these results indicate that the Omicron variants acquired mutations in RBD that not only facilitate their escape from antibody neutralization but also potentially expand their host range to mouse and perhaps mink. Active surveillance of these variants in both human and relevant animal species would be required to minimize potential cross-species transmission.

DISCUSSION

We performed comprehensive analysis on the impact of Omicron BA.1. BA.1.1 and BA.2 on neutralizing activity of therapeutic antibodies and convalescent plasma collected during the initial phase of pandemic in early 2020. Among the VOCs tested, we found Omicron BA.1 and BA.1.1 were the most capable of escaping from neutralization of convalescent plasma from early pandemic and a large number of therapeutic antibodies approved by the regulatory authorities, followed by Beta, BA.2, Gamma, Delta and Alpha. This resistance hierarchy is well correlated with the number of mutations in the NTD and RBD that led to the major antigenic shift in the spike protein. Particularly, Omicron variants has striking number of mutations across the entire spike, including 69-70del and 142-144del in the NTD and triple K417N-E484A-N501Y in RBD that previously found in Beta and Gamma and shown to jeopardize neutralizing activity of most therapeutic antibodies and plasma from convalescent and vaccinated individuals (1–3, 41–43). On top of these, Omicron variants also has additional mutations in the receptor-binding motif (RBM) (N440K, G446S, S477N, T478K, Q493R, G496S, Q498R, Y505H) and on the core domain of RBD (G339D, S371L, S373P, and S375F), which could facilitate Omicron escape from additional antibody and serum neutralization. No complete neutralizing data on BA.3 and BA.4/5 subvariants are currently available. However, given their similar degree of mutations with that found in BA.1, BA.1.1, and BA.2, it is reasonable to speculate that they are also capable of escaping from therapeutic antibodies and plasma

A

Fold changes in entry	D614G	Delta	Omicron BA.1	Omicron BA.1.1	Omicron BA.2	G339D	R346K	S371L	S371F	S373P	S375F	T376A	D405N
		Variants				RBD							
HeLa Human-ACE2	+1.0	+1.9	-4.3	-5.8	-9.4	+1.5	+1.4	-17.2	-11.1	+1.2	-401.9	-5.1	+1.0
HeLa Mink-ACE2	+1.0	+82.3	-1.5	-1.7	-6.3	+1.2	+1.8	-28.5	-18.8	-1.1	-71.6	-6.0	-1.7
HeLa Mouse-ACE2	+1.0	+131.7	+12.4	+8.2	+8.3	+1.3	+2.7	-93.7	-33.0	-1.3	-166.0	-10.5	-5.8
HeLa Deer-ACE2	+1.0	+3.4	-1.7	-3.8	-3.7	+1.5	+1.3	-18.9	-84.8	-1.1	-99.5	-4.0	-1.5
HeLa Hamster-ACE2	+1.0	+1.0	-15.0	-23.0	-19.2	+1.4	+1.2	-5.3	-2.4	-1.0	-193.6	-5.1	-1.2

Fold changes in entry	R408S	K417N	N440K	G446S	L452R	S477N	T478K	Q493R	Q493K	G496S	Q498R	N501Y	Y505H
	RBD												
HeLa Human-ACE2	+1.8	+1.3	-2.1	-3.0	-1.7	-2.5	+1.6	-1.8	-2.7	-2.9	-2.8	+1.3	-3.1
HeLa Mink-ACE2	+1.5	-3.4	+1.7	-3.0	+5.4	-1.7	+3.0	-1.1	-1.9	-6.0	-3.1	+7.1	-8.9
HeLa Mouse-ACE2	+30.1	+27.6	-1.0	-11.5	+6.1	-1.9	+7.5	+57.8	+76.4	+30.3	+32.7	+175.2	-12.2
HeLa Deer-ACE2	+1.9	-1.3	-1.4	-3.8	-1.6	-2.4	+2.2	-1.4	-1.8	-3.2	-2.1	+1.5	-3.6
HeLa Hamster-ACE2	-1.1	-1.6	-3.2	-4.6	-4.1	-3.2	-1.3	-3.8	-2.9	-4.2	-6.7	-1.5	-2.5

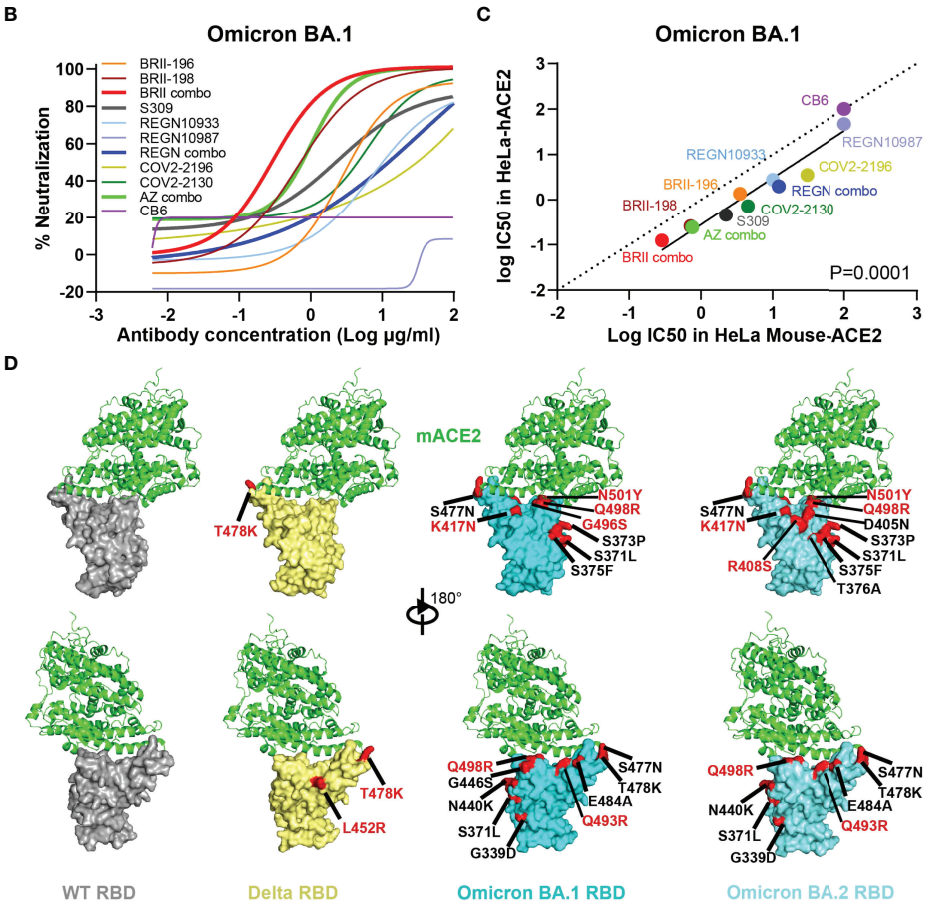

FIGURE 5 | Omicron variants acquire usage of mouse ACE2 and reduces sensitive to antibody neutralization. **(A)** Entry efficiency of SARS-CoV-2 Delta, Omicron BA.1, BA.1.1, BA.2, and 21 single mutant pseudoviruses into HeLa cell lines ectopically expressing various host ACE2. The values represent the fold changes in luciferase activity relative to D614G. The symbol "+" indicates an increase while "-" indicates a decrease in entry efficiency. Red color highlights at least threefold increase in entry efficiency; blue indicates at least threefold decrease in efficiency, while white indicates no change greater than threefold. Results were derived from two independent experiments. **(B)** Neutralizing sensitivity of Omicron BA.1 to each therapeutic antibody and designated combinations, measured in HeLa cells expressing mouse ACE2 (HeLa Mouse-ACE2). Results were calculated from two independent experiments. **(C)** Correlation between IC50 for each antibody and designated combinations against BA.1 pseudovirus measured in HeLa-hACE2 and HeLa Mouse-ACE2. The R^2 and P values for correlation were 0.9193 and 3.2e-6, determined by two-tailed Spearman correlation. Linear regression of experimental Log IC50 was estimated (solid line) and compared with a hypothetical regression (dotted line) for assumption of equal IC50s in both HeLa-hACE2 and HeLa Mouse-ACE2. Neutralizing activity was significantly higher in HeLa-hACE2 cells than that in HeLa Mouse-ACE2 ($P = 0.0001$). **(D)** Structural modeling of mouse ACE2 binding to RBD of WT, Delta, Omicron BA.1, and BA.2. Structure of mACE2 binding to a lethal mouse adapted SARS-CoV-2 RBD in grey (PDB:7FDK). Docking of mACE2 onto the Delta RBD in yellow (PDB:7WBQ), or onto Omicron BA.1 and BA.2 RBD in cyan (PDB:7WBP). The major substitutions found in the RBD of studied variants are indicated and those in red showed substantial enhancing effect on entry into HeLa Mouse-ACE2 cell line.

of convalescent and vaccinated individuals. Although the specific levels of neutralizing antibody required to confer protection remains uncertain, reductions in antibody titers raises concerns about their protective potentials against all Omicron variants analyzed here.

Among the tested therapeutic antibodies, a few remain active against Omicron variants such as BRII combo, S309, and AZ combo, although the underlying mechanisms might have been different. Despite substantially reduced activity of BRII-196 against Omicron variants, BRII-198 neutralizing and binding activity remained largely unaffected to BA.1, moderately decreased to BA.2, but severely reduced to BA.1.1. However, combination of BRII-196 and BRII-198 managed to maintain neutralizing activity to the Omicron variants up to single-digit μg/mL levels in both in HeLa-hACE2 and Huh7 cell lines. More importantly, BRII combo demonstrated strong protection against Omicron infection in a K18-hACE2 mouse model of SARS-CoV-2 infection, reinforcing its neutralizing activity *in vitro* could be translated into protectivity *in vivo*.

S309 maintained its potency and breadth against Omicron BA.1, BA.1.1 and BA.2, likely attributed to its highly conserved epitope across many VOCs identified so far (1, 2, 4, 43, 51, 52). However, S309 is the only antibody tested here that varied dramatically in its neutralizing activity between two different cell populations. In HeLa-hACE2 cells, S309 generally performed poorly and failed to reach 100% inhibitory effect (IC100) against Omicron variants and 90% inhibitory effect (IC90) against WT. Over expression of ACE2 in the HeLa cells could interfere the very inhibitory mechanism mediated by S309 (39). In this regard, selection of appropriate target cells is therefore fundamental for objectively evaluating antibody neutralization. Unfortunately, the FDA recently announced that the current S309 (sotrovimab) 500 mg dose would not be effective against the Omicron BA.2 subvariant and is therefore no longer authorized to treat COVID-19 in the US against BA.2 infection. In response, GSK/Vir have made public announcement that they are preparing materials and evidence in support of a higher dose of S309 (sotrovimab) for the treatment of Omicron BA.2 subvariant (https://us.gsk.com/en-us/media/press-releases/us-food-and-drug-administration-revises-emergency-use-authorization-for-sotrovimab-due-to-omicron-ba2-subvariant/). The final results have yet been released up till time of writing.

The most unexpected finding is the regaining neutralizing activity of AZ combo against Omicron variants despite each of the individual antibody (COV2-2196 and COV2-2130) markedly reduced or lost neutralizing activity. COV2-2196 and COV2-2130 failed to reach IC90 in HeLa-hACE2 cells so did COV2-2196 in Huh7 cell. However, in both cell types, COV2-2196 and COV2-2130 combo showed impressive synergistic effect and secured the effectiveness of AZ combo against Omicron particularly to subvariant BA.2. The synergistic effect between the two antibodies have also been reported elsewhere (22, 53).

Apart from neutralization escape, Omicron and Delta are found to acquire ability to use mouse ACE2, raising a serious concern of potential transmission to other animal species. Particularly, Omicron demonstrated improved tropism to HeLa Mouse-ACE2, perhaps due to N501Y, Q493K, or triple K417N-Q493H-N501Y mutations previously found to improve replication and cause more severe acute respiratory symptoms and mortality in standard laboratory mice (45, 48–50). The potential mechanism for enhanced entry of Delta remains unclear as K417N, Q493K/R, and N501Y were not found in its RBD (**Supplementary Figure 1**). It needs to be emphasized that our entry studies were conducted on ectopically expressed ACE2 that does not necessarily equal natural infection and transmission in the corresponding animals. However, the same K417N, Q493H/K, and/or N501Y mutations found in mouse adapted SARS-CoV-2 should raise enough concern about the potential spread of these new variants to mice and beyond. Indeed, recently identification of SARS-CoV-2 variants in the mink farm in Denmark (44), free-ranging white-tailed deer (46), and hamsters in pet shops and storage facilities (47) has raised alarming signal about the complexity of host range and cross-species transmission of SARS-CoV-2 variants. Rigorous and thorough monitoring of relevant animals would be required to better understand such complexity and to prevent future transmission to wildlife and spillback to humans.

MATERIALS AND METHODS

Study Approval

The study was approved by the Research Ethics Committee of Shenzhen Third People's Hospital (2020-084). Entire research was conducted following the rules and regulations of the Chinse government for the protection of human subjects. Blood samples were obtained with informed consent of the study subjects.

Human Blood Samples

A total of 18 SARS-CoV-2 infected and convalescent patients were enrolled into the study. Their infection status and related demographic information were previously reported (1). All these patients were cured although 7 individuals developed severe pneumonia and the remaining 11 individuals manifested mild symptom. Convalescent blood samples were collected during hospitalization or follow-up visits in Shenzhen Third People's Hospital, within two months after symptom onset. All blood samples were separated into plasma and peripheral blood mononuclear cells (PBMC) by Ficoll-Hypaque gradient (GE Healthcare) centrifugation. Plasma samples were heat-inactivated at 56 °C for 1h and stored at -80 °C until use.

Cell Lines

The following cell lines used in the current study were maintained at 37°C in 5% CO2 in Dulbecco's minimal essential medium (DMEM) containing 10% (v/v) heat-inactivated fetal bovine serum (FBS) and 100 U/mL of penicillin–streptomycin. They included HEK293T cells (ATCC, CRL-3216), Huh7 cells (JCRB, JCRB0403), HeLa cells (ATCC, CCL-2) and HeLa cells expressing ACE2 orthologs kindly provided by Dr. Qiang Ding at School of Medicine Tsinghua University. FreeStyle 293F cells (Thermo Fisher Scientific,

R79007) were maintained at 37°C in 5% CO2 in SMM 293-TII expression medium (Sino Biological, M293TII)

Production of Antibodies

Antibodies approved by the regulatory for clinical use include BRII-196/BRII-198, S309, REGN10933/REGN10987, COV2-2196/COV2-2130 and CB6 were selected for evaluation in the current study. All antibodies except BRII-196/BRII-198 were evaluated using parental IgG antibodies without Fc modification. Apart from BRII-196/BRII-198 derived from our own laboratory, the rest antibodies were synthesized according to the sequences released in Protein Data Bank (PDB) (52, 54–56). Antibodies were produced by co-transfection of the heavy and light chain expression vectors into 293F cells using polyethyleneimine (PEI) (Polysciences). After 96h, antibodies secreted into the cell supernatant were captured by AmMag Protein A Magnetic Beads (Genscript L00695) and eluted by solution buffer Glycine pH 3.0. All antibodies were further purified by gel-filtration chromatography with Superdex 200 High-Performance column (GE Healthcare). The final protein concentrations were determined by nanodrop 2000 Spectrophotometer (Thermo Scientific).

Production of Pseudoviruses Carrying Wildtype and Mutant Spike Protein

The wildtype pseudovirus used throughout the analysis was the prototype strain (GenBank: MN908947.3) (WT) or with a D614G mutation (D614G). The Alpha variant (Pango lineage B.1.1.7, GISAID: EPI_ISL_601443) included a total of 9 reported mutations in the spike protein (69-70del, 144del, N501Y, A570D, D614G, P681H, T716I, S982A and D1118H). The Beta variant (Pango lineage B.1.351, GISAID: EPI_ISL_700450) included 10 identified mutations in the spike such as L18F, D80A, D215G, 242-244del, S305T, K417N, E484K, N501Y, D614G and A701V. The Gamma variant (Pango lineage P.1, GISAID: EPI_ISL_792681) had 12 reported mutations in the spike including L18F, T20N, P26S, D138Y, R190S, K417T, E484K, N501Y, D614G, H655Y, T1027I and V1176F. The Delta variant (Pango lineage B.1.617.2, GISAID: EPI_ISL_1534938) included 10 reported mutations in the spike such as T19R, G142D, 156-157del, R158G, A222V, L452R, T478K, D614G, P681R, D950N. The Omicron BA.1 variant (Pango lineage BA.1, GISAID: EPI_ISL_6752027) was constructed with 32 mutations in the spike such as A67V, Δ69-70, T95I, G142D/Δ143-145, Δ211/L212I, ins214EPE, G339D, S371L, S373P, S375F, K417N, N440K, G446S, S477N, T478K, E484A, Q493R, G496S, Q498R, N501Y, Y505H, T547K, D614G, H655Y, N679K, P681H, N764K, D796Y, N856K, Q954H, N969K, and L981F. The Omicron BA.1.1 variant (Pango lineage BA.1.1, GISAID: EPI_ISL_7545692) was constructed based on BA.1 variant with additional of R346K substitution. The Omicron BA.2 variant (Pango lineage BA.2, GISAID: EPI_ISL_8515362) was constructed with 29 mutations in the spike such as T19I, 24-26del, A27S, G142D, V213G, G339D, S371F, S373P, S375F, T376A, D405N, R408S, K417N, N440K, S477N, T478K, E484A, Q493R, Q498R, N501Y, Y505H, D614G, H655Y, N679K, P681H, N764K, D796Y, N969K and Q954H.The full-length genes of spike variants were synthesized by Genwiz, Inc. and verified by sequencing. All the mutations in RBD domain of Delta and three Omicron variants were separately introduced into the pcDNA3.1 vector encoding WT D614G SARS-CoV-2. Pseudoviruses were generated by co-transfecting HEK-293T cells (ATCC) with human immunodeficiency virus backbones expressing firefly luciferase (pNL4-3-R-E-luciferase) and pcDNA3.1 vector encoding either wildtype or variant spike proteins. Viral supernatant was collected 48h or 72h later, centrifuged to remove cell lysis, and stored at -80°C until use.

HeLa Cell Lines Expressing ACE2 From Diverse Host Origin

HeLa cells expressing ACE2 orthologs were kindly provided by Dr. Qiang Ding at Tsinghua University School of Medicine as previously reported (1, 57). The species names and accession numbers of the ACE2 orthologs are listed below: Homo sapiens, NP_001358344.1; Mink, Mustela lutreola, MT560518.1; Mouse, Mus musculus, NP_001123985.1; Chinese hamster, Cricetulus griseus, XP_003503283.1; White-tailed fawn, Odocoileus virginianus texanus, XP_020768965.1. For studying entry efficiency of SARS-CoV-2 variants and WT D614G with single mutation, HeLa-ACE2 cells were added to 96 well plates, mixed with 50 μL of pseudovirus, and analyzed the luciferase activities 48 h after infection using Bright-Glo Luciferase Assay Vector System (Promega Bioscience). Fold changes between the variants and WT D614G were used to estimate the entry efficiency of SARS-CoV-2 variants.

Antibody and Plasma Neutralization Using Pseudoviruses

Therapeutic antibodies and convalescent plasma were serially diluted before mixing with wildtype or the variants pseudovirus at 37°C for 1h before added onto HeLa-hACE2 cells, Huh7 cells, or HeLa Mouse-ACE2 cells. After 48h, the infected cells were lysed and measured for luciferase-activity. The percent of neutralization was determined by comparing with that of virus control. To ensure properly measuring neutralizing activity, therapeutic antibodies were diluted starting from 100 μg/mL for Omicron pseudovirus and from 10μg/mL for WT pseudovirus. Convalescent plasma was diluted with the highest dilution of 1:60.

Binding of Antibodies and Convalescent Plasma to Cell Surface-Expressed Wildtype and Omicron Spike Proteins

The entire procedure was conducted as previously published (1, 58). Specifically, HEK 293T cells were transfected with expression plasmids encoding either wildtype or Omicron BA.1, BA.1.1, and BA.2 spike glycoproteins, and incubated at 37°C for 36 h. Cells were digested from the plate with trypsin and distributed onto 96-well plates. Cells were washed twice with 200 μL staining buffer (PBS with 2% heated-inactivated FBS) between each of the following steps. First, cells were stained with each antibody (1 μg/mL), relevant antibody combination (1 μg/mL +

1 μg/mL), diluted convalescent plasma (1:100), or S2-specific monoclonal antibody (1 μg/mL) (MP Biomedicals, Singapore 08720401) at 4°C for 30 min. PE-labeled anti-human IgG Fc (Biolegend 410718), anti-mouse IgG FITC (ThermoFisher Scientific A10673), or anti-his PE secondary antibody (Miltenyi 130120787) was added and incubated at 4°C for 30 min. After extensive washes, the cells were resuspended and analyzed with BD LSRFortassa (BD Biosciences, USA) and FlowJo 10 software (FlowJo, USA). HEK 293T cells with mock transfection were stained as background control. Fold changes in antibody binding were calculated by the ratio between the total fluorescence intensity (TFI) of Omicron over wildtype, normalized by that of S2 specific antibody (nTFI). TFI was calculated by multiplying the mean fluorescence intensity (MFI) and the number of positive cells in the selected gates.

Antibody Protection in hACE2 Transgenic Mice

Animal experiments were conducted in a Biosafety Level 3 (BSL-3) facility in accordance with the National University of Singapore (NUS) Institutional Animal Care and Use Committee (IACUC) (protocol no. R20-0504), and the NUS Institutional Biosafety Committee (IBC) and NUS Medicine BSL-3 Biosafety Committee (BBC) approved SOPs. Eight-week-old female K18-hACE2 transgenic mice (InVivos Ptd Ltd, Lim Chu Kang, Singapore) were used for this study. The mice were housed and acclimatized in an ABSL-3 facility for 72 h prior to the start of the experiment. K18-hACE2 transgenic mice were subjected to BRII combo (10 + 10 mg/kg) delivered through intraperitoneal injection a day prior to infection (n=12) or left untreated (n=12). The BRII combo was validated in live virus neutralization assay with IC50 0.168 μg/ml and IC90 0.828 μg/ml. The viral challenge was conducted through intranasal delivery in 25 μl of 1.7×10^3 PFU of the infectious SARS-CoV-2 Omicron BA.1. Body weights were measured prior to infection as baseline and monitored daily throughout the following 14 days. Mice were euthanized when their body weight fell below 75% of their baseline body weight. Six mice from each experimental group were sacrificed 3 days post inoculation, with lung and brain tissues harvested. Each organ was halved for the plaque assay and histology analysis, respectively.

For virus titer determination, supernatants from homogenized tissues were diluted 10-fold serially in DMEM supplemented with antibiotic and antimycotic and added to Vero E6 cells in 12-well plates. The inoculum was removed after 1 h of incubation for virus adsorption. Cells were washed once with PBS before 1.2% MCC-DMEM overlay media supplemented with antibiotic and antimycotic was added to each well. Then cells were incubated at 37°C, 5% CO2 for 72 h for plaque formation. The cells were fixed in 10% formalin overnight and counterstained with crystal violet. The number of plaques was determined, and the virus titers of individual samples were expressed in logarithm of PFU per organ.

For histopathological analyses, lung lobes were fixed in 3.7% formaldehyde solution prior to removal from BSL-3 containment. The tissues were routinely processed, embedded in paraffin blocks (Leica Surgipath Paraplast), sectioned at 4-μm thickness, and stained with H&E (Thermo Scientific) following standard histological procedures. For immunohistochemistry, sections were deparaffinized and rehydrated, followed by heat-mediated antigen retrieval, quenching of endogenous peroxidases and protein blocking. Sections were then covered with rabbit anti-SARS-CoV-2 N protein monoclonal antibody (Abcam; 1:1000) for 1 h at room temperature. Subsequently, sections were incubated with rabbit-specific HRP polymer (secondary antibody), visualized using chromogenic substrate DAB solution (Abcam), and counterstained with hematoxylin.

Structural Modeling of Mouse ACE2 Binding to RBD

The complex structure of mACE2 bound to a mouse adapted SARS-CoV-2 RBD (PDB:7FDK) was used to indicate critical residues that affected interaction between mACE2 and Delta RBD (PDB:7WBQ), and Omicron BA.1 and BA.2 RBD (PDB:7WBP). Pymol software was utilized for construction and demonstration of structural models.

Statistical Analysis

The technical and independent experiment replicates were indicated in the figure legends. Half-maximal inhibitory concentration (IC50) of mAb or dilutions (ID50) of convalescent plasma were calculated by the equation of four-parameter dose inhibition response using Graphpad Prism 8.0. The fold change of the variants relative to wildtype in neutralization were calculated by simple division of respective IC50 or ID50 values. The overall fold change in plasma neutralization to mutant over D614G pseudovirus was calculated by the geometric mean of the ID50 value of the 18 plasma samples. The significance of neutralizing and binding activities of convalescent plasma against each mutant pseudovirus relative to D614G was estimated using the paired t test by graphpad 8.0. Log IC50 of antibodies and the designated combinations between different cell types were fitted into linear regression model, and Spearman correlation was calculated by graphpad 8.0. The statistical differences between fitted regression model with hypothetical regression model was calculated using F test.

DATA AVAILABILITY STATEMENT

The original contributions presented in the study are included in the article/**Supplementary Material**. Further inquiries can be directed to the corresponding authors.

AUTHOR CONTRIBUTIONS

LZ and JC conceived and designed the study. RW, QZ, RZ, and ZA performed most of the experiments with assistance from PC, YW, JH, and XS. BJ provided plasmids of some of antibody production. QD provided HeLa cell lines expressing ACE2 from diverse origin. ZZ provided clinical care and management of infected patients, and particularly the recruitment and following

up the study subjects. RW, QZ, RZ, and LZ had full access to data in the study, generated figures and tables, and take responsibility for the integrity and accuracy of the data presentation. LZ and JC wrote the manuscript. All authors contributed to the article and approved the submitted version.

FUNDING

This study was funded by the National Key Plan for Scientific Research and Development of China (2020YFC0848800, 2020YFC0849900, 2021YFC0864500 and 2020YFC0861200), the National Natural Science Foundation (92169205, 81530065, 81661128042, 9216920007 and 32000661), Beijing Municipal Science and Technology Commission (D171100000517001, D171100000517003 and Z201100005420019), the Science and Technology Innovation Committee of Shenzhen Municipality (202002073000002 and JSGG20200807171401008), Beijing Advanced Innovation Center for Structural Biology, Tsinghua University Scientific Research Program (20201080053 and 2020Z99CFG004), Tencent Foundation, Shuidi Foundation, TH Capital, and the National Science Fund for Distinguished Young Scholars (82025022), Singapore National Medical Research Council Centre Grant Program (CGAug16M009), NUHSRO/2020/066/NUSMedCovid/01/BSL3 Covid Research Work, NUHSRO/2020/050/RO5+5/NUHS-COVID/4, Ministry of Education, Singapore MOE2017-T2-2-014; Singapore NMRC Centre Grant Program – Diabetes, Tuberculosis and Neuroscience CGAug16M009, Singapore Ministry of Health MOH-COVID19RF2-0001. The funders had no role in study design, data collection, data analysis, data interpretation or writing of the report.

ACKNOWLEDGMENTS

We thank Dr. Qing Zhu and Dr. Yun Ji from Brii Biosciences Inc. Durham, NC, USA for providing BRII-196 and BRII-198 antibodies. We acknowledge the work and contribution of all the health providers from Shenzhen Third People's Hospital. We thank patients for their active participation. We are also grateful to the National University of Singapore, Yong Loo Lin School of Medicine BSL-3 Core Facility for their support with this work. We thank Dr. Chee-Keng Mok in assisting with the initial omicron variant isolation and the animal study.

SUPPLEMENTARY MATERIAL

The Supplementary Material for this article can be found online at: https://www.frontiersin.org/articles/10.3389/fimmu.2022.854952/full#supplementary-material

REFERENCES

1. Wang R, Zhang Q, Ge J, Ren W, Zhang R, Lan J, et al. Analysis of SARS-CoV-2 Variant Mutations Reveals Neutralization Escape Mechanisms and the Ability to Use ACE2 Receptors From Additional Species. *Immunity* (2021) 54:1611–21.e1615. doi: 10.1016/j.immuni.2021.06.003
2. Wang P, Nair MS, Liu L, Iketani S, Luo Y, Guo Y, et al. Antibody Resistance of SARS-CoV-2 Variants B.1.351 and B.1.1.7. *Nature* (2021) 593:130–5. doi: 10.1038/s41586-021-03398-2
3. Lucas C, Vogels CBF, Yildirim I, Rothman JE, Lu P, Monteiro V, et al. Impact of Circulating SARS-CoV-2 Variants on mRNA Vaccine-Induced Immunity. *Nature* (2021) 600:523–9. doi: 10.1038/s41586-021-04085-y
4. Hastie KM, Li H, Bedinger D, Schendel SL, Dennison SM, Li K, et al. Defining Variant-Resistant Epitopes Targeted by SARS-CoV-2 Antibodies: A Global Consortium Study. *Sci (New York N.Y.)* (2021) 374:472–8. doi: 10.1126/science.abh2315
5. Liu C, Ginn HM, Dejnirattisai W, Supasa P, Wang B, Tuekprakhon A, et al. Reduced Neutralization of SARS-CoV-2 B.1.617 by Vaccine and Convalescent Serum. *Cell* (2021) 184:4220–36.e4213. doi: 10.1016/j.cell.2021.06.020
6. Kupferschmidt K, Wadman M. Delta Variant Triggers New Phase in the Pandemic. *Sci (New York N.Y.)* (2021) 372:1375–6. doi: 10.1126/science.372.6549.1375
7. Cov-lineage.org. *SARS-CoV-2 Lineages: B.1.617.2 Report* (2021). Available at: https://cov-lineages.org/global_report_B.1.617.2.html.
8. World Health Organization. *Tracking SARS-CoV-2 Variants* (2021). Available at: https://www.who.int/en/activities/tracking-SARS-CoV-2-variants/.
9. Li J, Lai S, Gao GF, Shi W. The Emergence, Genomic Diversity and Global Spread of SARS-CoV-2. *Nature* (2021) 600:408–18. doi: 10.1038/s41586-021-04188-6
10. van der Straten K, Guerra D, van Gils M, Bontjer I, Caniels TG, van Willigen HD, et al. Mapping the Antigenic Diversification of SARS-CoV-2. (2022). doi: 10.1101/2022.01.03.21268582
11. Public Health England. *SARS-CoV-2 Variants of Concern and Variants Under Investigation in England: Technical Briefing 14* (2021). Available at: https://assets.publishing.service.gov.uk/government/uploads/system/uploads/attachment_data/file/991343/Variants_of_Concern_VOC_Technical_Briefing_14.pdf.
12. Centers for Disease Control and Prevention. *Science Brief: Omicron (B.1.1.529) Variant* (2021). Available at: https://www.cdc.gov/coronavirus/2019-ncov/science/science-briefs/scientific-brief-omicron-variant.html.
13. World Health organization. *Classification of Omicron (B.1.1.529): SARS-CoV-2 Variant of Concern* (2021). Available at: https://www.who.int/news/item/26-11-2021-classification-of-omicron-(b.1.1.529)-sars-cov-2-variant-of-concern.
14. World Health Organization. *Statement on Omicron Sublineage BA.2*. (2022).
15. Collie S, Champion J, Moultrie H, Bekker LG, Gray G. Effectiveness of BNT162b2 Vaccine Against Omicron Variant in South Africa. *N Engl J Med* (2021) 386:494–6. doi: 10.1056/NEJMc2119270
16. Kuhlmann C, Mayer CK, Claassen M, Maponga T, Burgers WA, Keeton R, et al. Breakthrough Infections With SARS-CoV-2 Omicron Despite mRNA Vaccine Booster Dose. *Lancet (London England)* (2022) 399:625–6. doi: 10.1016/s0140-6736(22)00090-3
17. Yamasoba D, Kimura I, Nasser H, Morioka Y, Nao N, Ito J, et al. Virological Characteristics of SARS-CoV-2 BA.2 Variant. *bioRxiv* (2022) 2022. doi: 10.1101/2022.02.14.480335
18. Cameroni E, Bowen JE, Rosen LE, Saliba C, Zepeda SK, Culap K, et al. Broadly Neutralizing Antibodies Overcome SARS-CoV-2 Omicron Antigenic Shift. *Nature* (2021) 602:664–70. doi: 10.1038/d41586-021-03825-4
19. Wei C, Shan KJ, Wang W, Zhang S, Huan Q, Qian W. Evidence for a Mouse Origin of the SARS-CoV-2 Omicron Variant. *J Genet Genomics = Yi Chuan xue bao* (2021) 48:1111–21. doi: 10.1016/j.jgg.2021.12.003
20. Liu L, Iketani S, Guo Y, Chan JFW, Wang M, Liu L, et al. Striking Antibody Evasion Manifested by the Omicron Variant of SARS-CoV-2. *Nature* (2021) 602:676–81. doi: 10.1038/d41586-021-03826-3
21. Hoffmann M, Krüger N, Schulz S, Cossmann A, Rocha C, Kempf A, et al. The Omicron Variant Is Highly Resistant Against Antibody-Mediated Neutralization – Implications for Control of the COVID-19 Pandemic. *Cell* (2021) 185:447–56. doi: 10.1016/j.cell.2021.12.032
22. Dejnirattisai W, Huo J, Zhou D, Zahradník J, Supasa P, Liu C, et al. SARS-CoV-2 Omicron-B.1.1.529 Leads to Widespread Escape From Neutralizing Antibody Responses. *Cell* (2022) 185:467–484. doi: 10.1016/j.cell.2021.12.046

23. Planas D, Saunders N, Maes P, Guivel-Benhassine F, Planchais C, Buchrieser J, et al. Considerable Escape of SARS-CoV-2 Omicron to Antibody Neutralization. *Nature* (2021) 602:671–75. doi: 10.1038/d41586-021-03827-2
24. Cao Y, Wang J, Jian F, Xiao T, Song W, Yisimayi A, et al. Omicron Escapes the Majority of Existing SARS-CoV-2 Neutralizing Antibodies. *Nature* (2021) 602:657–63. doi: 10.1038/d41586-021-03796-6
25. Iketani S, Liu L, Guo Y, Liu L, Chan JF, Huang Y, et al. Antibody Evasion Properties of SARS-CoV-2 Omicron Sublineages. *Nature* (2022) 604:553–6s. doi: 10.1038/s41586-022-04594-4
26. Zhou H, Tada T, Dcosta BM, Landau NR. Neutralization of SARS-CoV-2 Omicron BA.2 by Therapeutic Monoclonal Antibodies. *bioRxiv* (2022). doi: 10.1101/2022.02.15.480166
27. Westendorf K, Žentelis S, Wang L, Foster D, Vaillancourt P, Wiggin M, et al. LY-CoV1404 (Bebtelovimab) Potently Neutralizes SARS-CoV-2 Variants. *Cell Rep* (2022). doi: 10.1101/2021.04.30.442182
28. Cele S, Jackson L, Khoury DS, Khan K, Moyo-Gwete T, Tegally H, et al. Omicron Extensively But Incompletely Escapes Pfizer BNT162b2 Neutralization. *Nature* (2021) 602:654–6. doi: 10.1038/d41586-021-03824-5
29. Garcia-Beltran WF, St Denis KJ, Hoelzemer A, Lam EC, Nitido AD, Sheehan ML, et al. mRNA-Based COVID-19 Vaccine Boosters Induce Neutralizing Immunity Against SARS-CoV-2 Omicron Variant. *medRxiv* (2021). doi: 10.1101/2021.12.14.21267755
30. Dejnirattisai W, Shaw RH, Supasa P, Liu C, Stuart AS, Pollard AJ, et al. Reduced Neutralisation of SARS-CoV-2 Omicron B.1.1.529 Variant by Post-Immunisation Serum. *Lancet (London England)* (2021) 399:234–6. doi: 10.1016/s0140-6736(21)02844-0
31. Bowen JE, Sprouse KR, Walls AC, Mazzitelli IG, Logue JK, Franko NM, et al. Omicron BA.1 and BA.2 Neutralizing Activity Elicited by a Comprehensive Panel of Human Vaccines. *bioRxiv* (2022). doi: 10.1101/2022.03.15.484542
32. Yu J, Collier AY, Rowe M, Mardas F, Ventura JD, Wan H, et al. Neutralization of the SARS-CoV-2 Omicron BA.1 and BA.2 Variants. *N Engl J Med* (2022) 386:1579–80. doi: 10.1056/NEJMc2201849
33. Wang P, Casner RG, Nair MS, Wang M, Yu J, Cerutti G, et al. Increased Resistance of SARS-CoV-2 Variant P.1 to Antibody Neutralization. *Cell Host Microbe* (2021) 29:747–751.e744. doi: 10.1016/j.chom.2021.04.007
34. Hoffmann M, Arora P, Gross R, Seidel A, Hornich BF, Hahn AS, et al. SARS-CoV-2 Variants B.1.351 and P.1 Escape From Neutralizing Antibodies. *Cell* (2021) 184:2384–2393.e2312. doi: 10.1016/j.cell.2021.03.036
35. Planas D, Veyer D, Baidaliuk A, Staropoli I, Guivel-Benhassine F, Rajah MM, et al. Reduced Sensitivity of SARS-CoV-2 Variant Delta to Antibody Neutralization. *Nature* (2021) 596:276–80. doi: 10.1038/s41586-021-03777-9
36. Chen RE, Winkler ES, Case JB, Aziati ID, Bricker TL, Joshi A, et al. *In Vivo* Monoclonal Antibody Efficacy Against SARS-CoV-2 Variant Strains. *Nature* (2021) 596:103–8. doi: 10.1038/s41586-021-03720-y
37. Arora P, Kempf A, Nehlmeier I, Graichen L, Sidarovich A, Winkler MS, et al. Delta Variant (B.1.617.2) Sublineages do Not Show Increased Neutralization Resistance. *Cell Mol Immunol* (2021) 18:2557–9. doi: 10.1038/s41423-021-00772-y
38. Ju B, Zhang Q, Ge J, Wang B, Sun J, Ge X, et al. Human Neutralizing Antibodies Elicited by SARS-CoV-2 Infection. *Nature* (2020) 584:115–9. doi: 10.1038/s41586-020-2380-z
39. Lempp FA, Soriaga LB, Montiel-Ruiz M, Benigni F, Noack J, Park YJ, et al. Lectins Enhance SARS-CoV-2 Infection and Influence Neutralizing Antibodies. *Nature* (2021) 598:342–7. doi: 10.1038/s41586-021-03925-1
40. Shan S, Mok CK, Zhang S, Lan J, Li J, Yang Z, et al. A Potent and Protective Human Neutralizing Antibody Against SARS-CoV-2 Variants. *Front Immunol* (2021) 12:766821. doi: 10.3389/fimmu.2021.766821
41. Jangra S, Ye C, Rathnasinghe R, Stadlbauer D, Krammer F, Simon V, et al. SARS-CoV-2 Spike E484K Mutation Reduces Antibody Neutralisation. *Lancet Microbe* (2021) 2:e283–4. doi: 10.1016/s2666-5247(21)00068-9
42. Li Q, Nie J, Wu J, Zhang L, Ding R, Wang H, et al. SARS-CoV-2 501y.V2 Variants Lack Higher Infectivity But Do Have Immune Escape. *Cell* (2021) 184:2362–2371.e2369. doi: 10.1016/j.cell.2021.02.042
43. Yuan M, Huang D, Lee CD, Wu NC, Jackson AM, Zhu X, et al. Structural and Functional Ramifications of Antigenic Drift in Recent SARS-CoV-2 Variants. *Sci (New York N.Y.)* (2021) 373:818–23. doi: 10.1126/science.abh1139
44. Oude Munnink BB, Sikkema RS, Nieuwenhuijse DF, Molenaar RJ, Munger E, Molenkamp R, et al. Transmission of SARS-CoV-2 on Mink Farms Between Humans and Mink and Back to Humans. *Sci (New York N.Y.)* (2021) 371:172–7. doi: 10.1126/science.abe5901
45. Leist SR, Dinnon KH 3rd, Schäfer A, Tse LV, Okuda K, Hou YJ, et al. A Mouse-Adapted SARS-CoV-2 Induces Acute Lung Injury and Mortality in Standard Laboratory Mice. *Cell* (2020) 183:1070–1085.e1012. doi: 10.1016/j.cell.2020.09.050
46. Hale VL, Dennis PM, McBride DS, Nolting JM, Madden C, Huey D, et al. SARS-CoV-2 Infection in Free-Ranging White-Tailed Deer. *Nature* (2021) 602:481–6. doi: 10.1038/s41586-021-04353-x
47. Yen HL, Sit THC, Brackman CJ, Chuk SSY, Gu H, Tam KWS, et al. Transmission of SARS-CoV-2 Delta Variant (AY.127) From Pet Hamsters to Humans, Leading to Onward Human-to-Human Transmission: A Case Study. *Lancet (London England)* (2022) 399:1070–8. doi: 10.1016/s0140-6736(22)00326-9
48. Sun S, Gu H, Cao L, Chen Q, Ye Q, Yang G, et al. Characterization and Structural Basis of a Lethal Mouse-Adapted SARS-CoV-2. *Nat Commun* (2021) 12:5654. doi: 10.1038/s41467-021-25903-x
49. Rathnasinghe R, Jangra S, Cupic A, Martinez-Romero C, Mulder LCF, Kehrer T, et al. The N501Y Mutation in SARS-CoV-2 Spike Leads to Morbidity in Obese and Aged Mice and Is Neutralized by Convalescent and Post-Vaccination Human Sera. *medRxiv* (2021). doi: 10.1101/2021.01.19.21249592
50. Gu H, Chen Q, Yang G, He L, Fan H, Deng YQ, et al. Adaptation of SARS-CoV-2 in BALB/c Mice for Testing Vaccine Efficacy. *Sci (New York N.Y.)* (2020) 369:1603–7. doi: 10.1126/science.abc4730
51. McCallum M, Czudnochowski N, Rosen LE, Zepeda SK, Bowen JE, Walls AC, et al. Structural Basis of SARS-CoV-2 Omicron Immune Evasion and Receptor Engagement. *Sci (New York N.Y.)* (2022) 375:864–8. doi: 10.1126/science.abn8652
52. Pinto D, Park YJ, Beltramello M, Walls AC, Tortorici MA, Bianchi S, et al. Cross-Neutralization of SARS-CoV-2 by a Human Monoclonal SARS-CoV Antibody. *Nature* (2020) 583:290–5. doi: 10.1038/s41586-020-2349-y
53. VanBlargan LA, Errico JM, Halfmann PJ, Zost SJ, Crowe JE Jr, Purcell LA, et al. An Infectious SARS-CoV-2 B.1.1.529 Omicron Virus Escapes Neutralization by Therapeutic Monoclonal Antibodies. *Nat Med* (2022) 28:490–5. doi: 10.1038/s41591-021-01678-y
54. Zost SJ, Gilchuk P, Case JB, Binshtein E, Chen RE, Nkolola JP, et al. Potently Neutralizing and Protective Human Antibodies Against SARS-CoV-2. *Nature* (2020) 584:443–9. doi: 10.1038/s41586-020-2548-6
55. Shi R, Shan C, Duan X, Chen Z, Liu P, Song J, et al. A Human Neutralizing Antibody Targets the Receptor-Binding Site of SARS-CoV-2. *Nature* (2020) 584:120–4. doi: 10.1038/s41586-020-2381-y
56. Hansen J, Baum A, Pascal KE, Russo V, Giordano S, Wloga E, et al. Studies in Humanized Mice and Convalescent Humans Yield a SARS-CoV-2 Antibody Cocktail. *Sci (New York N.Y.)* (2020) 369:1010–4. doi: 10.1126/science.abd0827
57. Liu Y, Hu G, Wang Y, Ren W, Zhao X, Ji F, et al. Functional and Genetic Analysis of Viral Receptor ACE2 Orthologs Reveals a Broad Potential Host Range of SARS-CoV-2. *Proc Natl Acad Sci USA* (2021) 118:e2025373118. doi: 10.1073/pnas.2025373118
58. Ge J, Wang R, Ju B, Zhang Q, Sun J, Chen P, et al. Antibody Neutralization of SARS-CoV-2 Through ACE2 Receptor Mimicry. *Nat Commun* (2021) 12:250. doi: 10.1038/s41467-020-20501-9

Conflict of Interest: The authors have filed patent applications on antibodies BRII-196 and BRII-198 described in the manuscript. LZ, QZ, and XS are shareholders of TSB Therapeutics.

Publisher's Note: All claims expressed in this article are solely those of the authors and do not necessarily represent those of their affiliated organizations, or those of the publisher, the editors and the reviewers. Any product that may be evaluated in this article, or claim that may be made by its manufacturer, is not guaranteed or endorsed by the publisher.

frontiers | Frontiers in Immunology

REVIEW
published: 27 June 2022
doi: 10.3389/fimmu.2022.904686

The Robustness of Cellular Immunity Determines the Fate of SARS-CoV-2 Infection

Esther Moga[1]*, *Elionor Lynton-Pons*[1] and *Pere Domingo*[2]

[1] Department of Immunology, Hospital de la Santa Creu i Sant Pau, Biomedical Research Institute Sant Pau (IIB Sant Pau), Universitat Autònoma de Barcelona, Barcelona, Spain, [2] Unidad de enfermedades infecciosas, Hospital de la Santa Creu i Sant Pau, Barcelona, Spain

Two years after the appearance of the SARS-CoV-2 virus, the causal agent of the current global pandemic, it is time to analyze the evolution of the immune protection that infection and vaccination provide. Cellular immunity plays an important role in limiting disease severity and the resolution of infection. The early appearance, breadth and magnitude of SARS-CoV-2 specific T cell response has been correlated with disease severity and it has been thought that T cell responses may be sufficient to clear infection with minimal disease in COVID-19 patients with X-linked or autosomal recessive agammaglobulinemia. However, our knowledge of the phenotypic and functional diversity of CD8+ cytotoxic lymphocytes, CD4+ T helper cells, mucosal-associated invariant T (MAIT) cells and CD4+ T follicular helper (Tfh), which play a critical role in infection control as well as long-term protection, is still evolving. It has been described how CD8+ cytotoxic lymphocytes interrupt viral replication by secreting antiviral cytokines (IFN-γ and TNF-α) and directly killing infected cells, negatively correlating with stages of disease progression. In addition, CD4+ T helper cells have been reported to be key pieces, leading, coordinating and ultimately regulating antiviral immunity. For instance, in some more severe COVID-19 cases a dysregulated CD4+ T cell signature may contribute to the greater production of pro-inflammatory cytokines responsible for pathogenic inflammation. Here we discuss how cellular immunity is the axis around which the rest of the immune system components revolve, since it orchestrates and leads antiviral response by regulating the inflammatory cascade and, as a consequence, the innate immune system, as well as promoting a correct humoral response through CD4+ Tfh cells. This review also analyses the critical role of cellular immunity in modulating the development of high-affinity neutralizing antibodies and germinal center B cell differentiation in memory and long-lived antibody secreting cells. Finally, since there is currently a high percentage of vaccinated population and, in some cases, vaccine booster doses are even being administered in certain countries, we have also summarized newer approaches to long-lasting protective immunity and the cross-protection of cellular immune response against SARS-CoV-2.

Keywords: SARS-CoV-2, cellular immunity, vaccine, COVID-19, helper T cells, cytotoxic T lymphocytes, severity, evasion

OPEN ACCESS

Edited by:
Penghua Wang,
University of Connecticut Health Center, United States

Reviewed by:
Emily S. J. Edwards,
Monash University, Australia
Masaaki Miyazawa,
Kindai University, Japan

***Correspondence:**
Esther Moga
mmoga@santpau.cat

Specialty section:
This article was submitted to Viral Immunology, a section of the journal Frontiers in Immunology

Received: *25 March 2022*
Accepted: *27 May 2022*
Published: *27 June 2022*

Citation:
Moga E, Lynton-Pons E and Domingo P (2022) The Robustness of Cellular Immunity Determines the Fate of SARS-CoV-2 Infection. Front. Immunol. 13:904686. doi: 10.3389/fimmu.2022.904686

HIGHLIGHTS

- The presence of cross-reactivity, either humoral or cellular, between common cold hCoV and SARS-CoV-2 does not prevent infection but may be associated with less severe COVID-19.
- The presence of SARS-CoV-2-specific CD4+ Th1 IFN-γ-producing cells and CD8+ CTLs cells were associated with reduced disease severity.
- T lymphocyte recruitment to infected lung tissues and T lymphocyte apoptosis/necrosis caused by the cytokine storm might be crucial determinants of CD4+ and CD8+ T-cell lymphopenia in severe COVID-19 cases.
- Severe/fatal disease presents with excessive hyperactivation of immune function with increased Tregs and Th2 and/or Th17 cell-biased phenotype, leading to T cell exhaustion and subsequently to a state of anergy.
- Functional memory B and T cells to SARS-CoV-2 have been detected 12 months after natural infection. SARS-CoV-2-specific T cell memory may be long lasting given that COVID-19 convalescent patients develop SARS-CoV-2-specific TSCM cells that display a non-exhausted phenotype.
- The immunogenicity of SARS-CoV-2 vaccines involves the humoral response (number of spike-specific antibodies, neutralizing antibodies, and antibody neutralization capacity) and the cellular response (IFN-γ-producing CD4+ and CD8+ T cells). Therefore, a combined analysis of humoral and cellular immunity is necessary for the identification of vaccine responders and the immune protection evolution.

INTRODUCTION

Coronaviruses (CoVs) are enveloped viruses containing non-segmented, single-stranded, positive-sense RNA genome whose primarily hosts are vertebrates (1, 2). Human Corovaniruses (HCoVs) have been responsible for significant health-related and economic costs worldwide for the last 20 years. The first time we received alarming information regarding HCoVs was with the appearance of severe acute respiratory syndrome coronavirus (SARS-CoV) in Guangdong Province (China) in November 2002 (3). By 2003, it had turned into a global infection with a mortality rate of 10% (4). The second HCoV outbreak occurred a decade later, in June 2012, with the Middle East respitatory syndrome coronavirus (MERS-CoV), which originated in Jeddah, Saudi Arabia (5). In the case of MERS-CoV, a 35% fatality rate was reported worldwide (6). Finally, the current pandemic, which is caused by severe acute respiratory syndrome coronavirus 2 (SARS-CoV-2), originated in Wuhan, China in December 2019 and causes the infection designated COVID-19 (Coronavirus Disease 2019) (7).

CoVs are classified in the realm Riboviria, order Nidovirales, suborder Cornidovirineae and family Coronaviridae with all 39 species of CoVs distributed in 27 subgenera, five genera, and two subfamilies (8, 9). HCoV are members of the Coronavirinae subfamily and are, in turn, categorized by the International Committee for the Taxonomy of Viruses into four major genera: AlphaCoV, BetaCoV, GammaCoV, and DeltaCoV (9). The AlphaCoV genera contains the common cold-causing HCoV-229E and HCoV-NL63 HCoVs, whereas in the BetaCoV genera are placed the common cold-causing HCoV-HKU1 and HCoV-OC43, as well as SARS-CoV, and MERS-CoV (10). SARS-CoV-2 sequence analysis has demonstrated a distant similarity of 79% to SARS-CoV and a 50% similarity to MERS-CoV with an 88% sequence identity to bat-SL-CoVZC45, bat-SLCoVZXC21 and bat-derived SARS-like CoV (11, 12).

The emergence of numerous SARS-CoV-2 variants of interest (VOI) and variants of concern (VOC) is one of the most important developments in the COVID-19 pandemic (13). The most important VOC variants reported to date are Alpha (B.1.1.7), Beta (B.1.351), Gamma (P.1) (14, 15), Mu (B.1.621) (16), Delta (B.1.617.2) (17) and Omicron (B.1.1.529), with the latest VOC reported in November 2021 (18). Understanding the impact of these variants on cellular immunity, in the context of COVID-19 infection and vaccination, is important for the development of effective strategies against future SARS-CoV-2 variants.

VIRAL INFECTIONS AND T CELL IMMUNE RESPONSES

A harmonized innate and adaptive immune response is crucial for the control and clearance of most viral infections. These two branches of the immune system collaborate to protect the body against infections. First, innate immunity includes evolutionarily primitive molecular and cellular mechanisms that recognize pathogens as common molecular patterns with the aim of preventing infection and quickly eliminating them. Second, the adaptive immune system takes longer to act but is characterised by a much more accurate response, as T and B lymphocytes undergo antigen-specific selection and proliferation. For many primary virus infections, it typically takes 7-10 days to prime and expand adaptive T cell immune responses in order to control the virus (19). Virus specific T cells have been shown to be protective against other viruses, like influenza (20), while heterologous immunity against diverse influenza strains is associated with conserved memory T-cell epitopes (21–23).

Coronaviruses and Immunity: Previous Knowledge

The innate immune system includes physical and chemical barriers to infection, as well as the germline-encoded receptors, known as pattern recognition receptors (PRRs), which recognise the common molecular structures of many pathogens. PRRs bind to pathogen-associated molecular patterns (PAMPs) and damage-associated molecular patterns (DAMPs) and trigger cellular responses. As we know from other CoVs, double-stranded RNA (dsRNA), which is a by-product of viral

genome replication and transcription, is a relevant PAMP model for CoVs (24, 25). It can be detected in the endosome by Toll-like receptor 3 (TLR3) and in the cytoplasm by RNA helicases retinoic acid-inducible gene I (RIG-I), melanoma differentiation-associated protein 5 (MDA5), and protein kinase R (PKR) (26–28). Single-stranded RNA (ssRNA) can also be detected in the endosome by Toll-like receptor 7 (TLR7) (29). Altogether, this allows for the detection of viral infection, activating signalling cascades like myeloid differentiation primary response 88 (MyD88) and inducing the production of type I interferons (IFNs) and nuclear factor kappa B (NF-κB) activation which, in turn, will induce the transcription of pro-inflammatory cytokines (30). Collectively, this triggers an antiviral immune response that constraints viral replication in infected and neighbouring cells.

However, CoVs are able to evade the mechanisms of innate immune detection, thereby preventing the generation of a proper immune response against viral infection (31). For example, the non-structural protein 3 (NSP3) of previous HCoVs has a papain-like protease domain that inhibits the activation of IFN regulatory factor 3 (IRF3) and the ubiquitination of TANK-binding kinase (TBK1), and RIG-I (32–35). Another example is the capacity of both SARS-CoV and MERS-CoV to prompt the production of double membrane vesicles lacking PRRs and their replication within them, thereby eluding the host viral dsRNA detection system (36, 37). Furthermore, the SARS-CoV and MERS-CoV M protein has previously been shown to interact with TNF receptor-associated factor 3 (TRAF3), disrupting TRAF3-TBK1 association and thus suppressing type I IFN production (38–40).

When the innate immune system is unable to control the viral infection, the adaptive immune system assumes a very important role. Previous studies of the adaptive immune response to earlier CoVs reported that antibody response decreases rapidly after infection or immunization, especially in cases of mild or subclinical disease such as that caused by common cold CoVs or mild MERS-CoVs, allowing for potential reinfection (41, 42). Moreover, SARS-CoV and MERS-CoV have been shown to impair T cell function and induce T cell apoptosis (43, 44). Thus, a commonly observed phenotype during acute phase disease in SARS-CoV and MERS-CoV patients, and also in COVID-19, was lymphopenia, which was seen particularly in patients with severe disease (43, 45, 46).

As is well known, the cytokine microenvironment generated by antigen presenting cells directs T cell phenotype differentiation and responses. Current evidence indicates that T helper 1 (Th1) response is crucial for the successful control of SARS-CoV and MERS-CoV (47).

There are a number of studies attempting to address the issue of the immune memory persistence conferred by infection with HCoVs. Some of those reveal that CD4+ and CD8+ memory T cell responses were identified in the blood of 70-100% of SARS-CoV patients four and six years after infection (48–50) and (51) even detected CD8+ T cell responses 11 years post-infection. These memory T cells may remain functionally active since another study revealed that they could proliferate, produce IFN-γ and induce delayed-type hypersensitivity (DTH) fast at antigen reencounter (48). Overall, T cell responses have been observed to have enhanced durability relative to antibody responses in SARS-CoV and MERS-CoV, hence it seems cellular response is crucial for the longevity of the immunity conferred by infection with CoVs.

Pre-Existing Immune Reactivity

At the beginning of the pandemic outbreak, many studies focused on the possibility of pre-existing immunity against SARS-CoV-2. Considering that more than 90% of the human population is seropositive for at least one out of three of the common cold-causing HCoVs (52), it is reasonable to hypothesize that there may be a degree of cross-reactivity between the immunity conferred against common cold HCoVs and immunity against SARS-CoV-2. Among unexposed donors, 20% to 50% had lymphocytes exhibiting significant reactivity to antigen peptide pools of SARS-CoV-2 (53–57).

Multiple investigations into early serological response to SARS-CoV-2 reported unconventional seroconversion patterns resembling those of secondary immune responses. During a secondary immune response, memory lymphocytes provide the necessary mechanisms for rapid, antigen-specific, effective immune responses, and when the same pathogen infects the body a second time, it often originates only mild symptoms or may not cause any symptoms at all. A large serological study of COVID-19 patients found IgM seroconversion before IgG (typical primary response), as expected in previously unexposed individuals, but also synchronous IgM and IgG, and IgM after IgG seroconversion, describing an uncommon pattern of seroconversion to SARS-CoV-2 infection (58). In COVID-19 convalescent subjects, IgG against the S protein of the HCoV-OC43 had higher titers than in unexposed subjects but that was not true for the S protein of HCoV-229E, which suggests a more significant cross-reactivity between betacoronaviruses (59). The same authors suggested that the early parallel production of IgM and IgG in response to SARS-CoV-2 infection might be mediated by the stimulation of IgG memory B cells, as well as by naïve B cells (59) indicating that the memory generated by previous infections with other HCoVs would trigger a response to infection by the current SARS-CoV-2.

However, although there are studies supporting the presence of pre-existing SARS-CoV-2 cross-reactive antibody neutralizing capacity (60), others found no association between the presence of pre-existing cross-reactive antibodies to SARS-CoV-2 and protection against SARS-CoV-2 infections and hospitalizations (61). That might be explained by the fact that those pre-existing cross-reactive antibodies share predominantly non-neutralizing antibodies against the epitopes of previously circulating HCoVs (61–63). Assuming that shared cross-reactive antibodies to SARS-CoV-2 had no neutralizing activity, pre-existing cellular immunity would play a crucial protective role.

Several studies have provided evidence of the cross-reactivity of T cell responses between SARS-CoV-2 and the common cold HCoVs (55–57, 64–67). Mateus J. et al. (64) detected cross-reactive CD4+ memory T cells with peptide pools selected on the

basis of homology between SARS-CoV-2 and other HCoVs and concluded that memory CD4+ T cells recognizing common cold HCoVs can exhibit substantial cross-reactivity to the homologous epitope in SARS-CoV-2. Cross-reactive CD8+ T cells also exist and, although they are less prevalent than cross-reactive CD4+ T cells (53), might be important determinants of immune protection at individual and population levels (68).

Nevertheless, pre-existing T cell immunity to SARS-CoV-2 has apparently low avidity when compared to that developed following infection with SARS-CoV-2 and may not participate in immunity very effectively (69). Thus, the immunity developed by previous HCoVs is not sufficient to prevent subsequent infection by SARS-CoV-2 but might be associated with less severe COVID-19 (70).

Interestingly, there seems to be an inverse association between cross-reactive antibody levels and age as shown by Shrwani K. et al. (63), who found children and younger people to have higher pre-existing cross-reactive antibodies to SARS-CoV-2 than older individuals. In line with that finding, a decrease in the magnitude and quality of SARS-CoV-2 cross-reactive CD4+ T-cells response with age has also been reported (71). Bearing this in mind, increased susceptibility to severe COVID-19 in elderly patients may at least in part be explained by a smaller pool of naïve T cells and the incapacity of the aged immune system to maintainthe SARS-CoV-2 cross-reactive T cells induced by previous HCoV infection.

SARS-COV-2 IMMUNE EVASION

Innate Immune System Evasion

As mentioned above, the first line of defense provided by our immune system against infection comes from the innate immune system. SARS-CoV-2, like other viruses and other HCoVs, attempts to evade the innate immune system and has been shown to do so by employing several different strategies.

Apparently, the main tactic by which viruses manage to evade the innate immune system is the inhibition of type I IFN response at different levels. It has been reported that SARS-CoV-2 may inhibit viral RNA recognition by modifying its own RNA and mimicking host RNA. The non-structural proteins NSP13, NSP14 and NSP16 perform this function by mediating the addition of a 7-methylguanyalte cap at the 5' end of viral RNA in order to elude RIG-I and MDA5 recognition (72, 73). SARS-CoV-2 can also inhibit type I IFN at different points of the signalling cascade, leading to IFN production after non-self nucleic acid detection. The SARS-CoV-2 NSP15 protein may reduce IFN production as there is evidence that NSP15 binds to NRDP1 (74), the E3 protein ubiquitin ligase, which is known to enhance TBK1 and IRF3 activation, thereby promoting IFN production (75). TBK1 activation can also be inhibited by the NSP13 SARS-CoV-2 protein (74, 76, 77), and is decreased, along with IRF3 activation, by open reading frame 9 (ORF9)- cyclic GMP–AMP synthase (cGAS)-stimulator of interferon genes (STING) interaction (78). The NSP12 SARS-CoV-2 protein seems to impair the nuclear translocation of IFR3 by inhibiting IFN-β promoter activity (79, 80). Some studies have reported the disruption of RIG-I-like receptor (RLR) signalosome binding to translocase of outer mitochondrial membrane 70 (TOM70) by ORF9b (74, 76, 81) and have suggested that ORF9b-TOM70 interaction may inhibit IFN-β promoter activity (82). Moreover, ORF9b expression by SARS-CoV-2 may prevent the ubiquitination of NEMO (NF-kB essential modulator), NF-kB activation and nuclear translocation (83). Furthermore, the ISGlyation (labelling with interferon-stimulated gene 15 (ISG15), an ubiquitin-like protein) of MDA5, which is required for downstream pathway activation to lead to IFN-β secretion, may be inhibited by the NSP3 protein of SARS-CoV-2 (84). The NSP3 protein also seems to antagonize IRF3 stabilization (85). Other investigations have proposed that SARS-CoV-2-M protein antagonizes RLR signaling by inhibiting IFN-β and IFN-k gene expression and IFN-β promoter activity (86, 87). In addition, Xia H. et al. (88) demonstrated that M protein reduces ISRE (interferon-stimulated response element) reporter activity after treatment with IFN activation. SARS-CoV-2 has been also shown to inhibit the IFN signalling cascade at the signal transducer and activation of transcription (STATs) phosphorialtion level. For example, the expression inhibition and lysosomal degradation of interferon-α/β receptor 1 (IFNAR1) by NSP14 and ORF3a SARS-CoV-2 proteins impairs STAT1 phosphorylation, as reported by Hayn M. et al. (89).

Adaptive Immune System Evasion

All the above-mentioned strategies allow SARS-CoV-2 to overcome the first line of defense of the host and this is when the host's second line of defense comes into play: the adaptive immune system. Unfortunately, SARS-CoV-2 has also developed evasion mechanisms to overcome the adaptive immune system.

Humoral

A certain degree of SARS-CoV-2 antibody neutralization escape has been detected in every variant of concern: Alpha or B.1.1.7 (90, 91), Beta or B.1.315 (92, 93), Gamma or P.1 (94, 95), Epsilon encompassing the lineages B.1.427 and B.1.429 (96, 97), Delta or B.1.617.2 (17, 98), as well as Omicron or B.1.1.529 (99–101). As expected given the unprecedented high infection (and reinfection) rate numbers of the Omicron variant, this VOC was able to easily evade past infection humoral immunity compared to the epidemiological surveillance data for Beta and Delta variants (102). However, although the neutralization ability of convalescent sera against Omicron is low, a certain degree of neutralization still exists, indicating that there is still a certain level of protective effect (102). Another relevant mechanism used by SARS-CoV-2 to evade humoral response is the ability of this virus to spread from cell to cell without exposure to the extracellular environment (103). This reduces the likelihood of SARS-CoV-2 detection by SARS-CoV-2-specific antibodies and therefore limits the role of humoral immunity in preventing viral spread within the host.

Cellular

Notwithstanding these considerations regarding neutralization escape, T-cell immunity against SARS-CoV-2 seems to be more robust, since SARS-CoV-2-CD4+ and CD8+ T cell responses are not substantially affected by the Alpha, Beta, Gamma and Epsilon variants of concern (B.1.429), likely because T cell

responses against SARS-CoV-2 are highly multi-antigenic and multi-specific, with many different epitopes being recognized by CD4+ and CD8+ T cells in a given individual (55, 67, 104–106). Nonetheless, a T-cell response reduction to SARS-CoV-2 variants of concern Alpha, Beta, and Gamma (107) has been demonstrated in vaccinated individuals and, as assessed in COVID-19 convalescent patients and vaccinated individuals, two SARS-CoV-2-spike mutations in the Delta (B.1.617.2) and the Delta plus (AY.2/B.1.617.2.2) may play a crucial role in HLA recognition and in reducing cellular immune response (108). In the case of vaccinated individuals, the above mentioned effect may be due to the fact that the multi-specificity conferred by natural SARS-CoV-2 infection cannot be achieved. Furthermore, SARS-CoV-2 is able to reduce T-cell response through a mechanism mediated by infected monocytes. These can directly reduce T cell response and inhibit epithelial cell survival through the hypoxia inducible factor 1-alpha (HIF-1a)/glycolysis-dependent axis, potentially contributing to immunopathology. This may explain why elevated glucose levels in diabetic individuals enhance viral replication and cytokine expression in monocytes (109).

Nevertheless, there are scarce studies investigating the T-cell immune escape of SARS-CoV-2 variants due to the difficulty of measuring T-cell response in clinical practice compared to antibody detection assays. More research needs to be conducted on this issue in order to draw firmer conclusions.

NATURAL INFECTION WITH SARS-COV-2 (COVID-19)

In natural infection, when innate immunity stimulates the adaptive response and sufficient effector T and B cells have proliferated and differentiated, they work together to rapidly and specifically eliminate infected cells and circulating virions. In an orchestrated immune response, the humoral branch alone cannot clear an ongoing infection and a cellular immune response will also be necessary. Thus, the presence of both T cells and antibodies is associated with the successful resolution of the average of cases of COVID-19 (53). T lymphocytes, the cells responsible for cell-mediated immunity, recognize the antigens present on antigen-presenting cells (APCs), and help phagocytes to destroy these microbes or to kill the infected cells. The best defined T lymphocytes are helper and cytotoxic (or cytolytic) T lymphocytes (CTLs), which present the cluster differentiation markers CD4+ and CD8+, respectively. T cells also assist B lymphocytes to proliferate and differentiate into plasma cells that secrete different classes of antibodies. This process requires a fairly well-defined time frame. In SARS-CoV-2 infection, following an incubation period of four to seven days before symptom onset, patients with COVID-19 progress towards recovery after seven to 10 days or else develop serious illness (110–112). The course of severe COVID-19 is characterised by an increased inflammatory response with a marked reduction in the number of T cells, frequently of both CD4+ and CD8+ T cells (113–116). In addition, symptomatic SARS-CoV-2 infection tends to elicit a higher peripheral blood T cell response with respect to asymptomatic infection (117, 118).The reduced frequencies of peripheral T cells during acute infection are likely to be associated with decreased CD4+ T cell proliferation and CD8+ T cell hyperactivation with T cell migration into the lungs (119). However, Liao L. et al. (120) have observed an increase of T cells in bronchoalveolar lavage fluids in mild patients but not in severe patients, suggesting a difference in T cell migration into the lungs in severe patients (120–122).

Meanwhile, arguments supporting the role of cellular immunity in the control of primary SARS-CoV-2 infection are supported by the fact that neutralizing antibody titers do not correlate with lessened disease severity in primary COVID-19 (123–125). Unlike neutralizing antibodies, SARS-CoV-2-specific CD4+ and CD8+ T cells were found to be associated with reduced disease severity in the same individuals (124). In agreement with these findings, there are reports of healthy individuals successfully controlling a SARS-CoV-2 infection with little to no neutralizing (or receptor binding domain -RBD- IgG) antibodies detectable post-infection, while having significant SARS-CoV-2-specific T cell memory (67, 68, 124, 126). On the other hand, neutralizing antibody titers (and total spike antibody titers) have indeed been positively correlated with COVID-19 disease severity (58, 127–129), possibly indicating that under normal conditions the adaptive immune response works in strict balance, but when one arm becomes unbalanced the other tries to compensate. Thus, a defect in the cellular response would cause a greater humoral response to correct this deficiency. The role of cellular response has also become evident in patients with agammaglobulinemia and no circulating B cells who have fully recovered from infection (130, 131) and subjects with pharmaceutical depletion of B cells who resolved COVID-19 infection without requiring intensive care (132–136). Moreover, in patients with haematological malignancy, CD8+ T cells appear to compensate for the lack of humoral immunity and were associated with improved outcomes, indicating a role for T cells in protection against SARS-CoV-2 infection (137).

CD4+ T cell responses to pathogens are divided into three major types: Th1, Th2, and Th17. Th1 immune response, which is characterized by T-bet-dependent responses and IFN-γ secretion, is generated against intracellular pathogens including viruses. In the Th1 response, pathogen clearance is mediated through effector cells including innate lymphoid cells 1 (ILC1), NK cells, and cytotoxic T lymphocytes (138–140). During SARS-CoV-2 acute infection, patients display a proliferation of IFN-γ-producing Th1 (IFN-γ, IL-12, IL-15, IL-2 and TNF) cells and it has been suggested that this Th1 cell-biased phenotype is associated with less severe disease (54, 141). In patients with moderate disease, the core COVID-19 inflammatory cytokine signature with IL-1a, IL-1b, IL-17A, and IFN-α observed in the first 10 days from symptom onset declined steadily (142) and the same happens with the innate cytokine IL-12, a key inducer of Th1 immune response, as well as IFN-γ (142). Early induction of IFN-γ-secreting SARS-CoV-2-specific T cells with accelerated viral clearance is present in these patients with mild disease (125) **Figure 1**.

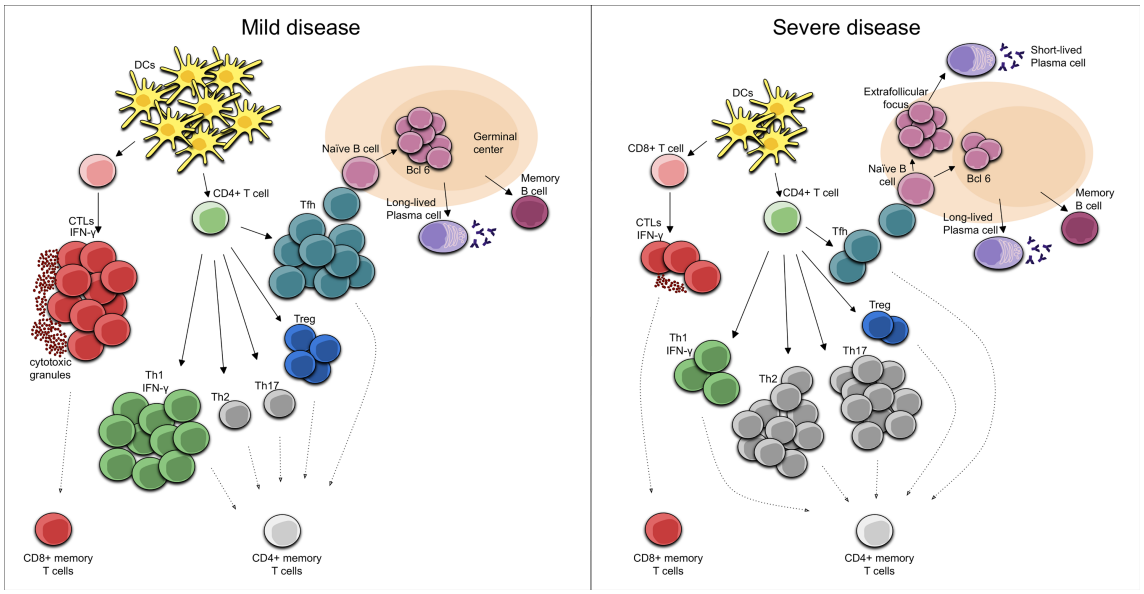

FIGURE 1 | Cellular immune response in Mild COVID-19. In mild COVID-19, there is an early induction of the Th1 cell-biased phenotype with IFN-γ secreting SARS-CoV-2-specific T cells. In turn, SARS-CoV-2-specific CD8+ T cells perform rapid responses, acting as CTLs, secreting cytotoxic granules and high levels of IFN-γ. Moreover, activated Tfh cells in the draining lymph nodes activate the naïve B cells that are necessary for the development of long-lived plasma cells and memory B cells. Cellular immune response in Severe COVID-19. During a severe course of COVID-19, there are reduced numbers and functions of DCs, leading to decreased numbers of CD4+ T cells. In this case, an elevation of Th2 phenotype and/or a dysregulation of the Treg/Th17 cell ratio toward the Th17 phenotype can be seen. Furthermore, decreased numbers of CD8+ T cells with an exhausted phenotype results in reduced CTL functionality while the T cell-mediated activation of B cells in extrafollicular focus induces their differentiation into short-lived plasma cells.

The effector cells of CD8+ lineage are CTLs, whose major function is to eliminate cells harboring viruses. SARS-CoV-2 CD8+ T cells are specific for a range of SARS-CoV-2 antigens, and spike, nucleocapsid, M, and ORF3a proteins are well represented (53, 56, 67, 126, 143, 144). CD8+ CTLs eliminate intracellular microbes mainly by killing infected cells by releasing cytotoxic proteins stored within cytoplasmic granules to the target cell and subsequently triggering cellular apoptosis. In acute COVID-19, SARS-CoV-2-specific CD8+ T cells exhibit high levels of IFN-γ, granzyme B, perforin, and CD107a molecules, some of which are present in the cytotoxic granules and are associated with potent cytotoxic effector functions (68, 124, 126, 145), developing fast CD8+ T cell responses (124). Patients with milder disease and recovery have been associated with a more robust clonal expansion of CD8+ T cells in peripheral blood (146). These findings would explain why, in SARS-CoV-2 infections, the presence of virus-specific CD8+ T cells has been associated with better COVID-19 outcomes (124, 144). Taken together, these observations suggest that cytotoxic activity is critical for the clearance of many viral infections and is therefore also important for the eradication of the infection reservoir. As with peripheral blood results, there is also an increase in SARS-CoV-2-specific CD8+ T cells in the respiratory tract of moderate COVID-19, as demonstrated in bronchoalveolar lavage fluid collected from COVID-19 patients. Bronchoalveolar lavage fluid CD8+ T cells showed clonal expansion, suggesting T cell migration to the infected site resulting in the overall peripheral counts (147).

The role of T folicular helper (Tfh) cells at germinal centers in the development of a long-lasting, high-affinity antibody response is well known (148, 149). In T cell-dependent immune responses, T cells are important in the formation of an extrafollicular focus, in which B cells proliferate and differentiate into plasma cells, most of which are short-lived. The activation of T cells in the extrafollicular focus will cause some of them to develop into Tfh cells and migrate into the germinal centers, where they perform their functions, which are necessary for the development of both the bone marrow resident plasma cells and the memory B cells that enter in the recirculating lymphocyte pool (150, 151). Importantly, it appears that the germinal center reaction in humans after vaccination persists over a longer period (152–154). Evidence suggesting that the above described process is indeed what occurs following SARS-CoV-2 infection have been provided by Mudd PA et al. (155) given that a high-magnitude, SARS-CoV-2-specific CD4+ T cell response in the draining lymph nodes is present during the development of high-titer neutralizing antibody responses in the setting of COVID-19 mRNA vaccination. The fact that CD4+ T cells in this type of response provide help to B cells for the production of antibodies has been demonstrated in other situations. For example, individuals with uncontrolled HIV and extremely low CD4+ T cell counts during vaccination lack seroconversion (156), and this has also been

observed in patients subjected to T cell-focused immunosuppressive regimens following solid organ transplantation who received a standard two-dose BNT162b2 regimen (157). Overall, there is direct and indirect evidence of the need for a robust T response for the generation of high-titer neutralizing antibody responses following COVID-19 infection or mRNA vaccination. However, a lower quality and lack of durability of humoral response has been observed during natural SARS-CoV-2 infection. Thus, although there is evidence of a robust T-cell-mediated activation of B cells in the non-germinal-center, this may be due to a loss of germinal centers through a specific block of germinal center type B cell-lymphoma 6 (Bcl-6)+ T follicular helper cell differentiation (158) **Figure 1**. This may compromise the early development of the high-affinity antibodies that could contribute to a certain attenuation of viral spread. Moreover, in COVID-19 patients, the relationship between plasmablasts and activated Tfh is weak, even though these individuals have a robust plasmablast response (114). At least part of the plasmablast response may be through activated (CD38+HLA-DR+) CD4+ T cells, which might play a role in providing B cell help as a part of an extrafollicular response (114).

Relation of Cellular Components With Disease Severity

As mentioned above, an immune response properly coordinated in time between the different components of innate and adaptive immunity is essential for it to be successful. In fact, if the adaptive immune response starts too late, fatal COVID-19 develops, defined as a situation in which the viral load is high (159).

IFN-γ has already been discussed as a cytokine secreted by CD4+ Th1 cells, but it is also secreted by differentiated CTLs. It contributes to classical macrophage activation and inflammation in the host's defense and in hypersensitivity reactions. It is likely that both CD4+ Th1 cells and CD8+ T cells contribute to the IFN-γ–induced phagocytic clearance of ingested microbes. These functions would explain the beneficial effect of rapid IFN-γ secretion in response to an infectious process. Thus, Zheng M. et al. (160) reported the secretion of IFN-γ by both CD8+ T cells and CD4+ Th1 cells under conditions of severe COVID-19 disease. Therefore, a poor T cell response contributes to SARS-CoV-2 viral persistence and COVID-19 mortality, whereas strong T cell responses are protective in the majority of individuals. As seen in SARS-CoV-2 infection in non-human primate models, the deletion of CD8+ T cells impairs this protection (161).Thus, human individuals with higher levels of IFN-γ secreting T cells (measured by enzyme-linked immunosorbent spot assay) against the SARS-CoV-2 S protein, nuclear proteins, and membrane proteins have a better protection against the virus (162), while a CD4+ T cell IFN-γ expression decrease has been reported in severe SARS-CoV-2 infection peripheral blood samples, and the T cells of these patients seemed to be unable to produce IFN-γ in response to viral proteins (163).

Patients with severe COVID-19 have marked reductions in the number and frequency of both CD4+ and CD8+ T cells, but increased activation of T cells (142, 145). Specifically, in an autopsy report, low levels of hyperactive T-cells in peripheral blood and an accumulation of mononuclear cells in the lungs of the individual were observed (164). In addition, the high proportion of M/NP-specific CD8+ T cell responses compared to the spike-specific CD4+ T cell response seen in mild disease is not found in severe disease (144). In fact, the percentages and absolute numbers of CD8+ T cells in severe disease were significantly reduced (163). This finding could suggest a protective role of CD8+ T-cell response in mild disease or a pathogenic role of the CD4+ T-cell response in severe disease (144). The same applies in the case of ICU (intensive care unit) patients: total T-cell, CD4+ and CD8+ T-cell counts in peripheral blood were significantly lower than in non-ICU COVID-19 cases, and the counts correlated negatively with patient survival (165). Some authors have observed an increased expression of the inhibitory receptor NKG2A, suggesting a decrease in CD8+ T cell functionality (160). NKG2A expression is upregulated on NK cells and CTLs in COVID-19 patients, with a decreased capacity to produce CD107a, IFN-γ, IL-2, granzyme B and TNF-α., which suggests functional exhaustion of cytotoxic lymphocytes in COVID-19 patients (160). The upregulation of NKG2A expression may be a consequence of and to compensate for the hyperactivation of CD8+ T cells in the severe stage of COVID-19.

There is a cellular subset composed mainly of mucosal-associated invariant T (MAIT) cells, the CD161+ CD8+ T cells which undergoes a strong reduction in frequency in individuals with severe COVID-19 (145). During viral infections, MAIT cells can become activated and migrate to infection sites (166, 167). The sharp decline in circulating MAIT cells in severe COVID-19 patients correlates with their presence in the airways of the patients (168). The reduction of this population in peripheral blood is likely to be indicative of sequestration in the lungs, potentially exacerbating tissue inflammation.

During many acute viral infections, the period of peak T-cell responses and plasmablast detection in peripheral blood is relatively short (169–171). However, there is a subgroup of COVID-19 disease patients with an over-aggressive immune response and/or a "cytokine storm" (172) due perhaps to a failure to regulate responses or a prolonged period of peak immune responses because there is a stability over time of CD8+ and CD4+ T-cell activation and plasmablast response (114). There has been speculation on possible causes for the well-known cytopenia occurring in COVID-19. One of these causes may be related to the recruitment of T cells to infected lung tissues to control viral infection (173). Another cause might be the apoptosis or necrosis of T cells caused by the cytokine storm that occurs in severe cases of COVID-19 (174). The severity of the disease also correlates with cytokine levels and these patients secrete higher levels of IL-6 and IL-10 (175). Thus, in ICU patients a further increase in IL-6 and IL-10 plus TNF-α (165) has been observed and has also been found to be higher in the bronchoalveolar lavage fluid of deceased patients than in those who survive IL-6 (120). The increase in TNF-α may explain why antibody levels correlate with disease severity, since this cytokine secreted by CD4+ T cells serves as a co-stimulatory signal for B cells. Furthermore, the expansion of plasma cells in severe disease

has been associated with large and oligoclonal B cell expansions (145).

The significant lymphopenia that COVID-19 patients present in the acute and severe phase is associated with a lower number and the functional impairment of dendritic cells (DCs), which are fundamental in T-cell antigenic presentation, compared to mild patients (119, 145, 176), and those cells are significantly decreased in fatal cases compared to survivors (177). Plasmacytoid DCs (pDCs), which is responsible for the production of the type I IFNs involved in virus defense, were also mainly reduced in abundance and impaired in function in severe COVID-19 patients (145). In fact, during COVID-19 infection, the rapid loss of DCs numbers and function may contribute to delayed T cell responses and the features of low level IFN-I/IFN-III (178).

This would partially explain the correlation of a fatal disease course with the age of the patients since we should not forget the process known as "immunosenescence", which features a reduction in the ability to fight novel infection (179) and a reduced abundance of DCs in elderly patients (180). Thus, the presence of an immunosenescent phenotype, demonstrated by an elevated neutrophils-to-lymphocytes ratio, was found in severe COVID-19 patients but not in mild disease (181).

Furthermore, patients with severe fatal disease up to 10 days from the onset of symptoms have a excessive hyperactivation of the immune function, demonstrated by significantly increased HLA-DR expression and IFN-γ synthesis. In fact, a robust T cell response in critical patients may contribute to hyperreactivity and immunophatogenesis (182). Moreover, the proportion of T regulatory (Treg) lymphocytes increases significantly in this phase, which negatively regulates immune response (112). As discussed previously, the Th1 cell-biased phenotype is associated with less severe disease (54, 141), but patients with SARS-CoV-2-induced acute respiratory distress syndrome (ARDS) often tend to have a Th1:Th2 ratio weighted towards the Th2 type, leading to substantial lung tissue damage (183, 184). In addition, a broad elevation of Th1, Th2 and Th17 signatures, including inflammasome-dependent cytokines such as IL-1b, IL-18 and Th2 and Th17 cytokines has been identified in patients with severe COVID-19 (142). Th2 and Th17 immunity depend on the transcription factors GATA-3 and RORγt, respectively, and the predominant response is driven by (IL-4, IL-5, IL-13) and (IL-17, IL-22) respectively (138–140). Also, dysregulation of the Treg/Th17 cell ratio toward the Th17 phenotype is an important contributor to disease severity. IL-17 secreted during SARS-CoV-2 infection can promote migration of neutrophils and monocytes into the pulmonary interstitium resulting in its consequent inflammation, as well as the activation of other cytokine cascades (G-CSF, TNFα, IL-1β and IL-6), which contribute to aggravating this inflammation and tissue damage (185). Thus, patients with severe COVID-19 showed a markedly high number of CCR6+ Th17 cells in peripheral blood (164), even though not all patients with severe COVID-19 have increased IL-17 expression (163). These data suggest that the dysregulation of Th polarization occurs in severe COVID-19 and a bias towards this type of Th response might define the disease course **Figure 1**.

Whether or not infection and hyperactivation persist, the immune system eventually enters an anergy state in which the number of lymphocytes (including T and B lymphocytes), NK cells and DCs continues decreasing in patients with a fatal outcome. CD4+ T cell function is impaired, as evidenced by decreased activating receptors and an increased expression of CD45RA and CD28 (112). Thus, deceased patients have lower frequencies of HLA-DR+ and IFN-γ-secreting cells within CD4+ and CD8+ T cells than survivors (186, 187).

Another important factor to be taken into account during any maintained immune response is a phenomenon called exhaustion, which is observed, for example, in some chronic viral infections when CTL effector responses gradually extinguish over time (188). Exhausted cells express increased levels of multiple inhibitory receptors, notably programmed cell death-1 (PD-1), since the programmed cell death-ligand 1 (PD-L1)/PD-1 immune checkpoint axis is the strongest T cell exhaustion inducer, alongside cytotoxic T lymphocyte-associated protein 4 (CTLA-4), T cell immunoglobulin mucin-3 (TIM-3), lymphocyte activation gene-3 (LAG-3), and others. It has been reported that increased T cell exhaustion, observed by the high level expression of PD-1 and TIM-3 (165) induced by IL-10 (189) and decreased functional diversity correlates with the degree of disease severity in patients with COVID-19 (190). In particular, Kreutmair S. et al. (191) showed that CD4+ T cells increased PD-1 expression during the first days following hospital admission and then normalized in moderate patients but remained elevated in severe disease (191). Likewise, as in memory CD4+ T cells, the frequency of PD-1 expressing cells were reported to be higher after one month in recovered patients with severe COVID-19, and correlated with the age of the patient (145). However, Rha M.S. et al. (192) reported that SARS-CoV-2-specific CD8+ T cells expressing PD-1 were found not to be exhausted but functional. This is explained by the fact that PD-1 is expressed on exhausted T cells but is also expressed on recently activated T cells (193–196) and the persistence of antigen encounter results in the maintenance of PD-1 expression, leading to exhausted T cells (197). PD-1 expression in the peripheral blood of COVID-19 patients is also increased in the exhaustion of other T cell subsets such as γδ T, mucosa-associated invariant T and invariant NKT cells which, in agreement with their exhausted phenotype, produce less IFN-γ than cells from healthy donors (168). Also, the T cells of ICU patients expressed increased PD-1 in bronchoalveolar lavage fluid as compared to peripheral blood T cells (198).

Regarding ligand PD-L1, both soluble and membrane-bound PD-L1 increased levels are associated with the degree of severity in COVID-19 (199–201). PD-L1/PD-1 overexpression in the white adipose tissue of obese individuals during IFN-γ secretion, which leads to the dysfunction of T cells and especially to a reduction in cytotoxic activity, explains why SARS-CoV-2 infection can worsen disease in obese individuals (202). Overall, we can outline that T cells of COVID-19 patients display a higher expression of PD-1 and that this elevated expression is correlated with disease severity, but whether or

not PD-1 expressing T cells in COVID-19 are functional needs to be investigated further. To assess exhaustion, it will be important to take into account not only the expression of PD-1, but other exhaustion markers and the time since a particular cell has encountered the antigen in order to differentiate an exhausted cell from a recently activated cell.

In the resolution of inflammation when the virus is eliminated, both adaptive regulatory cells, such as regulatory T and B cells and innate immune cells, such as macrophages and regulatory DCs, also contribute (203). In recovered patients, the number of peripheral blood lymphocytes gradually increases (186, 187) with a marked high frequency of spike specific CD4+ T cell response (53, 126, 144), while the effector function of T cells is not compromised (204). Two to four months after SARS-CoV-2 infection resolution, most of the components of cellular immunity return to normality (204), though with significant increases in regulatory T cell frequencies and TIM-3 expression on CD4+ and CD8+ T cells, while the cytotoxicity of T cells is significantly diminished (204). However, this immune response reversion is slower and the virus clearance time is prolonged in some critically ill patients even after entering the recovery stage (112).

BALANCE BETWEEN INNATE AND ADAPTIVE IMMUNITY

The first contact with pathogens is established by the host innate immune system. It is noteworthy that the innate immune system is indeed capable of eliminating some infections on its own, particularly when the infection is localized and caused by a low number of pathogens. But innate immunity is not sufficient to protect us fully from infectious diseases, in part because, as discussed earlier, many pathogens have features that allow them to evade innate immune responses. At this early stage, the innate cytokine IL-12 has been shown to stimulate the differentiation of naive CD8+ T cells into effector CTLs and it is involved in the differentiation of CD4+ T cells into Th1 cells, both contributing to the IFN-γ–induced phagocytic clearance of ingested microbes. However, in some circumstances, the innate immune response seeks to fill the gap left by the absence of a T cell response, attempting to assume t control of the immune response against the virus with an ever-expanding innate immunity activation. Following this thread, there are many studies that have identified innate cytokine/chemokine signatures of immunopathology (145, 205–209). The most common observation in this line is an elevated frequency of neutrophils in blood (145) and massive numbers of neutrophils in the lungs, both of which are associated with severe, end-stage COVID-19 disease (147, 206–208), as well as the cytokine storm (172). In severe COVID-19 patients, IL-12 and IFN-γ increased over time; however, T cell depletion was detected in these patients and the remaining T cells did not produce larger amounts of IFN-γ (142). This suggests that the secretion of IFN-γ by innate cells, such as ILCs and NK cells, or resident T cells in tissues were the primary contributors to the enhancement of the IL-12 and IFN-γ cytokine levels observed in severe patients.

The other finding reported is the role that the sex of the patient plays in the type of predominant immune response. It has been shown that male patients have higher plasma levels of innate immune cytokines, including IL-8 and IL-18, along with activated non-classical monocytes. In contrast, female patients seem to generate a more robust T cell activation during SARS-CoV-2 infection. A poor T cell response might be responsible for the worse outcomes observed in male patients, while in female patients, higher levels of cytokines related to innate immune response appear to be associated with worse disease evolution (210).

A recently published study in mice suggests that specific T cell and antibody responses develop independently of SARS-CoV-2 detection by some of the pattern recognition receptors (PRRs) of the innate immunity system: TLR2-5 and TLR7, STING-cGAS, NLRP3 (inflammasome activation), as well as RIP3 kinase (mediator of nedroptosis) and gasdermin D (mediator of pyroptosis). On the other hand, these specific T cell responses, mainly featuring CD8+ T cells, are affected by the altered recognition of SARS-CoV-2 by the MDA5-IFNAR1 signalling pathways (211). Airway epithelial cells from children appear to show an increased expression of MDA5 compared to its expression level in SARS-CoV-2 positive adult epithelial cells (212). Consistent with this, we found several studies showing that children eliminate SARS-CoV-2 faster than adults, probably by detaining viral replication earlier (213–216).

In general terms, we have sought to emphasize that a balance between the innate and the adaptive immune response is paramount for a favourable evolution and resolution of COVID-19 disease and its imbalance has detrimental consequences, including the inability to configure a competent adaptive response or the overactivation of the innate immune system which results in a cytokine storm.

IMMUNE MEMORY

The balance between naïve and memory T cells is crucial for infection control. Naïve T cells are responsible for primary infection response and memory T cells promote antigen-specific immune responses, being able to protect the host from re-infection with the same pathogen. Immune memory against SARS-CoV-2 correlates positively with patient disease severity during acute phase infection, both in humoral and cellular response (217). Thus, it has been shown that memory B cells percentages among hospitalized cases were significantly higher than among non-hospitalized cases following infection (218).

There are some studies that report relatively stable humoral immunity for up to 6-12 moths post-infection (217–221) and Zhang J. et al. (217) described the detection of neutralizing antibodies in convalescent COVID-19 patients even at 12 months following symptoms onset. However, further studies show a clear decline of SARS-CoV-2 neutralizing antibodies in the first months after infection (222–224), along with a progressive decline in total antibody levels eight months after SARS-CoV-2 infection (218, 225). These inconsistencies in the results of humoral immunity longevity may be due to variations

between the studied cohorts and the use of different techniques or distinct antibody-detection epitopes in the assays.

In a longitudinal study, Rodda L.B. et al. (226) detected memory T cells, which secrete IFN-γ and are able to clonally expand following SARS-CoV-2-antigen re-exposure, at least three months after disease onset. Further investigations have detected maintained SARS-CoV-2-specific memory T cell responses in COVID-19 convalescent patients at least 7-12 months after infection (217, 221, 227) and this has been found to be true regardless of disease severity (227). Considering immune memory at the tissue level, SARS-CoV-2-specific lung resident memory T cell can be detected at least 10 months following infection (228). Lung resident memory T cells may be key players in limiting the severity of COVID-19 or the potential for reinfection. In this regard, it has been described that a higher number of these resident memory T cells in the lungs corresponds with a higher degree of clinical protection (229).

Therefore, both B and T memory cells exhibit robust memory response (225), indicating that, in the event of a re-encounter with SARS-CoV-2, the levels of total and neutralizing antibodies and effector T cells necessary to respond efficiently to infection might be rapidly recovered. In fact, B and T cell memory functional responses to SARS-CoV-2 are still detectable 12 months after natural infection (230).

Immune Memory Phenotypes

Individuals who have undergone mild symptomatic SARS-CoV-2 infection show, after a few months, an increase in circulating Th1 cytokine-producing CXCR5+ Tfh and CXCR5- non-Tfh cells, CD4+ CXCR3+ proliferative memory T cells and IFN-γ-producing CD8+ T cells (226). In these mild COVID-19 cases, CD8+ T memory cell responses predominate over CD4+ T memory cell responses and, additionally, the memory CD8+ T cells specific for SARS-CoV-2 M and NP proteins exhibit the highest frequency of multiple cytokine production (144). Additionally, the SARS-CoV-2-specific memory CD4+ T cells of recovered individuals have the capacity to express CXCR5, ICOS, CD40L and proliferate at spike-protein re-exposure (226). The expression of these markers and a variety of cytokines is important for T-B cells interaction (231) as they enable memory CD4+ T cells to help reactivate memory B cells and therefore start producing antibodies against SARS-CoV-2 since, as discussed above, their levels may have decreased over time. This may serve to explain why, during the memory phase, an abundance of Tfh cells correlates with antibody response (232–234).

Regarding the immune memory to SARS-CoV-2 in convalescent individuals, a number of authors have underlined the contribution of a subtype of terminally differentiated memory cells: the terminally differentiated effector memory T cells re-expressing marker CD45-RA (T_{EMRA}). T_{EMRA} have generally been associated with protection against viral infection (22, 235–238). During the memory phase following SARS-CoV-2 infection, a high prevalence (218, 227) and a progressive enrichment of the T_{EMRA} phenotype and T stem cell memory (T_{SCM}) phenotype in SARS-CoV-2-specific CD8+ T cells (239) has been described. The same authors postulate that the differentiation towards one phenotype or the other might be associated with disease severity with a bias towards T_{SCM} in mild disease and increased T_{EMRA} in severe disease. In agreement with previous studies that highlight the role of type I IFN in memory development (240), Adamo S. et al. (239) reported an expression enrichment of the genes involved in IFN signaling pathways in SARS-CoV2-specific memory CD8+ T cells. Thus, type I IFN signaling might be a key driver directing cells to become long-lived memory cells. While it has already been mentioned that T_{EMRA} cells are associated with protection against viruses, it has also been shown that they can accumulate during chronic viral infections (241). In Long COVID syndrome, when compared to COVID-19 convalescent individuals, an increase in CD8+ T effector memory (T_{EM}) and CD8+ T_{EMRA} cell number, accompanied by a decrease in their functional activity, has been reported (242).

The success of long-term memory T cells depends on the generation of T_{SCM} cells (243) since they have a higher self-renewal ability and are multipotent cells, being able to reconstitute several memory phenotypes (244). T cell memory developed during SARS-CoV-2 infection may be long-lasting since COVID-19 convalescent patients develop SARS-CoV-2-specific T_{SCM} cells (192, 227, 239). Cohen K.W. et al. (245) defined most SARS-CoV-2 CD4+ T cells as displaying a central memory profile. Furthermore, Gurevich M. et al. (221) reported the presence of IL-2-secreting and IFN-γ+IL-2-secreting SARS-CoV-2-specific central memory T cells that might be long-lasting memory phenotypes in accordance with previous studies (246). There are two different subsets of CCR7+ stem cell-like progenitors: CCR7+PD-1−TIGIT− cells are observed to display stem cell-like features, whereas CCR7+PD-1+TIGIT+ cells seem to exhibit exhausted traits (192, 247). SARS-CoV-2-specific T_{SCM} cells rarely express PD-1 and TIGIT, making them non-exhausted-like progenitors but functional memory T cells (227).

VACCINATION

A good adaptive immune response and immune memory are vital to the success of vaccines and the achievement of a low degree of reinfection. When studying natural immunity to the virus, including the role of SARS-CoV-2 specific T cells, it is critical to fill in the current gaps in our knowledge for improved vaccine design. The generation of a robust cellular immune response is a desirable attribute for a vaccine against SARS-CoV-2 because, as we have referred to throughout this report, following natural infection, t T-cell response is activated rapidly to control disease progression (53, 55, 144, 248), and these virus-specific T-cell response have been shown to be associated with milder disease in COVID-19 patients (126).

mRNA vaccination leads to the development of both humoral and cellular immunity against the Covid-19 spike protein (249, 250) **Figure 2**. The onset of protection for mRNA vaccines has been observed as early as 10-12 days after the first dose (251) and during this phase T cells and spike-specific antibodies are detectable (250, 252) but neutralizing antibodies do not appear until after the second vaccine dose (253–256). In fact, the presence of anti-S reactive T cells secreting IFN-γ or IL-2 is

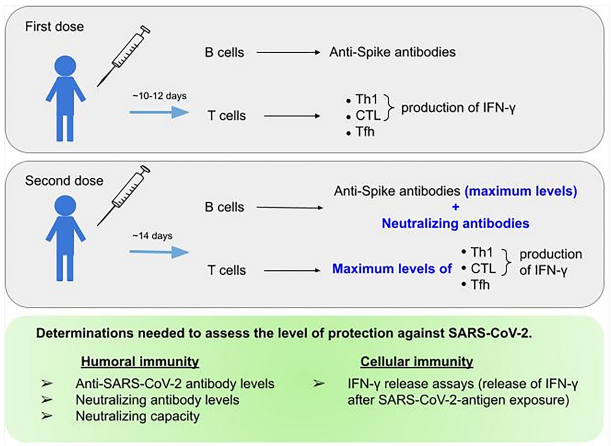

FIGURE 2 | Parameters to be assessed regarding humoral and cellular response to SARS-CoV-2 mRNA vaccine. The top and middle figure outline the immunological response achieved after the first and second doses of mRNA vaccines, respectively. The bottom figure summarizes the parameters needed to assess protection against SARS-CoV-2.

remarkable as early as three days post-vaccination, but it is not until 14 days after completing the vaccination schedule that they reach their maximum levels (121). The development of humoral responses is gradual and they only consistently reach peak levels after the second vaccination dose (257, 258). In fact, the highest frequencies of spike-binding germinal centre B cells and plasmablasts in draining lymph nodes were reached at twelve weeks after the second immunization (152). However, the natural course of humoral immunity is to decrease over time, with reductions in neutralizing antibody titers (259, 260). At three months post-vaccination, the neutralization capacity was significantly decreased, in agreement with lower S-RBD antibody levels (261) in all variants described to date, from Alpha to Omicron (260). This may, feasibly, be due to the fact that not all vaccine-induced plasmablasts commit or are maintained as long-lived memory plasma cells (123, 262, 263). However, these reductions do not necessarily correspond to proportional reductions in vaccine efficacy over time, and neither do reductions in vaccine efficacy against mild disease necessarily predict reductions in efficacy against severe disease. This may be because protection against severe disease is mediated not only by antibody response, which might be relatively short lived for some vaccines, but also by cell-mediated immunity and memory responses, which are generally longer lived (152). In fact, memory humoral and cellular responses are still detectable in vaccinated individuals who have not undergone COVID-19, and in those who have recovered from COVID-19, eight months after vaccination, despite a progressive decline in antibody levels (230). At six months, although vaccinated individuals show a decreased level of anti-S IgG, all of them present cell-mediated immune responses. The decrease in antibody titers is apparently compensated by an increased neutralization capacity and a robust cellular immune response, which is reflected by a high level of IFN-γ synthesis by the stimulated T-cells (264). In mice, the primary source of serum IFN-γ one day after secondary immunization are CD4+ and CD8+ T cells, which results in improved myeloid cell activation after secondary immunization (211). Given all of the information mentioned above, the assessment of humoral immune response as determined by the measurement of antibodies against the receptor-binding domain of the spike protein after vaccination underestimates the immunogenicity of SARS-CoV-2 vaccines and a combined analysis of humoral and cellular immunity was proposed for the identification of vaccine responders (265).

The type of response that vaccines should trigger must always be Th1 cell response or balanced T-cell responses, because when the response is Th2 cell, it has been associated with enhanced respiratory disease (266–270). Moreover, we have looked at how T cells also play a critical role in B-cell maturation and therefore the induction of a strong and durable antibody response (150). In most of the current COVID-19 vaccines that have reported clinical trial results, the induction of cellular response in humans has a Th1 bias and/or is characterized by IFN-γ expression and appears to be substantially protective against severe disease in all the major viral variants (271). Thus, in a longitudinal study, Painter M. M. et al. (250) show that mRNA vaccines induce Th1 and Tfh cell responses following the first dose, correlated with post-boost CD8+T cells and neutralizing antibodies, respectively, which is expected since Th1 cells predominantly facilitate CD8+ T cell response, while Tfh cells help promote optimal B cell, germinal center, and antibody responses (150, 272–274). At three months, 87% of vaccinated individuals developed either CD4+ or CD8+ T cell responses (261) but after the first dose, in subjects who had no previous contact with SARS-CoV-2, vaccination induced rapid and robust SARS-CoV-2-specific CD4+ T cell responses compared with CD8+T cell responses, which developed gradually and were variable in magnitude (250). However, other authors observed a robust, stable and fully functional response of Spike-specific CD8 T cells after primary vaccination (275). Differences in cohort or methodology may have affected the discrepancy in these findings, but these observations indicate that SARS-CoV-2-specific CD4+ T cells are largely contributors to the protection observed early after the first vaccine dose (251, 276).

CD4+ T cell responses were detected after immunization with ChAdOx-1 S, Ad26.COV2.S, mRNA-1273 or BNT162b2 vaccines, and did not show significant differences between the different variants of concern, including the Omicron variant (143). One or two doses of vaccine elicited a persistent and robust cellular immune memory response even when vaccinated individuals had been infected previously (277–279), with an homogeneity in the magnitude (264). Although previous infected individuals had similar frequencies of vaccine-induced CD4+ T cells as non-infected individuals, the former produced greater IFN-γ following spike-stimulation (230) In addition, T cell reactivity following vaccination or natural infection proved to be similar across early strains (Alpha, Beta and Gamma) given that 93% and 97% of CD4 and CD8 epitopes are 100% conserved across these variants, potentially reducing the severity of

COVID-19 if a progression of infection occurs, even though neutralizing antibodies for emerging variants might be reduced in comparison with the original strain of SARS-CoV-2 (280). The same applies to the latest variants, since SARS-CoV-2 vaccination induces immunological CD4+ and CD8+ T cell memory able to cross-recognize variants from Alpha to Omicron (281). Furthermore, CD4+ and CD8+ SARS-CoV-2 spike-specific T cell responses triggered by prior infection with the original strain or BNT 162b2 vaccination, remain largely intact against the Omicron strain (282). This is due to the fact that the vast majority of T cell epitopes are fully conserved (279–281, 283–286), which suggests that the continued evolution of variants has not been associated with increased viral escape from T cell responses at the population level, and HLA binding of the mutated epitopes has been well conserved for the majority of the epitopes in Alpha to Omicron variants (281). Furthermore, it has been proposed that the phenotype of memory and the helper subset distribution of SARS-CoV-2-specific CD4+ and CD8+ T cells responses elicited by second dose vaccine are similar to the ones detected in individuals who have gone through a natural SARS-CoV-2 infection (250).

The effect of the booster dose (a third vaccination dose) is different in naïve individuals than in recovered COVID-19 individuals. In naïve individuals, this booster significantly increased the levels of spike-specific antibodies and B and CD4+ T cells, while in recovered COVID-19 individuals, the booster dose has minor effects (230), in line with what was observed for the second vaccine dose (249, 250). Moreover, the second vaccine dose in individuals who have undergone symptomatic infection with SARS-CoV-2 is associated with lower neutralizing antibody levels, in addition to T and B cell spike-specific frequencies, which suggests that a vaccine over-boost strategy may lead to anergy and exhaustion (249, 257). It is important to differentiate between the immune response driven by the spike protein vaccine and the response resulting from SARS-CoV-2 infection, where the innate immune response triggers the adaptive immune response, and many more elements come into play in a much more complex process. In addition, the effect of repeated doses on overactivation and the role played in its regulatory mechanisms, as well as the appearance of exhausted cells, merits further study.

Age is an important factor influencing vaccine responses, and there have been studies that report elderly people responding poorly to influenza, Hepatitis A and B, and pneumococcal vaccines as they develop lower antibody levels and weaker cell-mediated responses (287). Immunosenescense is likely to affect the vaccine response to SARS-CoV-2, as spike-specific IFN-γ T cell responses to vaccines were impaired in the age group over 80 years (288, 289) and individuals with a higher number of immunosenescent CD8+ T_{EMRA} cells have lower spike-specific CD4+ T cell responses (261). For example, a study of COVID-19-naïve nursing-home residents found that both humoral and cellular responses declined after four weeks and remained lower than those of healthcare workers after 24 weeks (290). These data emphasize the need for additional measures for the fragile elderly population.

Considering this information, to ensure that responses mediated by antibodies with neutralizing capacity are complemented by T cell responses, an alternative parallel strategy in vaccine generation should involve the inclusion of additional antigens and T cell epitopes. This needs to be taken into account since early functional T cells specific to SARS-CoV-2- have a prognostic value with important implications for vaccine design and immune monitoring (125).

DISCUSSION

SARS-CoV-2, the coronavirus responsible for the last global pandemic, which originated in December 2019, is the causative agent of the disease called COVID-19. The existence of cross-reactivity between the immunity created by the common cold coronaviruses and SARS-CoV-2 has not avoided infection but may have possibly reduced the severity of the disease in some individuals. SARS-CoV-2, like other viruses, has evolved immune evasion mechanisms. In fact, multiple evasion mechanisms have been observed at the level of innate and adaptive humoral immune response; however, the evasion mechanisms involved in cellular response, although existing, require further study.

SARS-CoV-2 infection triggers a potent immune response that directs CD4+ T cellular adaptive response towards Th1 polarization and an activation of CD8+ CTLs, both IFN-γ producers, as well as an antibody-producing humoral response. Different mechanisms cause an imbalance in this response, leading to an overactivation of the innate immune system and resulting in a cytokine storm, together with a hyperactivation of the adaptive immune response that will consequently cause an exhaustion of the latter. The fundamental role played by cellular immunity as the main axis of the immune response against SARS-CoV-2, directing the different components involved, such as the innate response and the humoral response, is evidenced throughout this review.

Many efforts are being made during this pandemic to avoid both primoinfections and reinfections, using massive vaccination strategies. Both natural infection and vaccines produce long-term memory T cells, CD4+ and CD78+, which would protect the population particularly by avoiding severe infections and being associated with a better prognosis. Even so, the immunity provided by vaccination is more limited than the one provided by natural infection. This is because the immune response in vaccination is limited to the spike protein, which affects the variety of the T cell response and, notably, CD8+ T cell memory, which seems to be associated with a better prognosis in the case of non-spike-specific CD8+ T cells. Thus, a future vaccination strategy should include antigens, which are also important for the cellular response, to fill in these gaps.

A successful vaccination strategy requires knowledge of the previous immunity of the individual to SARS-CoV-2 since the cellular immune response to the vaccine is different in naïve individuals and in those who have been previously infected. In the latter, there is a faster and more robust response, which is already detectable with the first vaccine dose. The different studies

TABLE 1 | Up-to-date key concepts to consider regarding natural infection or vaccination immunity against SARS-CoV-2.

KEY CONCEPTS
• The presence of cross-reactivity, either humoral or cellular, between common cold hCoV and SARS-CoV-2 does not prevent infection but may be associated with less severe COVID-19.
• The presence of SARS-CoV-2-specific CD4+ Th1 IFN-γ-producing cells and CD8+ CTLs cells were associated with reduced disease severity.
• T lymphocyte recruitment to infected lung tissues and T lymphocyte apoptosis/necrosis caused by the cytokine storm might be crucial determinants of CD4+ and CD8+ T-cell lymphopenia in severe COVID-19 cases.
• Severe /fatal disease presents with excessive hyperactivation of immune function with increased Tregs and Th2 and/or Th17 cell-biased phenotype, leading to T cell exhaustion and subsequently to a state of anergy.
• Functional memory B and T cells to SARS-CoV-2 have been detected 12 months after natural infection. SARS-CoV-2-specific T cell memory may be long lasting given that COVID-19 convalescent patients develop SARS-CoV-2-specific TSCM cells that display a non-exhausted phenotype.
• The immunogenicity of SARS-CoV-2 vaccines involves the humoral response (number of spike-specific antibodies, neutralizing antibodies, and antibody neutralization capacity) and the cellular response (IFN-γ-producing CD4+ and CD8+ T cells). Therefore, a combined analysis of humoral and cellular immunity is necessary for the identification of vaccine responders and the immune protection evolution.

performed to date make it possible to reach some conclusions concerning the role of cell-mediated immunity in SARS-CoV-2 infection/vaccination (**Table 1**). Hopefully, in the future, the analysis of cellular immunological memory generated by a previous infection or by vaccination will provide us with the tools required to fight against future variants of SARS-CoV-2 in terms of infection control, as well as future revaccination programs.

AUTHOR CONTRIBUTIONS

EM and EL-P contributed to the conception and design of the article, the interpretation of the relevant literature, and the writing of the manuscript and prepared the figures. PD contributed to the critical revision of the article for intellectual content and funding acquisition. All authors contributed to the article and approved the submitted version.

FUNDING

This work was partially supported by the grant COV20/00070 (to PD), Instituto de Salud Carlos III, Madrid, Spain. PD is supported by a grant from the Programa de Intensificación de Investigadores (INT19/00036)-ISCIII.

REFERENCES

1. Jakubowiak AJ, Dytfeld D, Griffith KA, Lebovic D, Vesole DH, Jagannath S, et al. A Phase 1/2 Study of Carfilzomib in Combination With Lenalidomide and Low-Dose Dexamethasone as a Frontline Treatment for Multiple Myeloma. *Blood* (2012) 120(9):1801–9. doi: 10.1182/blood-2012-04-422683
2. Masters PS. The Molecular Biology of Coronaviruses. *Adv Virus Res* (2006) 65:193–292. doi: 10.1016/S0065-3527(06)66005-3
3. Zhong NS, Zheng BJ, Li YM, Poon LLM, Xie ZH, Chan KH, et al. Epidemiology and Cause of Severe Acute Respiratory Syndrome (SARS) in Guangdong, People's Republic of China, in February, 2003. *Lancet* (2003) 362(9393):1353–8. doi: 10.1016/S0140-6736(03)14630-2
4. Lee N, Hui D, Wu A, Chan P, Cameron P, Joynt GM, et al. A Major Outbreak of Severe Acute Respiratory Syndrome in Hong Kong. *N Engl J Med* (2003) 348(20):1986–94. doi: 10.1056/NEJMoa030685
5. Zaki AM, van Boheemen S, Bestebroer TM, Osterhaus ADME, Fouchier RAM. Isolation of a Novel Coronavirus From a Man With Pneumonia in Saudi Arabia. *N Engl J Med* (2012) 367(19):1814–20. doi: 10.1056/NEJMoa1211721
6. de Groot RJ, Baker SC, Baric RS, Brown CS, Drosten C, Enjuanes L, et al. Middle East Respiratory Syndrome Coronavirus (MERS-CoV): Announcement of the Coronavirus Study Group. *J Virol* (2013) 87 (14):7790–2. doi: 10.1128/JVI.01244-13
7. Zhu N, Zhang D, Wang W, Li X, Yang B, Song J, et al. A Novel Coronavirus From Patients With Pneumonia in China, 2019. *N Engl J Med* (2020) 382 (8):727–33. doi: 10.1056/NEJMoa2001017
8. Siddell SG, Walker PJ, Lefkowitz EJ, Mushegian AR, Adams MJ, Dutilh BE, et al. Additional Changes to Taxonomy Ratified in a Special Vote by the International Committee on Taxonomy of Viruses (October 2018). *Arch Virol* (2019) 164(3):943–6. doi: 10.1007/s00705-018-04136-2
9. Gorbalenya AE, Baker SC, Baric RS, de Groot RJ, Drosten C, Gulyaeva AA, et al. The Species Severe Acute Respiratory Syndrome-Related Coronavirus: Classifying 2019-Ncov and Naming it SARS-CoV-2. *Nat Microbiol* (2020) 5 (4):536–44. doi: 10.1038/s41564-020-0695-z
10. Woo PCY, Lau SKP, Lam CSF, Lau CCY, Tsang AKL, Lau JHN, et al. Discovery of Seven Novel Mammalian and Avian Coronaviruses in the Genus Deltacoronavirus Supports Bat Coronaviruses as the Gene Source of Alphacoronavirus and Betacoronavirus and Avian Coronaviruses as the Gene Source of Gammacoronavirus and Deltacoronavi. *J Virol* (2012) 86 (7):3995–4008. doi: 10.1128/JVI.06540-11
11. Lu R, Zhao X, Li J, Niu P, Yang B, Wu H, et al. Genomic Characterisation and Epidemiology of 2019 Novel Coronavirus: Implications for Virus Origins and Receptor Binding. *Lancet* (2020) 395(10224):565–74. doi: 10.1016/S0140-6736(20)30251-8
12. Zhou P, Yang XL, Wang XG, Hu B, Zhang L, Zhang W, et al. A Pneumonia Outbreak Associated With a New Coronavirus of Probable Bat Origin. *Nature* (2020) 579(7798):270–3. doi: 10.1038/s41586-020-2012-7
13. Callaway E. Beyond Omicron: What's Next for COVID's Viral Evolution. *Nature* (2021) 600(7888):204–7. doi: 10.1038/d41586-021-03619-8
14. Harvey WT, Carabelli AM, Jackson B, Gupta RK, Thomson EC, Harrison EM, et al. SARS-CoV-2 Variants, Spike Mutations and Immune Escape. *Nat Rev Microbiol* (2021) 19(7):409–24. doi: 10.1038/s41579-021-00573-0
15. Walensky RP, Walke HT, Fauci AS. SARS-CoV-2 Variants of Concern in the United States-Challenges and Opportunities. *JAMA - J Am Med Assoc* (2021) 325(11):1037–8. doi: 10.1001/jama.2021.2294
16. Uriu K, Kimura I, Shirakawa K, Takaori-Kondo A, Nakada T, Kaneda A, et al. Neutralization of the SARS-CoV-2 Mu Variant by Convalescent and Vaccine Serum. *N Engl J Med* (2021) 385(25):2397–9. doi: 10.1056/NEJMc2114706

17. Mlcochova P, Kemp S, Dhar MS, Papa G, Meng B, Ferreira IATM, et al. SARS-CoV-2 B.1.617.2 Delta Variant Replication and Immune Evasion. *Nature* (2021) 599:114–9. doi: 10.1038/s41586-021-03944-y
18. Karim SSA, Karim QA. Omicron SARS-CoV-2 Variant: A New Chapter in the COVID-19 Pandemic. *Lancet* (2021) 398(10317):2126–8. doi: 10.1016/S0140-6736(21)02758-6
19. St. John AL, Rathore APS. Adaptive Immune Responses to Primary and Secondary Dengue Virus Infections. *Nat Rev Immunol* (2019) 19(4):218–30. doi: 10.1038/s41577-019-0123-x
20. Hayward AC, Wang L, Goonetilleke N, Fragaszy EB, Bermingham A, Copas A, et al. Natural T Cell-Mediated Protection Against Seasonal and Pandemic Influenza: Results of the Flu Watch Cohort Study. *Am J Respir Crit Care Med* (2015) 191(12):1422–31. doi: 10.1164/rccm.201411-1988OC
21. Greenbaum JA, Kotturi MF, Kim Y, Oseroff C, Vaughan K, Salimi N, et al. Pre-Existing Immunity Against Swine-Origin H1N1 Influenza Viruses in the General Human Population. *Proc Natl Acad Sci U S A* (2009) 106 (48):20365–70. doi: 10.1073/pnas.0911580106
22. Sridhar S, Begom S, Bermingham A, Hoschler K, Adamson W, Carman W, et al. Cellular Immune Correlates of Protection Against Symptomatic Pandemic Influenza. *Nat Med* (2013) 19(10):1305–12. doi: 10.1038/nm.3350
23. Wilkinson TM, Li CKF, Chui CSC, Huang AKY, Perkins M, Liebner JC, et al. Preexisting Influenza-Specific CD4 + T Cells Correlate With Disease Protection Against Influenza Challenge in Humans. *Nat Med* (2012) 18 (2):274–80. doi: 10.1038/nm.2612
24. Weber F, Wagner V, Rasmussen SB, Hartmann R, Paludan SR. Double-Stranded RNA Is Produced by Positive-Strand RNA Viruses and DNA Viruses But Not in Detectable Amounts by Negative-Strand RNA Viruses. *J Virol* (2006) 80(10):5059–64. doi: 10.1128/JVI.80.10.5059-5064.2006
25. Zielecki F, Weber M, Eickmann M, Spiegelberg L, Zaki AM, Matrosovich M, et al. Human Cell Tropism and Innate Immune System Interactions of Human Respiratory Coronavirus EMC Compared to Those of Severe Acute Respiratory Syndrome Coronavirus. *J Virol* (2013) 87(9):5300–4. doi: 10.1128/JVI.03496-12
26. Rasmussen SB, Reinert LS, Paludan SR. Innate Recognition of Intracellular Pathogens: Detection and Activation of the First Line of Defense. *Apmis* (2009) 117(5–6):323–37. doi: 10.1111/j.1600-0463.2009.02456.x
27. Yim HCH, Williams BRG. Protein Kinase R and the Inflammasome. *J Interf Cytokine Res* (2014) 34(6):447–54. doi: 10.1089/jir.2014.0008
28. Yoneyama M, Jogi M, Onomoto K. Regulation of Antiviral Innate Immune Signaling by Stress-Induced RNA Granules. *J Biochem* (2015) 159(3):279–86. doi: 10.1093/jb/mvv122
29. Lund JM, Alexopoulou L, Sato A, Karow M, Adams NC, Gale NW, et al. Recognition of Single-Stranded RNA Viruses by Toll-Like Receptor 7. *Proc Natl Acad Sci U S A* (2004) 101(15):5598–603. doi: 10.1073/pnas.0400937101
30. De Wit E, Van Doremalen N, Falzarano D, Munster VJ. SARS and MERS: Recent Insights Into Emerging Coronaviruses. *Nat Rev Microbiol* (2016) 14 (8):523–34. doi: 10.1038/nrmicro.2016.81
31. de Wilde AH, Snijder EJ, Kikkert M, van Hemert MJ. Host Factors in Coronavirus Replication. *Curr Top Microbiol Immunol* (2018) 419:1–42. doi: 10.1007/82_2017_25
32. Ratia K, Kilianski A, Baez-Santos YM, Baker SC, Mesecar A. Structural Basis for the Ubiquitin-Linkage Specificity and Deisgylating Activity of SARS-CoV Papain-Like Protease. *PLoS Pathog* (2014) 10(5):e1004113. doi: 10.1371/journal.ppat.1004113
33. Devaraj SG, Wang N, Chen Z, Chen Z, Tseng M, Barretto N, et al. Regulation of IRF-3-Dependent Innate Immunity by the Papain-Like Protease Domain of the Severe Acute Respiratory Syndrome Coronavirus. *J Biol Chem* (2007) 282(44):32208–21. doi: 10.1074/jbc.M704870200
34. Frieman M, Ratia K, Johnston RE, Mesecar AD, Baric RS. Severe Acute Respiratory Syndrome Coronavirus Papain-Like Protease Ubiquitin-Like Domain and Catalytic Domain Regulate Antagonism of IRF3 and NF-κb Signaling. *J Virol* (2009) 83(13):6689–705. doi: 10.1128/JVI.02220-08
35. Sun L, Xing Y, Chen X, Zheng Y, Yang Y, Nichols DB, et al. Coronavirus Papain-Like Proteases Negatively Regulate Antiviral Innate Immune Response Through Disruption of STING-Mediated Signaling. *PLoS One* (2012) 7(2):e30802. doi: 10.1371/journal.pone.0030802
36. de Wilde AH, Raj VS, Oudshoorn D, Bestebroer TM, van Nieuwkoop S, Limpens RWAL, et al. MERS-Coronavirus Replication Induces Severe In Vitro Cytopathology and Is Strongly Inhibited by Cyclosporin A or Interferon-α Treatment. *J Gen Virol* (2013) 94(PART8):1749–60. doi: 10.1099/vir.0.052910-0
37. Knoops K, Kikkert M, Van Den Worm SHE, Zevenhoven-Dobbe JC, van der Meer Y, Koster AJ, et al. SARS-Coronavirus Replication Is Supported by a Reticulovesicular Network of Modified Endoplasmic Reticulum. *PLoS Biol* (2008) 6(9):1957–74. doi: 10.1371/journal.pbio.0060226
38. Siu KL, Chan CP, Kok KH, Chiu-Yat Woo P, Jin DY. Suppression of Innate Antiviral Response by Severe Acute Respiratory Syndrome Coronavirus M Protein is Mediated Through the First Transmembrane Domain. *Cell Mol Immunol* (2014) 11(2):141–9. doi: 10.1038/cmi.2013.61
39. Lui PY, Wong LYR, Fung CL, Siu KL, Yeung ML, Yuen KS, et al. Middle East Respiratory Syndrome Coronavirus M Protein Suppresses Type I Interferon Expression Through the Inhibition of TBK1-Dependent Phosphorylation of IRF3. *Emerg Microbes Infect* (2016) 5(1):1–9. doi: 10.1038/emi.2016.33
40. Siu KL, Kok KH, Ng MHJ, Poon VKM, Yuen KY, Zheng BJ, et al. Severe Acute Respiratory Syndrome Coronavirus M Protein Inhibits Type I Interferon Production by Impeding Theformation of TRAF3·TANK·Tbk1/Ikkε Complex. *J Biol Chem* (2009) 284(24):16202–9. doi: 10.1074/jbc.M109.008227
41. Drosten C, Meyer B, Müller MA, Corman VM, Al-Masri M, Hossain R, et al. Transmission of MERS-Coronavirus in Household Contacts. *N Engl J Med* (2014) 371(9):828–35. doi: 10.1056/NEJMoa1405858
42. Zhao J, Alshukairi AN, Baharoon SA, Ahmed WA, Bokhari AA, Nehdi AM, et al. Recovery From the Middle East Respiratory Syndrome is Associated With Antibody and T Cell Responses. *Sci Immunol* (2017) 2(14):eaan5393. doi: 10.1126/sciimmunol.aan5393
43. Chu H, Zhou J, Wong BHY, Li C, Chan JFW, Cheng ZS, et al. Middle East Respiratory Syndrome Coronavirus Efficiently Infects Human Primary T Lymphocytes and Activates the Extrinsic and Intrinsic Apoptosis Pathways. *J Infect Dis* (2016) 213(6):904–14. doi: 10.1093/infdis/jiv380
44. Yang Y, Xiong Z, Zhang S, Yan Y, Nguyen J, Ng B, et al. Bcl-xL Inhibits T-Cell Apoptosis Induced by Expression of SARS Coronavirus E Protein in the Absence of Growth Factors. *Biochem J* (2005) 392(1):135–43. doi: 10.1042/BJ20050698
45. Cameron MJ, Bermejo-Martin JF, Danesh A, Muller MP, Kelvin DJ. Human Immunopathogenesis of Severe Acute Respiratory Syndrome (SARS). *Virus Res* (2008) 133(1):13–9. doi: 10.1016/j.virusres.2007.02.014
46. He Z, Zhao C, Dong Q, Zhuang H, Song S, Peng G, et al. Effects of Severe Acute Respiratory Syndrome (SARS) Coronavirus Infection on Peripheral Blood Lymphocytes and Their Subsets. *Int J Infect Dis* (2005) 9(6):323–30. doi: 10.1016/j.ijid.2004.07.014
47. Li CK, Wu H, Yan H, Ma S, Wang L, Zhang M, et al. T Cell Responses to Whole SARS Coronavirus in Humans. *J Immunol* (2008) 181(8):5490–500. doi: 10.4049/jimmunol.181.8.5490
48. Fan YY, Huang ZT, Li L, Wu MH, Yu T, Koup RA, et al. Characterization of SARS-CoV-Specific Memory T Cells From Recovered Individuals 4 Years After Infection. *Arch Virol* (2009) 154(7):1093–9. doi: 10.1007/s00705-009-0409-6
49. Oh H-LJ, Chia A, Chang CXL, Leong HN, Ling KL, Grotenbreg GM, et al. Engineering T Cells Specific for a Dominant Severe Acute Respiratory Syndrome Coronavirus CD8 T Cell Epitope. *J Virol* (2011) 85(20):10464–71. doi: 10.1128/JVI.05039-11
50. Tang F, Quan Y, Xin Z-T, Wrammert J, Ma M-J, Lv H, et al. Lack of Peripheral Memory B Cell Responses in Recovered Patients With Severe Acute Respiratory Syndrome: A Six-Year Follow-Up Study. *J Immunol* (2011) 186(12):7264–8. doi: 10.4049/jimmunol.0903490
51. Ng OW, Chia A, Tan AT, Jadi RS, Leong HN, Bertoletti A, et al. Memory T Cell Responses Targeting the SARS Coronavirus Persist Up to 11 Years Post-Infection. *Vaccine* (2016) 34(17):2008–14. doi: 10.1016/j.vaccine.2016.02.063
52. Gorse GJ, Patel GB, Vitale JN, O'Connor TZ. Prevalence of Antibodies to Four Human Coronaviruses is Lower in Nasal Secretions Than in Serum. *Clin Vaccine Immunol* (2010) 17(12):1875–80. doi: 10.1128/CVI.00278-10
53. Grifoni A, Weiskopf D, Ramirez SI, Mateus J, Dan JM, Moderbacher CR, et al. Targets of T Cell Responses to SARS-CoV-2 Coronavirus in Humans

With COVID-19 Disease and Unexposed Individuals. *Cell* (2020) 181 (7):1489–501.e15. doi: 10.1016/j.cell.2020.05.015
54. Weiskopf D, Schmitz KS, Raadsen MP, Grifoni A, Okba NMA, Endeman H, et al. Phenotype and Kinetics of SARS-CoV-2-Specific T Cells in COVID-19 Patients With Acute Respiratory Distress Syndrome. *Sci Immunol* (2020) 5 (48):eabd2071. doi: 10.1126/sciimmunol.abd2071
55. Braun J, Loyal L, Frentsch M, Wendisch D, Georg P, Kurth F, et al. SARS-CoV-2-Reactive T Cells in Healthy Donors and Patients With COVID-19. *Nature* (2020) 587(7833):270–4. doi: 10.1038/s41586-020-2598-9
56. Le Bert N, Tan AT, Kunasegaran K, Tham CYL, Hafezi M, Chia A, et al. SARS-CoV-2-Specific T Cell Immunity in Cases of COVID-19 and SARS, and Uninfected Controls. *Nature* (2020) 584(7821):457–62. doi: 10.1038/s41586-020-2550-z
57. Meckiff BJ, Ramírez-Suástegui C, Fajardo V, Chee SJ, Kusnadi A, Simon H, et al. Imbalance of Regulatory and Cytotoxic SARS-CoV-2-Reactive CD4+ T Cells in COVID-19. *Cell* (2020) 183(5):1340–53.e16. doi: 10.1016/j.cell.2020.10.001
58. Long QX, Liu BZ, Deng HJ, Wu GC, Deng K, Chen YK, et al. Antibody Responses to SARS-CoV-2 in Patients With COVID-19. *Nat Med* (2020) 26 (6):845–8. doi: 10.1038/s41591-020-0897-1
59. Nguyen-Contant P, Embong AK, Kanagaiah P, Chaves FA, Yang H, Branche AR, et al. S Protein-Reactive IGG and Memory B Cell Production After Human SARS-CoV-2 Infection Includes Broad Reactivity to the S2 Subunit. *MBio* (2020) 11(5):1–11. doi: 10.1128/mBio.01991-20
60. Ng KW, Faulkner N, Cornish GH, Rosa A, Harvey R, Hussain S, et al. Preexisting and *De Novo* Humoral Immunity to SARS-CoV-2 in Humans. *Sci (80-)* (2020) 370(6522):1339–43. doi: 10.1126/science.abe1107
61. Anderson EM, Goodwin EC, Verma A, Arevalo CP, Bolton MJ, Weirick ME, et al. Seasonal Human Coronavirus Antibodies are Boosted Upon SARS-CoV-2 Infection But Not Associated With Protection. *Cell* (2021) 184 (7):1858–64.e10. doi: 10.1016/j.cell.2021.02.010
62. Poston D, Weisblum Y, Wise H, Templeton K, Jenks S, Hatziioannou T, et al. Absence of Severe Acute Respiratory Syndrome Coronavirus 2 Neutralizing Activity in Prepandemic Sera From Individuals With Recent Seasonal Coronavirus Infection. *Clin Infect Dis* (2021) 73(5):E1208–11. doi: 10.1093/cid/ciaa1803
63. Shrwani K, Sharma R, Krishnan M, Jones T, Mayora-Neto M, Cantoni D, et al. Detection of Serum Cross-Reactive Antibodies and Memory Response to SARS-CoV-2 in Prepandemic and Post-COVID-19 Convalescent Samples. *J Infect Dis* (2021) 224(8):1305–15. doi: 10.1093/infdis/jiab333
64. Mateus J, Grifoni A, Tarke A, Sidney J, Ramirez SI, Dan JM, et al. Selective and Cross-Reactive SARS-CoV-2 T Cell Epitopes in Unexposed Humans. *Sci* (2020) 370(6512):89–94. doi: 10.1126/science.abd3871
65. Sette A, Crotty S. Pre-Existing Immunity to SARS-CoV-2: The Knowns and Unknowns. *Nat Rev Immunol* (2020) 20(8):457–8. doi: 10.1038/s41577-020-0389-z
66. Saletti G, Gerlach T, Jansen JM, Molle A, Elbahesh H, Ludlow M, et al. Older Adults Lack SARS CoV-2 Cross-Reactive T Lymphocytes Directed to Human Coronaviruses OC43 and NL63. *Sci Rep* (2020) 10(1):21447. doi: 10.1038/s41598-020-78506-9
67. Nelde A, Bilich T, Heitmann JS, Maringer Y, Salih HR, Roerden M, et al. SARS-CoV-2-Derived Peptides Define Heterologous and COVID-19-Induced T Cell Recognition. *Nat Immunol* (2021) 22(1):74–85. doi: 10.1038/s41590-020-00808-x
68. Schulien I, Kemming J, Oberhardt V, Wild K, Seidel LM, Killmer S, et al. Characterization of Pre-Existing and Induced SARS-CoV-2-Specific CD8+ T Cells. *Nat Med* (2021) 27(1):78–85. doi: 10.1038/s41591-020-01143-2
69. Bacher P, Rosati E, Esser D, Martini GR, Saggau C, Schiminsky E, et al. Low-Avidity CD4+ T Cell Responses to SARS-CoV-2 in Unexposed Individuals and Humans With Severe COVID-19. *Immunity* (2020) 53(6):1258–71.e5. doi: 10.1016/j.immuni.2020.11.016
70. Sagar M, Reifler K, Rossi M, Miller NS, Sinha P, White LF, et al. Recent Endemic Coronavirus Infection is Associated With Less-Severe COVID-19. *J Clin Invest* (2021) 131(1):e143380. doi: 10.1172/JCI143380
71. Loyal L, Braun J, Henze L, Kruse B, Dingeldey M, Reimer U, et al. Cross-Reactive CD4+ T Cells Enhance SARS-CoV-2 Immune Responses Upon Infection and Vaccination. *Sci (80-)* (2021) 374(6564):eabh1823. doi: 10.1126/science.abh1823
72. Viswanathan T, Arya S, Chan SH, Qi S, Dai N, Misra A, et al. Structural Basis of RNA Cap Modification by SARS-CoV-2. *Nat Commun* (2020) 11(1):3718. doi: 10.1038/s41467-020-17496-8
73. Rosas-Lemus M, Minasov G, Shuvalova L, Inniss NL, Kiryukhina O, Brunzelle J, et al. High-Resolution Structures of the SARS-CoV-2 2′-O-Methyltransferase Reveal Strategies for Structure-Based Inhibitor Design. *Sci Signal* (2020) 13(651):eabe1202. doi: 10.1126/scisignal.abe1202
74. Gordon DE, Jang GM, Bouhaddou M, Xu J, Obernier K, White KM, et al. A SARS-CoV-2 Protein Interaction Map Reveals Targets for Drug Repurposing. *Nature* (2020) 583(7816):459–68. doi: 10.1038/s41586-020-2286-9
75. Wang C, Chen T, Zhang J, Yang M, Li N, Xu X, et al. The E3 Ubiquitin Ligase Nrdp1 "Preferentially" Promotes TLR-Mediated Production of Type I Interferon. *Nat Immunol* (2009) 10(7):744–52. doi: 10.1038/ni.1742
76. Gordon DE, Hiatt J, Bouhaddou M, Rezelj VV, Ulferts S, Braberg H, et al. Comparative Host-Coronavirus Protein Interaction Networks Reveal Pan-Viral Disease Mechanisms. *Science* (2020) 370(6521):eabe9403. doi: 10.1126/science.abe9403
77. Vazquez C, Swanson SE, Negatu SG, Dittmar M, Miller J, Ramage HR, et al. SARS-CoV-2 Viral Proteins NSP1 and NSP13 Inhibit Interferon Activation Through Distinct Mechanisms. *PLoS One* (2021) 16(6):e0253089. doi: 10.1371/journal.pone.0253089
78. Han L, Zhuang MW, Deng J, Zheng Y, Zhang J, Nan ML, et al. SARS-CoV-2 ORF9b Antagonizes Type I and III Interferons by Targeting Multiple Components of the RIG-I/MDA-5–MAVS, TLR3–TRIF, and cGAS–STING Signaling Pathways. *J Med Virol* (2021) 93(9):5376–89. doi: 10.1002/jmv.27050
79. Lei X, Dong X, Ma R, Wang W, Xiao X, Tian Z, et al. Activation and Evasion of Type I Interferon Responses by SARS-CoV-2. *Nat Commun* (2020) 11 (1):3810. doi: 10.1038/s41467-020-17665-9
80. Wang W, Zhou Z, Xiao X, Tian Z, Dong X, Wang C, et al. SARS-CoV-2 Nsp12 Attenuates Type I Interferon Production by Inhibiting IRF3 Nuclear Translocation. *Cell Mol Immunol* (2021) 18(4):945–53. doi: 10.1038/s41423-020-00619-y
81. Gao X, Zhu K, Qin B, Olieric V, Wang M, Cui S. Crystal Structure of SARS-CoV-2 Orf9b in Complex With Human TOM70 Suggests Unusual Virus-Host Interactions. *Nat Commun* (2021) 12(1):2843. doi: 10.1038/s41467-021-23118-8
82. Jiang HW, Zhang HN, Meng QF, Xie J, Li Y, Chen H, et al. SARS-CoV-2 Orf9b Suppresses Type I Interferon Responses by Targeting TOM70. *Cell Mol Immunol* (2020) 17(9):998–1000. doi: 10.1038/s41423-020-0514-8
83. Wu J, Shi Y, Pan X, Wu S, Hou R, Zhang Y, et al. SARS-CoV-2 ORF9b Inhibits RIG-I-MAVS Antiviral Signaling by Interrupting K63-Linked Ubiquitination of NEMO. *Cell Rep* (2021) 34(7):108761. doi: 10.1016/j.celrep.2021.108761
84. Liu GQ, Lee JH, Parker ZM, Acharya D, Chiang JJ, van Gent M, et al. ISG15-Dependent Activation of the Sensor MDA5 is Antagonized by the SARS-CoV-2 Papain-Like Protease to Evade Host Innate Immunity. *Nat Microbiol* (2021) 6(4):467–78. doi: 10.1038/s41564-021-00884-1
85. Moustaqil M, Ollivier E, Chiu HP, Van Tol S, Rudolffi-Soto P, Stevens C, et al. SARS-CoV-2 Proteases PLpro and 3clpro Cleave IRF3 and Critical Modulators of Inflammatory Pathways (NLRP12 and TAB1): Implications for Disease Presentation Across Species. *Emerg Microbes Infect* (2021) 10 (1):178–95. doi: 10.1080/22221751.2020.1870414
86. Zheng Y, Zhuang MW, Han L, Zhang J, Nan ML, Zhan P, et al. Severe Acute Respiratory Syndrome Coronavirus 2 (SARS-CoV-2) Membrane (M) Protein Inhibits Type I and III Interferon Production by Targeting RIG-I/MDA-5 Signaling. *Signal Transduct Target Ther* (2020) 5(1):299. doi: 10.1038/s41392-020-00438-7
87. Fu YZ, Wang SY, Zheng ZQ, Huang Y, Li WW, Xu ZS, et al. SARS-CoV-2 Membrane Glycoprotein M Antagonizes the MAVS-Mediated Innate Antiviral Response. *Cell Mol Immunol* (2021) 18(3):613–20. doi: 10.1038/s41423-020-00571-x
88. Xia H, Cao Z, Xie X, Zhang X, Chen JYC, Wang H, et al. Evasion of Type I Interferon by SARS-CoV-2. *Cell Rep* (2020) 33(1):108234. doi: 10.1016/j.celrep.2020.108234
89. Hayn M, Hirschenberger M, Koepke L, Nchioua R, Straub JH, Klute S, et al. Systematic Functional Analysis of SARS-CoV-2 Proteins Uncovers Viral

Innate Immune Antagonists and Remaining Vulnerabilities. *Cell Rep* (2021) 35(7):109126. doi: 10.1016/j.celrep.2021.109126
90. Collier DA, De Marco A, Ferreira IATM, Meng B, Datir R, Walls AC, et al. SARS-CoV-2 B.1.1.7 Sensitivity to mRNA Vaccine-Elicited, Convalescent and Monoclonal Antibodies. *medRxiv Prepr Serv Heal Sci* (2021) 593:136–41. doi: 10.1038/s41586-021-03412-7
91. Graham C, Seow J, Huettner I, Khan H, Kouphou N, Acors S, et al. Neutralization Potency of Monoclonal Antibodies Recognizing Dominant and Subdominant Epitopes on SARS-CoV-2 Spike is Impacted by the B.1.1.7 Variant. *Immunity* (2021) 54(6):1276–89.e6. doi: 10.1016/j.immuni.2021.03.023
92. Wibmer CK, Ayres F, Hermanus T, Madzivhandila M, Kgagudi P, Oosthuysen B, et al. SARS-CoV-2 501y.V2 Escapes Neutralization by South African COVID-19 Donor Plasma. *Nat Med* (2021) 27(4):622–5. doi: 10.1038/s41591-021-01285-x
93. Li Q, Nie J, Wu J, Zhang L, Ding R, Wang H, et al. SARS-CoV-2 501y.V2 Variants Lack Higher Infectivity But do Have Immune Escape. *Cell* (2021) 184(9):2362–71.e9. doi: 10.1016/j.cell.2021.02.042
94. Wang P, Casner RG, Nair MS, Wang M, Yu J, Cerutti G, et al. Increased Resistance of SARS-CoV-2 Variant P.1 to Antibody Neutralization. *Cell Host Microbe* (2021) 29(5):747–51.e4. doi: 10.1016/j.chom.2021.04.007
95. Hoffmann M, Arora P, Groß R, Seidel A, Hörnich BF, Hahn AS, et al. SARS-CoV-2 Variants B.1.351 and P.1 Escape From Neutralizing Antibodies. *Cell* (2021) 184(9):2384–93.e12. doi: 10.1016/j.cell.2021.03.036
96. Garcia-Beltran WF, Lam EC, St. Denis K, Nitido AD, Garcia ZH, Hauser BM, et al. Multiple SARS-CoV-2 Variants Escape Neutralization by Vaccine-Induced Humoral Immunity. *Cell* (2021) 184(9):2372–83.e9. doi: 10.1016/j.cell.2021.03.013
97. Deng X, Garcia-Knight MA, Khalid MM, Servellita V, Wang C, Morris MK, et al. Transmission, Infectivity, and Antibody Neutralization of an Emerging SARS-CoV-2 Variant in California Carrying a L452R Spike Protein Mutation. *medRxiv* (2021) 9:2021.03.07.21252647. doi: 10.1101/2021.03.07.21252647
98. Planas D, Veyer D, Baidaliuk A, Staropoli I, Guivel-Benhassine F, Rajah MM, et al. Reduced Sensitivity of SARS-CoV-2 Variant Delta to Antibody Neutralization. *Nature* (2021) 596(7871):276–80. doi: 10.1038/s41586-021-03777-9
99. Schmidt F, Muecksch F, Weisblum Y, Da Silva J, Bednarski E, Cho A, et al. Plasma Neutralization of the SARS-CoV-2 Omicron Variant. *N Engl J Med* (2022) 386(6):599–601. doi: 10.1056/NEJMc2119641
100. Zou J, Xia H, Xie X, Kurhade C, Machado RRG, Weaver SC, et al. Neutralization Against Omicron SARS-CoV-2 From Previous non-Omicron Infection. *Cell Host Microbe* (2022) 30(4):485–8.e3. doi: 10.1038/s41467-022-28544-w
101. Planas D, Saunders N, Maes P, Guivel-Benhassine F, Planchais C, Buchrieser J, et al. Considerable Escape of SARS-CoV-2 Omicron to Antibody Neutralization. *Nature* (2021) 602: 671–67. doi: 10.1038/s41586-021-04389-z
102. Wang Y, Zhang L, Li Q, Liang Z, Li T, Liu S, et al. The Significant Immune Escape of Pseudotyped SARS-CoV-2 Variant Omicron. *Emerg Microbes Infect* (2022) 11(1):1–5. doi: 10.1080/22221751.2021.2017757
103. Fenrich M, Mrdenovic S, Balog M, Tomic S, Zjalic M, Roncevic A, et al. SARS-CoV-2 Dissemination Through Peripheral Nerves Explains Multiple Organ Injury. *Front Cell Neurosci* (2020) 14. doi: 10.3389/fncel.2020.00229
104. Tarke A, Sidney J, Methot N, Zhang Y, Dan JM, Goodwin B, et al. Negligible Impact of SARS-CoV-2 Variants on CD4 + and CD8 + T Cell Reactivity in COVID-19 Exposed Donors and Vaccinees. *bioRxiv* (2021) 1:2021.02.27.433180. doi: 10.1101/2021.02.27.433180
105. Tarke A, Sidney J, Kidd CK, Dan JM, Ramirez SI, Yu ED, et al. Comprehensive Analysis of T Cell Immunodominance and Immunoprevalence of SARS-CoV-2 Epitopes in COVID-19 Cases. *Cell Rep Med* (2021) 2(2):100204. doi: 10.1016/j.xcrm.2021.100204
106. Ferretti AP, Kula T, Wang Y, Nguyen DMV, Weinheimer A, Dunlap GS, et al. Unbiased Screens Show CD8+ T Cells of COVID-19 Patients Recognize Shared Epitopes in SARS-CoV-2 That Largely Reside Outside the Spike Protein. *Immunity* (2020) 53(5):1095–107.e3. doi: 10.1016/j.immuni.2020.10.006
107. Gallagher KME, Leick MB, Larson RC, Berger TR, Katsis K, Yam JY, et al. MGH COVID-19 Collection & Processing Team, Maus MV. SARS -CoV-2 T-Cell Immunity to Variants of Concern Following Vaccination. *bioRxiv [Preprint]* (2021) 3:2021.05.03.442455. doi: 10.1101/2021.05.03.442455
108. Zhang H, Deng S, Ren L, Zheng P, Hu X, Jin T, et al. Profiling CD8+ T Cell Epitopes of COVID-19 Convalescents Reveals Reduced Cellular Immune Responses to SARS-CoV-2 Variants. *Cell Rep* (2021) 36(11):109708. doi: 10.1016/j.celrep.2021.109708
109. Codo AC, Davanzo GG, de Brito Monteiro L, de Souza GF, Muraro SP, Virgilio-da-Silva JV, et al. Elevated Glucose Levels Favor SARS-CoV-2 Infection and Monocyte Response Through a HIF-1α/Glycolysis-Dependent Axis. *Cell Metab* (2020) 32(3):437–46.e5. doi: 10.2139/ssrn.3606770
110. ECDC. 2020 EC for DP and C (ECDC). *Q & A on Novel Coronavirus. S. European Centre for Disease Prevention and Control (ECDC). Q & A on Novel Coronavirus*. Stockholm: ECDC (2020). Available at: https://www.ecdc.europa.eu/en/covid-19/questions-answers.
111. He W, Yi GY, Zhu Y. Estimation of the Basic Reproduction Number, Average Incubation Time, Asymptomatic Infection Rate, and Case Fatality Rate for COVID-19: Meta-Analysis and Sensitivity Analysis. *J Med Virol* (2020) 92(11):2543–50. doi: 10.1002/jmv.26041
112. Zhou X, Ye Q. Cellular Immune Response to COVID-19 and Potential Immune Modulators. *Front Immunol* (2021) 12. doi: 10.3389/fimmu.2021.646333
113. Huang C, Wang Y, Li X, Ren L, Zhao J, Hu Y, et al. Clinical Features of Patients Infected With 2019 Novel Coronavirus in Wuhan, China. *Lancet* (2020) 395(10223):497–506. doi: 10.1016/S0140-6736(20)30183-5
114. Mathew D, Giles JR, Baxter AE, Oldridge DA, Greenplate AR, Wu JE, et al. Deep Immune Profiling of COVID-19 Patients Reveals Distinct Immunotypes With Therapeutic Implications. *Science* (2020) 369(6508):eabc8511. doi: 10.1126/science.abc8511
115. Giamarellos-Bourboulis EJ, Netea MG, Rovina N, Akinosoglou K, Antoniadou A, Antonakos N, et al. Complex Immune Dysregulation in COVID-19 Patients With Severe Respiratory Failure. *Cell Host Microbe* (2020) 27(6):992–1000.e3. doi: 10.1016/j.chom.2020.04.009
116. Zhou Z, Ren L, Zhang L, Zhong J, Xiao Y, Jia Z, et al. Heightened Innate Immune Responses in the Respiratory Tract of COVID-19 Patients. *Cell Host Microbe* (2020) 27(6):883–90.e2. doi: 10.1016/j.chom.2020.04.017
117. Reynolds CJ, Swadling L, Gibbons JM, Pade C, Jensen MP, Diniz MO, et al. Discordant Neutralizing Antibody and T Cell Responses in Asymptomatic and Mild SARS-CoV-2 Infection. *Sci Immunol* (2020) 5(54):eabf3698. doi: 10.1126/sciimmunol.abf3698
118. Zuo J, Dowell AC, Pearce H, Verma K, Long HM, Begum J, et al. Robust SARS-CoV-2-Specific T Cell Immunity is Maintained at 6 Months Following Primary Infection. *Nat Immunol* (2021) 22(5):620–6. doi: 10.1038/s41590-021-00902-8
119. Zhou R, To KKW, Wong YC, Liu L, Zhou B, Li X, et al. Acute SARS-CoV-2 Infection Impairs Dendritic Cell and T Cell Responses. *Immunity* (2020) 53(4):864–77.e5. doi: 10.1016/j.immuni.2020.07.026
120. Liao L, Yang Gh. Clinical Significance of Cellular Immunity Function and Inflammatory Factors Assays in Alveolar Lavage Fluid for Severe COVID-19 Pneumonia. *J Med Virol* (2021) 93(5):2979–87. doi: 10.1002/jmv.26827
121. Gil-Manso S, Carbonell D, López-Fernández L, Miguens I, Alonso R, Buño I, et al. Induction of High Levels of Specific Humoral and Cellular Responses to SARS-CoV-2 After the Administration of Covid-19 mRNA Vaccines Requires Several Days. *Front Immunol* (2021) 12. doi: 10.3389/fimmu.2021.726960
122. Domingo P, Mur I, Pomar V, Corominas H, Casademont J, de Benito N. The Four Horsemen of a Viral Apocalypse: The Pathogenesis of SARS-CoV-2 Infection (COVID-19). *EBioMedicine* (2020) 58:102887. doi: 10.1016/j.ebiom.2020.102887
123. Baumgarth N, Nikolich-Žugich J, Lee FE-H, Bhattacharya D. Antibody Responses to SARS-CoV-2: Let's Stick to Known Knowns. *J Immunol* (2020) 205(9):2342–50. doi: 10.4049/jimmunol.2000839
124. Rydyznski Moderbacher C, Ramirez SI, Dan JM, Grifoni A, Hastie KM, Weiskopf D, et al. Antigen-Specific Adaptive Immunity to SARS-CoV-2 in Acute COVID-19 and Associations With Age and Disease Severity. *Cell* (2020) 183(4):996–1012.e19. doi: 10.1016/j.cell.2020.09.038

125. Tan AT, Linster M, Tan CW, Le Bert N, Chia WN, Kunasegaran K, et al. Early Induction of Functional SARS-CoV-2-Specific T Cells Associates With Rapid Viral Clearance and Mild Disease in COVID-19 Patients. *Cell Rep* (2021) 34(6):108728. doi: 10.1016/j.celrep.2021.108728
126. Sekine T, Perez-Potti A, Rivera-Ballesteros O, Strålin K, Gorin J-B, Olsson A, et al. Cell Immunity in Convalescent Individuals with Asymptomatic or Mild COVID-19. *Cell* (2020) 183(1):158–68.e14. doi: 10.1016/j.cell.2020.08.017
127. Piccoli L, Park YJ, Tortorici MA, Czudnochowski N, Walls AC, Beltramello M, et al. Mapping Neutralizing and Immunodominant Sites on the SARS-CoV-2 Spike Receptor-Binding Domain by Structure-Guided High-Resolution Serology. *Cell* (2020) 183(4):1024–42.e21. doi: 10.1016/j.cell.2020.09.037
128. Robbiani DF, Gaebler C, Muecksch F, Lorenzi JCC, Wang Z, Cho A, et al. Convergent Antibody Responses to SARS-CoV-2 in Convalescent Individuals. *Nature* (2020) 584(7821):437–42. doi: 10.1038/s41586-020-2456-9
129. Liu A, Li Y, Peng J, Huang Y, Xu D. Antibody Responses Against SARS-CoV-2 in COVID-19 Patients. *J Med Virol* (2021) 93(1):144–8. doi: 10.1002/jmv.26241
130. Soresina A, Moratto D, Chiarini M, Paolillo C, Baresi G, Focà E, et al. Two X-Linked Agammaglobulinemia Patients Develop Pneumonia as COVID-19 Manifestation But Recover. *Pediatr Allergy Immunol* (2020) 31(5):565–9. doi: 10.1111/pai.13263
131. Quinti I, Lougaris V, Milito C, Cinetto F, Pecoraro A, Mezzaroma I, et al. A Possible Role for B Cells in COVID-19? Lesson From Patients With Agammaglobulinemia. *J Allergy Clin Immunol* (2020) 146(1):211–13.e4. doi: 10.1016/j.jaci.2020.04.013
132. Montero-Escribano P, Matías-Guiu J, Gómez-Iglesias P, Porta-Etessam J, Pytel V, Matias-Guiu JA. Anti-CD20 and COVID-19 in Multiple Sclerosis and Related Disorders: A Case Series of 60 Patients From Madrid, Spain. *Mult Scler Relat Disord* (2020) 42:102185. doi: 10.1016/j.msard.2020.102185
133. Novi G, Mikulska M, Briano F, Toscanini F, Tazza F, Uccelli A, et al. COVID-19 in a MS Patient Treated With Ocrelizumab: Does Immunosuppression Have a Protective Role? *Mult Scler Relat Disord* (2020) 42:102120. doi: 10.1016/j.msard.2020.102120
134. Safavi F, Nourbakhsh B, Azimi AR. B-Cell Depleting Therapies May Affect Susceptibility to Acute Respiratory Illness Among Patients With Multiple Sclerosis During the Early COVID-19 Epidemic in Iran. *Mult Scler Relat Disord* (2020) 43:102195. doi: 10.1016/j.msard.2020.102195
135. Creed MA, Ballesteros E, Greenfield LJ Jr, Imitola J. Mild COVID-19 Infection Despite Chronic B Cell Depletion in a Patient With Aquaporin-4-Positive Neuromyelitis Optica Spectrum Disorder. *Mult Scler Relat Disord* (2020) 44:102199. doi: 10.1016/j.msard.2020.102199
136. Avouac J, Airó P, Carlier N, Matucci-Cerinic M, Allanore Y. Severe COVID-19-Associated Pneumonia in 3 Patients With Systemic Sclerosis Treated With Rituximab. *Ann Rheum Dis* (2020) annrheumdis-2020-217864. doi: 10.1136/annrheumdis-2020-217864
137. Bange EM, Han NA, Wileyto P, Kim JY, Gouma S, Robinson J, et al. CD8+ T Cells Contribute to Survival in Patients With COVID-19 and Hematologic Cancer. *Nat Med* (2021) 27(7):1280–9. doi: 10.1038/s41591-021-01386-7
138. Annunziato F, Romagnani C, Romagnani S. The 3 Major Types of Innate and Adaptive Cell-Mediated Effector Immunity. *J Allergy Clin Immunol* (2015) 135(3):626–35. doi: 10.1016/j.jaci.2014.11.001
139. Iwasaki A, Medzhitov R. Control of Adaptive Immunity by the Innate Immune System. *Nat Immunol* (2015) 16(4):343–53. doi: 10.1038/ni.3123
140. O'Shea J, Paul WE. Mechanisms Underlying Lineage Commitment and Plasticity of Helper CD4 + T Cells. *Science* (2010) 327(5969):1098–102. doi: 10.1126/science.1178334
141. Chen G, Wu D, Guo W, Cao Y, Huang D, Wang H, et al. Clinical and Immunological Features of Severe and Moderate Coronavirus Disease 2019. *J Clin Invest* (2020) 130(5):2620–9. doi: 10.1172/JCI137244
142. Lucas C, Wong P, Klein J, Castro TBR, Silva J, Sundaram M, et al. Longitudinal Analyses Reveal Immunological Misfiring in Severe COVID-19. *Nature* (2020) 584(7821):463–9. doi: 10.1038/s41586-020-2588-y
143. GeurtsvanKessel CH, Geers D, Schmitz KS, Mykytyn AZ, Lamers MM, Bogers S, et al. Divergent SARS CoV-2 Omicron-Specific T- and B-Cell Responses in COVID-19 Vaccine Recipients. *Sci Immunol* (2022) 7(69):eabo2202. doi: 10.1126/sciimmunol.abo2202
144. Peng Y, Mentzer AJ, Liu G, Yao X, Yin Z, Dong D, et al. Broad and Strong Memory CD4+ and CD8+ T Cells Induced by SARS-CoV-2 in UK Convalescent Individuals Following COVID-19. *Nat Immunol* (2020) 21(11):1336–45. doi: 10.1038/s41590-020-0782-6
145. Kuri-Cervantes L, Pampena MB, Meng W, Rosenfeld AM, Ittner CAG, Weisman AR, et al. Comprehensive Mapping of Immune Perturbations Associated With Severe COVID-19. *Sci Immunol* (2020) 5(49):eabd7114. doi: 10.1126/sciimmunol.abd7114
146. Wen W, Su W, Tang H, Le W, Zhang X, Zheng Y, et al. Immune Cell Profiling of COVID-19 Patients in the Recovery Stage by Single-Cell Sequencing. *Cell Discov* (2020) 6(1):31. doi: 10.1038/s41421-020-00187-5
147. Liao M, Liu Y, Yuan J, Wen Y, Xu G, Zhao J, et al. Single-Cell Landscape of Bronchoalveolar Immune Cells in Patients With COVID-19. *Nat Med* (2020) 26(6):842–4. doi: 10.1038/s41591-020-0901-9
148. Ripperger TJ, Bhattacharya D. Transcriptional and Metabolic Control of Memory B Cells and Plasma Cells. *Annu Rev Immunol* (2021) 39:345–68. doi: 10.1146/annurev-immunol-093019-125603
149. Victora GD, Nussenzweig MC. Germinal Centers. *Annu Rev Immunol* (2012) 30:429–57. doi: 10.1146/annurev-immunol-020711-075032
150. Crotty S. Follicular Helper CD4 T Cells (T Fh). *Annu Rev Immunol* (2011) 29:621–63. doi: 10.1146/annurev-immunol-031210-101400
151. Ueno H, Banchereau J, Vinuesa CG. Pathophysiology of T Follicular Helper Cells in Humans and Mice. *Nat Immunol* (2015) 16(2):142–52. doi: 10.1038/ni.3054
152. Turner JS, O'Halloran JA, Kalaidina E, Kim W, Schmitz AJ, Zhou JQ, et al. SARS-CoV-2 mRNA Vaccines Induce Persistent Human Germinal Centre Responses. *Nature* (2021) 596(7870):109–13. doi: 10.1038/s41586-021-03738-2
153. Turner JS, Zhou JQ, Han J, Schmitz AJ, Rizk AA, Alsoussi WB, et al. Human Germinal Centres Engage Memory and Naive B Cells After Influenza Vaccination. *Nature* (2020) 586(7827):127–32. doi: 10.1038/s41586-020-2711-0
154. Kim W, Zhou JQ, Sturtz AJ, Horvath SC, Schmitz AJ, Lei T, et al. Germinal Centre-Driven Maturation of B Cell Response to SARS-CoV-2 Vaccination. *bioRxiv* (2021) 2:2021.10.31.466651. doi: 10.1101/2021.10.31.466651
155. Mudd PA, Minervina AA, Pogorelyy MV, Turner JS, Kim W, Kalaidina E, et al. SARS-CoV-2 mRNA Vaccination Elicits a Robust and Persistent T Follicular Helper Cell Response in Humans. *Cell* (2022) 185(4):603–13.e15. doi: 10.1016/j.cell.2021
156. Touizer E, Alrubayyi A, Rees-Spear C, Fisher-Pearson N, Griffith SA, Muir L, et al. Failure to Seroconvert After Two Doses of BNT162b2 SARS-CoV-2 Vaccine in a Patient With Uncontrolled HIV. *Lancet HIV* (2021) 8(6):e317–8. doi: 10.1016/S2352-3018(21)00099-0
157. Kamar N, Abravanel F, Marion O, Couat C, Izopet J, Del Bello A. Three Doses of an mRNA Covid-19 Vaccine in Solid-Organ Transplant Recipients. *N Engl J Med* (2021) 385(7):661–2. doi: 10.1056/NEJMc2108861
158. Kaneko N, Kuo HH, Boucau J, Farmer JR, Allard-Chamard H, Mahajan VS, et al. Loss of Bcl-6-Expressing T Follicular Helper Cells and Germinal Centers in COVID-19. *Cell* (2020) 183(1):143–57.e13. doi: 10.1016/j.cell.2020.08.025
159. Magleby R, Westblade LF, Trzebucki A, Simon MS, Rajan M, Park J, et al. Impact of Severe Acute Respiratory Syndrome Coronavirus 2 Viral Load on Risk of Intubation and Mortality Among Hospitalized Patients With Coronavirus Disease 2019. *Clin Infect Dis* (2021) 73(11):e4197–205. doi: 10.1093/cid/ciaa851
160. Zheng M, Gao Y, Wang G, Song G, Liu S, Sun D, et al. Functional Exhaustion of Antiviral Lymphocytes in COVID-19 Patients. *Cell Mol Immunol* (2020) 17(5):533–5. doi: 10.1038/s41423-020-0402-2
161. McMahan K, Yu J, Mercado NB, Loos C, Tostanoski LH, Chandrashekar A, et al. Correlates of Protection Against SARS-CoV-2 in Rhesus Macaques. *Nature* (2021) 590(7847):630–4. doi: 10.1038/s41586-020-03041-6
162. Wyllie DH, Mulchandani R, Jones HE, Taylor-Phillips S, Brooks T, Charlett A, et al. Responsive T Cell Numbers Are Associated With Protection From COVID-19: A Prospective Cohort Study in Keyworkers. *medRxiv* (2020) 04:2020.11.02.20222778. doi: 10.1101/2020.11.02.20222778.
163. Ni L, Cheng ML, Feng Y, Zhao H, Liu J, Ye F, et al. Impaired Cellular Immunity to SARS-CoV-2 in Severe COVID-19 Patients. *Front Immunol* (2021) 12. doi: 10.3389/fimmu.2021.603563

164. Xu Z, Shi L, Wang Y, Zhang J, Huang L, Zhang C, et al. Pathological Findings of COVID-19 Associated With Acute Respiratory Distress Syndrome. *Lancet Respir Med* (2020) 8(4):420–2. doi: 10.1016/S2213-2600(20)30076-X
165. Diao B, Wang C, Tan Y, Chen X, Liu Y, Ning L, et al. Reduction and Functional Exhaustion of T Cells in Patients With Coronavirus Disease 2019 (COVID-19). *Front Immunol* (2020) 11. doi: 10.3389/fimmu.2020.00827
166. Billerbeck E, Kang YH, Walker L, Lockstone H, Grafmueller S, Fleming V, et al. Analysis of CD161 Expression on Human CD8+ T Cells Defines a Distinct Functional Subset With Tissue-Homing Properties. *Proc Natl Acad Sci USA* (2010) 107(7):3006–11. doi: 10.1073/pnas.0914839107
167. Van Wilgenburg B, Scherwitzl I, Hutchinson EC, Leng T, Kurioka A, Kulicke C, et al. MAIT Cells are Activated During Human Viral Infections. *Nat Commun* (2016) 7:11653. doi: 10.1038/ncomms11653
168. Jouan Y, Guillon A, Gonzalez L, Perez Y, Boisseau C, Ehrmann S, et al. Phenotypical and Functional Alteration of Unconventional T Cells in Severe COVID-19 Patients. *J Exp Med* (2020) 217(12):e20200872. doi: 10.1084/jem.20200872
169. Blanchard-Rohner G, Pulickal AS, Jol-van Der Zijde CM, Snape MD, Pollard AJ. Appearance of Peripheral Blood Plasma Cells and Memory B Cells in a Primary and Secondary Immune Response in Humans. *Blood* (2009) 114 (24):4998–5002. doi: 10.1182/blood-2009-03-211052
170. Lee FE-H, Halliley JL, Walsh EE, Moscatiello AP, Kmush BL, Falsey AR, et al. Circulating Human Antibody-Secreting Cells During Vaccinations and Respiratory Viral Infections Are Characterized by High Specificity and Lack of Bystander Effect. *J Immunol* (2011) 186(9):5514–21. doi: 10.4049/jimmunol.1002932
171. Wrammert J, Onlamoon N, Akondy RS, Perng GC, Polsrila K, Chandele A, et al. Rapid and Massive Virus-Specific Plasmablast Responses During Acute Dengue Virus Infection in Humans. *J Virol* (2012) 86(6):2911–8. doi: 10.1128/JVI.06075-11
172. Moore JB, June CH. Cytokine Release Syndrome in Severe COVID-19. *Sci (80-)* (2020) 368(6490):473–4. doi: 10.1126/science.abb8925
173. Tay MZ, Poh CM, Rénia L, MacAry PA, Ng LFP. The Trinity of COVID-19: Immunity, Inflammation and Intervention. *Nat Rev Immunol* (2020) 20 (6):363–74. doi: 10.1038/s41577-020-0311-8
174. Guo XzJ, Thomas PG. New Fronts Emerge in the Influenza Cytokine Storm. *Semin Immunopathol* (2017) 39(5):541–50. doi: 10.1007/s00281-017-0636-y
175. Wan S, Yi Q, Fan S, Lv J, Zhang X, Guo L, et al. Relationships Among Lymphocyte Subsets, Cytokines, and the Pulmonary Inflammation Index in Coronavirus (COVID-19) Infected Patients. *Br J Haematol* (2020) 189 (3):428–37. doi: 10.1111/bjh.16659
176. Lee JS, Park S, Jeong HW, Ahn JY, Choi SJ, Lee H, et al. Immunophenotyping of Covid-19 and Influenza Highlights the Role of Type I Interferons in Development of Severe Covid-19. *Sci Immunol* (2020) 5(49):eabd1554. doi: 10.1126/sciimmunol.abd1554
177. Zhang Q, Liu Z, Moncada-Velez M, Chen J, Ogishi M, Bigio B, et al. Inborn Errors of Type I IFN Immunity in Patients With Life-Threatening COVID-19. *Science* (2020) 370(6515):eabd4570. doi: 10.1126/science.abd4570
178. Blanco-Melo D, Nilsson-Payant BE, Liu WC, Uhl S, Hoagland D, Møller R, et al. Imbalanced Host Response to SARS-CoV-2 Drives Development of COVID-19. *Cell* (2020) 181(5):1036–45.e9. doi: 10.1016/j.cell.2020.04.026
179. Ferrucci L, Fabbri E. Inflammageing: Chronic Inflammation in Ageing, Cardiovascular Disease, and Frailty. *Nat Rev Cardiol* (2018) 15(9):505–22. doi: 10.1038/s41569-018-0064-2
180. Shaw AC, Goldstein DR, Montgomery RR. Age-Dependent Dysregulation of Innate Immunity. *Nat Rev Immunol* (2013) 13(12):875–87. doi: 10.1038/nri3547
181. Qin C, Zhou L, Hu Z, Zhang S, Yang S, Tao Y, et al. Dysregulation of Immune Response in Patients With Coronavirus 2019 (COVID-19) in Wuhan, China. *Clin Infect Dis* (2020) 71(15):762–8. doi: 10.1093/cid/ciaa248
182. Thieme CJ, Anft M, Paniskaki K, Blazquez-Navarro A, Doevelaar A, Seibert FS, et al. Robust T Cell Response Toward Spike, Membrane, and Nucleocapsid SARS-CoV-2 Proteins Is Not Associated With Recovery in Critical COVID-19 Patients. *Cell Rep Med* (2020) 1(6):100092. doi: 10.1016/j.xcrm.2020.100092
183. Vaz de Paula CB, de Azevedo MLV, Nagashima S, Martins APC, Malaquias MAS, Miggiolaro A, et al. IL-4/IL-13 Remodeling Pathway of COVID-19 Lung Injury. *Sci Rep* (2020) 10(1):18689. doi: 10.1038/s41598-020-75659-5
184. Melgaço JG, Brito E Cunha D, Azamor T, Da Silva AMV, Tubarão LN, Gonçalves RB, et al. Cellular and Molecular Immunology Approaches for the Development of Immunotherapies Against the New Coronavirus (SARS-CoV-2): Challenges to Near-Future Breakthroughs. *J Immunol Res* (2020) 2020:8827670. doi: 10.1155/2020/8827670
185. Martonik D, Parfieniuk-Kowerda A, Rogalska M, Flisiak R. The Role of Th17 Response in COVID-19. *Cells* (2021) 10(6):1550. doi: 10.3390/cells10061550
186. Schulte-Schrepping J, Reusch N, Paclik D, Baßler K, Schlickeiser S, Zhang B, et al. Severe COVID-19 Is Marked by a Dysregulated Myeloid Cell Compartment. *Cell* (2020) 182(6):1419–40.e23. doi: 10.1016/j.cell.2020.08.001
187. Deng Z, Zhang M, Zhu T, Zhili N, Liu Z, Xiang R, et al. Dynamic Changes in Peripheral Blood Lymphocyte Subsets in Adult Patients With COVID-19. *Int J Infect Dis* (2020) 98:353–8. doi: 10.1016/j.ijid.2020.07.003
188. Wherry EJ. T Cell Exhaustion. *Nat Immunol* (2011) 12(6):492–9. doi: 10.1038/ni.2035
189. Brooks DG, Trifilo MJ, Edelmann KH, Teyton L, McGavern DB, Oldstone MBA. Interleukin-10 Determines Viral Clearance or Persistence In Vivo. *Nat Med* (2006) 12(11):1301–9. doi: 10.1038/nm1492
190. Zheng HY, Zhang M, Yang CX, Zhang N, Wang XC, Yang XP, et al. Elevated Exhaustion Levels and Reduced Functional Diversity of T Cells in Peripheral Blood may Predict Severe Progression in COVID-19 Patients. *Cell Mol Immunol* (2020) 17(5):541–3. doi: 10.1038/s41423-020-0401-3
191. Kreutmair S, Unger S, Núñez NG, Ingelfinger F, Alberti C, De Feo D, et al. Distinct Immunological Signatures Discriminate Severe COVID-19 From non-SARS-CoV-2-Driven Critical Pneumonia. *Immunity* (2021) 54 (7):1578–93.e5. doi: 10.1016/j.immuni.2021.05.002
192. Rha MS, Jeong HW, Ko JH, Choi SJ, Seo IH, Lee JS, et al. PD-1-Expressing SARS-CoV-2-Specific CD8+ T Cells Are Not Exhausted, But Functional in Patients With COVID-19. *Immunity* (2021) 54(1):44–52.e3. doi: 10.1016/j.immuni.2020.12.002
193. Doering TA, Crawford A, Angelosanto JM, Paley MA, Ziegler CG, Wherry EJ. Network Analysis Reveals Centrally Connected Genes and Pathways Involved in CD8+ T Cell Exhaustion Versus Memory. *Immunity* (2012) 37 (6):1130–44. doi: 10.1016/j.immuni.2012.08.021
194. Fuertes Marraco SA, Neubert NJ, Verdeil G, Speiser DE. Inhibitory Receptors Beyond T Cell Exhaustion. *Front Immunol* (2015) 6(JUN). doi: 10.3389/fimmu.2015.00310
195. Singer M, Wang C, Cong L, Marjanovic ND, Kowalczyk MS, Zhang H, et al. A Distinct Gene Module for Dysfunction Uncoupled From Activation in Tumor-Infiltrating T Cells. *Cell* (2016) 166(6):1500–11.e9. doi: 10.1016/j.cell.2016.08.052
196. Tirosh I, Izar B, Prakadan SM, Wadsworth MH, Treacy D, Trombetta JJ, et al. Dissecting the Multicellular Ecosystem of Metastatic Melanoma by Single-Cell RNA-Seq. *Sci* (2016) 352(6282):189–96. doi: 10.1126/science.aad0501
197. Youngblood B, Oestreich KJ, Ha SJ, Duraiswamy J, Akondy RS, West EE, et al. Chronic Virus Infection Enforces Demethylation of the Locus That Encodes PD-1 in Antigen-Specific CD8+ T Cells. *Immunity* (2011) 35 (3):400–12. doi: 10.1016/j.immuni.2011.06.015
198. Saris A, Reijnders TDY, Nossent EJ, Schuurman AR, Verhoeff J, Van Asten S, et al. Distinct Cellular Immune Profiles in the Airways and Blood of Critically Ill Patients With COVID-19. *Thorax* (2021) 76(10):1010–9. doi: 10.1136/thoraxjnl-2020-216256
199. Vitte J, Diallo AB, Boumaza A, Lopez A, Michel M, Allardet-Servent J, et al. A Granulocytic Signature Identifies COVID-19 and its Severity. *J Infect Dis* (2020) 222(12):1985–96. doi: 10.1093/infdis/jiaa591
200. Chen J, Vitetta L. Increased PD-L1 Expression may be Associated With the Cytokine Storm and CD8+T-Cell Exhaustion in Severe COVID-19. *J Infect Dis* (2021) 223(9):1659–60. doi: 10.1093/infdis/jiab061
201. Sabbatino F, Conti V, Franci G, Sellitto C, Manzo V, Pagliano P, et al. PD-L1 Dysregulation in COVID-19 Patients. *Front Immunol* (2021) 12. doi: 10.3389/fimmu.2021.695242
202. Eljaafari A, Pestel J, Le Magueresse-Battistoni B, Chanon S, Watson J, Robert M, et al. Adipose-Tissue-Derived Mesenchymal Stem Cells Mediate PD-L1 Overexpression in the White Adipose Tissue of Obese Individuals, Resulting in T Cell Dysfunction. *Cells* (2021) 10(10):2645. doi: 10.3390/cells10102645

203. Dorward DA, Russell CD, Um IH, Elshani M, Armstrong SD, Penrice-Randal R, et al. Tissue-Specific Immunopathology in Fatal COVID-19. *Am J Respir Crit Care Med* (2021) 203(2):192–201. doi: 10.1164/rccm.202008-3265OC
204. Liu J, Yang X, Wang H, Li Z, Deng H, Liu J, et al. Analysis of the Long-Term Impact on Cellular Immunity in COVID-19-Recovered Individuals Reveals a Profound Nkt Cell Impairment. *MBio* (2021) 12(2):e00085–21. doi: 10.1128/mBio.00085-21
205. Aid M, Busman-Sahay K, Vidal SJ, Maliga Z, Bondoc S, Starke C, et al. Vascular Disease and Thrombosis in SARS-CoV-2-Infected Rhesus Macaques. *Cell* (2020) 183(5):1354–66.e13. doi: 10.1016/j.cell.2020.10.005
206. Li S, Jiang L, Li X, Lin F, Wang Y, Li B, et al. Clinical and Pathological Investigation of Patients With Severe COVID-19. *JCI Insight* (2020) 5(12): e138070. doi: 10.1172/jci.insight.138070
207. Radermecker C, Detrembleur N, Guiot J, Cavalier E, Henket M, d'Emal C, et al. Neutrophil Extracellular Traps Infiltrate the Lung Airway, Interstitial, and Vascular Compartments in Severe COVID-19. *J Exp Med* (2020) 217 (12):e20201012. doi: 10.1084/jem.20201012
208. Schurink B, Roos E, Radonic T, Barbe E, Bouman CSC, de Boer HH, et al. Viral Presence and Immunopathology in Patients With Lethal COVID-19: A Prospective Autopsy Cohort Study. *Lancet Microbe* (2020) 1(7):e290–9. doi: 10.1016/S2666-5247(20)30144-0
209. Del Valle DM, Kim-Schulze S, Huang HH, Beckmann ND, Nirenberg S, Wang B, et al. An Inflammatory Cytokine Signature Predicts COVID-19 Severity and Survival. *Nat Med* (2020) 26(10):1636–43. doi: 10.1038/s41591-020-1051-9
210. Takahashi T, Ellingson MK, Wong P, Israelow B, Lucas C, Klein J, et al. Sex Differences in Immune Responses That Underlie COVID-19 Disease Outcomes. *Nature* (2020) 588(7837):315–20. doi: 10.1038/s41586-020-2700-3
211. Li C, Lee A, Grigoryan L, Arunachalam PS, Scott MKD, Trisal M, et al. Mechanisms of Innate and Adaptive Immunity to the Pfizer-BioNTech BNT162b2 Vaccine. *Nat Immunol* (2022) 23:543–555. doi: 10.1038/s41590-022-01163-9
212. Loske J, Röhmel J, Lukassen S, Stricker S, Magalhães VG, Liebig J, et al. Pre-Activated Antiviral Innate Immunity in the Upper Airways Controls Early SARS-CoV-2 Infection in Children. *Nat Biotechnol* (2021) 40:319–24. doi: 10.1101/2021.06.24.21259087
213. Dufort EM, Koumans EH, Chow EJ, Rosenthal EM, Muse A, Rowlands J, et al. Multisystem Inflammatory Syndrome in Children in New York State. *N Engl J Med* (2020) 383(4):347–58. doi: 10.1056/NEJMoa2021756
214. Feldstein LR, Rose EB, Horwitz SM, Collins JP, Newhams MM, Son MBF, et al. Multisystem Inflammatory Syndrome in U.S. Children and Adolescents. *N Engl J Med* (2020) 383(4):334–46. doi: 10.1056/NEJMoa2021680
215. Weisberg SP, Connors TJ, Zhu Y, Baldwin MR, Lin WH, Wontakal S, et al. Distinct Antibody Responses to SARS-CoV-2 in Children and Adults Across the COVID-19 Clinical Spectrum. *Nat Immunol* (2021) 22(1):25–31. doi: 10.1038/s41590-020-00826-9
216. Whittaker E, Bamford A, Kenny J, Kaforou M, Jones CE, Shah P, et al. Clinical Characteristics of 58 Children With a Pediatric Inflammatory Multisystem Syndrome Temporally Associated With SARS-CoV-2. *JAMA - J Am Med Assoc* (2020) 324(3):259–69. doi: 10.1001/jama.2020.10369
217. Zhang J, Lin H, Ye B, Zhao M, Zhan J, Dong S, et al. One-Year Sustained Cellular and Humoral Immunities of COVID-19 Convalescents. *Clin Infect Dis* (2021) ciab884. doi: 10.1093/cid/ciab884
218. Dan JM, Mateus J, Kato Y, Hastie KM, Yu ED, Faliti CE, et al. Immunological Memory to SARS-CoV-2 Assessed for Up to 8 Months After Infection. *Science* (2021) 371(6529):eabf4063. doi: 10.1126/science.abf4063
219. Bilich T, Nelde A, Heitmann JS, Maringer Y, Roerden M, Bauer J, et al. T Cell and Antibody Kinetics Delineate SARS-CoV-2 Peptides Mediating Long-Term Immune Responses in COVID-19 Convalescent Individuals. *Sci Transl Med* (2021) 13(590):eabf7517. doi: 10.1126/scitranslmed.abf7517
220. He Z, Ren L, Yang J, Guo L, Feng L, Ma C, et al. Seroprevalence and Humoral Immune Durability of Anti-SARS-CoV-2 Antibodies in Wuhan, China: A Longitudinal, Population-Level, Cross-Sectional Study. *Lancet* (2021) 397 (10279):1075–84. doi: 10.1016/S0140-6736(21)00238-5
221. Gurevich M, Zilkha-Falb R, Sonis P, Magalashvili D, Menascu S, Flechter S, et al. SARS-CoV-2 Memory B and T Cell Profiles in Mild COVID-19 Convalescent Patients. *Int J Infect Dis* (2022) 115:208–14. doi: 10.1016/j.ijid.2021.12.309
222. Bonifacius A, Tischer-Zimmermann S, Dragon AC, Gussarow D, Vogel A, Krettek U, et al. COVID-19 Immune Signatures Reveal Stable Antiviral T Cell Function Despite Declining Humoral Responses. *Immunity* (2021) 54 (2):340–54.e6. doi: 10.1016/j.immuni.2021.01.008
223. Huang C, Huang L, Wang Y, Li X, Ren L, Gu X, et al. 6-Month Consequences of COVID-19 in Patients Discharged From Hospital: A Cohort Study. *Lancet* (2021) 397(10270):220–32. doi: 10.1016/S0140-6736(20)32656-8
224. Wheatley AK, Juno JA, Wang JJ, Selva KJ, Reynaldi A, Tan HX, et al. Evolution of Immune Responses to SARS-CoV-2 in Mild-Moderate COVID-19. *Nat Commun* (2021) 12(1):1162. doi: 10.1038/s41467-021-21444-5
225. Sherina N, Piralla A, Du L, Wan H, Kumagai-Braesch M, Andréll J, et al. Persistence of SARS-CoV-2-Specific B and T Cell Responses in Convalescent COVID-19 Patients 6–8 Months After the Infection. *Med* (2021) 2(3):281–95.e4. doi: 10.1016/j.medj.2021.02.001
226. Rodda LB, Netland J, Shehata L, Pruner KB, Morawski PA, Thouvenel CD, et al. Functional SARS-CoV-2-Specific Immune Memory Persists After Mild COVID-19. *Cell* (2021) 184(1):169–83.e17. doi: 10.1016/j.cell.2020.11.029
227. Jung JH, Rha MS, Sa M, Choi HK, Jeon JH, Seok H, et al. SARS-CoV-2-Specific T Cell Memory Is Sustained in COVID-19 Convalescent Patients for 10 Months With Successful Development of Stem Cell-Like Memory T Cells. *Nat Commun* (2021) 12(1):4043. doi: 10.1038/s41467-021-24377-1
228. Grau-Expósito J, Sánchez-Gaona N, Massana N, Suppi M, Astorga-Gamaza A, Perea D, et al. Peripheral and Lung Resident Memory T Cell Responses Against SARS-CoV-2. *Nat Commun* (2021) 12(1):3010. doi: 10.1038/s41467-021-23333-3
229. Szabo PA, Dogra P, Gray JI, Wells SB, Connors TJ, Weisberg SP, et al. Longitudinal Profiling of Respiratory and Systemic Immune Responses Reveals Myeloid Cell-Driven Lung Inflammation in Severe COVID-19. *Immunity* (2021) 54(4):797–814.e6. doi: 10.1016/j.immuni.2021.03.005
230. Mazzoni A, Vanni A, Spinicci M, Lamacchia G, Kiros ST, Rocca A, et al. SARS-CoV-2 Infection and Vaccination Trigger Long-Lived B and CD4+ T Lymphocytes: Implications for Booster Strategies. *J Clin Invest* (2022) 132(6): e157990. doi: 10.1172/JCI157990
231. Vinuesa CG, Linterman MA, Yu D, Maclennan ICM. Follicular Helper T Cells. *Annu Rev Immunol* (2016) 34:335–68. doi: 10.1146/annurev-immunol-041015-055605
232. Juno JA, Tan HX, Lee WS, Reynaldi A, Kelly HG, Wragg K, et al. Humoral and Circulating Follicular Helper T Cell Responses in Recovered Patients With COVID-19. *Nat Med* (2020) 26(9):1428–34. doi: 10.1038/s41591-020-0995-0
233. Boppana S, Qin K, Files JK, Russell RM, Stoltz R, Bibollet-Ruche F, et al. SARS-CoV-2-Specific Circulating T Follicular Helper Cells Correlate With Neutralizing Antibodies and Increase During Early Convalescence. *PLoS Pathog* (2021) 17(7):e1009761. doi: 10.1371/journal.ppat.1009761
234. Stephenson E, Reynolds G, Botting RA, Calero-Nieto FJ, Morgan MD, Tuong ZK, et al. Single-Cell Multi-Omics Analysis of the Immune Response in COVID-19. *Nat Med* (2021) 27(5):904–16. doi: 10.1038/s41591-021-01329-2
235. Northfield JW, Loo CP, Barbour JD, Spotts G, Hecht FM, Klenerman P, et al. Human Immunodeficiency Virus Type 1 (HIV-1)-Specific CD8 + T EMRA Cells in Early Infection Are Linked to Control of HIV-1 Viremia and Predict the Subsequent Viral Load Set Point. *J Virol* (2007) 81(11):5759–65. doi: 10.1128/JVI.00045-07
236. Lilleri D, Fornara C, Revello MG, Gerna G. Human Cytomegalovirus-Specific Memory CD8+ and CD4+ T Cell Differentiation After Primary Infection. *J Infect Dis* (2008) 198(4):536–43. doi: 10.1086/590118
237. Akondy RS, Monson ND, Miller JD, Edupuganti S, Teuwen D, Wu H, et al. The Yellow Fever Virus Vaccine Induces a Broad and Polyfunctional Human Memory CD8 + T Cell Response. *J Immunol* (2009) 183(12):7919–30. doi: 10.4049/jimmunol.0803903
238. Dunne PJ, Faint JM, Gudgeon NH, Fletcher JM, Plunkett FJ, Soares MVD, et al. Epstein-Barr Virus-Specific CD8+ T Cells That Re-Express CD45RA are Apoptosis-Resistant Memory Cells That Retain Replicative Potential. *Blood* (2002) 100(3):933–40. doi: 10.1182/blood-2002-01-0160

239. Adamo S, Michler J, Zurbuchen Y, Cervia C, Taeschler P, Raeber ME, et al. Signature of Long-Lived Memory CD8+ T Cells in Acute SARS-CoV-2 Infection. *Nature* (2022) 602(7895):148–55. doi: 10.1038/s41586-021-04280-x
240. Kolumam GA, Thomas S, Thompson LJ, Sprent J, Murali-Krishna K. Type I Interferons Act Directly on CD8 T Cells to Allow Clonal Expansion and Memory Formation in Response to Viral Infection. *J Exp Med* (2005) 202 (5):637–50. doi: 10.1084/jem.20050821
241. Derhovanessian E, Maier AB, Hähnel KH, Beck R, de Craen AJM, Slagboom EP, et al. Infection With Cytomegalovirus But Not Herpes Simplex Virus Induces the Accumulation of Latedifferentiated CD4 + and CD8 + T-Cells in Humans. *J Gen Virol* (2011) 92(12):2746–56. doi: 10.1099/vir.0.036004-0
242. Visvabharathy L, Hanson B, Orban Z, Lim PH, Palacio N, Jain R, et al. Neuro-COVID Long-Haulers Exhibit Broad Dysfunction in T Cell Memory Generation and Responses to Vaccination. *medRxiv* (2021) 29:2021.08.08.21261763. doi: 10.1101/2021.08.08.21261763
243. Gattinoni L, Speiser DE, Lichterfeld M, Bonini C. T Memory Stem Cells in Health and Disease. *Nat Med* (2017) 23(1):18–27. doi: 10.1038/nm.4241
244. Gattinoni L, Lugli E, Ji Y, Pos Z, Paulos CM, Quigley MF, et al. A Human Memory T Cell Subset With Stem Cell-Like Properties. *Nat Med* (2011) 17 (10):1290–7. doi: 10.1038/nm.2446
245. Cohen KW, Linderman SL, Moodie Z, Czartoski J, Lai L, Mantus G, et al. Longitudinal Analysis Shows Durable and Broad Immune Memory After SARS-CoV-2 Infection With Persisting Antibody Responses and Memory B and T Cells. *Cell Rep Med* (2021) 2(7):100354. doi: 10.1101/2021.04.19.21255739
246. Forthal D. Adaptive Immune Responses to SARS-CoV-2. *Adv Drug Delivery Rev* (2021) 172:1–8. doi: 10.1016/j.addr.2021.02.009
247. Galletti G, De Simone G, Mazza EMC, Puccio S, Mezzanotte C, Bi TM, et al. Two Subsets of Stem-Like CD8+ Memory T Cell Progenitors With Distinct Fate Commitments in Humans. *Nat Immunol* (2020) 21(12):1552–62. doi: 10.1038/s41590-020-0791-5
248. Cox RJ, Brokstad KA. Not Just Antibodies: B Cells and T Cells Mediate Immunity to COVID-19. *Nat Rev Immunol* (2020) 20(10):581–2. doi: 10.1038/s41577-020-00436-4
249. Mazzoni A, Di Lauria N, Maggi L, Salvati L, Vanni A, Capone M, et al. First-Dose mRNA Vaccination is Sufficient to Reactivate Immunological Memory to SARS-CoV-2 in Subjects Who Have Recovered From COVID-19. *J Clin Invest* (2021) 131(12):e149150. doi: 10.1172/JCI149150
250. Painter MM, Mathew D, Goel RR, Apostolidis SA, Pattekar A, Kuthuru O, et al. Rapid Induction of Antigen-Specific CD4+ T Cells is Associated With Coordinated Humoral and Cellular Immunity to SARS-CoV-2 mRNA Vaccination. *Immunity* (2021) 54(9):2133–42.e3. doi: 10.1016/j.immuni.2021.08.001
251. Polack FP, Thomas SJ, Kitchin N, Absalon J, Gurtman A, Lockhart S, et al. Safety and Efficacy of the BNT162b2 mRNA Covid-19 Vaccine. *N Engl J Med* (2020) 383(27):2603–15. doi: 10.1056/NEJMoa2034577
252. Kalimuddin S, Tham CYL, Qui M, de Alwis R, Sim JXY, Lim JME, et al. Early T Cell and Binding Antibody Responses are Associated With COVID-19 RNA Vaccine Efficacy Onset. *Med* (2021) 2(6):682–88.e4. doi: 10.1016/j.medj.2021.04.003
253. Sahin U, Muik A, Derhovanessian E, Vogler I, Kranz LM, Vormehr M, et al. COVID-19 Vaccine BNT162b1 Elicits Human Antibody and TH1 T Cell Responses. *Nature* (2020) 586(7830):594–9. doi: 10.1038/s41586-020-2814-7
254. Sahin U, Muik A, Vogler I, Derhovanessian E, Kranz LM, Vormehr M, et al. BNT162b2 Vaccine Induces Neutralizing Antibodies and Poly-Specific T Cells in Humans. *Nature* (2021) 595(7868):572–7. doi: 10.1038/s41586-021-03653-6
255. Collier DA, De Marco A, Ferreira IATM, Meng B, Datir RP, Walls AC, et al. Sensitivity of SARS-CoV-2 B.1.1.7 to mRNA Vaccine-Elicited Antibodies. *Nature* (2021) 593(7857):136–41. doi: 10.1038/s41586-021-03412-7
256. Wang Z, Schmidt F, Weisblum Y, Muecksch F, Barnes CO, Finkin S, et al. mRNA Vaccine-Elicited Antibodies to SARS-CoV-2 and Circulating Variants. *Nature* (2021) 592(7855):616–22. doi: 10.1038/s41586-021-03324-6
257. Goel RR, Apostolidis SA, Painter MM, Mathew D, Pattekar A, Kuthuru O, et al. Distinct Antibody and Memory B Cell Responses in SARSCoV-2 Naïve and Recovered Individuals Following mRNA Vaccination. *Sci Immunol* (2021) 6(58):1–19. doi: 10.1126/sciimmunol.abi6950
258. Jackson LA, Anderson EJ, Rouphael NG, Roberts PC, Makhene M, Coler RN, et al. An mRNA Vaccine Against SARS-CoV-2 — Preliminary Report. *N Engl J Med* (2020) 383(20):1920–31. doi: 10.1056/NEJMoa2022483
259. Saadat S, Rikhtegaran Tehrani Z, Logue J, Newman M, Frieman MB, Harris AD, et al. Binding and Neutralization Antibody Titers After a Single Vaccine Dose in Health Care Workers Previously Infected With SARS-CoV-2. *JAMA - J Am Med Assoc* (2021) 325(14):1467–9. doi: 10.1001/jama.2021.3341
260. McDade TW, Demonbreun AR, Sancilio A, Mustanski B, D'Aquila RT, McNally EM. Durability of Antibody Response to Vaccination and Surrogate Neutralization of Emerging Variants Based on SARS-CoV-2 Exposure History. *Sci Rep* (2021) 11(1):17325. doi: 10.1038/s41598-021-96879-3
261. Naaber P, Tserel L, Kangro K, Sepp E, Jürjenson V, Adamson A, et al. Dynamics of Antibody Response to BNT162b2 Vaccine After Six Months: A Longitudinal Prospective Study. *Lancet Reg Health Eur* (2021) 10:100208. doi: 10.1016/j.lanepe.2021.100208
262. Quast I, Tarlinton D. B Cell Memory: Understanding COVID-19. *Immunity* (2021) 54(2):205–10. doi: 10.1016/j.immuni.2021.01.014
263. Khodadadi L, Cheng Q, Radbruch A, Hiepe F. The Maintenance of Memory Plasma Cells. *Front Immunol* (2019) 10. doi: 10.3389/fimmu.2019.00721
264. Chivu-Economescu M, Bleotu C, Grancea C, Chiriac D, Botezatu A, Iancu IV, et al. Kinetics and Persistence of Cellular and Humoral Immune Responses to SARS-CoV-2 Vaccine in Healthcare Workers With or Without Prior COVID-19. *J Cell Mol Med* (2022) 26(4):1293–305. doi: 10.1111/jcmm.17186
265. Schmidt T, Klemis V, Schub D, Schneitler S, Reichert MC, Wilkens H, et al. Cellular Immunity Predominates Over Humoral Immunity After Homologous and Heterologous mRNA and Vector-Based COVID-19 Vaccine Regimens in Solid Organ Transplant Recipients. *Am J Transplant* (2021) 21(12):3990–4002. doi: 10.1111/ajt.16818
266. Zhu J. T Helper 2 (Th2) Cell Differentiation, Type 2 Innate Lymphoid Cell (ILC2) Development and Regulation of Interleukin-4 (IL-4) and IL-13 Production. *Cytokine* (2015) 75(1):14–24. doi: 10.1016/j.cyto.2015.05.010
267. Bolles M, Deming D, Long K, Agnihothram S, Whitmore A, Ferris M, et al. A Double-Inactivated Severe Acute Respiratory Syndrome Coronavirus Vaccine Provides Incomplete Protection in Mice and Induces Increased Eosinophilic Proinflammatory Pulmonary Response Upon Challenge. *J Virol* (2011) 85(23):12201–15. doi: 10.1128/JVI.06048-11
268. Agrawal AS, Tao X, Algaissi A, Garron T, Narayanan K, Peng BH, et al. Immunization With Inactivated Middle East Respiratory Syndrome Coronavirus Vaccine Leads to Lung Immunopathology on Challenge With Live Virus. *Hum Vaccines Immunother* (2016) 12(9):2351–6. doi: 10.1080/21645515.2016.1177688
269. Yasui F, Kai C, Kitabatake M, Inoue S, Yoneda M, Yokochi S, et al. Prior Immunization With Severe Acute Respiratory Syndrome (SARS)-Associated Coronavirus (SARS-CoV) Nucleocapsid Protein Causes Severe Pneumonia in Mice Infected With SARS-CoV. *J Immunol* (2008) 181(9):6337–48. doi: 10.4049/jimmunol.181.9.6337
270. Iwata-Yoshikawa N, Uda A, Suzuki T, Tsunetsugu-Yokota Y, Sato Y, Morikawa S, et al. Effects of Toll-Like Receptor Stimulation on Eosinophilic Infiltration in Lungs of BALB/c Mice Immunized With UV-Inactivated Severe Acute Respiratory Syndrome-Related Coronavirus Vaccine. *J Virol* (2014) 88(15):8597–614. doi: 10.1128/JVI.00983-14
271. Xu K, Dai L, Gao GF. Humoral and Cellular Immunity and the Safety of COVID-19 Vaccines: A Summary of Data Published by 21 May 2021. *Int Immunol* (2021) 33(10):529–40. doi: 10.1093/intimm/dxab061
272. Krawczyk CM, Shen H, Pearce EJ. Memory CD4 T Cells Enhance Primary CD8 T-Cell Responses. *Infect Immun* (2007) 75(7):3556–60. doi: 10.1128/IAI.00086-07
273. Luckheeram RV, Zhou R, Verma AD, Xia B. CD4 +T Cells: Differentiation and Functions. *Clin Dev Immunol* (2012) 2012:925135. doi: 10.1155/2012/925135
274. Williams MA, Tyznik AJ, Bevan MJ. Interleukin-2 Signals During Priming are Required for Secondary Expansion of CD8+ Memory T Cells. *Nature* (2006) 441(7095):890–3. doi: 10.1038/nature04790
275. Oberhardt V, Luxenburger H, Kemming J, Schulien I, Ciminski K, Giese S, et al. Rapid and Stable Mobilization of CD8+ T Cells by SARS-CoV-2 mRNA Vaccine. *Nature* (2021) 597(7875):268–73. doi: 10.1038/s41586-021-03841-4

276. Baden LR, El Sahly HM, Essink B, Kotloff K, Frey S, Novak R, et al. Efficacy and Safety of the mRNA-1273 SARS-CoV-2 Vaccine. *N Engl J Med* (2021) 384(5):403–16. doi: 10.1056/NEJMoa2035389
277. Lustig Y, Nemet I, Kliker L, Zuckerman N, Yishai R, Alroy-Preis S, et al. Neutralizing Response Against Variants After SARS-CoV-2 Infection and One Dose of BNT162b2. *N Engl J Med* (2021) 384(25):2453–4. doi: 10.1056/NEJMc2104036
278. Goel RR, Painter MM, Apostolidis SA, Mathew D, Meng W, Rosenfeld AM, et al. mRNA Vaccines Induce Durable Immune Memory to SARS-CoV-2 and Variants of Concern. *Sci* (2021) 374(6572):abm0829. doi: 10.1126/science.abm0829
279. Collier A-RY, Brown CM, Mcmahan K, Yu J, Liu J, Jacob-Dolan C, et al. Immune Responses in Fully Vaccinated Individuals Following Breakthrough Infection With the SARS-CoV-2 Delta Variant in Provincetown, Massachusetts. *medRxiv* (2021) 20:2021.10.18.21265113. doi: 10.1101/2021.10.18.21265113
280. Tarke A, Sidney J, Methot N, Yu ED, Zhang Y, Dan JM, et al. Impact of SARS-CoV-2 Variants on the Total CD4+ and CD8+ T Cell Reactivity in Infected or Vaccinated Individuals. *Cell Rep Med* (2021) 2(7):100355. doi: 10.1016/j.xcrm.2021.100355
281. Tarke A, Coelho CH, Zhang Z, Dan JM, Yu ED, Methot N, et al. SARS-CoV-2 Vaccination Induces Immunological T Cell Memory Able to Cross-Recognize Variants From Alpha to Omicron. *Cell* (2022) 185(5):847–59.e11. doi: 10.1101/2021.12.28.474333
282. Gao Y, Cai C, Grifoni A, Müller TR, Niessl J, Olofsson A, et al. Ancestral SARS-CoV-2-Specific T Cells Cross-Recognize the Omicron Variant. *Nat Med* (2022) 28:472–6. doi: 10.1038/s41591-022-01700-x
283. Geers D, Shamier MC, Bogers S, den Hartog G, Gommers L, Nieuwkoop NN, et al. SARS-CoV-2 Variants of Concern Partially Escape Humoral But Not T-Cell Responses in COVID-19 Convalescent Donors and Vaccinees. *Sci Immunol* (2021) 6(59):eabj1750. doi: 10.1126/sciimmunol.abj1750
284. Keeton R, Richardson SI, Moyo-Gwete T, Hermanus T, Tincho MB, Benede N, et al. Prior Infection With SARS-CoV-2 Boosts and Broadens Ad26.COV2.S Immunogenicity in a Variant-Dependent Manner. *Cell Host Microbe* (2021) 29(11):1611–19.e5. doi: 10.1016/j.chom.2021.10.003
285. Melo-González F, Soto JA, González LA, Fernández J, Duarte LF, Schultz BM, et al. Recognition of Variants of Concern by Antibodies and T Cells Induced by a SARS-CoV-2 Inactivated Vaccine. *Front Immunol* (2021) 12. doi: 10.3389/fimmu.2021.747830
286. Riou C, Keeton R, Moyo-Gwete T, Hermanus T, Kgagudi P, Baguma R, et al. Escape From Recognition of SARS-CoV-2 Variant Spike Epitopes But Overall Preservation of T Cell Immunity. *Sci Transl Med* (2022) 14(631):eabj6824. doi: 10.1126/scitranslmed.abj6824
287. Zimmermann P, Curtis N. Factors That Influence the Immune Response to Vaccination. *Clin Microbiol Rev* (2019) 32(2):e00084-18. doi: 10.1128/CMR.00084-18
288. Collier DA, Ferreira IATM, Kotagiri P, Datir RP, Lim EY, Touizer E, et al. Age-Related Immune Response Heterogeneity to SARS-CoV-2 Vaccine BNT162b2. *Nature* (2021) 596(7872):417–22. doi: 10.1038/s41586-021-03739-1
289. Witkowski W, Gerlo S, De Smet E, Wejda M, Acar D, Callens S, et al. Humoral and Cellular Responses to COVID-19 Vaccination Indicate the Need for Post-Vaccination Testing in Frail Population. *Vaccines* (2022) 10(2):260. doi: 10.3390/vaccines10020260
290. Van Praet JT, Vandecasteele S, De Roo A, Vynck M, De Vriese AS, Reynders M. Dynamics of the Cellular and Humoral Immune Response After BNT162b2 Messenger Ribonucleic Acid Coronavirus Disease 2019 (COVID-19) Vaccination in COVID-19-Naive Nursing Home Residents. *J Infect Dis* (2021) 224(10):1690–3. doi: 10.1093/infdis/jiab458

Conflict of Interest: The authors declare that the research was conducted in the absence of any commercial or financial relationships that could be construed as a potential conflict of interest.

Publisher's Note: All claims expressed in this article are solely those of the authors and do not necessarily represent those of their affiliated organizations, or those of the publisher, the editors and the reviewers. Any product that may be evaluated in this article, or claim that may be made by its manufacturer, is not guaranteed or endorsed by the publisher.

frontiers | Frontiers in Immunology

TYPE Original Research
PUBLISHED 28 July 2022
DOI 10.3389/fimmu.2022.889372

OPEN ACCESS

EDITED BY
Penghua Wang, University of Connecticut Health Center, United States

REVIEWED BY
Ciro Leonardo Pierri, University of Bari Aldo Moro, Italy
Tilman Schlothauer, Roche, Germany

*CORRESPONDENCE
P. Mark Hogarth
mark.hogarth@burnet.edu.au

SPECIALTY SECTION
This article was submitted to Viral Immunology, a section of the journal Frontiers in Immunology

RECEIVED 04 March 2022
ACCEPTED 27 June 2022
PUBLISHED 28 July 2022

CITATION
Wines BD, Kurtovic L, Trist HM, Esparon S, Lopez E, Chappin K, Chan L-J, Mordant FL, Lee WS, Gherardin NA, Patel SK, Hartley GE, Pymm P, Cooney JP, Beeson JG, Godfrey DI, Burrell LM, van Zelm MC, Wheatley AK, Chung AW, Tham W-H, Subbarao K, Kent SJ and Hogarth PM (2022) Fc engineered ACE2-Fc is a potent multifunctional agent targeting SARS-CoV2.
Front. Immunol. 13:889372.
doi: 10.3389/fimmu.2022.889372

Fc engineered ACE2-Fc is a potent multifunctional agent targeting SARS-CoV2

Bruce D. Wines[1,2,3,4], Liriye Kurtovic[2,3], Halina M. Trist[1], Sandra Esparon[1], Ester Lopez[5], Klasina Chappin[1], Li-Jin Chan[6,7], Francesca L. Mordant[5], Wen Shi Lee[5], Nicholas A. Gherardin[5], Sheila K. Patel[8], Gemma E. Hartley[3], Phillip Pymm[6,7], James P. Cooney[6,7], James G. Beeson[2,3,9,10], Dale I. Godfrey[5], Louise M. Burrell[8], Menno C. van Zelm[3,11], Adam K. Wheatley[5,12], Amy W. Chung[5], Wai-Hong Tham[6,7], Kanta Subbarao[5,13], Stephen J. Kent[5,12,14] and P. Mark Hogarth[1,2,3]*

[1]Immune therapies Laboratory, Burnet Institute, Melbourne, VIC, Australia, [2]Life Sciences, Burnet Institute, Melbourne, VIC, Australia, [3]Department of Immunology and Pathology, Central Clinical School, Monash University, Melbourne, VIC, Australia, [4]Department of Clinical Pathology, The University of Melbourne, Parkville, VIC, Australia, [5]Department of Microbiology and Immunology, The Peter Doherty Institute for Infection and Immunity, The University of Melbourne, Melbourne, VIC, Australia, [6]Infectious Diseases and Immune Defence Division, The Walter and Eliza Hall Institute of Medical Research, Parkville, VIC, Australia, [7]Department of Medical Biology, The University of Melbourne, Melbourne, VIC, Australia, [8]Department of Medicine, Austin Health, The University of Melbourne, Melbourne, VIC, Australia, [9]Department of Medicine, Royal Melbourne Hospital, The University of Melbourne, Parkville, VIC, Australia, [10]Department of Microbiology, Monash University, Clayton VIC, Australia, [11]Department of Allergy, Immunology and Respiratory Medicine, Central Clinical School, Alfred Hospital, Melbourne, VIC, Australia, [12]Australian Research Council Centre for Excellence in Convergent Bio-Nano Science and Technology, The University of Melbourne, Melbourne, VIC, Australia, [13]World Health Organization (WHO) Collaborating Centre for Reference and Research on Influenza, The Peter Doherty Institute for Infection and Immunity, The University of Melbourne, Melbourne, VIC, Australia, [14]Melbourne Sexual Health Centre and Department of Infectious Diseases, Alfred Hospital and Central Clinical School, Monash University, Melbourne, VIC, Australia

Joining a function-enhanced Fc-portion of human IgG to the SARS-CoV-2 entry receptor ACE2 produces an antiviral decoy with strain transcending virus neutralizing activity. SARS-CoV-2 neutralization and Fc-effector functions of ACE2-Fc decoy proteins, formatted with or without the ACE2 collectrin domain, were optimized by Fc-modification. The different Fc-modifications resulted in distinct effects on neutralization and effector functions. H429Y, a point mutation outside the binding sites for FcγRs or complement caused non-covalent oligomerization of the ACE2-Fc decoy proteins, abrogated FcγR interaction and enhanced SARS-CoV-2 neutralization. Another Fc mutation, H429F did not improve virus neutralization but resulted in increased C5b-C9 fixation and transformed ACE2-Fc to a potent mediator of complement-dependent cytotoxicity (CDC) against SARS-CoV-2 spike (S) expressing cells. Furthermore, modification of the Fc-glycan enhanced cell activation *via* FcγRIIIa. These different immune profiles demonstrate the capacity of Fc-based agents to be engineered to

optimize different mechanisms of protection for SARS-CoV-2 and potentially other viral pathogens.

KEYWORDS

coronavirus, SARS-CoV-2, COVID-19, ACE2-Fc, neutralization, antibody effector function, ADCC, complement

Introduction

Recent history has seen regular deadly zoonotic coronavirus spillover events with the emergence of severe acute respiratory syndrome coronavirus (SARS-CoV) in 2002 (1), Middle East respiratory syndrome (MERS) coronavirus in 2012 (2) and SARS-CoV-2 in December 2019 (3). SARS related coronaviruses are found in bats throughout Southeast Asia (4) and the serology of people living in proximity to a Rhinolophus spp bat colony suggests these zoonotic infections are not uncommon (5). Since the publication of the SARS-CoV-2 genome in January 2020 (3) there has been rapid development and deployment of vaccines for SARS-CoV-2 (6) and the clinical development of multiple SARS-CoV-2 spike specific neutralizing monoclonal antibodies (mAbs) from convalescent patients or animals, reviewed in (7).

Evolution of the SARS-COV-2 spike protein has selected for increased transmissibility, for example by increased affinity for host cells (8), with the emergence and then dominance of many new variants of concern (VOC) including Alpha, B.1.1.7; Beta, B.1.351; Gamma, P.1; Delta, B.1.617.2 (9) and most recently, Omicron, B.1.1.529 (WHO) that impact the neutralization efficacy of antibodies generated against the spike antigen of earlier strains (10). This includes profound escape from neutralization by some mAbs (11–15) and significant loss of neutralization activity of convalescent sera (13, 16, 17) and of humoral responses to first generation vaccines (12, 18, 19) reviewed in (10). Reinfection by neutralization-escape variants (20, 21) and break-through infection in vaccinees is now a feature of the pandemic (13, 19). Furthermore, protective antibody responses in humans are largely restricted to specific coronavirus species since few Abs to SARS-CoV-2 receptor binding domain (RBD) cross-neutralize SARS-CoV or MERS-CoV (22) but the recent identification of spike-specific broadly neutralizing mAbs may be a key to future pan-beta-coronavirus pandemic preparedness (23). Overall, despite increased surveillance and biosecurity (24) and the development of SARS-CoV-2 vaccines and mAbs, a critical vulnerability to variants of concern (VOC) and future pandemic novel coronaviruses persists. There is a need for prophylactic and therapeutic approaches that are more broadly effective against Sarbecoviruses.

Decoy proteins, based on the host entry receptor, inhibit viral entry, and achieve cross neutralization of multiple virus species or strains (25–31). Angiotensin-converting enzyme 2 (ACE2), is the principal entry receptor for the major human pathogenic coronaviruses, SARS-CoV and SARS-CoV-2 (32, 33), as well as the human endemic coronavirus NL63 (34). ACE2 is a transmembrane carboxypeptidase (35) with the ectodomain comprised of a catalytic domain, as well as a collectrin domain likely involved in dimerization (36). It normally plays a role in cardiovascular homeostasis by cleaving angiotensin II, the key agonist of the renin–angiotensin–aldosterone system (RAAS) that regulates blood pressure and electrolytes (37, 38). SARS-CoV-2 entry into host cells is blocked by the recombinant soluble ACE2 catalytic ectodomain in its native form (39, 40) or when engineered for higher avidity (31, 41, 42) or affinity (28, 29, 31, 41–45) for the ancestral spike, which has thus far been retained against later VOC (28, 29, 31, 41). Enzyme inactive forms of antiviral ACE2 decoy proteins have also been developed (26, 46, 47). However, ACE2 enzymatic activity, by cleaving angiotensin II, is protective in lung injury models and may therefore be beneficial to retain in an ACE2-based biological for COVID19 (38, 39, 48, 49).

To improve virus neutralization potency or pharmacokinetic properties of SARS-CoV-2 decoys, the ACE2 ectodomain, with or without the collectrin domain, has been fused to the Fc portion of IgG (26, 28, 29, 42–47, 50–55), which results in increased neutralisation potency by bivalency and increased serum half-life (56). In mAb studies using *in vivo* SARS-CoV-2 challenge models, Fc-dependent immune effector functions, which include antibody-dependent cellular cytotoxicity (ADCC), phagocytosis and clearance of viruses, bolstered protection against infection and pathology above that provided by neutralization alone (57–61). Similarly, ACE-Fc decoys have demonstrated protective activity in human ACE2 transgenic mouse models (29, 49, 62) and in hamsters (28) challenged with SARS-CoV-2.

We report the development of multifunctional antiviral proteins by applying novel mutations of the Fc and glycan modification to manipulate the Fc component of ACE2-Fc which resulted variously in increased virus neutralization, complement directed killing and activation of FcγRIIIa.

10.3389/fimmu.2022.889372

Materials and methods

Constructs and proteins

-trACE2 and *trACE2-Fc* Truncated ACE2 (trACE2) comprised the catalytic portion of the ACE2 ectodomain and a sequence encoding trACE2 (aa 19-615, Accession BAB40370) in pHLsec (63) was a gift from Merlin Thomas (64). This trACE2 sequence was fused to a synthetic DNA for human IgG1 Fc (Accession AXN93652.1) in pcDNA3.4 (ThermoFisher) with an encoded linker sequence D^{615}-GSGSGSG-T^{223}, where D^{615} is the last residue of ACE2 and T^{223} (Eu numbering) is the fusion point to IgG1-Fc on the amino terminal side of the Fc core hinge containing the inter-heavy chain disulfides (for full amino acid sequences see Supplementary Text). *-flACE2-Fc* comprised the full-length ACE2 ectodomain fused to human IgG1-Fc. The incorporation of a synthetic DNA encoding the collectrin domain (GeneArt, ThermoFisher) formed a full length ACE2 ectodomain encoding sequence (aa 19-740) fused to the human IgG1-Fc *via* a linker with the sequence S^{740}-GGGGS-T^{223}, where S^{740} is the last residue of ACE2 and T^{223} is the fusion point to IgG1-Fc. *EflACE2-Fc.* EflACE2-Fc was equivalent to the flACE2-Fc, except it incorporated the three mutations, T27Y, L79T, N330Y reported as sACE2.v2.4 and having enhanced affinity for SARS-CoV-2 spike RBD (43). The EflACE2-Fc construct was a synthetic DNA (GeneArt) in pcDNA3.4 (ThermoFisher). The mutations H429F, H429Y and E430G in the Fc were introduced using cleavage at a unique Afe *I* (New England Biolabs) site within codons for E430-L432 and the insertion of appropriate mutagenic oligos with NEBuilder according to the manufacturer's instructions (NEB).

ACE2-Fc protein expression used transient transfection of Expi293 cells (Thermo Fisher Scientific). The supernatant of Expi293 transiently transfected for the expression of ACE2-Fc was extensively dialysed against 10mM TrisHCl pH 8 and applied to a High-Q column (BioRad Laboratories). Bound proteins were eluted with the indicated gradient to buffer A with 0.4 M NaCl and washed with 1 M NaCl. Fractions were examined by SDS-PAGE, fractions containing ACE2-Fc were pooled and concentrated using a 30 kDa cut-off filtration device (Merck) and separated by SEC using a Superose 6 column (GE Lifesciences). Lamelli native PAGE (150V, 2.5 h, 4°C), was performed according to (65).

Recombinant Spike receptor binding domain (RBD; aa328-514, GenBank: MN908947.3) of SARS-CoV-2 Wuhan strain was produced with the N-terminal Fel d 1 leader sequence and C-terminal biotin ligase (BirA) AviTag and a hexahistidine affinity tag (Hartley et al., 2020). Specific mutations were introduced in this construct to generate SARS-CoV-2 variant RBD proteins, representing those from three lineages of concern: B.1.351 (beta; N501Y, E484K, K417N), P.1 (gamma; N501Y, E4848K, K417T) and B.1.167.2 (delta; T478K, L452R). The DNA constructs were codon-optimized for *H. sapiens* and cloned into a pCR3 expression vector. Plasmid DNA was purified from *E. coli* by Maxiprep (Zymo Research, Irvine, CA), and 30 µg DNA was transfected into Expi 293F cells using the Expi293 Expression system (Thermo Fisher, Waltham, MA). Supernatants from 25 ml cell cultures were collected 5 days post-transfection and purified by application to a Talon NTA-cobalt affinity column (Takara Bio, Kusatsu, Shiga, Japan) with elution in 200 mM Imidazole. Eluted proteins were then dialyzed against 10 mM Tris for 48 hours at 4°C.

Virus neutralization assays

Antiviral activity was determined using SARS-CoV-2 (CoV/Australia/VIC01/2020) in a microneutralization assay where cytopathic effect was titred to limiting dilution on Vero cells as described previously (64, 66).

Bio-layer interferometry

Measurements of the affinity of ACE2 proteins for S protein RBD (64) were performed on the Octet RED96e (FortéBio). All assays were performed at 25°C using anti-human IgG Fc capture (AHC) biosensor tips (FortéBio) in kinetics buffer (PBS pH 7.4 supplemented with 0.1% (w/v) BSA and 0.05% (v/v) Tween-20). After a 60 second (60s) biosensor baseline step, ACE2-Fc recombinant proteins (20 µg/mL) were loaded onto the AHC sensors by submerging sensor tips for 200s and then washing in kinetics buffer for 60s. For most ACE2-Fc recombinant proteins, association measurements were performed by dipping into a two-fold dilution series of SARS-CoV-2 spike RBD (64) from 16–250 or 500nM for 180s and dissociation was measured in kinetics buffer for 180s. For EflACE2-Fc WT a two-fold dilution series of 2 – 31 or 63nM was used. Sensor tips were regenerated five times using a cycle of 5s in 10 mM glycine pH 1.5 and 5 s in kinetics buffer. Baseline drift was corrected by subtracting the average shift of an ACE2-Fc-loaded sensor not incubated with SARS-CoV-2 spike RBD, and an unloaded sensor incubated with SARS-CoV-2 spike RBD. Curve fitting analysis was performed with Octet Data Analysis 10.0 software using a global fit 1:1 model to determine K_D values and kinetic parameters. Curves that could not be fitted were excluded from the analyses.

ACE2-Fc binding ELISA

ELISA plates were coated with 5µg/ml CoV-2 receptor binding domain fused to mIgGFc (RBD-Ig, RBD aa residues 334-527) and blocked with phosphate buffered saline (PBS) containing 0.05% (w/v) Tween-20 and 2% (w/v) bovine serum albumin (BSA). RBD-Ig was reacted with ACE2-Fc proteins diluted in ½ log titrations (1 hour, 25°C) followed by washing 5 times with PBS, 0.05% Tween-20. Bound ACE2-Fc was detected with sequential incubation with mouse anti-human IgG1-biotin (Thermo MH1515, clone HP6070, at 1µg/ml for 1 hour, 25°C),

high sensitivity streptavidin-HRP (1/10,000 dil, 1 hour, 25°C, Pierce, Thermo Scientific) and TMB substrate.

ACE2-Fc and dimeric recombinant soluble (rs) FcγR binding by flow cytometry

The ACE2-Fc proteins or the anti-CD20 mAb, Rituximab, at 5μg/ml, or the indicated concentrations were incubated with Ramos cells expressing transfected spike proteins (Ramos-S cells) (67) at $5x10^6$ cells/ml in 25μl in fluorescence activated cell sorting (FACS) buffer- PBS containing 0.5% (w/v) BSA, 1mM glucose (PBS/BSA/G), for 30 min on ice. Cells were washed twice with FACS-buffer, incubated with APC conjugated anti-human IgG-Fc for thirty minutes on ice, washed again and resuspended in 25 μl of FACS-buffer.

Evaluation of the binding of dimeric rsFcγR was performed as described in (68). ACE2-Fc opsonized Ramos-S cells were resuspended in 0.5μg/ml of dimeric rsFcγRIIIa (V158 form) or FACS-buffer and incubated for 30 min on ice followed by 1/500 streptavidin-APC (or anti-hIgG-Fc labelled with fluorescein isothiocyanate for confirmation of ACE2-Fc opsonization) for 20 min on ice. The cells were washed, resuspended in FACS buffer and analyzed on a Canto II flow cytometer (Becton Dickinson).

Complement fixation immunoassay for ACE2-Fc

Ninety-six well flat-bottom MaxiSorp Nunc plates (ThermoFischer Scientific) were coated with 5 μg/ml Avidin in PBS overnight, blocked, and then incubated with either two-fold dilution of biotinylated RBD (69) or 2.5 μg/ml in 0.1% casein for 1 hour at RT. The ACE2-Fc proteins were then added over the indicated concentration range. In experiments to measure C5b-C9 fixation, the plates were incubated with 10% fresh human serum for 30 minutes at RT followed by 1/2000 dilution of rabbit anti-C5b-C9 (Millipore) for 1 hour at RT, washed and then incubated with goat anti-rabbit IgG conjugated to HRP (Millipore) at 1/2000 dilution for 1 hour at RT, followed by TMB substrate for 15-20 minutes at RT (70). Reactivity was stopped using 1 M sulfuric acid and absorbance was measured at 450 nm. Test samples and reagents were prepared in PBS 0.1% (w/v) casein and plates washed thrice between each step using PBS, 0.05% (v/v) Tween 20. Samples were tested in duplicate and corrected for background reactivity using negative control wells from which ACE2-Fc proteins were omitted. The mean and SEM from independent experiments are shown.

Complement dependent cytotoxicity

CDC was measured by opsonizing Ramos-S cells as above ($5x10^6$ cells/ml in 25μl in PBS/BSA/G for 30 min on ice) before resuspending in 1/3 diluted normal human serum for 30 min at 37°C. Cells were washed twice with PBS and the dead cells were enumerated by staining with 1/500 Zombie green (BioLegend) before fixing with 2% paraformaldehyde in PBS and analysis on a Canto II flow cytometer.

FcγRIIIa-NF-κB-RE nanoluciferase reporter assay

This assay used IIA1.6/FcR-γ/FcγRIIIa V158 cells expressing a NF-κB response element driven nanoluciferase (NanoLuc, pNL3.2.NF-κB-RE[NlucP/NF-κB-RE/Hygro], Promega N111) and was performed essentially as described previously (67). Briefly, Ramos cells expressing the Spike-IRES-orange2 were used as target cells and were incubated with agonists and the FcγRIIIa/NF-κB-RE reporter cells for 5h before measurement of induced nanoluciferase with Nano-Glo substrate (Promega).

RBD variants and coronavirus S multiplex ACE2-Fc inhibition assay

A custom coronavirus multiplex array (71) was performed using SARS-S1 subunit (S1N-S52H5, Acrobiosystems), SARS-CoV-2 S1 (40591-V08B1) and HCoV NL63 S1 and S2 subunits (40604-V08B, Sino Biological), NL63 S trimer [100788, bpsbioscience], and hexahistidine tagged RBD WT (SARS CoV-2, isolate Wuhan-Hu-1, NCBI Reference Sequence: YP_009724390.1, aa residues 319-541 (72),) and 24 variants identified from the GISAID RBD surveillance repository (71). TrACE2-Fc was biotinylated using EZ-Link® Sulfo-NHS-LC-Biotin (ThermoFisher Scientific) according to the manufacturer's instructions. Biotinylated trACE2-Fc (70 nM) was incubated with a concentration series, eight two-fold dilutions from 282 nM, of unlabelled trACE2-Fc, flACE2-Fc, EflACE2-Fc fusion proteins or the inhibitory human mAb S35 (AcroBiosystems) and binding to RBD or S proteins coupled to beads was determined using first Streptavidin, R-Phycoerythrin Conjugate (SAPE) (Thermo Fisher) at 4μg/ml (1 h), followed by 10μg/ml of R-Phycoerythrin, Biotin-XX Conjugate (Thermo Fisher) (1 h) and multiplex analysis. Apparent IC50 (nM) values are indicated from curve fits.

Modelling of ACE2-Fc decoy proteins

Alphafold v2.2 (73, 74) was run on the EflACE2-Fc sequence using five models and specifying two homo-oligomers. The output of this recapitulated the observed structure of the ACE2 homodimer (PDB ID: 6M17, ACE2 residues 19-729) with an RMSD of 1.378 Å, however, the IgG1-Fc domains did not pair. The IgG1-Fc plus the G4S linker and collectrin domain of ACE2 (residues 615-729) was therefore run on Alphafold v2.2 specifying two homo-oligomers and an output of five models. Of these, one model showed correctly paired IgG1 Fc domains and a collectrin domain folded as in the full-length ACE2 structure (PDB ID: 6M17) with an RMSD of 0.718 Å. Superimposition of the collectrin domains of the model with the ACE2 homodimer and that with the paired IgG1-Fc allowed reconstruction for the complete EflACE2-Fc sequence. Positioning of the linkers was manually modelled based on the human B12 IgG crystal structure (PDB ID: 1HZH) to allow the correct pairing of the Fc-hinge disulphide residues at positions 749 and 752

(Figures 1A, B). The trACE2-Fc structure was modelled manually on the EflACE2-Fc model, maintaining the relative position of the ACE2 catalytic domains as in the full-length homodimer. Coordinate files are available from the authors on request.

Docking of the SARS-CoV-2 spike RBD to the EflACE2-Fc construct was modelled using HADDOCK v2.4 (75, 76) and the best model from the top scoring cluster was taken, having a HADDOCK score of -151 ± 4.2 and an RMSD from the overall lowest energy structure of 0.7 Å ± 0.5 (Figure 1E). The SARS-CoV-2 spike RBD and ACE2 catalytic domain (residues 19-614) had an overall RMSD of 2.733 Å from the observed SARS-CoV-2 binding to native ACE2 (PDB ID: 6M0J), with the SARS-CoV-2 and ACE2 chains aligning more closely with RMSDs of 0.400 Å and 1.400 Å respectively. A HADDOCK SARS-CoV-2 spike RBD docking model generated using an Alphafold prediction of the native ACE2 structure aligned similarly with the observed structure (PDB ID: 6M0J) with an RMSD of 2.940 Å, and overlayed the EflACE2-Fc structure with an RMSD of 0.573 Å.

Data and Statistical analysis used the Prism software package (GraphPad Software 9.0.2, San Diego, CA). Curve fitting to agonist(inhibitor) response curves for EC_{50} (IC_{50}) determination and ANOVA with multiple comparisons tests were used as indicated in the Figure legends.

Results

A series of ACE2-Fc fusion proteins (Table 1) were produced and analyzed for improved capacity to neutralize SARS-CoV-2 infection and to enhance or transform Fc-dependent effector functions attributed normally to the mechanisms of action of antibodies. Three versions of the ACE2 ectodomain were fused to the human IgG1 Fc portion. The first ACE2 fusion comprised the full length ACE2 ectodomain (flACE2-Fc, aa 19-740), including both the catalytic and collectrin domains (Figure 1A) and the second, an enhanced full length ACE2 ectodomain, EflACE2-Fc, with enhanced binding to SARS-CoV-2 S protein-RBD resulting from three amino acid mutations in the RBD binding site of the ACE2 protein (T27Y, L79T and N330Y) (43) and the third comprised a truncated ectodomain (trACE2-Fc, aa 19-615) containing the ACE2 catalytic domain but lacking the collectrin domain. Models of the trACE2-Fc (Figures 1C, D) and EflACE2-Fc (Figures 1A, B) decoy proteins were generated using Alphafold 2 (73, 74) and EflACE2-Fc was docked to SARS-CoV-2 spike RBD (Figure 1E). A comparison of the RBD docked to the Alphafold prediction of the EflACE2 and native ACE2 structures aligned similarly with the observed structure (PDB ID: 6M0J) with an RMSD of 2.733 Å and 2.940 Å respectively, and overlayed the RBD-EflACE2-Fc docked structure with an RMSD of 0.573 Å. This indicates that the affinity enhancing mutations do not impact the docking position of the SARS-CoV-2 spike RBD using this modelling approach. To evaluate the interaction with trimeric spike and assess the relative distance between ACE2 catalytic domains and adjacent RBD, the EflACE2-Fc-SARS-CoV-2 spike RBD or the trACE2-Fc-SARS-CoV-2 spike RBD model was overlayed on the RBD of chain A of the observed Spike-ACE2 complex structure (PDB ID: 7VXM) (Figures 1F, G). This showed that the ACE2 dimer in the EflACE2-Fc construct is not able to bind adjacent RBD on a single spike trimer due to distance restraints. Though the two ACE2 catalytic domains in the trACE2-Fc construct are likely not dimeric, through the lack of a collectrin domain (36), restraints imposed by disulphide bonding at the N-terminus of the Fc similarly act to restrict the distance between the ACE2 domains and likely also prevent binding to adjacent RBD for this construct (Figure 1G).

The key rationale for the development of a ACE2 decoy antiviral protein as a biosecurity agent against a future pandemic is the presumption it will similarly inhibit SARS-CoV-2 variants and ACE2 tropic coronaviruses generally. Indeed, using an ELISA flACE2-Fc bound near equally to both the ancestral RBD and RBD from the beta, gamma and delta VOCs (Figure 1H).

The activity of ACE2-Fc against SARS-CoV-2 variants was further addressed using a bead array. The inhibition of binding of biotinylated trACE2-Fc to an established array of 24 SARS-CoV-2 spike RBD variants (71) by unlabeled ACE2-Fc decoys was examined. Inhibition of binding to RBD-WT followed the hierarchy trACE2-Fc-WT < flACE2-Fc-WT < EflACE2-Fc-WT (IC_{50} = 114, 80, 10 nM respectively) with effective inhibition of binding to all the individual RBD variants reached, with IC_{50} values within two-fold of that observed with the ancestral RBD (Figure 2). Thus, across the array of RBD variants the average IC_{50} values (110 ± 4; 86 ± 4 nM; 9.5 ± 0.9 nM) simply replicated this hierarchy of increasing neutralization potency over trACE2-Fc-WT as variants with increased affinity for ACE2 have equivalent increased susceptibility to inhibition by ACE2, including the N439K, S477N and E484K RBDs and other variants associated with escape from neutralizing antibodies (11, 54, 77). This contrasted sharply with the neutralizing mAb S35 where binding to the L455F and A475V RBD variants was abrogated. Furthermore, the decoy proteins were also effective inhibitors of binding to the spike proteins of the SARS and NL63 beta-coronaviruses (Figure 2). This illustrates the intrinsic resistance of ACE2 based antiviral decoys to escape by spike mutation and their applicability to other viruses that also use ACE2 for entry.

In addition to fusion to wild-type (WT) IgG1-Fc, these ACE2 formats were also fused to a Fc carrying novel substitutions of histidine 429 (Eu numbering) with phenylalanine (H429F) or tyrosine (H429Y), or in the adjacent residue, a known IgG hexamerising mutation E430G (78, 79). A glycan-modified form of trACE2-Fc was also produced in the presence of the mannosidase inhibitor kifunensine (trACE2-Fc-*kif*). The recombinant ACE2-Fc fusion proteins were purified first by anion exchange followed by size exclusion chromatography (SEC) and comprised largely a single species

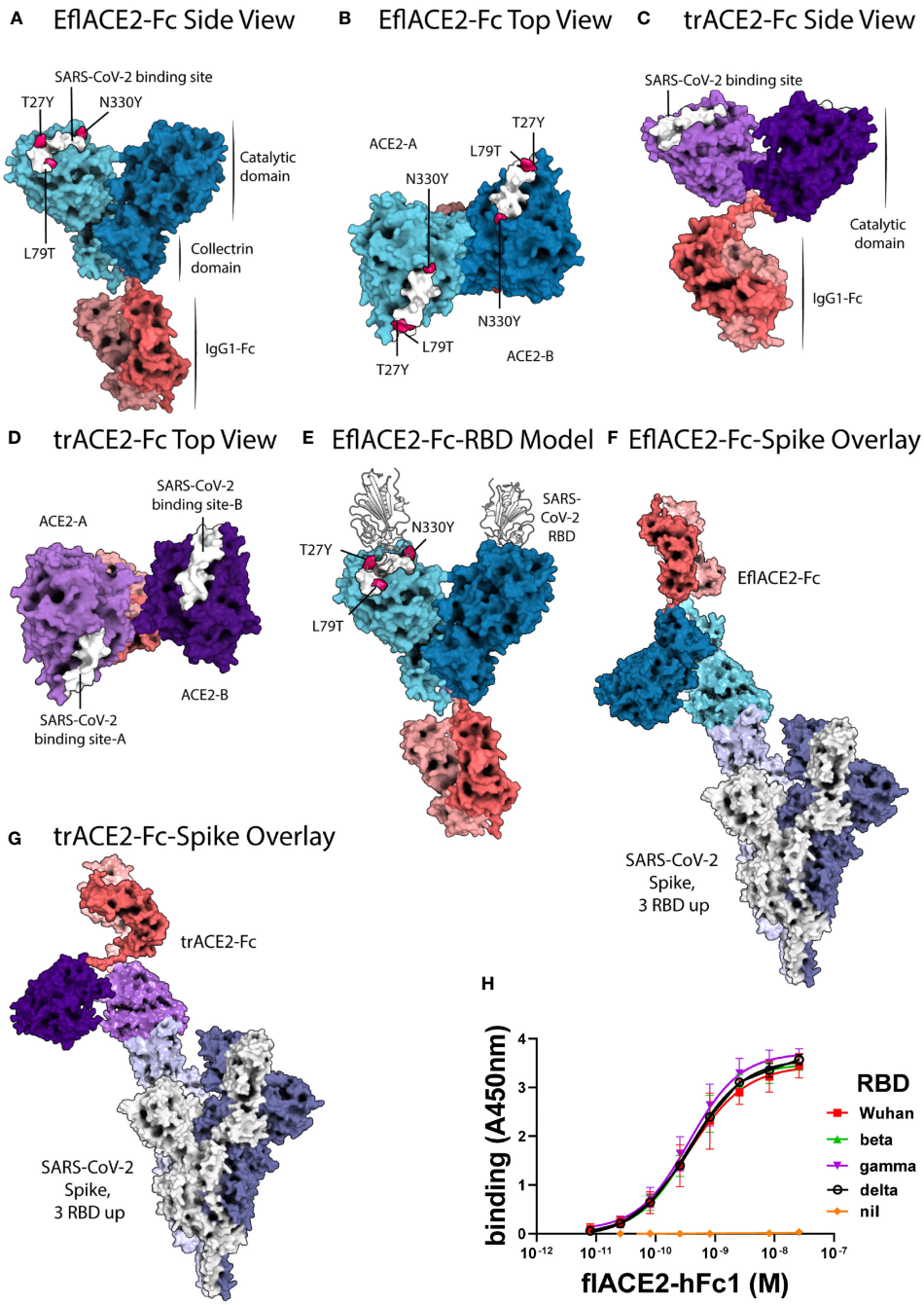

FIGURE 1
ACE2-Fc protein modelling and the interaction with SARS-CoV-2. **(A-E)** SARS-CoV-2 spike RBD binding footprint in white. The flACE2-Fc comprised a full-length ACE2 ectodomain (aa 19-740) fused to human IgG1-Fc. **(A, B)** EflACE2-Fc, having improved RBD binding is a variant of flACE2-Fc wherein three-point mutations, T27Y, L79T and N330Y, have been incorporated into ACE2 component (43) to enhance binding affinity to SARS-CoV-2 spike RBD. **(C, D)** The truncated ACE2 ectodomain (aa 19-615) was fused to human IgG1 Fc generating the trACE2-Fc fusion protein. **(E)** HADDOCK model of SARS-CoV-2 spike RBD binding to EflACE2 SARS-CoV-2 spike RBD shown in cartoon representation in white. **(F)** EflACE2-Fc shown overlayed on, and aligned by, ACE2 residues 19-614 of the 7VXM cryo-EM complex of SARS-CoV-2 spike and ACE2. **(G)** trACE2-Fc shown overlayed on, and aligned by, ACE2 residues 19-614 of the 7VXM cryo-EM complex of SARS-CoV-2 Spike and ACE2. In **(F, G)**, Positioning of the ACE2 dimer and Fc disulfides respectively indicate the ACE2-Fc constructs are unlikely to bind multiple RBD on a single spike trimer. **(H)** ACE2-Fc binding to variant SARS-CoV-2 spike RBD. The flACE2-Fc-WT fusion protein binds to the ancestral Wuhan RBD, and the beta, gamma and delta VOC RBDs with equivalent EC_{50} values. Plotted values are mean ± SD, n = 3, except for delta RBD n = 2. Agonist versus response curve fitting EC_{50} ranged from 0.31 to 0.40 nM.

TABLE 1 ACE2 proteins used in this study.

Protein name	ACE2 ectodomain form(amino acid sequence)	ACE2 modification	Fc modification (IgG1 EU numbering)
trACE2	Truncated ACE2 (aa 19-615)	Not modified	N/A*
trACE2-Fc WT	Truncated ACE2 (aa 19-615)	Not modified	Not modified
trACE2-Fc-H429F	Truncated ACE2 (aa 19-615)	Not modified	His 429 Phe
trACE2-Fc-H429Y	Truncated ACE2 (aa 19-615)	Not modified	His 429 Tyr
trACE2-Fc-E430G	Truncated ACE2 (aa 19-615)	Not modified	Glu 430 Gly
trACE2-Fc-*kif*	Truncated ACE2 (aa 19-615)	Modified glycans	Modified glycan at Asn 297
flACE2-Fc-WT	Full length ACE2 (amino acids 19-740)	Not modified	Not modified
flACE2-Fc-H429F	Full length ACE2 (amino acids 19-740)	Not modified	His 429 Phe
flACE2-Fc-H429Y	Full length ACE2 (amino acids 19-740)	Not modified	His 429 Tyr
flACE2-Fc-E430G	Full length ACE2 (amino acids 19-740)	Not modified	Glu 430 Gly
EflACE2-Fc-WT	Full length ACE2 (amino acids 19-740)	Thr 27 Tyr Leu 79 Thr Asn 330 Tyr	Not modified
EflACE2-Fc-H429F	Full length ACE2 (amino acids 19-740)	Thr 27 Tyr Leu 79 Thr Asn 330 Tyr	His 429 Phe
EflACE2-Fc-H429Y	Full length ACE2 (amino acids 19-740)	Thr 27 Tyr Leu 79 Thr Asn 330 Tyr	His 429 Tyr
EflACE2-Fc-E430G	Full length ACE2 (amino acids 19-740)	Thr 27 Tyr Leu 79 Thr Asn 330 Tyr	Glu 430 Gly

*N/A, not applicable as no Fc present i.e truncated ACE2 ectodomain only.

by SEC (Figure 3A) except the H429Y mutant Fc proteins which in all formats were resolved by SEC as oligomeric and monomeric species (Figure 3B).

Fc modification did not affect the intrinsic affinity for the SARS-CoV-2 spike RBD (e.g. trACE2-Fc-WT, K_D = 28.6nM; flACE2-Fc-WT, 25.2 nM; flACE2-Fc-H429F, K_D = 23.2 nM, Figures 3C-E) which was comparable with that of the reported affinity 22nM for the flACE2 (43). As expected, the EflACE2-Fc WT protein with the enhanced RBD-binding mutant ACE2 domain showed a ~30-fold increase in affinity to K_D = 0.7 nM (Figure 3F) (43) compared to the flACE2-Fc.

Native PAGE (N-PAGE) analysis showed that ACE2-Fc WT fusion proteins migrate as a single species, at ~ 260 kDa for trACE2-Fc and at > 260 kDa for the flACE2-Fc and EflACE2-Fc fusion proteins, reflecting the additional presence of the collectrin domain (Figure 3G). Notably the ACE2-Fc-H429Y variants (e.g. trACE2-Fc-H429Y Fc, Figure 3G, 5th trACE2-Fc lane "Y") migrated in N-PAGE as several distinct higher molecular weight oligomer species, that were not apparent in denaturing SDS-PAGE, i.e. these comprise non-covalent oligomers. N-PAGE shift analysis showed that the normal and enhanced ACE2 (e.g. trACE2-Fc and EflACE2-Fc) proteins, and the Fc mutants, had high-specific binding activity for SARS-CoV-2 spike RBD, visualized by their shift to high molecular weight complexes following interaction with SARS-CoV-2 spike RBD-Ig (RBD-Ig "+" lanes, Figure 3G). When quantified by ELISA the ACE2-Fc proteins bound the bivalent ligand RBD-Ig with subnanomolar avidity and were unaffected by mutation of the Fc, excepting the oligomer forming H429Y Fc mutants which exhibited weaker binding (Figure 3H).

The antiviral activities of the ACE2-Fc fusion proteins were determined in a microneutralization assay using SARS-CoV-2 infection of Vero cells (64) where the EC_{50} endpoint corresponds to neutralization of ~99% of the inoculum virions (66). The SARS-CoV-2 neutralization endpoint (EC_{50} 2.70 μM) of the unfused truncated ectodomain (trACE2 alone) was improved ~10-fold by its fusion with the unmodified wildtype Fc region of IgG1 (trACE2-Fc-WT, EC_{50} 283 nM), consistent with its improved binding avidity (Figure 4A). In accord with its increased intrinsic affinity for the RBD (Figure 3F), the

10.3389/fimmu.2022.889372

VIRAL LIGAND		INHIBITOR IC50 (nM)			
		trACE2-Fc	flACE2-Fc	EflACE2-Fc	mAb S35
CoV-2 RBD	RBD WT	114.3	80.4	10.3	14.8
	R403K	100.8	84.6	9.7	13.5
	N439K	91.5	79.3	6.9	33.7
	K444R	115.8	81.6	9.1	14.1
	V445I	115.1	84.0	10.6	14.3
	G446S	113.7	87.2	6.8	24.8
	G446V	125.5	125.3	5.1	35.1
	S477N	66.2	73.5	11.3	18.9
	L455F	130.6	68.8	3.5	>>200
	A475V	122.7	81.9	3.8	>200
	G476S	115.4	85.2	10.9	14.8
	T478I	122.6	86.0	8.9	11.0
	V483A	106.4	75.1	8.5	18.1
	V483F	100.7	86.3	7.7	19.4
	V483I	101.6	80.6	9.8	14.9
	E484A	124.2	78.6	13.6	23.6
	E484D	124.1	75.4	7.5	18.4
	E484K	112.0	88.0	6.2	25.5
	E484Q	101.0	62.7	6.8	16.0
	F490L	167.8	155.6	17.0	99.0
	F490S	101.8	83.0	5.1	28.3
	Q493L	92.8	91.4	13.4	128.8
	S494P	115.3	90.0	15.5	13.5
	N501Y	84.5	86.1	23.3	43.5
	V503F	94.8	76.8	6.7	21.3
SARS-1	S1	140.7	45.0	5.0	NB
CoV-2	S1	111.8	71.8	7.2	26.0
NL63	S1 and S2	112.9	61.1	15.6	NB
NL63	trimer	100.1	52.7	13.2	NB

Scale (nM)				
	0	25.0	50.0	75.0
	100	125.0	150.0	175.0

FIGURE 2
Human ACE2-Fc decoy proteins broadly inhibit binding to RBD variants and S from variants and related Sarbecoviruses. Biotinylated trACE2-Fc was incubated with a concentration series of unlabelled trACE2-Fc, flACE2-Fc, EflACE2-Fc fusion proteins or the inhibitory human mAb S35. Binding to RBD or S proteins coupled to beads was determined. Apparent IC50 (nM) values are indicated. NB, no binding.

EflACE2-Fc-WT (EC_{50} 11 nM) was a further ~11 and 25-fold more inhibitory than the unmodified flACE2-Fc-WT (EC_{50} 124 nM) and trACE2-Fc-WT respectively (Figures 4A–C). Thus overall, EflACE2-Fc-WT (Figure 4C) was ~240-fold more active in virus neutralization than trACE2 alone (Figure 4A).

Of the five Fc modifications, the oligomeric (og) form of the H429Y Fc mutants fused with any ACE2 format, consistently displayed superior neutralization activity within its ACE2 format class. Thus, the oligomeric trACE2-Fc-H429Y_{og}, isolated by SEC, had a neutralization activity (EC_{50} 21.9 nM) that was 13-fold improved over the monomeric trACE2-Fc-WT (EC_{50} 283nM, Figure 4A). Similarly, flACE2-Fc-H429Y_{og} (EC_{50} 10.0 nM) showed greater potency than flACE2-Fc-WT (EC_{50} 124 nM) (Figure 4B). Indeed, it was equivalent in neutralization activity to the EflACE2-Fc WT neutralization (EC_{50} 10.6 nM). Finally, the most potent inhibitor, EflACE2-Fc-H429Y_{og} (EC_{50} 4.23 nM) (Figure 4C), was ~ 600-fold more active than the monovalent trACE2 (Figure 4A). This improved neutralization by the H429Y decoy contrasted with the H429F and the E430G modifications which did not significantly alter SARS-CoV-2 neutralization

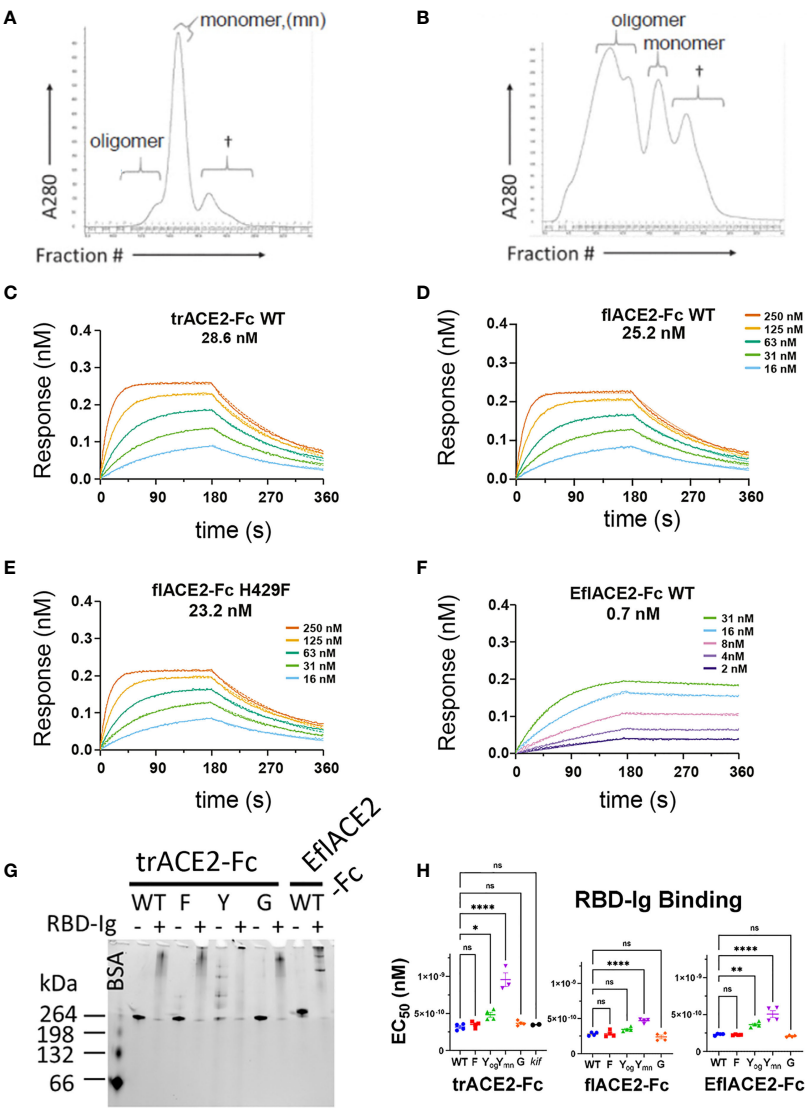

FIGURE 3
Characterization of engineered human flACE2-Fc and trACE2–Fc fusion proteins. **(A)** Size-exclusion chromatography (SEC) of IEX fractions containing flACE2-Fc-WT using a Superose 6 column, with oligomeric, monomeric forms and low mw impurities (†) indicated; and **(B)** SEC of IEX fractions containing flACE2-Fc H429Y, showing the high proportion of oligomeric species. **(C–F)** Biolayer interferometry (BLI) analysis of ACE2-Fc proteins which were immobilized on anti-human Fc (BLI) sensors and reacted with the indicated concentrations of RBD. The dissociation constants, KD (nM), are derived from global fitting of the association and dissociation curves to a Langmuir binding model. The ACE2-Fc proteins were, **(C)** trACE2-Fc WT **(D)** flACE2-Fc WT, **(E)** flACE2-Fc H429F and **(F)** the RBD binding-enhanced triple mutant of ACE2 fused to Fc; EflACE2-Fc WT (representative of n = 2 independent experiments). **(G)** Native Gel-shift analysis of ACE2-Fc proteins (1 mg, ~ 5 pmol) alone or combined with SARS-CoV-2 spike RBD-Ig (0.5 mg, ~ 5 pmol) and analyzed by native PAGE. The resulting shift in size of the proteins in the mixtures demonstrated the formation of ACE2-Fc: Cov2-RBD complexes. **(H)** Binding of different formats of ACE2-Fc-WT, and their Fc variants to immobilized RBD-Ig was determined by ELISA. EC_{50} (nM) values are from agonist versus response curve fits,mean ± SD, n is indicated by individual symbols for each independent experiment. One-way ANOVA with Dunnett's multiple comparisons test, p > 0.05 (ns), ≤ 0.05 (*), ≤0.01 (**), ≤ 0.0001 (****).

activity in any ACE2-Fc format (Figures 4A-C). As a comparator the laboratory equivalent of the therapeutic mAb REGN 10933 (casirivimab) had an EC_{50} of 3.6 nM, (n = 2).

The Fc receptors of leukocytes and serum complement provide the two major effector systems harnessed normally by the Fc portion of antibodies. FcγR functions, which may include ADCC, phagocytosis and clearance of opsonized viruses are important antiviral effector mechanisms and are increasingly found to play a protective role during SARS-CoV-2 infection (57, 58, 60, 61, 80, 81). The interaction of FcγRIIIa with the ACE2-Fc fusion proteins was evaluated by flow cytometry using Ramos cells expressing SARS-CoV-2 spike protein (Ramos-S cells)

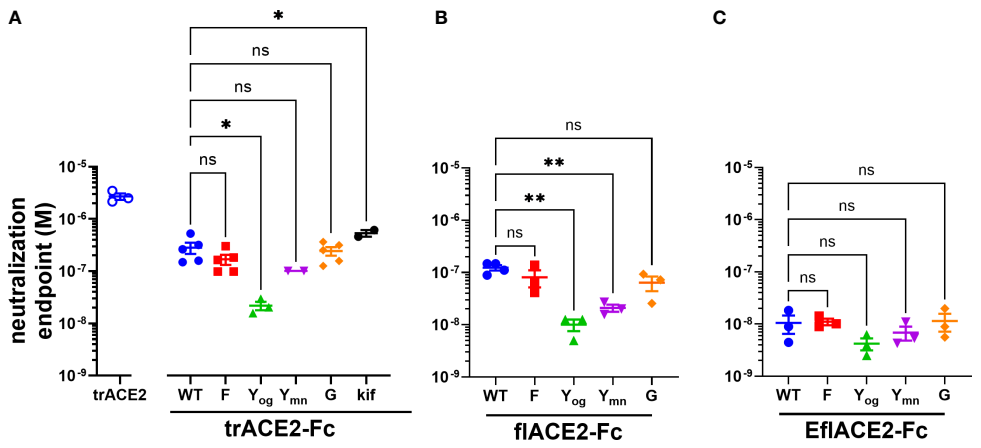

FIGURE 4
(A–C) SARS-CoV-2 neutralization potency of ACE2-Fc fusion proteins is increased by both the ACE2 scaffold and the H429Y Fc mutation. Neutralization potencies of the ACE2 enzymatic ectodomain polypeptide (trACE2) and the three formats of ACE2-Fc-WT fusion and variant proteins were determined by titration of the cytopathic effect to endpoint in a micro-neutralization assay. The fusion proteins were **(A)** trACE2-Fc-WT, **(B)** flACE2-Fc-WT and **(C)** EflACE2-Fc-WT, incorporating triple mutation of ACE2 engineered (43) for enhanced affinity to RBD and their Fc variants (Eu numbering), E430G, G; H429F, F; H429Y oligomers on SEC, Yog; and H429Y monomers on SEC, Ymn. A further variant trACE2-Fc fusion protein is the glycan-modified trACE2-Fc-kif produced in the presence of kifunensine. Mean ± SEM, one-way ANOVA with Dunnett's multiple comparisons test, $p < 0.05$ (ns), ≤ 0.05 (*), ≤ 0.01 (**), independent experiments (n) are indicated as individual symbols.

opsonized with the different formats of ACE2-Fc. Dimeric recombinant soluble FcγRIIIa (68) bound the Fc-WT and H429F and E430G mutant fusion proteins within each ACE2 format class near equivalently. However, the H429Y mutation of the Fc largely ablated FcγR binding in all the ACE2-Fc formats (Supplementary Figure S1A). The loss of FcγRIIIa binding was not due to lack of opsonization of the Ramos-S cells by the H429Y variants as all ACE2-Fc proteins showed similar binding of the SARS-CoV-2 spike protein on the cell surface (Table 2).

Next, FcγRIIIa activation by ACE2-Fc fusion proteins was evaluated as a validated surrogate of ADCC (67). FcγRIIIa was activated by Ramos-S cells opsonized with a Fc-WT fusion of any ACE2 format (Figure 5A). The flACE2-Fc-WT induced FcγRIIIa-mediated activation of the reporter cell at 2.7-fold lower concentration than the trACE2-Fc-WT (EC_{50} 1.7 nM) (Figure 4A, $p < 0.0001$, Supplementary Figures S1B, C), indicating that inclusion of the ACE2 collectrin domain, improved FcγRIIIa activation. Notably, the increased affinity of the EflACE2-Fc WT for SARS-CoV-2 spike protein, did not increase FcγRIIIa activation above that of flACE2-Fc WT (Figure 5A).

However, the most potent FcγRIIIa activation was achieved following glycan-modification by kifunensine (82) during the production of the trACE2-Fc. Thus, despite the lower activity of the trACE2-Fc format, FcγRIIIa activation by trACE2-Fc-*kif* exceeded that of the flACE2-Fc and EflACE2-Fc and approached that of the therapeutic anti-CD20 mAb rituximab used as a comparator on the $CD20^+$ Ramos-S cells (Figure 5A; Supplementary Figure S1B). Thus, the hierarchy of FcγRIII activation by the proteins was trACE2-Fc-*kif* > EflACE2-Fc WT ~ flACE2-Fc- WT > trACE2-Fc-WT.

In accord with the FcγRIIIa binding data (Supplementary Figure S1A), modification of ACE2-Fc decoys by the H429F or E430G mutation had only modest effects on FcγRIIIa activation (Figure 5A; Supplementary Figures S1B, C). In contrast, the H429Y mutation in all ACE2-Fc formats ablated FcγRIIIa activation of cells which is consistent with their abrogated binding to FcγRIIIa (Supplementary Figure S1A). Thus, while enhancing virus neutralization, the H429Y modified Fc in trACE2-Fc, flACE2-Fc and EflACE2-Fc formats were largely inactive in FcγR binding and consequently unable to activate cells *via* FcγRIIIa (Figure 5A).

TABLE 2 Flow cytometric analysis of Ramos-S cells by opsonized ACE2-Fc proteins*.

	WT	H429F	$H429Y_{mn}$	E430G	*kif*
trACE2-Fc	15455 (1.00†)	16268 (1.05)	11586 (0.75)	16730 (1.08)	16382 (1.06)
flACE2-Fc	17246 (1.00)	16887 (0.98)	12496 (0.72)	17286 (1.00)	ND
EflACE2-Fc	19576 (1.00)	20472 (1.05)	15065 (0.77)	20961 (1.07)	ND

*ACE2-Fc and Fc variant fusion proteins (5 μg/ml) were reacted with Ramos-S cells and binding determined by flow cytometry.
†Median fluorescence intensity value (normalized to WT). ND, not determined.

10.3389/fimmu.2022.889372

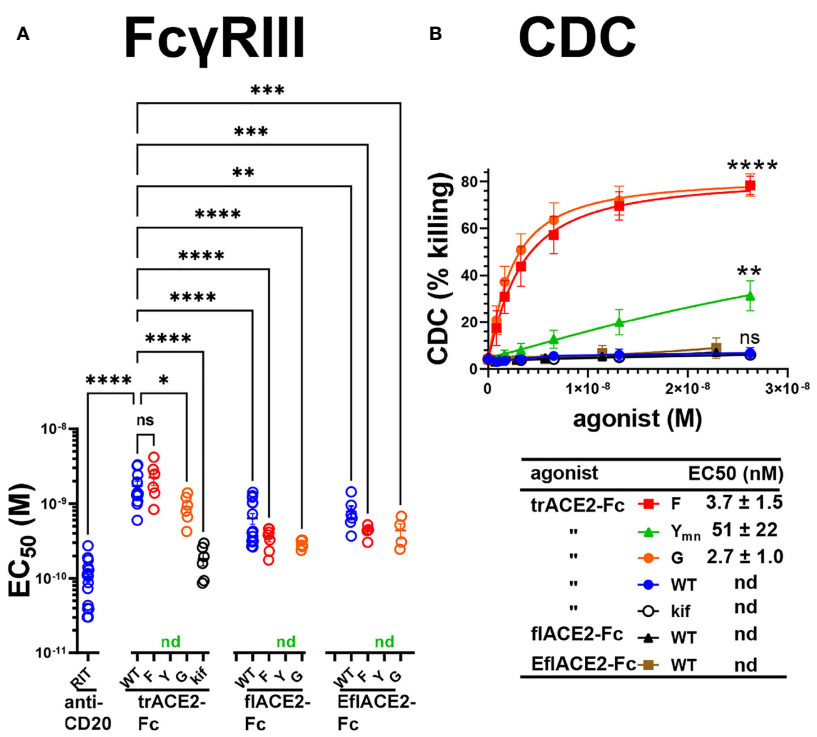

FIGURE 5
FcγR and complement dependent effector functions of the ACE2-Fc decoy proteins. **(A)** Activation of FcγRIIIa by ACE2-Fc proteins. ACE2-Fc proteins activated FcγRIIIa, except for the Fc H429Y mutants which failed to stimulate in any ACE2 format either as oligomeric or monomeric forms. Ramos-S target cells were opsonized with trACE2-Fc, flACE2-Fc and EflACE2-Fc, WT and Fc variants, including H429F, F; H429Y, Y; E430G, G or trACE2-Fc-*kif*, produced from trACE2-Fc WT in 293Expi cells in the presence of the mannosidase inhibitor kifunensine. In some experiments Ramos-S target cells were separately opsonized with Rituximab, RIT. These opsonized targets were incubated with FcγRIIIa/NF-κB-RE nanoluciferase reporter cells and FcγRIIIa activation measured by the induction of nanoluciferase (RLU). Activation data (**Supplementary Figures S1B, C**) were fitted to agonist response curves to estimate EC_{50}(nM); nd, not determined as there was insufficient activity for the data to be fitted. EC_{50} values from the curve fits are shown. Mean ± SEM, n is indicated by individual symbols for each independent experiment, one-way ANOVA with Dunnett's multiple comparisons test, comparing to trACE2-Fc WT. p > 0.05 (ns), ≤ 0.05 (*), ≤ 0.01 (**), ≤ 0.001 (***), ≤ 0.0001 (****). **(B)** H429F, and E430G Fc mutant ACE2-Fc proteins are potent mediators of complement lysis of SARS-CoV-2 S expressing cells. Flow cytometric analysis of complement-dependent cytotoxicity (CDC) of opsonized Ramos-S cells was determined in the presence of a 1/3 dilution of a pool of normal human serum (from >5 individuals) as a source of complement. Plots are mean ± SEM, n = 3 independent experiments. Two-way ANOVA with Dunnett's multiple comparisons test comparing to trACE2-Fc-WT for main column effect, p > 0.05 (ns), ≤ 0.01 (**), ≤ 0.0001 (****). EC_{50} (nM) values are mean ± SEM each from 3 curve fits.

The second major Fc-dependent effector system is the classical complement pathway. The activation of complement by the ACE2-Fc proteins was tested initially by ELISA for the capacity to fix complement components C5b-9 and then to mediate complement-dependent killing of cells expressing SARS-CoV-2 spike protein. The fixing of C5b-9 (Supplementary Figure S1D) which forms the membrane attack complex, was achieved by all Fc fusions but was enhanced by both the H429F Fc mutation and the hexamerising E430G mutation of trACE2-Fc compared to unmodified Fc-WT. Despite the H429Y mutated Fc preforming oligomers, which might be anticipated to confer superior complement fixation, this was not apparent and the trACE2-Fc-H429Y oligomer form, showed similar C5b-9 fixation as the trACE2-Fc-WT and glycomodifed trACE2-Fc-*kif*, (Supplementary Figure S1D).

Despite the ELISA showing that the trACE2-Fc-WT fusions with an unmodified Fc fix C5b-9, analysis of cell killing showed that the unmodified Fc-WT fusion proteins of any ACE2 format failed to mediate significant CDC (Figure 5B). In stark contrast to this CDC inactivity, both the H429F and the hexamerising E430G Fc mutants of trACE2-Fc fusion proteins were remarkably active in mediating complement lysis of Ramos-S cells (Figure 5B). The monomeric form of trACE2-Fc-H429Y_{mn} was active, although substantially less potent than the H429F mutant. H429 in the Fc is thus a site for modification that remarkably potentiates the Fc's capacity for stimulating complement-mediated target lysis.

Discussion

In this study we examined different antiviral functions of ACE2-Fc virus decoy proteins. As in IgG antibodies, the Fc-

region drives the effector responses mediated by the IgG-Fc fusion proteins. *In vivo* SARS-CoV-2 challenge models (57–61) have found Fc immune functions of antibodies decreased virus load, spread from nasal tissue to major organ systems, cytokine storm and inflammation, and mortality. In contrast, ablating Fc function resulted in increased disease severity or mortality (58–60, 83). Recently a non-neutralizing human mAb with Fc-enhanced ADCC activity conferred partial protection in a SARS-CoV-2 infection model and contributed to complete protection in combination with a neutralizing mAb (80). Indeed, ADCC potency is an indicator of humoral responses that protect against severe disease in humans (81). While complement activation features in the pathophysiology of severe COVID-19 it is likely to be initially protective (84) and is an identified function of anti-SARS-CoV-2 therapeutic antibodies (85). The Fc portion is thus an important element to optimize for the development of ACE2-Fc as an anti-SARS-CoV-2 antiviral molecule and for viral entry receptors fused to Fc more generally.

Hence, we have manipulated three major antiviral activities of ACE2-Fc by modifying its Fc portion to enhance the existing decoy (neutralization) action of the ACE2 component, complement mediated killing and activation of FcγR. Firstly, the H429Y mutation, in the Fc CH3 domain outside the Fcγ receptor or complement contact sites of the CH2 domain, resulted in the formation of oligomers of the decoy protein which resulted in improved neutralization potency. The improved neutralization activity and oligomeric nature of the H429Y Fc mutant decoys mimic the polymeric antibody classes, IgA (86) and IgM (87) where avidity contributes to the efficacy of SARS-CoV-2 neutralization. Fc : Fc interactions are a recognized property of IgG antibodies (88) and their stabilization by mutation can lead to the formation of in solution oligomers (89). In contrast, the E430G modification of IgG is known to promote "on-target" oligomerization (hexamerization) of IgG (79), but did not significantly alter SARS-CoV-2 neutralization activity in any ACE2-Fc format. In contrast, the H429Y Fc mutation enhanced neutralization potency of all formats of the ACE2-Fc decoy proteins. H429Y Fc mutation in combination with the inclusion of the collectrin domain and the triple ACE2 mutations enhancing affinity for S (43), (i.e. EflACE2-Fc-H429Y) resulted in an overall 600-fold increased SARS-CoV-2 neutralization potency over that of the monomeric truncated ACE2 domain. The neutralization potency of EflACE2-Fc-H429Y (4.2 nM) was comparable to that of the laboratory equivalent of the therapeutic mAb REGN 10933 (casirivimab, 3.6 nM). A feature of the H429Y mutation was the loss of binding by FcγRIIIa. Mutations at the CH2/CH3 interface can affect low affinity FcγR binding to the Fc (90), suggesting these sites, though distant, can affect each other (91).

Secondly, the phenylalanine substitution of histidine 429 (H429F) of the ACE2-Fc proteins did not enhance neutralization but did transform CDC against S expressing targets. This improved CDC activity was like that of E430G mutated ACE2-Fc, a known "on-target" Fc-hexamerising mutation, a format optimal for C1 binding and activation (78, 79). Lastly, FcγR potency of trACE2-Fc was improved by modifying the Fc glycan (82) to enhance FcγRIII binding (92). It is likely that similar treatment of flACE2-Fc WT and EflACE2-Fc WT, or alternatively, amino acid substitution to increase affinity for FcγRIIIa (93), would similarly further improve their FcγRIII activating potency. Notably, FcγRIII activation was a little reduced for the decoy lacking the collection domain, indicating the formatting of Fc-fusion proteins can impact Fc-mediated activity.

We have demonstrated ACE2-Fc to be a potent agent against SARS-CoV-2, not only for neutralization but also for the harnessing of Fc-mediated effector functions. The exemplar Fc modifications demonstrated herein illustrate the potential for the tuning of Fc function to optimize virus neutralization, FcγR interaction and complement activation. This selection of desired functional profiles could aid the deployment of broadly effective ACE2-Fc, mAbs and other Fc therapeutics. There has been a rapid progression of multiple different SARS-CoV-2 mAbs to clinical use that is likely to herald increased deployment of mAbs clinically for infectious diseases. The optimization of Fc functions will make a significant difference to their clinical success. Furthermore, the world remains susceptible to new pandemics and vaccine escape variants. Thus, an antiviral decoy comprising optimized Fc fusion to a viral entry receptor such as ACE2-Fc, is an important option for deploying a rapid first line of defense to contain new zoonotic viral threats while vaccines, mAbs and antiviral drugs are being developed.

Data availability statement

The raw data supporting the conclusions of this article will be made available by the authors, without undue reservation. PDB coordinate files are available from the authors on request.

Author contributions

BW and PMH conceived and planned the experiments. BW, LK, HT, SE, EL, KC, L-JC, FM, WL, NG, SP, GH, PP, and JC performed the experiments and analyzed the data. JB, DG, LB, MvZ, AW, AC, W-HT, KS, SK, and PMH provided supervision and analyzed the data. BW and PMH wrote the manuscript with input from all other authors. All authors contributed to the article and approved the submitted version.

Funding

The Medical Research Future Fund (MRFF 2002073) and Victorian State Government COVID research funding

supported the research of AW, DG, W-HT, SK, PH, and SP, LB (1175865) with contribution from the Victorian Operational Infrastructure Support Program and Australian Government NHMRC Independent Research Institutes Infrastructure Support Scheme. NHMRC project grants supported PH, BW. (1145303). Investigator Grants are held by JB (1173046), KS (1177174) and DG (2008913) and program grants by SK (1149990), LB (1055214). DG (1117766), W-HT, SK, MZ (1117687) and AW receive National Health and Medical Research Council (NHMRC) fellowships. DG is supported by the Australian Research Council (ARC; CE140100011). NG was supported by an ARC DECRA Fellowship (DE210100705). SP and LB funded by a Heart Foundation Vanguard Grant (105798). The Melbourne WHO Collaborating Centre for Reference and Research on Influenza is supported by the Australian Government Department of Health. W-HT is a Howard Hughes Medical Institute–Wellcome Trust International Research Scholar (208693/Z/17/Z).

Acknowledgments

We thank Dr Gaoqian Feng for pooled human serum. Thanks to Reema Bajaj for reading the manuscript.

Conflict of interest

Authors PMH and BW are inventors on a provisional patent filing by the Burnet Institute.

The remaining authors declare that the research was conducted in the absence of any commercial or financial relationships that could be construed as a potential conflict of interest.

Publisher's note

Supplementary material

The Supplementary Material for this article can be found online at: https://www.frontiersin.org/articles/10.3389/fimmu.2022.889372/full#supplementary-material

SUPPLEMENTARY FIGURE 1

Human ACE2-Fc proteins activate FcγRIIIa and Complement. **(A)** FcγRIIIa binding. The ACE2-Fc WT fusion proteins and their variants (5 µg/ml) were reacted with Ramos-S cells (Ramos cells expressing spike protein) and Fc receptor binding evaluated by flow cytometry using biotinylated dimeric rsFcγRIIIa, followed by streptavidin-APC. (mean of 3 replicates). **(B, C)** Activation of FcγRIIIa. ACE2-Fc proteins are potent activators of FcγRIIIa apart from the Fc H429Y mutants which fail to stimulate FcγRIIIa in any ACE2 format. Ramos-S target cells were opsonized with **(B)** trACE2-Fc and **(C)** flACE2-Fc, WT and separately with Fc variants, including H429F, F; H429Y unfractionated, Y; H429Y oligomers, Y_{og}; H429Y monomer, Y_{mn}; E430G, G or trACE2-Fc *kif* produced from trACE2-Fc WT in 293Expi cells in the presence of the mannosidase inhibitor kifunensine. Ramos-S target cells were separately opsonized with Rituximab, RIT. These opsonized targets were incubated with FcγRIIIa-NF-κB-RE nanoluciferase reporter cells and FcγRIIIa activation measured by the induction of nanoluciferase (RLU). Representative activation data showing fitting to agonist response curves to determine each EC_{50} (nM) data point shown in **Figure 5A**. **(D)** ACE2-Fc fusion proteins comprising Fc regions with either of the H429F and E430G mutations, strongly fix complement C5b-9. In ELISA analysis the indicated concentration series of trACE2-Fc or its Fc variants, was bound to SARS-CoV-2 spike RBD-biotin (2.5 µg/ml) captured by plate bound avidin (2 µg/ml). Following incubation with human serum the formation of C5b-9 was determined, (mean ± SD); two independent experiments.

References

1. Zhong NS, Zheng BJ, Li YM, Poon ZH, Chan KH, Li PH, et al. Guan: Epidemiology and cause of severe acute respiratory syndrome (SARS) in guangdong, people's republic of China, in February, 2003. *Lancet* (2003) 362 (9393):1353–8. doi: 10.1016/s0140-6736(03)14630-2

2. Zaki AM, van Boheemen S, Bestebroer TM, Osterhaus AD, Fouchier RA. Isolation of a novel coronavirus from a man with pneumonia in Saudi Arabia. *N Engl J Med* (2012) 367(19):1814–20. doi: 10.1056/NEJMoa1211721

3. Zhu N, Zhang D, Wang W, Li X, Yang B, Song J, et al. A novel coronavirus from patients with pneumonia in China, 2019. *N Engl J Med* (2020) 382(8):727–33. doi: 10.1056/NEJMoa2001017

4. Wacharapluesadee S, Tan CW, Maneeorn P, Duengkae P, Zhu F, Joyjinda Y, et al. Evidence for SARS-CoV-2 related coronaviruses circulating in bats and pangolins in southeast Asia. *Nat Commun* (2021) 12(1):972. doi: 10.1038/s41467-021-21240-1

5. Wang N, Li SY, Yang XL, Huang HM, Zhang YJ, Guo H, et al. Serological evidence of bat SARS-related coronavirus infection in humans, China. *Virol Sin* (2018) 33(1):104–7. doi: 10.1007/s12250-018-0012-7

6. Heinz FX, Stiasny K. Distinguishing features of current COVID-19 vaccines: knowns and unknowns of antigen presentation and modes of action. *NPJ Vaccines* (2021) 6(1):104. doi: 10.1038/s41541-021-00369-6

7. Corti D, Purcell LA, Snell G, Veesler D. Tackling COVID-19 with neutralizing monoclonal antibodies. *Cell* (2021) 184(12):3086–108. doi: 10.1016/j.cell.2021.05.005

8. Tragni V, Preziusi F, Laera L, Onofrio A, Mercurio I, Todisco S, et al. Modeling SARS-CoV-2 spike/ACE2 protein-protein interactions for predicting the binding affinity of new spike variants for ACE2, and novel ACE2 structurally related human protein targets, for COVID-19 handling in the 3PM context. *EPMA J* (2022) 13(1):149–75. doi: 10.1007/s13167-021-00267-w

9. Tegally H, Wilkinson E, Giovanetti M, Iranzadeh A, Fonseca V, Giandhari J, et al. Detection of a SARS-CoV-2 variant of concern in south Africa. *Nature* (2021) 592(7854):438–43. doi: 10.1038/s41586-021-03402-9

10. Harvey WT, Carabelli AM, Jackson B, Gupta RK, Thomson EC, Harrison EM, et al. SARS-CoV-2 variants, spike mutations and immune escape. *Nat Rev Microbiol* (2021) 19(7):409–24. doi: 10.1038/s41579-021-00573-0

11. Yuan M, Huang D, Lee CD, Wu NC, Jackson AM, Zhu X, et al. Structural and functional ramifications of antigenic drift in recent SARS-CoV-2 variants. *Science* (2021) 373(6556):818–23. doi: 10.1126/science.abh1139

12. Collier DA, De Marco A, Ferreira I, Meng B, Datir RP, Walls AC, et al. Sensitivity of SARS-CoV-2 B.1.1.7 to mRNA vaccine-elicited antibodies. *Nature* (2021) 593(7857):136–41. doi: 10.1038/s41586-021-03412-7

13. Wang P, Nair MS, Liu L, Iketani S, Luo Y, Guo Y, et al. Antibody resistance of SARS-CoV-2 variants B.1.351 and B.1.1.7. *Nature* (2021) 593(7857):130–5. doi: 10.1038/s41586-021-03398-2

14. Chen RE, Winkler ES, Case JB, Aziati ID, Bricker TL, Joshi A, et al. *In vivo* monoclonal antibody efficacy against SARS-CoV-2 variant strains. *Nature* (2021) 596(7870):103–8. doi: 10.1038/s41586-021-03720-y

15. Liu H, Wei P, Zhang Q, Chen Z, Aviszus K, Downing W, et al. 501Y.V2 and 501Y.V3 variants of SARS-CoV-2 lose binding to bamlanivimab *in vitro*. *MAbs* (2021) 13(1):1919285. doi: 10.1080/19420862.2021.1919285

16. Cele S, Gazy I, Jackson L, Hwa SH, Tegally H, Lustig G, et al. Escape of SARS-CoV-2 501Y.V2 from neutralization by convalescent plasma. *Nature* (2021) 593(7857):142–6. doi: 10.1038/s41586-021-03471-w

17. Wibmer CK, Ayres F, Hermanus T, Madzivhandila M, Kgagudi P, Oosthuysen B, et al. SARS-CoV-2 501Y.V2 escapes neutralization by south African COVID-19 donor plasma. *Nat Med* (2021) 27(4):622–5. doi: 10.1038/s41591-021-01285-x

18. Wang Z, Schmidt F, Weisblum Y, Muecksch F, Barnes CO, Finkin S, et al. mRNA vaccine-elicited antibodies to SARS-CoV-2 and circulating variants. *Nature* (2021) 592(7855):616–22. doi: 10.1038/s41586-021-03324-6

19. Kustin T, Harel N, Finkel U, Perchik S, Harari S, Tahor M, et al. Evidence for increased breakthrough rates of SARS-CoV-2 variants of concern in BNT162b2-mRNA-vaccinated individuals. *Nat Med* (2021) 27(8):1379–84. doi: 10.1038/s41591-021-01413-7

20. Sabino EC, Buss LF, Carvalho MPS, Prete CAJr., Crispim MAE, Fraiji NA, et al. Resurgence of COVID-19 in manaus, Brazil, despite high seroprevalence. *Lancet* (2021) 397(10273):452–5. doi: 10.1016/S0140-6736(21)00183-5

21. Pulliam JRC, van Schalkwyk C, Govender N, von Gottberg A, Cohen C, Groome MJ, et al. Increased risk of SARS-CoV-2 reinfection associated with emergence of Omicron in South Africa. *Science* (2022) 76(6593):eabn4947. doi: 10.1126/science.abn4947

22. Ju B, Zhang Q, Ge J, Wang R, Sun J, Ge X, et al. Human neutralizing antibodies elicited by SARS-CoV-2 infection. *Nature* (2020) 584(7819):115–9. doi: 10.1038/s41586-020-2380-z

23. Zhou P Fau - Yuan M, Yuan G, Auid M, Song G, Beutler N, Shaabani N, et al. A human antibody reveals a conserved site on beta-coronavirus spike proteins and confers protection against SARS-CoV-2 infection. *Sci Transl Med* (2022) 14 (637):eabi9215. doi: 10.1126/scitranslmed.abi9215

24. Daszak P, Olival KJ, Li H. A strategy to prevent future epidemics similar to the 2019-nCoV outbreak. *Biosaf Health* (2020) 2(1):6–8. doi: 10.1016/j.bsheal.2020.01.003

25. Stegmann C, Hochdorfer D, Lieber D, Subramanian N, Stohr D, Laib Sampaio K, et al. A derivative of platelet-derived growth factor receptor alpha binds to the trimer of human cytomegalovirus and inhibits entry into fibroblasts and endothelial cells. *PloS Pathog* (2017) 13(4):e1006273. doi: 10.1371/journal.ppat.1006273

26. Zhang Z, Zeng E, Zhang L, Wang W, Jin Y, Sun J, et al. Potent prophylactic and therapeutic efficacy of recombinant human ACE2-Fc against SARS-CoV-2 infection in vivo. *Cell Discovery* (2021) 7(1):65. doi: 10.1038/s41421-021-00302-0

27. Zhang L, Narayanan KK, Cooper L, Chan KK, Devlin CA, Aguhob A, et al. An engineered ACE2 decoy receptor can be administered by inhalation and potently targets the BA.1 and BA.2 omicron variants of SARS-CoV-2. *bioRxiv* (2022) 2022:3.28.486075. doi: 10.1101/2022.03.28.486075

28. Higuchi Y, Suzuki T, Arimori T, Ikemura N, Mihara E, Kirita Y, et al. Engineered ACE2 receptor therapy overcomes mutational escape of SARS-CoV-2. *Nat Commun* (2021) 12(1):3802. doi: 10.1038/s41467-021-24013-y

29. Sims JJ, Greig JA, Michalson KT, Lian S, Martino RA, Meggersee R, et al. Intranasal gene therapy to prevent infection by SARS-CoV-2 variants. *PloS Pathog* (2021) 17(7):e1009544. doi: 10.1371/journal.ppat.1009544

30. Ikemura N, Taminishi S, Inaba T, Arimori T, Motooka D, Katoh K, et al. Engineered ACE2 counteracts vaccine-evading SARS-CoV-2 omicron variant. *bioRxiv* (2022) 2021:12.22.473804. doi: 10.1101/2021.12.22.473804

31. Tanaka S, Nelson G, Olson CA, Buzko O, Higashide W, Shin A, et al. An ACE2 triple decoy that neutralizes SARS-CoV-2 shows enhanced affinity for virus variants. *Sci Rep* (2021) 11(1):12740. doi: 10.1038/s41598-021-91809-9

32. Walls AC, Park YJ, Tortorici MA, Wall A, McGuire AT, Veesler D. Structure, function, and antigenicity of the SARS-CoV-2 spike glycoprotein. *Cell* (2020) 183(6):1735. doi: 10.1016/j.cell.2020.11.032

33. Zhou P, Yang XL, Wang XG, Hu B, Zhang L, Zhang W, et al. A pneumonia outbreak associated with a new coronavirus of probable bat origin. *Nature* (2020) 579(7798):270–3. doi: 10.1038/s41586-020-2012-7

34. Devarakonda CKV, Meredith E, Ghosh M, Shapiro LH. Coronavirus receptors as immune modulators. *J Immunol* (2021) 206(5):923–9. doi: 10.4049/jimmunol.2001062

35. Obukhov AG, Stevens BR, Prasad R, Li Calzi S, Boulton ME, Raizada MK, et al. SARS-CoV-2 infections and ACE2: Clinical outcomes linked with increased morbidity and mortality in individuals with diabetes. *Diabetes* (2020) 69(9):1875–86. doi: 10.2337/dbi20-0019

36. Yan R, Zhang Y, Li Y, Xia L, Guo Y, Zhou Q. Structural basis for the recognition of SARS-CoV-2 by full-length human ACE2. *Science* (2020) 367 (6485):1444–8. doi: 10.1126/science.abb2762

37. Bourgonje AR, Abdulle AE, Timens W, Hillebrands JL, Navis GJ, Gordijn SJ, et al. Angiotensin-converting enzyme 2 (ACE2), SARS-CoV-2 and the pathophysiology of coronavirus disease 2019 (COVID-19). *J Pathol* (2020) 251 (3):228–48. doi: 10.1002/path.5471

38. Liu P, Wysocki J, Souma T, Ye M, Ramirez V, Zhou B, et al. Novel ACE2-Fc chimeric fusion provides long-lasting hypertension control and organ protection in mouse models of systemic renin angiotensin system activation. *Kidney Int* (2018) 94(1):114–25. doi: 10.1016/j.kint.2018.01.029

39. Zoufaly A, Poglitsch M, Aberle JH, Hoepler W, Seitz T, Traugott M, et al. Human recombinant soluble ACE2 in severe COVID-19. *Lancet Respir Med* (2020) 8(11):1154–8. doi: 10.1016/S2213-2600(20)30418-5

40. Monteil V, Kwon H, Prado P, Hagelkruys A, Wimmer RA, Stahl M, et al. Inhibition of SARS-CoV-2 infections in engineered human tissues using clinical-grade soluble human ACE2. *Cell* (2020) 181(4):905–913 e7. doi: 10.1016/j.cell.2020.04.004

41. Xiao T, Lu J, Zhang J, Johnson RI, McKay LGA, Storm N, et al. A trimeric human angiotensin-converting enzyme 2 as an anti-SARS-CoV-2 agent. *Nat Struct Mol Biol* (2021) 28(2):202–9. doi: 10.1038/s41594-020-00549-3

42. Li Y, Wang H, Tang X, Fang S, Ma D, Du C, et al. SARS-CoV-2 and three related coronaviruses utilize multiple ACE2 orthologs and are potently blocked by an improved ACE2-ig. *J Virol* (2020) 94(22):e01283–20. doi: 10.1128/JVI.01283-20

43. Chan KK, Dorosky D, Sharma P, Abbasi SA, Dye JM, Kranz DM, et al. Engineering human ACE2 to optimize binding to the spike protein of SARS coronavirus 2. *Science* (2020) 369(6508):1261–5. doi: 10.1126/science.abc0870

44. Glasgow A, Glasgow J, Limonta D, Solomon P, Lui I, Zhang Y, et al. Engineered ACE2 receptor traps potently neutralize SARS-CoV-2. *Proc Natl Acad Sci U.S.A.* (2020) 117(45):28046–55. doi: 10.1073/pnas.2016093117

45. Cohen-Dvashi H, Weinstein J, Katz M, Eilon M, Mor Y, Shimon A, et al. Coronacept – a potent immunoadhesin against SARS-CoV-2. *bioRxiv* (2020) 2020:8.12.247940. doi: 10.1101/2020.08.12.247940

46. Lei C, Qian K, Li T, Zhang S, Fu W, Ding M, et al. Neutralization of SARS-CoV-2 spike pseudotyped virus by recombinant ACE2-ig. *Nat Commun* (2020) 11 (1):2070. doi: 10.1038/s41467-020-16048-4

47. Liu P, Xie X, Gao L, Jin J. Designed variants of ACE2-Fc that decouple anti-SARS-CoV-2 activities from unwanted cardiovascular effects. *Int J Biol Macromol* (2020) 165(Pt B):1626–33. doi: 10.1016/j.ijbiomac.2020.10.120

48. Abd El-Aziz TM, Al-Sabi A, Stockand JD. Human recombinant soluble ACE2 (hrsACE2) shows promise for treating severe COVID-19. *Signal Transduct Target Ther* (2020) 5(1):258. doi: 10.1038/s41392-020-00374-6

49. Zhang L, Dutta S, Xiong S, Chan M, Chan KK, Fan TM, et al. Engineered ACE2 decoy mitigates lung injury and death induced by SARS-CoV-2 variants. *Nat Chem Biol* (2022) 18(3):342–51. doi: 10.1038/s41589-021-00965-6

50. Iwanaga N, Cooper L, Rong L, Maness NJ, Beddingfield B, Qin Z, et al. ACE2-IgG1 fusions with improved *in vitro* and *in vivo* activity against SARS-CoV-2. *iScience* (2022) 25(1):103670. doi: 10.1016/j.isci.2021.103670

51. Tada T, Fan C, Chen JS, Kaur R, Stapleford KA, Gristick H, et al. An ACE2 microbody containing a single immunoglobulin Fc domain is a potent inhibitor of SARS-CoV-2. *Cell Rep* (2020) 33(12):108528. doi: 10.1016/j.celrep.2020.108528

52. Huang KY, Lin MS, Kuo TC, Chen CL, Lin CC, Chou YC, et al. Humanized COVID-19 decoy antibody effectively blocks viral entry and prevents SARS-CoV-2 infection. *EMBO Mol Med* (2020) 13(1):e12828. doi: 10.15252/emmm.202012828

53. Svilenov HL, Sacherl J, Reiter A, Wolff LS, Cheng CC, Stern M, et al. Picomolar inhibition of SARS-CoV-2 variants of concern by an engineered ACE2-IgG4-Fc fusion protein. *Antiviral Res* (2021) 196:105197. doi: 10.1016/j.antiviral.2021.105197

54. Liu Z, VanBlargan LA, Bloyet LM, Rothlauf PW, Chen RE, Stumpf S, et al. Identification of SARS-CoV-2 spike mutations that attenuate monoclonal and serum antibody neutralization. *Cell Host Microbe* (2021) 29(3):477–488 e4. doi: 10.1016/j.chom.2021.01.014

55. Jing W, Procko E. ACE2-based decoy receptors for SARS coronavirus 2. *Proteins* (2021) 89(9):1065–78. doi: 10.1002/prot.26140

56. Stapleton NM, Einarsdottir HK, Stemerding AM, Vidarsson G. The multiple facets of FcRn in immunity. *Immunol Rev* (2015) 268(1):253–68. doi: 10.1111/imr.12331

57. Schafer A, Muecksch F, Lorenzi JCC, Leist SR, Cipolla M, Bournazos S, et al. Antibody potency, effector function, and combinations in protection and therapy for SARS-CoV-2 infection in vivo. *J Exp Med* (2021) 218(3):e20201993. doi: 10.1084/jem.20201993

58. Ullah I, Prevost J, Ladinsky MS, Stone H, Lu M, Anand SP, et al. Live imaging of SARS-CoV-2 infection in mice reveals that neutralizing antibodies require Fc function for optimal efficacy. *Immunity* (2021) 54(9):2143–2158 e15. doi: 10.1016/j.immuni.2021.08.015

59. Suryadevara N, Shrihari S, Gilchuk P, VanBlargan LA, Binshtein E, Zost SJ, et al. Neutralizing and protective human monoclonal antibodies recognizing the n-terminal domain of the SARS-CoV-2 spike protein. *Cell* (2021) 184(9):2316–2331 e15. doi: 10.1016/j.cell.2021.03.029

60. Yamin R, Jones AT, Hoffmann HH, Schafer A, Kao KS, Francis RL, et al. Fc-engineered antibody therapeutics with improved anti-SARS-CoV-2 efficacy. *Nature* (2021) 599(7885):465–70. doi: 10.1038/s41586-021-04017-w

61. Li D, Edwards RJ, Manne K, Martinez DR, Schafer A, Alam SM, et al. *In vitro* and *in vivo* functions of SARS-CoV-2 infection-enhancing and neutralizing antibodies. *Cell* (2021) 184(16):4203–4219 e32. doi: 10.1016/j.cell.2021.06.021

62. Chen Y, Sun L, Ullah I, Beaudoin-Bussières G, Anand SP, Hederman AP, et al. Engineered ACE2-Fc counters murine lethal SARS-CoV-2 infection through direct neutralization and Fc-effector activities. *bioRxiv* (2021) 2021:11.24.469776. doi: 10.1101/2021.11.24.469776

63. Aricescu AR, Lu W, Jones EY. A time- and cost-efficient system for high-level protein production in mammalian cells. *Acta Crystallogr D Biol Crystallogr* (2006) 62(Pt 10):1243–50. doi: 10.1107/S0907444906029799

64. Juno JA, Tan HX, Lee WS, Reynaldi A, Kelly HG, Wragg K, et al. Humoral and circulating follicular helper T cell responses in recovered patients with COVID-19. *Nat Med* (2020) 26(9):1428–34. doi: 10.1038/s41591-020-0995-0

65. Wines BD, Hulett MD, Jamieson GP, Trist HM, Spratt JM, Hogarth PM. Identification of residues in the first domain of human Fc alpha receptor essential for interaction with IgA. *J Immunol* (1999) 162(4):2146–53.

66. Khoury DS, Wheatley AK, Ramuta MD, Reynaldi A, Cromer D, Subbarao K, et al. Measuring immunity to SARS-CoV-2 infection: comparing assays and animal models. *Nat Rev Immunol* (2020) 20(12):727–38. doi: 10.1038/s41577-020-00471-1

67. Lee WS, Selva KJ, Davis SK, Wines BD, Reynaldi A, Esterbauer R, et al. Decay of Fc-dependent antibody functions after mild to moderate COVID-19. *Cell Rep Med* (2021) 2(6):100296. doi: 10.1016/j.xcrm.2021.100296

68. Wines BD, Vanderven HA, Esparon SE, Kristensen AB, Kent SJ, Hogarth PM. Dimeric FcgammaR ectodomains as probes of the Fc receptor function of anti-influenza virus IgG. *J Immunol* (2016) 197(4):1507–16. doi: 10.4049/jimmunol.1502551

69. Hartley GE, Edwards ESJ, Aui PM, Varese N, Stojanovic S, McMahon J, et al. Rapid generation of durable b cell memory to SARS-CoV-2 spike and nucleocapsid proteins in COVID-19 and convalescence. *Sci Immunol* (2020) 5(54): eabf8891. doi: 10.1126/sciimmunol.abf8891

70. Kurtovic L, Agius PA, Feng G, Drew DR, Ubillos I, Sacarlal J, et al. Induction and decay of functional complement-fixing antibodies by the RTS,S malaria vaccine in children, and a negative impact of malaria exposure. *BMC Med* (2019) 17(1):45. doi: 10.1186/s12916-019-1277-x

71. Lopez E, Haycroft ER, Adair A, Mordant FL, O'Neill MT, Pymm P, et al. Simultaneous evaluation of antibodies that inhibit SARS-CoV-2 variants *via* multiplex assay. *JCI Insight* (2021) 6(16):e150012. doi: 10.1172/jci.insight.150012

72. Amanat F, Stadlbauer D, Strohmeier S, Nguyen THO, Chromikova V, McMahon M, et al. A serological assay to detect SARS-CoV-2 seroconversion in humans. *Nat Med* (2020) 26(7):1033–6. doi: 10.1038/s41591-020-0913-5

73. Jumper J, Evans R, Pritzel A, Green T, Figurnov M, Ronneberger O, et al. Highly accurate protein structure prediction with AlphaFold. *Nature* (2021) 596 (7873):583–9. doi: 10.1038/s41586-021-03819-2

74. Varadi M, Anyango S, Deshpande M, Nair S, Natassia C, Yordanova G, et al. AlphaFold protein structure database: massively expanding the structural coverage of protein-sequence space with high-accuracy models. *Nucleic Acids Res* (2022) 50 (D1):D439–44. doi: 10.1093/nar/gkab1061

75. Honorato RV, Koukos PI, Jimenez-Garcia B, Tsaregorodtsev A, Verlato M, Giachetti A, et al. Structural biology in the clouds: The WeNMR-EOSC ecosystem. *Front Mol Biosci* (2021) 8:729513. doi: 10.3389/fmolb.2021.729513

76. van Zundert GCP, Rodrigues J, Trellet M, Schmitz C, Kastritis PL, Karaca E, et al. The HADDOCK2.2 web server: User-friendly integrative modeling of biomolecular complexes. *J Mol Biol* (2016) 428(4):720–5. doi: 10.1016/j.jmb.2015.09.014

77. Prevost J, Finzi A. The great escape? SARS-CoV-2 variants evading neutralizing responses. *Cell Host Microbe* (2021) 29(3):322–4. doi: 10.1016/j.chom.2021.02.010

78. Diebolder CA, Beurskens FJ, de Jong RN, Koning RI, Strumane K, Lindorfer MA, et al. Complement is activated by IgG hexamers assembled at the cell surface. *Science* (2014) 343(6176):1260–3. doi: 10.1126/science.1248943

79. Strasser J, de Jong RN, Beurskens FJ, Wang G, Heck AJR, Schuurman J, et al. Unraveling the macromolecular pathways of IgG oligomerization and complement activation on antigenic surfaces. *Nano Lett* (2019) 19(7):4787–96. doi: 10.1021/acs.nanolett.9b02220

80. Beaudoin-Bussières G, Chen Y, Ullah I, Prévost J, Tolbert WD, Symmes K, et al. A Fc-enhanced NTD-binding non-neutralizing antibody delays virus spread and synergizes with a nAb to protect mice from lethal SARS-CoV-2 infection. *Cell Rep* (2022) 38(7):110368. doi: 10.1016/j.celrep.2022.110368

81. Zohar T, Loos C, Fischinger S, Atyeo C, Wang C, Slein MD, et al. Compromised humoral functional evolution tracks with SARS-CoV-2 mortality. *Cell* (2020) 183(6):1508–1519 e12. doi: 10.1016/j.cell.2020.10.052

82. van Berkel PH, Gerritsen J, van Voskuilen E, Perdok G, Vink T, van de Winkel JG, et al. Rapid production of recombinant human IgG with improved ADCC effector function in a transient expression system. *Biotechnol Bioeng* (2010) 105(2):350–7. doi: 10.1002/bit.22535

83. Winkler ES, Gilchuk P, Yu J, Bailey AL, Chen RE, Chong Z, et al. Human neutralizing antibodies against SARS-CoV-2 require intact Fc effector functions for optimal therapeutic protection. *Cell* (2021) 184(7):1804–1820 e16. doi: 10.1016/j.cell.2021.02.026

84. Afzali B, Noris M, Lambrecht BN, Kemper C. The state of complement in COVID-19. *Nat Rev Immunol* (2022) 22(2):77–84. doi: 10.1038/s41577-021-00665-1

85. Yu J, Tostanoski LH, Peter L, Mercado NB, McMahan K, Mahrokhian SH, et al. DNA Vaccine protection against SARS-CoV-2 in rhesus macaques. *Science* (2020) 369(6505):806–11. doi: 10.1126/science.abc6284

86. Wang Z, Lorenzi JCC, Muecksch F, Finkin S, Viant C, Gaebler C, et al. Enhanced SARS-CoV-2 neutralization by dimeric IgA. *Sci Transl Med* (2021) 13 (577):eabf1555. doi: 10.1126/scitranslmed.abf1555

87. Gasser R, Cloutier M, Prevost J, Fink C, Ducas E, Ding S, et al. Major role of IgM in the neutralizing activity of convalescent plasma against SARS-CoV-2. *Cell Rep* (2021) 34(9):108790. doi: 10.1016/j.celrep.2021.108790

88. Moller NP. Fc-mediated immune precipitation. i. a new role of the Fc-portion of IgG. *Immunology* (1979) 38(3):631–40.

89. de Jong RN, Beurskens FJ, Verploegen S, Strumane K, van Kampen MD, Voorhorst M, et al. A novel platform for the potentiation of therapeutic antibodies based on antigen-dependent formation of IgG hexamers at the cell surface. *PloS Biol* (2016) 14(1):e1002344. doi: 10.1371/journal.pbio.1002344

90. Shields RL, Namenuk AK, Hong K, Meng YG, Rae J, Briggs J, et al. High resolution mapping of the binding site on human IgG1 for Fc gamma RI, Fc gamma RII, Fc gamma RIII, and FcRn and design of IgG1 variants with improved binding to the Fc gamma R. *J Biol Chem* (2001) 276(9):6591–604. doi: 10.1074/jbc.M009483200

91. Orlandi C, Deredge D, Ray K, Gohain N, Tolbert W, DeVico AL, et al. Antigen-induced allosteric changes in a human IgG1 Fc increase low-affinity Fcgamma receptor binding. *Structure* (2020) 28(5):516–527 e5. doi: 10.1016/j.str.2020.03.001

92. Shinkawa T, Nakamura K, Yamane N, Shoji-Hosaka E, Kanda Y, Sakurada M, et al. The absence of fucose but not the presence of galactose or bisecting n-acetylglucosamine of human IgG1 complex-type oligosaccharides shows the critical role of enhancing antibody-dependent cellular cytotoxicity. *J Biol Chem* (2003) 278 (5):3466–73. doi: 10.1074/jbc.M210665200

93. Wang X, Mathieu M, Brezski RJ. IgG Fc engineering to modulate antibody effector functions. *Protein Cell* (2018) 9(1):63–73. doi: 10.1007/s13238-017-0473-8

Frontiers in Immunology

Explores novel approaches and diagnoses to treat immune disorders.

The official journal of the International Union of Immunological Societies (IUIS) and the most cited in its field, leading the way for research across basic, translational and clinical immunology.

Discover the latest Research Topics

See more →

Frontiers

Avenue du Tribunal-Fédéral 34
1005 Lausanne, Switzerland
frontiersin.org

Contact us

+41 (0)21 510 17 00
frontiersin.org/about/contact